



UNIVERSITY OF STAVANGER

FACULTY OF SCIENCE AND TECHNOLOGY

## MASTER'S THESIS

Study programme / specialisation: <b>MSc. in Petroleum Engineering / Drilling and Well Engineering</b>	The spring semester, 2022  Open / <del>Confidential</del>
---	---

Author: <b>Golam Morshed Kadery</b>	 (Author's signature)
--	--

Course coordinator: <b>Dr. Mesfin Belayneh Agonafir, Assoc. Prof.</b> Supervisor(s): <b>Dr. Mesfin Belayneh Agonafir, Assoc. Prof.</b>
---

<b>Title of the Master's Thesis:</b>
--------------------------------------

<i><b>Effects of Nanoparticles (<math>Al_2O_3</math> and <math>TiO_2</math>), Fibers and Fly Ash on Cementitious and Non-cementitious Materials at Room Temperature and 80°C Curing Temperature: Experimental and Empirical Modelling Studies</b></i>
---

Credits (ECTS): <b>30</b>
---------------------------

Keywords:	
-----------	--

<b>OPC, Geopolymer, CF, WF, Nanoparticles, <math>Al_2O_3</math>, <math>TiO_2</math>, FA, UCS, Young's modulus, Resilience, M-modulus, SEM, EDS, Rheology, Viscosity, Pumpability, Temperature, Microstructure, Porosity, Impermeability, Pore Structure, Gel Structure</b>	
--	--

Number of pages: <b>161</b>
-----------------------------

+ Supplemental materials/ Appendices: <b>81</b>
---

Stavanger, 12 <sup>th</sup> of August, 2022
---

## **Acknowledgement**

First and foremost, I would like to praise ALLAH for granting me his hallowed grace and blessings throughout my academic and personal life and, indeed, in completing my thesis. His benevolence has enabled me to accomplish all of my academic endeavours.

I want to express my infinite and most profound appreciation to my supervisor, Dr. Mesfin Belayneh Agonafir, who deserves my most heartfelt gratitude. It would not have been possible to complete this thesis without the directions, supervision and assistance he offered throughout the process. I am eternally grateful to my supervisor. He is always delighted to be of help and very enthusiastic about having a conversation about thesis work, be it early in the morning or late in the evening. His incomparable dedication to his thesis candidates and his regular students alike is something that everyone admires.

Additionally, I would like to thank Dr. Andreas Delimitis for assisting me with SEM and EDS analyses of my test samples during the course of the experimental works of this thesis.

Furthermore, I would like to express my gratitude to the University of Stavanger for permitting me to use the facilities, including the equipment and laboratories, during the experimental work conducted for this thesis. My time spent studying at the University of Stavanger has been both illuminating and instructive during the years that I have attended.

In conclusion, I would like to convey my unconditional love and affection to my parents, A B M Azad and Laila Masuda, who have raised me to be a good and mentally strong person and who have been a constant source of inspiration and motivation for me throughout my life, particularly in my academic endeavours abroad. I want to thank two extraordinary friends of mine, Dipanjan and Ashiq, whom I got to know when I came to study in Norway. Their wonderful company is what I am grateful for whenever the times were difficult.

I am dedicating my thesis to my loving parents, who are my north stars.

Golam Morshed Kadery  
University of Stavanger  
Stavanger, August 2022.

## **Preface**

This thesis was completed at The Department of Energy and Petroleum Engineering (IEP) at the University of Stavanger, following the rules and regulations set by the university in spring 2022.

The candidate with this declares that all copyrighted information has been properly referenced and cited to the best of his abilities but should anyone be an owner of a copyright and believe that your rights have been infringed upon, please contact at [kadery.a20.2019@gmail.com](mailto:kadery.a20.2019@gmail.com) and the situation will be remedied readily.

General information regarded as public knowledge or not copyrighted by individuals has not been cited. Sources can be located in the [References](#) section, nevertheless.

## Abstract

Cement constitutes undoubtedly one of the most important well barrier elements, in terms of maintaining well integrity by preventing undesired flow of reservoir fluid into the wellbore. NORSOK D-010 standard dictates that well cement must be impermeable, non-shrinking, ductile and resistant to corrosion among other requirements to ensure long term integrity of the wells [1]. Although, various surveys have found that conventional well cement have serious shortcomings that are the reasons for compromising well integrity globally. It was discovered in 2003 that 8000 to 11000 wells in GOM experienced SCP due to compromised cement integrity as the ages of the wells increased [2]. In 2008, cement failure induced well integrity issues were detected in around 10.7% of 75 NCS wells from a total of 406 well that were included in this study [3]–[4]. Poor cement qualities affect the environment as well. Reported in 2013, authorities in Pennsylvania had issued notices of environmental violations to 1144 wells out of 3533 wells, where 8.7% violations originated from poor cement and casing quality that led to environmental pollution [5]. These investigations reveal that cement in its neat form fails to maintain permanent zonal isolation in wells. It goes without saying, the current cement properties do not meet the regulatory requirements. This is why investigations were conducted to improve the mechanical and rheological properties.

Applications of nanotechnology have spread over numerous industries. Numbers of research publications concerning the implementations of nanotechnology are ever growing with time and some studies have shown to have obtained promising results using different metallic nanoparticles. Consequently,  $\text{Al}_2\text{O}_3$  and  $\text{TiO}_2$  nanoparticles (NPs) were considered to be investigated in conjunction with G-class Ordinary Portland Cement (OPC), fly ash (FA), geopolymers, carbon fibers (CF) and white glass fibers (WF). Moreover, two different curing environments of room temperature of  $20^\circ\text{C}$  and oven temperature of  $80^\circ\text{C}$  were introduced to study the temperature effects on the nano-modified cementitious and non-cementitious materials. Because the conventional cement gets degraded when exposed to high temperature for a long time. In terms of experimental structures, total of five test designs were constructed. Four test designs were made with OPC had curing ages of 3, 7 and 28 days and they were cured in both room and oven. One design consisting of geopolymers were mainly cured in room temperature for a period of 10 days.

Lower concentration of  $\text{Al}_2\text{O}_3$  NPs seemed to improve the uniaxial compressive strength (UCS) of OPC by 100.1% in room and 24.8% in oven after 28 days of curing. OPC modified with solitary FA and binary hybrid of FA and intermediate  $\text{Al}_2\text{O}_3$  had shown improvement in early strength after 3 and 7 days. However, after 28 days, solitary and binary blend of FA showed opposing results. Medium concentration of  $\text{TiO}_2$  NPs significantly improved the UCS of geopolymers by 41.8%. When applied in OPC, lowest dosage of  $\text{TiO}_2$  improved the strength of OPC plug by 19.2% in room temperature after 28 days, whereas the highest concentration performed the best in oven with 42.1% UCS raise. With an intention to potentially reducing cement's brittleness, CF and WF were added with  $\text{TiO}_2$  as respective binary hybrids to OPC, which had presented with very optimistic results. Generally,  $\text{TiO}_2$  with highest dosage of CF had shown the most improvements in OPC strength developments in both curing environments. The stiffness, energy absorption capacity and modulus of elasticity of the samples were also analysed, however there were no clear trends of the developments of these properties. Rheological properties for the additives-modified OPC slurries were determined to have workability and slurries were comparatively pumpable, whilst nano-added geopolymers cement was highly viscous for the given LSR. The internal structures of nano-added OPC and geopolymers plugs were analysed with SEM. An empirical UCS vs compressional wave velocity ( $v_p$ ) model was developed from the experimental data from this thesis and it was subsequently tested with three other models to verify its competence and was found to be quite fitting.

## **Table of contents**

<b>Title of the Master’s Thesis .....</b>	<b>1</b>
<b>Acknowledgement .....</b>	<b>2</b>
<b>Preface .....</b>	<b>3</b>
<b>Abstract .....</b>	<b>4</b>
<b>Table of contents.....</b>	<b>5</b>
<b>Table of figures .....</b>	<b>8</b>
<b>List of tables.....</b>	<b>11</b>
<b>List of acronyms .....</b>	<b>12</b>
<b>List of equations .....</b>	<b>13</b>
<b>Nomenclatures .....</b>	<b>14</b>
<b>1 Introduction .....</b>	<b>15</b>
1.1 Background and research motivation .....	15
1.2 Studies on cement related well integrity issues.....	19
1.3 Research questions formulation .....	25
1.4 Scope and objectives of the thesis .....	25
<b>2 Literature Study .....</b>	<b>26</b>
2.1 Ordinary Portland Cement (OPC) .....	27
2.1.1 Hydration process of cement.....	28
2.1.2 Factors affecting hydration process.....	29
2.1.3 Portland cement classifications .....	31
2.1.4 Additives used in Portland Cement .....	32
2.2 Fly Ash .....	32
2.3 Geopolymer cement .....	33
2.3.1 Portland cement chemistry vs Geopolymer cement chemistry .....	34
2.3.2 Geopolymer cement categories .....	35
2.3.3 Potential geopolymer cement application in wellbore cementing operation .....	36
2.3.4 Workability issues of geopolymer cement .....	37
2.4 Fibers .....	38
2.4.1 Carbon fibers (CF) .....	38
2.4.2 White glass fibers (WF) .....	41
2.5 Nanotechnology .....	46
2.5.1 Nanoparticles.....	48
2.5.2 Applications of nanotechnology in petroleum industry .....	49
2.5.3 Potential use of nanotechnology in well cementing in the forms of nanoparticles. 53	
<b>3 Experimental Programs.....</b>	<b>63</b>
3.1 Materials.....	63

3.1.1 Cement .....	64
3.1.2 Water .....	64
3.1.3 Al <sub>2</sub> O <sub>3</sub> Nanoparticles .....	65
3.1.4 TiO <sub>2</sub> Nanoparticles .....	65
3.1.5 Fly Ash .....	66
3.1.6 Geopolymers .....	66
3.1.7 Carbon fibers (CF) .....	68
3.1.8 White glass fibers (WF) .....	68
3.2 Test Designs .....	69
3.2.1 Experimental designs .....	69
3.2.2 Constants and variables .....	70
3.2.3 Cement slurry synthesis .....	70
3.2.4 Test design process and their compositions .....	72
3.2.5 Test Design 1 .....	72
3.2.6 Test Design 2 .....	73
3.2.7 Test Design 3 .....	74
3.2.8 Test Design 4 .....	75
3.2.9 Test Design 5 .....	75
<b>4 Characterization Mechanisms .....</b>	<b>77</b>
4.1 Experimental works .....	79
4.1.1 Destructive tests .....	79
4.1.2 Non-destructive tests .....	87
4.2 Empirical UCS modelling .....	93
4.2.1 Horsrud's (2001) empirical UCS model .....	93
4.2.2 Nerhus's (2020) empirical UCS model .....	93
4.2.3 Titlestad's (2021) empirical UCS model .....	93
<b>5 Results and Discussions .....</b>	<b>94</b>
5.1 General information .....	94
5.2 Test Design 1 (Effect of Al <sub>2</sub> O <sub>3</sub> nanoparticles on OPC) .....	95
5.2.1 Impact of Al <sub>2</sub> O <sub>3</sub> nanoparticles on uniaxial compressive strength (UCS) .....	95
5.2.2 Impact of Al <sub>2</sub> O <sub>3</sub> nanoparticles on Young's modulus (E-modulus) .....	97
5.2.3 Impact of Al <sub>2</sub> O <sub>3</sub> nanoparticles on resilience (R) .....	98
5.2.4 Impact of Al <sub>2</sub> O <sub>3</sub> nanoparticles on P-wave modulus (M-modulus) .....	100
5.3 Test Design 2 (Effect of Al <sub>2</sub> O <sub>3</sub> nanoparticles and fly ash on OPC) .....	102
5.3.1 Impact of Al <sub>2</sub> O <sub>3</sub> nanoparticles and fly ash on uniaxial compressive strength (UCS) .....	102
5.3.2 Impact of Al <sub>2</sub> O <sub>3</sub> nanoparticles and fly ash on Young's modulus (E-modulus) ....	104

5.3.3 Impact of Al <sub>2</sub> O <sub>3</sub> nanoparticles and fly ash on resilience (R) .....	105
5.3.4 Impact of Al <sub>2</sub> O <sub>3</sub> nanoparticles and fly ash on P-wave modulus (M-modulus).....	107
5.4 Test Design 3 (Effect of TiO <sub>2</sub> nanoparticles on geopolymer cement) .....	109
5.4.1 Impact of TiO <sub>2</sub> nanoparticles on uniaxial compressive strength UCS .....	109
5.4.2 Impact of TiO <sub>2</sub> nanoparticles on Young's modulus (E-modulus).....	110
5.4.3 Impact of TiO <sub>2</sub> nanoparticles on resilience (R).....	110
5.4.4 Impact of TiO <sub>2</sub> nanoparticles on P-wave modulus (M modulus).....	111
5.5 Test Design 4 (Effect of TiO <sub>2</sub> nanoparticles on OPC) .....	113
5.5.1 Impact of TiO <sub>2</sub> nanoparticles on uniaxial compressive strength UCS .....	113
5.5.2 Impact of TiO <sub>2</sub> nanoparticles on Young's modulus (E-modulus).....	115
5.5.3 Impact of TiO <sub>2</sub> nanoparticles on resilience (R).....	116
5.5.4 Impact of TiO <sub>2</sub> nanoparticles on P-wave modulus (M modulus).....	118
5.6 Test Design 5 (Effect of TiO <sub>2</sub> nanoparticles, CF and WF on OPC) .....	120
5.6.1 Impact of TiO <sub>2</sub> NPs, CF and WF on uniaxial compressive strength (UCS) .....	120
5.6.2 Impact of TiO <sub>2</sub> NPs, CF and WF on Young's modulus (E-modulus).....	122
5.6.3 Impact of TiO <sub>2</sub> NPs, CF and WF on resilience (R).....	124
5.6.4 Impact of TiO <sub>2</sub> NPs, CF and WF on P-wave modulus (M modulus).....	125
5.7 Rheology of the nano-systems .....	127
5.7.1 Ordinary Portland cement batch 1 .....	128
5.7.2 Geopolymer test design .....	129
5.7.3 Ordinary Portland cement batch 2.....	129
5.8 SEM and EDS analyses .....	131
5.8.1 SEM and EDS analyses for TD-3 samples.....	131
5.8.2 SEM and EDS analyses for TD-4 samples.....	135
5.9 Uncertainties and challenges .....	138
<b>6 Empirical UCS Modelling .....</b>	<b>140</b>
6.1 Development of a new model.....	140
6.2 Testing of the new model .....	141
<b>7 Summary and Conclusions .....</b>	<b>144</b>
<b>8 Future Work Recommendations.....</b>	<b>149</b>
<b>References .....</b>	<b>150</b>
<b>Appendix A – Percentile changes in the results.....</b>	<b>162</b>
<b>Appendix B – Load vs deformation diagrams .....</b>	<b>180</b>
<b>Appendix C – Measured non-destructive test results .....</b>	<b>224</b>
<b>Appendix D – Supplementary pictures of cement plugs and equipment from the experiments .....</b>	<b>240</b>

## Table of figures

Figure 1.1 Typical well construction and the primary cement job [6].....	15
Figure 1.2 Illustration of the barriers throughout a well’s lifecycle [9].....	17
Figure 1.3 Overview of potential leakage pathways along an existing wellbore [10].....	19
Figure 1.4 Various well integrity issues of the 75 wells [3] .....	20
Figure 1.5 Analysis of casing corrosion due to poor cement quality [12] .....	21
Figure 1.6 Location of (a) SCVF/GM source compared to cement top and (b) corrosion failure (casing failure compared to cement top) [12] .....	22
Figure 1.7 A breakdown of the 1144 environmental violations issues for the 3533 wells in Pennsylvania from 2008 to 2011 (Red font indicates those related to well barrier and integrity failure) [5] .....	23
Figure 2.1 Overview of the literature study .....	26
Figure 2.2 Mineralogical Composition of Classic Portland Cement Clinker [2].....	27
Figure 2.3 Hydration of C <sub>2</sub> S and C <sub>3</sub> S versus time [2].....	28
Figure 2.4 Schematic representation of hydration stages and heat development [2].....	29
Figure 2.5 Effect of temperature on hydration kinetics of Class G Portland cement [2].....	30
Figure 2.6 The chemical requirements for fly ashes .....	33
Figure 2.7 Creation of geopolymers [22] .....	34
Figure 2.8 Hardening of OPC (left) and geopolymers (right) [22] .....	34
Figure 2.9 Alkaline-reagents classifications [22].....	35
Figure 2.10 Effect of different concentration of NaOH on the compressive strength [25].....	36
Figure 2.11 Strength of geopolymers at 60°C and 90°C [26].....	37
Figure 2.12 Carbon fibers.....	38
Figure 2.13 A 6 µm diameter carbon fiber filament (running from bottom left to top right) compared to a human hair [31] .....	39
Figure 2.14 Carbon fiber preparation [31] .....	39
Figure 2.15 Compressive strength as a function of fiber mass fractions (a) good dispersion of carbon fibers and (b) poor dispersion of carbon fibers [32].....	40
Figure 2.16 Load extension curve of a target system compared to the response of an unreinforced system and representative fiber-reinforced composites [34] .....	41
Figure 2.17 White glass fiber .....	41
Figure 2.18 Classifications and physical properties of various glass fibers [36].....	42
Figure 2.19 Mechanical properties of various glass fibers [36].....	42
Figure 2.20 Flow chart of fiberglass manufacturing process [39]–[40].....	43
Figure 2.21 Compressive strength at a) 60°C and b) 38°C [41].....	44
Figure 2.22 Dose of the manufactured GRC mortars (values in grams) [42] .....	45
Figure 2.23 Modulus of rupture (bending strength) of the GRC composites. (SC, standard curing for 28 days at 20°C; Acc, short curing for 7 days at 20°C plus Acc for 21 days at 55°C; SC+Ag, 28 days SC plus aging for 28 days at 55°C) [42] .....	45
Figure 2.24 Toughness of the GRC composites. (SC, standard curing for 28 days at 20°C; Acc, short curing for 7 days at 20°C plus Acc for 21 days at 55°C; SC+Ag, 28 days SC plus aging for 28 days at 55°C) [42].....	46
Figure 2.25 Comparison of nanomaterials’ sizes [47] .....	47
Figure 2.26 Schematic diagrams showing some shapes for nano-objects [50].....	47
Figure 2.27 The top-down and bottom-up approach for making nanoparticles [55] .....	48
Figure 2.28 Number of publications per year [60].....	49
Figure 2.29 (a) Distribution of investigation for the different NP in the oil and gas applications; (b) Targeted property of improvement by means of NP [60].....	51
Figure 2.30 Percentage of investigations of NPs across the oil and gas industry [60] .....	51



Figure 2.31 Summary of nanofluids' field trials [77] .....	52
Figure 2.32 UCS for various concentrations of Al <sub>2</sub> O <sub>3</sub> on 0.44 WCR G-class cement [78].....	54
Figure 2.33 The bond strength of the reference case and all repair materials [81].....	55
Figure 2.34 Microscopic images of shale-1.0% ANPs-epoxy polymer nanocomposite interface with two different levels of magnification showing the ability of the epoxy repair material to completely fill the gap at the shale-cement interface [81] .....	56
Figure 2.35 UCS for various concentrations of TiO <sub>2</sub> on 0.52 WCR G-class cement [78] .....	57
Figure 2.36 a) Compressive strength; b) Setting time of the slurry [83] .....	58
Figure 2.37 a) Compressive strengths; b) Shear-bond strengths for the ternary systems [72]	59
Figure 2.38 a) Shear stress and b) UCS of nano-modified rock-based geopolymers [85].....	60
Figure 2.39 a) Compressive and b) splitting tensile strength [86] .....	61
Figure 2.40 Load v/s Deflection graph [88] .....	62
Figure 3.1 Ordinary Portland Cement G-class [91] .....	64
Figure 3.2 Al <sub>2</sub> O <sub>3</sub> Nanoparticles [92] .....	65
Figure 3.3 TiO <sub>2</sub> Nanoparticles [93] .....	65
Figure 3.4 Fly Ash.....	66
Figure 3.5 Silica Fume .....	66
Figure 3.6 10M NaOH [96].....	67
Figure 3.7 Na <sub>2</sub> SiO <sub>3</sub> [97] .....	67
Figure 3.8 Carbon fibers.....	68
Figure 3.9 White glass fibers.....	68
Figure 3.10 Cement Mould .....	71
Figure 4.1 Characterization mechanisms summarized.....	77
Figure 4.2 Characterization of experimental works .....	78
Figure 4.3 Modelling of experimental works.....	78
Figure 4.4 Customized hand-operated hydraulic shop press.....	80
Figure 4.5 Uniaxial compressive strength.....	81
Figure 4.6 Young's modulus of a cement sample .....	82
Figure 4.7 Resilience of a cement sample.....	84
Figure 4.8 a) Leica EM ACE600 sputter coater; b) Copper coated samples .....	85
Figure 4.9 Schematic of a SEM [113].....	85
Figure 4.10 a) Zeiss Gemini Supra 35 VP SEM; b) Samples inside SEM; c) Computer screen .....	86
Figure 4.11 Digital Vernier Caliper .....	87
Figure 4.12 Kern PRJ 1200-3N mass balance.....	88
Figure 4.13 CNS Farnell PUNDIT-7 .....	89
Figure 4.14 OFITE 8-Speed Fann viscometer used in rheology testing .....	92
Figure 5.1 UCS of TD-1 samples cured in room temperature .....	95
Figure 5.2 UCS of TD-1 samples cured in oven temperature .....	96
Figure 5.3 Young's moduli of TD-1 samples cured in room temperature .....	97
Figure 5.4 Young's moduli of TD-1 samples cured in oven temperature.....	98
Figure 5.5 Resilience of TD-1 samples cured in room temperature .....	99
Figure 5.6 Resilience of TD-1 samples cured in oven temperature .....	100
Figure 5.7 P-wave moduli of TD-1 samples cured in room temperature.....	100
Figure 5.8 P-wave moduli of TD-1 samples cured in oven temperature .....	101
Figure 5.9 UCS of TD-2 samples cured in room temperature .....	102
Figure 5.10 UCS of TD-2 samples cured in oven temperature.....	103
Figure 5.11 Young's moduli of TD-2 samples cured in room temperature .....	104
Figure 5.12 Young's moduli of TD-2 samples cured in oven temperature.....	105
Figure 5.13 Resilience of TD-2 samples cured in room temperature .....	106

Figure 5.14 Resilience of TD-2 samples cured in oven temperature .....	106
Figure 5.15 P-wave moduli of TD-2 samples cured in room temperature.....	107
Figure 5.16 P-wave moduli of TD-2 samples cured in oven temperature .....	108
Figure 5.17 UCS of TD-3 geopolymer cement samples .....	109
Figure 5.18 Young's moduli of TD-3 geopolymer cement samples .....	110
Figure 5.19 Resilience of TD-3 geopolymer cement samples .....	111
Figure 5.20 P-wave moduli of TD-3 geopolymer cement samples.....	112
Figure 5.21 UCS of TD-4 samples cured in room temperature .....	113
Figure 5.22 UCS of TD-4 samples cured in oven temperature .....	114
Figure 5.23 Young's moduli of TD-4 samples cured in room temperature .....	115
Figure 5.24 Young's moduli of TD-4 samples cured in oven temperature.....	116
Figure 5.25 Resilience of TD-4 samples cured in room temperature .....	117
Figure 5.26 Resilience of TD-4 samples cured in oven temperature .....	117
Figure 5.27 P-wave moduli of TD-4 samples cured in room temperature.....	118
Figure 5.28 P-wave moduli of TD-4 samples cured in oven temperature .....	119
Figure 5.29 UCS of TD-5 samples cured in room temperature .....	120
Figure 5.30 UCS of TD-5 samples cured in oven temperature .....	121
Figure 5.31 Young's moduli of TD-5 samples cured in room temperature .....	122
Figure 5.32 Young's moduli of TD-5 samples cured in oven temperature.....	123
Figure 5.33 Resilience of TD-5 samples cured in room temperature .....	124
Figure 5.34 Resilience of TD-5 samples cured in oven temperature .....	125
Figure 5.35 P-wave moduli of TD-5 samples cured in room temperature.....	125
Figure 5.36 P-wave moduli of TD-5 samples cured in oven temperature .....	126
Figure 5.37 Shear stress of the tested cement slurries of OPC-1 .....	128
Figure 5.38 Shear stress of the tested cement slurries of OPC-2 .....	129
Figure 5.39 SEM images of (a) Geopolymer Reference; (b) Geopolymer Ref. + 0.4g TiO <sub>2</sub> NPs .....	132
Figure 5.40 SEM image of crystallized TiO <sub>2</sub> nanoparticles in geopolymer cement.....	133
Figure 5.41 EDS results of (a) Geopolymer Reference; (b) Geopolymer Ref. + 0.4g TiO <sub>2</sub> NPs .....	134
Figure 5.42 SEM images of (a) Reference and (b) Ref. + 0.25g TiO <sub>2</sub> NPs.....	135
Figure 5.43 EDS results of (a) Reference and (b) Ref. + 0.25g TiO <sub>2</sub> NPs.....	136
Figure 5.44 TiO <sub>2</sub> NPs fused OPC sample .....	137
Figure 6.1 Newly developed UCS– $v_p$ model .....	140
Figure 6.2 Kadery's UCS experimental data (2022) vs models' estimations .....	141
Figure 6.3 Titlestad's UCS experimental data (2021) vs models' estimations.....	142
Figure 6.4 Nerhus's UCS experimental data (2020) vs models' estimations .....	142

## List of tables

Table 3.1 Test designs in the experimental works of this thesis .....	69
Table 3.2: Constants and variables.....	70
Table 3.3 Test design 1 .....	72
Table 3.4 Composition of TD-1 .....	72
Table 3.5 Test design 2 .....	73
Table 3.6 Composition of TD-2 .....	73
Table 3.7 Test design 3 .....	74
Table 3.8 Composition of TD-3 .....	74
Table 3.9 Test design 4 .....	75
Table 3.10 Composition of TD-4 .....	75
Table 3.11 Test design 5 .....	76
Table 3.12 Composition of TD-5 .....	76
Table 5.1 Standard deviations (SD, MPa) for TD-1 samples in room temperature.....	96
Table 5.2 Standard deviations (SD, MPa) for TD-1 samples in oven temperature.....	97
Table 5.3 Standard deviations (SD, MPa) for TD-2 samples in room temperature.....	103
Table 5.4 Standard deviations (SD, MPa) for TD-2 samples in oven temperature.....	104
Table 5.5 Standard deviations (SD, MPa) for TD-3 geopolymer cement samples.....	109
Table 5.6 Standard deviations (SD, MPa) for TD-4 samples in room temperature.....	114
Table 5.7 Standard deviations (SD, MPa) for TD-4 samples in oven temperature.....	115
Table 5.8 Standard deviations (SD, MPa) for TD-5 samples in room temperature.....	121
Table 5.9 Standard deviations (SD, MPa) for TD-5 samples in oven temperature.....	122
Table 5.10 Selected nano-systems and their references for rheology testing .....	127
Table 5.11 Casson yield stress (YS, $\tau_c$ ) and plastic viscosity (PV, $\mu_c$ ) .....	128
Table 5.12 Viscometer readings for Geopolymer slurries .....	129
Table 5.13 Casson yield stress ( $\tau_c$ ) and plastic viscosity ( $\mu_c$ ) .....	130
Table 7.1 Summary of the experimental results based on UCS developments.....	144

## List of acronyms

%bwoc – By weight of cement  
Acc – Accelerated curing  
ASV– Annular safety valve  
BOP– Blowout preventor  
BP– British Petroleum  
CF– Carbon fibers  
DEP– Department of Environmental Protection of the US state of Pennsylvania  
DSC – Differential scanning calorimetry  
EDS – Energy Dispersive X-ray Spectroscopy  
EOR– Enhanced oil recovery  
ERCB– Alberta Energy Resources Conservation Board  
GM– Gas migration  
GOM– Gulf of Mexico  
HSR– High sulfate resistance  
LSR– Liquid-Solid Ratio  
MSR– Moderate sulfate resistance  
NCS– Norwegian continental shelf  
NORSOK– Norsk Søkkel Konkurransesjjon (Norwegian Shelf’s Competitive Position)  
NPs– Nanoparticles  
OBM – Oil-based mud  
OPC– Ordinary Portland cement G-class  
P&A– Plug and abandonment  
PSA– Petroleum Safety Authority of Norway  
PV– Plastic viscosity  
SC – Standard curing  
SC+Ag – Standard curing + Accelerated aging  
SCP– Sustained casing pressure  
SCVF– Surface casing vent flow  
SD – Standard Deviation  
SEM – Scanning Electron Microscope  
TB– Test batch  
TD– Test design  
TG – Thermogravimetric analysis  
UCS– Uniaxial compressive strength  
USA– United States of America  
WBE– Well barrier element  
WBM – Water-based mud  
WCR– Water-Cement Ratio  
WF– White glass fibers for reinforcement  
Wt.%– Weight percent  
wt%– Weight percent  
X-mas tree– Christmas tree  
XRD – X-ray diffraction  
YS– Yield stress

## List of equations

[Equation 2.1].....	28
[Equation 2.2].....	28
[Equation 4.1].....	81
[Equation 4.2].....	82
[Equation 4.3].....	82
[Equation 4.4].....	83
[Equation 4.5].....	83
[Equation 4.6].....	87
[Equation 4.7].....	87
[Equation 4.8].....	88
[Equation 4.9].....	90
[Equation 4.10].....	90
[Equation 4.11].....	91
[Equation 4.12].....	91
[Equation 4.13].....	91
[Equation 4.14].....	92
[Equation 4.15].....	92
[Equation 4.16].....	93
[Equation 4.17].....	93
[Equation 4.18].....	93
[Equation 6.1].....	140

## Nomenclatures

$A_{\text{cross-section}}$  – Original cross-sectional area of a cement plug, [m<sup>2</sup>]  
 $E$  – Young's Modulus, [GPa]  
 $F_{\text{max}}$  – Maximum load applied at fracture point, [kN]  
 $G$  – Shear modulus, [GPa]  
 $K$  – Bulk modulus, [GPa]  
 $L_0$  – Original plug length, [mm]  
 $m$  – Mass, [g]  
 $M$  – P-wave modulus, [GPa]  
 $m$  – Slope of a stress-strain curve  
 $OD$  – Outer diameter, [mm]  
 $R$  – Modulus of resilience, [kJ/m<sup>3</sup>]  
 $V$  – Volume, [m<sup>3</sup>]  
 $v_p$  – Compressional wave (P-wave) velocity, [m/s]  
 $\gamma$  – Shear rate, [sec<sup>-1</sup>]  
 $\Delta t$  – Sound transit time, [ $\mu$ s]  
 $\Delta \epsilon$  – Change in uniaxial strain, [dimensionless]  
 $\Delta \sigma$  – Change in uniaxial stress, [MPa]  
 $\epsilon$  – Strain, [dimensionless]  
 $\epsilon_y$  – Yield strain, [dimensionless]  
 $\epsilon_{zz}$  – Axial strain [dimensionless] in the same direction as axial stress  
 $\mu_c$  – Casson plastic viscosity, [(lb<sub>f</sub> \* sec) / (100 ft<sup>2</sup>)]  
 $\rho$  – Density, [kg/m<sup>3</sup>]  
 $\sigma$  – Stress, [MPa]  
 $\sigma_{\text{UCS}}$  – Uniaxial compressive strength, [MPa]  
 $\sigma_y$  – Yield stress, [MPa]  
 $\sigma_{zz}$  – Axial stress [MPa] in the longitudinal direction  
 $\tau$  – Shear stress, [lb<sub>f</sub> / (100 ft<sup>2</sup>)]  
 $\tau_c$  – Casson yield stress, [lb<sub>f</sub> / (100 ft<sup>2</sup>)]

## 1 Introduction

Ordinary Portland G-class cement (OPC) is frequently used in the development of oil and gas wells, as well as in plug and abandonment operations. The principal functions are to maintain the integrity of the well and to prevent undesirable fluid leaks from reaching the surface. However, well integrity surveys reveal that conventional cement fails to meet regulatory standards specified in NORSOK D-010, most accepted well integrity standard. This demonstrates the need of improving G-class cement and it is the most widely utilized well cement. As such, this thesis includes an experimental investigation into the impacts of fly ash, different nanoparticles and fibers additions on 0.44 WCR pristine G-class cement and on geopolymer. The cement's characteristics were determined using destructive and non-destructive testing. Additionally, the literature reviews on the application of nanotechnology to cement are offered, as well as the theory used to define the cement's characteristics. Additionally, an empirical model was created from the recorded test data that may be utilized to predict the cement's uniaxial compressive strength (UCS) using the compressional wave velocity ( $v_p$ ).

### 1.1 Background and research motivation

The operationally efficient, environmentally safe and cost-effective recovery of hydrocarbons from a reservoir should be the primary concern of every oil or gas well. To do this, the well must have an appropriate design and construction, with special attention paid to ensuring the well's continued structural soundness throughout time. Typical components of a well's construction are seen in *figure 1.1*, including the conductor casing, surface casing, intermediate casing, production casing, a production tubing and surrounding cement. In general, the structural parts of the well should be constructed to handle operational and geological loadings induced by temperature and pressure in order to survive a variety of failure modes including collapse, burst, corrosion, and deformation, which are most often seen.

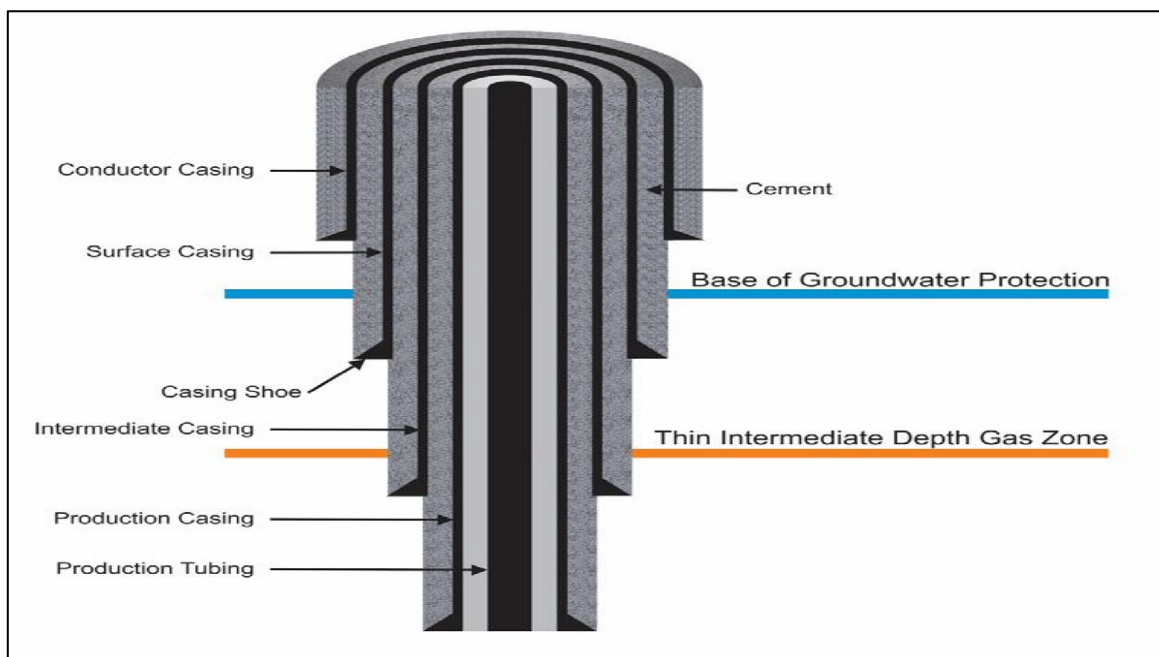


*Figure 1.1 Typical well construction and the primary cement job [6]*

According to NORSOK D-010, well barrier is defined as “Envelope of one or several well barrier elements preventing fluids from flowing unintentionally from the formation into the wellbore, into another formation or to the external environment” and well barrier element as “A physical element which in itself does not prevent flow but in combination with other well barrier elements forms a well barrier” [1].

Cement constitutes one of the most important well barrier elements in the primary and secondary well barrier envelopes depending on the operational stage of a well and that is why it is covered under the definitions of well integrity, which is supported by physical well barrier elements.

The definition of well integrity according to NORSOK D-010 follows as “Application of technical, operational and organizational solutions to reduce risk of uncontrolled release of formation fluids and well fluids throughout the life cycle of a well” [1]. This is the most accepted well integrity definition by the industry. ISO/TS 16530-2 gives other accepted definition, which finds well integrity as “Containment and the prevention of the escape of fluids (i.e., liquids or gases) to subterranean formations or surface” [7]. NORSOK D-010 also sets the following requirements for the properties of cement [1]:

- Provide long term integrity (eternal perspective)
- Impermeable
- Non-shrinking
- Able to withstand mechanical loads/impact
- Resistant to chemicals/ substances (H<sub>2</sub>S, CO<sub>2</sub> and hydrocarbons)
- Ensure bonding to steel
- Not harmful to the steel tubulars integrity

Pertaining to well integrity, as a WBE, cement is used to hold casings in place and to prevent fluid migration between subsurface formations. In addition, cement provides corrosion protection for the casing by isolating the steel casing from aggressive fluids and gases such as H<sub>2</sub>S, brine and CO<sub>2</sub>, thus extending the well's lifespan. Cementing operations can be divided into two broad categories: primary cementing and remedial cementing [8].

Primary cementing is a technique for placing cement slurries in the annular space between the casing and the borehole, shown in *figure 1.1*. After placement, the cement hardens to form a hydraulic seal in the wellbore, preventing the migration of formation fluids in the annulus. Therefore, primary cementing is one of the most critical stages during the drilling and completion of a well. This procedure must be planned and executed carefully, because there is only one chance to complete the job successfully. During the life of a producing oil and gas well, the quality of the cement job has a direct impact on the economic longevity of the well. From the time the well is first produced until the well is abandoned, proper cement-slurry design and placement techniques will affect well productivity, both physically and economically [2].

Remedial cementing is a general term to describe operations that employ cementitious fluids to cure a variety of well problems. Such problems may occur at any time during the life of the well, from well construction to well stimulation, production, and abandonment. Remedial cementing is commonly divided into two broad categories: plug cementing and squeeze cementing. Plug cementing consists of placing cement slurry in a wellbore and allowing it to set. Squeeze cementing consists of forcing cement slurry through holes, splits, or fissures in the casing/wellbore annular space [2].



To further demonstrate the significance of cement in a well, we must understand that cement has several applications inside a well. Cement is considered a primary and secondary well barrier element depending on the life stage of a well in NORSOK D-010. Throughout regular operations, it is considered a secondary barrier. In some instances, however, the liner cement serves as the principal barrier, such as during a temporary P&A operation in which the X-mas tree and BOP are removed [1]. Some barriers are primary barriers, while others are secondary since there should always be at least two in place according to the NORSOK D-010 standard [1].

Besides well completion and well intervention usages, cement is used widely in P&A operations, both temporarily and permanently. During a permanent P&A operation, the plugging materials are frequently made of cement because of its inexpensiveness and reasonable availability, albeit it might not be the most optimal in the neat form, particularly in the eternal aspects. The reasons behind the potential ineffectiveness of the cement plugs in the grand scheme of time will be discussed momentarily. **Figure 1.2** depicts the use of cement throughout the lifecycle of a well including permanent P&A operation [9].

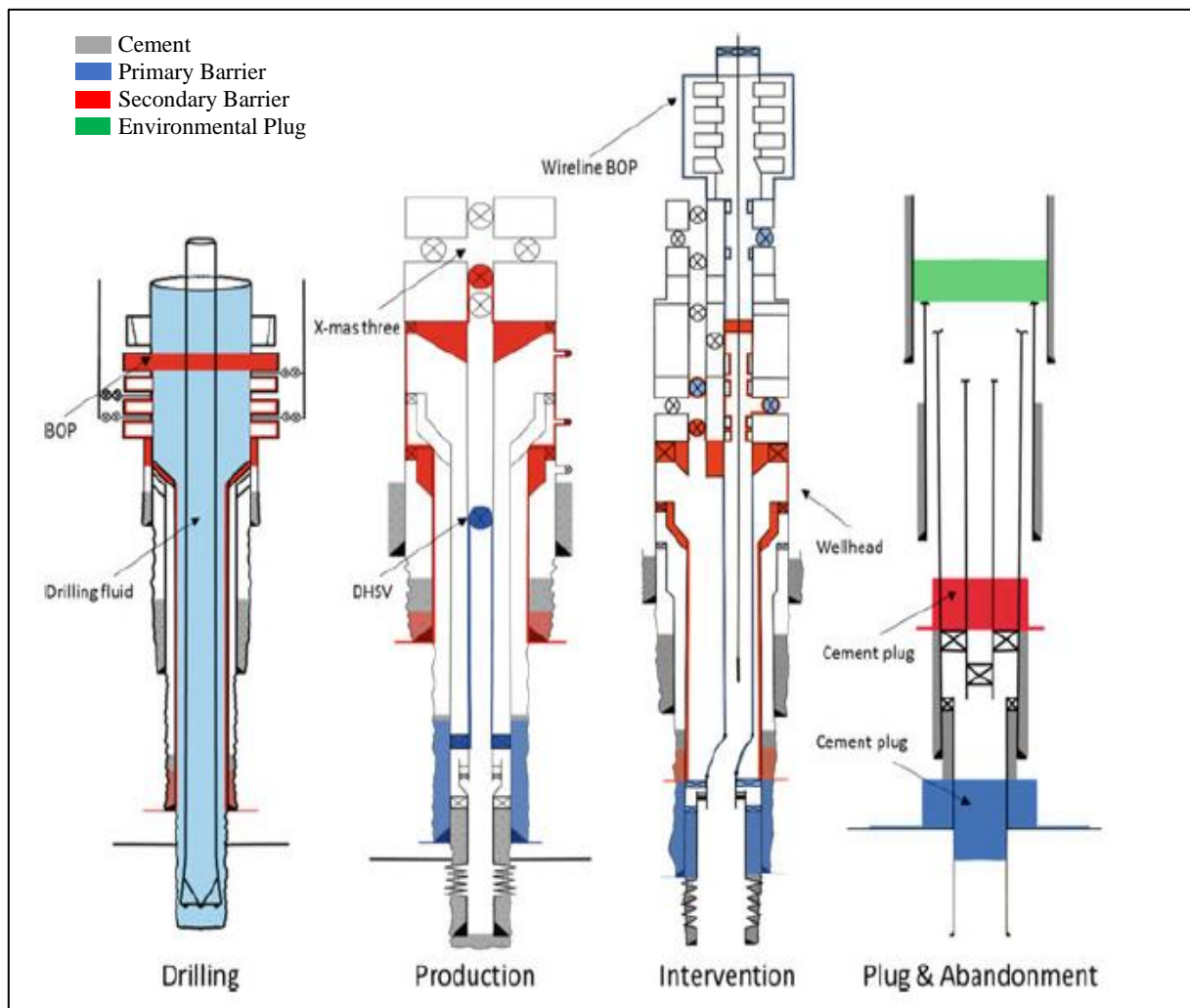


**Figure 1.2** Illustration of the barriers throughout a well's lifecycle [9]

As it has been discussed already, it is known that oil and gas wells are exposed to enormously harsh environments i.e., high pressures and temperatures, toxic and corrosive fluids and gases which cause failure in wellbore cement. These can be occurring both naturally and introduced intentionally due to operational necessity. The failures in cement can be characterized by the following terms as [2]:

- **Cracking:** The first condition, termed ‘cracking’, is caused by thermal or pressure fluctuations in the well caused by the production process. For example, gas wells are subjected to large variations in drawdown pressure and temperature as the gas demand changes. Depending on the magnitude and frequency of these production variables, the casing and cement sheath expand and contract in different ways. This causes stress gradients that gradually crack cement, with the subsequent loss of cement integrity.
- **Debonding:** The second condition, termed ‘debonding’, occurs when the bond between either the cement/rock or the pipe/cement interface fails. Several production practices can cause debonding:
  - The gradual decrease in pressure as a well is produced
  - Casing movement as subsidence occurs
  - Cement shrinkage with time
  - Temperature and pressure fluctuations
  - Stimulation practices, such as hydraulic fracturing
- **Shear failure:** The third condition, called ‘shear failure’, typically results in complete failure of the cement sheath. Shear failure is normally caused by effective stress increases around a wellbore caused by rock subsidence and movement as the reservoir is depleted. This effect can also be caused by vibrations from downhole pumps or gas-lift operations.

Any of these conditions will result in flow paths in the form of discrete conductive fractures in the cement or micro-annuli. These paths, and their effective widths, create cement permeabilities that far exceed the intrinsic permeability of the undisturbed cement. Even a small micro-annulus results in a large effective permeability along the cement sheath.

*Figure 1.3 shows* overview of potential leakage pathways along an existing wellbore, which are listed in the following [10]:

**Path (1)** – through the casing

**Path (2)** – through fractures on the cement wall

**Path (3)** – between the cement wall and formation rock

**Paths (4 and 5)** – between cement and casing

**Path (6)** – through the cement plugs (modified from [3])

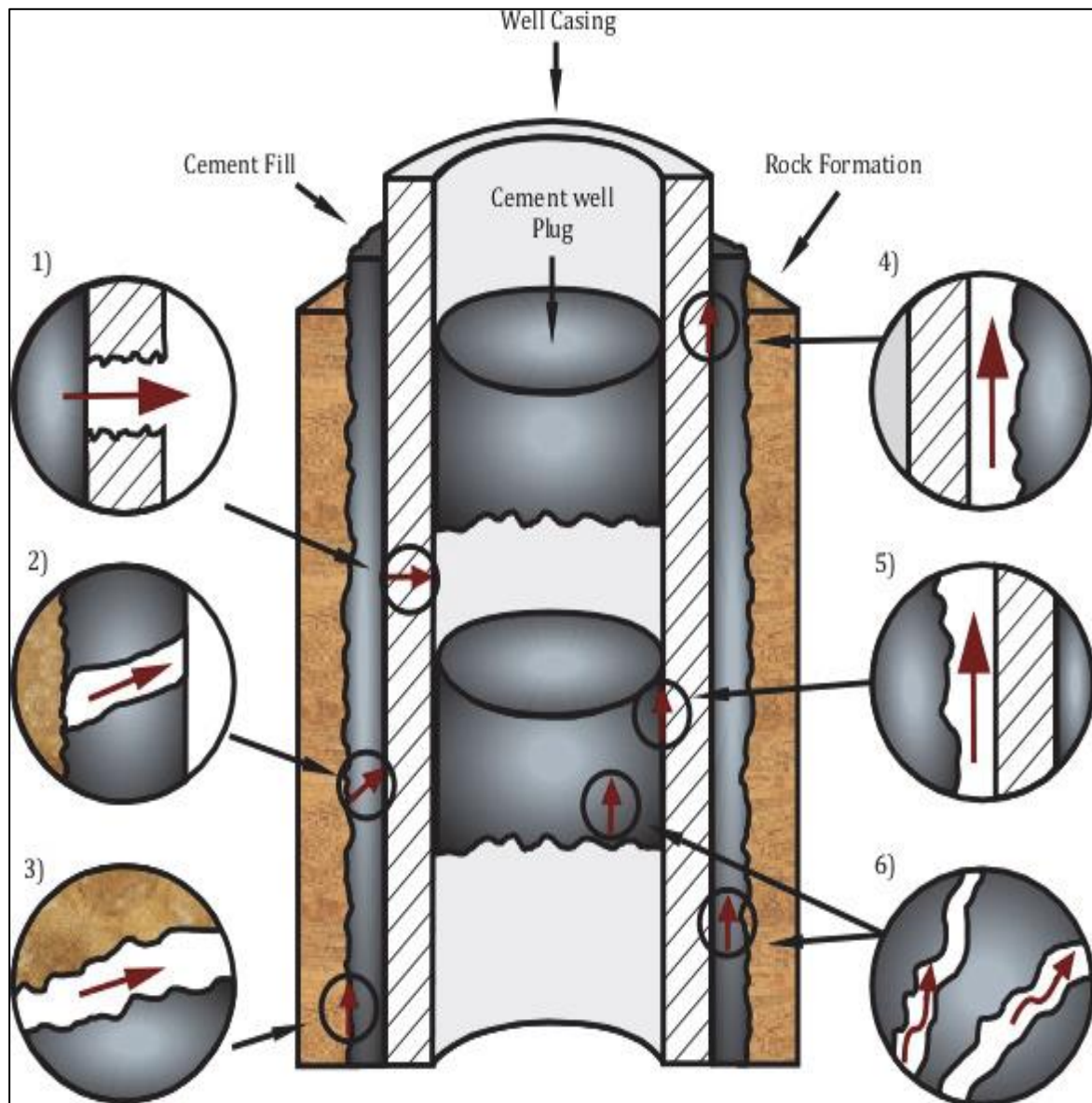


*Figure 1.3 Overview of potential leakage pathways along an existing wellbore [10]*

## **1.2 Studies on cement related well integrity issues**

There are several studies and surveys that have been conducted by various entities to pursue the knowledge of the real-world consequences of cement utilizations in wells and the reasons behind the failure of cement and their ramifications. In addition to the above discussions, these studies and surveys can motivate us to research more on cement to obtain solutions towards solving the well integrity issues rooting from cement to make hydrocarbon production futureproof.

➤ Offshore Norway

In one study by Vignes and Aadnøy (March, 2008), titled “Well-Integrity Issues Offshore Norway”, it is shown that cement failure has been one of the most widespread reasons for well integrity issues in the wells on the Norwegian Continental Shelf (NCS). It was found that out of 406 production and injection wells, 75 wells (18% of 406 wells) reported well integrity issues in terms of well barrier elements failure [3]. It is observed from the following **figure 1.4**, cement failure (10.7%) along with tubing (38.7%), ASV (12%) and casing (10.7%) related issues cause the most numbers of issues in wells [3]. Cement problems range from no cement behind the casing and above the production packer to leaks likely along cement bonds, or leak through cement micro-annulus.

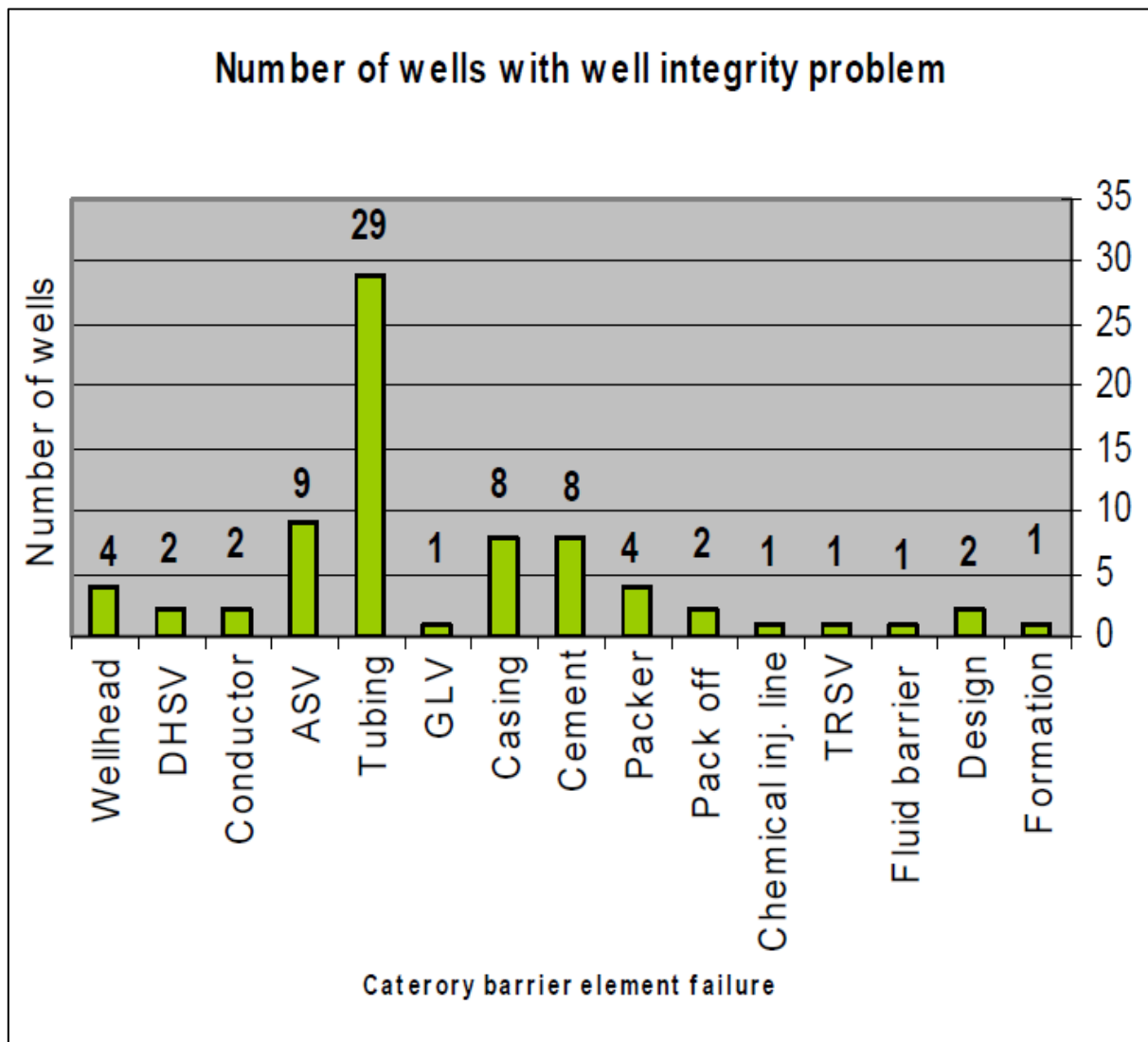
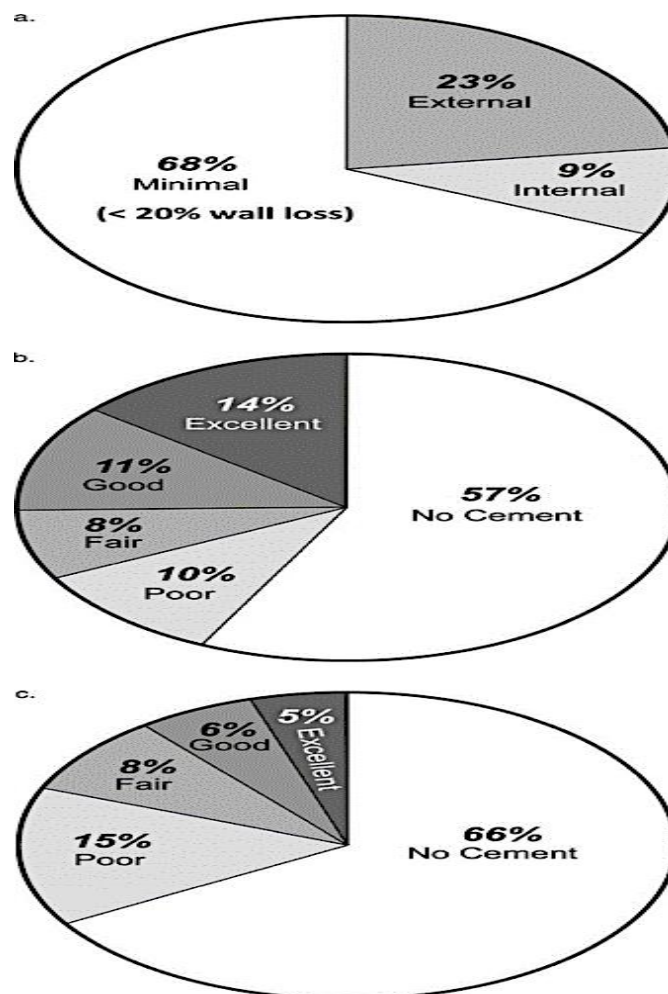


Figure 1.4 Various well integrity issues of the 75 wells [3]

➤ **Alberta, Canada**

The Alberta Energy Resources Conservation Board (ERCB), the regulatory agency for energy resources production and conservation in Alberta, collects and stores information about all the deep wells in the province (oil, gas, injection, and disposal). At the end of 2004, there were approximately 316,500 wells. Casing-inspection logs that indicated both internal and external corrosion were evaluated against cement-bond logs (or equivalent). Data were collected for approximately 500 wells. These wells were selected for analysis on the basis of the existence of both surface casing vent flow (SCVF) [11] or gas migration (GM) and casing failure in the same well or on the basis of geographic location in fields known to have a high incidence of SCVF/GM or casing failure. Information on casing and cement condition were recorded against a depth register to determine the effects of cementing on casing corrosion. A smaller subset of these wells (142) had adequate data to conduct full evaluations. The following conclusions were obtained [12]:

- a) The majority of significant corrosion occurs on the external wall of the casing (*figure 1.5.a*)
- b) A significant portion of wellbore length is uncemented (*figure 1.5.b*)
- c) External corrosion is most likely to occur in areas where there is no or poor cement (*figure 1.5.c*)



*Figure 1.5 Analysis of casing corrosion due to poor cement quality [12]*

Another important determination was made in relation to casing failure due sub-optimum cement placement in the wells, which is most of the casings' issues stemming from SCVF/GM took place in shallower depths and it is comprehensible that lack of cement in those depths was to be blamed as it did not isolate the casings from formation sufficiently. Following *figure 1.6* will give a clear picture of the situation [12].

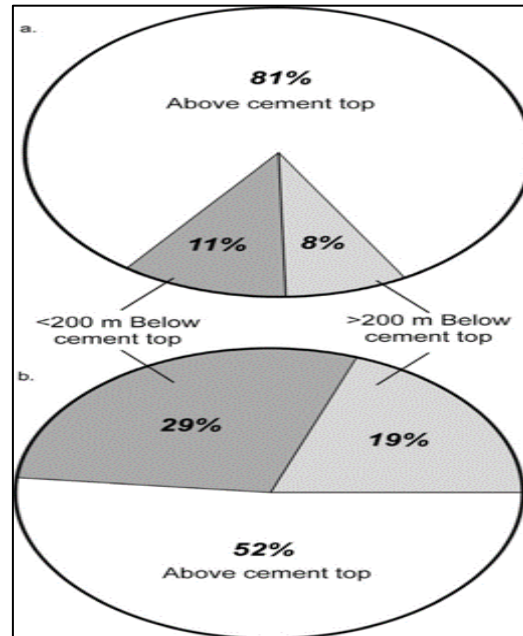


*Figure 1.6 Location of (a) SCVF/GM source compared to cement top and (b) corrosion failure (casing failure compared to cement top) [12]*

#### ➤ Pennsylvania, USA

The online database collated by the Department of Environmental Protection (DEP) in the US state of Pennsylvania allows oil and gas well archived by various criteria, such as well status, operator and drilling date. Using this database, Considine et al. (March, 2013) identified 2.58% of 3533 individual wells as having some forms of barrier or integrity failure. This consisted of 0.17% of wells that have experienced blowouts (4 wells), venting or gas migration (2) and 2.41% having experienced casing or cementing failures. Measurable concentrations of gas were present at the surface for most wells with casing or cementing violations. *Figure 1.7* shows a breakdown of the 1144 environmental violations issues for the 3533 wells [5].

In this study, the search criteria used to categorize leakage incidents in Pennsylvania are based on code violations reported during site inspections. Code violations that would constitute a well failure is those likely to result in a significantly increased risk of contaminants reaching either the surface or potable water sources. They include [5]: (a) failure to case and cement the well properly; (b) excessive casing seat pressure; (c) failure to case and cement sufficiently to prevent migrations into fresh groundwater; and (d) insufficient cement and steel casings between the wellbore and the near-surface aquifer to prevent seepage of fluids. Using the Pennsylvania state database, a well barrier or integrity failure rate of 6.3% is found for the years 2005–2013.

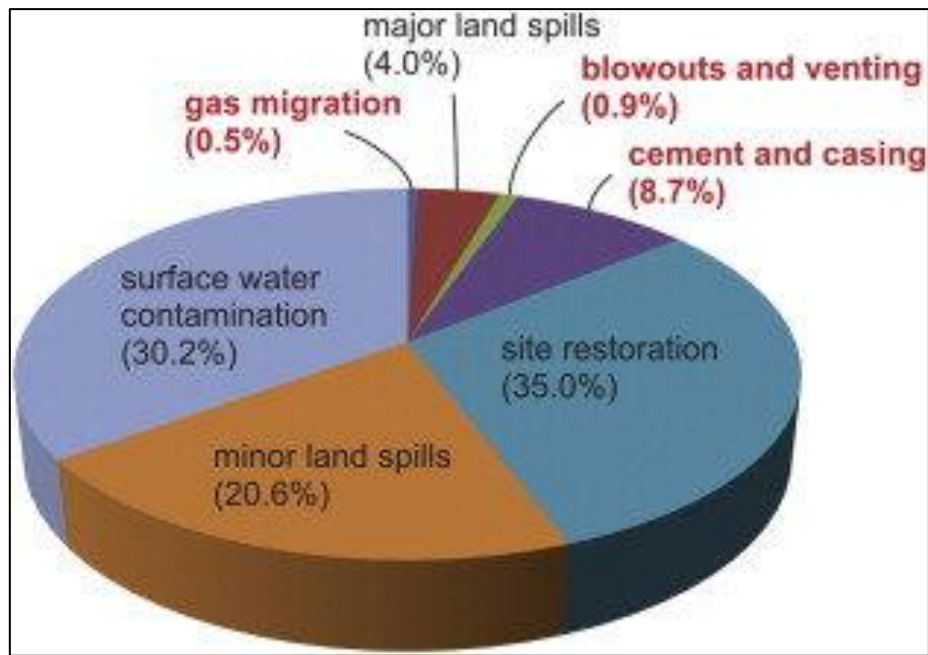


**Figure 1.7** A breakdown of the 1144 environmental violations issues for the 3533 wells in Pennsylvania from 2008 to 2011 (Red font indicates those related to well barrier and integrity failure) [5]

➤ **Gulf of Mexico, USA**

Data from the US Minerals Management Service show that of 15,500 producing, shut in and temporarily abandoned wells in the outer continental shelf of the Gulf of Mexico (GOM), 6692 (43%) have sustained casing pressure (SCP) on at least one casing annulus. Of these incidents, 47.1% occurred in the production strings, 26.2% in the surface casing, 16.3% in the intermediate casing, and 10.4% in the conductor pipe [13]. SCP is excessive casing pressures in wells that persistently rebuilds after bleed-down. SCP is caused by gas migration from a high-pressured subsurface formation through the leaking cement sheath in one of the well's casing annuli. It may also be caused by defect and leaking tubing connections, downhole accessories or wellhead seals [14]. In eventuality, SCP poses a serious HSE risk and effectively renders wells short-lived.

All the surveys that have been presented above provide evidence that the loss of well integrity occurs on a regular basis globally in spite of taking necessary precautions, using innovative technologies and highly trained personnel. Cement related issues play a significant role in contributing to the integrity problems. It is possible that severe leakages from a well might have severe implications for the environment, as well as be the cause of serious harm to personnel and in the worst-case scenario, the loss of human life. In addition to this, the loss of cement integrity may contribute to reduced production from wells, a significantly shorter longevity for wells, complicated and expensive remedial operations and sometimes even penalties from regulatory authorities depending on the magnitude of a situation. Improving composition compositions of cementitious and non-cementitious materials can help reduce the number of well integrity concerns by minimizing the number of occurrences where cement-related difficulties are the primary cause. The research is not only of paramount importance for the petroleum industry but also for other industries where cementitious and non-cementitious materials are often used.

British Petroleum's (BP) "Statistical Review of World Energy of 2022" reveals that energy demand and emissions bounced back to around pre-pandemic levels in 2021, reversing the temporary reduction in 2020 resulting from the COVID-19 pandemic. It was recorded that oil and natural gas still hold the biggest shares with more than 50% shares among the global primary energy. Renewable energy had gradual increase in energy shares, while coal and nuclear energy shares plummeted [15]. From this review, it is unequivocally clear that petroleum products are still in high demand and will be for much longer than anticipated.

The reason behind discussing the scale of the energy consumption by types of energy source is to show that the hydrocarbon industry is still the primary energy industry in the world. Even though, this industry is not the most favourite industry presently, owing to greater emphasis and renewed consciousness around climate change, the environment and the long-term viability of our energy supplies and eventually there might come a time when a full transition may happen from the usage of hydrocarbon to renewable and alternative energy sources, but for the foreseeable future we are greatly dependent on oil and gas. That is exactly why maintaining the integrity of wells has become a concern on a worldwide scale. Therefore, we can say in an unambiguous conclusion that cement is an important component of the well integrity equation and it plays a critical part in ensuring that we will be able to continue to meet our ever-increasing need for energy. It should be compelling enough for continuous research on cementitious and non-cementitious materials.



### **1.3 Research questions formulation**

As one of the most suitable options, cement and cementation remain fundamental parts of well construction, intervention and plugging materials in P&A operations. Albeit cement related well integrity issues have been reported at an alarmingly high rate globally as discussed in the earlier section. A failure of cement could result in an unmitigated disaster. This leads one to believe that the ordinary Portland cement used in wells does not fulfill all the requirements specified by the NORSOK D-010 standard. Eventually, enhancing cement's material qualities is indispensable.

In recent years, the use of nanotechnology in the petroleum sector has demonstrated promising outcomes for applications such as well cementing, drilling fluids, and enhanced oil recovery (EOR). These achievements have been achieved using nanoparticles. However, usage of nanoparticles in the petroleum sector are not yet ready for commercial use since this field is still in the research and development stage. For the purpose of this thesis, G-class OPC as cementitious material and alkaline-activated fly ash based geopolymer as non-cementitious material will be used to evaluate the impacts of various nanoparticles, fibers and fly ash on these chosen materials. The following research questions are going to be addressed:

- The effects of the separate fly ash and nanoparticles on cement and non-cementitious materials' mechanical and rheological parameters
- The effects of binary hybrids of fly ash, nanoparticles and fibers on cement and non-cementitious materials' mechanical and rheological parameter

### **1.4 Scope and objectives of the thesis**

The following subjects will also be discussed in depth inside the thesis in addition to the questions mentioned in the [section 1.3](#):

- Literature review of the theories on relevant materials (*figure 2.1*)
- Experimental characterizations of the following in room temperature and 80°C curing temperature (*figure 4.2*):
  - Effect of Al<sub>2</sub>O<sub>3</sub> nanoparticles on G-class OPC
  - Effect of Al<sub>2</sub>O<sub>3</sub> nanoparticles on Fly ash and G-class OPC blended system
  - Effect of TiO<sub>2</sub> nanoparticles on alkaline-activated fly ash based geopolymer cement
  - Effect of TiO<sub>2</sub> nanoparticles on G-class OPC
  - Effect of binary blend of TiO<sub>2</sub> and either with carbon fibers or white glass fibers for reinforcement nanoparticles on G-class OPC
- Empirical modelling of uniaxial compressive strength (UCS) vs compressional wave velocity ( $v_p$ ) (*figure 4.3*)

## 2 Literature Study

The purpose of this upcoming sections is to provide a theoretical foundation by conducting a comprehensive literature review of pertinent materials and procedures used in the experimental efforts presented in this thesis. The following *figure 2.1* will show the overview of the literature study path.

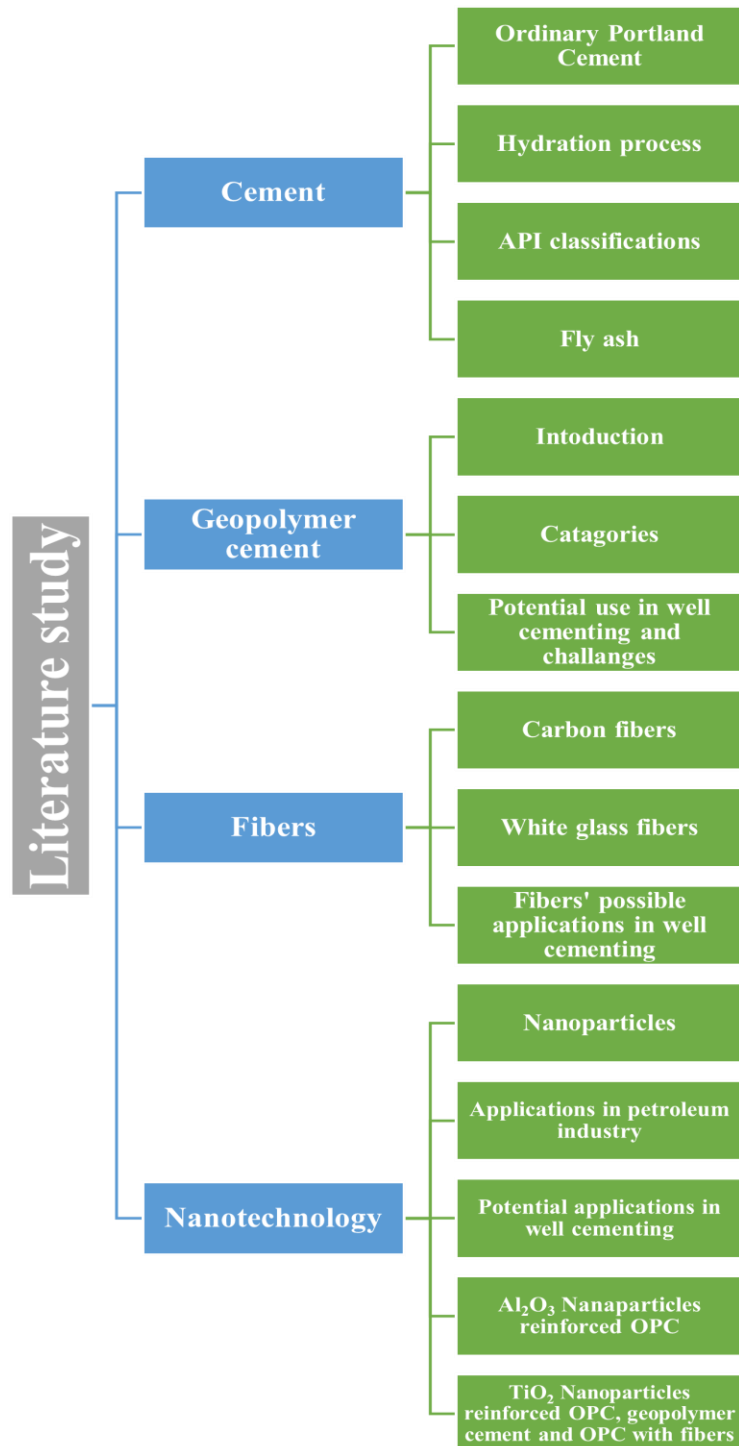


Figure 2.1 Overview of the literature study

## 2.1 Ordinary Portland Cement (OPC)

Ordinary Portland cement (OPC) is by far the most important oilwell binding material in terms of quantity produced and indeed, it is possibly the most abundant manufactured material. The term “ordinary” indicates that the cement is manufactured in a rotary kiln from a molten matrix of suitably proportioned ingredients. OPC is used in nearly all well cementing operations, therefore, throughout this thesis, the terms *OPC* and *Ordinary Portland Cement* shall be used interchangeably. The conditions to which Portland cements are exposed in a well differ significantly from those encountered at ambient conditions during construction operations; as a result, special Portland cements are manufactured for use as well cements [2].

OPC is the most common example of a hydraulic cement. Such types of cement set and develop compressive strength due to hydration, involving chemical reactions between water and the compounds present in the cement. The setting and hardening occur not only if the cement/water mixture is left to stand in the air but also if it is placed underwater. The development of strength is predictable, uniform, and relatively rapid. The set cement also has low permeability and is nearly insoluble in water; therefore, exposure to water does not destroy the hardened material. Such attributes are essential to achieving and maintaining zonal isolation [2]. It is easy to appreciate why Portland cement is utilized in such high quantities in the petroleum sector when these features are considered in conjunction with its availability and the relative economic feasibility of the material.

Portland cement is produced by pulverizing clinker. Clinker is the calcined (burned) material that exits the rotary kiln in a cement plant. Clinker consists primarily of hydraulic calcium silicates, calcium aluminates, and calcium aluminoferrites. One or more forms of calcium sulfate are interground with the clinker to make the finished product. Materials used in the manufacture of Portland cement clinker must contain appropriate amounts of calcium, silica, alumina, and iron compounds. During manufacture, frequent chemical analyses of all materials are made to ensure uniformity and high quality [2].

Two types of raw materials are needed to prepare a mixture that will produce Portland cement clinker: calcareous materials, which contain lime, and argillaceous materials, which contain alumina, silica, and iron oxide. The properties of Portland cement are determined by the mineralogical composition of the clinker. The mineralogical composition of conventional Portland cement clinker is shown in *figure 2.2*. For special cements, the content of  $C_3A$  and  $C_4AF$  can differ significantly. The main oxides make up about 95%:  $CaO$  (60-70%);  $SiO_2$  (18–22%);  $Al_2O_3$  (4–6%) and  $Fe_2O_3$  (2–4%) [2].

Oxide Composition	Cement Notation	Common Name	Concentration (wt%)
$3CaO \cdot SiO_2$	$C_3S$	Alite	55–65
$2CaO \cdot SiO_2$	$C_2S$	Belite	15–25
$3CaO \cdot Al_2O_3$	$C_3A$	Aluminate	8–14
$4CaO \cdot Al_2O_3 \cdot Fe_2O_3$	$C_4AF$	Ferrite phase	8–12

*Figure 2.2 Mineralogical Composition of Classic Portland Cement Clinker* [2]

### 2.1.1 Hydration process of cement

The compounds present in Portland cement are anhydrous. When brought into contact with water, they are attacked or decomposed, forming hydrated compounds. Supersaturated and unstable solutions form, gradually depositing their excess solids. Because the solubilities of the original anhydrous compounds are much higher than those of the hydration products, complete hydration should ultimately occur [2].

The silicate phases in Portland cement are the most abundant, often comprising more than 80% of the total material.  $C_3S$  is the principal constituent, with a concentration as high as 68%. The quantity of  $C_2S$  typically does not exceed 30%. As shown in the idealized chemical equations below, the hydration products for both phases are calcium silicate hydrate and calcium hydroxide (also known as portlandite) [2].



The calcium silicate hydrate does not have the exact composition of  $C_3S_2H_3$ ; instead, the C:S and H:S ratios are variables depending upon such factors as the calcium concentration in the aqueous phase, temperature, the presence of additives and aging. The material is quasi-amorphous and it is therefore commonly called the “C-S-H phase”. The C-S-H phase makes up roughly 65% of fully hydrated Portland cement at ambient conditions and is considered the principal binder of hardened cement. By contrast, the calcium hydroxide is highly crystalline and occurs as hexagonal plates. Its concentration in hardened cement is usually between 15% and 20% [2].

After a brisk but brief initial hydration when added to water, the silicate phases experience a period of low reactivity, called the “induction period.” During this stage, they do not significantly influence the rheology of the cement slurry. Substantial hydration eventually resumes and as shown in *figure 2.3*, the hydration rate of  $C_3S$  exceeds that of  $C_2S$  by a wide margin. Because of the  $C_3S$  abundance and the massive formation of the C-S-H phase, the hydration of  $C_3S$  is mainly responsible for the beginning of the set and early strength development. The hydration of  $C_2S$  is significant only in terms of the final strength of the hardened cement [2].

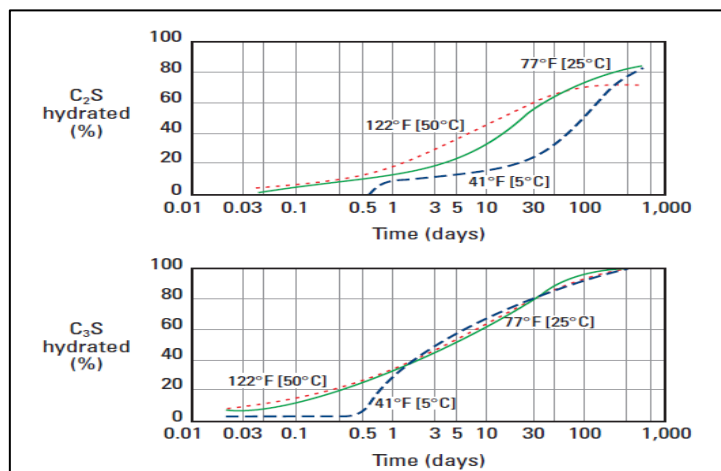


*Figure 2.3 Hydration of  $C_2S$  and  $C_3S$  versus time [2]*

The hydration of  $C_3S$  (OPC) is an exothermic process; therefore, the hydration rate can be followed by conduction calorimetry. Five hydration stages are arbitrarily defined from the thermogram given in *figure 2.4* [2].

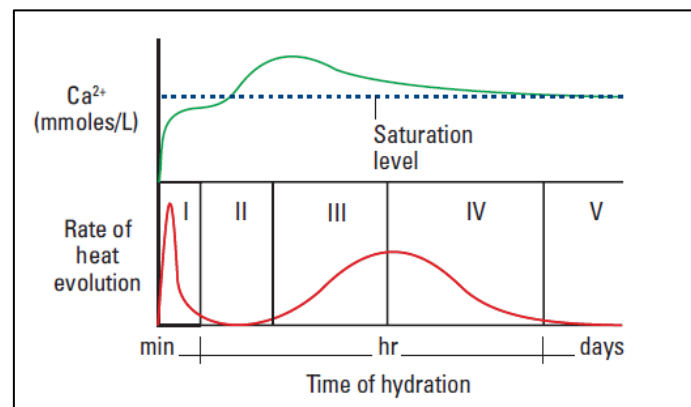


*Figure 2.4 Schematic representation of hydration stages and heat development* [2]

The five stages from the schematic of hydration stages and heat development are stated below according to the roman numerals [2]:

- I.** Preinduction period
- II.** Induction period
- III.** Acceleration period
- IV.** Deceleration period
- V.** Diffusion period

### **2.1.2 Factors affecting hydration process**

The hydration of Portland cement is a sequence of overlapping chemical reactions between clinker components, calcium sulfate, and water, leading to continuous cement-slurry thickening and hardening. Although the hydration of  $C_3S$  is often used as a model for the hydration of Portland cement, it must be kept in mind that many additional parameters are involved. The following is a list of potential elements that have an impact on the hydration process [2]:

- **Volume changes during setting:** When Portland cement reacts with water, the combined system of cement and water goes through a process that results in a net reduction in volume. This results in a reduction in the volume in absolute terms. This happens because of the fact that the hydrated material has a higher absolute density than the reactants that were used initially.
- **Effect of temperature:** Temperature is one of the significant factors affecting the hydration of Portland cement. The hydration rate of the cement and the nature, stability, and morphology of the hydration products are strongly dependent upon this parameter. Elevated hydration temperatures accelerate the hydration of cement. As illustrated by the calorimetry curves in *figure 2.5*, the duration of the induction and setting periods is shortened, and the rate of hydration during the setting period is much higher. However, upon extended curing, the degree of hydration and the ultimate strength are often reduced. This is most probably related to forming a dense layer of the C-S-H phase around the  $C_3S$  surfaces, hindering their complete hydration.

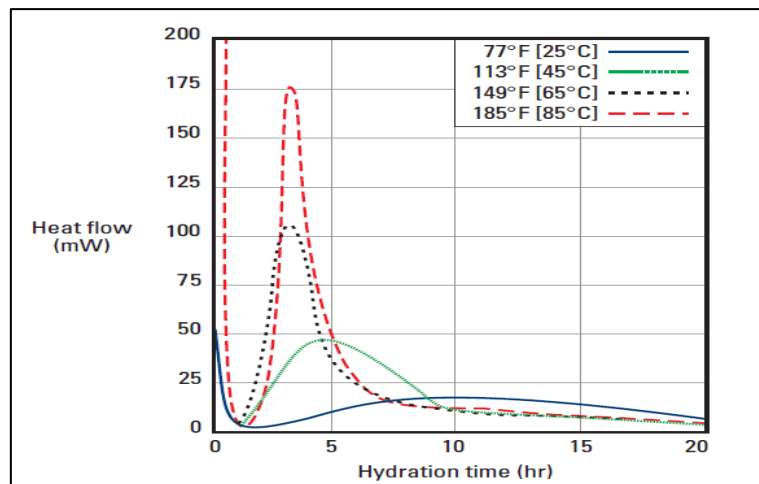


**Figure 2.5** Effect of temperature on hydration kinetics of Class G Portland cement [2]

Up to 40°C, the hydration products are the same as those that occur under ambient conditions. Certain changes occur in the microstructure and morphology of the C-S-H phase at higher temperatures. The material becomes more fibrous, and a higher degree of silicate polymerization is observed. At curing temperatures exceeding 110°C, the C-S-H phase is no longer stable, and crystalline calcium silicate hydrates eventually form.

- **Flash set and false set:** When Portland cement clinker is ground alone (i.e., without calcium sulfates) and mixed with water, the C<sub>3</sub>A and C<sub>4</sub>AF rapidly react. The slurry temperature markedly increases and an irreversible stiffening occurs followed quickly by a pseudoset. This phenomenon is called a “flash set” or sometimes a “quick set”. In the context of well cementing, a flash set could prevent the proper placement of the cement slurry in the annulus. To avoid uncontrolled C<sub>3</sub>A and C<sub>4</sub>AF hydration, calcium sulfates (usually gypsum) are ground in with the clinker while manufacturing Portland cement. For optimal cement performance, the quantity of calcium sulfates must be balanced according to the reactivity of the clinker.
- **Effects of aging:** The performance of Portland cement can be affected significantly by exposure to the atmosphere and high temperatures or both during storage in sacks or silos. The principal effects upon neat cement slurries (no additives) include the following: increased thickening time; decreased compressive strength; decreased heat of hydration and increased slurry viscosity.
- **Influence of alkalis:** The principal alkaline elements found in Portland cement are sodium and potassium. They affect setting and strength development; thus, the amounts of these substances are usually held below 1% (expressed as oxides). In well cements, the maximum concentration of total alkalis is 0.75% (as a convention, these are expressed as total equivalent Na<sub>2</sub>O). Total alkalis are the sum of insoluble alkalis (impurities in the lattices of clinker phases) and soluble alkalis (in the form of alkali sulfates). The effects of alkalis upon strength development are unpredictable. Alkalis demonstrate a positive effect upon early strength but an adverse effect upon long-term strength.
- **Sulfate resistance:** Downhole brines commonly contain magnesium sulfate and sodium sulfate, and detrimental effects can result when such solutions react with certain cement hydration products. These sulfates react with precipitated calcium hydroxide to form magnesium hydroxide, sodium hydroxide and calcium sulfate. The calcium sulfate can in turn react with the aluminates to form secondary ettringite.

- **Influence of surface area:** The surface area (sometimes called fineness, measured in  $\text{cm}^2/\text{g}$  or  $\text{m}^2/\text{kg}$ ) is an essential parameter concerning cement reactivity and slurry rheology. The fineness of cement is usually determined by measuring the air permeability of a small layer of lightly compacted cement (Blaine method [16]). With the assumption that the cement particles are spherical, such information is used to calculate a theoretical surface area.

The water-to-cement ratio required to wet the cement particles and prepare a pumpable slurry is directly related to the surface area. Thus, for consistency of performance, the fineness is controlled by the cement manufacturer.

Compressive strength development is often correlated with the cement's surface area. Generally, the results indicate that cements with high fineness tend to develop greater compressive strength.

### **2.1.3 Portland cement classifications**

Portland cements are manufactured to meet specific chemical and physical standards that depend upon their application. To promote consistency of performance among cement manufacturers, various user groups have established classification systems and specifications. The best-known systems are those of ASTM International (formerly the American Society for Testing and Materials) (ASTM C 150, *Standard Specification for Portland Cement*) and API (API Spec 10A, *Specification for Cements and Materials for Well Cementing*). The ISO has adopted the API classification scheme as Standard 10426-1, *Petroleum and natural gas industries - Cements and materials for well cementing - Part 1: Specification* [2].

The requirements for well cements are more rigorous than those for construction cements. Well cements must perform over a wide range of temperatures and pressures and are exposed to subterranean conditions that construction cements do not encounter. Well cements require greater consistency from batch to batch to ensure predictable performance when various cement additives are introduced. There are currently eight classes of API-ISO Portland cements, designated A through H. They are arranged according to the depths at which they are placed and the temperatures and pressures to which they are exposed. Within some classes, cements with varying degrees of sulfate resistance (as determined by  $\text{C}_3\text{A}$  content) are sanctioned: ordinary (O), moderate sulfate resistance (MSR), and high sulfate resistance (HSR) [2]. Below given are the short descriptions of the API Portland cement classes [2]:

- **Class A:** Intended for use when special properties are not required. Available only in O grade (similar to ASTM C 150, Type I).
- **Class B:** Intended for use when conditions require moderate or high sulfate resistance. Available in both MSR and HSR grades (similar to ASTM C 150, Type II)
- **Class C:** Intended for use when conditions require high early strength. Available in O, MSR, and HSR grades (similar to ASTM C 150, Type III).
- **Classes D, E, and F:** The products obtained by grinding Portland cement clinker, consisting essentially of hydraulic calcium silicates, usually contain one or more of the forms of calcium sulfate as an interground addition. Provided materials used in manufacturing meet the requirements of ASTM C 465, classes D, E, and F are intended for use under moderately high temperatures and pressures. They are available in MSR and HSR grades. Classes D, E, and F are also known as “retarded cements”, intended for use in deeper wells. The retardation is accomplished by significantly reducing the amount of faster-hydrating phases ( $\text{C}_3\text{S}$  and  $\text{C}_3\text{A}$ ) and increasing the particle size of the cement grains.
- **Classes G and H:** The products obtained by grinding Portland cement clinker, consisting essentially of hydraulic calcium silicates, usually containing one or more of the forms of calcium sulfate as an interground addition. No additions other than calcium sulfate or water

or both shall be interground or blended with clinker during Class G well cement manufacture. These products are intended for use as basic well cements. Available in MSR and HSR grades. Classes G and H were developed in response to the improved technology in slurry acceleration and retardation by chemical means. The cement manufacturer is prohibited from adding special chemicals, such as glycols or acetates, to the clinker. Such chemicals improve grinding efficiency but have been shown to interfere with various cement additives. Classes G and H are by far the most commonly used well cements today. In this thesis, the class G cement is considered for the experimental investigations.

- **Classes K and L:** Class K is a composite cement that reflects the oilfield industry practice of blending 35% to 40% bwoc silica in blends where preventing strength retrogression is required and available in O, MSR and HSR grade intended for use as a basic well cement. Class L composite well cement is obtained by intergrinding Portland cement clinker and one or more forms of calcium sulfate with fly ash. This product is intended for use under conditions when a lower density cement slurry is desired [17].

#### **2.1.4 Additives used in Portland Cement**

Portland cement systems for well cementing are routinely designed to perform at temperatures ranging from below freezing in permafrost zones to 350°C [700°F] in thermal-recovery and geothermal wells. Well cements encounter the pressure range from near ambient in shallow wells to more than 30,000 psi [200 MPa] in deep wells. In addition to severe temperatures and pressures, well cements must often be designed to contend with weak or porous formations, corrosive fluids, and over-pressured formation fluids. Cement additives make it possible to accommodate such a wide range of conditions. Additives modify the behavior of the cement system, ideally allowing successful slurry placement between the casing and the formation, rapid compressive strength development, and adequate zonal isolation during the lifetime of the well. Today more than 100 additives for well cements are available, many of which can be supplied in solid or liquid forms. There are eight major categories of additives with different performances such as accelerators, retarders, extenders, weighting agents, dispersants, fluid-loss control agents, and specialty additives [2].

However, in this thesis work, due to the unavailability of all the additives, only cement along with water and this thesis additives will be evaluated.

#### **2.2 Fly Ash**

Fly ash is the residue from power plants that burn pulverized coal. The ash is suspended in flue gases as fused particles solidify into a roughly spherical shape. The ash is very finely divided, with a surface area roughly approximating that of Portland cement. The principal constituent of fly ash is a glass chiefly composed of silica and alumina with some iron oxide, lime, alkalis, and magnesia. Quartz, mullite, hematite, magnetite and some combustible matters are also found. The composition and properties of fly ash can vary widely depending upon the coal's source and the power plant's efficiency; accordingly, the specific gravities of fly ashes can vary from about 2.0 to 2.7 [2].

Fly ash is by far the most widely used of the pozzolanic materials. Pozzolans are a broad class of siliceous and aluminous materials which, in themselves, possess little or no cementitious value but which will, in finely divided form and in the presence of water, react chemically with  $\text{Ca}(\text{OH})_2$  (calcium hydroxide) at ordinary temperature to form compounds possessing cementitious properties [18]. The quantification of the capacity of a pozzolan to react with calcium hydroxide and water is given by measuring its pozzolanic activity [19].



According to ASTM International Standard C618, three types of fly ash are recognized: Types N, F, and C. As shown in **figure 2.6**, the distinction is made on chemical grounds. Types N and F are normally produced from burning anthracite or bituminous coals. Type C fly ashes, made from lignite or sub-bituminous coals, are less siliceous and some contain more than 10% lime; as a result, many of them are cementitious and do not fit the strict definition of a pozzolanic material. In well cementing, Type F fly ash is used most frequently [2].

	Mineral Admixture Class		
	N	F	C
Min. silicon dioxide (SiO <sub>2</sub> ) + aluminum oxide (Al <sub>2</sub> O <sub>3</sub> ) + iron oxide (Fe <sub>2</sub> O <sub>3</sub> ) (%)	70	70	50
Max. sulfur trioxide (SO <sub>3</sub> ) (%)	4	5	5
Max. moisture content (%)	3	3	3
Max. loss on ignition (%)	10	12	6

**Figure 2.6** The chemical requirements for fly ashes

Moreover, fly ash is used as pozzolanic material with an alkaline activator to create geopolymer cement, which comparatively a new material developed to use as a substitute of OPC. Geopolymer is basically a non-cementitious material without fly ash. Geopolymer is considered a significant environmentally alternative to OPC. The use of fly ash reduces the CO<sub>2</sub> emission enormously. FA is the main largest binding material in geopolymer cement. Since this being produced as results of other industrial process, using fly ash abundantly can be enormously cost-effective and globally sustainable [20]. However, as of this moment in the experimental stages of the geopolymer, there are some serious practical disadvantages. It is evident that geopolymer does have the potential to the ultimate OPC alternative but further developments are paramount to achieve that goal.

### 2.3 Geopolymer cement

Geopolymer cement is an innovative material and a real alternative to conventional Portland cement for use in transportation infrastructure, construction, petroleum engineering and offshore applications. It relies on minimally processed natural materials or industrial byproducts to significantly reduce its carbon footprint. It has been estimated that one ton of cement was produced per year for every human being [21]. It is also very resistant to many of the durability issues that can plague conventional concretes. From a terminological point of view, geopolymer cement is a binding system that hardens at room temperature, like OPC [22].

Creating geopolymer cement [**figure 2.7**] requires an alumina silicate material, a user-friendly alkaline reagent (sodium or potassium soluble silicates with a molar ratio (MR) SiO<sub>2</sub>:M<sub>2</sub>O>1,65, M being Na or K) and water. Room temperature hardening relies on the addition of calcium cations, essentially iron blast furnace slag. Geopolymer cements cure more rapidly than Portland-based cements. They gain most of their strength within 24 hours. However, they set slowly enough that they can be mixed at a batch plant and delivered in a concrete mixer. Geopolymer cement also has the ability to form a strong chemical bond with all kinds of rock-based aggregates [22].

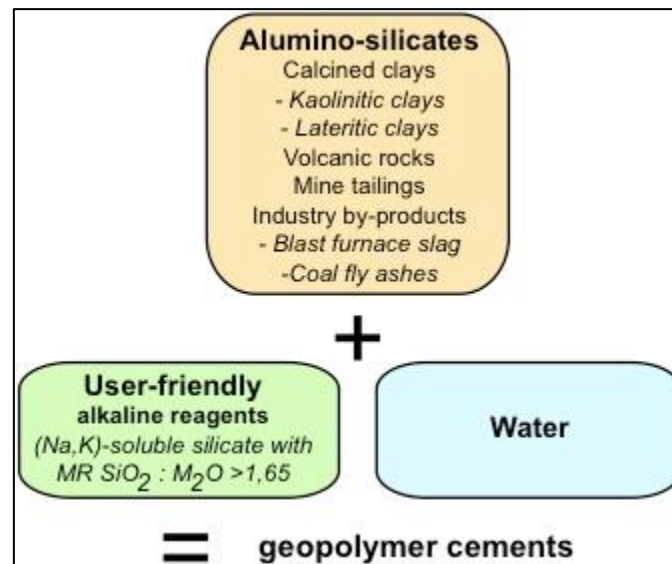


Figure 2.7 Creation of geopolymer cement [22]

On March 2010, the US Department of Transportation Federal Highway Administration released a TechBrief titled “Geopolymer Concrete” that states [23]: *The production of versatile, cost-effective geopolymer cements that can be mixed and hardened essentially like Portland cement would represent a **game-changing** advancement, revolutionizing the construction of transportation infrastructure.*

### 2.3.1 Portland cement chemistry vs Geopolymer cement chemistry

Understanding the distinctions between geopolymer and OPC, in terms of their chemical constitution is very important while conducting experiments. That is why basic chemical process during hardening of both types of cement is shown in *figure 2.8*.

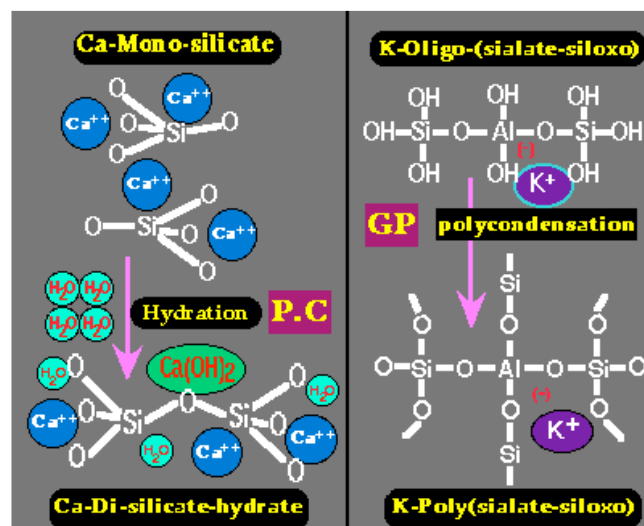




Figure 2.8 Hardening of OPC (left) and geopolymer cement (right) [22]

The hardening processes described in *figure 2.8* is accompanied by following commentary [22]:

**Left:** Hardening of OPC (PC) through simple hydration of calcium silicate into calcium di-silicate hydrate (CSH) and lime ( $\text{Ca}(\text{OH})_2$ ).

**Right:** Hardening of Geopolymer cement (GP) through polycondensation of potassium oligo-(sialate-siloxo) into potassium poly(sialate-siloxo) cross linked network.

Although geopolymerization does not rely on toxic organic solvents but only on water, it needs chemical ingredients that may be dangerous and therefore requires some safety procedures. Material Safety rules classify the alkaline products in two categories: corrosive products (named here: hostile) and irritant products (named here: friendly). The two classes are recognizable through their respective logos. The *figure 2.9* below lists some alkaline chemicals and their corresponding safety label. The corrosive products must be handled with gloves, glasses and masks. They are user-hostile and cannot be implemented in mass applications without the appropriate safety procedures. In the second category one finds Portland cement or hydrated lime, typical mass products. Geopolymeric alkaline reagents belonging to this class may also be termed as user-friendly [22].

 <b>hostile</b>	<b>friendly</b> 
CaO (quick lime) NaOH, KOH	$\text{Ca}(\text{OH})_2$ Portland cement, Iron slag
Sodium metasilicate $\text{SiO}_2:\text{Na}_2\text{O} = 1.0$	Slurry soluble silicate/kaolin $1.25 < \text{SiO}_2:\text{Na}_2\text{O} < 1.45$
Any soluble silicate $\text{SiO}_2:\text{Na}_2\text{O} < 1.45$	Any soluble silicate $\text{SiO}_2:\text{Na}_2\text{O} > 1.45$

*Figure 2.9 Alkaline-reagents classifications* [22]

### 2.3.2 Geopolymer cement categories

The categories of geopolymer cement will be described below [22]:

- Slag-based geopolymer cement
- Rock-based geopolymer cement
- Fly ash-based geopolymer cement
  - Type-1: alkali-activated fly ash geopolymer
  - Type-2: slag/fly ash-based geopolymer cement
- Ferro-sialate-based geopolymer cement

In this thesis, we considered only alkali-activated fly ash based geopolymer for the experimental purposes. That is why we are choosing type-1 FA based geopolymer for further elaboration.

For alkali-activated fly ash geopolymer (user-hostile), in general requires heat hardening at 60-80°C and is not manufactured separately and becomes part of the resulting fly-ash based concrete. NaOH (user-hostile) + fly ash: fly ash particles embedded in an aluminosilicate gel with Si:Al = 1 to 2, zeolitic type (chabazite-Na and sodalite).

### **2.3.3 Potential geopolymer cement application in wellbore cementing operation**

Various studies have been done on FA-based geopolymer cement to further check its viability and feasibility in cementing applications for oil and gas wells. Until this point in time, geopolymer cement has not been used in real wellbore operations. That is why it is important to mention some relevant studies to establish the base of our experiments in this thesis.

It was reported by Adjei et al. (2022) in a review published in Journal of Petroleum Science and Engineering that geopolymer cement has many vital advantages compared to OPC. These advantages include having lower permeability than OPC, being more resistant in acidic and high saline environments, more compatible with OBM and experiencing lower shrinkage rate and higher shear bond strength than OPC making it an ideal candidate for zonal isolation and P&A operation. However, they reported few limitations as well, which include being more susceptible to WBM, conventional geopolymer cement exhibiting higher brittleness and rapid gelation at elevated temperatures in comparison with OPC [24].

In terms of formulating a new geopolymer cement for oil well cementing, Suppiah et al. (2016) presented a recipe for geopolymer cement, which is particularly relevant for this thesis due to the ingredients used to make geopolymer cement. They investigated the effects of sodium hydroxide (NaOH) concentration on compressive strength of geopolymer cement system that could be used in oil well. Different ratios of Class F fly ash were mixed with different ratios of sodium silicate to sodium hydroxide ratio (2.5, 1, 0.5 and 0.25) to produce different geopolymer slurry densities. The NaOH solution was prepared by diluting NaOH pellets with distilled water according to the specified molarity (8M, 10M, 12M and 14M). The solution was then mixed with sodium silicate to form the alkaline solution. The mixture was placed in a 50 mm mould and cured at 93°C and 3000 psia for 24 hours and the cubes were tested for destructive compressive strength. The results showed that the compressive strength increases as the NaOH molarity increases, however when it reaches 14M, the adverse effect to the strength development was observed as in *figure 2.10* [25].

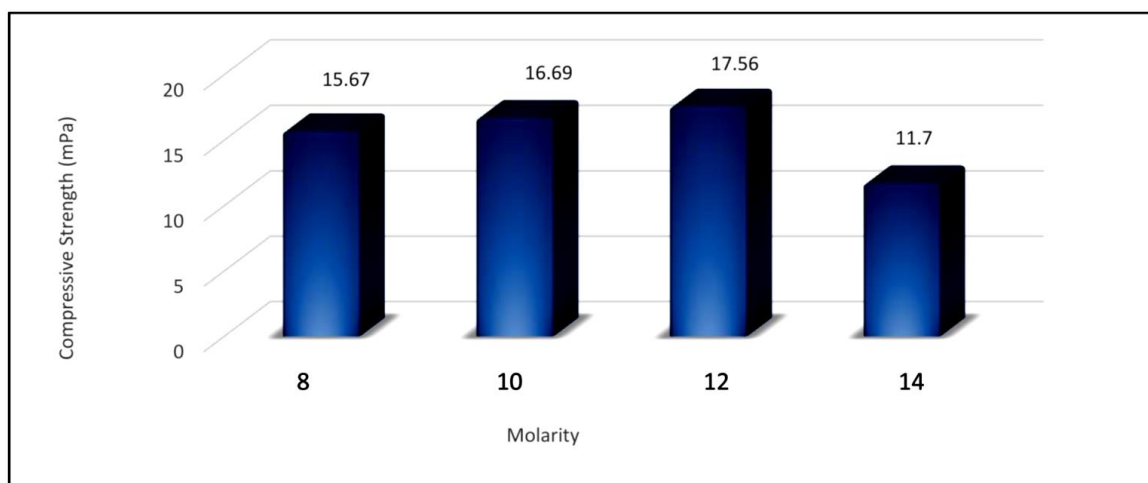


*Figure 2.10 Effect of different concentration of NaOH on the compressive strength* [25]

Downhole temperature is a big issue to current OPC. Over time, high temperature degrades the integrity of the OPC. That is why it is important that geopolymer cement can withstand high temperature to be considered as a workable alternative.

Suppiah et al. (2020) investigated the temperature effects on geopolymer cement. Geopolymer cement samples were cured in the potable water heated at 60°C and 90°C for 24 hours before testing for uniaxial compressive strength. Samples cured at 90°C showed the higher value of UCS as compared to the samples cured at 60°C and it was because heat is required to stimulate the polymeric reaction [26]. **Figure 2.11** illustrates the results obtained from the study.

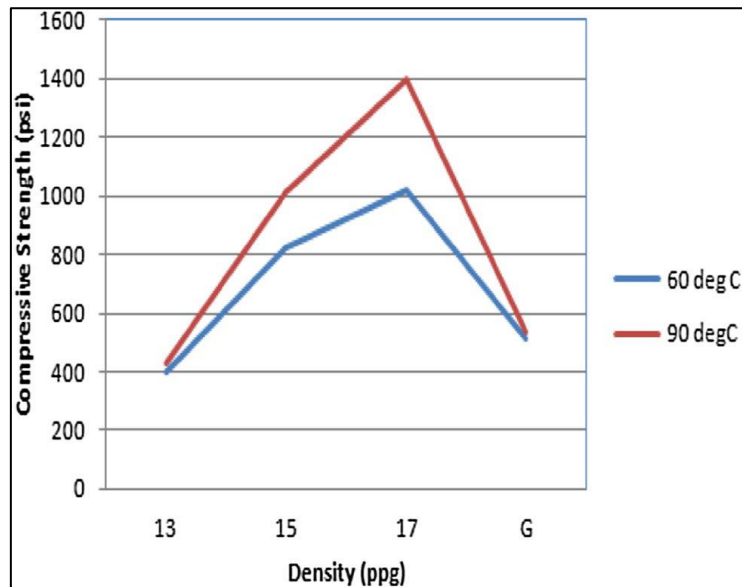


**Figure 2.11** Strength of geopolymer at 60°C and 90°C [26]

Some studies have found attributions in the FA-based geopolymer cement that can be useful in P&A operations of well. In such one study, Salehi et al. (2017) was reported to have found various positive findings, i.e., geopolymer showed more ductile behaviour than Portland cement and have good pumpability. They also reported that geopolymers shows lower shrinkage compared to cement. It should be noted that in this investigation API Class H Portland cement and Class F Fly Ash were used [27].

### **2.3.4 Workability issues of geopolymer cement**

Although, geopolymer cement is found to be environmentally friendly when manufacturing by having a reduction in CO<sub>2</sub> emission in the range of 40% to 80-90% [22], they have some serious workability issues until now.

Generally, one of the main problems with geopolymer binder is its poor workability: Alkali-activated Fly Ash has a much greater plastic viscosity than OPC [28] and is prone to fast setting. In a matter of minutes, it can produce “highly viscous, unmanageable concrete mixtures” [29].

These problems were faced with Portland cement as well, leading to the development of mix designs and admixtures that increase workability; to a limited extent, those techniques can be applied to geopolymer binder.

## **2.4 Fibers**

In the subsequent sections, we will shed some light on relevant information from literature for the types of fibers used in this thesis.

### **2.4.1 Carbon fibers (CF)**

Carbon fibers (alternatively CF, graphite fiber) are fibers about 5 to 10 micrometers (0.00020–0.00039 in) in diameter and composed mostly of carbon atoms [30]. Carbon fibers have several advantages: high stiffness, high tensile strength, high strength to weight ratio, high chemical resistance, high-temperature tolerance, and low thermal expansion. These properties have made carbon fiber very popular in aerospace, civil engineering, military, motorsports, and other competition sports. However, they are relatively expensive compared to similar fibers, such as glass fiber, basalt fibers, or plastic fibers [31]. *Figure 2.12* displays the CF used in the experiments of this thesis before it was cut.



*Figure 2.12 Carbon fibers*

To produce a carbon fiber, the carbon atoms are bonded together in crystals that are more or less aligned parallel to the fiber's long axis as the crystal alignment gives the fiber a high strength-to-volume ratio (in other words, it is strong for its size). Several thousand carbon fibers are bundled together to form a tow, which may be used by itself or woven into a fabric [31].

Carbon fibers are usually combined with other materials to form a composite. For example, when permeated with a plastic resin and baked, it forms carbon-fiber-reinforced polymer (often referred to as carbon fiber), which has a very high strength-to-weight ratio and is extremely rigid although somewhat brittle. Carbon fibers are also composited with other materials, such as graphite, to form reinforced carbon-carbon composites, which have a very high heat tolerance [31].

The atomic structure of carbon fiber is similar to that of graphite, consisting of sheets of carbon atoms arranged in a regular hexagonal pattern (graphene sheets), the difference being in the way these sheets interlock. Graphite is a crystalline material in which the sheets are stacked parallel to one another in regular fashion. The intermolecular forces between the sheets are relatively weak Van der Waals forces, giving graphite its soft and brittle characteristics [31].

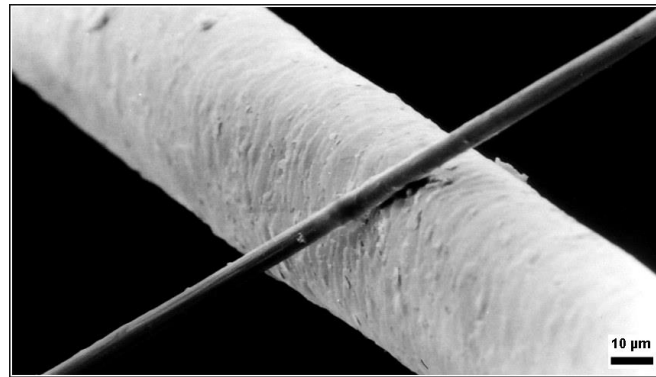


**Figure 2.13** A 6  $\mu\text{m}$  diameter carbon fiber filament (running from bottom left to top right) compared to a human hair [31]

Depending upon the precursor to make the fiber, carbon fiber may be turbostratic or graphitic, or have a hybrid structure with both graphitic and turbostratic parts present. In turbostratic carbon fiber the sheets of carbon atoms are haphazardly folded, or crumpled, together. Carbon fibers derived from polyacrylonitrile (PAN) are turbostratic, whereas carbon fibers derived from mesophase pitch are graphitic after heat treatment at temperatures exceeding 2200 °C. Turbostratic carbon fibers tend to have high ultimate tensile strength, whereas heat-treated mesophase-pitch-derived carbon fibers have high Young's modulus (i.e., high stiffness or resistance to extension under load) and high thermal conductivity [31].

Carbon fiber is prepared by producing carbon filament from a polymer such as polyacrylonitrile (PAN), rayon, or petroleum pitch. **Figure 2.14** will show CF preparation steps comprehensively [31].

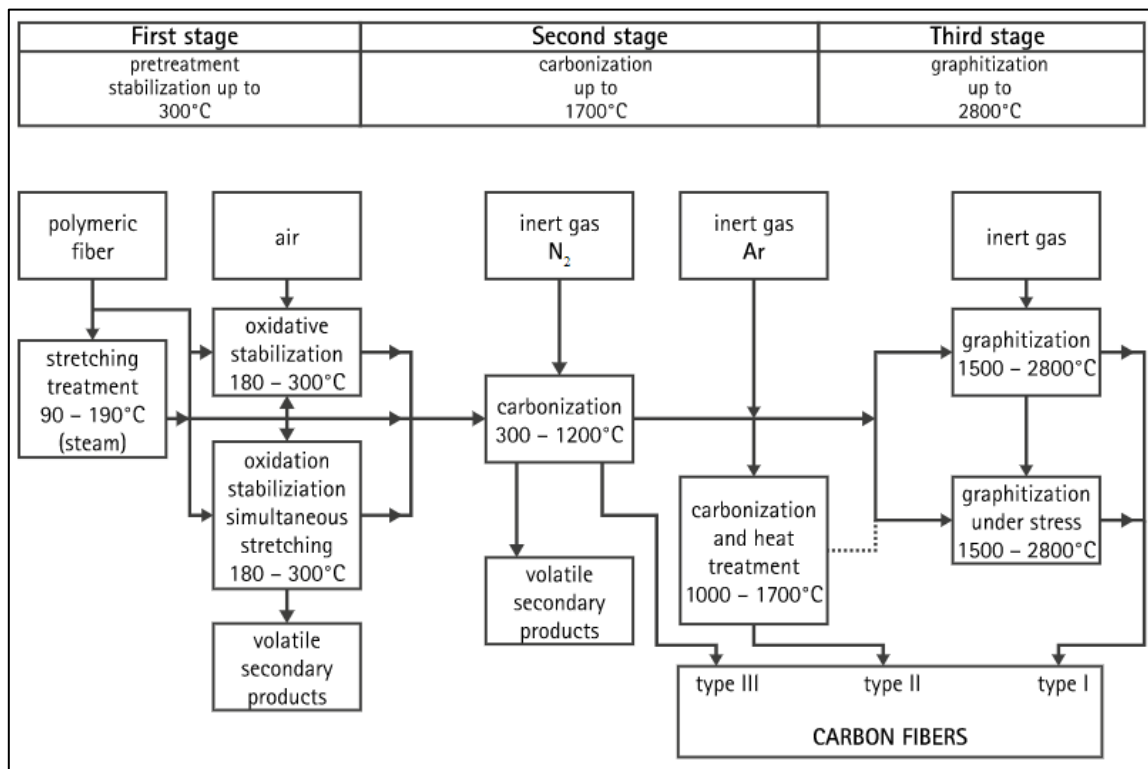


**Figure 2.14** Carbon fiber preparation [31]

### 2.4.1.1 Viability of applying carbon fibers in wellbore cementing operations

Various entities have studied the potentiality of using CF in oil well cement to improve the properties of OPC with the aim to have a more sustainable cement in the wells in the long run. A few of those investigations will be mentioned below to show our sources of inspirations for the experimental works.

When comes to Portland cement, mechanical and workability properties are equally important because they are reliant on each other. One such workability property is the how well a material can be dispersed in the cement slurry while mixing due to the material's ability to impact the cement's pumpability and UCS after hardening. This property, thus, was studied by Wang et al. (2008), where they demonstrated the effect of dispersion of CF in the slurry and in the hardened cement matrix as shown in *figure 2.15* [32].

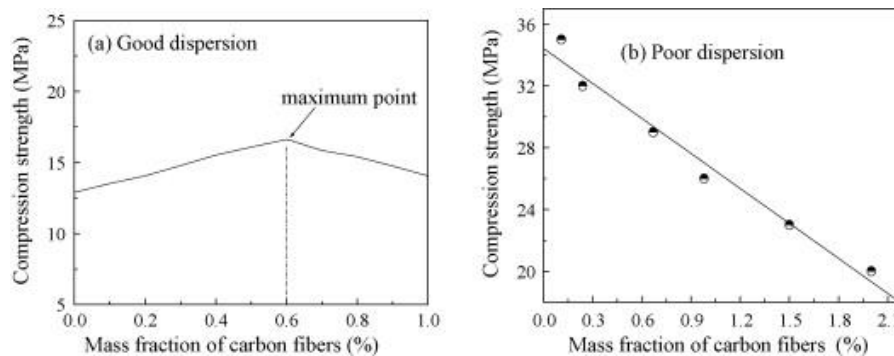


**Figure 2.15 Compressive strength as a function of fiber mass fractions (a) good dispersion of carbon fibers and (b) poor dispersion of carbon fibers [32]**

In this study, it was found that when CF are well dispersed in the cement matrix, the compressive strength increases with the increasing fiber contents gradually before the percentage of 0.6% as illustrated in *figure 2.15 (a)*. It has been increased by 20% at this percentage. For comparison, *figure 2.15 (b)* is provided to demonstrate that the compressive strength decreases dramatically with the increasing fiber content when carbon fibers are not well dispersed. The deteriorating strength is caused by holes and pores in the composites. The study also showed that CF can stop the appearance of micro-cracks in the cement and their free expansion. Therefore, they can not only enhance the compressive strength, but improve the toughness [32].

While conducting a study on the mechanical properties of G-class OPC, Yu et al. (2020) found that the maximum tensile strength, maximum compressive strength and ultimate strain of the enhanced cement stone of the CFs treated with sodium hypochlorite (P1) increased by 68.2%, 12.0%, and 4.4%, respectively. The maximum tensile strength, maximum compressive strength and ultimate strain of the enhanced cement stone of the CFs treated with concentrated nitric acid (P2) increased by 72.7%, 14.7%, and 4.5%, respectively. They study showed that the unprocessed CF (P0) also had increase in compressive and tensile strength [33].

In a comparative study on the mechanical behaviours of API H-class cement reinforced with CF, mineral and polypropylene fibers, Martín-Del-Río et al. (2019) showed that in relation to the mechanical behavior, short carbon fibers are advantageous when compared to the other selected fiber types; in fact, only the API class H cement reinforced with 1–2 wt% carbon fibers is found to have appreciable improvements in tensile and compressive strengths, as well as the other mechanical properties under study as shown in *figure 2.16* [34].



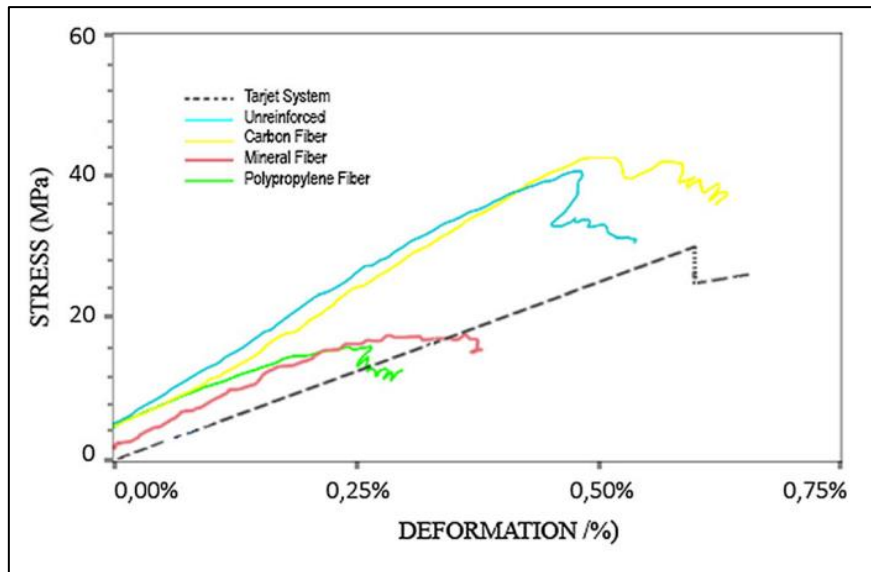


*Figure 2.16 Load extension curve of a target system compared to the response of an unreinforced system and representative fiber-reinforced composites [34]*

#### **2.4.2 White glass fibers (WF)**

Glass fiber is a material consisting of numerous extremely fine fibers of glass [35]. Usually, the glass fibers are white in colour. Glass fiber has roughly comparable mechanical properties to other fibers such as polymers and carbon fiber. Although not as rigid as carbon fiber, it is much cheaper and significantly less brittle when used in composites. Glass fiber reinforced composites are used in marine industry and piping industries because of good environmental resistance, better damage tolerance for impact loading, high specific strength and stiffness [36]. White glass fiber will be denoted with WF.

Below shown in *figure 2.17* the glass fiber used in the experiments in this thesis, before it was cut. This WF was in the form of woven mat. The WF was found to be very weakened in tensile direction but relatively stronger in compression. Additionally, it was highly soluble in the cement slurry and there was no visible trace of the WF in the hardened cement matrix.

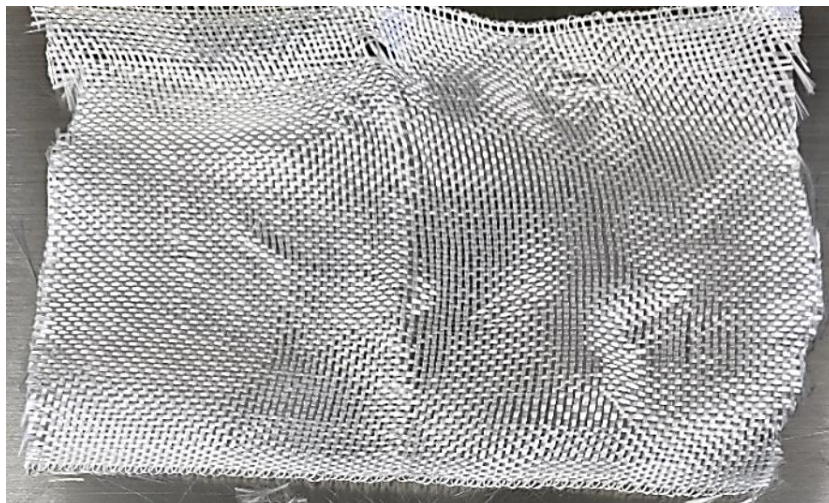


*Figure 2.17 White glass fiber*

Depending on the operational needs, WF is classified in different types and *figure 2.18* will display the classifications of WF with their physical properties [36].

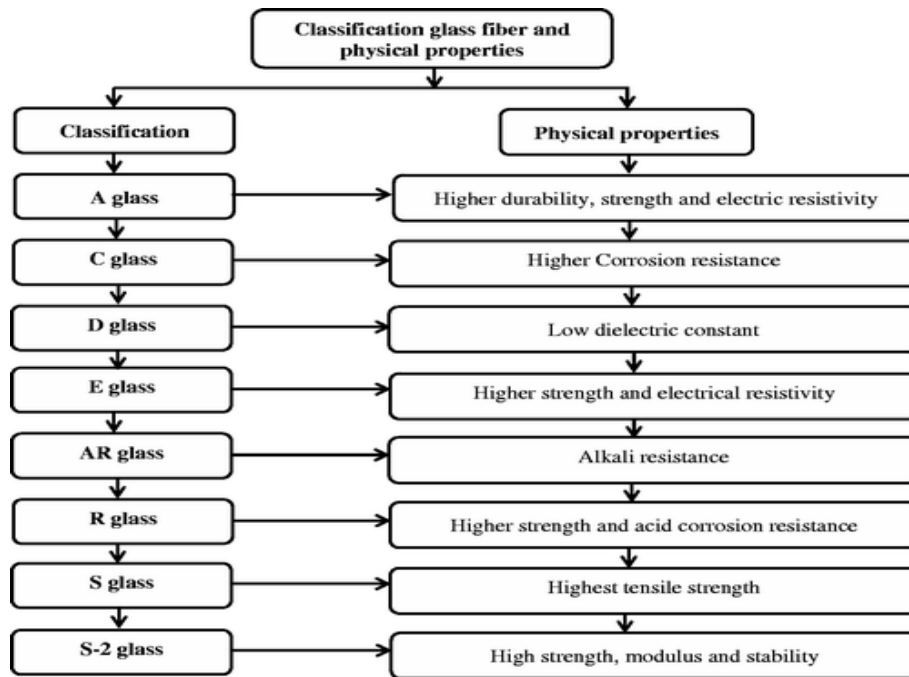


*Figure 2.18 Classifications and physical properties of various glass fibers* [36]

The mechanical properties of WF are vital to understand if it is to be applied in developing cement slurry. The strength of glass is usually tested and reported for "virgin" or pristine fibers—those that have just been manufactured. The freshest, thinnest fibers are the strongest because the thinner fibers are more ductile. The more the surface is scratched, the less the resulting tenacity [37]. Because glass has an amorphous structure, its properties are the same along the fiber and across the fiber [38]. Humidity is an important factor in the tensile strength. Moisture is easily adsorbed and can worsen microscopic cracks, surface defects and lessen tenacity.

In contrast to carbon fiber, glass can undergo more elongation before it breaks [38]. Thinner filaments can bend further before they break [35]. The viscosity of the molten glass is very important for manufacturing success. During drawing, the process where the hot glass is pulled to reduce the diameter of the fiber, the viscosity must be relatively low. If it is too high, the fiber will break during drawing. However, if it is too low, the glass will form droplets instead of being drawn out into a fiber. Mechanical properties of some of the WF are shown in *figure 2.19*.

Fiber	Density (g/cm <sup>3</sup> )	Tensile strength GPa	Young's modulus (GPa)	Elongation (%)	Coefficient of thermal expansion (10 <sup>-7</sup> /°C)	Poisson's ratio	Refractive index	Ref.
E-glass	2.58	3.445	72.3	4.8	54	0.2	1.558	17
C-glass	2.52	3.310	68.9	4.8	63	—	1.533	
S <sub>2</sub> -glass	2.46	4.890	86.9	5.7	16	0.22	1.521	
A-glass	2.44	3.310	68.9	4.8	73	—	1.538	
D-glass	2.11–2.14	2.415	51.7	4.6	25	—	1.465	
R-glass	2.54	4.135	85.5	4.8	33	—	1.546	
EGR-glass	2.72	3.445	80.3	4.8	59	—	1.579	
AR glass	2.70	3.241	73.1	4.4	65	—	1.562	

*Figure 2.19 Mechanical properties of various glass fibers* [36]

There are two main types of glass fiber manufacture and two main types of glass fiber product. First, fiber is made either from a direct melt process or a marble remelt process [35]. *Figure 2.20* will exhibit manufacturing process in a flow chart [39]–[40].

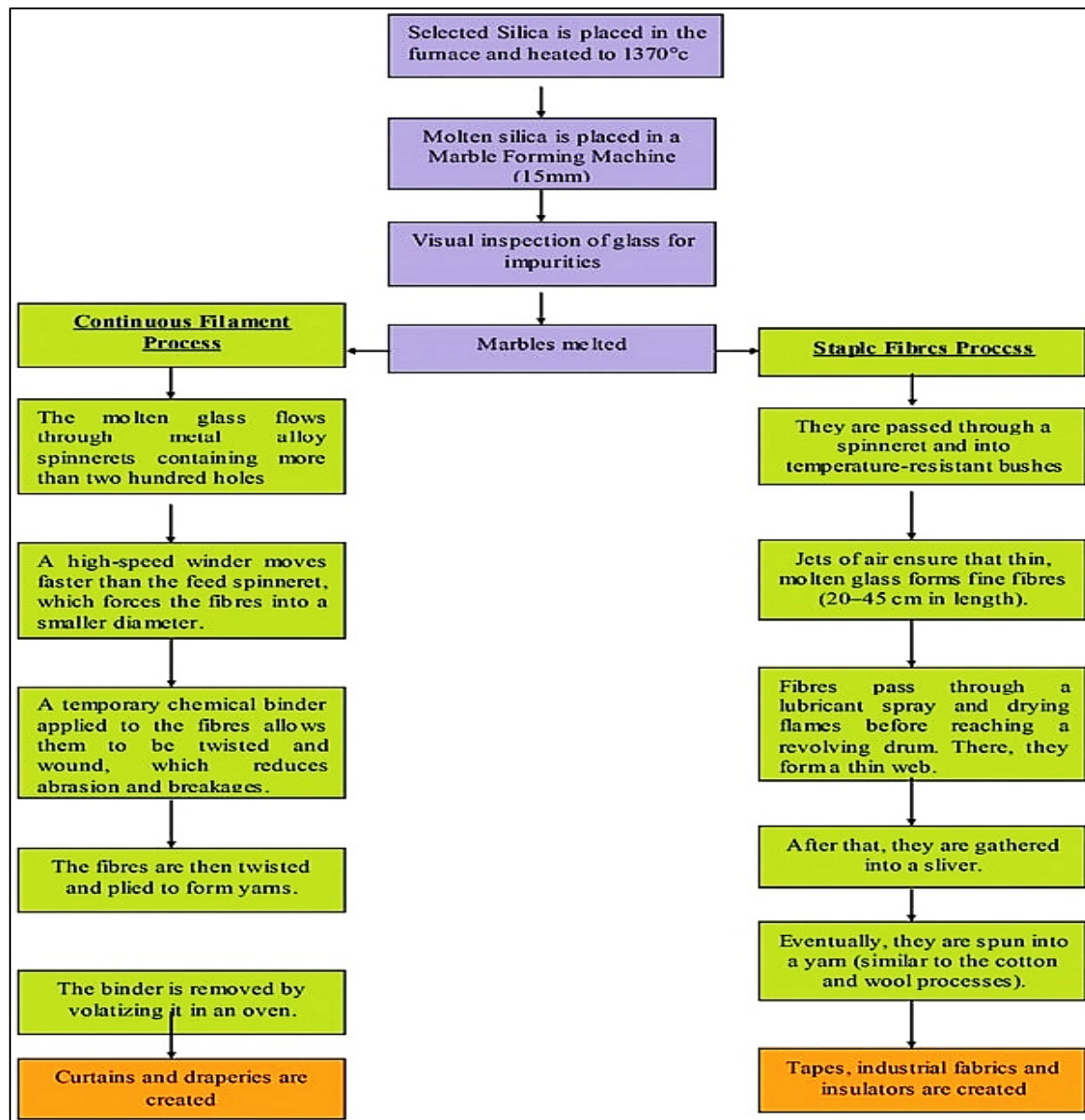


*Figure 2.20 Flow chart of fiberglass manufacturing process [39]–[40]*

Currently, the applications of WF are widespread. The high strength-to-weight ratio of fiberglass makes it a superior material in applications where high strength and minimum weight are required. In textile form, this strength can be unidirectional or bidirectional, allowing flexibility in design and cost. It is extensively used in automotive market, civil construction, sporting goods, aviation and aerospace, boats and marine, electronics, home and wind energy. They are also used in the manufacture of structural composites, printed circuit boards and a wide range of special-purpose products. The world production of glass fibers is around 4.5 million ton annually. Major producers are China, the United States and the European Union [39].

### 2.4.2.1 Potential use of glass fibers (WF) in cementing of oil and gas wells

From the discussions above, it is evident that WF has the potential of being used in the petroleum sector, especially in formulation of better cement by improving various mechanical and physical properties of OPC. In this thesis, we also experimented with WF to establish the sustainable possibility of utilizing glass fiber reinforced OPC in wells having been inspired by various studies conducted by different entities.

Assi et al. (2021) reported on a study conducted on G-class OPC with glass fiber and milled glass fiber, where it was tried to improve tensile and compressive strength of OPC. They conducted these experiments at 60°C and 38°C with glass fibers and milled glass fibers of 0.125%, 0.25%, 0.5%, 0.75%, 1% and 2% bwoc, respectively. The samples were cured for 8 hours at these temperatures before they were tested. These evaluations showed that slurries with less than 1% glass fiber content gave a higher compressive strength than a sample containing more than 1% glass fiber. Also, the slurry mixed with equal or less than 1% milled glass fiber is higher compressive than the sample mixed with more than 1% milled glass fiber. So, the optimal concentration for glass fiber is less than 1% bwoc and for milled glass fiber, it is less or equal to 1% bwoc [41]. **Figure 2.21** will display the results on the basis of temperature.

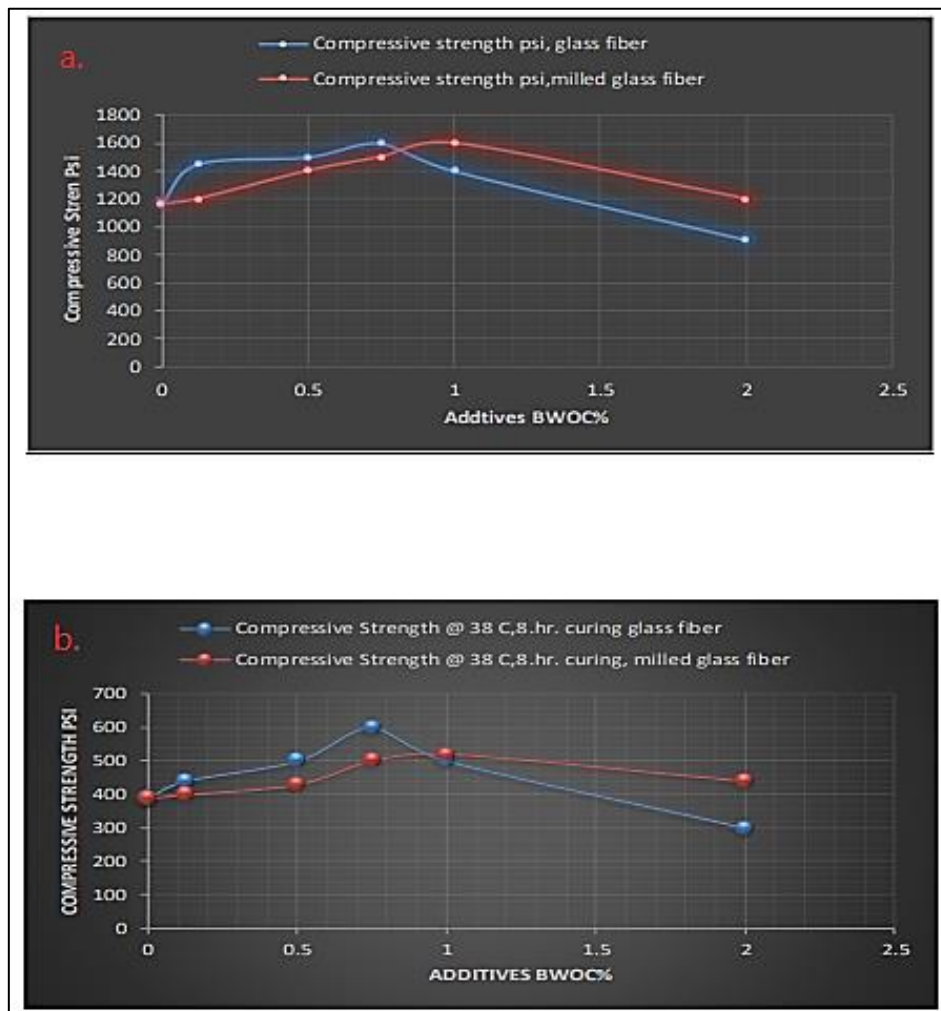


Figure 2.21 Compressive strength at a) 60°C and b) 38°C [41]

In another study done by Lalinde et al. (2022) on the durability of glass fiber reinforced cement (GRC), OPC of CEM I/52.5R grade was experimented on with alkali-resistant (AR) glass fibers. It is interesting to mention that this OPC contained high proportion of pozzolans (ground fly ash or a mixture of ground fly ash and sonicated silica fume) in order to reduce the corrosion of the fibers due to OPC having aggressive alkaline medium during hydration. The modulus of rupture and toughness were determined. Sample compositions are shown in *figure 2.22* [42].

Sample	CEM I 52.5R	Limestone Filler	Pozzolan	Siliceous Sand	AR Fiber	Superplastizicer	Mixing Water
C	1153.7	384.6	0	1025.5	93	15.4	529.8
GFA60	461.5	153.8	923	1025.5	93	12.3	531.6
GFA50+SSF10	461.5	153.8	769.1 + 153.8	1025.5	93	20	527.0

*Figure 2.22 Dose of the manufactured GRC mortars (values in grams)* [42]

The density of composite C increased with aging, but its modulus of rupture did not (*figure 2.23*). For the pozzolanic composites, an increase in both density and strength took place with aging. This means that increasing density was not the key to strength development for the C composite because fiber deterioration occurred. For the pozzolan composites, fiber integrity was maintained, and increasing density favored an increase in mechanical properties [42].

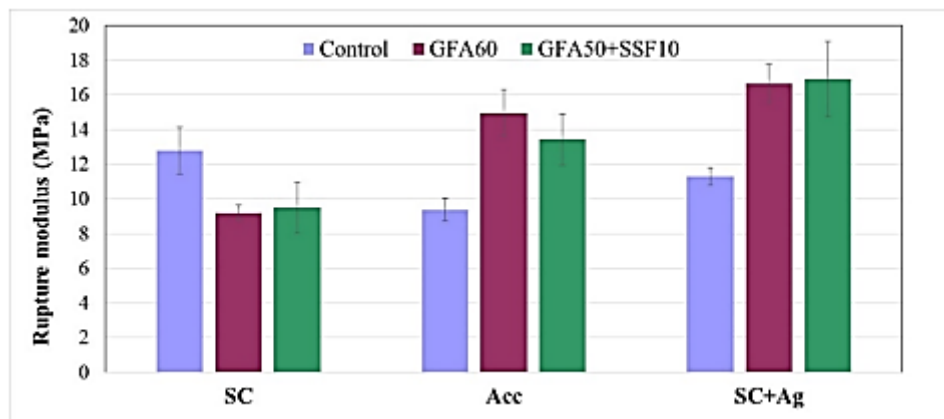


*Figure 2.23 Modulus of rupture (bending strength) of the GRC composites. (SC, standard curing for 28 days at 20°C; Acc, short curing for 7 days at 20°C plus Acc for 21 days at 55°C; SC+Ag, 28 days SC plus aging for 28 days at 55°C)* [42]

*Figure 2.24* shows the toughness of the studied composites. For SC (28 days at 20 °C), composite C obtained a significant toughness value (1.35 J), which was only exceeded by pozzolanic composite GFA50+SSF10 (1.48 J). During the acceleration and aging processes, the toughness for C drastically dropped, but toughness was maintained for the pozzolanic composites [42].

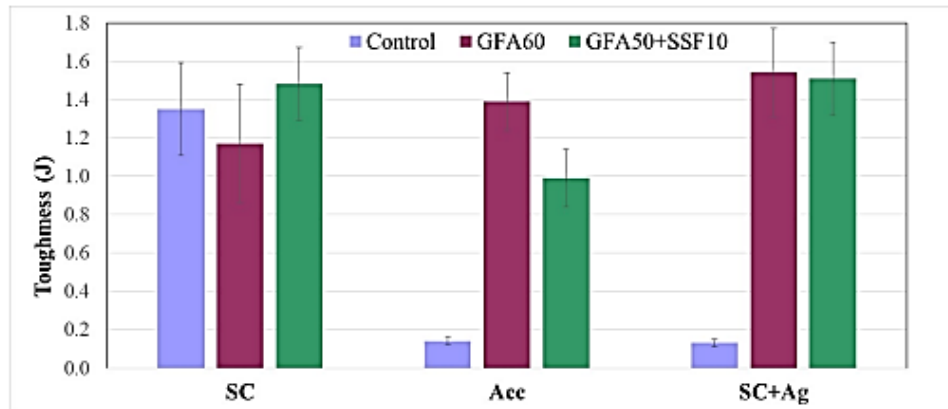


**Figure 2.24 Toughness of the GRC composites.** (SC, standard curing for 28 days at 20°C; Acc, short curing for 7 days at 20°C plus Acc for 21 days at 55°C; SC+Ag, 28 days SC plus aging for 28 days at 55°C) [42]

Composite behavior showed that the samples with pozzolans not only presented a better modulus of rupture and toughness, but also better resisted aging, physical and chemical attacks than the samples prepared with 100% Portland cement (control specimens) [42]. Due to the good behavior in durability terms, the high pozzolan content GRC products are suitable in potential corrosive environments, namely in a wellbore's downhole environment.

## 2.5 Nanotechnology

Nanotechnology is the use of matter on an atomic, molecular, and supramolecular scale for industrial purposes. The earliest, widespread description of nanotechnology referred to the particular technological goal of precisely manipulating atoms and molecules for fabrication of macroscale products, also now referred to as molecular nanotechnology [43]– [45].

Nanotechnology is science, engineering, and technology conducted at the nanoscale, which is about 1 to 100 nanometers. Nanoscience and nanotechnology are the study and application of extremely small things and can be used across all the other science fields, such as chemistry, biology, physics, materials science, and engineering [46]. **Figure 2.25** shows the comparison of nanomaterials' sizes against other objects for context [47].

Nanotechnology as defined by size is naturally broad, including fields of science as diverse as surface science, organic chemistry, molecular biology, semiconductor physics, energy storage, engineering, microfabrication and molecular engineering. The associated research and applications are equally diverse, ranging from extensions of conventional device physics to completely new approaches based upon molecular self-assembly, from developing new materials with dimensions on the nanoscale to direct control of matter on the atomic scale [45].

One nanometer (nm) is one billionth or  $10^{-9}$  of a meter. By comparison, typical carbon-carbon bond lengths, or the spacing between these atoms in a molecule, are in the range 0.12–0.15 nm, and a DNA double-helix has a diameter around 2 nm. On the other hand, the smallest cellular life-forms, the bacteria of the genus *Mycoplasma*, are around 200 nm in length. By convention, nanotechnology is taken as the scale range 1 to 100 nm following the definition used by the National Nanotechnology Initiative in the US. The lower limit is set by the size of atoms (hydrogen has the smallest atoms, which are approximately a quarter of a nm kinetic diameter) since nanotechnology must build its devices from atoms and molecules. The upper

limit is more or less arbitrary but is around the size below which the phenomena not observed in larger structures start to become apparent and can be made use of in the nano device [48].

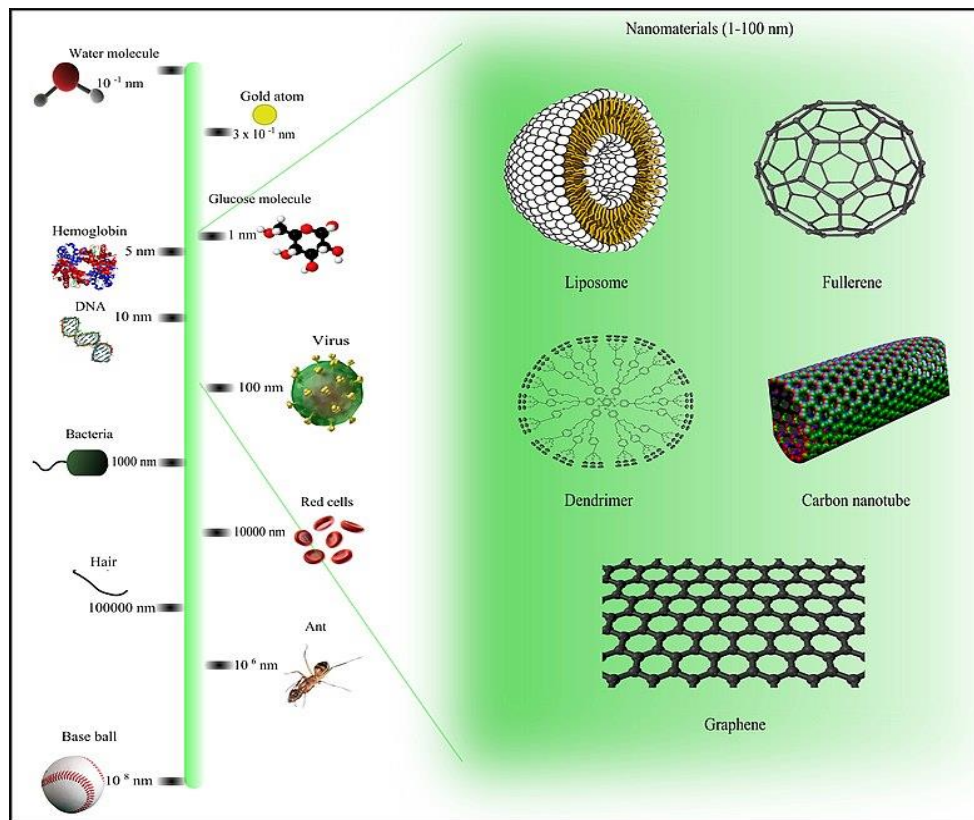


**Figure 2.25 Comparison of nanomaterials' sizes [47]**

Nanomaterials with a minimum of one dimension in the nanoscale are known as nanolayers. Examples are thin films and surface coatings. Nanomaterials with two dimensions in the nanoscale are referred to as nanotubes or nanowires. Examples of these include carbon nanotubes and carbon nanofibers. Nanomaterials with all three dimensions in the nanoscale are called nanoparticles [49]. Nanomaterials can further be broken down into four types: carbon-based materials, metal-based materials, dendrimers and composites. The unique properties of intentionally produced nanomaterials falling into these four main categories give them imaging, thermal, mechanical, medical and commercial features highly sought after in applications across various industrial sectors [49].

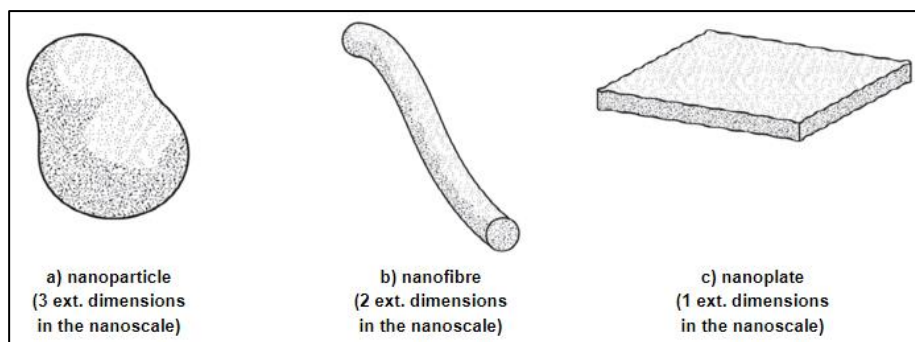


**Figure 2.26 Schematic diagrams showing some shapes for nano-objects [50]**

### 2.5.1 Nanoparticles

A nanoparticle or ultrafine particle is usually defined as a particle of matter that is between 1 and 100 nanometers (nm) in diameter [51]. According to the International Standards Organization (ISO) technical specification 80004, a nanoparticle is an object with all three external dimensions in the nanoscale, whose longest and shortest axes do not differ significantly, with a significant difference typically being a factor of at least 3 [50].

At the lowest range, metal particles smaller than 1 nm are usually called atom clusters instead. Being more subject to the Brownian motion, they usually do not sediment, like colloidal particles that conversely are usually understood to range from 1 to 1000 nm. [52].

The characterization of nanoparticles is a branch of nanometrology that deals with the characterization, or measurement, of the physical and chemical properties of nanoparticles. Microscopy and spectroscopy methods are usually used in characterizations. Nanoparticles measure less than 100 nanometers in at least one of their external dimensions and are often engineered for their unique properties. Nanoparticles are unlike conventional chemicals in that their chemical composition and concentration are not sufficient metrics for a complete description, because they vary in other physical properties such as size, shape, surface properties, crystallinity and dispersion state [53].

Nanoparticle synthesis refers to methods for creating nanoparticles [54]. Nanoparticle synthesis can be divided in traditional methods and green methods [57]. We will be focusing on the traditional methods.

Nanoparticles are typically synthesized from a top-down or bottom-up approach. A bottom-up approach relies on nucleating atomic-sized materials into the eventual nanoparticles. While the exact synthesis method depends on the material being generated, some common methods include the Turkevich method (citrate reduction) [56], gas phase synthesis, block copolymer synthesis, and more recently, microbial synthesis. Top-down methods, where a bulk material is physically broken down to make smaller molecules, include milling, laser ablation, and spark ablation. *Figure 2.27* illustrates the nanoparticles synthesis approaches [55].

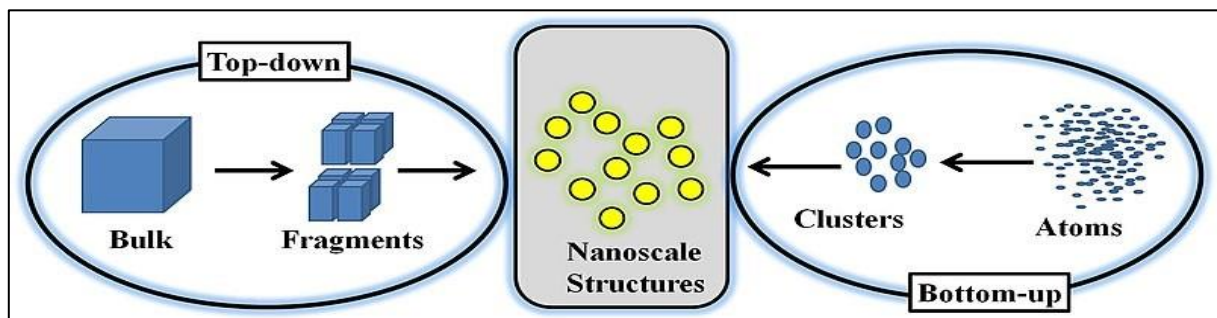


*Figure 2.27 The top-down and bottom-up approach for making nanoparticles [55]*

Bottom-up synthesis methods are often termed “wet” methods since they involve batches of solvents and other chemicals. Additionally, the particles often must be stabilized or capped in solution to ensure that they do not continue to grow past the nanoscale range. The particles then usually need to be moved or transferred from their solutions for their application or characterization. This can be accomplished by drop-casting the solution onto the substrate of interest. However, in some applications, such as catalysis, it may also be necessary to remove the stabilizers from the surface of the nanoparticles after they have been immobilized on the final support of interest. The removal process can prove difficult or even impossible, leading these particles to be unusable for their intended purpose [55].



## 2.5.2 Applications of nanotechnology in petroleum industry

Nanotechnology has become the buzz word of the decade! The precise manipulation and control of matter at dimensions of (1-100) nanometers have revolutionized many industries including the Oil and Gas industry. Its broad impact on more than one discipline is making it of increasing interest to concerned parties [58].

The tiny nature of nanoparticles results in some useful characteristics, such as an increased surface area to which other materials can bond in ways that make for stronger or more lightweight materials. At the nanoscale, size does matter when it comes to how molecules react to and bond with each other. Suspensions of nanoparticles are possible because the interaction of the particle surface with the solvent is strong enough to overcome differences in density, which usually result in a material either sinking or floating in a liquid forming ‘Nanofluid’ [58].

Nowadays, due to the different challenges presented in the oil and gas industry, different and modern technologies have arisen to accomplish production goals and environmental requirements. Nanotechnology in oil and gas industry is a fascinating subject of recent origin. Nanomaterials are involved in almost all stages in the oil and gas industry, including searching, drilling, cementing, production, processing, transport, and refining [59].

With this growing attention and development of nanotechnology in the oil and gas industry, which can be clearly observed through the number of related publications (*figure 2.28*), it is crucial to review the available application and summarize what has been done up to date [60]. Few of these study areas will be discussed shortly.

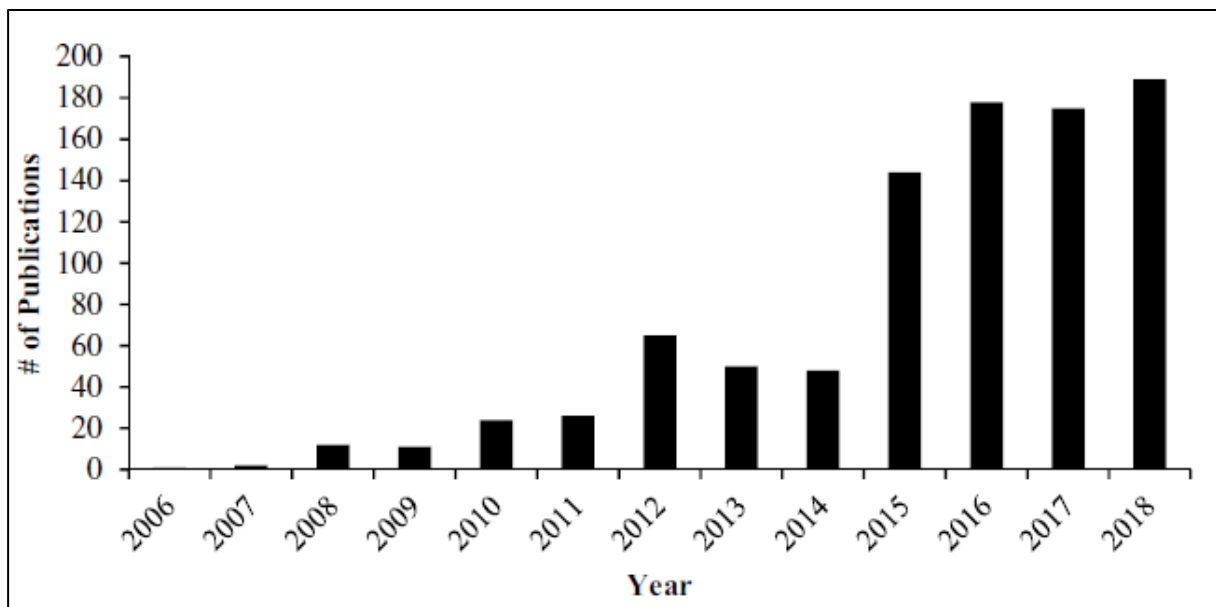


*Figure 2.28 Number of publications per year [60]*

- **Enhanced oil recovery applications:** Due to the fact that two-thirds of the oil in place is left behind after the primary and secondary recovery and based on the significant increase observed in oil recovery using EOR techniques, which includes chemical injection, thermal recovery, and gas injection, a good number of researches have been conducted to improve the different EOR techniques by the addition of nanoparticles. The main objective of these investigations is to study the effect of nanoparticles in improving oil recovery by improving one of the parameters related to oil recovery [60].

Hogeweg et al. (2018) found that aluminium oxide and titanium dioxide reduced oil viscosity and improved the stability of the injected water for EOR applications [61]. Various other nanoparticles including SiO<sub>2</sub>, ZnO, MgO and graphene oxide improved many other properties regarding EOR including rheological properties of oil, stability of oil in water emulsions, reducing mobility ratio [60]. Even though NPs might improve some parameters, it could also negatively affect some other parameters. Adding NP to brine or ethanol could result in poor recovery compared to brine or ethanol alone. Injection blockage and settling issues have also been reported previously [62]. NPs could modify the permeability up to a certain limit when all contact surfaces are covered with NP and at that point, a reduction in porosity and absolute permeability would initiate [60].

- **Drilling fluids applications:** Drilling fluids can be simply defined as a heavy viscous fluid mixture that is used during the drilling stage to perform different tasks including lifting the drilled cuttings, controlling the formation pressure, maintaining wellbore stability, etc. Different additives are used to enhance the different properties of drilling fluids such as the rheological properties, filtration properties. There are different limitations that are faced when designing drilling fluids using conventional additives such as the temperature and the additives particle size limitations. Therefore, nanoparticles were investigated extensively to study their applicability in overcoming these limitations [60].

It was found that high NP concentration is not recommended due to the insignificant performance increase observed between low and high NP concentrations [63]. High concentration could also result in increasing the particles friction coefficient, which may alter lubricity and hole cleaning efficiency [64]. At high temperatures, some NP could result in a negative effect on filtration characteristics. Alsaba et al. (2018) showed that copper oxide has better thermal stability when compared to magnesium oxide and aluminum oxide in terms of rheological properties [65]. In addition, it was found that silicon dioxide NP might increase the pressure losses in bentonite water-based mud due to the increase in the frictional forces [60].

- **Well stimulation applications:** Well stimulation can be simply defined as treatments used to enhance the well productivity either by hydraulic fracturing and matrix acidizing to increase the permeability or by increasing the well production. Few investigations showed an improvement in the well stimulation jobs by means of nontechnology [60].

Gurluk et al. (2013) found that the salt concentration greatly affects the viscoelastic surfactant fracturing fluid including NP and causes some viscosity stability. The addition of magnesium oxide NP causes a decrease in apparent viscosity of the fracturing fluid [66]. Silicon dioxide acid showed different behavior in limestone compared to shale. Fracture conductivity of shale rock showed better improvements when compared to limestone rock (Singh et al. 2018) [67]. Fakoya and Shah (2018) found that there is an optimum concentration to improve rheological properties of surfactant-based fluids for hydraulic fracturing applications, where higher concentration was not recommended [68].

Utilizations of nanoparticles in various investigations are accumulated from literature in *figure 2.29(a)*. It is evident that silicon dioxide is the most widely used nanoparticles across the oil and gas industry followed by aluminum oxide [60]. *Figure 2.29(b)* shows the highest targeted property for improvement by means of nanoparticles. It can be clearly seen that nanoparticles have been investigated heavily to study their effect on increasing the oil recovery, which falls down under EOR applications followed by improving the filtration characteristics of drilling fluids and improving cementing, while the least investigated property was found to be the lubricity of drilling fluids [60].

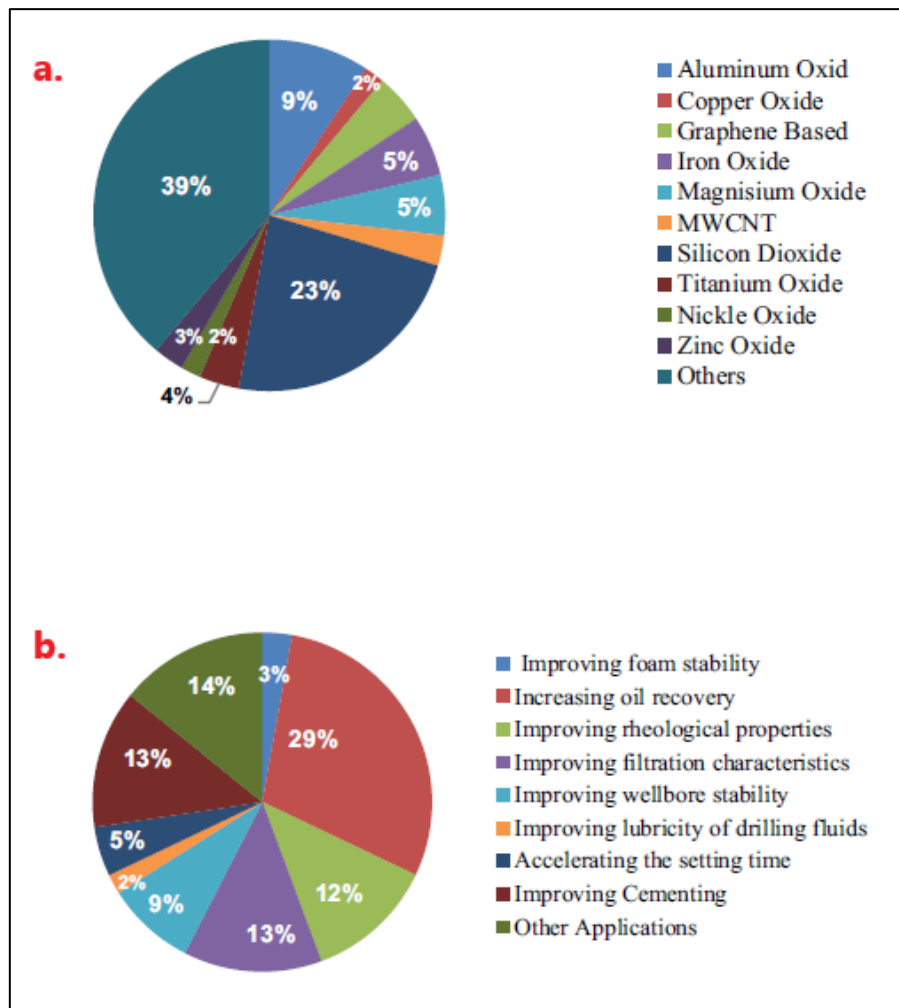


Figure 2.29 (a) Distribution of investigation for the different NP in the oil and gas applications; (b) Targeted property of improvement by means of NP [60]

The percentage of the conducted investigations of nanoparticles across the oil and gas industry for the four applications discussed above is shown in *figure 2.30*. It can be observed that nanoparticles have attracted researchers in EOR, drilling, and cementing applications. However, the application of nanoparticles for stimulation applications is still not as high as the other applications [60].

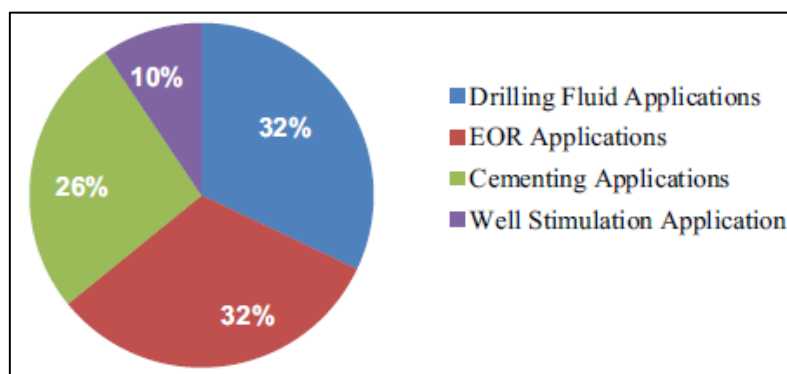


Figure 2.30 Percentage of investigations of NPs across the oil and gas industry [60]

## Effects of nanoparticles, fibers and fly ash on cementitious and non-cementitious materials

For the oil and gas industry, in particular, different nanotechnology applications have been proposed based on laboratory experiments. Most of the reported results in the literature showed the potential of nanoparticles in improving the evaluated parameters. Nevertheless, few field trials have been reported [60]. Few of these field trials of nanoparticles and nanofluids that shows the potential of nanotechnology applications is given in *figure 2.31* [77].

application	year	location	nanofluid/nanoparticle type and concentration	main findings
asphaltene formation damage inhibition	2012 (first field trial) ongoing expansion	Cupiagua field (first field trial), Colombia expansion in Colombian oilfields	generally ~30 nm Al <sub>2</sub> O <sub>3</sub> nanoparticles in a carrier fluid composed of a mixture of solvents and alcohols; concentration (up to 500 mg/L) may vary, depending on the field	for the first trial, increases in cumulative oil production of more than 270 000 barrels. Currently, expansion has been made to six fields in Colombia, resulting in a reserve increase of ~1.5 Mbbl with high cost-effectiveness
finest migration formation damage	2014	Colombia	SiO <sub>2</sub> nanoparticles of 30 nm in a carrier fluid composed of a mixture of solvents and alcohols; nanoparticles concentration was 500 mg/L	production increase of 48 bbl oil per day and 1000 thousand standard cubic feet per day regarding the baseline
inorganic scale (CaCO <sub>3</sub> ) formation damage	2017 (first field trial) ongoing expansion	Colombia expansion in Colombian oilfields	a nanofluid composed of a phosphonate-based carrier fluid with 50 mg/L of Ca-diethylenetriamine pentamethylene phosphonic acid (Ca-DTPMP, 66 nm) nanoparticles	incremental in oil productivity of 66 bbl per day three additional interventions have been made in Colombia, resulting in a reserves increase of ~20 000 bbl
drilling (filtrate reduction)	2014	Alberta, Canada	concentrated solution at 5 wt % of calcium-based nanoparticles (51 ± 11 nm) in the form of an invert emulsion	filtrate reductions up to 34% regarding tween applications without nanoparticles
drilling (shale stabilization)	2018	Reconcavo Bainano basin, Brazil	unknown chemical nature	higher well stability; a second field trial implementation using the recycled fluid, leading to a cost reduction of 15%
drilling (drilling fluid improvement)	2020	Iran	functionalized nanoporous graphene (FNPG, 50 nm) and/or functionalized multiwalled carbon nanotubes (FMWCNT, 14 nm) in a dosage of 3 wt % in a bentonite slurry	improvement in drilling fluid properties such as rheology, filtration, lubricant, and shale hydration inhibition; nanomaterials led to a more economical operation
drilling (filtrate reduction and finest migration inhibition)	2020	Colombia	nanocarbonate and alumina nanoparticles (1000 mg/L) of unspecified size	lower filtrate invasion when using the nanotechnology-based nanofluid compared with homologue wells in the field; regarding inhibition of finest migration, the results were not conclusive
heavy and extra-heavy oil mobility enhancement ( <i>huff-n-puff</i> )	2013 (first field trial) ongoing expansion	Castilla and Chichimene fields in Colombia (first field trial) expansion in Colombian oilfields	Al <sub>2</sub> O <sub>3</sub> -based nanoparticles of ~25 nm dispersed in an oil-based/alcohol carrier fluid in concentrations up to 500 mg/L depending on the reservoir	in Castilla and Chichimene fields production increase up to 310 bopd; some cases showed reduction in BSW; the technology has been applied in more than eight fields with a reserves increase close to 1 MM bbls
heavy and extra-heavy oil mobility enhancement (injection through the capillary of the pump)	2019	Colombia	nanofluids composed of Al <sub>2</sub> O <sub>3</sub> -based nanoparticles (~25 nm) with an oil-based/alcohol carrier fluid at concentrations up to 2000 mg/L	the efficiency of the lifting system increased in terms of reducing the temperature and pressure of the pump
water shutoff	2017	Algyo field, Hungary	silica nanoparticles at 1000 mg/L in a silicate/polymer gel system	reduction of ~45% of the water cut in two years; oil cut increased up to 80%
wettability alteration	2020	Colombia	nanocapsules of a shell composed of a nonpolar material with a surfactant core	in one well, a decrease in total fluid production in 300 BFPD, positive impact on OPEX with constant crude oil production in another well, a decrease of 360 bfpd in total production with constant oil production was observed; 7% increase in the productivity index

*Figure 2.31 Summary of nanofluids' field trials* [77]

There are various challenges regarding implementation of nanotechnology in actual field operations. In regard to the economic feasibility of nanoparticles versus conventional materials, the main reason behind this issue is basically the relatively higher cost of producing some nanoparticles compared to conventional material. Additionally, the availability of nanoparticles for widescale oil gas application is under scrutiny. The other challenge with respect to their effectiveness when applied to a larger scale in the field rather than the laboratory-scale requires better collaboration between oil companies and researchers to validate their performance through pilot testing [60]. When it comes to the impact of nanoparticles on health, environment, and safety, they can be very hazardous and might lead to severe health issues since they have higher potential of being inhaled or absorbed through skin (Lau et al., 2017) due to their unique properties of nanoparticles in terms of size and surface-to area ratio [69]. Based on the challenges discussed, more research should be conducted in order to reduce the cost of producing nanoparticles and make NPs less harmful to health.

### **2.5.3 Potential use of nanotechnology in well cementing in the forms of nanoparticles**

Good cement integrity is essential for safe completion and production operations, as the cement between casing and formation prevents borehole collapse, holds the casing in place, and prevents flow between subsurface formations. Poor cement integrity has been cited as one of the most prominent contributing factors in overall wellbore integrity. Cement with good integrity should have low permeability, high tensile and compressive strengths and a relatively low Young's modulus to accommodate in-situ shear deformation without failure. These properties may be controlled with chemical additives. The role of nanoparticles in improving cement properties has garnered interest in industry for several years and is the subject of a number of studies and patents [74].

Well cementing, which can be defined as the process of mixing and pumping cement slurry downhole in the annuls and allowing it to cure and bond between the formation and the casing, is a crucial element in well construction. There are at least six common API classes of cement that meet certain requirements such as sulfate resistance or high early strength. Cement additives are added to improve specific parameters such as density, setting time, filtration, and viscosity [60]. Statistics of studies addressed the use of nanoparticles in well cementing to enhance cement properties as it was discussed in *section 2.5.2*.

Vipulanandan et al. (2018) reported that using Al<sub>2</sub>O<sub>3</sub> NPs increased the electrical resistivity and enhanced the compressive strength of Portland cement [70]. Alkhamis and Imqam (2018) showed in another study that graphene nanoplatelets (GNP) reduced chemical shrinkage and improved mechanical properties of cement [71]. Mabeyo and Gu (2021) presented the coupled effects of hydrophilic nano silica oxide and anatase nano titanium oxide on strengths of oilwell cement at 80°C. The results revealed that both nano-SiO<sub>2</sub> and nano-TiO<sub>2</sub> increased strength evolution [72]. Baig et al. (2017) attested that nano zeolite can be an effective oil well cement additive because it enhances early strength, and the final compressive strength helps improve cement durability. The accelerated compressive strength development can help decrease wait-on-cement (WOC) time, thus lowering operation costs. Additionally, denser microstructure can help restrain the invasion of corrosive formation fluids [73].

The curing fluid, such as limewater or water, can greatly affect the cement compressive strength. It was found that cement can be preferably replaced with 2% aluminum oxide NP when cured in limewater and 1% aluminum oxide NP when cured in water. However, the addition of the NP can reduce the workability of the cement where different materials need to be added such as plasticizers [75]. Alkhamis and Imqam (2018) found that graphene nanoplatelets cause a reduction in cement sheath thermal gradient, which may cause thermal cracks when acceding the tensile stress [71]. Experimental evaluation performed by Santra et al. (2012) using multiwalled carbon nanotubes (MWNTs) did not show an improvement in cement mechanical properties [76].

It was noticeable that studies with aluminium oxide and titanium dioxide did not have a large portion in the percentile status shown in *figure 2.29 (a)*. This is why we were inspired to conduct studies in this thesis with aluminium and titanium nanoparticles on cementitious and non-cementitious material. In the following subsections, reviews of studies conducted with these nanoparticles and their effects on the relevant materials for this thesis will be summarized. For better clarifications regarding the materials involved in the thesis, it is recommended to refer to *chapter 1*. It should be noted that the review will only contain findings related to Al<sub>2</sub>O<sub>3</sub> and TiO<sub>2</sub> NPs with relation to OPC, geopolymers, cement, fly ash, carbon fibers and white glass fibers with their cementing applications, which means if a study contains other additives, they will not be mentioned.

### 2.5.3.1 Al<sub>2</sub>O<sub>3</sub> in use with OPC and fly ash

In this thesis, the effect of nano-aluminium on OPC and OPC with fly ash was studied. Hence the following studies will give some insights into the potentials of this nanoparticles.

- Nerhus (2020) had conducted experiments with Al<sub>2</sub>O<sub>3</sub> NPs on OPC of WCR 0.44 to observe the effects. They reported that addition of aluminium nanoparticles showed a clear trend of increasing in UCS as the concentrations of nanoparticles increased. Although, it was observed that percentile increase over their reference neat OPC was very small and it was asserted that, in future even higher UCS could be achieved if the concentrations of nano-aluminium were increased. This made us curious to see developments of nano-Al in OPC by increasing the dosages [78]. *Figure 2.32* is showing the UCS development from the study.

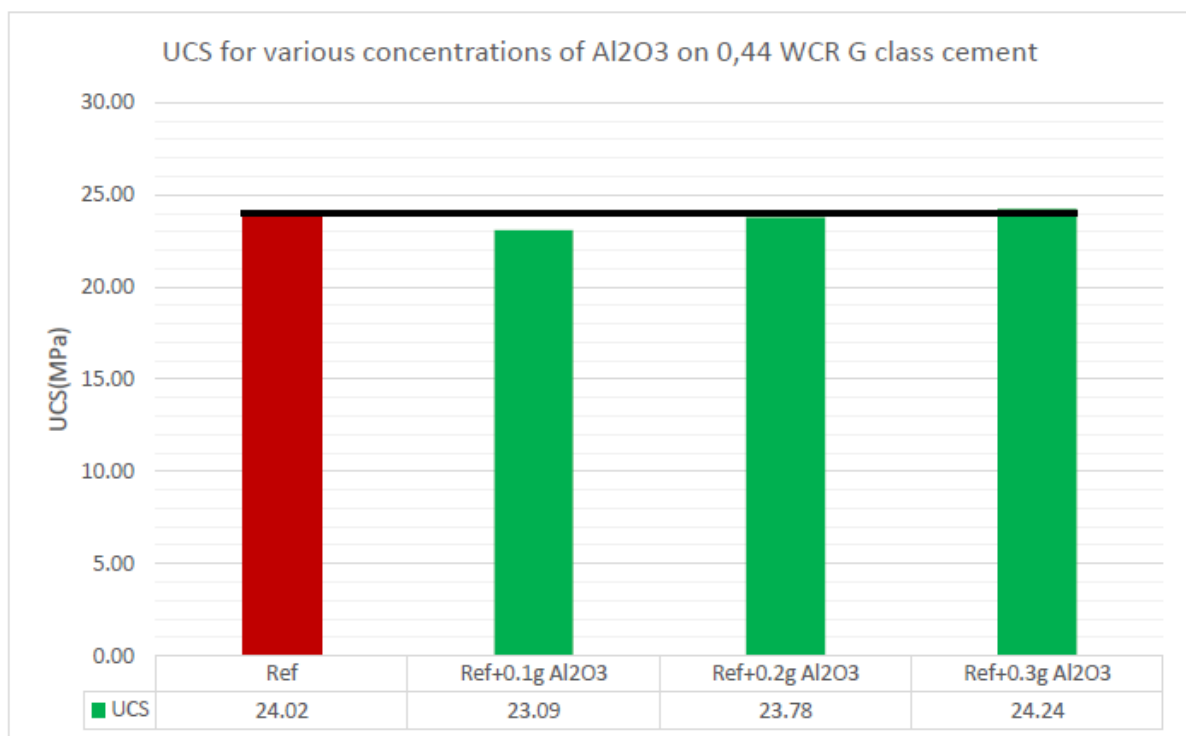


*Figure 2.32 UCS for various concentrations of Al<sub>2</sub>O<sub>3</sub> on 0.44 WCR G-class cement [78]*

- Titlestad (2021) studied the effects of fly ash as standalone additive and in conjunction with SiO<sub>2</sub> nanoparticles. Even though nano-Si was not used in this thesis, this study interested us because of the use of FA. They documented that FA as a standalone additive showed weak early strength, although it significantly improved the OPC mechanical properties after 28 days. On the other hand, it was shown that FA and SiO<sub>2</sub> blend did not perform favourably when compared to neat OPC. Rheological properties seemed to be improved by nanoparticles, whereas FA reduce shear stress and Casson PV. It was also suggested that FA alone could be a promising additive to be blended with OPC due to its inexpensiveness and apparent high performance [79].

- Farzadnia et al. (2013) detailed a study where the effect of elevated temperatures on chemical composition, microstructure and mechanical properties of high strength mortars with nano alumina was investigated. Mortars with 1%, 2% and 3% nano alumina as cement replacement were prepared and then exposed to 100°C, 200°C, 300°C, 400°C, 600°C, 800°C and 1000°C. They reported that nano alumina enhanced compressive strength of samples up to 16% and improved residual compressive strength. An increase in the relative elastic modulus, higher energy absorption and lower permeability were also observed when 1% nano alumina was added. It should be mentioned that Portland cement type I graded 32.5 was used to make samples that cured for 28 days [80].
- Genedy et al. (2017) reported on an experiment, with a focus on restoring wellbore seal integrity applying a new polymer nanocomposite repair material through the micro-annuli. They studied the efficiency of Novolac epoxy incorporating aluminum nanoparticles (ANPs) and microfine cement with shale as G-class OPC being the reference. **Figure 2.33** is displaying the bond strength results achieved in the study [81].

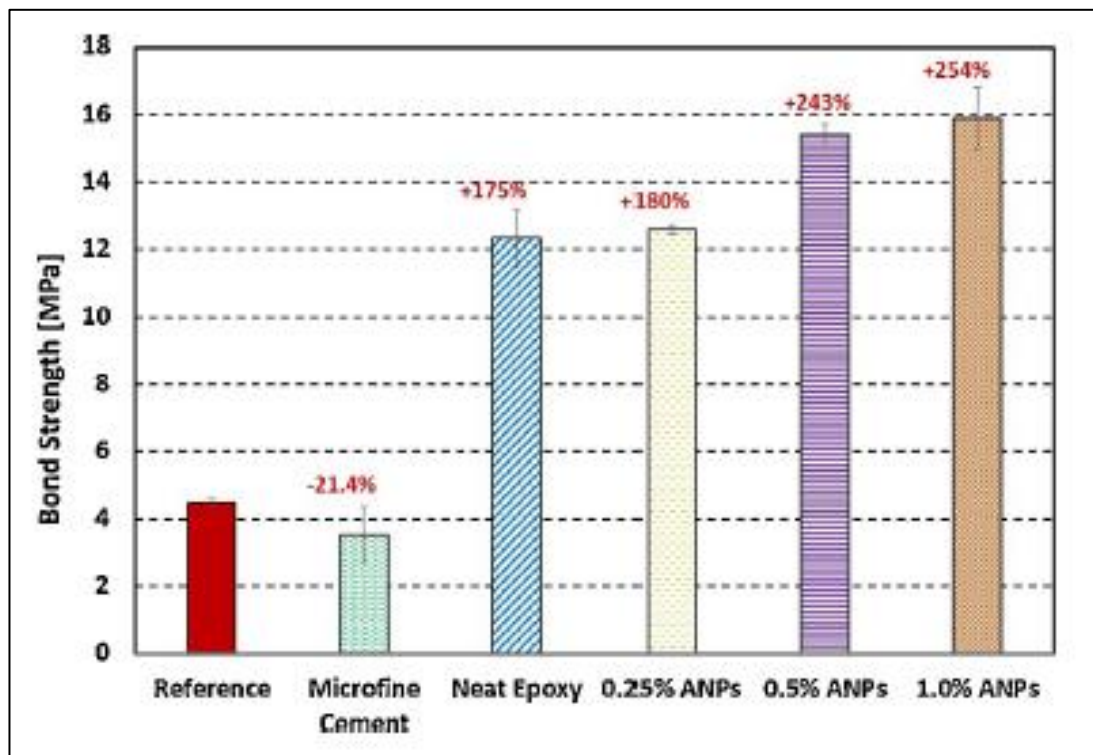


**Figure 2.33** The bond strength of the reference case and all repair materials [81]

Novolac epoxy nanocomposite incorporating ANPs proved to be a good repair material for shale micro-annulus with improved bond strength and excellent flexibility. The microfine cement has a bond strength that is 21% lower than the reference case. In contrast, ANPs-epoxy nanocomposites had a bond strength that is 250% higher than the reference case. Microscopic investigation of the shale-cement interface shows microfine cement was unable to completely fill the gap and microcracks along the inter-face with widths up to 40  $\mu\text{m}$  remaining open. However, no gap was observed with ANPs-epoxy nanocomposites. **Figure 2.34** exhibits shale- 1.0% ANPs-epoxy polymer nanocomposite interface [81].

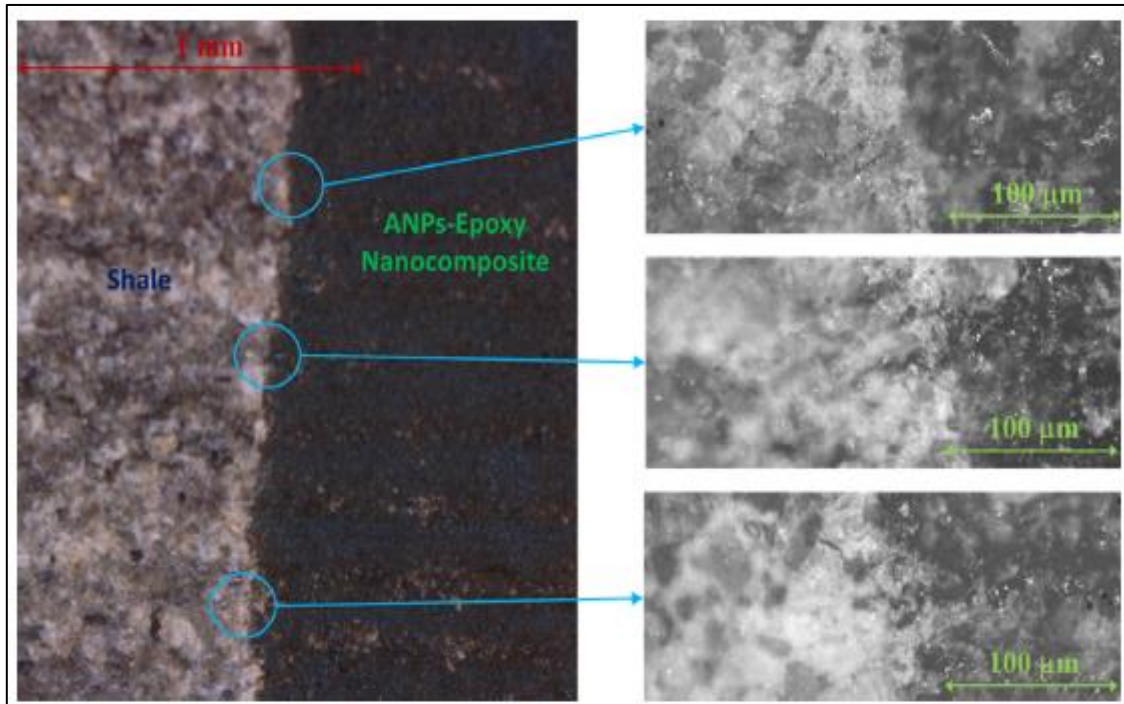


**Figure 2.34** Microscopic images of shale-1.0% ANPs-epoxy polymer nanocomposite interface with two different levels of magnification showing the ability of the epoxy repair material to completely fill the gap at the shale-cement interface [81]

The study goes to show that nanoparticles have a highly potential capability to aid in remedial cementing of wells with issues of integrity issues concerning cement. This avenue was not particularly investigated in this thesis, however certainly there is opening for future works.

- Maagi et al. (2019) examined effect of Nano-SiO<sub>2</sub>, Nano-TiO<sub>2</sub> and nano-Al<sub>2</sub>O<sub>3</sub> addition on fluid loss in oil-well cement slurry. They reported that ternary combination of nanoparticles (NSTA) showed effective properties as a fluid loss reducing material compared to the control specimens. It was clearly observed that there was a trend of decreasing fluid loss depending on the ratio of nano-scale particles and temperature variations. The out-flow of liquid decreased gradually with the cumulative nanoparticles content. Conversely, the filtration loss was noticeably found to increase progressively as temperature was adjusted to 90 °C. However, the samples with ternary combination of nanoparticles showed an effective performance on restricting fluid loss. In general, the fluid collected in all ternary samples was less than 100 ml. It seems that, the nano-scale particles were well able to place between the empty pore of cement matrix and did not let the solid part of the slurry to be separated from the liquid, thus stopping the escapement of water from the cement matrix. This phenomenon helps to diminish the loss of fluids from the cement slurry [82]. This is a very interesting finding in terms of required properties of cement being impermeable in the long run to maintain well integrity.



### 2.5.3.2 TiO<sub>2</sub> use with OPC, geopolymer cement and OPC reinforced with fibers

The second nanoparticles used in our studies is TiO<sub>2</sub> nanoparticles. Studies were conducted on OPC, geopolymer cement and OPC reinforced with carbon fibers and glass fibers. To understand the feasibility of using nano-Ti to improve the properties of cement, previous investigations can be useful.

- Nerhus (2020) conducted studies on 0.52 WCR G-class OPC. They reported that relatively high concentrations of titanium NPs did not perform well and the increment in UCS was very low. They documented that both 0.1g and 0.2g of added TiO<sub>2</sub> lead to a decrease in compressive strength, where the latter has the lowest UCS of the two. The highest UCS observed is obtained through the addition of 0.3g of titanium dioxide, which leads to an increase of approximately 8% compared to the control. **Figure 2.35** will display the UCS below [78].

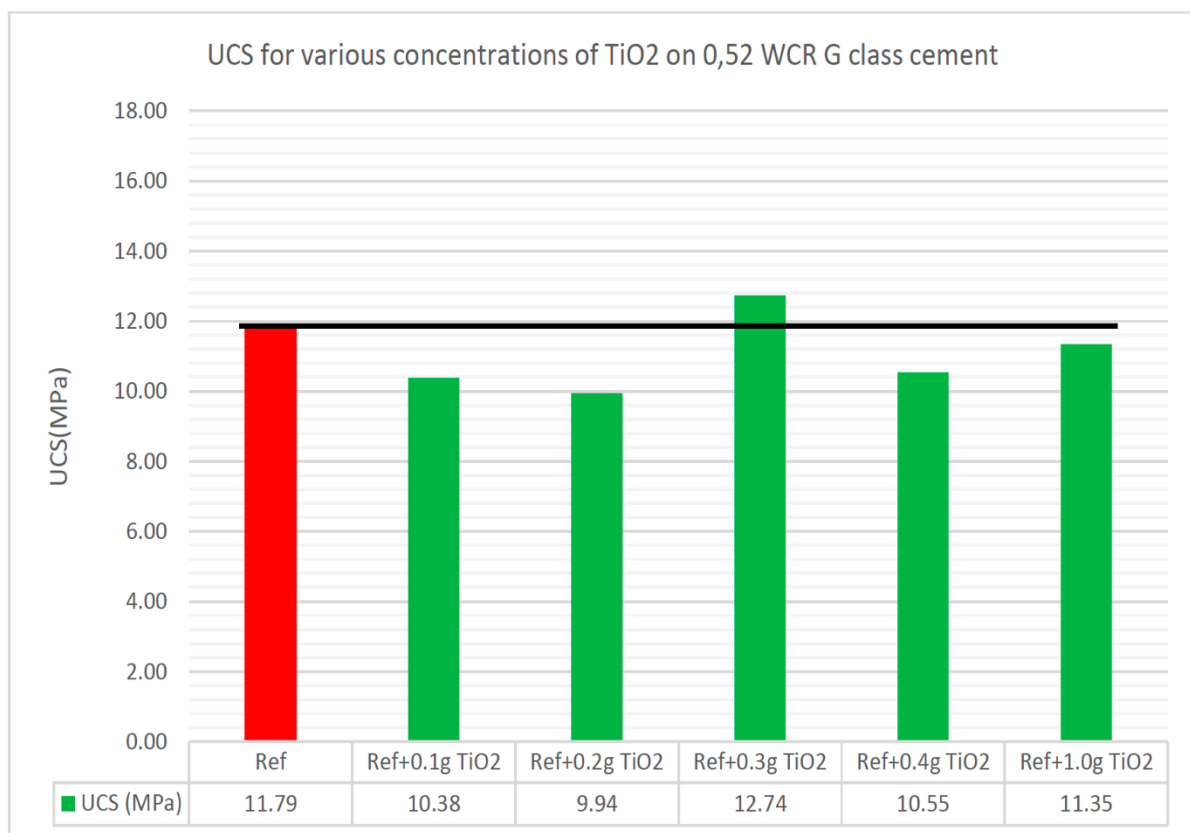


**Figure 2.35 UCS for various concentrations of TiO<sub>2</sub> on 0.52 WCR G-class cement [78]**

For both 0.4g and 1.0g added, the strength decreases. There appears to be no definite trend displayed from the graph in terms of strength increase versus dosage, but it is possible that the peak dosage lies in the proximity of 0.3g. They also reported that the highest E-modulus is observed from the addition of 0.3g of nano-TiO<sub>2</sub>, which causes an increase of 5.9% compared to the control. They also showed that few of dosages had massive reduction in resilience as well [78].

- Khan et al. (2022) reported on a study focusing on the application of titanium dioxide nanoparticles for the design of oil well cement slurry. The experimental investigation reveals that the mixing of the diminutive amount of TiO<sub>2</sub> nanoparticles (0.5%, 0.1%, 1.5%, and 2.0% BWOC) can simultaneously enhance the compressive strength and reduce the setting time of the cement slurry. **Figure 2.36** depicts **a)** the UCS and **b)** setting time [83].

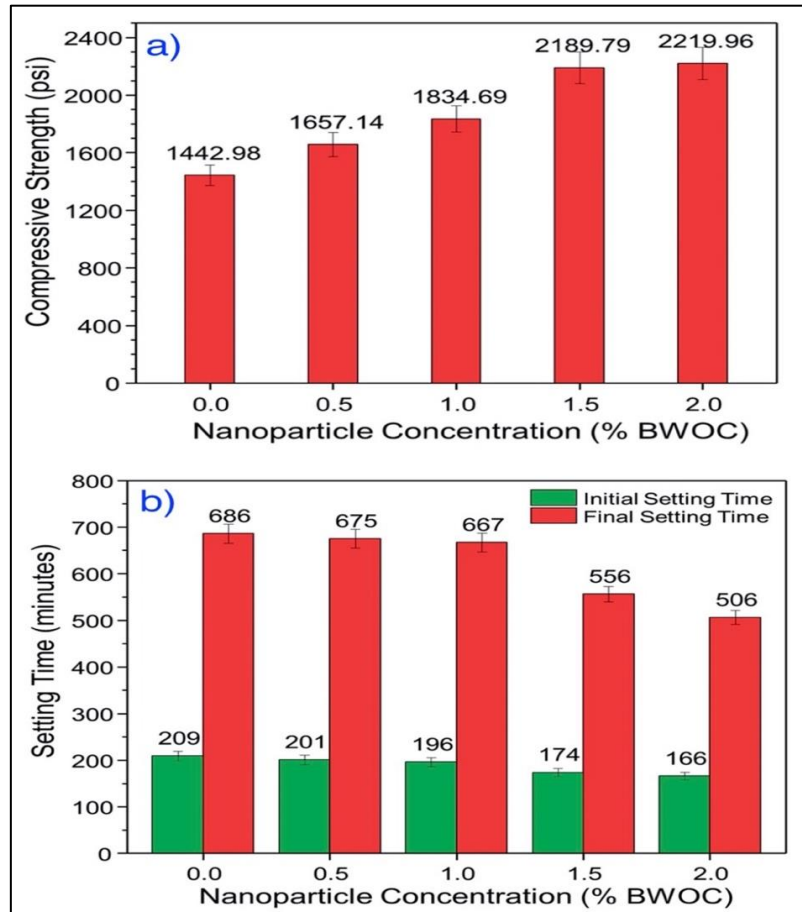


**Figure 2.36 a) Compressive strength; b) Setting time of the slurry** [83]

The increment of 2% BWOC of TiO<sub>2</sub> nanoparticles in the cement slurry increases the compressive strength by almost 54% while the final setting time reduces by nearly 26%. The compressive strength of the cement mixture was seen to be increasing with the increment of TiO<sub>2</sub> nanoparticles concentration in the slurry, while the setting time was found to be reduced. The cement slurry's viscosity was also found to be increased with the addition of nanoparticles. The study shows that the TiO<sub>2</sub> nanoparticles can be used as an additive to oil well cement slurry as an accelerator and at the same time strength enhancer [83].

- Mabeyo and Gu (2021) studied the effects of nano-SiO<sub>2</sub> and nano-TiO<sub>2</sub> on oil well cement's compressive and shear bond strengths at 80°C for 3, 7, 14 and 28 days of hydration. The XRD, TG and DSC were used for the analysis of cement hydration products. The results revealed that both nano-SiO<sub>2</sub> and nano-TiO<sub>2</sub> increased strength evolution. A ternary system made with 2% nano-SiO<sub>2</sub> and 2% nano-TiO<sub>2</sub> improved compressive strength by 22.6% and 48.4%, while the shear bond strength increased by 110.6% and 55% at age of 3 days and

28 days, respectively, compared to their corresponding binary systems. Therefore, these results remark the potential of replacing an appropriate proportion of oilwell cement with coupled nano-SiO<sub>2</sub> and nano-TiO<sub>2</sub> to ensure cement sheath structure durability in the annular and long-lasting zonal isolation. The compressive strengths and shear-bond strengths for the ternary systems are illustrated below in **figure 2.37** [72].

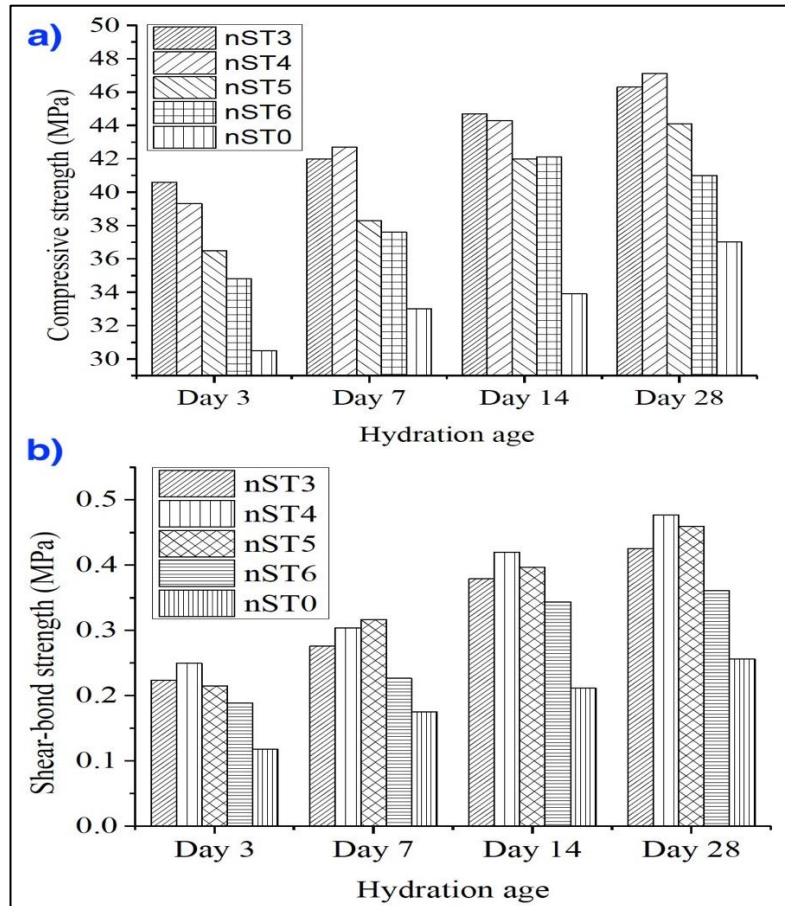


**Figure 2.37 a) Compressive strengths; b) Shear-bond strengths for the ternary systems** [72]

- Döndüren and Al-Hagri (2022) detailed a review study of the effect and optimization of use of nano-TiO<sub>2</sub> in cementitious composites. In their summary, it was reported that incorporation of nano-titanium (NT) into cementitious composites can remarkably reduce their workability and reduce their initial and final setting time. Use of nano-titania can also improve the compressive strength, split tensile strength and flexural strength of mortar and concrete, especially at early ages (1-7 days). This might be ascribed to the nano-filler effect and hydration acceleration effect of NT. Replacement of cement with an appropriate percentage of NT can improve the ultrasonic pulse velocity (UPV), electrical sensitivity and sulfate attack resistance of cementitious composites. However, NT might lead to a reduction in the resistance of cement-based materials to carbonation. They also described that it has been found in numerous studies that incorporation of high percentage of NT might lead to a reverse effect on the properties of cementitious composites due to the unsuitable dispersion and agglomeration of nanoparticles. Additionally, an allusion was made concerning the optimum dosages of titanium nanoparticles being within the range of 1.0-5.0 wt% [84].

- Khalifeh et al. (2019) examined the capability of nano-modified rock-based geopolymers as supplement to Portland cement for oil well cementing. In this study, the effect of nano titanium dioxide and nanocarbon graphene is considered on the rock-based geopolymers. Their findings show that the nanoparticles prolonged the pumpability and the nano-TiO<sub>2</sub> had the most effect. However, both types of the nanoparticles increased the viscosity of the geopolymeric slurry. The nano-TiO<sub>2</sub> had an adverse effect on strength development of the geopolymers, at low concentration (the first seven days of curing), when compared to nanocarbon. **Figure 2.38** will show the shear stress and UCS development at 2000 psi and 70°C [85].

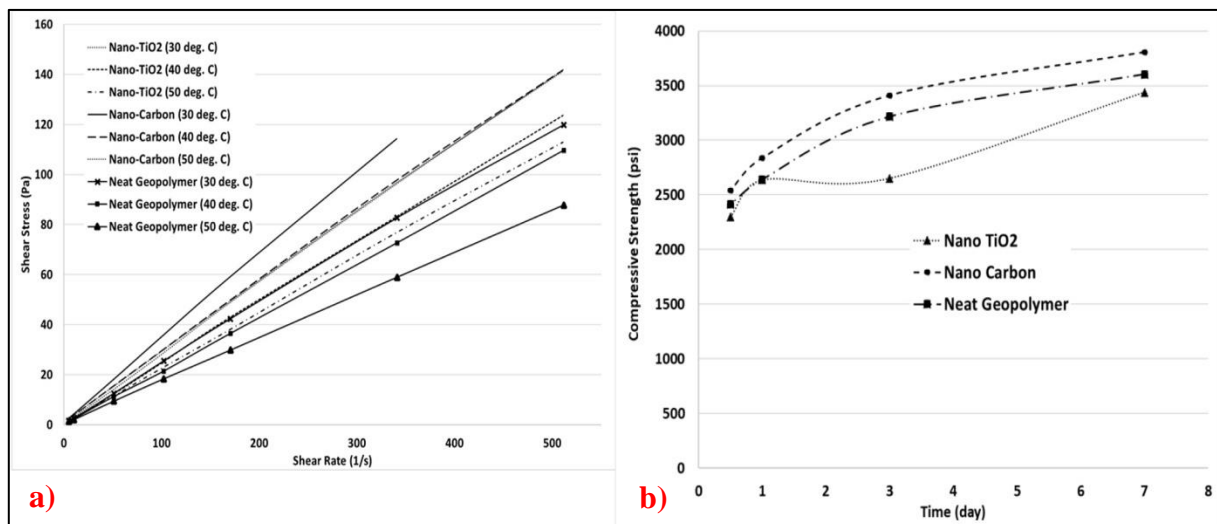


**Figure 2.38 a) Shear stress and b) UCS of nano-modified rock-based geopolymers [85]**

They reported as well that strength development of geopolymers is a continuous process although the strength development rate is not as rapid as it is in the initial stage. The nanocarbon particles increased both the tensile strength and the tensile to compressive strength ratio. SEM analysis and element mapping showed that the nano particles were not distributed homogenously in the geopolymers [85].

- Jumaa et al. (2022) strived to ascertain strength and microstructural properties of binary and ternary blends of NPs in fly ash-based geopolymer concrete. NPs used in this study were nano-clay (NC) and nano-TiO<sub>2</sub> (NT). Mixtures with constant water to FA (12%) and different alkaline contents of 40%, 45% and 50% by FA were made. The study was divided into three groups. In the first group, only FA was used as a binder, meanwhile, a combination of (FA+NC- MBC) and (FA+NT- MBT) was used separately in group two (binary). In the third group, (FA+NC+NT- MR) were mixed together (ternary). The findings revealed that the addition of nanomaterials obviously enhanced the density of the microstructure, reducing the pores of the produced geopolymer concrete. Moreover, the compressive strength was enhanced up to 24 % for nano-Ti in the binary blends compared to control mix (MC) while the improvement reached 55 % in the ternary blends. The splitting tensile strength results showed nano-TiO<sub>2</sub> had increased tensile strength of geopolymer concrete by 29%, 17% and 18% at alkaline doses of 40%, 45% and 50% respectively. **Figure 2.39** shows the a) compressive and b) splitting tensile strength results from the experiments [86].

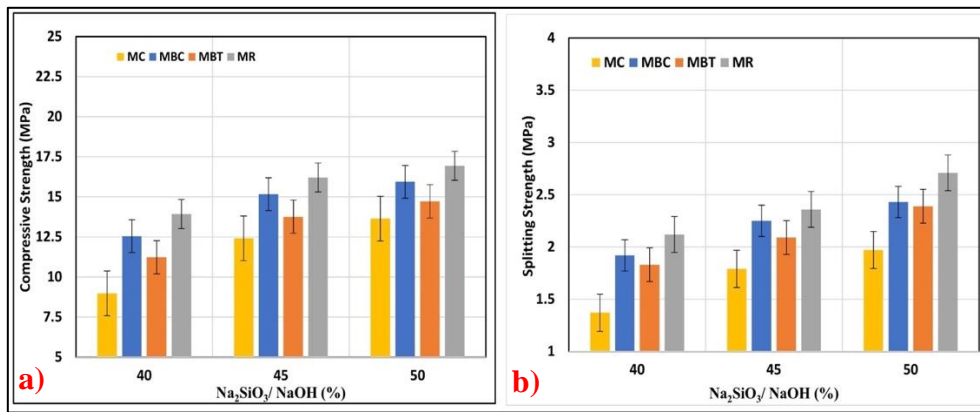


**Figure 2.39 a) Compressive and b) splitting tensile strength [86]**

- Xu et al. (2021) reviewed research progress on key problems of nanomaterials-modified geopolymer concrete (GPC). The raw materials of geopolymer come from industrial wastes, which have the advantages of lower carbon emissions and less energy consumption compared with traditional cement products. However, it still has the disadvantages of low strength, easy cracking and low production efficiency, which limit its engineering application and development. They summarized few bottlenecks of geopolymer cement that need to be resolved for the geopolymer to be applicable in field operations. It was described that due to nanomaterials' excellent physical and chemical mechanism, nanomaterials can improve the properties of geopolymer cement, thus broad varieties of NPs should be tested on geopolymer cement. More efforts need to be made to develop more admixtures in material selection to improve the working performance of GPC. Importantly, systematic study of how the mechanical properties of NPs improve the all-over properties of GPC must be widened to better characterize it. Most researches on GPC modified by nanomaterials being on the initial stage of exploration, it is paramount to conduct more researches to make up for the research gap in nanomaterial, dispersion effect and performance, to promote the field of nanomaterial- modified GPC and to develop its application value rapidly [87].
- Hunashyal et al. (2015) investigated the behaviour of OPC reinforced with TiO<sub>2</sub> and CFs. TiO<sub>2</sub> was varied at 0.1% and 0.5% by weight of cement and that of CFs was fixed at 0.25%. Load carrying capacity of composites reached high value with dosage of 0.5% by weight of TiO<sub>2</sub>. Composites with 0.5% of TiO<sub>2</sub> showed higher deflections. They underwent large deformation with increased load carrying capacity. Composite with 0.5% TiO<sub>2</sub> and 0.25% CFs showed the lesser amount of deflection compared to other nano composites. This may be due to the crack propagation inhibition by CFs [figure 2.40] [88].

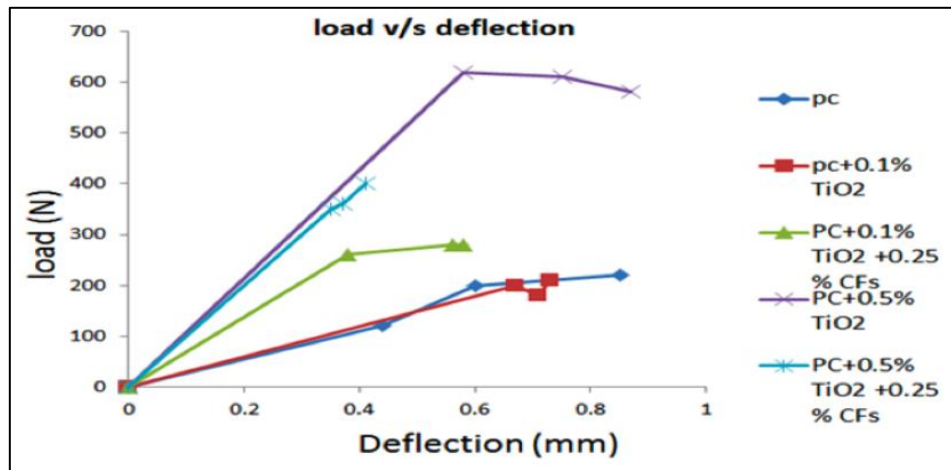


**Figure 2.40 Load v/s Deflection graph [88]**

- Joshaghani (2018) evaluated the effects of titanium dioxide (TiO<sub>2</sub>) and carbon-nanofibers (CNF) as cement partial replacement on concrete properties. It was reported that concrete containing CNF is also improved in mechanical properties. It can be attributed to the bridging effect of the CNFs for microcracks and filler effect. Compared TiO<sub>2</sub> with the CNF, the mixtures containing CNF had slightly higher compressive strength. CNF could recover the particle packing density and bridge the gel pores, which results in the volume of larger pores reduction. They also asserted that the addition of nanoparticles increases the amounts of harmless pores and reduces the amounts of harmful pores. The effectiveness of CNF in improving the pore structure is much better than TiO<sub>2</sub>. The total numbers of the harmless in mixtures containing CNF were increased to the largest extent. The reduction shrinkage in nanoparticles is accredited to microstructure. The performance of CNF in controlling shrinkage was better than TiO<sub>2</sub>. However, the largest shrinkage values were recorded for the mixture that contains CNF at opening hours due to free shrinkage. The nanoparticles addition in the mixture results in lower shrinkage values [89].
- Park et al. (2020) aims to examine the mechanical, shrinkage and chemical properties of photocatalytic cementitious materials containing synthetic fibers and a shrinkage-reducing admixture (SRA). Two types of titanium dioxide (TiO<sub>2</sub>) powders and white Portland cement were considered along with ordinary Portland cement (OPC) as a control. Two types of synthetic fibers, i.e., glass and polyethylene (PE) and an SRA with contents varying from 0% to 3% were also considered. Using the TiO<sub>2</sub> powders and the white Portland cement was successful in reducing the nitrogen oxides concentration in cement composites. The use of PE fibers was more effective than glass fibers in terms of the mechanical properties, i.e., the compressive strength and tensile performance. With the addition of TiO<sub>2</sub> powders and SRA or the replacement of OPC with white cement, the mechanical properties of the cement mortar generally deteriorated. The total shrinkage of the mortar could be reduced by incorporating the fibers at volume fractions greater than 1% and the glass fiber was more effective than the PE fiber in this regard. The TiO<sub>2</sub> powders had no significant impact on the shrinkage reduction of the cement mortar, whereas the SRA and the white Portland cement efficiently reduced shrinkage. The addition of 3% SRA decreased the total shrinkage by 43%, while the replacement of the OPC with white cement resulted in a 20% reduction in the shrinkage [90].

## **3 Experimental Programs**

This chapter presents the descriptions of materials utilized in all the experimental designs along with and the rationalizations behind the various test batches.

### **3.1 Materials**

The materials used for the experiments are cementations and non-cementations materials.

The first investigation is on Portland cement, which is cementations. When it is in contact with water, the hydration process undergoes. In this system, the effect of fly ash, fibers, nanoparticles and their mixtures have been evaluated.

The second study is the formulation of synthetic rock, which is formulated based on non-cementitious solids (silica fume, fly ash) and alkaline activators (10M NaOH, Na<sub>2</sub>SiO<sub>3</sub>). The effect of nanoparticles on the base geopolymer here was also evaluated.

The following sub-section presents chemical and physical properties of the materials along with the company providers.

Experiments were conducted in various laboratories of the University of Stavanger and the instruments used in the experimental works were acquired by the University from different providers.

### 3.1.1 Cement

The G-class OPC used in experiments was provided by NORCEM AS in Lilleaker, Norway. *Figure 3.1* shows the composition of the cement [91].

PRODUCT DATA SHEET  
**NORWELL**  
**CLASS G (HSR)**  
 LAST VERSION JANUARY 2021

The cement satisfies the requirements according to API Spec. 10A Class G (HSR) cement

Properties		Declared values	Requirements according to API Spec. 10A
Fineness (Blaine m <sup>2</sup> /kg)		330	NR
Specific weight (kg/dm <sup>3</sup> )		3.25	NR
Free lime (%)		1.2	NR
MgO (%)		2.1	≤ 6.0 %
SO <sub>3</sub> (%)		2.1	≤ 3.0 %
LOI (%)		1.0	≤ 3.0 %
I.R. (%)		0.2	≤ 0.75 %
C <sub>3</sub> S (%)		54	48 - 65 %
C <sub>2</sub> A (%)		2	≤ 3 %
C <sub>4</sub> AF + 2*C <sub>2</sub> A (%)		15	≤ 24 %
Na <sub>2</sub> O-eq (%)		0.6	≤ 0.75 %
Free fluid (%)		4.0	≤ 5.9 %
Compressive strength at 8 hrs (psi)	38°C	500	≥ 300
	60°C	1900	≥ 1500
Thickening time - Schedule 5 (min)		105	90 - 120
Max consistence 15 - 30 min (Bc)		19	≤ 30
Water soluble Cr (VI) (ppm)		< 2	≤ 2 <sup>1</sup>

<sup>1</sup> According to EU-regulation REACH Annex XVII point 47 Chromium VI-compounds

**NORCEM**  
 HEIDELBERGCEMENT Group  
 Norcem AS, P.O.Box 142, Lilleaker, NO-0216 Oslo  
 Tel +47-22 87 84 00 firmapost@norcem.no www.norcem.no



*Figure 3.1 Ordinary Portland Cement G-class [91]*

### 3.1.2 Water

Freshwater from the laboratory's faucet was utilized to make cement slurries. It was used with the idea that it was pure and free of any kind of contamination. Furthermore, it is also realistic to use localized source of freshwater in a sense that in the oil and gas fields, regular freshwater is used in mixing cement slurry most often.



### **3.1.3 Al<sub>2</sub>O<sub>3</sub> Nanoparticles**

U.S. Research Nanomaterials Inc., located in the city of Houston, Texas, provided the Al<sub>2</sub>O<sub>3</sub>. The particles are around 30 nm in size and have a purity of 99.99%. Particles' structure is characterized as "Alpha". The particles are also dispersed in water that contains roughly 20% by weight of the particles and a pH range from 6-8 [92].

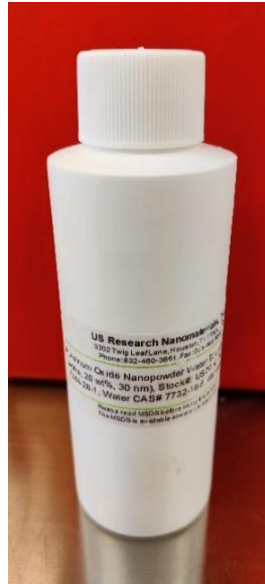


*Figure 3.2 Al<sub>2</sub>O<sub>3</sub> Nanoparticles [92]*

### **3.1.4 TiO<sub>2</sub> Nanoparticles**

The anatase TiO<sub>2</sub> nanoparticle was obtained from U.S. Research Nanomaterials Inc.. The size of TiO<sub>2</sub> nanoparticles is in the range of 5 to 15 nm. The solution comprises approximately of 15,3 wt.% of titanium dioxide and dispersed in water. The aqueous solution that was added to the water before it was mixed with the cement powder is depicted in the illustration below [93].



*Figure 3.3 TiO<sub>2</sub> Nanoparticles [93]*

### **3.1.5 Fly Ash**

Norcem in Lilleaker, Norway contributed the Class-F fly ash for this thesis. Class-F FA is used here because it has negligible pozzolanic properties on its own but develops them when exposed to moisture [94]. The density of the FA is  $2.3 \text{ g/cm}^3$ . The fly ash was pale brown in color and very fine powder, shown is *figure 3.4*.



*Figure 3.4 Fly Ash*

### **3.1.6 Geopolymers**

Short descriptions of the materials used in geopolymer design are given below in the following sub-sections.

#### **3.1.6.1 Silica Fume**

Norcem in Lilleaker, Norway supplied the silica fume [*figure 3.5*]. It is a highly pozzolanic material that is used to enhance mechanical and durability properties of a non-cementitious material like geopolymer. It is essentially defined as very fine noncrystalline silica produced in electric arc furnaces as a by-product of the production of elemental silicon or alloys containing silicon [95]. Physically, it had powder-like general appearance with small round ball-like structures and bluish gray coloration.



*Figure 3.5 Silica Fume*

#### **3.1.6.2 Fly Ash**

Class-F FA was used in making geopolymer cement. The characteristics were described in *section 3.1.5*.

### 3.1.6.3 10M NaOH

NaOH pellet was supplied by VWR Chemicals of VWR International s.r.o. from the Czech Republic. Sodium hydroxide (98.5-100.5%) of  $2.13 \text{ g/cm}^3$  ( $20^\circ\text{C}$ ) had colour of white pastilles. From the pallets, 10M NaOH solution was made by mixing with water [96].

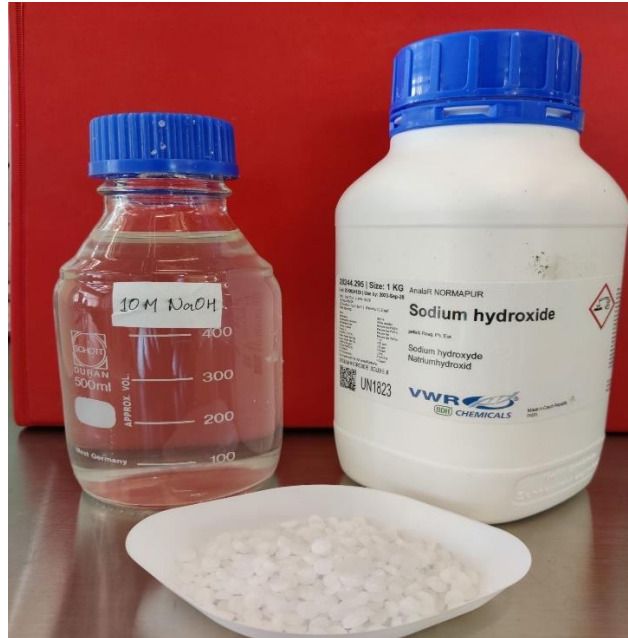


*Figure 3.6 10M NaOH [96]*

### 3.1.6.4 $\text{Na}_2\text{SiO}_3$

Sodium Silicate, also known as Water Glass, is an alkaline liquid that was used in the geopolymer synthesis. It was syrupy in appearance and in terms of visibility, the liquid was semi-transparent. The solution has 45-65% of water content and molar ratio of 1.6-2.6 [97].

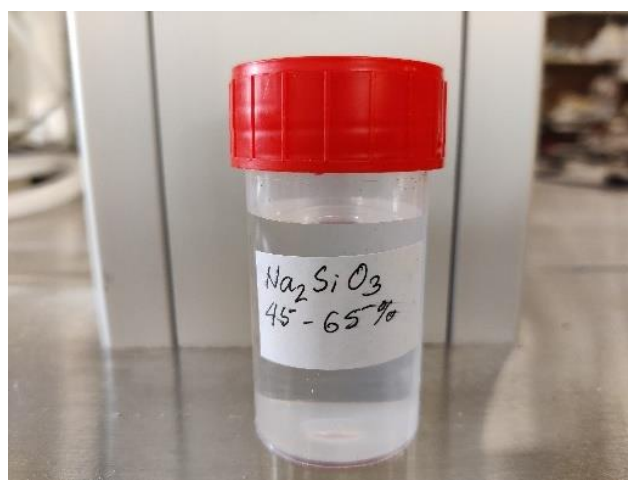


*Figure 3.7  $\text{Na}_2\text{SiO}_3$  [97]*

### **3.1.7 Carbon fibers (CF)**

Carbon Fiber is a long, thin strand of material about 0.0002-0.0004 in (0.005-0.010 mm) in diameter and composed mostly of carbon atoms. The carbon atoms are bonded together in microscopic crystals that are more or less aligned parallel to the long axis of the fiber. The crystal alignment makes the fiber incredibly strong for its size [98].

The carbon fiber used in the experiment was obtained by my thesis supervisor for past experiments. However, the details of the material's characterizations were not available. The fiber is black in color and very lightweight. It had a hair-like structural attribution [figure 3.8]. The fiber was cut according to the convenience so that the dispersion was done as evenly as possible in the cement slurry.



*Figure 3.8 Carbon fibers*

### **3.1.8 White glass fibers (WF)**

This fiber in white colour is a type of glass fiber for reinforcement which was acquired by my supervisor from SCANOX AS in Drammen, Norway. The detail of the materials characterization was not available from the manufacturer. From the picture below [figure 3.9] and in the section above, we observe that the white glass fibers are in smaller volumes than the carbon fibers despite having the same mass. This shows that the white glass fibers are denser than carbon fiber [99].



*Figure 3.9 White glass fibers*

### 3.2 Test Designs

The subsequent section will provide information on the test matrices and test batches that were designed. The compositions and design backgrounds for the matrices will be expounded upon in the sections that follow.

#### 3.2.1 Experimental designs

Five test designs (TDs) were constructed in total. TD-1, TD-2, TD-4 and TD-5 consist of test batches (TBs) that were aged for three, seven, or twenty-eight days, respectively. TD-3 consists of TB which was cured for ten days. **Table 3.1** shows the summary of the TDs along with their respective TBs and their curing time and environments.

**Table 3.1 Test designs in the experimental works of this thesis**

Test designs (TDs)	Test batches (TBs)	Curing environment and time					
		Room temperature, 20°C			Oven temperature, 80°C		
		Batch No.	Time	No. of Plugs	Batch No.	Time	No. of Plugs
TD-1	TB-1	TB-1-R	3 days	8	TB-1-O	3 days	8
	TB-2	TB-2-R	7 days	8	TB-2-O	7 days	8
	TB-3	TB-3-R	28 days	8	TB-3-O	28 days	8
TD-2	TB-4	TB-4-R	3 days	14	TB-4-O	3 days	14
	TB-5	TB-5-R	7 days	14	TB-5-O	7 days	14
	TB-6	TB-6-R	28 days	14	TB-6-O	28 days	14
TD-3*	TB-7*	TB-7-R*	8 days	8	TB-7-R*	2 days	8
TD-4	TB-8	TB-8-R	3 days	10	TB-8-O	3 days	10
	TB-9	TB-9-R	7 days	10	TB-9-O	7 days	10
	TB-10	TB-10-R	28 days	10	TB-10-O	28 days	10
TD-5	TB-11	TB-11-R	3 days	16	TB-11-O	3 days	16
	TB-12	TB-12-R	7 days	16	TB-12-O	7 days	16
	TB-13	TB-13-R	28 days	16	TB-13-O	28 days	16

**NB.** TD-3\* — It has the same 8 plugs from the room temperature.

- **Test design 1:** Analyzed the effects of Al<sub>2</sub>O<sub>3</sub> nanoparticles on 0.44 WCR neat G-class OPC with curing ages of 3, 7, 28 days.
- **Test design 2:** Studied the efficacy of Al<sub>2</sub>O<sub>3</sub> nanoparticles and fly ash blending on 0.44 WCR neat G-class OPC with curing ages of 3, 7, 28 days.
- **Test design 3:** Examined the developments of a Geopolymer based design with TiO<sub>2</sub> curing ages of 10 days.
- **Test design 4:** Evaluated the outcome of TiO<sub>2</sub> nanoparticles on 0.44 WCR neat G-class OPC with curing ages of 3,7, 28 days.
- **Test design 5:** Investigated the implications of TiO<sub>2</sub> nanoparticles, carbon fibers and white glass fibers for reinforcement on 0.44 WCR neat G-class OPC with curing ages of 3,7, 28 days.

### 3.2.2 Constants and variables

In order to maintain certain levels of consistency and avoid disproportionate changes in the test designs and obtained results, few parameters were kept constant throughout the experimental phases of certain designs and few were kept throughout the whole experimental phases of all the designs. In the following *table 3.2*, these constants and variables are displayed.

**Table 3.2: Constants and variables**

TBs	Constants		Variables			
TB-1	WCR = 0.44	G-class OPC	Al <sub>2</sub> O <sub>3</sub>			48 plugs
TB-2						
TB-3						
TB-4	WCR = 0.44	G-class OPC	Al <sub>2</sub> O <sub>3</sub> + FA	FA	84 plugs	
TB-5						
TB-6						
TB-7	Calculated LSR = 0.54	n/a	TiO <sub>2</sub>			8 plugs
TB-8	WCR = 0.44	G-class OPC	TiO <sub>2</sub>			60 plugs
TB-9						
TB-10						
TB-11	WCR = 0.44	G-class OPC	TiO <sub>2</sub>	TiO <sub>2</sub> + CF	TiO <sub>2</sub> + WF	96 plugs
TB-12						
TB-13						

### 3.2.3 Cement slurry synthesis

Prior to mixing the slurries, all the necessary materials were collected and measured in the relevant amount for the respective TDs., which helped maximize the working efficiency and minimize the unnecessary time spending between mixing subsequent specimens.

- For TBs 1–6 and 8–13, following procedures were maintained:
  - ⇒ The procedure to construct cement plugs was to measure 227.27±0,05 g of neat G-class cement with 100 g of liquid which results in a 0.44 WCR.
    - a) In all the relevant batches (*table 3.2*) where fly ash was utilized as an additive, a dry cement-like ingredient in appearance, the amount of fly ash was then subtracted from the cement in mass. Fly ash was mixed with cement very carefully to ensure a very homogeneous blend before any liquid was added.
    - b) The liquid mix in the above-mentioned batches is composed of water and nanoparticles. The decided upon mass of nanoparticles was subtracted from the 100 g water to maintain 0.44 WCR.
    - c) The batches (*table 3.2*) where CF and WF were added in the plugs, no modifications were made to the solid mass but for liquid mass (*b*) was followed.
- For TB-7, procedures are shown below:
  - ⇒ The cement plugs constructed in this batch are geopolymer based, in which NP were added as an additive. Geopolymer as non-cementitious material, no specific LSR was maintained. However, liquid-solid ratio (LSR) was calculated to be 0.54. The amount of water added in the base design was to make slurry less viscous and more pumpable. The composition of the slurry will be discussed in the future corresponding section.

It is important to note that while making all the TBs, first two plugs were reference specimens which had no additives at all, which is followed by two plugs for every concentration of additives.

Furthermore, the solid parts were put in a mixing container and then the liquid parts including the NPs were added in the mixture. Before the solid and liquid combination could be poured into the cement moulds (*figure 3.10*), it was mixed with a stirrer until it was completely smooth. Usually before pouring the slurry, moulds were glazed with a little cooking oil to have an easier retrieval of the hardened plugs after they were cured. The moulds were regularly and gently tapped against a flat surface while the slurry was being poured to prevent air bubbles from forming in the cement plugs. This was done to avoid the cement plug from being riddled with air pockets. The cement plugs may crack if air gets trapped inside them. The corks that were originally part of the moulds were not placed on top after pouring the slurry into the moulds to ease the water evaporation. It is essential to note that the cork was not screwed on top because doing so could cause the slurry to become contaminated with air and compromise the specimen's structural integrity. The moulds were then left to be cured in room temperature and put in an oven at 80°C without the moulds' corks for their relevant curing ages.

In this thesis, we are experimenting with the temperature effects on the samples. Except for TB-7, the exact number of plugs were made in every batch for two different curing environments- **a)** at room temperature, 20°C and **b)** in an oven at 80°C, which is a realistic temperature for downhole in both NCS and globally [100]. After each successive batch was made, it was allowed to cure at the earlier temperatures and under normal atmospheric pressure for either 3, 7 or 28 days, depending on which option was selected based on the availability of materials and time. After the allotted time for each TB's curing time had passed, the top of each specimen was then smoothed out to create a level surface. This would exclude the possibility of any point-loading occurring when they would later be crushed. Because point-loading can substantially reduce the samples' compressive load, the top had to be unmistakably flat. After measuring each specimen's length, weight and ultrasonic time, the specimens were eventually crushed so that their UCS values could be determined. The tests were conducted immediately on the next day after the designated curing time had passed.

In the exceptional case of TB-7 as shown in *table 3.1*, the same specimens were cured for 10 days, among which 8 days were in room temperature and 2 days in the oven to dry the excess water. They were only cured to increase hardness and quicken the water drying [101]–[102].

The specimens were cured in plastic cylinder moulds with a 69 mm height and a 34 mm diameter. To remove the plugs without damaging the samples, the plastic mould was carefully cut when the plugs had achieved the curing age. To remove the plug from their moulds, the plastic moulds were cut with a blade.



*Figure 3.10 Cement Mould*

### 3.2.4 Test design process and their compositions

The design process is based on the issues addressed in [chapter 1](#) and specifically, based on the research questions in [section 1.3](#). That is to try to study the separate additives' effects and their amalgamations to investigate if there exist synergies on the positive and negative impacts.

For TDs 1-2 and 4-5, the effects of a single NPs blend on OPC were studied. Based on that, the hybrid effects were investigated by combining NPs with FA (TD-2) and with different fibers (TD-5) from TD-1 and TD-4, respectively.

In TD-3, we first analyzed the base reference composition with various ingredients of corresponding concentration. After obtaining optimistic reference results, we decided to employ a NP system for final analysis.

### 3.2.5 Test Design 1

Test design 1 (TD-1) consists of test batches- 1, 2 and 3. It was designed to examine how Al<sub>2</sub>O<sub>3</sub> NPs react with the neat G-class OPC. **Table 3.3** shows the TD-1 test batches.

**Table 3.3 Test design 1**

Test design (TD)	Test batches (TBs)	Curing environment and time					
		Room temperature, 20°C			Oven temperature, 80°C		
		Batch No.	Time	No. of Plugs	Batch No.	Time	No. of Plugs
TD-1	TB-1	TB-1-R	3 days	8	TB-1-O	3 days	8
	TB-2	TB-2-R	7 days	8	TB-2-O	7 days	8
	TB-3	TB-3-R	28 days	8	TB-3-O	28 days	8

Additionally, the compositions of cement slurries that were tested in TD-1 are provided in **table 3.4**. Although the batches have identical additives in identical concentrations and they are divided in same numbers for two different curing environments. The only differentiating factor is the curing time which is valid for TDs-2, 4 and 5 as well.

**Table 3.4 Composition of TD-1**

Samples	Cement, g	Water, g	Al <sub>2</sub> O <sub>3</sub> NPs, g
TD-1– Ref.-1	227.27	100	0
TD-1– Ref.-2	227.27	100	0
TD-1– Ref.+1.2g Al <sub>2</sub> O <sub>3</sub> -1	227.27	98.8	1.2
TD-1– Ref.+1.2g Al <sub>2</sub> O <sub>3</sub> -2	227.27	98.8	1.2
TD-1– Ref.+1.4g Al <sub>2</sub> O <sub>3</sub> -1	227.27	98.6	1.4
TD-1– Ref.+1.4g Al <sub>2</sub> O <sub>3</sub> -2	227.27	98.6	1.4
TD-1– Ref.+1.6g Al <sub>2</sub> O <sub>3</sub> -1	227.27	98.4	1.6
TD-1– Ref.+1.6g Al <sub>2</sub> O <sub>3</sub> -2	227.27	98.4	1.6

**NB.** “Ref.”– shown in the table 3.4 is short for **Reference**, which refers to the reference plugs mentioned in the [section 3.2.3](#). It is valid all the other TDs as well.



The slurries for each batch are synthesized according to the methods outlined in *section 3.2.3*. In addition, Al<sub>2</sub>O<sub>3</sub> nanoparticles were added in quantities of 1.2g, 1.4g and 1.6g. For each batch, sixteen cement plugs were produced, among which eight were cured at room temperature of 20°C and eight were cured in the oven at 80°C. Each nano-Al<sub>2</sub>O<sub>3</sub> concentration family consisted of two plugs and two reference plugs were made with no additives. Additional information will be available in the corresponding result discussion section.

### 3.2.6 Test Design 2

As shown in *table 3.5*, test design 2 consists of TBs-4,5 and 6. The purpose of the test design was to investigate the effects of Al<sub>2</sub>O<sub>3</sub> NPs on OPC and fly ash blended system. WCR of 0.44 is maintained here as well.

**Table 3.5 Test design 2**

Test design (TD)	Test batches (TBs)	Curing environment and time					
		Room temperature, 20°C			Oven temperature, 80°C		
		Batch No.	Time	No. of Plugs	Batch No.	Time	No. of Plugs
TD-2	TB-4	TB-4-R	3 days	14	TB-4-O	3 days	14
	TB-5	TB-5-R	7 days	14	TB-5-O	7 days	14
	TB-6	TB-6-R	28 days	14	TB-6-O	28 days	14

In *table 3.6*, cement slurry compositions are shown which were chosen to conduct the experiments. It was created keeping in mind the obtained results from TD-1.

**Table 3.6 Composition of TD-2**

Samples	Cement, g	Water, g	Al <sub>2</sub> O <sub>3</sub> NPs, g	Fly Ash (FA), g
TD-2– Ref.-1	227.27	100	0	0
TD-2– Ref.-2	227.27	100	0	0
TD-2– 1.4g Al <sub>2</sub> O <sub>3</sub> / 1g FA-1	226.27	98.6	1.4	1
TD-2– 1.4g Al <sub>2</sub> O <sub>3</sub> / 1g FA-2	226.27	98.6	1.4	1
TD-2– 1.4g Al <sub>2</sub> O <sub>3</sub> / 2g FA-1	225.27	98.6	1.4	2
TD-2– 1.4g Al <sub>2</sub> O <sub>3</sub> / 2g FA-2	225.27	98.6	1.4	2
TD-2– 1.4g Al <sub>2</sub> O <sub>3</sub> / 3g FA-1	224.27	98.6	1.4	3
TD-2– 1.4g Al <sub>2</sub> O <sub>3</sub> / 3g FA-2	224.27	98.6	1.4	3
TD-2–1g FA-1	226.27	100	0	1
TD-2–1g FA-2	226.27	100	0	1
TD-2–2g FA-1	225.27	100	0	2
TD-2–2g FA-2	225.27	100	0	2
TD-2–3g FA-1	224.27	100	0	3
TD-2–3g FA-2	224.27	100	0	3

Results from Test design 1 showed that the 1.4g Al<sub>2</sub>O<sub>3</sub> improved the UCS significantly. Based on this information, test design 2 was designed to investigate if FA improved the neat OPC and its blending with the 1.4g Al<sub>2</sub>O<sub>3</sub> as well. To maintain the WCR of 0.44, part of cement has been replaced by solid fly ash and part of the water has been replaced by nano-solution.

### 3.2.7 Test Design 3

The main objective of Test Design 3 was to investigate the impact of TiO<sub>2</sub> on geopolymer. It is an environment-friendly material that could be potentially used as the best alternative for OPC in the future. The design is provided below in *table 3.7*. It consists of only one batch, TB-7.

**Table 3.7 Test design 3**

Test design (TD)	Test batches (TBs)	Curing environment and time					
		Room temperature, 20°C			Oven temperature, 80°C		
		Batch No.	Time	No. of Plugs	Batch No.	Time	No. of Plugs
TD-3*	TB-7*	TB-7-R*	8 days	8	TB-7-R*	2 days	8

*NB. TD-3\* — It has the same 8 plugs from the room temperature.*

The composition of this design was based on the visual inspection of the slurry. Due to materials and research times, the detail geopolymer formulation process on the potential pumpability, viscosity and the setting time of the slurry have not been studied. The design intention here is to formulate the base geopolymer and see how TiO<sub>2</sub> NPs chemically interact. The ingredients were also chosen based on the available materials that can be used to create a reference or base geopolymer. The selected compositions are described in *table 3.8*. In this design, the calculated liquid (alkaline activator + water) to solid (FA + silica fume) ratio was found to be 0.54 and the TiO<sub>2</sub> concentrations varies from 0.3g to 0.5g.

**Table 3.8 Composition of TD-3**

Samples	TiO <sub>2</sub> NPs, g	Solid, Wt. %	Liquid, Wt. %
Geopolymer Ref.-1	0	64.74%	35.26%
Geopolymer Ref.-2	0	64.74%	35.26%
Geopolymer Ref.+0.3g TiO <sub>2</sub> -1	0.3	64.74%	35.32%
Geopolymer Ref.+0.3g TiO <sub>2</sub> -2	0.3	64.74%	35.32%
Geopolymer Ref.+0.4g TiO <sub>2</sub> -1	0.4	64.74%	35.34%
Geopolymer Ref.+0.4g TiO <sub>2</sub> -2	0.4	64.74%	35.34%
Geopolymer Ref.+0.5g TiO <sub>2</sub> -1	0.5	64.74%	35.36%
Geopolymer Ref.+0.5g TiO <sub>2</sub> -2	0.5	64.74%	35.36%

### 3.2.8 Test Design 4

This design is very much like TD-1, which means that we experimented on OPC with TiO<sub>2</sub> as the single additive in various concentrations. This design is made up of TBs-8,9 and 10. We maintained 0.44 WCR for G-class cement. Inspiration for utilizing TiO<sub>2</sub> as an additive was taken from previous experiments by different entities. The formulation is demonstrated in *table 3.9*.

**Table 3.9 Test design 4**

Test design (TD)	Test batches (TBs)	Curing environment and time					
		Room temperature, 20°C			Oven temperature, 80°C		
		Batch No.	Time	No. of Plugs	Batch No.	Time	No. of Plugs
TD-4	TB-8	TB-8-R	3 days	10	TB-8-O	3 days	10
	TB-9	TB-9-R	7 days	10	TB-9-O	7 days	10
	TB-10	TB-10-R	28 days	10	TB-10-O	28 days	10

TD-4 compositions will be shown in *table 3.10* to clarify the distribution of the chemical components in details. Each concentration having two plugs including two reference samples with no additives are also divided equally for two different curing environments.

**Table 3.10 Composition of TD-4**

Samples	Cement, g	Water, g	TiO <sub>2</sub> NPs, g
TD-4–Ref.-1	227.27	100	0
TD-4–Ref.-2	227.27	100	0
TD-4–Ref.+ 0.15g TiO <sub>2</sub> -1	227.27	99.85	0.15
TD-4–Ref.+ 0.15g TiO <sub>2</sub> -2	227.27	99.85	0.15
TD-4–Ref.+ 0.25g TiO <sub>2</sub> -1	227.27	99.75	0.25
TD-4–Ref.+ 0.25g TiO <sub>2</sub> -2	227.27	99.75	0.25
TD-4–Ref.+ 0.35g TiO <sub>2</sub> -1	227.27	99.65	0.35
TD-4–Ref.+ 0.35g TiO <sub>2</sub> -2	227.27	99.65	0.35
TD-4–Ref.+ 0.45g TiO <sub>2</sub> -1	227.27	99.55	0.45
TD-4–Ref.+ 0.45g TiO <sub>2</sub> -2	227.27	99.55	0.45

Due to the damage on the surface of the samples, samples from TB-9-R containing 0.15g, 0.25g and 0.45g TiO<sub>2</sub> were made again to get reproducible results.

### 3.2.9 Test Design 5

TD-5 studies the effects of TiO<sub>2</sub> on OPC G-class induced with two different kinds of fibers to reduce the brittleness of OPC and increase strength. The two fibers are *a)* carbon fibers and *b)* white glass fibers for reinforcement. The decision to keep using TiO<sub>2</sub> was made after observing relatively promising results in TD-4. The model is explained in the following *table 3.11*. Same numbers of plugs were created for each curing environments.

Table 3.11 Test design 5

Test design (TD)	Test batches (TBs)	Curing environment and time					
		Room temperature, 20°C			Oven temperature, 80°C		
		Batch No.	Time	No. of Plugs	Batch No.	Time	No. of Plugs
TD-5	TB-11	TB-11-R	3 days	16	TB-11-O	3 days	16
	TB-12	TB-12-R	7 days	16	TB-12-O	7 days	16
	TB-13	TB-13-R	28 days	16	TB-13-O	28 days	16

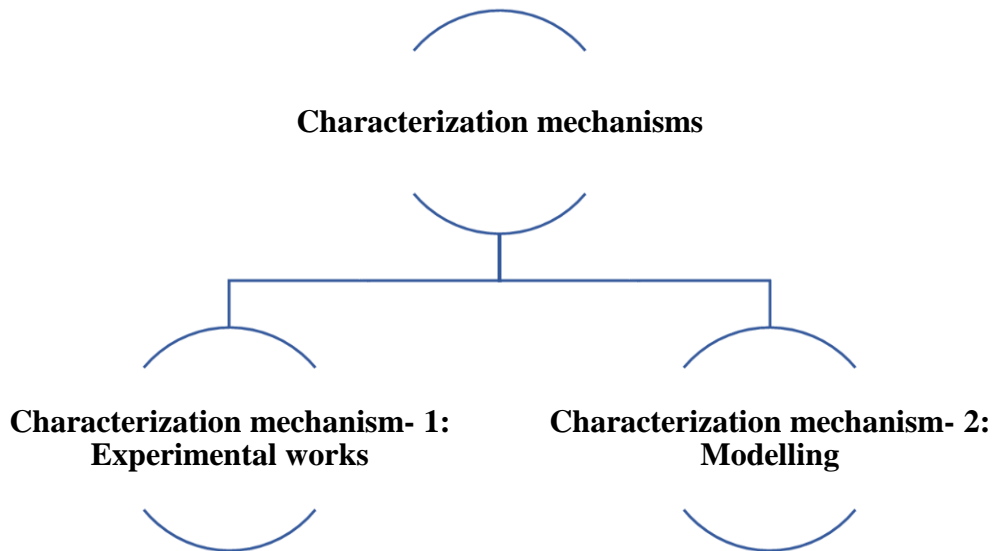
The specific concentration of TiO<sub>2</sub>, which was kept constant throughout the design was 0.45g because it showed good potential for reproducibility in room temperature. In an exceptional case, two reference points were considered in this instance which were just OPC without additives and OPC with only TiO<sub>2</sub>. The rest of the design was equally divided between two fibers having the same numbers of specimens. Below shown the compositions of the design in *table 3.12*. As it was done in the all the previous designs, here as well demonstrably all the concentration family have two plugs each.

Table 3.12 Composition of TD-5

Samples	Cement, g	Water, g	TiO <sub>2</sub> NPs, g	CF, g	WF, g
TD-5–Ref.-0/0-1	227.27	100	0	0	0
TD-5–Ref.-0/0-2	227.27	100	0	0	0
TD-5–Ref.+0/0.45g TiO <sub>2</sub> -1	227.27	99.55	0.45	0	0
TD-5–Ref.+0/0.45g TiO <sub>2</sub> -2	227.27	99.55	0.45	0	0
TD-5–Ref.+0.1g CF/0.45g TiO <sub>2</sub> -1	227.27	99.55	0.45	0.1	0
TD-5–Ref.+0.1g CF/0.45g TiO <sub>2</sub> -2	227.27	99.55	0.45	0.1	0
TD-5–Ref.+0.2g CF/0.45g TiO <sub>2</sub> -1	227.27	99.55	0.45	0.2	0
TD-5–Ref.+0.2g CF/0.45g TiO <sub>2</sub> -2	227.27	99.55	0.45	0.2	0
TD-5–Ref.+0.3g CF/0.45g TiO <sub>2</sub> -1	227.27	99.55	0.45	0.3	0
TD-5–Ref.+0.3g CF/0.45g TiO <sub>2</sub> -2	227.27	99.55	0.45	0.3	0
TD-5–Ref.+0.1g WF/0.45g TiO <sub>2</sub> -1	227.27	99.55	0.45	0	0.1
TD-5–Ref.+0.1g WF/0.45g TiO <sub>2</sub> -2	227.27	99.55	0.45	0	0.1
TD-5–Ref.+0.2g WF/0.45g TiO <sub>2</sub> -1	227.27	99.55	0.45	0	0.2
TD-5–Ref.+0.2g WF/0.45g TiO <sub>2</sub> -2	227.27	99.55	0.45	0	0.2
TD-5–Ref.+0.3g WF/0.45g TiO <sub>2</sub> -1	227.27	99.55	0.45	0	0.3
TD-5–Ref.+0.3g WF/0.45g TiO <sub>2</sub> -2	227.27	99.55	0.45	0	0.3

## 4 Characterization Mechanisms

The cement plugs and cement slurries synthesized in [chapter 3](#) are going to be characterized through different mechanisms, which are depicted below in [figure 4.1](#). The theories and procedures for these characterization mechanisms will be discussed in this chapter.



*Figure 4.1 Characterization mechanisms summarized*

### ➤ Characterization mechanism- 1: Experimental works

The experimental works in this mechanism are the primary tasks completed to obtain data which took place at once after the curing time had passed. Initially, they are divided into two methods mainly. They are classified as *a)* Destructive tests and *b)* Non-Destructive tests. In-depth classifications are shown in [figure 4.2](#).

*a)* From the uniaxial compressive destructive methods, the cement plug's elastic and mechanical properties are quantified. These are uniaxial compressive strength, the Young's modulus and the energy absorption property (i.e., resilience) of the plugs. After the plugs have been crushed, some of the specimens have been further analyzed through Scan Electron Microscope (SEM) to study the internal structure of the plugs.

*b)* Under the non-destructive methods, the compressional wave velocity and the density of the plugs are calculated. These properties describe how the cement plugs are well compacted indirectly. Moreover, from these two properties, the modulus of elasticity of the plugs are calculated. In addition, to study the pumpability of the cement slurries, the rheological properties of the slurries are measured.

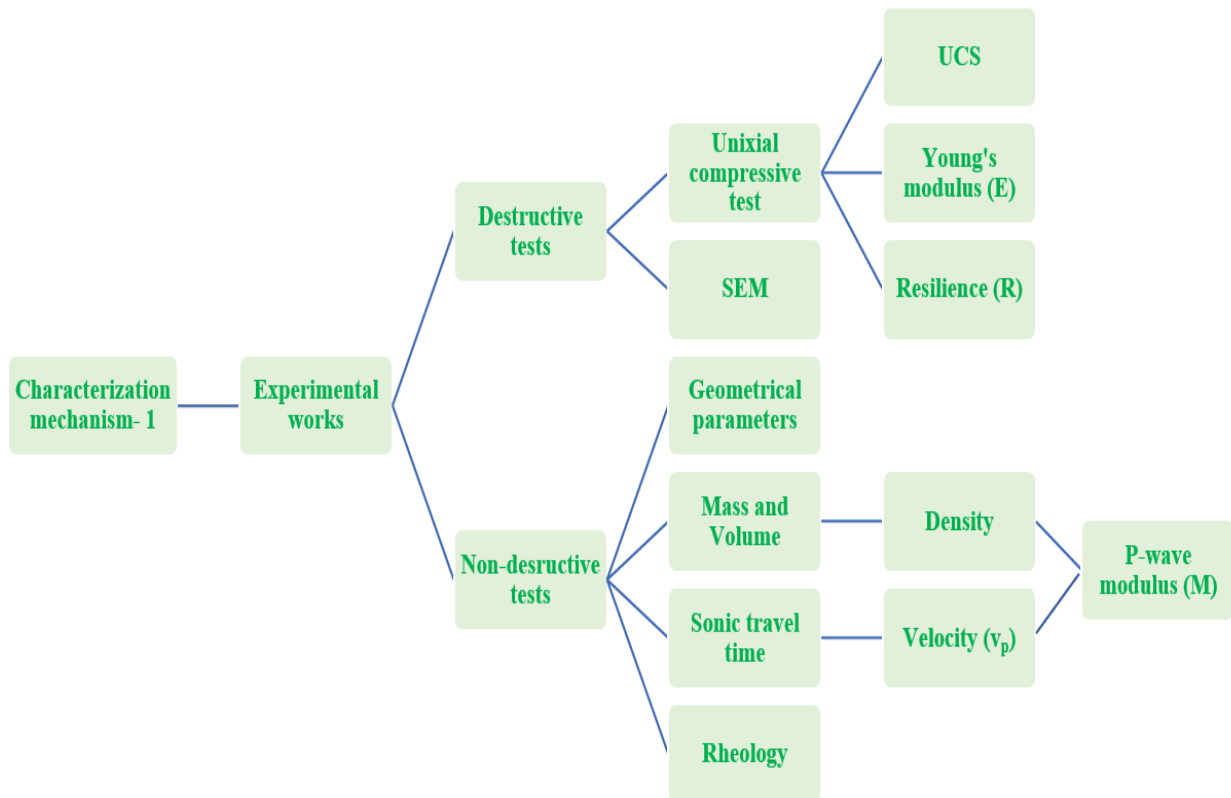


Figure 4.2 Characterization of experimental works

➤ **Characterization mechanism- 2: Modelling with data obtained from “Experimental works”**

As outlined in *figure 4.3*, the second mechanism of the characterization is modelling of the experimental data obtained from destructive method (UCS) and the non-destructive method ( $v_p$ ). Several models are available in literature that relates the UCS and  $v_p$ . Among others, the Horsrud’s (2001), Nerhus’s (2020) and Titlestad’s (2021) empirical models relate UCS- $v_p$  with power law behavior. In this thesis work, all possible modelling options will be evaluated including the power law:  $UCS = a \cdot v_p^b$ , where the empirical constants ‘a’ and ‘b’ will be determined from curve fitting between the model and the measured datasets.

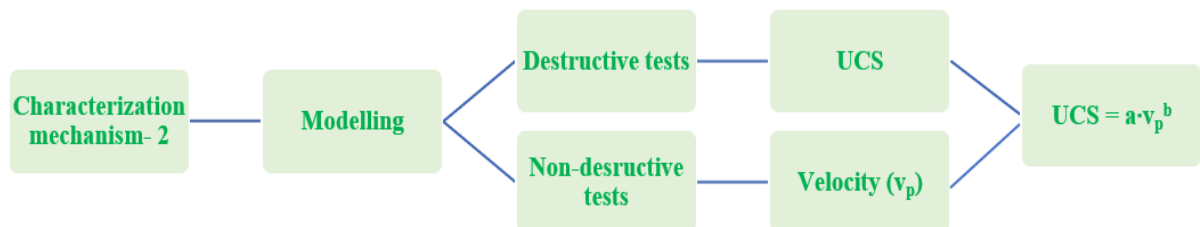


Figure 4.3 Modelling of experimental works

## **4.1 Experimental works**

In this section, all the experimental works will be discussed in details and graphical representations will be provided, when needed. As described earlier, destructive and non-destructive tests are conducted according to the classifications depicted in *figure 4.2*.

### **4.1.1 Destructive tests**

The following sections will provide information concerning the destructive aspects of the experimental works. As its title indicates, destructive testing is the method of testing a material's strength to its yield (failure) point by subjecting it to heavy mechanical loads. The findings of destructive testing are the maximum mechanical loads and specimens' deformation data. This can quantify the specimen's various mechanical properties, such as uniaxial compressive strength, Young's modulus and resilience. Additionally, the internal structure of the cement plugs can be ascertained by SEM after the cement plugs have been crushed in the destructive tests.

#### **4.1.1.1 Measurement process and equipment for the destructive methods**

The principal equipment which was used for crushing all the cement plugs was a customized hand-operated hydraulic shop press purchased from Biltema in Stavanger, Norway. This press was equipped with a load cell and a deformation sensor, which enabled the recording of load and deformation data and ensured the accuracy of data output. The press was connected to a computer. Using data acquisition (DAQ) software, the computer collected all load and deformation measurements.

Before any testing could begin, the top and bottom surfaces of the plugs had to be flat to prevent point-loading. In fact, the surfaces' being flat is also valid for the non-destructive tests, which take place before the destructive tests chronologically. After confirming this by using a spirit level, the samples were positioned under the load cell in the center on a small round stage. The load cell was subsequently lowered to be positioned just above the cement plug. Before lowering the load cell further, some short and sturdy metal plates were positioned beneath the deformation sensor until the sensor's tip touched the metal plates, ensuring that deformation data would be recorded accurately. Finally, a plastic protective cover was put in front of the cement plug to guard against cement splinters and dust containing nanoparticles; this allowed manual loading of the cement plug to begin until mechanical failure was achieved.

The loading rate was maintained as consistently as feasible. In addition to visually seeing failure, the program clearly displayed the load difference when failure was achieved. The final step involved exporting several thousand data cells from the DAQ software to an Excel spreadsheet for future calculations. The DAQ software also found the maximum loads from the load data cells, after which the yielding of a plug happens.

The exact hydraulic press that was used in the experiments is depicted below in *figure 4.4*.

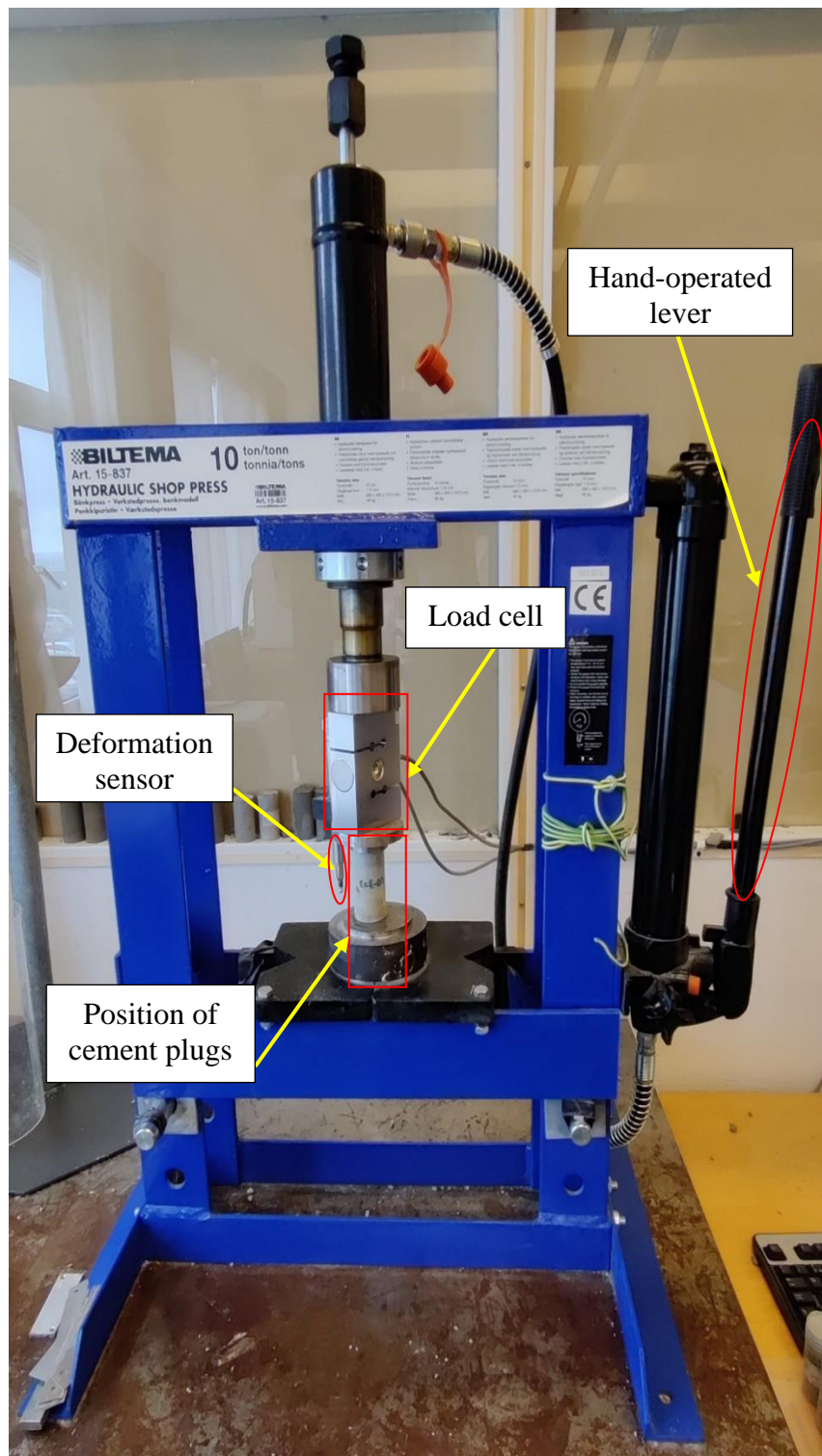


*Figure 4.4 Customized hand-operated hydraulic shop press*



#### 4.1.1.2 Uniaxial compressive strength (UCS)

UCS is a measure of a material's strength. The uniaxial compressive strength (UCS) is the maximum axial compressive stress that a right-cylindrical sample of a material can withstand before failing [103]. The uniaxial compressive strength is also referred to as the unconfined compressive strength because, during loading of the cylindrical sample, only the top and bottom surface areas will be in contact with the compressing device and there will be no forces acting in other directions, resulting in zero confining stress. In industrial applications, axial loads are one of the most frequent, which is why the UCS is such a crucial parameter of cement's strength. **Figure 4.5** graphically presents UCS of a cement sample. UCS can be determined with typical engineering stress formula [2], [104]–[107]:

$$\sigma_{UCS} = \frac{F_{max}}{A_{cross-section}} \quad [Equation 4.1]$$

Where:  $\sigma_{UCS}$  = Uniaxial compressive strength, [MPa]

$F_{max}$  = Maximum load applied at fracture point, [kN]

$A_{cross-section}$  = Original cross – sectional area of a cement plug, [m<sup>2</sup>]

**Figure 4.5** displays uniaxial compressive strength of a cement sample in a stress-strain diagram. This particular sample had UCS of 28.4 MPa. This data was taken from an actual specimen's destructive test result of this thesis.

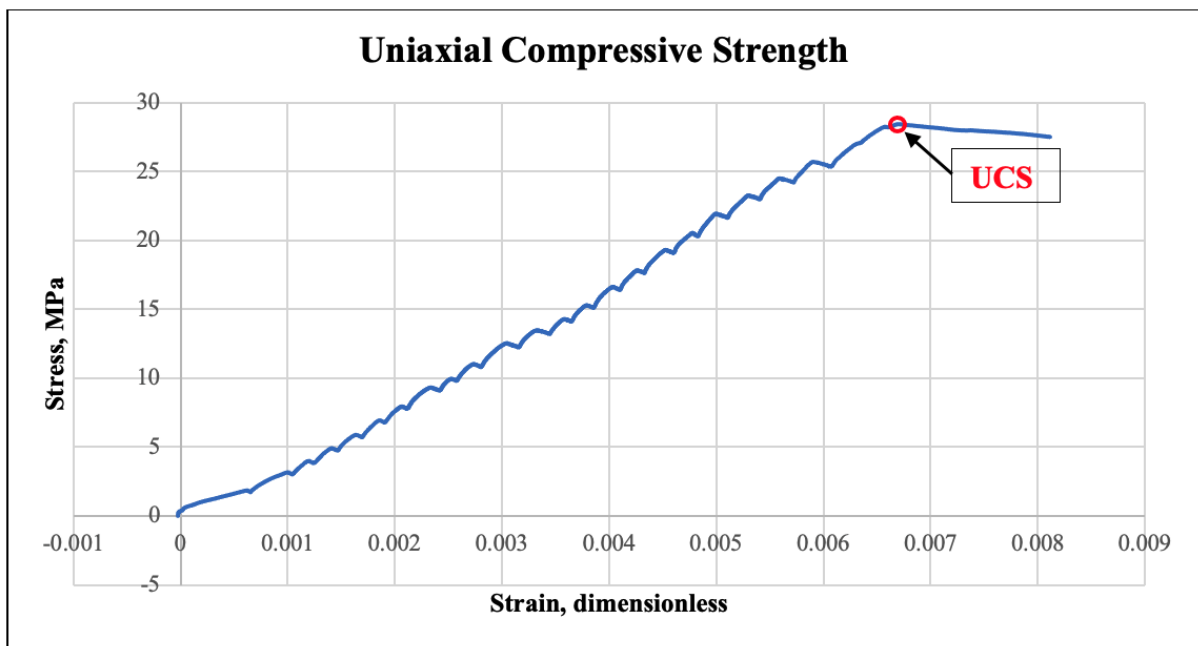


**Figure 4.5 Uniaxial compressive strength**

### 4.1.1.3 Young's Modulus (E-modulus)

Young's modulus (E), a numerical constant, describes the elastic properties of a material undergoing tension or compression in only one direction, as in the case of a material that returns to its original length after being stretched or compressed axially. It is dependent on temperature and pressure, however. The E-modulus is, in essence, the stiffness of a material. In other words, it is how easily it is bent or stretched. E-moduli of materials are determined from the linear-elastic deformation, where the Hooke's law is valid. E-moduli are typically so large that they are expressed not in pascals but gigapascals (GPa) [2], [107]–[109].

The E-modulus is the slope of the line as depicted in **figure 4.6** and calculated as [107]:

$$E = \frac{\Delta\sigma}{\Delta\varepsilon} \quad \text{[Equation 4.2]}$$

Where: E = Young's Modulus, [GPa]

$\Delta\sigma$  = Change in uniaxial stress, [MPa]

$\Delta\varepsilon$  = Change in uniaxial strain, [dimensionless]

Using an equation for a straight line, we can figure out the E-moduli, often called the modulus of elasticity, of samples from stress-strain diagrams [**figure 4.6**]:

$$y = mx + c \quad \text{[Equation 4.3]}$$

Where **m** is the slope of a straight line, which is also the E-modulus [110]. Cement plug chosen in [section 4.1.1.2](#) is shown with its E-modulus of 4.6945 GPa in **figure 4.6**.

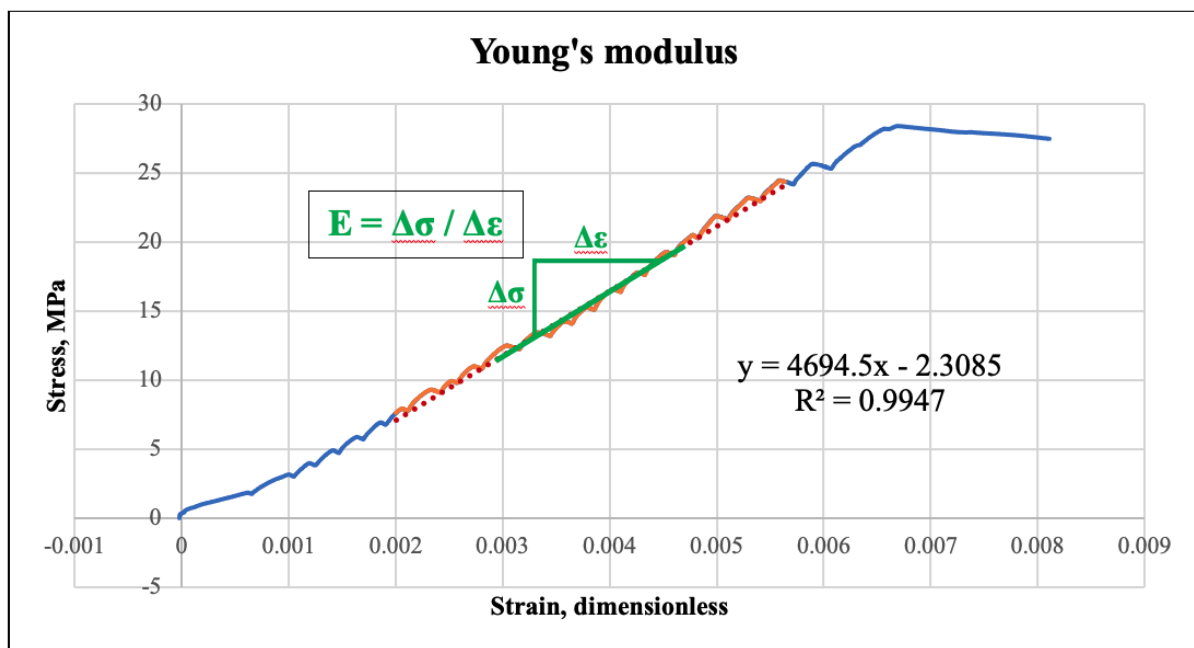


**Figure 4.6** Young's modulus of a cement sample

#### 4.1.1.4 Resilience (R)

In material science, resilience is the ability of a material to absorb energy when it is deformed elastically and release that energy upon unloading. The modulus of resilience is expressed as the maximum energy that can be absorbed per unit volume without creating a permanent distortion. After the elastic limit is reached, permanent deformation occurs, otherwise known as the plastic region. For the materials' deformation that show the proportionality limit is equal to the yield stress, the energy absorption is calculated by the following formula [107], [111]:

$$R = \frac{\sigma_y^2}{2E} = \frac{\sigma_y \cdot \epsilon_y \cdot 10^3}{2} \quad [\text{Equation 4.4}]$$

Where: R = Modulus of resilience, [ $\frac{\text{kJ}}{\text{m}^3}$ ]

E = Young's Modulus, [GPa]

$\sigma_y$  = Yield stress, [MPa]

$\epsilon_y$  = Yield strain, [dimensionless]

However, since most of the samples do not show a clear transition between the elastic and plastic region, which is why it is difficult to quantify the yield stress of the material. Therefore, the above equation was not used. Instead, based on the observation assuming that the yield stress is nearly equal to the UCS, the resilience is calculated by integrating the area under the stress-strain curve until the UCS value as [111]:

$$R = \left| \sum \frac{(\epsilon_{(i+1)} - \epsilon_{(i)}) \cdot (\sigma_{(i+1)} + \sigma_{(i)})}{2} \right| \quad [\text{Equation 4.5}]$$

Where:  $\epsilon$  = Strain, [dimensionless]

$\sigma$  = Stress, [MPa]

For the following *figure 4.7*, stress-strain diagram of the same sample chosen in [section 4.1.1.2](#) is displayed with its resilience, which is in 94.7 kJ/m<sup>3</sup>.

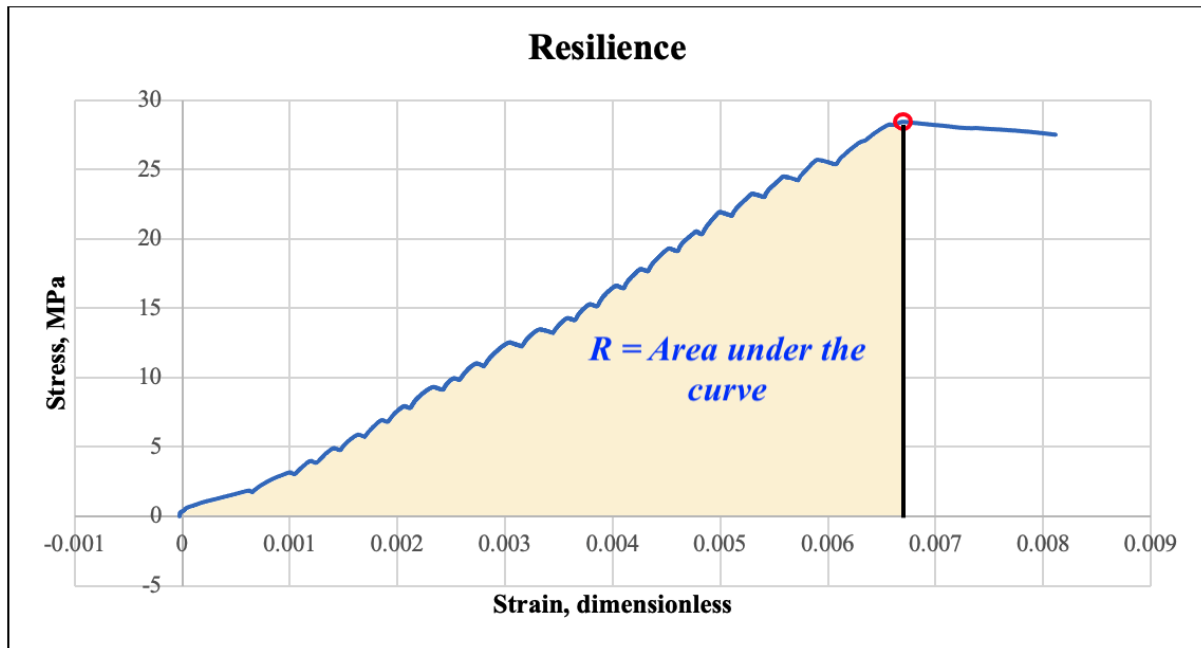


Figure 4.7 Resilience of a cement sample

#### 4.1.1.5 Analysis of internal structure using SEM and EDS

SEM stands for scanning electron microscope. The SEM is a microscope that uses electrons instead of light to form an image. The scanning electron microscope has many advantages over traditional microscopes. It has a large depth of field, which allows more of a specimen to be in focus at one time. SEM also has much higher resolution, so closely spaced specimens can be magnified at much higher levels. Some SEMs can achieve resolutions better than 1nm [112]. Because the SEM uses electromagnets rather than lenses, the researcher has much more control over the degree of magnification. All these advantages make the scanning electron microscope one of the most useful instruments in research today.

##### 4.1.1.5.1 Sample preparation

Because the SEM utilizes vacuum conditions and electrons to form an image, special preparations must be made to the sample. Humidity must be removed from the samples because the water would vaporize in the vacuum. All metals are conductive and require no preparation before being used. That is why all non-metals must be made conductive by covering the sample with a thin layer of conductive material. This is done by using a device called a “sputter coater” [113].

The sputter coater uses an electric field and argon gas. The sample is placed in a small chamber that is at a vacuum. Argon gas and an electric field cause an electron to be removed from the argon, making the atoms positively charged. The argon ions then become attracted to a negatively charged gold or palladium foil. The argon ions knock gold atoms from the surface of the gold or palladium foil. These atoms fall and settle onto the surface of the sample producing a thin gold or palladium coating [113]. In our case, copper (Cu) was used for coating, which is also a very conductive material.

After the samples were crushed, samples for SEM analysis were selected. It is important to denote that the chosen samples were kept as thin and flat as possible to obtain good scans.

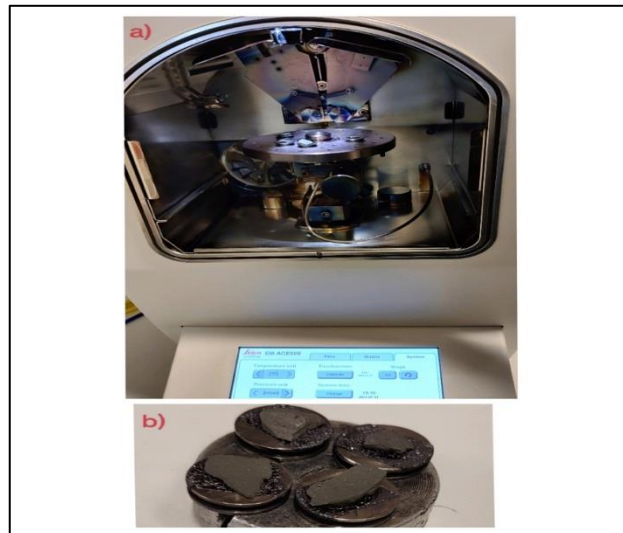


**Figure 4.8 a) Leica EM ACE600 sputter coater; b) Copper coated samples**

To remove the humidity as well as possible, the chosen samples were kept in an oven inside cement moulds for up to 5 hrs. at 100°C. They were kept un the moulds until they were made ready for coating. **Figure 4.8** shows the sputter coater used in the process and the copper-coated samples.

#### 4.1.1.5.2 Scanning process and image formation

The SEM is an instrument that produces a vastly magnified image by using electrons instead of light to form an image. An electron gun produces a beam of electrons at the top of the microscope. **Figure 4.9** is depicting the schematic of an SEM and its operational directions [113].

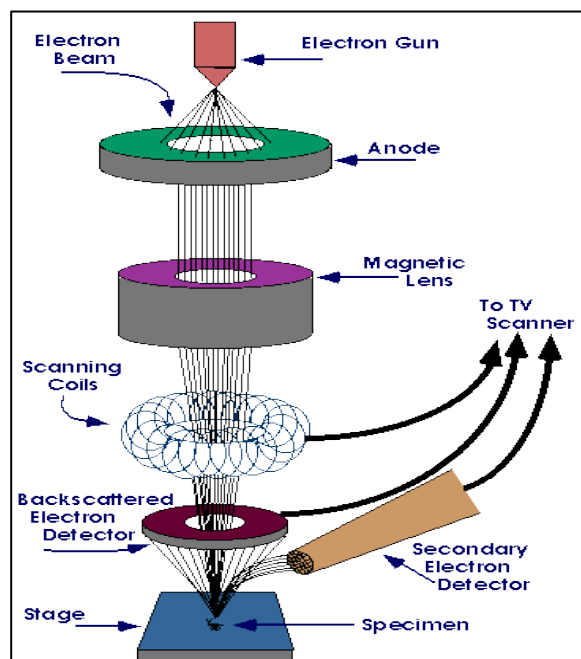


**Figure 4.9 Schematic of a SEM [113]**

## *Effects of nanoparticles, fibers and fly ash on cementitious and non-cementitious materials*

The electron beam follows a vertical path through the microscope, which is held within a vacuum. The beam travels through electromagnetic fields and lenses, focusing the beam down toward the sample. Once the beam hits the sample, electrons and X-rays are ejected from the sample. Detectors collect these X-rays, backscattered electrons, and secondary electrons and convert them into a signal sent to a screen similar to a television screen. This produces the final image [113].

In *figure 4.10* the scanning process is shown including the equipment itself. After putting the samples inside SEM, vacuuming process started by using nitrogen gas and subsequently 20 kV was used to accelerate electrons to start imaging of the samples. To provide supporting evidence for the nanoparticles' presence in the samples, EDS analyses (element analysis) were performed as well.

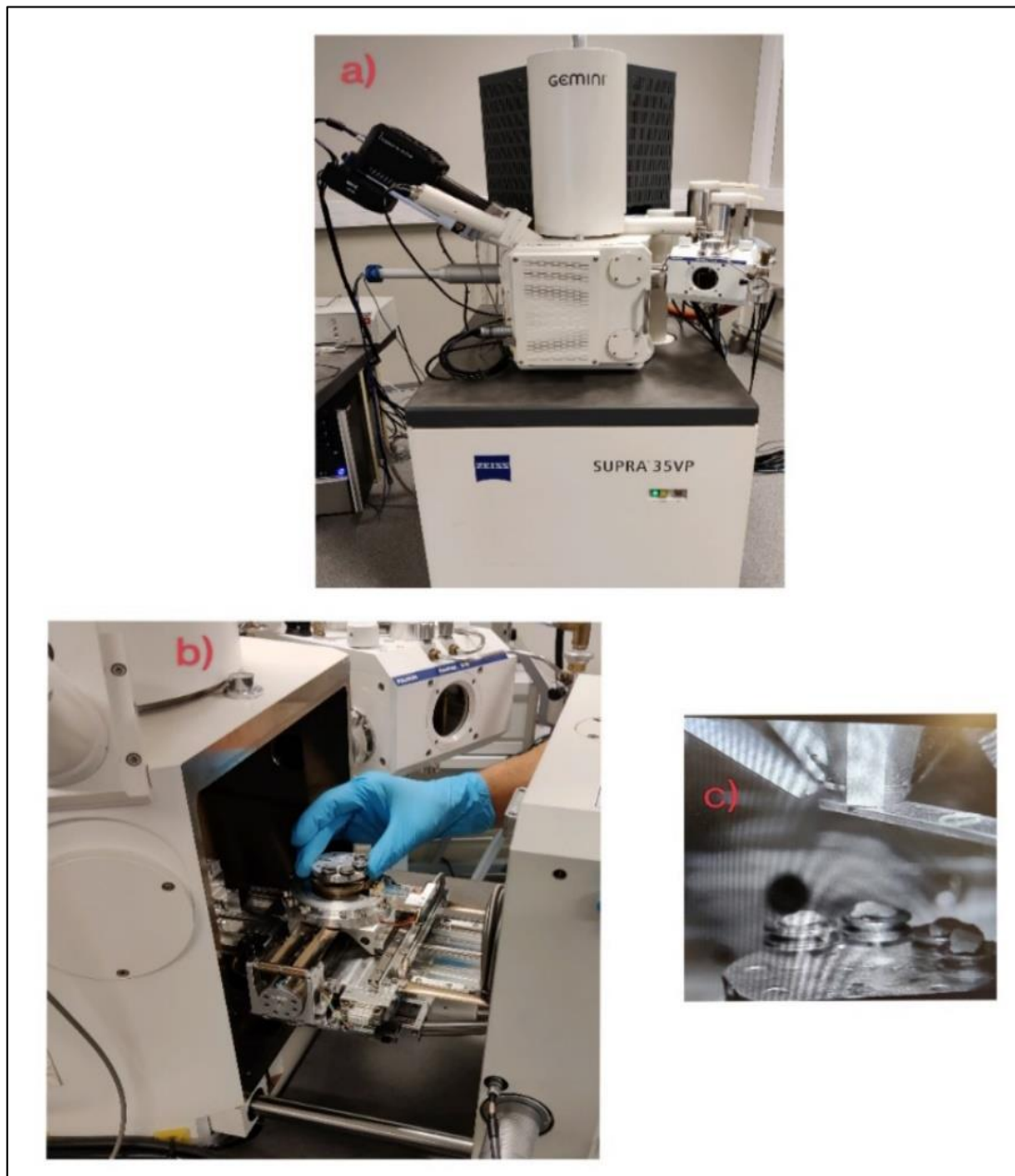


*Figure 4.10 a) Zeiss Gemini Supra 35 VP SEM; b) Samples inside SEM; c) Computer screen*

#### 4.1.2 Non-destructive tests

In the subsequent sections, the methodology for the non-destructive testing that was performed on the cement specimens as well as the parameter determination are discussed. The non-destructive tests are conducted before the destructive tests for obvious reasons. In this portion, we measured few very important parameters of plugs and they are described below sequentially.

##### 4.1.2.1 Geometrical parameters

In geometrical parameters, we recorded outer diameters and lengths of the cement plugs using a Vernier caliper to get as accurate data as possible. The cross-sectional areas and volumes of the cement plugs were calculated directly from this information. Following formulas were used for cross-sectional area and volume calculation respectively:

$$A_{\text{cross-section}} = \frac{\pi}{4} \cdot \left(\frac{OD}{1000}\right)^2 \quad [\text{Equation 4.6}]$$

$$V = \frac{\pi}{4} \cdot \left(\frac{OD}{1000}\right)^2 \cdot \left(\frac{L_0}{1000}\right) \quad [\text{Equation 4.7}]$$

Where:  $A_{\text{cross-section}}$  = Original cross – sectional area of cement plug, [m<sup>2</sup>]

OD = Outer diameter, [mm]

V = Volume, [m<sup>3</sup>]

L<sub>0</sub> = Original plug length, [mm]

The exact digital Vernier caliper that was used is illustrated below in *figure 4.11*.

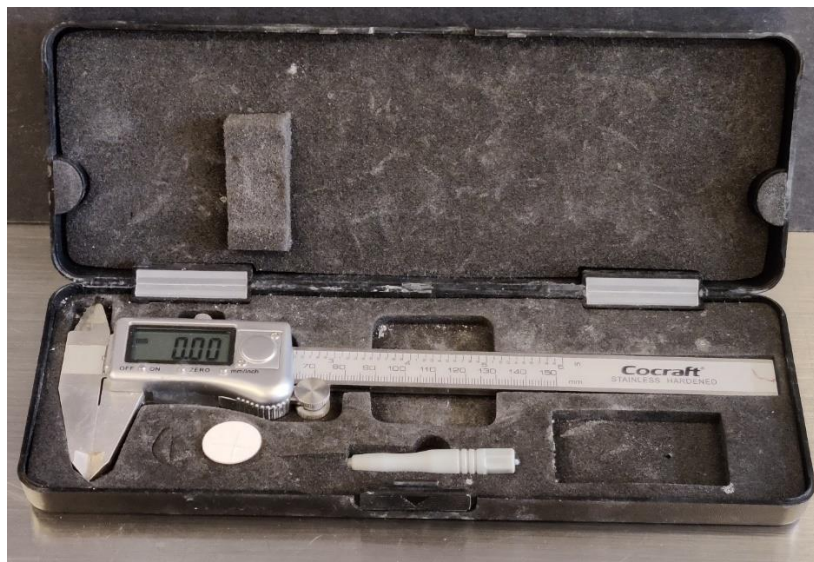


*Figure 4.11 Digital Vernier Caliper*

#### 4.1.2.2 Physical Attributions

In characterizing physical attributions, mass and density of the cement plugs were recorded. Density was calculated using the formula stated below:

$$\rho = \frac{m}{\frac{1000}{V}} \quad [Equation 4.8]$$

Where:  $\rho$  = Density, [ $\frac{kg}{m^3}$ ]  
 $m$  = Mass, [g]  
 $V$  = Volume, [ $m^3$ ]

In the following *figure 4.12* will be shown the mass balance which was used in the experiments.

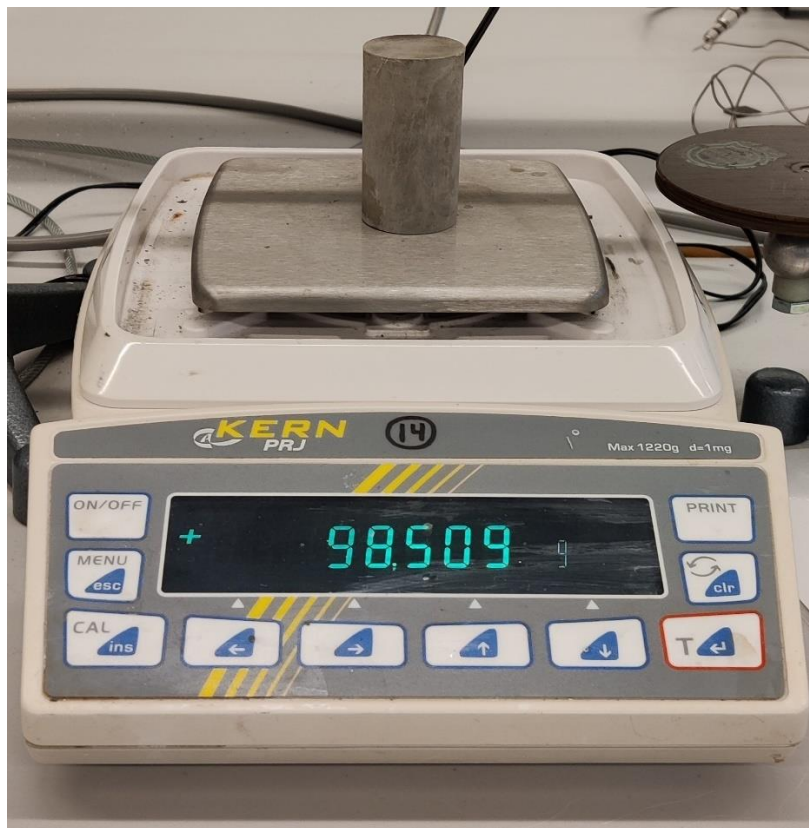


*Figure 4.12 Kern PRJ 1200-3N mass balance*



### 4.1.2.3 Sonic Measurements

The sonic measurements are done on two steps and they are *1<sup>st</sup> step*) collecting sound transit time and *2<sup>nd</sup> step*) using the time to divide the original length of a cement plug to determine the ultrasonic velocity. This information may offer indicators as to how effectively the cement plug has dried and how well the bonding is, as well as whether or not there is air trapped in the specimen and if there are substantial cracks on the surface of the sample. As we know that sound travels the fastest through the solid medium, getting a relatively short travel time gives a positive indication of the potential quality of the plugs and obviously, longer travel time expresses the opposite.

#### 4.1.2.3.1 Sonic transit time measuring process

In order to get an accurate reading of the sonic time, a plug has to be positioned between an emitter and a receiver. A sonic pulse is transmitted by the emitter and the receiver keeps track of the amount of time it takes for the pulse to propagate through the whole length of the cement plugs, which is then used to determine the velocity. Below shown in *figure 4.13* is the exact portable ultrasonic nondestructive digital indicating tester (PUNDIT) [2] and the test set-up that was used in these sonic experiments for this thesis.

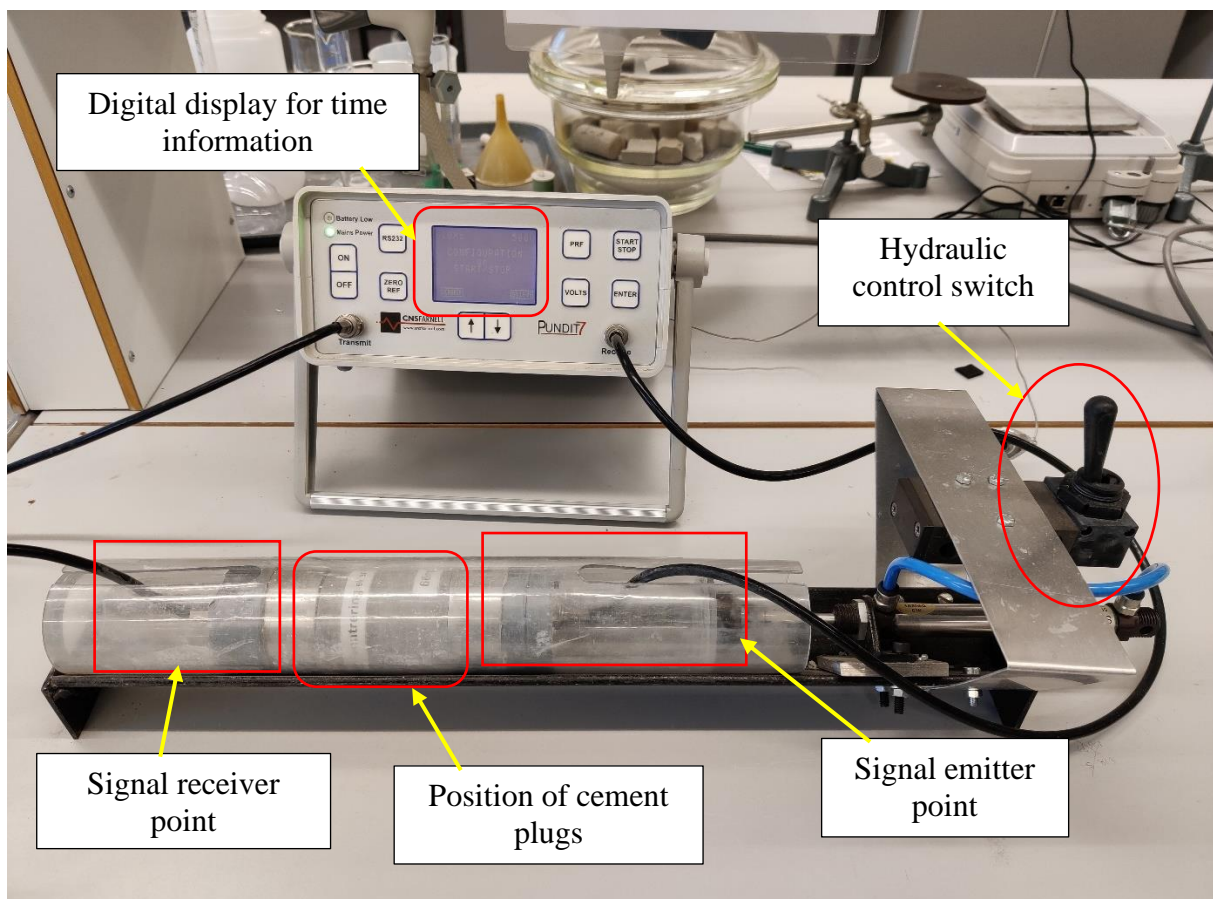


*Figure 4.13 CNS Farnell PUNDIT-7*

In the apparatus shown above, there are two tubes and each connected with the emitter and receiver on the opposite sides. There is a hydraulic control switch to make sure that the sensors are in tightly in contact with the cement plug placed between them to reduce any potential measuring error. Then the device measures the travel time through the cement plugs and displays the value on screen in the unit of  $\mu\text{s}$  (microseconds).

The whole process of measuring time starts by calibrating the device with a homogeneous medium with an established travel time of  $25.2\mu\text{s}$ . When it is done being calibrated to the known time, then we start inserting the cement plugs into the plastic tube between the emitter and receiver. Subsequently the hydraulic switch is flipped to keep them firmly together as a unit. It is very important to note that to keep the uniformity of the experiment, the bottom of the plug was always maintained connected with the emitter and the top of the plug with the receiver.

#### 4.1.2.3.2 Sonic transit velocity measuring process

In due course, after measuring the travel time, we have enough data to determine the transit velocity of the sound through the plugs. We do this by using the following formula:

$$v_p = \frac{L_0}{\frac{\Delta t}{10^6}} \quad [Equation 4.9]$$

Where:  $v_p$  = Compressional wave velocity, [ $\frac{\text{m}}{\text{s}}$ ]  
 $L_0$  = Original plug length, [mm]  
 $\Delta t$  = Sound transit time, [ $\mu\text{s}$ ]

#### 4.1.2.3.3 P-wave modulus (M-modulus)

There are two kinds of seismic body waves in solids, pressure waves (P-waves) and shear waves. In this thesis, we are only measuring P-wave. In linear elasticity, the P-wave modulus (M), also known as the longitudinal modulus or the constrained modulus, is one of the elastic moduli available to describe isotropic homogeneous materials [114]–[115].

It is defined as the ratio of axial stress to axial strain in a uniaxial strain state [114]–[115]:

$$\sigma_{zz} = M \cdot \epsilon_{zz} ; \epsilon_{xx} = \epsilon_{yy} = \epsilon_{xy} = \epsilon_{xz} = \epsilon_{yz} = 0 \quad [Equation 4.10]$$

Where: M = P – wave modulus, [GPa]

$\sigma_{zz}$  = Axial stress [MPa] in the longitudinal direction

$\epsilon_{zz}$  = Axial strain [dimensionless] in the same direction as axial stress

M-modulus can be expressed in terms of shear modulus (G) and bulk modulus (K) as well, which are two other elastic moduli, by the following relationship [114]–[115]:

$$M = K + \frac{4G}{3} \quad [\text{Equation 4.11}]$$

Where: M = P – wave modulus, [GPa]  
K = Bulk modulus, [GPa]  
G = Shear modulus, [GPa]

Moreover, the P-wave modulus can be described by velocity of a P-wave and the travelling medium's density with the equation below [114]–[115]:

$$v_p^2 \cdot \rho = K + \frac{4G}{3} \quad [\text{Equation 4.12}]$$

Where:  $v_p$  = compressional wave velocity, [ $\frac{m}{s}$ ]  
 $\rho$  = Density, [ $\frac{kg}{m^3}$ ]

The P-wave modulus is finally found as [114]–[115]:

$$M = \frac{v_p^2 \cdot \rho}{10^9} \quad [\text{Equation 4.13}]$$

Where: M = P – wave modulus, [GPa]  
 $v_p$  = compressional wave velocity, [ $\frac{m}{s}$ ]  
 $\rho$  = Density of the cement plug, [ $\frac{kg}{m^3}$ ]

#### **4.1.2.4 Rheological study**

Rheology is the study of the deformation and flow of materials. In this particular case, rheology can be described as the science that attempts to determine the intrinsic fluid properties—mainly viscosity— necessary to determine the relationships between the flow rate (shear rate) element and the pressure gradient (shear stress) element that causes fluid movement [2]. Obtaining rheological information about cement slurry is particularly important because it is the rheological parameters that will determine the workability of the cement slurry.

##### **4.1.2.4.1 Rheology experiment procedure**

The rheometer that was used for the experiment was an OFITE 8-Speed viscometer, depicted in *figure 4.14*. Before pouring into the measurement cup, cement slurries were mixed until achieved smooth mixture ensuring that there were no lumps of cement left. Subsequently, viscometer readings of the slurry were recorded at 300, 200, 100, 60, 30, 6,3 RPM. Notably, cement slurries were not tested at 600 RPM as this is not a practical measurement for material intended for cementation.

#### 4.1.2.4.2 Rheology model

There are many established rheological model to characterize rheology of the materials. But there is a model named “Casson rheological model” very much associated with evaluating cement slurry’s rheology, which will be considered in this thesis. It reads as [2]:

$$\sqrt{\tau} = \sqrt{\tau_c} + \sqrt{\mu_c \cdot \gamma}, \text{ for } \tau < \tau_c \quad [\text{Equation 4.14}]$$

$$\gamma = 0, \text{ for } \tau \geq \tau_c \quad [\text{Equation 4.15}]$$

Where:  $\tau$  = Shear stress,  $[\frac{\text{lb}_f}{100 \text{ ft}^2}]$

$\tau_c$  = Casson yield stress,  $[\frac{\text{lb}_f}{100 \text{ ft}^2}]$

$\mu_c$  = Casson plastic viscosity,  $[\frac{\text{lb}_f \cdot \text{sec}}{100 \text{ ft}^2}]$

$\gamma$  = Shear rate,  $[\text{sec}^{-1}]$

In clarification, viscosity is the property of fluids and slurries that indicates their resistance to flow, defined as the ratio of shear stress to shear rate [116] and plastic viscosity is the slope of the shear stress/shear rate line above the yield point [117]. Additionally, the minimum force per unit area required to sustain a constant rate of fluid movement is noted as the shear stress [118]. In a connected manner, yield stress is the stress that must be applied to a material to make it begin to flow (or to yield) [119]. Finally, Shear rate is the rate of change of velocity at which one layer of fluid passes over an adjacent layer [120].

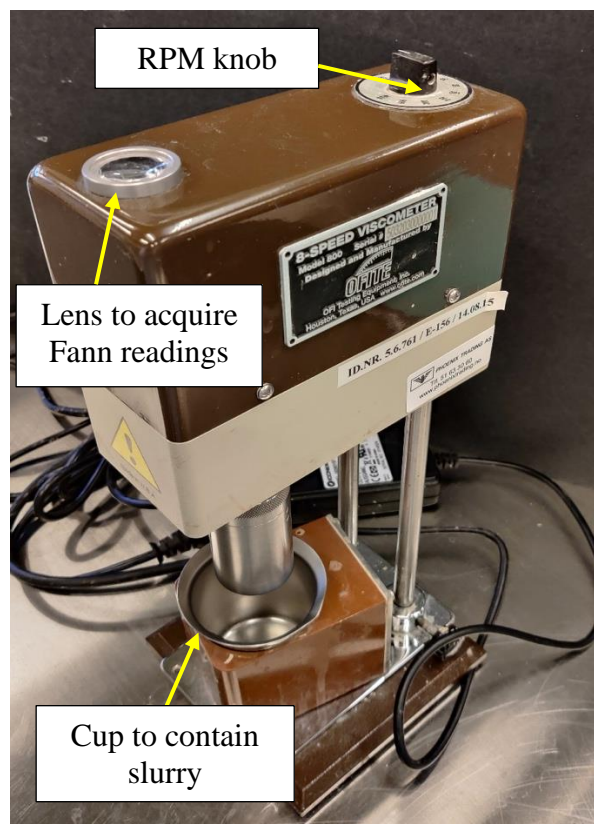


*Figure 4.14 OFITE 8-Speed Fann viscometer used in rheology testing*

## **4.2 Empirical UCS modelling**

The following sections will contain discussions regarding methods and principles for creating an empirical UCS- $v_p$  model from the data obtained during the experimental phases.

One of the most common loading scenarios for cement in industry is uniaxial compressive stress (UCS), which indicates the maximum load carrying capacity of the formation before failure. The parameter is normally determined from UCS test as outlined in [section 4.1.1.2](#). However, in literature, several investigators have developed empirical models that relate the UCS-destructive test results with the non-destructive compressional wave velocity ( $v_p$ ). Provided that the models are good enough, the UCS can be estimated from the measured compressional wave velocity and vice versa. Few previously created models will be discussed in the following subsections to establish the base for the new model.

### **4.2.1 Horsrud's (2001) empirical UCS model**

Horsrud (2001) developed UCS- $v_p$  model that uses sonic log data to estimate the UCS of the drilling formations. He developed the model based on several shale rock samples obtained from North Sea. The model reads [121]:

$$UCS = 0.77 * v_p^{2.93} \quad [Equation 4.16]$$

Where: UCS = Uniaxial compressive stress, [MPa]

$v_p$  = P – wave velocity through the material, [ $\frac{km}{s}$ ]

Even though, the Horsrud's model was developed from shale, the predictive power of the model will be tested on cement data and will be compared with the empirical model developed in this thesis. The model developed in this thesis will have the same shape, as well.

To test the newly developed model in this thesis, two other models created previously using the same principle stated above will be used as well. Important thing to note is that they were developed with experimental data obtained from cement specimens. The models are Nerhus's (2020) [78] and Titlestad's (2021) [79] empirical UCS models. The models are described below.

### **4.2.2 Nerhus's (2020) empirical UCS model**

$$UCS = 0.0954 * v_p^{4.7184} \quad [Equation 4.17]$$

### **4.2.3 Titlestad's (2021) empirical UCS model**

$$UCS = 0.2191 * v_p^{3.9503} \quad [Equation 4.18]$$

## **5 Results and Discussions**

In this chapter, all the results obtained in the experimental works of the thesis, which entail destructive (UCS, Young's modulus, resilience and SEM) and non-destructive (P-wave modulus and rheology) tests, will be presented. "Appendix A" will illustrate the change in the obtained results in percentage to decipher the data better and "Appendix B" will contain the load vs. deformation profiles for the samples. "Appendix C" will show the achieved results from the non-destructive tests. "Appendix D" will illustrate various pictures of the experimental process.

### **5.1 General information**

Here, the general information will provide a clear picture of the presentation of the results, which are displayed in charts and tabular forms. From the diagrams, one can visually read the neat cement/reference result deviations from this thesis work on additives-based cement results. The diagrams combine the data in tabular form and display them according to the curing age and environment. On the chart, the Y-axis shows the values of the cement plugs' properties and the X-axis denotes the cement plugs' compositions in grams. The results are also discussed by comparing the samples with and without additives based on their respective curing age and environments.

For statistical purposes, the results presented in this thesis are the average of two plug samples. The standard deviation of the Uniaxial compressive strength data is also calculated and presented in tabular form. In some cases, the results are also based on one plug, as its pair of cement plugs were compromised and damaged or measuring instruments malfunctioned. The damage on samples results in a value that does not represent the property of the cement slurry. The defects on the sample are either due to surface irregularities that create point-loadings and result in early failure or had defects internally, which is due to creation of two phases or air gaps, which in general result in uncompacted and non-uniform structure in the cement plugs. The sample, therefore, does not represent the cement slurry properties.

In particular, when analysing and discussing the samples' Young's moduli and resilience, it should be noted that some datasets are missing due to the deformation sensor malfunctioning sometimes during the collection of the detailed load and deformation data. They are always from the same datasets because each sample has its own stress-strain graph, from where the stated parameters are determined.

Furthermore, various colour codes are applied in the diagrams to identify the different curing days. The diagrams will also contain the values of the experimental parameters against the respective cement samples with additives.

Finally, it is essential to clarify that we have received cement from different cement providers of NORCEM AS. Since their ages and duration of exposure to air are not known, the results obtained for these neat cements will be reported independently. Experimental test results have also shown that both neat cements have recorded different values.

## 5.2 Test Design 1 (Effect of Al<sub>2</sub>O<sub>3</sub> nanoparticles on OPC)

In this section, we are going to discuss results obtained from TD-1, where experiments were conducted to observe the impacts of 1.2g, 1.4g and 1.6g Al<sub>2</sub>O<sub>3</sub> NPs on OPC of 0.44 WCR. The design consists of TBs-1,2,3 in both room temperature of 20°C and oven temperature of 80°C. For easier clarifications, various colour codes are used in the bar graphs and they are red, yellow and gray for 3, 7 and 28 days, respectively.

### 5.2.1 Impact of Al<sub>2</sub>O<sub>3</sub> nanoparticles on uniaxial compressive strength (UCS)

To understand the load carrying capacity of cement in wells and its ability to withstand harsh environments without failing, we need to analyse uniaxial compressive strength or UCS of cement. For UCS, the higher the value is, the higher strength the cement has, which means a very competent cement.

**Figure 5.1** displays the UCS results obtained from specimens aged in room temperature for 3, 7 and 28 days. As shown in the figure, the strength build-up for the plugs with NPs additives varies over the period of 28 days as compared to the reference plugs. Noticeably, the reference plugs after curing 3 and 7 days had biggest improvement over the nano systems with average strengths of 18.7 MPa and 29.4 MPa in their respective batches. During the 28 days batches, compressive strength of the nanoparticles bases plugs has increased significantly over the respective reference sample. The NPs additives of 1.2g, 1.4g and 1.6g have improved UCS of the neat cement by 100%, 45.8% and 47.4%, respectively [[Appendix A](#)]. Detailed percentage development of the strength can be found in Appendix A.

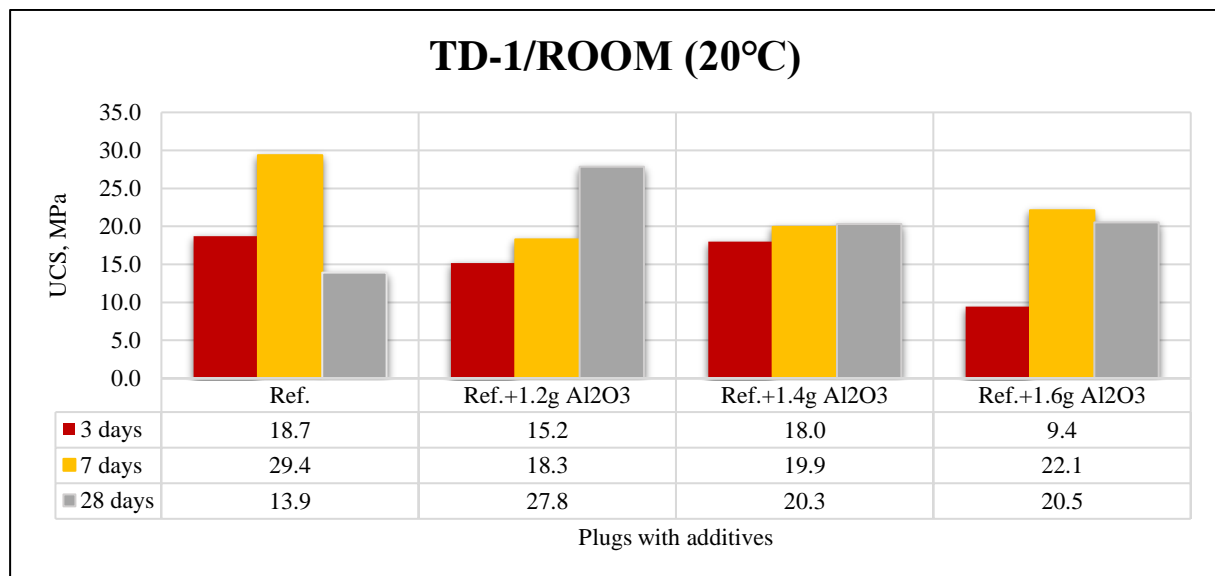


**Figure 5.1** UCS of TD-1 samples cured in room temperature

**Table 5.1** shows the standard deviation values for all the samples. Here, the lower the values are, the more consistent UCS results the samples have. The standard deviation of the neat cement after 28 days showed about 0.3 MPa. Both the samples' strengths are very close. On the other hand, In the 28 days batch, the plugs with 1.2g, 1.4g and 1.6g additives have the highest standard deviations of 7.2 MPa, 4.6 MPa and 8.1 MPa respectively, although they have the highest strength with 27.8 MPa, 20.3 MPa and 20.5 MPa. The reason for this was that one of the samples recorded lower strength and the other sample recorded higher values.

The lower strength was due to possible defects mentioned earlier. Provided that the sample had reduced defect or no defect, the strength could have been comparable with the stronger sample value. Hence, the overall mean strength value due to nanoparticle additive system could have been even higher than the one reported in *figure 5.1*.

**Table 5.1 Standard deviations (SD, MPa) for TD-1 samples in room temperature**

Curing age \ Plugs	Ref.	Ref.+1.2g Al <sub>2</sub> O <sub>3</sub>	Ref.+1.4g Al <sub>2</sub> O <sub>3</sub>	Ref.+1.6g Al <sub>2</sub> O <sub>3</sub>
3 days	0.1	1.8	0.1	1.8
7 days	0.9	2.3	6.7	5.2
28 days	0.3	7.2	4.6	8.1

When considering results from oven temperature of 80°C presented in *figure 5.2*, we see that after 28 days of curing the nano concentration had the highest improvement compared to the reference OPC samples is 1.2g with 25 MPa, which translates into 24.8% increase in strength. After 3 days of curing, 1.6g shows an increase of 7.1% with compared to reference. In contrast, 1.6g plugs show poor strength development with only 10.8 MPa having a 46.4% decrease in strength compared to reference plugs after 28 days. It is possible to decide that when cured under a relatively high temperature, 1.2g dosage may perform better than 1.6g.

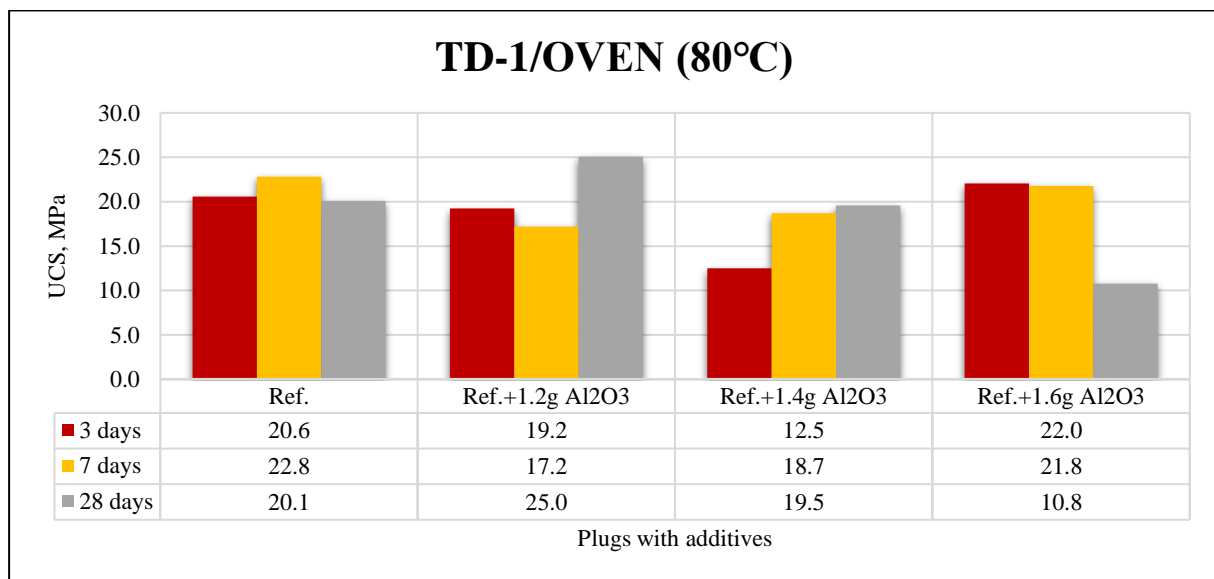


**Figure 5.2 UCS of TD-1 samples cured in oven temperature**

*Table 5.2* describes the standard deviations for UCS measurements for the samples cured at 80°C. As shown, except for the 1.6g nanoparticle blending, all plugs show a higher standard deviation. This was due to the higher difference between the recorded value of the plugs. Here again, provided that the lower value was associated due to damage on the sample, the nanoparticle mixed systems still have shown strength improvement as compared with the reference system. From this as well, we can say that higher concentration of aluminium NPs may have been degraded due to high temperature.



**Table 5.2 Standard deviations (SD, MPa) for TD-1 samples in oven temperature**

Curing age \ Plugs	Ref.	Ref.+1.2g Al <sub>2</sub> O <sub>3</sub>	Ref.+1.4g Al <sub>2</sub> O <sub>3</sub>	Ref.+1.6g Al <sub>2</sub> O <sub>3</sub>
3 days	0.5	4.5	3.9	1.4
7 days	2.7	3.9	5.9	6.7
28 days	7.4	6.9	13.7	0.9

**5.2.2 Impact of Al<sub>2</sub>O<sub>3</sub> nanoparticles on Young’s modulus (E-modulus)**

Young's modulus (E) or the modulus of elasticity is a mechanical property that measures stiffness of a solid material when the force is applied lengthwise. It quantifies the relationship between tensile/compressive stress and axial strain (proportional deformation) in the linear elastic region of a material [109]. Higher Young's Modulus corresponds to greater axial stiffness. High stiffness with ductility can help well cement resist any permanent deformation that might be incurred upon by harsh downhole environments.

Ideally, high stiffness with ductility is sought after in cement properties but seldom is found. It is due to the brittle nature of cement. When the UCS tests are conducted, we can analyse and establish a relationship between UCS and stiffness of the cement, which can give valuable insights. Logically, when UCS increases, Young’s modulus should increase as well, as they are directly proportional [equation 4.2].

Depicted in *figure 5.3* are Young’s moduli for cement samples cured in room temperature are depicted according to their curing ages and concentrations. Some results are absent here due to the malfunction of deformation sensor while recording data as it showed miniscule deformation, which resulted in unrealistic Young’s moduli. For clarification, it is recommended to refer to [Appendix B](#), which contains the load vs deformation graphs for relevant samples.

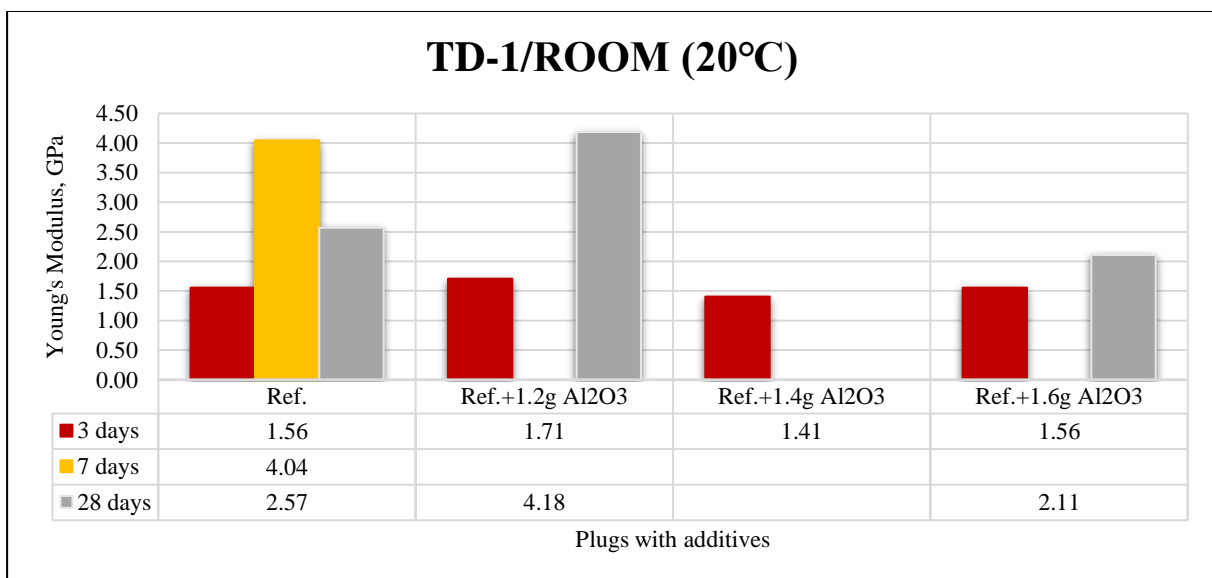


**Figure 5.3 Young’s moduli of TD-1 samples cured in room temperature**

We can observe in **figure 5.3** that the reference plugs after 7 days have the stiffness of 4.04 GPa but it decreased to 2.57 GPa after curing for 28 days. It is important note that the stated reference plugs had a decrease in UCS [[section 5.2.1](#)] in same manner. It can be attested to the fact the UCS and Young’s modulus are directly proportional, shown in [section 4.1.1.3](#). The plugs with 1.2g aluminium nanoparticles after 28 days have Young’s modulus of 4.18 GPa, which translates into an increase of 62.76% as compared to reference plugs in same curing period. Moreover, 1.6g samples suffered a decrease in Young’s modulus by 17.97%, which is also the largest loss of stiffness in this curing environment.

The following **figure 5.4** pictures the analysed E-modulus for samples cured in oven at 80°C for 3, 7 and 28 days. After 3 days of curing the nano-systems of 1.2g, 1.4g, 1.6g had the respective Young’s moduli of 1.8 GPa, 2.6 GPa and 2.7 GPa, which means all the concentrations had negative results compared to reference plugs having Young’s modulus of 3.9 GPa. From the [Appendix A](#), the decreases in percentiles are 54.4%, 33.3% and 30.2% correspondingly. After 28 days of curing, nano-systems with 1.2g and 1.4g of Al<sub>2</sub>O<sub>3</sub> NPs had

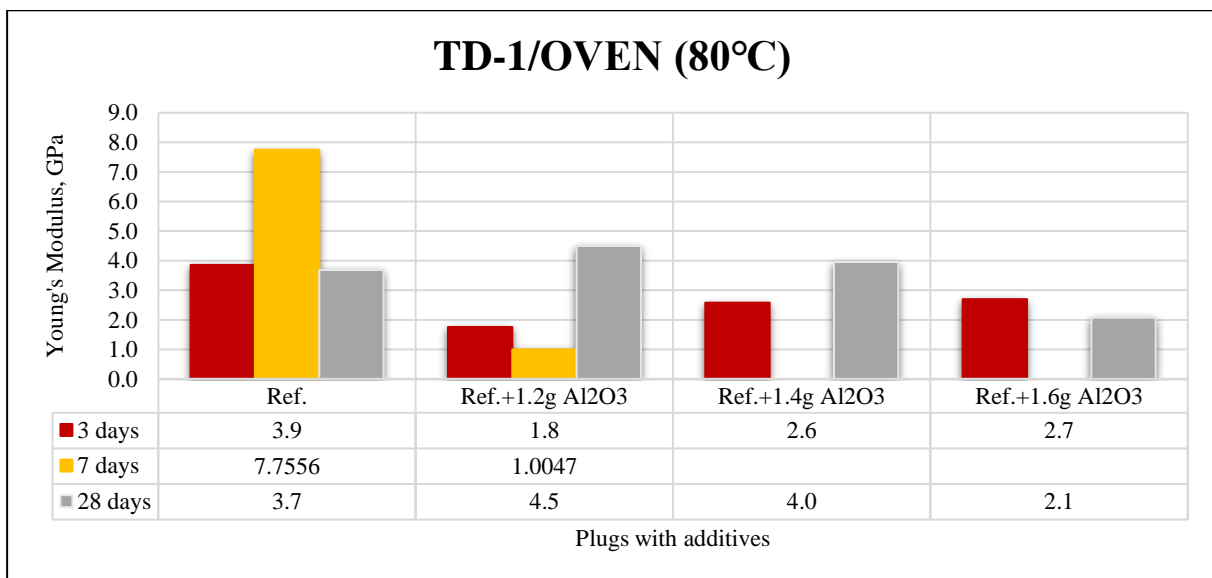


**Figure 5.4 Young’s moduli of TD-1 samples cured in oven temperature**

respective increases of 22.1% and 7.3% compared to reference samples. Although 1.6g plugs suffered a significant loss of E-modulus by 43.7%. Here as well, we can observe that E-modulus increase and decreased as the UCS [[section 5.2.1](#)] increased and decreased. It can be said in conclusion that higher concentration nano-system do not perform better in the high temperature environment during a long curing period as it possibly slows down the hydration process making it overwhelmingly less stiff than that nano-systems with lower concentrations.

### **5.2.3 Impact of Al<sub>2</sub>O<sub>3</sub> nanoparticles on resilience (R)**

Resilience is measured by integrating the area under the stress-strain curve starting from the point where loadings started and finishing to the point where UCS is the highest, as was formulated in [section 4.1.1.4](#). Resilience is the highest energy absorbed by a material when applied load before permanent deformation. Since cement is a brittle material, it has a very short plastic region. In the majority of the cases, it fails immediately after UCS has reached its peak. Resilience is directly proportional to UCS and inversely proportional to Young’s modulus.

In *figure 5.5*, resilience data for the samples cured in room temperature are shown. Unfortunately, some data are missing due to deformation sensor not recording data properly [*Appendix B*]. The data are from the same sets, where Young’s moduli [*section 5.2.2*] data were absent due to same reason.

We can observe that after 3 days of curing all the samples had poor results compared to reference sample. The plugs with 1.2g, 1.4g, 1.6g dosages respectively had 49.2%, 39.7% and 84.7% negative developments in resilience. It is to be noted that this trend is consistent with UCS [*section 5.2.1*] trend for the batch. After 28 days of curing, it is noticeable that 1.2g plug had a promising resilience of 156.7 kJ/m<sup>3</sup>, which is an astonishing increase of 89.8% compared to reference plugs with 82.5 kJ/m<sup>3</sup>. The reference plugs have shown a gradual decreasing trend over the periods of 3, 7 and 28 days, which can be interpreted as OPC losing its load bearing capacity over a long period and this is a very realistic scenario in wellbore cement.

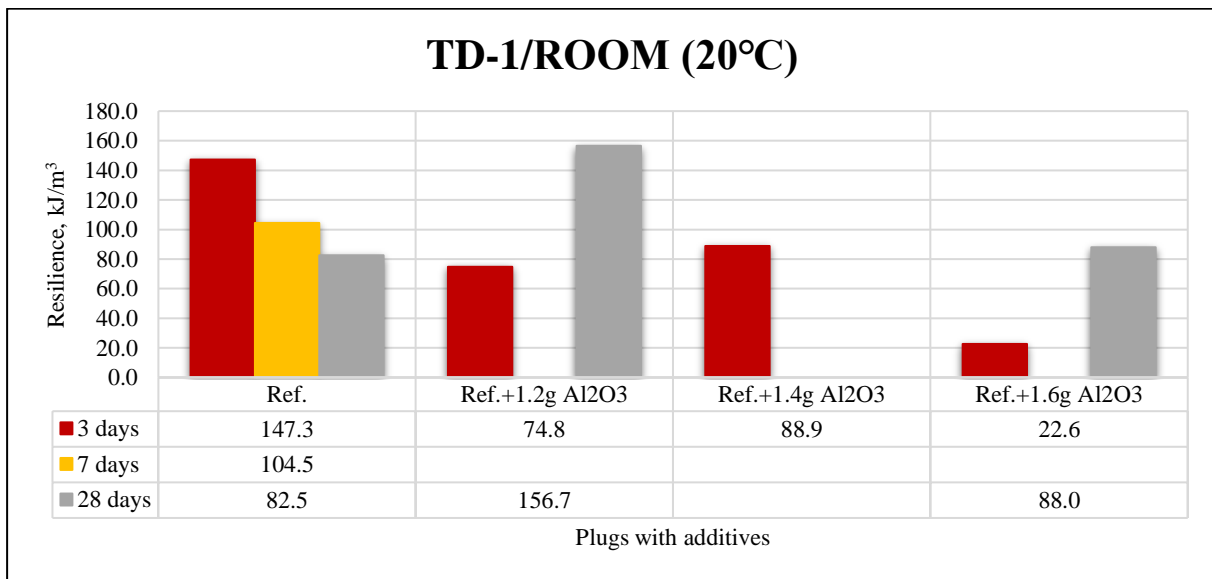


*Figure 5.5 Resilience of TD-1 samples cured in room temperature*

Shown below in *figure 5.6* are resilience data from oven-cured samples. The plugs with 1.2g aluminium nano-system perform the best with 120 kJ/m<sup>3</sup> and 23% increase compared to the corresponding batch reference plugs after 28 days of curing with a trend of gradual increase in high temperature environment, although it had a significant early resilience decrease of 43.1% after 3 days of curing.

When analysed with Young’s modulus [*section 5.2.2*] data, there are some anomalies that can be noticed in the nano-systems in both room and oven curing environments. The increase in resilience for 1.2g plugs should have meant a decrease in the E-modulus [*section 5.2.2*], when compared to their respective reference values. But the opposite happened, which can only be explained with uncertainty of nanoparticles’ reactions with OPC.

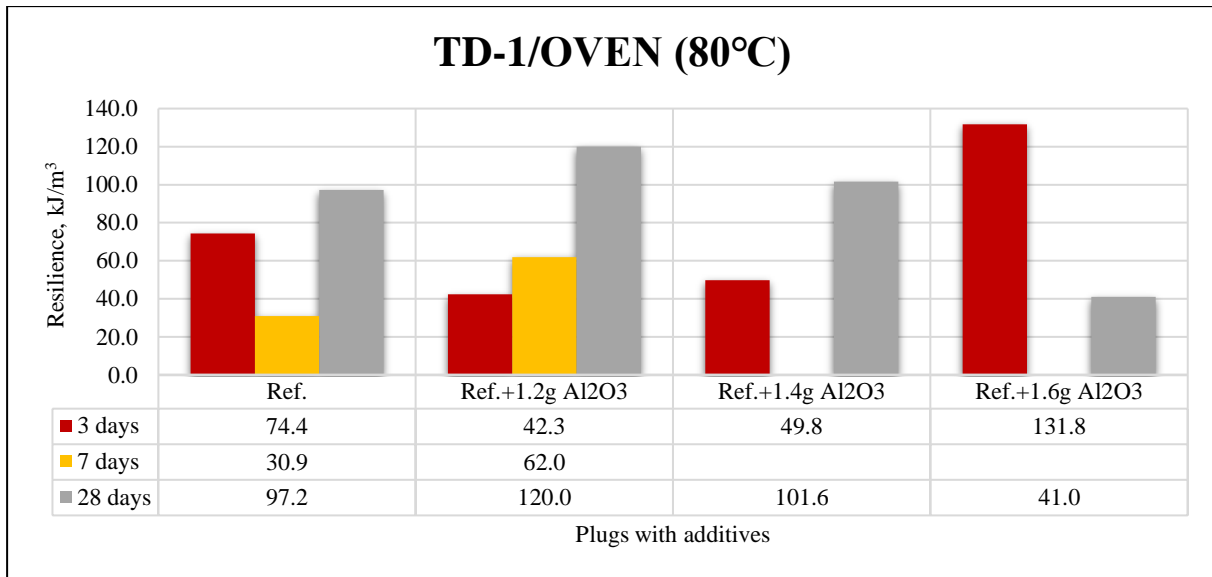


Figure 5.6 Resilience of TD-1 samples cured in oven temperature

#### 5.2.4 Impact of Al<sub>2</sub>O<sub>3</sub> nanoparticles on P-wave modulus (M-modulus)

P-wave modulus or M-modulus are found from the velocity of the compressional waves through the medium and the density of the medium. High M-modulus is associated with low wave transit time and higher velocity through the medium. High M-modulus means the medium is sufficiently packed. A compact medium provides evidence that the microstructure is in excellent form since it demonstrates no substantial fractures or pore gaps present. Because of this, it is often assumed that a high M-modulus correlates with high UCS values, as it represents a more refined microstructure.

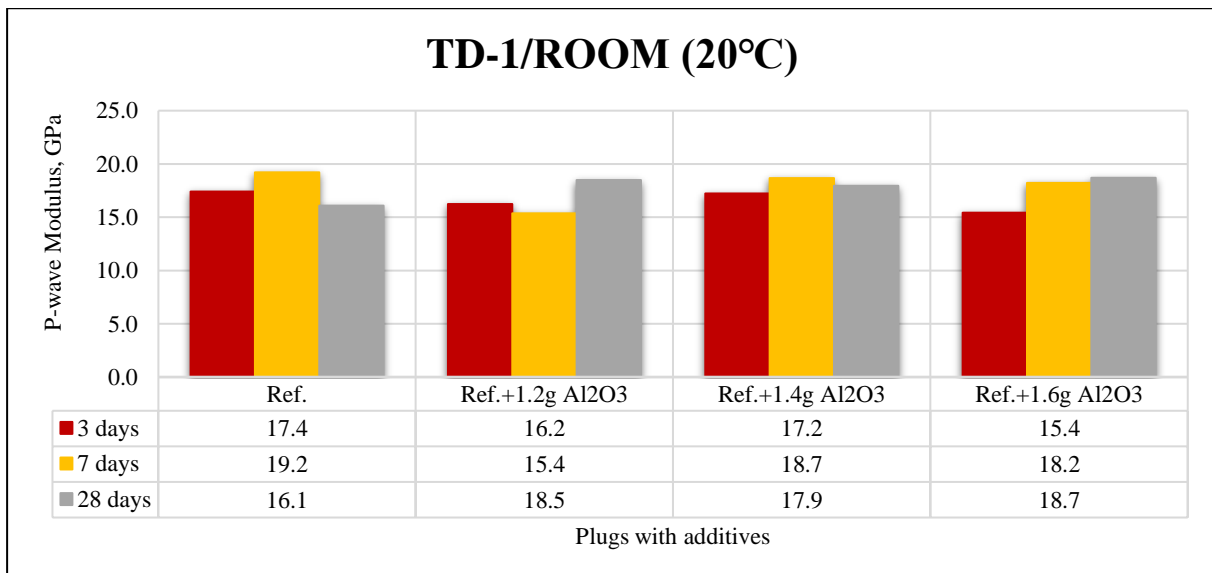
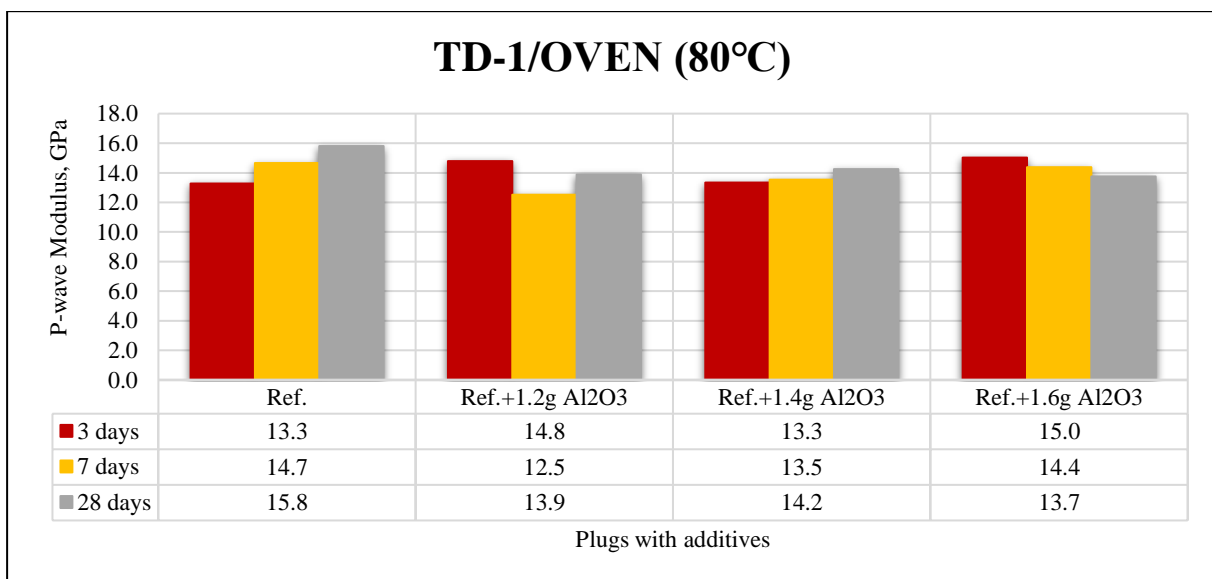


Figure 5.7 P-wave moduli of TD-1 samples cured in room temperature

UCS and M-modulus are connected because they are functions of velocity of sound in the samples. In *figure 5.7*, the reference plugs in room temperature after curing 7 days have the highest M-modulus value of 19.2 GPa, which coincides with the UCS [[section 5.2.1](#)] trend of the same plugs.

All the nano-systems shown in *figure 5.7* show negative developments after 3 and 7 days. Please refer to [Appendix A](#) for percentile change data. Most of the samples' M-moduli in this curing environment follow the same trend as that of UCS in room temperature with one exception of plugs with 1.6g addition after curing 7 days. The 1.6g plugs with 18.2 GPa were supposed to follow the UCS [[section 5.2.1](#)] trend of increasing towards the reference value of the respective batch, but it decreased away from the reference. The 28 days batch adheres to the UCS trend of the of the same batch as compared to the reference values with the best performing plugs of 1.2g and 1.6g, which has M-modulus of 18.5 GPa and 18.7 GPa and an increase in performance by 14.9% and 16.3% respectively [[Appendix A](#)].

*Figure 5.8* shows the M-moduli oven-cured samples. It can be observed that the modulus developments among the samples vary differently over the curing days. There are three anomalies, where samples behave differently than the UCS [[section 5.2.1](#)] values. The 1.2g plugs from 3 days batch had a M-modulus of 14.8 GPa (11.5% increase), which had increased as opposed to decreasing. After curing 28 days, the 1.2g and 1.4g had decreased by 12.2% and 9.9% accordingly and when compared to the respective UCS trends, they are inconsistent [[Appendix A](#)].



*Figure 5.8 P-wave moduli of TD-1 samples cured in oven temperature*

Since there are no major fluctuations of the M-modulus values for the both room-cured and oven-cured samples, their combined density and velocity properties could be the reason for this. Up to this level of research, the thesis could not provide explanations other than this. The main reason is that the M-moduli have been determined by the density and velocity measurement values.

### 5.3 Test Design 2 (Effect of Al<sub>2</sub>O<sub>3</sub> nanoparticles and fly ash on OPC)

In the subsequent sections, results obtained from TD-2, where effects of binary hybrid of aluminium NPs and fly ash (FA) on OPC of 0.44 WCR was investigated. As mentioned in [section 3.2.6](#), 1.4g Al<sub>2</sub>O<sub>3</sub> was kept constant throughout the design. TBs-4,5,6 constitute this test design, where samples were cured in room temperature and at 80°C in an oven for 3, 7 and 28 days, correspondingly. Colour codes used here are the same as TD-1, which are red, yellow and gray for respective curing ages.

#### 5.3.1 Impact of Al<sub>2</sub>O<sub>3</sub> nanoparticles and fly ash on uniaxial compressive strength (UCS)

UCS results for samples cured in room temperature for 3,7 and 28 days are displayed in [figure 5.9](#). It is evident from the figure that most of the samples cured for 28 days had the largest strength improvement over the reference sample. Among them, best performing dosage was with 2g FA and 1.4g NPs had UCS of 32.5 MPa, which is an increase of 23.6% over the reference plug [[Appendix A](#)]. If compared with results from TD-1/Room, this is a quite significant development in strength. From the only FA systems, the results are very close and 2g FA system had the best result of 28.4 MPa, which translates into 7.9% increase from the neat OPC reference, as depicted in [Appendix A](#).

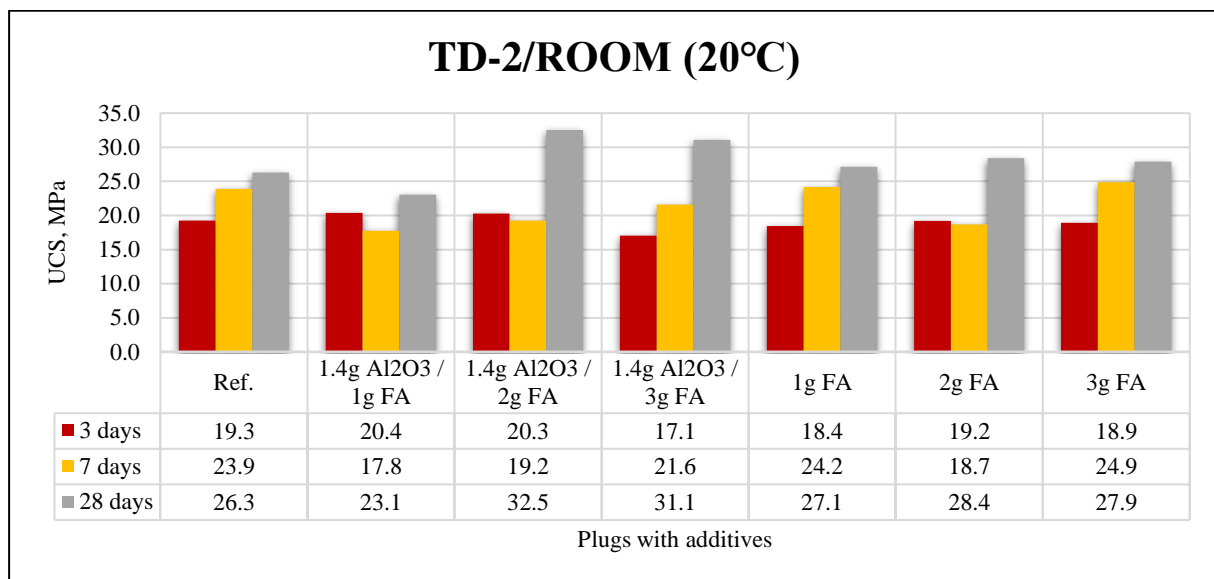


**Figure 5.9 UCS of TD-2 samples cured in room temperature**

Strength build-up after 3 days seems to be very slow, as there are small fluctuations among the values [2], [122]. Figure 5.9 also displays UCS development of samples after being cured for 7 days. It is noticeable that most of the samples had significant decrease in strength, as compared to reference sample. 3g FA with and without NPs had very smooth transition in hydration process, which is apparent in the [figure 5.9](#).

[Table 5.3](#) of standard deviations present the reproducibility of data. This table portrays how reliable the data is. Lower the standard deviation, more reliable the data is. For example, 3g FA with NPs have very the highest standard deviation after being cured for 28 days, which tells us that the data may not be reproduced due to various uncertainties. On the other hand, 3g FA system without NPs have one of the lowest deviations from the mean value, which alludes to having the highest reliability of data.

**Table 5.3 Standard deviations (SD, MPa) for TD-2 samples in room temperature**

Curing age\ Plugs	Ref.	1.4g Al <sub>2</sub> O <sub>3</sub> / 1g FA	1.4g Al <sub>2</sub> O <sub>3</sub> / 2g FA	1.4g Al <sub>2</sub> O <sub>3</sub> / 3g FA	1g FA	2g FA	3g FA
3 days	1.4	2.4	0.7	0.8	1.2	1.0	0.5
7 days	2.6	8.0	1.6	0.3	0.2	2.1	3.0
28 days	0.9	2.8	1.5	3.2	1.4	2.1	0.9

UCS development for cement plugs cured at 80°C in are documented in *figure 5.10*. Significant development in UCS after being cured 7 days, where 3g FA with and 2g FA without NPs had the biggest raise in strength with 23.8 MPa (32% increase) and 25.8 MPa (43.3% increase) compared to the reference plugs. Astonishingly, on the other end of the spectrum, all the samples cured for 28 days in oven had negative development in strength in comparison with the reference [*Appendix A*]. When compared with high temperature results from TD-1, we also see that most samples have adverse effects in UCS. It should be noted that lowest drops in performances occurred in the nano-system with 1g FA and 3g FA, having 40.2% and 37.1% decrease respectively.

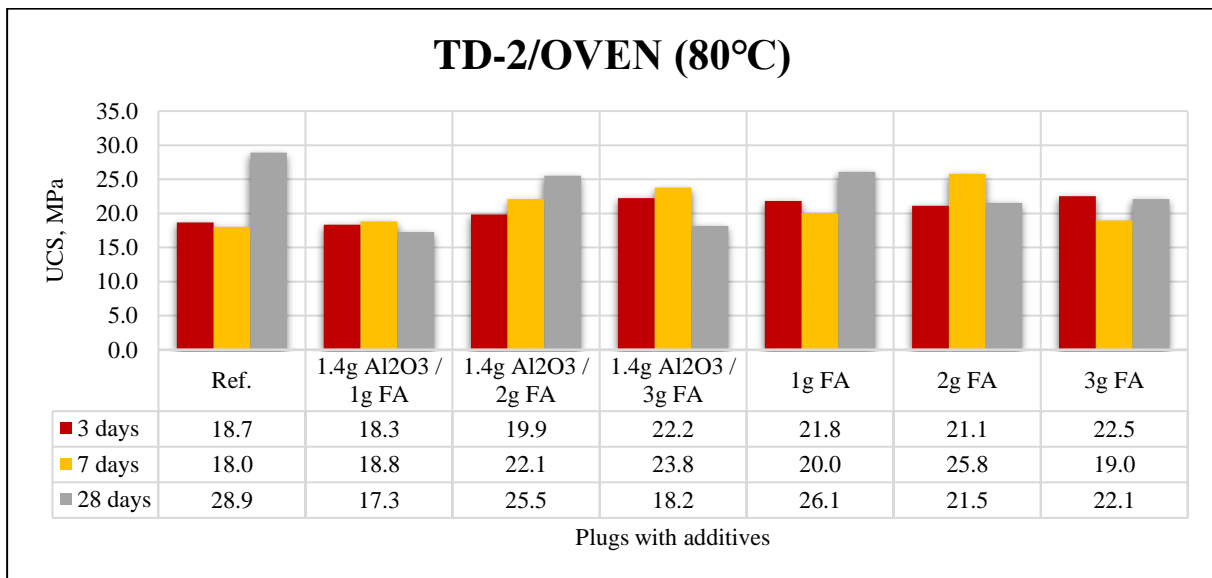


**Figure 5.10 UCS of TD-2 samples cured in oven temperature**

*Table 5.4* shows the standard deviations of UCS results for oven-cured samples. Here, as well, it is observed that due to degradation of nanoparticles under high temperature after 28 days, high standard deviations were found. Although, the samples with only FA had relatively lower deviations, which could mean that cement plugs with only FA have more reliable data. For 7 days, 3g FA with the lowest SD of 0.1 MPa, which is congruent with the reliability of data. Reference plug after 7 days had an SD of 7 MPa, which translates into plugs having defects internally leading to huge differences in values. Solitary FA systems after being cured in oven for 7 days had relatively large SDs, as well. It is an indication that the positive development in the UCS may not be reproducible. However, all the cement additions had positive development in compressive strength after 7 days compared to the reference plug.

Table 5.4 Standard deviations (SD, MPa) for TD-2 samples in oven temperature

Curing age \ Plugs	Ref.	1.4g Al <sub>2</sub> O <sub>3</sub> / 1g FA	1.4g Al <sub>2</sub> O <sub>3</sub> / 2g FA	1.4g Al <sub>2</sub> O <sub>3</sub> / 3g FA	1g FA	2g FA	3g FA
3 days	0.8	0.1	2.3	1.5	1.9	1.1	1.3
7 days	7.0	5.5	3.5	0.1	14.7	4.4	3.0
28 days	2.9	5.6	3.4	9.1	2.5	2.2	3.5

### 5.3.2 Impact of Al<sub>2</sub>O<sub>3</sub> nanoparticles and fly ash on Young’s modulus (E-modulus)

Due to unfortunate and unforeseen events during UCS testing, the detailed deformation and load data of the samples “TD-2–3g FA–1” and “TD-2– Ref.-2” from room and oven environment respectively were not correctly recorded [Appendix B]. Only the maximum loads could be recorded. But due to the lack of time and materials at that point of the experimental process, the samples were not recreated and single sample results in both cases were used to figure out E-modulus and resilience. By being more efficient in the future, however, such events were avoided.

Young’s moduli for the TD-2 samples cured in room temperature are presented in figure 5.11. We observe that after curing for 3 days, all the dosages had significant increases in their stiffness, which is not congruent with UCS trends of the same plugs. For example, samples with solitary blend of FA had negative development in UCS, but high increase in E-modulus as compared to their reference plug. It is noticeable that two of the best performing samples in UCS after 28 days had opposite developments in their E-moduli as compared to their reference plug. These plugs are nano-systems with 2g and 3g FA having 3.3 GPa (26.3% increase) and 2.3 GPa (12.4% decrease), respectively [Appendix A]. For solitary FA blend after 28 days curing period, samples’ E-moduli were found to be consistent with UCS measurements.

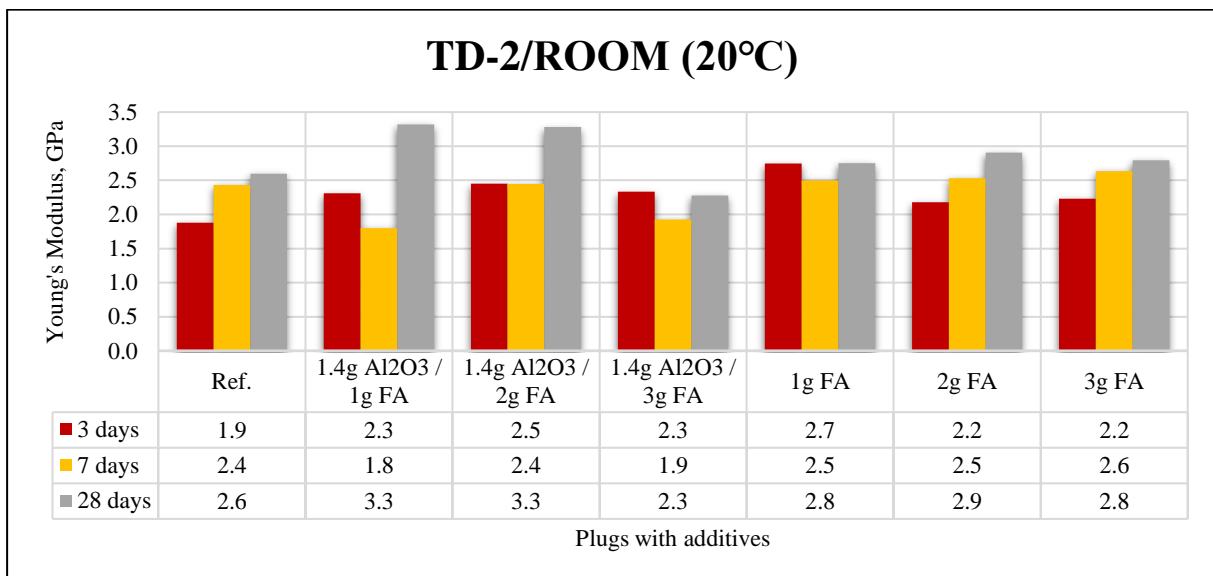
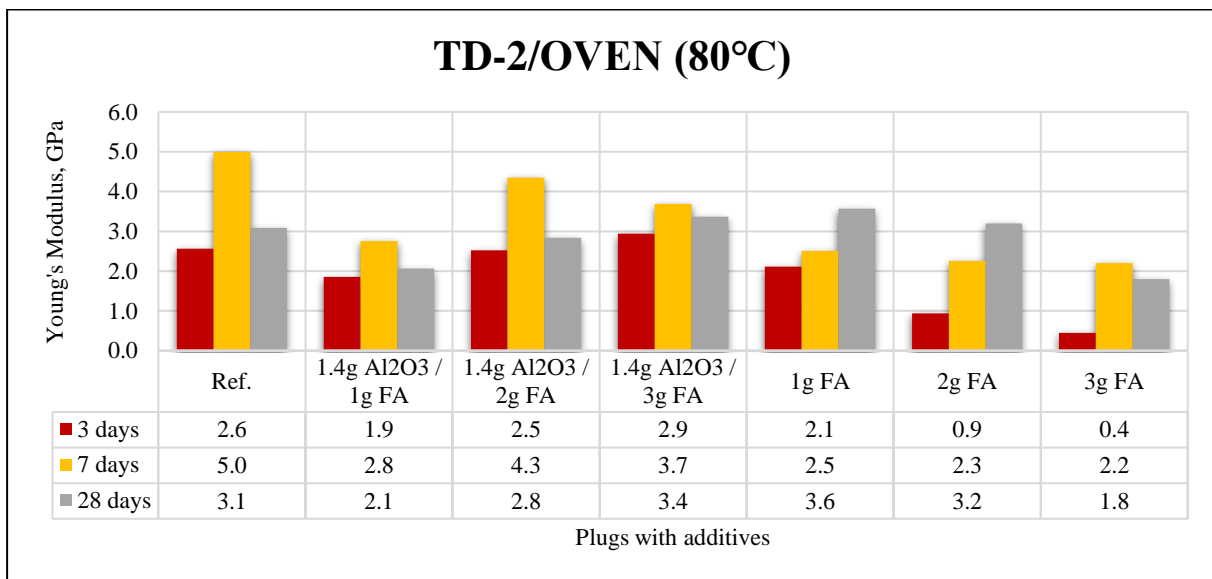


Figure 5.11 Young’s moduli of TD-2 samples cured in room temperature



**Figure 5.12** is displaying E-moduli of the oven-cured samples of TD-2. Compared to reference plug results, most of the dosages had very low stiffness values after being cured for 3 and 7 days at 80°C, among which solitary 3g FA plugs performed the worst with 82.6% and 55.9% loss in stiffness correspondingly for 3 and 7 days. E-moduli results are contrary to UCS results of the relevant batches, where for 3 and 7 days, instead of improving stiffness along with UCS, they worsened. For plugs aged 28 days in the oven, it is observed that samples have some improvements compared to the reference sample, the negative results also exist here. It is visible that 1g FA with 1.4g aluminium nanoparticles and solitary 3g FA blend had the lowest E-moduli among other plugs with respective stiffness of 2.1 GPa (33.1% decrease) and 1.8 GPa (41.5% decrease). Interestingly, 3g FA with NPs and 1g FA without NPs had the highest stiffness after 28 days having 9.2% and 15.8% increase respectively [[Appendix A](#)]. It is to be noted that the lowest dosage of 1g FA with NPs and the highest concentration of 3g FA solitary blend did not interact with OPC very well resulting in very low stiffnesses.



**Figure 5.12** Young’s moduli of TD-2 samples cured in oven temperature

### 5.3.3 Impact of Al<sub>2</sub>O<sub>3</sub> nanoparticles and fly ash on resilience (R)

In this section, resilience results for plugs from TD-2 will analysed. As mentioned in [section 5.3.2](#), resilience data are missing for the same plugs due to human error [[Appendix B](#)].

Since cement is a brittle material, the resilience or energy absorbed by a sample under load is found by integrating the area under UCS. Resilience is shown in **figure 5.13** for the samples cured in room temperature for 3, 7 and 28 days from TD-2. For 3 days aged plugs, it is apparent that most plugs had adverse results in resilience development, which is congruent with the UCS trend of the same plugs, where the plugs could not absorb much energy leading them to be weaker and stiffer, when combining with E-moduli from [section 5.3.2](#). Solitary 3g FA plug after being cured for 7 days had the highest resilience of 154.9 kJ/m<sup>3</sup> with an increase of 22.3% compared to the reference plug. For the curing period of 28 days, nano-system with 2g and 3g FA had the two highest peaks of 186.5 kJ/m<sup>3</sup> (171.4% increase) and 193.4 kJ/m<sup>3</sup> (181.4% increase). It should be mentioned that all the single FA blends had significant increment over their corresponding reference plug and they are consistent with the trend of having low E-moduli.

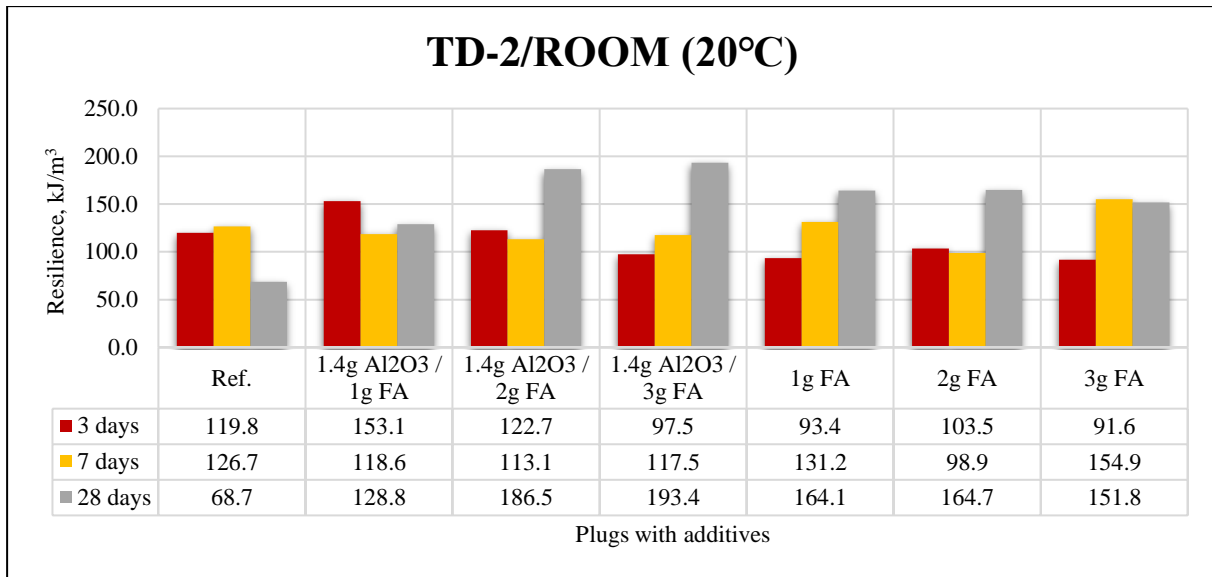


**Figure 5.13 Resilience of TD-2 samples cured in room temperature**

**Figure 5.14** shows the resilience of the oven-cured samples for TD-2. From the percentile change diagrams in [Appendix A](#), we can observe that after curing 3 and 28 days, most of the samples encountered negative development in comparison with their particular references, which indeed follow the UCS trend, where developments were also unfavourable. Only significant positive increment in resilience was recorded for solitary 2g FA after being cured for 7 days, which meant 57.9% increase (157.4 kJ/m<sup>3</sup>).

One can easily ascertain the disparities in results between two curing environments from the above discussions. It is evident that Al<sub>2</sub>O<sub>3</sub> nano-system with FA and solitary FA system do not perform well under high temperature over a long curing period. While there are multiple clear peaks in 28 days performance, there is a single peak for 3 and 7 days each.

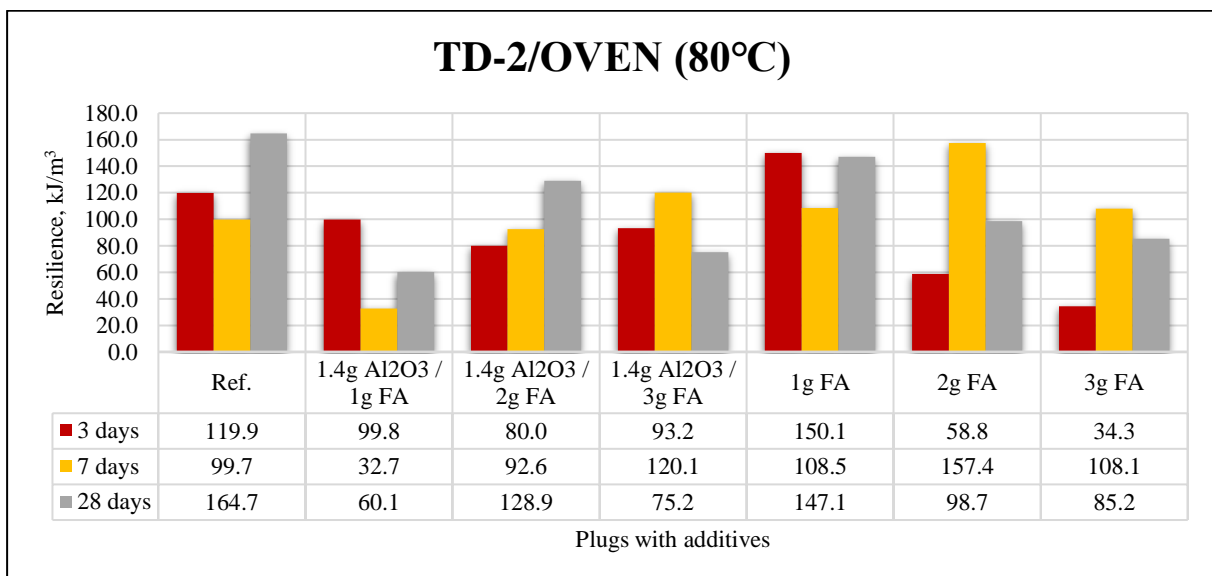


**Figure 5.14 Resilience of TD-2 samples cured in oven temperature**

### 5.3.4 Impact of Al<sub>2</sub>O<sub>3</sub> nanoparticles and fly ash on P-wave modulus (M-modulus)

The microstructure analysis is useful to understand the strength build-up of cement plugs. M-modulus can give us insights into the microstructure. As mentioned earlier, UCS and M-modulus are functions of velocity.

M-moduli for room-cured samples from TD-2 are displayed in *figure 5.15*. Most of the plugs after being cured for 3 and 7 days had positive developments in M-moduli. Although, OPC did not perform well in 28 days curing period having negative results in general as compared to their reference plug. Concerning fluctuations in results, plugs in 3 and 28 days batches are quite stable, however ups and downs can be visible in 7 days aged plugs, where 2g FA with nanoparticles had the largest M-modulus of 21.1 GPa (5.2% increase over reference) and solitary 3g FA with the smallest M-modulus of 18 GPa (10.1% decrease from reference).

In terms of following the UCS strength build-up, majority of the plugs followed the trends, however not without exceptions. For example, in TB-6-R, 2g and 3g FA with 1.4g Al<sub>2</sub>O<sub>3</sub> NPs and solitary 2g FA blend had opposite trends in comparison with UCS. Such occurrences in TB-4-R and TB-5-R can also be observed in [Appendix A](#) of percentile change diagrams.

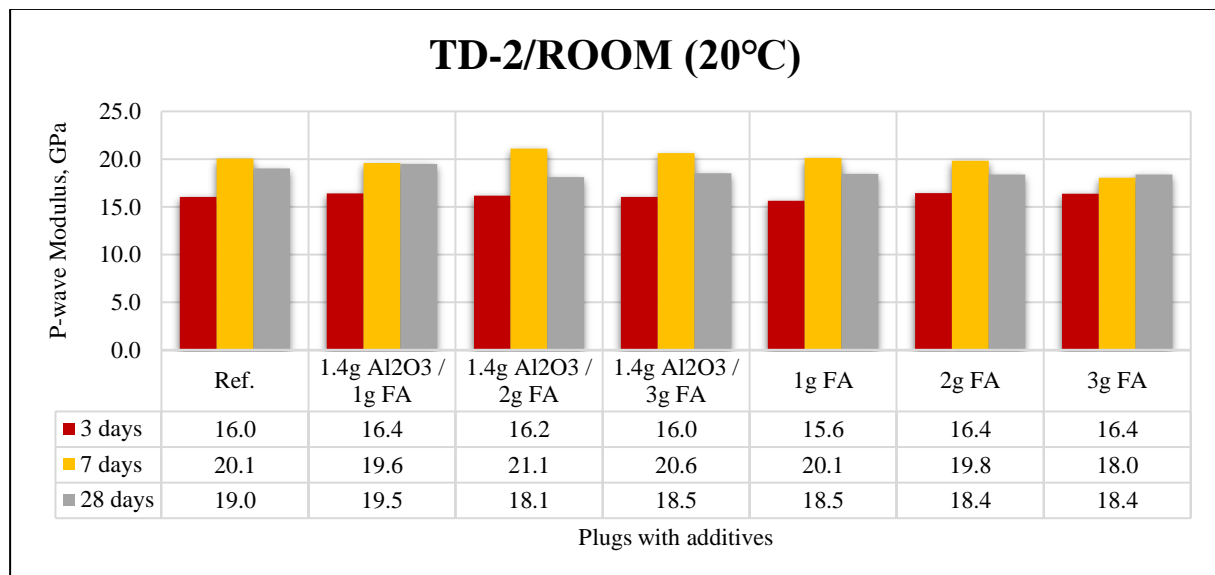


*Figure 5.15 P-wave moduli of TD-2 samples cured in room temperature*

*Figure 5.16* is showing the obtained M-modulus results of oven-cured cement samples from TD-2 after they were cured at 80°C for 3, 7 and 28 days. Cement plugs cured for 3 and 7 days did not have very variations in their M-moduli and in general, they suffered poor results compared to their respective reference plugs. Although, all the plugs in 28 days batch had visible increments over their base plug and it is important to mention that M-moduli of the samples fluctuates clearly. In TB-6-O, nano-system with 2g FA had the highest M-modulus, which is 16 GPa and it translates into 26.8% increment from the reference plug, which had the lowest M-modulus of 12.6 GPa in the whole batch.

Anomalies exist here as well, as they did in batches from the room temperature. In 28 days batch, for example, 1g FA with NPs and single 2g FA blend were supposed to go down in transition according to UCS trend but they went up in values. In the same batch, single 1g FA plug was expected to have an upward facing trend as UCS, instead it went down in values. The opposite trends for some plugs in TB-4-O and TB-5-O were found as well.

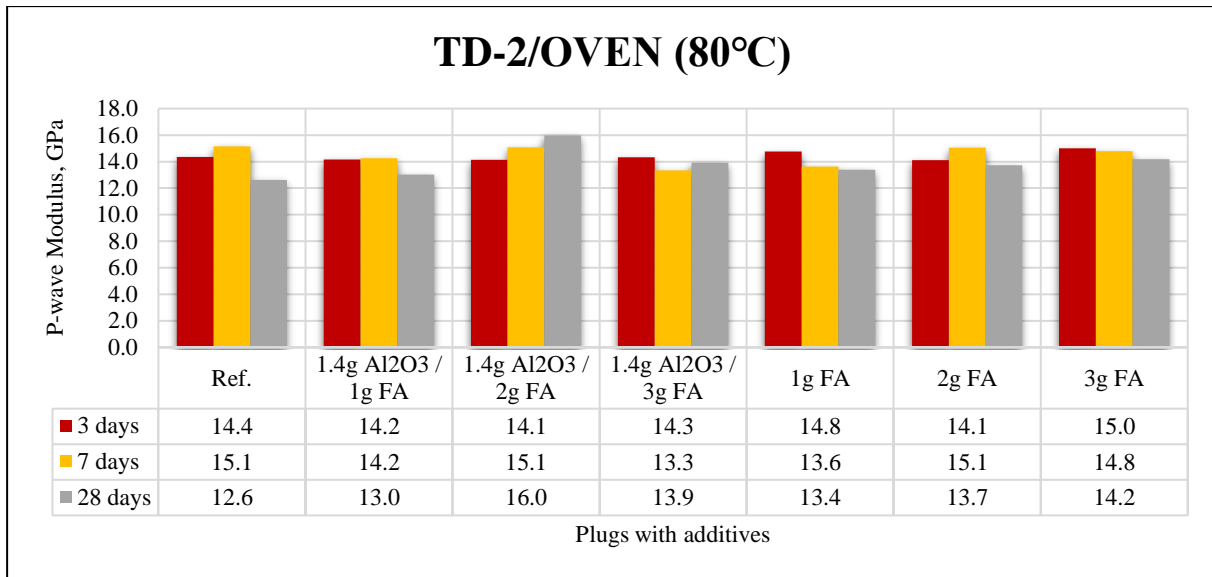


**Figure 5.16 P-wave moduli of TD-2 samples cured in oven temperature**

As it can be noticed in both TD-1 [section 5.2.4] and TD-2 that M-moduli results are usually lower among oven-cured samples in comparison with the room-cured samples. These disparities in results between room and oven curing environments can be explained with the variations in sonic velocity. After being cured in oven at 80°C for 3, 7 and 28 days, samples are much drier than respective room-cured samples, which could still have humidity in their microstructures. Due to this reason, sonic waves propagate through room-cured plugs in higher velocity compared to their respective plugs from oven environment, where the pore spaces are filled with air.

### 5.4 Test Design 3 (Effect of TiO<sub>2</sub> nanoparticles on geopolymer cement)

The following subsections will comprise of results obtained from TD-3, where investigations were conducted on API Class F FA-based geopolymer cement to examine the effects of TiO<sub>2</sub> NPs with dosages of 0.3g, 0.4g and 0.5g. In this test design, the samples cured for 8 days in room temperature were the same samples that were cured in oven at 80°C for 2 days, as mentioned in [section 3.2.1](#). Since there is only one batch of samples, different colour codes were used in the diagrams. The colour green was used to mark the reference plug and the colour blue was used to denote samples with additions of NPs.

#### 5.4.1 Impact of TiO<sub>2</sub> nanoparticles on uniaxial compressive strength UCS

UCS results obtained from destructive tests conducted on geopolymer cement plugs in TD-3 are exhibited in [figure 5.17](#). It is found that plug with the lowest concentration of 0.3g titanium had bare minimum improvement with 23.6 MPa (4.7% increase) as compared with the reference plug. The intermedial concentration of 0.4g TiO<sub>2</sub> gave the highest positive development in UCS of 32 MPa, having 41.8% rise in strength compared to reference. The highest concentration of titanium NPs had the worst result with 15.7 MPa leading to significant 30.2% reduction in strength in comparison with its reference and other concentrations of NPs [[Appendix A](#)].

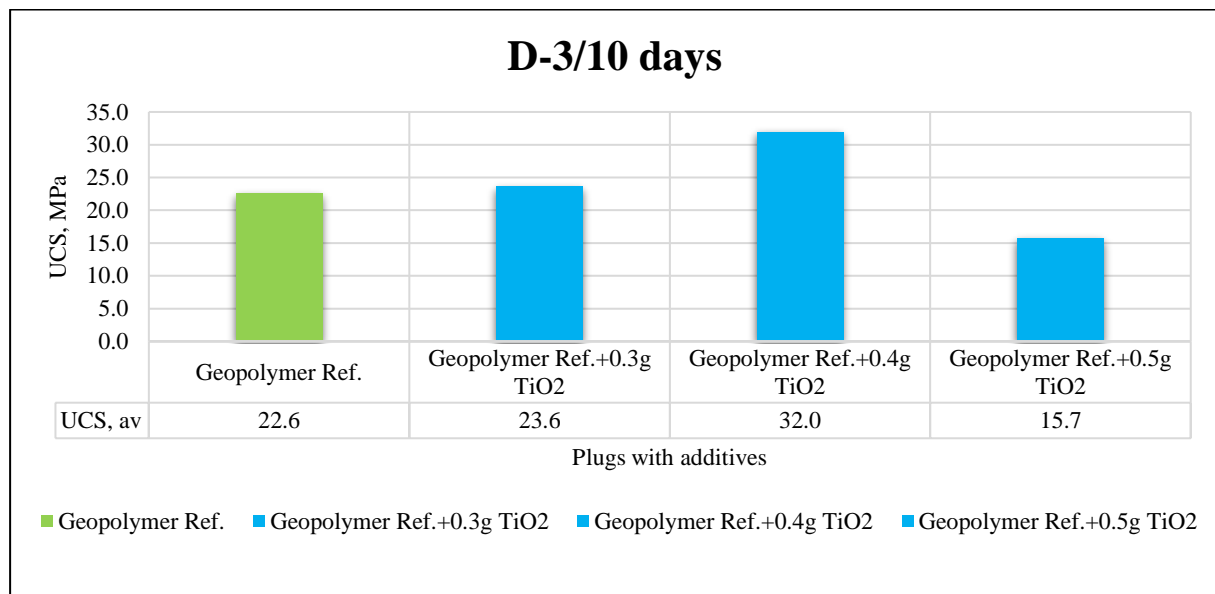


*Figure 5.17 UCS of TD-3 geopolymer cement samples*

The [table 5.5](#) contains the SDs for the geopolymer plugs with hints of the reliability of the data. It is observed that geopolymer cement reference plug and 0.3g nano-system have the highest SDs making them potentially unreliable data due to many possible challenges

**Table 5.5 Standard deviations (SD, MPa) for TD-3 geopolymer cement samples**

Curing age\ Plugs	Geopolymer Ref.	Geopolymer Ref.+0.3g TiO <sub>2</sub>	Geopolymer Ref.+0.4g TiO <sub>2</sub>	Geopolymer Ref.+0.5g TiO <sub>2</sub>
10 days	10.2	4.1	0.9	0.4

mentioned earlier. In contrast, we can distinguish between SDs from another spectrum, where the nano-systems with relatively higher dosages had the lowest standard deviations, which make their data much more reliable and in terms of reproducibility, the future outcomes could be the same as results found here.

#### 5.4.2 Impact of TiO<sub>2</sub> nanoparticles on Young’s modulus (E-modulus)

Young’s moduli for the geopolymer cement samples are displayed in *figure 5.18*, where the reference sample found to be the stiffest compared to the nano-systems. The geopolymer plugs with 0.3g, 0.4g and 0.5g TiO<sub>2</sub> nanoparticles had respective E-moduli of 3.6 GPa, 3.8 GPa and 3.3 GPa, which translate into corresponding 56.7%, 53.6% and 59.9% decrease in stiffness as compared to the reference plug [[Appendix A](#)].

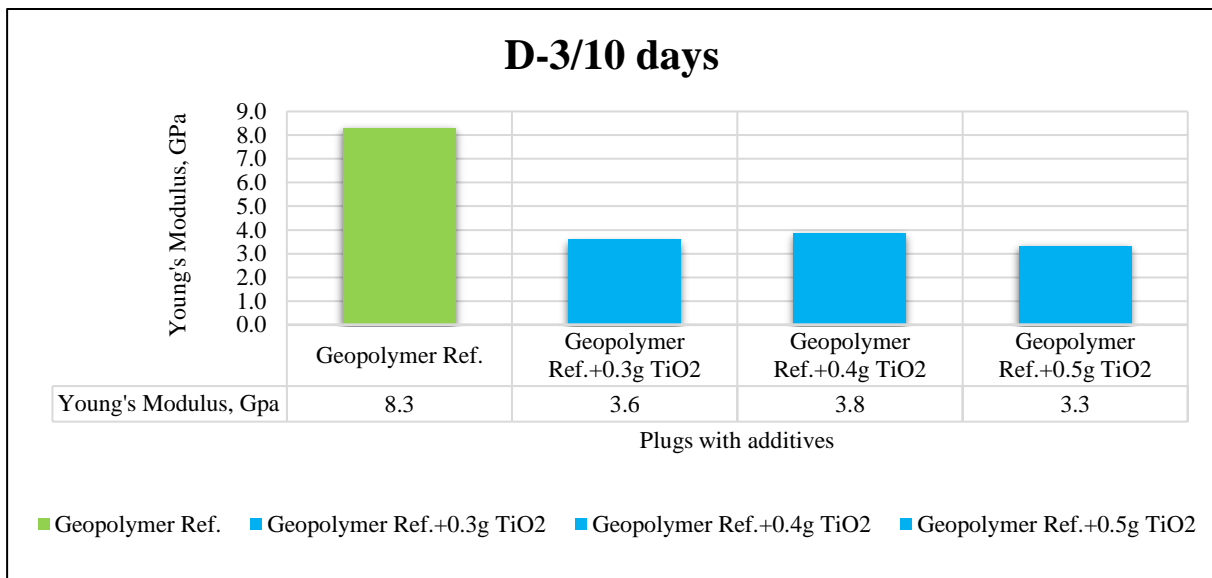


*Figure 5.18 Young’s moduli of TD-3 geopolymer cement samples*

As it is known that usually with increase of UCS, stiffness of the materials also relatively increases. From the discussion in [section 5.4.1](#) and here, we observe the previously mentioned correlation between UCS and E-moduli, where the nano-system with highest UCS has the highest E-moduli among the nano-systems and for the weakest nano-system had the lowest stiffness. Although the reference seems to be the exception to this rule, which can be explained by considering the high brittleness of conventional geopolymer cement. Therefore, it can be concluded that the addition of the nanoparticles stabilized the E-moduli of samples by reducing fluctuations in data among the nano-systems compared to their reference plug. However, it should be mentioned that plugs with NPs did not have any conventional positive development over the reference despite having higher UCS.

#### 5.4.3 Impact of TiO<sub>2</sub> nanoparticles on resilience (R)

*Figure 5.19* displays the resilience results achieved from the TD-3. It is visible that there is clear fluctuation in the results. Here 0.3g nano-system does not adhere to the conventional rule of following the UCS trend, as it was supposed to have higher resilience compared to its reference plug but it was recorded to be the opposite.

Naturally, plugs with 0.4g and 0.5g NPs followed the expected trend with 129 kJ/m<sup>3</sup> and 49 kJ/m<sup>3</sup>, respectively having increased up 48.2% and decreased by 43.7% as compared to the reference plug [Appendix A]. The aforementioned plugs had the energy absorption rate in the opposite direction.

When compared against E-moduli, the resilience of the plugs improved noticeably, as high resilience is associated with low stiffness. However, the nano-systems did not have in most cases compared to the reference sample. Only plug with 0.4g titanium NPs had significant development, which is proportional to UCS development.

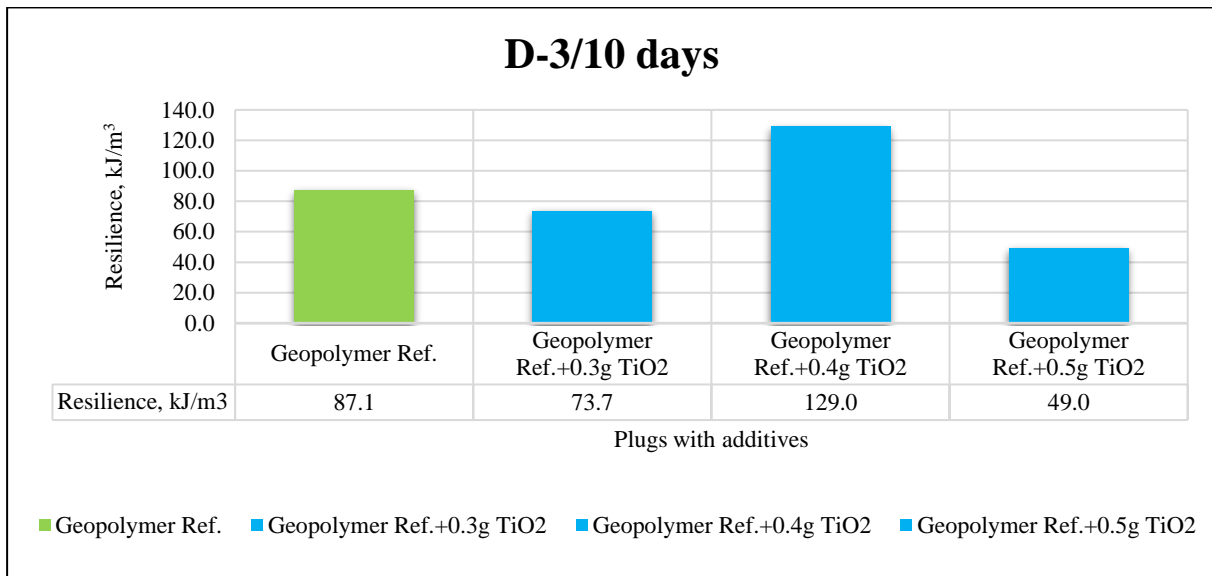


*Figure 5.19 Resilience of TD-3 geopolymer cement samples*

#### **5.4.4 Impact of TiO<sub>2</sub> nanoparticles on P-wave modulus (M modulus)**

M-moduli of the geopolymer cement samples are shown in *figure 5.20*. As discussed in previous sections, it has been shown that in most cases M-moduli follow the UCS trend, although exceptions do occur from time to time. The plugs with 0.4g and 0.5g TiO<sub>2</sub> NPs were found to be the best and worst performing dosages respectively. The former had an M-modulus of 12.6 GPa with 16.1% increase and the latter suffered adverse results with 9.2 GPa having decreased by 15.6% in elasticity in comparison with the reference plug [Appendix A].

The exception was the plug with 0.3g NPs having M-modulus of 9.8 GPa, which instead of performing better than its reference, it had a reduction in elasticity making it a divergent result.

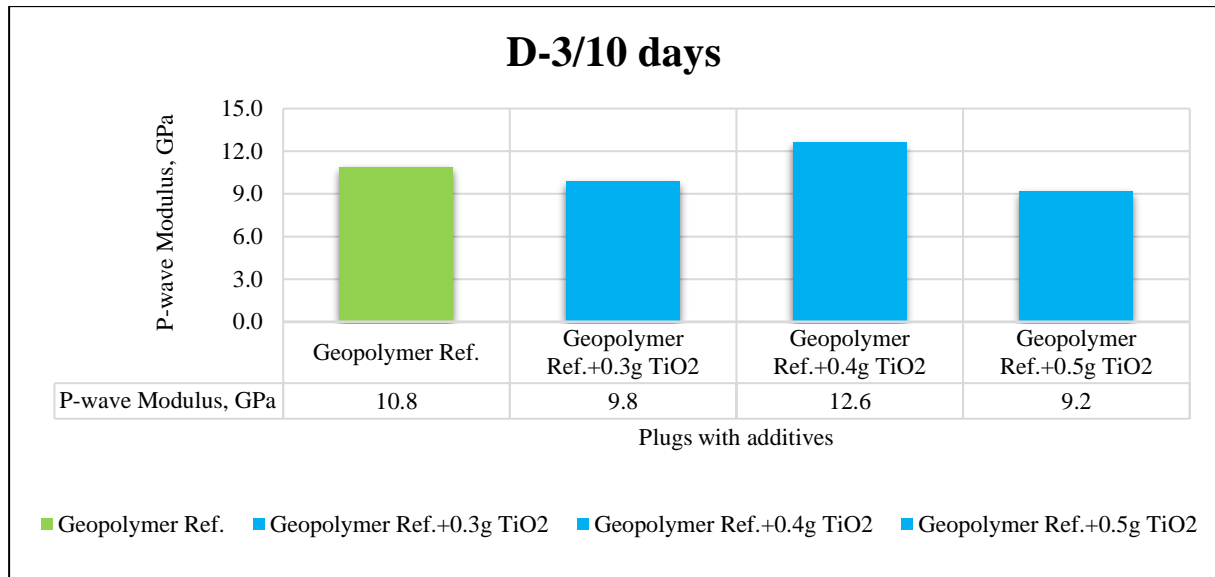


*Figure 5.20 P-wave moduli of TD-3 geopolymer cement samples*



### 5.5 Test Design 4 (Effect of TiO<sub>2</sub> nanoparticles on OPC)

The following sub-sections holds the discussions regarding the effects of 0.15g, 0.25g, 0.35g and 0.45g TiO<sub>2</sub> NPs on G-class OPC. These experiments took place in TD-4, which consists of TBs-8,9,10 having curing environments of 20°C and 80°C. The applied colour codes in the bar graphs for 3, 7 and 28 days are red, yellow and gray, respectively.

#### 5.5.1 Impact of TiO<sub>2</sub> nanoparticles on uniaxial compressive strength UCS

UCS test results for samples cured in room temperature in TD-4 are displayed in *figure 5.21*. It can be seen that after 3 days of curing, nano-added samples performed poorly compared with the reference with 0.15g and 0.35g plugs having strength reduced by 1.4% (16 MPa) and 11.5% (14.3 MPa) [[Appendix A](#)]. In contrast, most samples cured for 7 days have seen significant strength development as compared to the reference. The samples with the positive developments are 0.15g, 0.25g and 0.45g nano-added plugs with correspondingly 26.4 MPa, 23.6 MPa and 23 MPa. Plugs after 28 days had decreased in strength compared to their 7 days strength development, except for the neat OPC reference plug having gradual increase in strength over 3, 7 and 28 days period as the hydration process matured. It should be noted that the only plugs with NPs had continuous positive UCS was plugs with 0.45g nano-Ti.

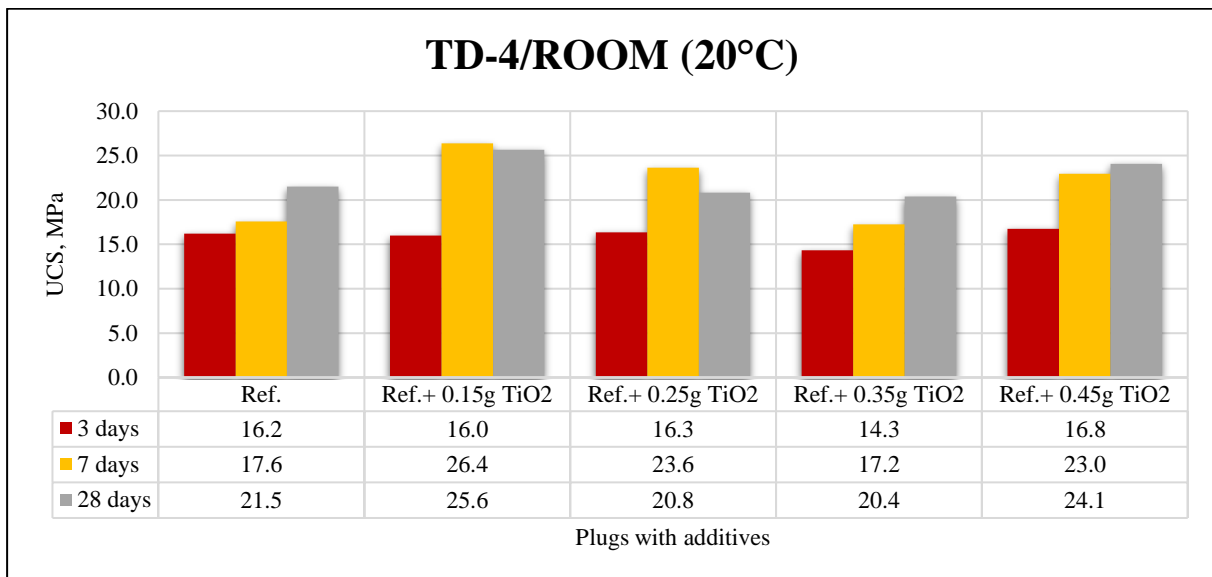


*Figure 5.21 UCS of TD-4 samples cured in room temperature*

We can also observe in *figure 5.21* that TiO<sub>2</sub> NPs can improve early strength by boosting the hydration process, especially after 7 days, although the performance dipped after 28 days. The possible explanation could be for this is the reduction in C-S-H gel in the cement matrix.

*Table 5.6* details the standard deviations for the room cured samples in this design. One can observe that, in general, the SDs are quite small, making the UCS data reliable. This reliability indicates that the if manufactured for industrial applications, in room temperature, nano-modified OPC could show the same trends in the strength development. For example, the plug with 0.35g NPs performed consistently below par throughout all the curing periods is reflective of the determined SDs.

**Table 5.6 Standard deviations (SD, MPa) for TD-4 samples in room temperature**

Curing age \ Plugs	Ref.	Ref.+ 0.15g TiO <sub>2</sub>	Ref.+ 0.25g TiO <sub>2</sub>	Ref.+ 0.35g TiO <sub>2</sub>	Ref.+ 0.45g TiO <sub>2</sub>
3 days	0.6	0.2	0.9	1.8	1.9
7 days	1.7	1.0	2.4	1.9	0.4
28 days	0.1	0.2	1.5	0.3	2.9

Displayed in *figure 5.22* are the UCS results for the oven-cured samples from TD-4. After being cured at 80°C for 28 days, all the nano-added plugs had significant strength improvement in comparison their reference. Among them, plug with 0.45g NPs had the highest strength with 28.2 MPa, which translates into 42.1% increase in strength over the reference. The other additions of NPs had increments of 34.3%, 38.5% and 12.8% respectively for plugs with 0.15g, 0.23g and 0.35g nano-Ti [Appendix A]. When comparing between two curing environments, it was found interesting that in room temperature, most improvements happened after being cured for 7 days, however, samples cured at 80°C had seen the highest peaks in UCS after 28 days. To elucidate, it is possible that elevated temperature could slow down the early strength build-up. But as the time went by, high temperature helped increase bonding between the titanium nanoparticles and OPC by increased gelation. Additionally, strength build-up could also mean that the TiO<sub>2</sub> NPs are reducing the pore spaces by occupying them in comparatively higher rate.

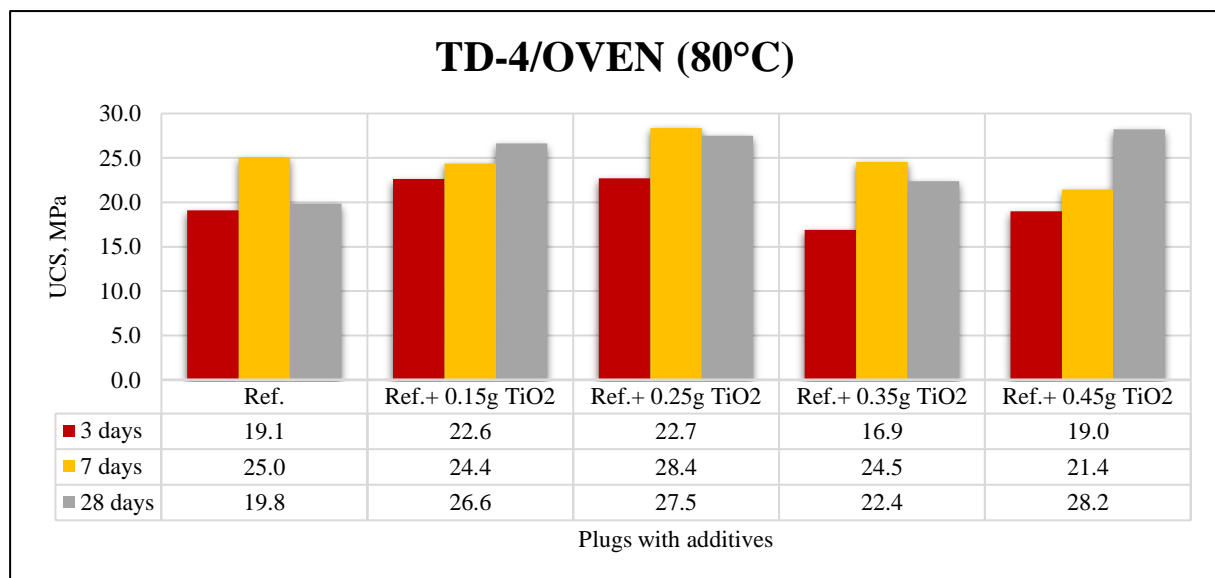


**Figure 5.22 UCS of TD-4 samples cured in oven temperature**

To realize the reproducibility of the cement plugs discussed above, it is highly necessary to look at the standard deviations of the said samples. For instance, the 0.45g plug being the best performing plug after being cured for 28 days in an oven had the descriptive SD of 0.8 MPa, which makes this UCS data quite reliable. On the other hand, on the same batch the reference sample had the highest SD of 4.7 MPa, which makes the data a little undependable. Because in room temperature, the neat OPC had the lowest SD after 28 days. It goes to show that the degradation of neat OPC due to high temperature might be underlying reason for the unreliable data.

**Table 5.7 Standard deviations (SD, MPa) for TD-4 samples in oven temperature**

Curing age\ Plugs	Ref.	Ref.+ 0.15g TiO <sub>2</sub>	Ref.+ 0.25g TiO <sub>2</sub>	Ref.+ 0.35g TiO <sub>2</sub>	Ref.+ 0.45g TiO <sub>2</sub>
3 days	6.6	0.1	2.6	2.0	0.1
7 days	0.2	0.0	1.2	3.6	4.6
28 days	4.7	2.9	1.6	0.1	0.8

This consistency of 0.45g nano-added samples in strength developments inspired us to make binary amalgamation of carbon fibers and glass fibers to improve the mechanical and petrophysical properties of OPC in the later test design, results from which will be discussed in the [section 5.6](#).

### 5.5.2 Impact of TiO<sub>2</sub> nanoparticles on Young’s modulus (E-modulus)

Young’s moduli for the samples cured in room temperature in TD-4 are shown in [figure 5.23](#), where it can be seen that E-moduli for the samples after 3 days of curing did not fluctuate greatly. Although, samples with nano addition had developed very high stiffness as compared to the reference after 7 days. In percentile development, plugs with 0.15g, 0.25g, 0.35g and 0.45g nano-Ti had corresponding massive increase in stiffness over reference by 244.9% (3.7 GPa), 222% (3.4 GPa), 308% (4.3 GPa) and 153% (2.7 GPa) [[Appendix A](#)]. These unrealistic values can be explicated by samples having very low deformation as shown in [Appendix B](#) due to cement’s inherent brittleness. However, it should be noted that for most samples, the stiffness

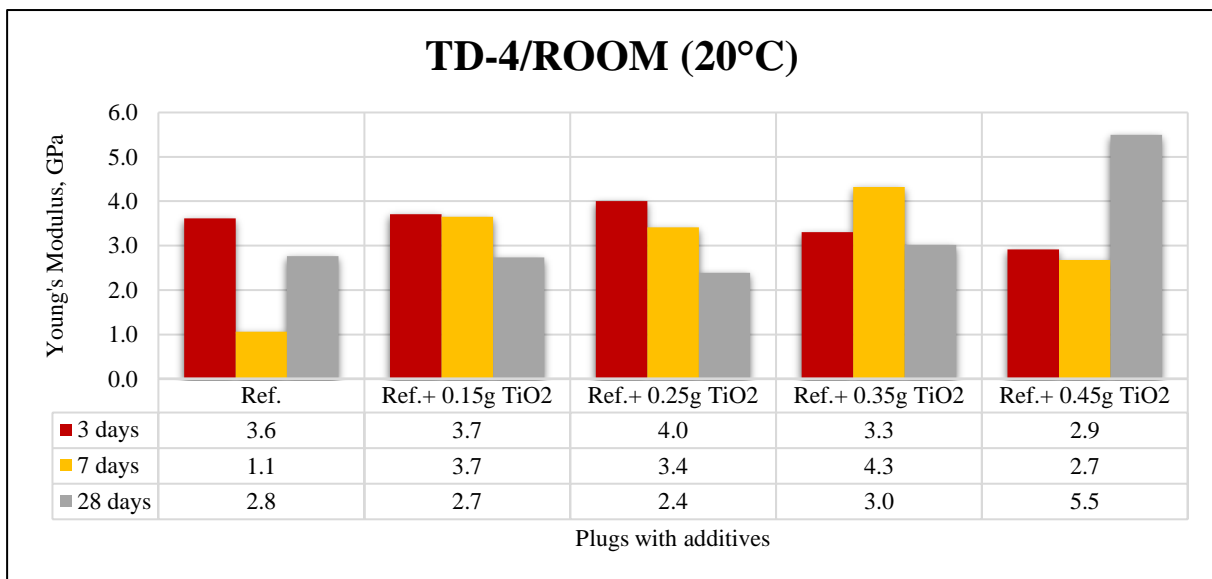


**Figure 5.23 Young’s moduli of TD-4 samples cured in room temperature**

development followed the UCS development. After 28 days of curing period in room temperature, the plug with 0.45g TiO<sub>2</sub> NPs was the stiffest having 5.5 GPa E-modulus with 98.8% increase over the neat OPC plug. The exception in the 28 days batch in terms of not having an increase in stiffness along with improved strength is the plug with 0.15g NPs being reduced in stiffness compared to the reference by 1.1% [[Appendix A](#)].

All the samples cured at 80°C for 3 and 7 days suffered adverse effects in E-moduli [figure 5.24]. Especially for 7 days batch, it is the opposite development in stiffness of what was recorded in the room-cured batch’s stiffness development. In the other end of the spectrum of E-moduli, samples cured for 28 days in an oven had progressive developments for all the nano dosages in comparison with the reference. The plugs with 0.15g, 0.25g, 0.35g and 0.45g NPs had particular stiffness of 3.6 GPa, 5.6 GPa, 5.9 GPa and 6.5 GPa, having been increase by 7.8%, 64.8%, 75% and 91.1% over the reference. It is essential to remark that the stiffness trend of 28 days oven-cured samples generally adheres to that of UCS development.

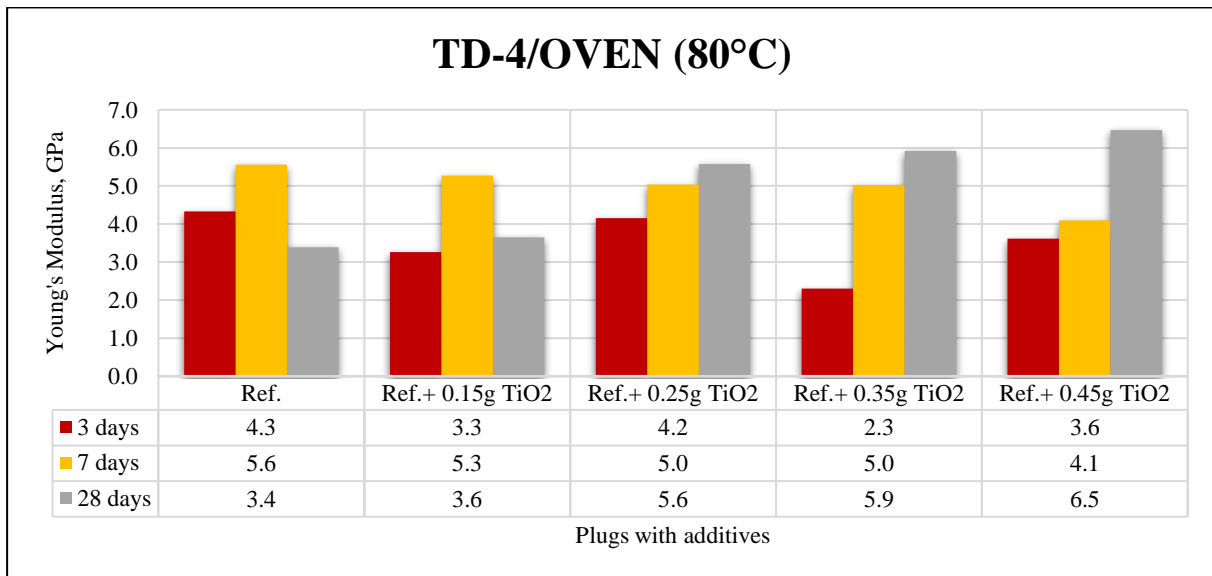


*Figure 5.24 Young’s moduli of TD-4 samples cured in oven temperature*

### 5.5.3 Impact of TiO<sub>2</sub> nanoparticles on resilience (R)

Resilience data obtained from TD-4 samples cured in room temperature are presented in figure 5.25. It is noticeable that after 3 days curing period, the fluctuations are not that great among the samples. Most nano dosages had positive resilience compared to their reference, except 0.25g plug. Predictably, most samples from the curing periods of 7 and 28 days had suffered unfavorable results, as found in section 5.5.2, most samples had positive E-moduli development.

It is predictable because resilience is inversely proportional to stiffness. The sole sample to have positive resilience development compared to reference is the sample with 0.15g NPs from 28 days curing period having a resilience of 121.8 kJ/m<sup>3</sup>, which is interpreted into 46.9% raise over the reference [Appendix A].

The reason behind calling the results predictable because low resilience is associated with high E-modulus [107] and resilience is influenced by deformation of the samples as well. If the deformation is very low, stiffness tends to be large and as a results cement samples will absorb low energy before being crushed. Since brittle materials, such as cement, do not have a plastic region to deform, the deformation inclines to be very small, which can be seen in Appendix B.

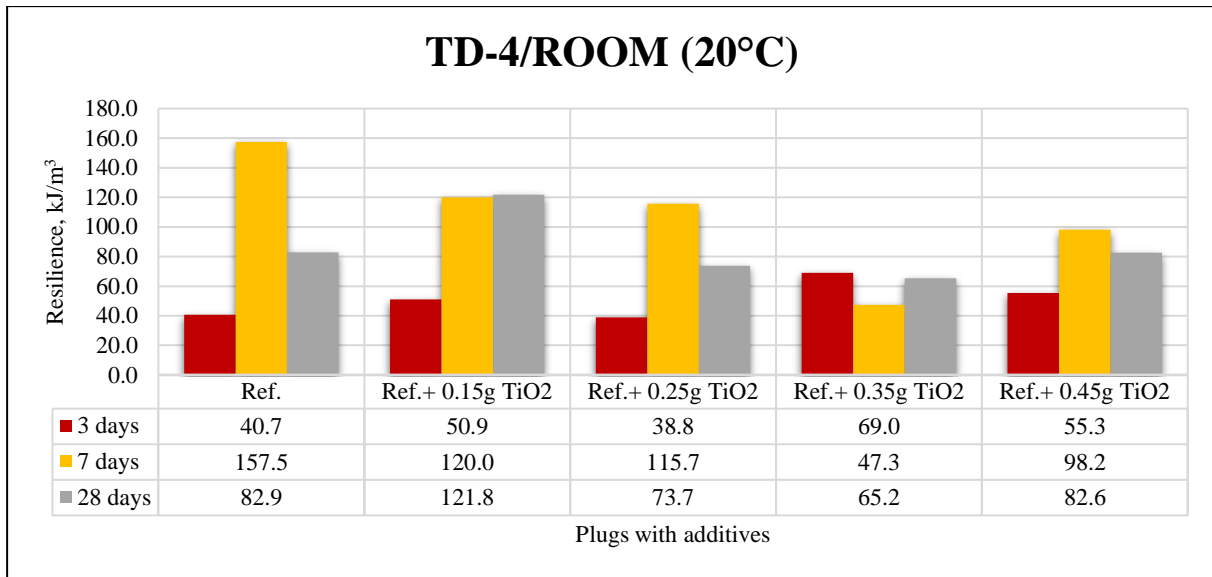


**Figure 5.25 Resilience of TD-4 samples cured in room temperature**

Resilience for the oven-cured samples tested in TD-4 are shown in **figure 5.26**, where most samples developed greater resilience than their respective reference plugs. If we consider the 28 days curing period, all the nano-added plugs had advantageous resilience improvement as compared to the reference plug, among which the plug with 0.45g NPs had the highest resilience with 239.7 kJ/m<sup>3</sup>, meaning a 248.1% growth over the reference [[Appendix A](#)]. These data are very positive because when combining with UCS and E-moduli development of the same samples, they turn out to be quite strong, tough and relatively less brittle than other samples created in 3 days and 7 days batches.

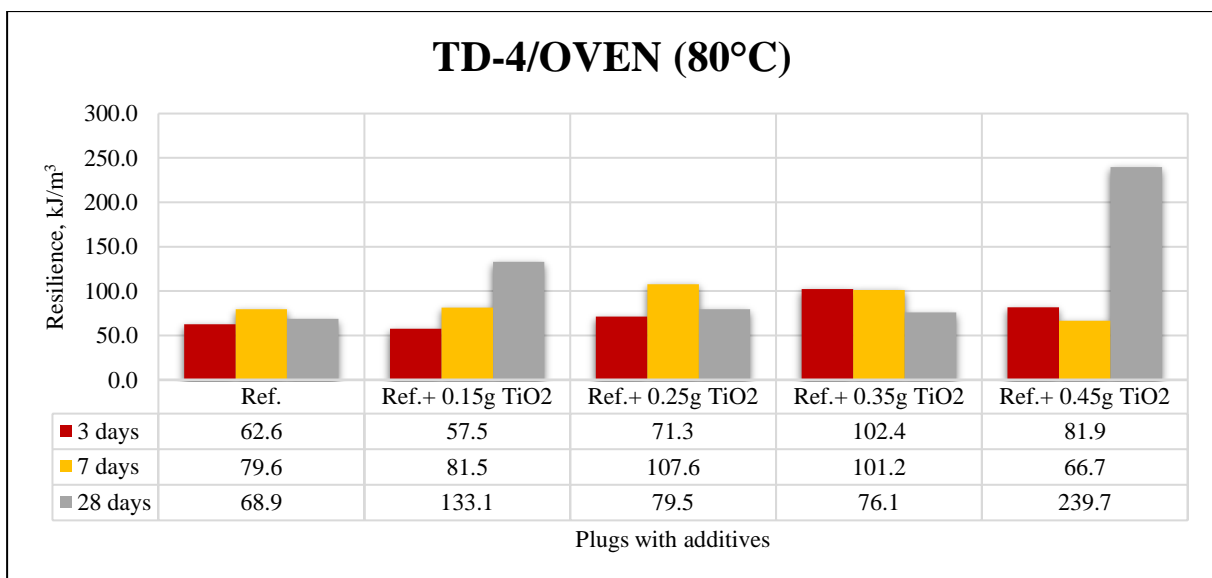


**Figure 5.26 Resilience of TD-4 samples cured in oven temperature**

### 5.5.4 Impact of TiO<sub>2</sub> nanoparticles on P-wave modulus (M modulus)

In *figure 5.27*, M-moduli for the TD-4 room-cured samples are shown. It is apparent from the diagram is that the elastic moduli do not vary significantly. Although, the M-moduli development had been largely negative in comparison with their specific references. From the whole room temperature curing environment, there are only two nano-added plugs were recorded to have increased M-moduli against their references. They are 0.25g plug from 7 days curing period with 19.7 GPa (4.3% raise) and 0.15g plug from 28 days batch with 17.4 GPa (0.7% raise) [[Appendix A](#)].

In general, the M-moduli follow the UCS trend of the same samples, but the magnitude of values may differ. As discussed previously, due to defects on the samples' surfaces and due to being non-homogeneous internally, there happen to be some anomalies in the datasets. For example, 0.15g and 0.25g plugs with NPs from 7 days had deviating trends from the UCS's trends.

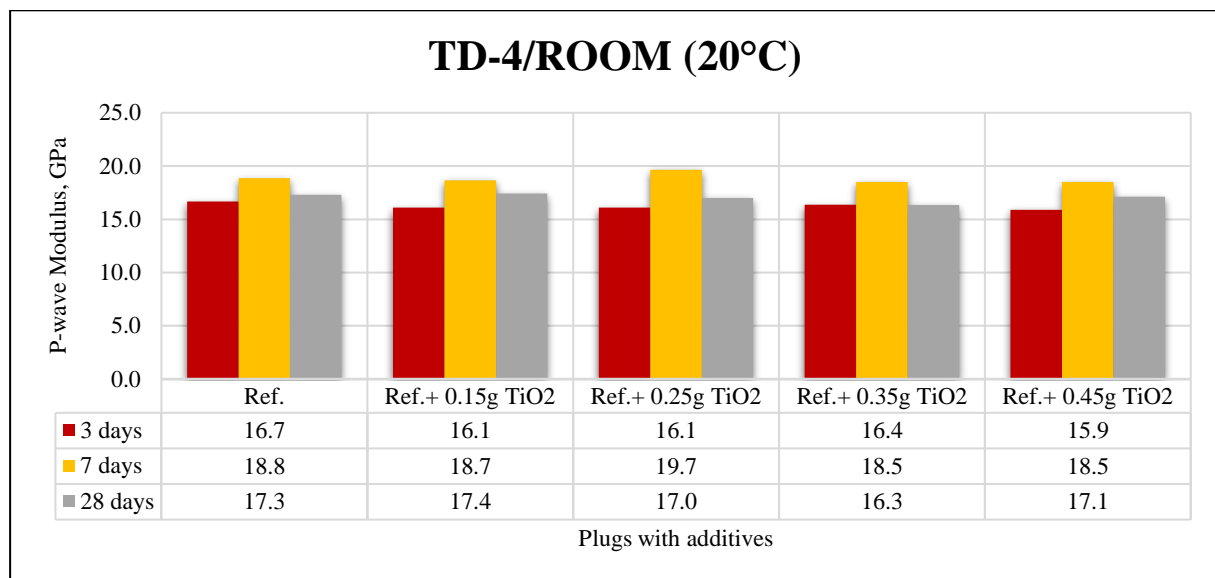


*Figure 5.27 P-wave moduli of TD-4 samples cured in room temperature*

It is evident from *figure 5.28*, which displays the M-moduli results for samples cured at 80°C in TD-4, that the elasticity of the cement samples varies decimally in the large portion of the data. Nano-modified OPC plugs from 3 days and 7 days show totally contrastive results, where the 3 days M-moduli for the samples are negative in comparison with the reference, whilst the 7 days samples had all positive developments in M-moduli.

For 28 days batch, two best performing nano-modified plugs are also the best performer here. The 0.25g and 0.45g plugs with NPs had respectively 13.1 GPa and 12.8 GPa of M-moduli, interpreting them into 3.7% and 1.3% raise in elasticity compared to their reference [[Appendix A](#)].

Furthermore, concerning the adherence to the UCS oscillating trends, predominantly M-moduli follow the patterns despite having different magnitudes of values. However, it is not completely without contradictions. I.e., plugs with 0.15g nano-Ti have veered away in the opposite directions of the UCS in 3, 7 and 28 days batches. The likely reasons could be for these anomalies, in addition to what was described earlier, the nonuniform hydration process taking place internally and how the titanium nanoparticles have integrated within the cement matrix.

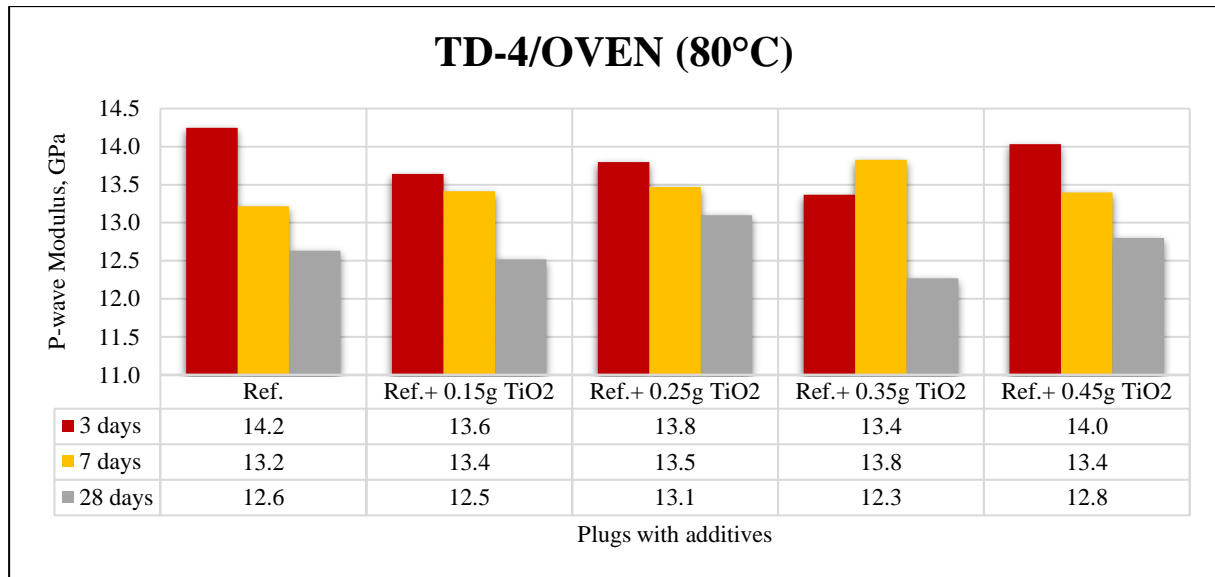


*Figure 5.28 P-wave moduli of TD-4 samples cured in oven temperature*

### 5.6 Test Design 5 (Effect of TiO<sub>2</sub> nanoparticles, CF and WF on OPC)

Experimental results obtained from TD-5 will be deliberated in this segment. CF and WF were added to the G-class OPC modified with 0.45g TiO<sub>2</sub> NPs to improve the mechanical and rheological properties and the samples were cured indeed in room temperature and at 80°C in an oven. It is important to note that for the whole design 0.45g nano-Ti was kept constant with varying dosages of CF and WF in the range of 0.1g to 0.3g for both fibers. TD-5 comprises of TBs-11,12,13 having relevant batches for both curing environments. Red, yellow and gray are the designated colour schemes specifically for 3, 7 and 28 days.

#### 5.6.1 Impact of TiO<sub>2</sub> NPs, CF and WF on uniaxial compressive strength (UCS)

**Figure 5.29** is displaying the UCS data for room-cured samples from TD-5. After 3 days of curing period, only the 0.3g WF reinforced plug with NPs had the largest improvement in UCS with 19.2 MPa (17.8% increase) [[Appendix A](#)], albeit it failed to perform better than the reference in both 7 days and 28 days. Most samples suffered adverse results after being cured for 7 days in room temperature, except for the plug with 0.3g CF with nano-Ti having 27.6 MPa with 9.1% increase as compared to the neat OPC. In contrast, samples in general had positive development in strength after they were cured for 28 days. Here as well, nano-added sample with 0.3g CF was found to have the best UCS with 31.9 MPa, meaning a 23.2% growth over the reference plug [[Appendix A](#)]. It is also evident from the **figure 5.29** that nano-modified OPC reinforced with 0.3g CF had continuous positive development over the 3 days, 7 days and 28 days of curing period. However, the sample with only 0.45g NPs had negative results after all of the curing periods, which is inexplicable because in UCS in TD-4 for the same dosage in room temperature was recorded to have relatively positive developments in strength [[section 5.5.1](#)].

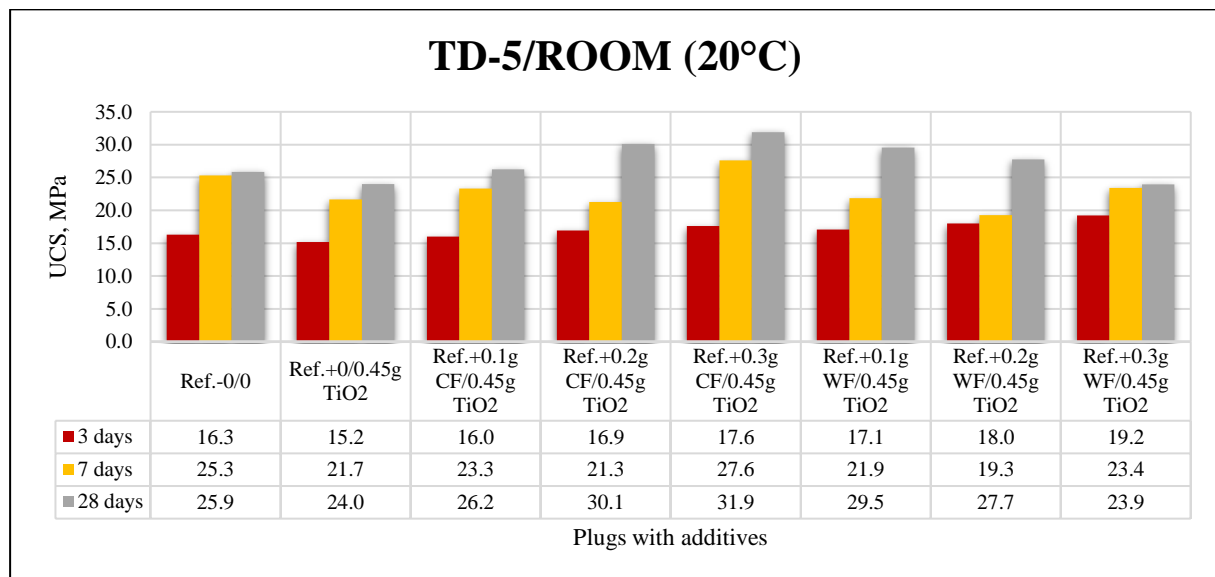


**Figure 5.29 UCS of TD-5 samples cured in room temperature**

For samples cured for 3 days at 20°C, the UCS data are quite reliable as visible in **table 5.8**. It is possible that if reproduced, the UCS trends of these plugs may remain the same. For 7 and 28 days batches, some plugs had very low SDs and some were found to have relatively high SDs. For instance, plug with binary blend of NPs and 0.1g WF had an SD of 7.9 MPa from



7 days batch, which is the highest in the batch. Additionally, from 28 days curing period, solitary NPs blend and binary 0.3g WF and NPs blend had respective SDs of 8.8 MPa and 7.1 MPa, which constitute potentially unreliable data. Conversely, if we consider the plug with binary blending of NPs and 0.3g CF having standard deviations of 1.2 MPa and 3.9 MPa from respectively 7 and 28 days, it can be accepted as very dependable and reproducible data. It is necessary to mention that neat OPC plugs for 7 days and 28 days curing periods had relatively high standard deviations.

**Table 5.8 Standard deviations (SD, MPa) for TD-5 samples in room temperature**

Curing age\ Plugs	Ref.-0/0	Ref.+0/0.45g TiO <sub>2</sub>	Ref.+0.1g CF/0.45g TiO <sub>2</sub>	Ref.+0.2g CF/0.45g TiO <sub>2</sub>	Ref.+0.3g CF/0.45g TiO <sub>2</sub>	Ref.+0.1g WF/0.45g TiO <sub>2</sub>	Ref.+0.2g WF/0.45g TiO <sub>2</sub>	Ref.+0.3g WF/0.45g TiO <sub>2</sub>
3 days	0.3	0.7	1.2	3.0	0.2	0.6	0.6	0.5
7 days	4.5	3.4	0.1	0.7	1.2	7.9	3.5	2.8
28 days	4.5	8.8	2.3	2.2	3.9	2.5	2.2	7.1

UCS variations for the oven-cured samples in TD-5 are presented in *figure 5.30*. It can be observed that samples after being cured for 3 days at 80°C had mostly positive early strength development. However, for 7 days batch, most samples with solitary and binary blends saw vast reduction in strength compared to their reference and where there were some improvements in UCS, the margins were relatively small. In a very different picture, all but one sample cured in oven for 28 days had huge improvements over their reference. Among the samples, binary blending of titanium NPs and 0.3g CF reinforced OPC had the highest progression in UCS, which is 30.8 MPa carrying an increase by 41.7% as compared to the OPC reference [[Appendix A](#)]. Additionally, carbon fibers and NP added OPC plugs performed distinctly better than the WF reinforced cement plugs after 28 days in an oven, as can be seen from *figure 5.30*.

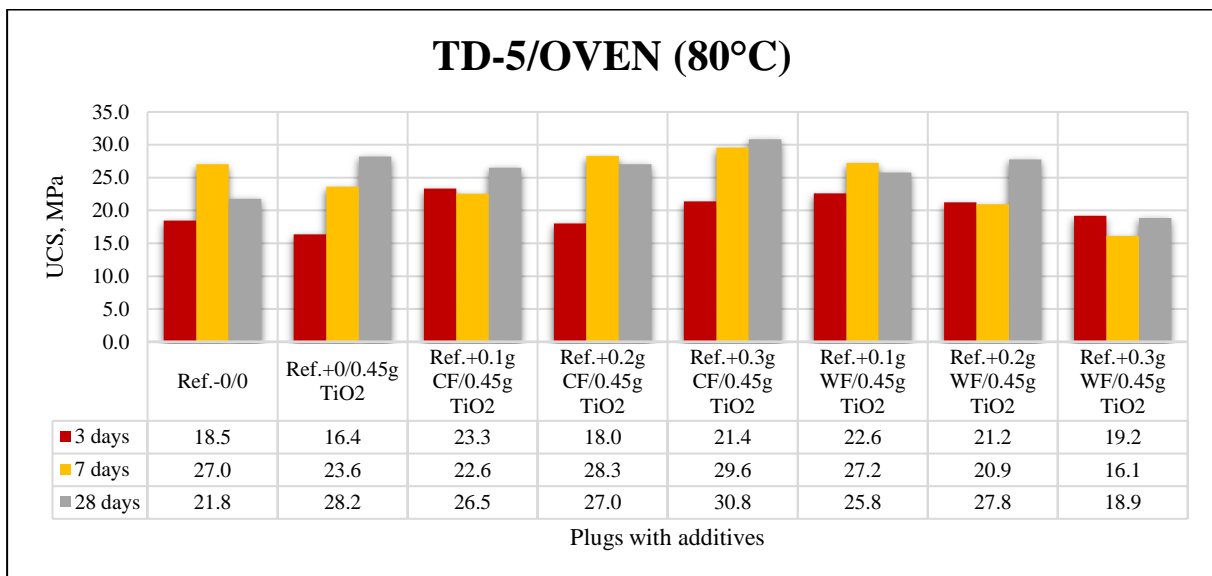


**Figure 5.30 UCS of TD-5 samples cured in oven temperature**

Furthermore, reinforcing 0.45g TiO<sub>2</sub> nano-modified OPC with CF have shown very positive improvement in both curing environments over the neat OPC and solitary NPs addition to OPC, which had been the intention when 0.45g dosage was chosen after showing optimistic development of the OPC properties in TD-4 [[section 5.5](#)].

Data reliability and quality of the oven-cured samples in TD-5 are discussed with the analyses of standard deviations in **table 5.9**, where it is observed that SDs for most samples from 3 days and 28 days have comparatively reproducible data. Contrarily, the variations in SDs among the plugs from 7 days happen to be some the highest across the whole curing environment, i.e., 0.3g CF and 0.1g WF with NPs have 6.8 MPa and 9.3 MPa standard deviations, rendering the data slightly irreplicable. It should be considered that the binary blend of NPs and 0.3g CF in OPC was found to be best performing plug in 7 days batch notwithstanding the relatively large SD and the situation had repeated in the 28 days batch as well.

**Table 5.9 Standard deviations (SD, MPa) for TD-5 samples in oven temperature**

Curing age\ Plugs	Ref.-0/0	Ref.+0/0.45g TiO <sub>2</sub>	Ref.+0.1g CF/0.45g TiO <sub>2</sub>	Ref.+0.2g CF/0.45g TiO <sub>2</sub>	Ref.+0.3g CF/0.45g TiO <sub>2</sub>	Ref.+0.1g WF/0.45g TiO <sub>2</sub>	Ref.+0.2g WF/0.45g TiO <sub>2</sub>	Ref.+0.3g WF/0.45g TiO <sub>2</sub>
3 days	4.8	1.6	0.3	2.5	1.9	1.2	1.9	1.0
7 days	3.6	1.6	3.0	2.0	6.8	9.3	1.0	3.9
28 days	2.1	0.8	0.1	0.8	5.4	3.7	0.7	6.2

From the observations made above in UCS development, it can be alluded that the addition of CF including with the constant dosage of 0.45g NPs have improved the UCS due to enhancement of the internal structure. When comparing the effects from the two curing environments, the elevated temperature presents a more realistic downhole environment. This makes it apparent from the results above that even after facing high temperature degradation for an extended period of time, 0.3g CF in combination with 0.45g TiO<sub>2</sub> NPs in OPC had shown the most encouraging results.

**5.6.2 Impact of TiO<sub>2</sub> NPs, CF and WF on Young’s modulus (E-modulus)**

**Figure 5.31** displays the E-moduli of the samples from TD-5, which were cured in room temperature. Due to the malfunctioning of the deformation sensor, E-modulus of the plug with

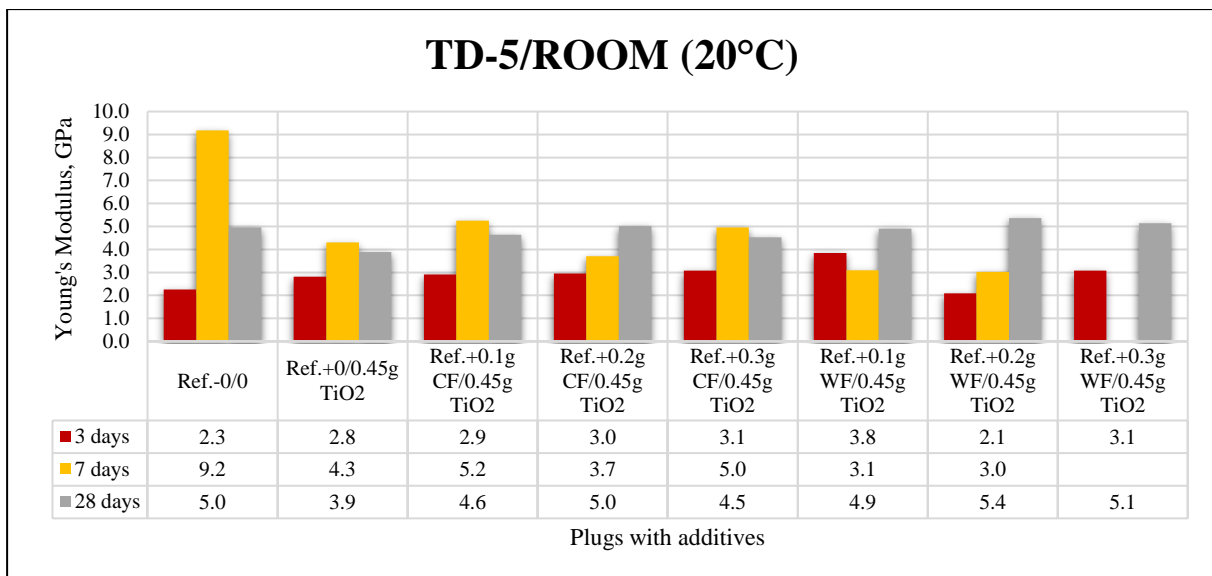


**Figure 5.31 Young’s moduli of TD-5 samples cured in room temperature**

binary blend of 0.3g WF and 0.45g nano-Ti from 7 days was found to be unrealistic, thus it was not included for discussion in the **figure 5.31**, however, for clarification, it was included in the **Appendix B**. Young’s moduli for samples after they were cured for 3 days were found to have higher stiffness than the reference plug. But surprisingly, all samples cured for 7 days in room temperature had much lower E-moduli than their base sample following the UCS trends for the same batch with varying scales. The plugs from 28 days batch had mixed results, where most plugs were less stiff than the reference sample, binary combinations of NPs with 0.2g CF, 0.2g WF and 0.3g WF managed to obtain stiffness higher than the neat OPC, in percentile changes the E-moduli are 1%, 8% and 3.5% [**Appendix A**].

When focusing on E-moduli data from samples cured at 80°C for 3, 7 and 28 days in TD-5, we can observe that most samples’ stiffness improved frequently as compared to their respective references, as depicted in **figure 5.32**. The stiffest samples after 3 days and 7 days are correspondingly binary blends of 0.3g WF and 0.3g CF with nano-Ti having particularly 4.8 GPa (97.7% increase) and 10.7 GPa (101.8% increase) [**Appendix A**]. All except one sample after 28 days developed significantly higher stiffness in comparison with the reference sample. Plug with solitary addition of nano-Ti with 6.6 GPa and 69.6% raise was the stiffest and on other hand, 0.2g WF with NPs had the worst stiffness with 3.7 GPa and 5.3% reduction compared reference [**Appendix A**].

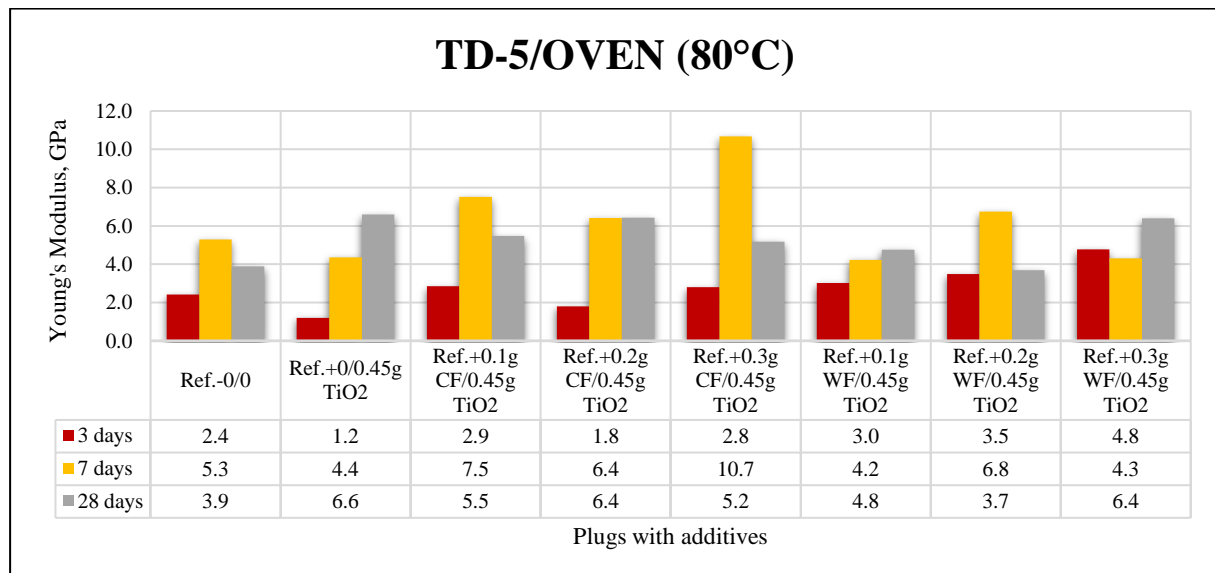


**Figure 5.32 Young’s moduli of TD-5 samples cured in oven temperature**

Evidently, no clear trends were observed in **figure 5.32**. However, E-moduli improvements are noteworthy, if compared to the E-moduli data from room temperature batch. Since, Young’s modulus is a mechanical property that can be influence by temperature, these developments can be explained as the effects of elevated temperature.

### 5.6.3 Impact of TiO<sub>2</sub> NPs, CF and WF on resilience (R)

Figure 5.33 shows the resilience results obtained from room-cured samples in TD-5. The resilience data for 0.3g WF with NPs from 7 days is absent due to the same reason, which was illuminated in section 5.6.2 and for further clarification, it is recommended to refer to Appendix B, which contains the load vs deformation diagrams. All the samples from 3 days batch had suffered negative effects in resilience with varying magnitudes. Although, majority of the samples from 7 days and 28 days had positive developments in resilience compared to their respective references. From both these batches, plugs reinforced with 0.3g CF and 0.45g TiO<sub>2</sub> NPs were recorded as the most resilient plugs with 122.1 kJ/m<sup>3</sup> and 208 kJ/m<sup>3</sup> respectively, interpreting them into 60.5% and 91% increment compared to their particular references [Appendix A]. One possible way these improvements can be explained is the assistance of CF and NPs to reduce pore spaces and increase bonding with to help OPC absorb more energy prior to fail. Lower stiffness of these particular plugs also supports this notion as elaborated in section 5.6.2.

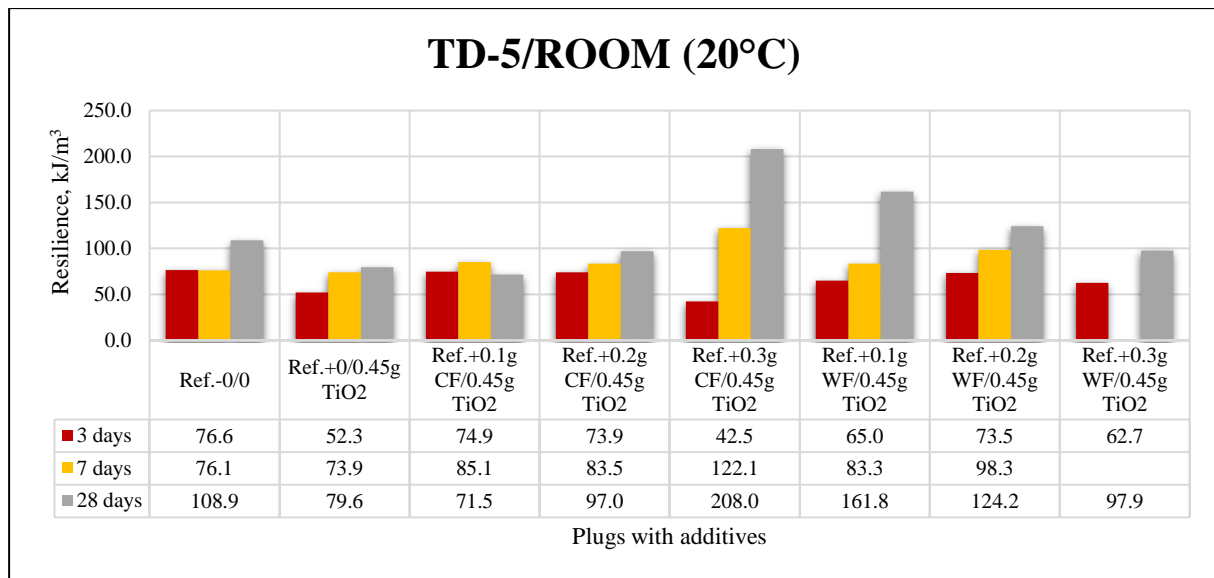


Figure 5.33 Resilience of TD-5 samples cured in room temperature

Elevated temperature of 80°C in oven denotes the second curing environment in TD-5, where the samples were cured for 3, 7 and 28 days and the obtained resilience results are displayed in figure 5.34. It is visible that no clear trends can be noticed here and the values fluctuate a lot. Astonishingly, absolute majority of the samples across all three curing periods suffered some of the most significant reduction in resilience when compared to neat OPC. Few samples managed to absorb more energy than their specific references. For instance, from the 28 days batch, plug with binary blend of NPs and 0.2g WF in OPC had the most resilience with 183.7 kJ/m<sup>3</sup>, which meant the resilience increased by 28.2% compared to the reference.

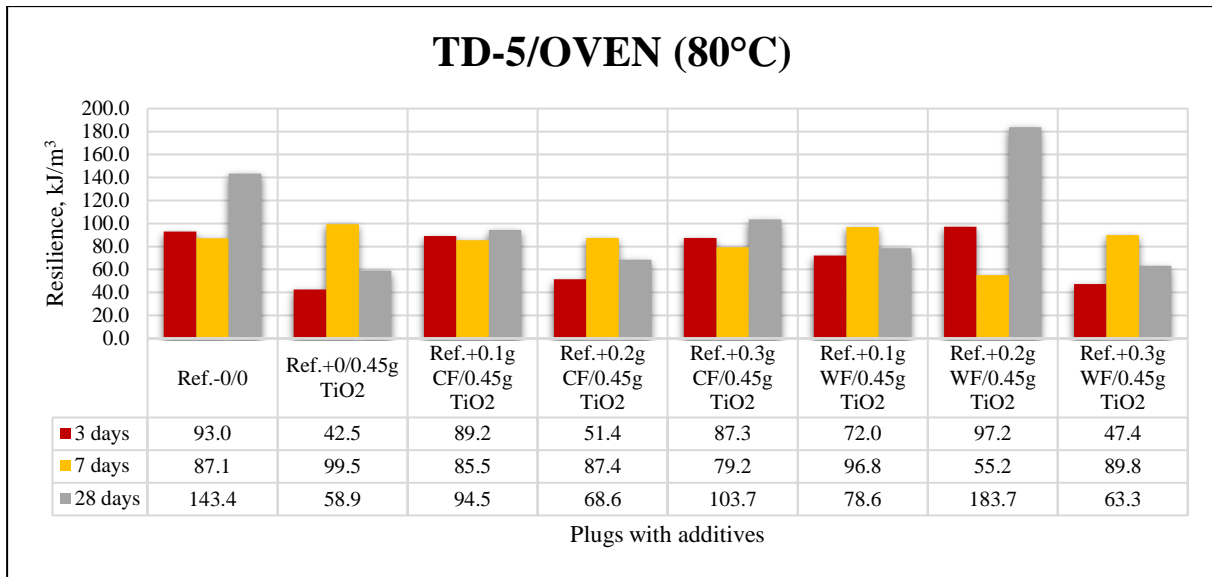


Figure 5.34 Resilience of TD-5 samples cured in oven temperature

#### 5.6.4 Impact of TiO<sub>2</sub> NPs, CF and WF on P-wave modulus (M modulus)

Compressional wave modulus results obtained from TD-5 samples cured in room temperature are presented in *figure 5.35*. It is observed that all the samples after 3 days of curing showed positive development in their elasticity. Moreover, samples from 7 days and 28 days have shown M-moduli development in contrasting directions, where samples from 7 days had generally negative results compared to their reference and complete 28 days batch had shown higher M-moduli enhancement than their base. Naturally, the best performing additions varied by curing periods. Binary blend of NPs with 0.3g WF from 3 and 7 days was the best performing additive in OPC with 15 GPa (15.1% raise) and 21.6 GPa (7.5% increment), while from 28 days, binary blend of NPs and 0.2g CF had been the best with 18.9 GPa (8.8% increase) [[Appendix A](#)].

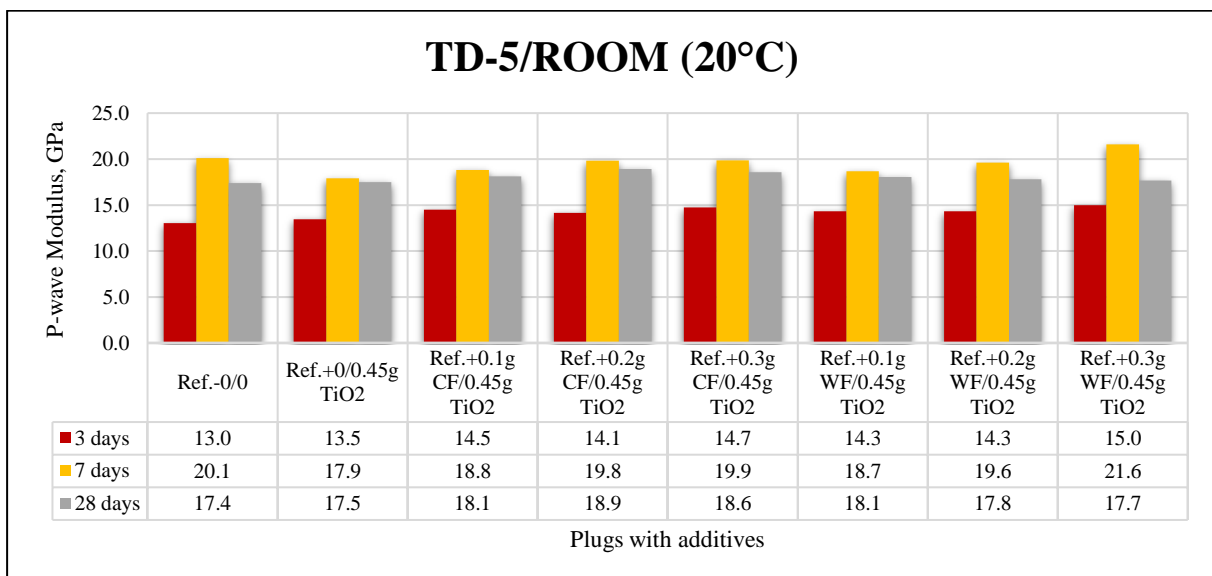
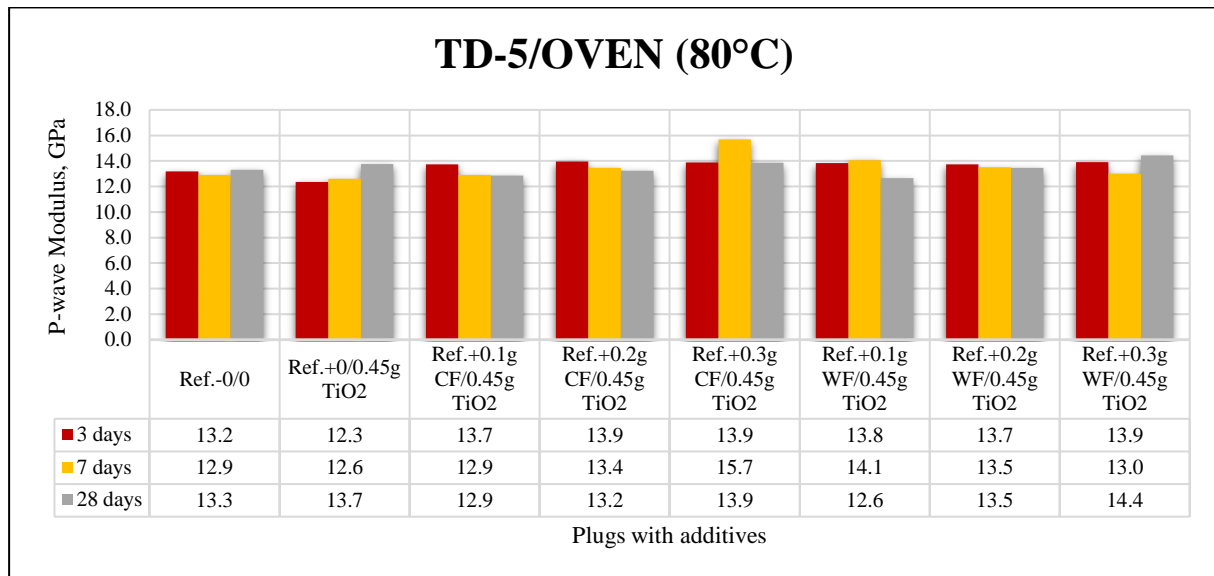


Figure 5.35 P-wave moduli of TD-5 samples cured in room temperature

M-moduli for oven-cured samples from TD-5 are shown in **figure 5.36**, the elasticity of the samples does not differentiate greatly. However, it is noteworthy that just like the previous curing environments, here as well not a single concentration family performed consistently over all three curing ages resulting in different concentration family being the best in different curing period. Such that, binary blend of NPs and 0.2g CF with 13.9 GPa (5.8% increase) from 3 days, plug with 0.3g CF and nano-Ti having 15.7 GPa (21.5% raise) from 7 days and titanium nano-modified OPC reinforced with 0.3g WF gaining 14.4 GPa (8.5% growth) from 28 days are the concentration families that had most elasticity performance [[Appendix A](#)].



**Figure 5.36 P-wave moduli of TD-5 samples cured in oven temperature**

UCS and M-modulus being a function of the compressional wave velocity, their testing mechanisms are different, the former being the destructive and the latter non-destructive. As a result, most of the time M-modulus follows the trend that of UCS, albeit not without a few ambiguities. In this design as well, there exist a few anomalies to the norm, which is the parallel trend of UCS and M-moduli. As the sound propagates through the nonhomogeneous medium of the cement samples, it faces different densities and microstructures, as this has been explained to be the likely cause for the existences of anomalies including surface defects of cement plugs.

### 5.7 Rheology of the nano-systems

Rheology is of the utmost importance because a significant quantity of fluid transfer is involved in the petroleum business. This gives information crucial for determining the flow and deformation of flowing materials. Rheological characteristics will assist in the planning and carrying out the primary cement job during the well construction, where it is crucial to do it correctly on the first effort. If one is familiar with the rheological characteristics of a cement slurry, one will be better equipped to calculate the necessary pump pressure and rate for pumping the cement slurry downhole. In addition, rheology helps estimate the frictional pressure present in the wellbore during the process of pumping cement downhole, and it contributes to the optimization of the cement slurry placement.

For further characterization, we tested rheological parameters of the cementitious and non-cementitious materials with nanoparticles. The nano-systems that performed best in UCS testing after being cured in an oven at 80°C for 28 days were chosen for rheological testing, except for geopolymer test design. Two OPC batches acquired on two different occasions from the provider based on necessity, which also impacted the classifications. Reasons behind this choice was described in [section 5.1](#). The selected nano-systems are given below in *table 5.10*.

**Table 5.10 Selected nano-systems and their references for rheology testing**

Samples	Test design	Test batch	OPC batch
Reference (neat OPC G-class)	TD-1	TB-3-O	OPC-1
1.2g Al <sub>2</sub> O <sub>3</sub>	TD-1	TB-3-O	OPC-1
Geopolymer reference	TD-3	TB-7	n/a
Geopolymer reference + 0.4g TiO <sub>2</sub>	TD-3	TB-7	n/a
Reference (neat OPC G-class)	TD-4,5	TB-10,13-0	OPC-2
0.45g TiO <sub>2</sub>	TD-4	TB-10-O	OPC-2
0.3g CF / 0.45g TiO <sub>2</sub>	TD-5	TD-13-O	OPC-2

As it can be seen in *table 5.10*, no nano-system has been chosen from TD-2. This is because of no additive systems showing positive development compared to their references.

Rheological modelling is done according to Casson model as stated in [section 4.1.2.4.2](#), which is often used by the cement industry to determine the rheological characteristics of cement. As mentioned there, the data were recorded at 300, 200, 100, 60, 30, 6 and 3 RPM, which translate into the following shear rate ( $\gamma$ ,  $\text{sce}^{-1}$ ) respectively: 510.9, 340.6, 170.3, 102.2, 51.1, 10.2 and 5.1  $\text{sce}^{-1}$ . The shear rates are constant for all the rheological tests.

### 5.7.1 Ordinary Portland cement batch 1

Figure 5.37 shows the measured shear stress ( $\tau$ ) of the samples taken from TD-1. It is noticeable that the nano-system has relatively higher shear stress in low shear rates than the reference sample. Although the opposite happens when the shear rate is the highest at 510.9  $\text{sec}^{-1}$ . At 340.6  $\text{sec}^{-1}$ , the shear stress for both samples is same, which is 98.2  $\text{lb}_f/100 \text{ft}^2$ .

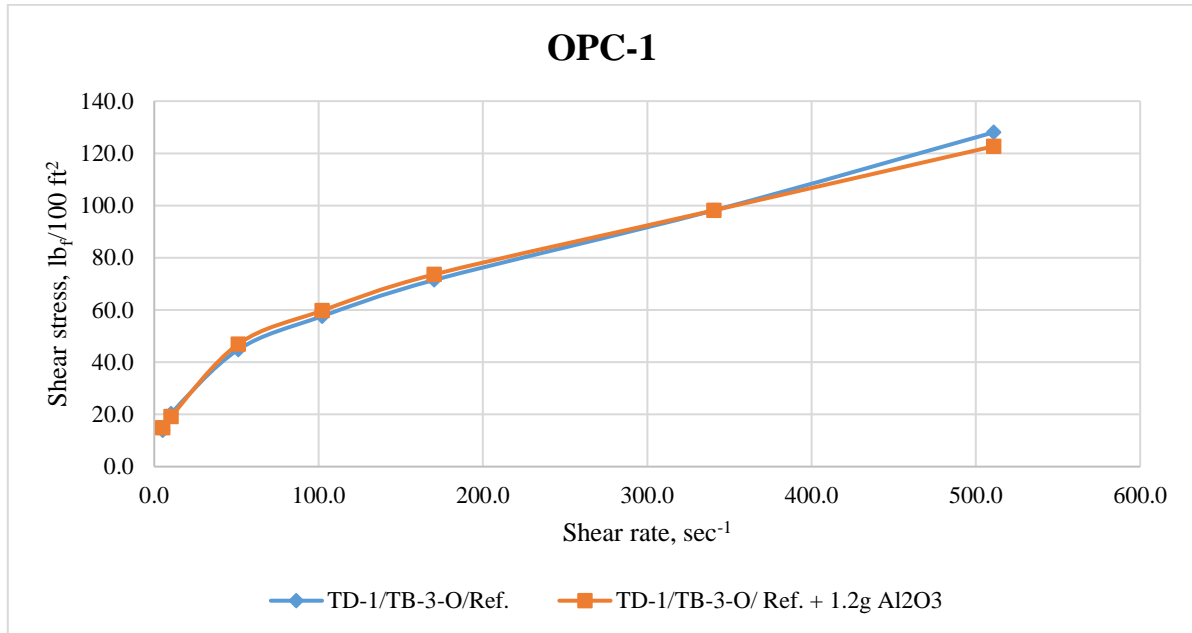


Figure 5.37 Shear stress of the tested cement slurries of OPC-1

Additionally, table 5.11 presents the Casson yield stress and plastic viscosity. It can be observed that nano-system has higher yield stress compared the reference system, which means the nano-system slurry will require more force to start flowing. In practice, this implies that in order to pump the slurry downhole, high pump pressure will be required. On the other hand, the nanoparticles induced slurry's PV is decreased in comparison to the OPC slurry. In oilfield applications, it means the flow of slurry in pipes will have low friction making it efficiently pumpable. Low viscosity slurry might also improve the place of cement in the narrow annuli [123].

Table 5.11 Casson yield stress (YS,  $\tau_c$ ) and plastic viscosity (PV,  $\mu_c$ )

Parameters	TD-1/TB-3-O/Ref.	TD-1/TB-3-O/ Ref. + 1.2g $\text{Al}_2\text{O}_3$
Yield stress ( $\tau_c$ , $\text{lb}_f/100 \text{ft}^2$ )	12.61	13.63
Plastic viscosity ( $\mu_c$ , $\text{lb}_f \text{sec}/100 \text{ft}^2$ )	0.13	0.12



### 5.7.2 Geopolymer test design

The addition of TiO<sub>2</sub> in geopolymer based cement made it highly viscous. **Table 5.12** presents the viscometer reading for the geopolymer slurries. We can see that both slurries have impractical high Fann readings at very low RPM. This alludes to unpumpable slurries. This is why modelling was not done with geopolymer slurries measured data.

**Table 5.12** Viscometer readings for Geopolymer slurries

Slurry \ RPM	300	200	100	60	30	6	3
	Measured Fann data						
Geopolymer Reference	–	–	–	245	125	27	16
Geopolymer Reference + 0.4g TiO <sub>2</sub>	–	–	–	234	126	28	17

### 5.7.3 Ordinary Portland cement batch 2

In this section, slurries made with the second batch of Portland cement will be discussed. In **figure 5.38** is presented rheological test data of slurries from TD-4 and 5 having only one reference slurry. Addition of only TiO<sub>2</sub> with OPC had a very recognizable low shear stress compared to its reference slurry and the binary hybrid slurry, as well. In contrast, slurry with binary hybrid of titanium NPs and CF had a gradual increase in shear stress having the highest value compared to other slurries. It is noticeable that the reference slurry had relatively larger shear stress at most of the recorded shear rates but at the highest shear rate it was surpassed by the slurry with CF and NPs blending.

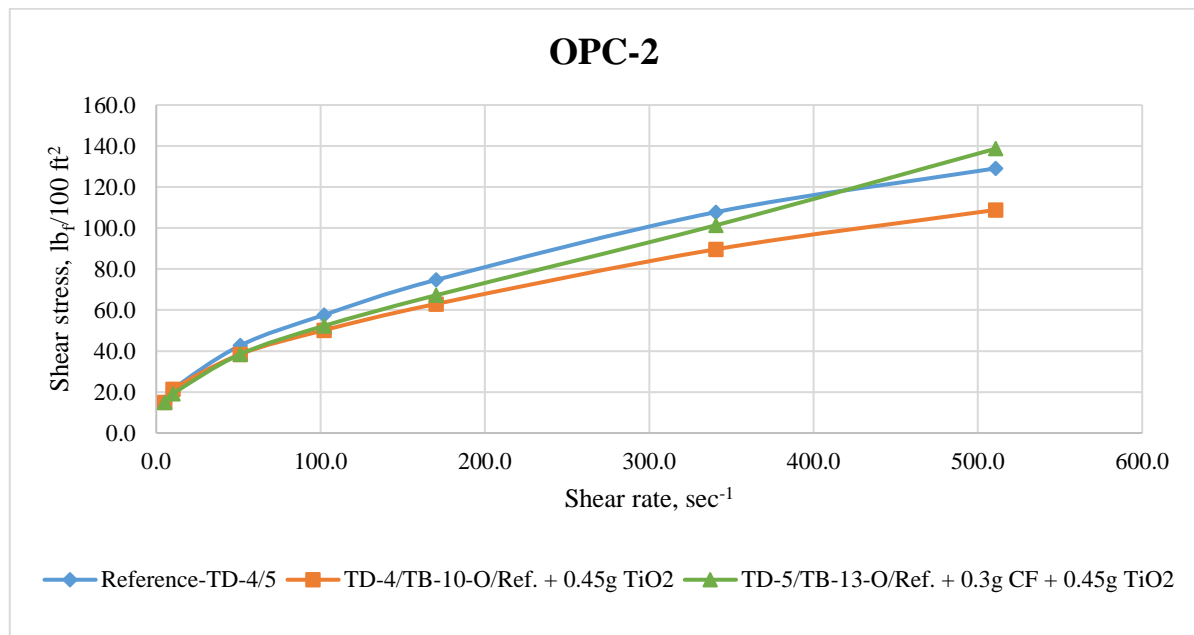


**Figure 5.38** Shear stress of the tested cement slurries of OPC-2

Casson YS found from the analysis of the viscometer data show that solitary blend of titanium NPs have largest YS compared to all the other slurries making it slurry which would require more force to start flowing, however this slurry is the least viscous of all three slurries making it the most pumpable comparatively, as presented in **table 5.13**. The hybrid binary blend

of NPs and CF in cement has the exact opposite characteristics than the solitary NPs blend. It means that while having lowest YS, this slurry is most viscous compared to other slurries. In real life application in oil and gas wells, it indicates that low pump pressure could be sufficient to commence flowing the slurry downhole and at the same time it could be beneficial in hole cleaning.

**Table 5.13 Casson yield stress ( $\tau_c$ ) and plastic viscosity ( $\mu_c$ )**

<b>Parameters</b>	<b>Reference-TD-4/5</b>	<b>TD-4/TB-10-O/Ref. + 0.45 TiO<sub>2</sub></b>	<b>TD-5/TB-13-O/Ref. + 0.3g CF + 0.45g TiO<sub>2</sub></b>
Yield stress ( $\tau_c$ , lb <sub>f</sub> /100 ft <sup>2</sup> )	12.76	13.23	10.45
Plastic viscosity ( $\mu_c$ , lb <sub>f</sub> ·sec/100 ft <sup>2</sup> )	0.13	0.10	0.14

From the figures above, it is discernable that there are no clear trends YS and PV. The results are not fully conclusive as sometimes it is preferable to have a highly viscous slurry for i.e., hole cleaning and cutting transport, while sometimes it is recommended to pump low viscosity slurry for convenient for its pumpability.

It is crucial to remember that these rheological criteria cannot, on their own, tell us whether a cement slurry is suitable for a particular well operation. To obtain a comprehensive perspective, running well simulations using the rheological parameters determined earlier is necessary. This will allow one to learn about all the challenges involved. In this thesis, this task was not performed.

## 5.8 SEM and EDS analyses

In this section, we are going to shed some light on the microstructures for some of the cement samples. The SEM and EDS analyses processes were discussed comprehensively in [section 4.1.1.5](#).

The SEM-analysis provides very high-resolution images of the surface of a material (better than 1mm) whilst the EDS-analysis provides an element content analysis for a specific point. The aim with these analyses was to analyze the internal structure of the cement slurry and how nanoparticles are deposited in the pore structure and how they are distributed in cement [124].

Titanium nanoparticles used in this thesis are in the range of 5nm - 15nm in size. The chosen samples are from TD-3 and TD-4/Oven (80°C)/7days. The samples were collected after they were crushed in destructive tests. They were chosen on the basis of availability and their UCS strength. Plugs with nano additions were accompanied with their respective references. They are listed below:

- TD-3: Geopolymer Reference; UCS of 22.6 MPa
- TD-3: Geopolymer Ref. + 0.4g TiO<sub>2</sub>; UCS of 32 MPa
  
- TD-4/Oven (80°C)/7days: Reference; UCS of 25 MPa
- TD-4/Oven (80°C)/7days: Ref. + 0.25g TiO<sub>2</sub>; UCS of 28.4 MPa

Ideally, the cement plugs chosen from OPC batch should be from 28 days and oven-cured. However, at the time of test, we were not able to keep the samples due to unforeseen events and human error. The reason for choosing geopolymer plugs are due to their potentiality of being an alternative to OPC because studying the internal structure is vital to improve the geopolymer properties.

### 5.8.1 SEM and EDS analyses for TD-3 samples

SEM images at the magnification of 2000 times for (a) Geopolymer Reference and (b) Geopolymer Ref. + 0.4g TiO<sub>2</sub> NPs are shown in [figure 5.39](#). At first glance, the surfaces very much look like “the surface of the moon”.

As shown, both geopolymers contain a lot of unreacted fly ash as well as a lot of bubbles that had been generated during geopolymerization process. Moreover, we can observe cracks that pass through the air bubbles and along the grain boundaries.

The more unreacted fly ash reduces the degrees of the geopolymerization and hence they do not contribute on the mechanical strength of the geopolymer. However, taking a closer look at the structures around the unreacted fly ash, we can observe gel structures and needle-like structures in the TiO<sub>2</sub> blended geopolymer. For instance, if we consider the fly as in red circles, the shape of unreacted fly ash is not a spherical ball shape, but deformed and structure at the top and at the bolt.

For a brief elemental analyses for both samples, EDS results are shown in [figure 5.41](#). By comparing the two results, we have the evidence of titanium’s presence in one of the samples, albeit the peak is not very high. Additionally, it can be observed that the reference sample and the plug with NPs are showing the elements used in creating the geopolymer plugs. It should be denoted that EDS results are not representative of the whole sample, because the dispersion of elements is not always homogeneous.

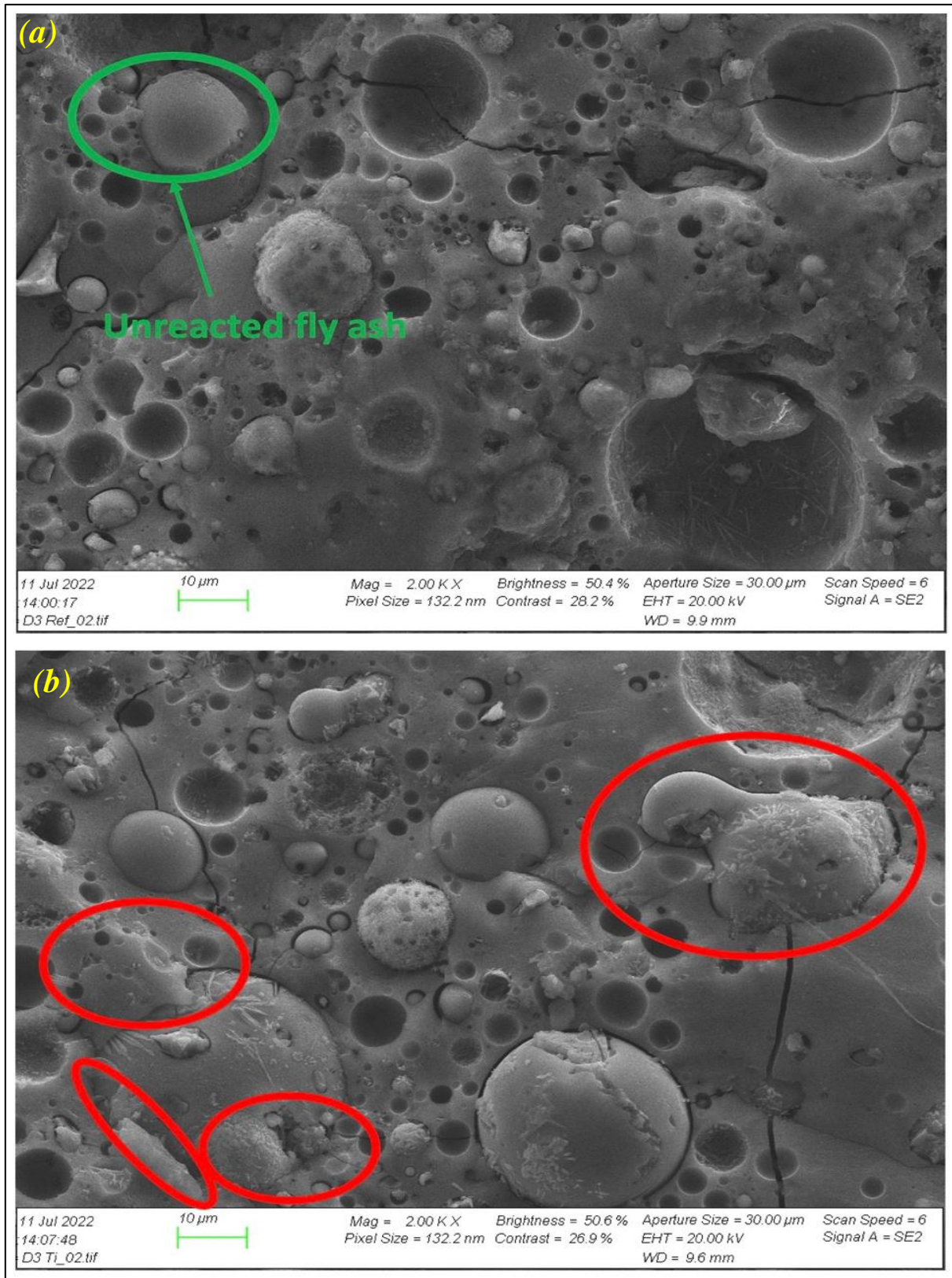
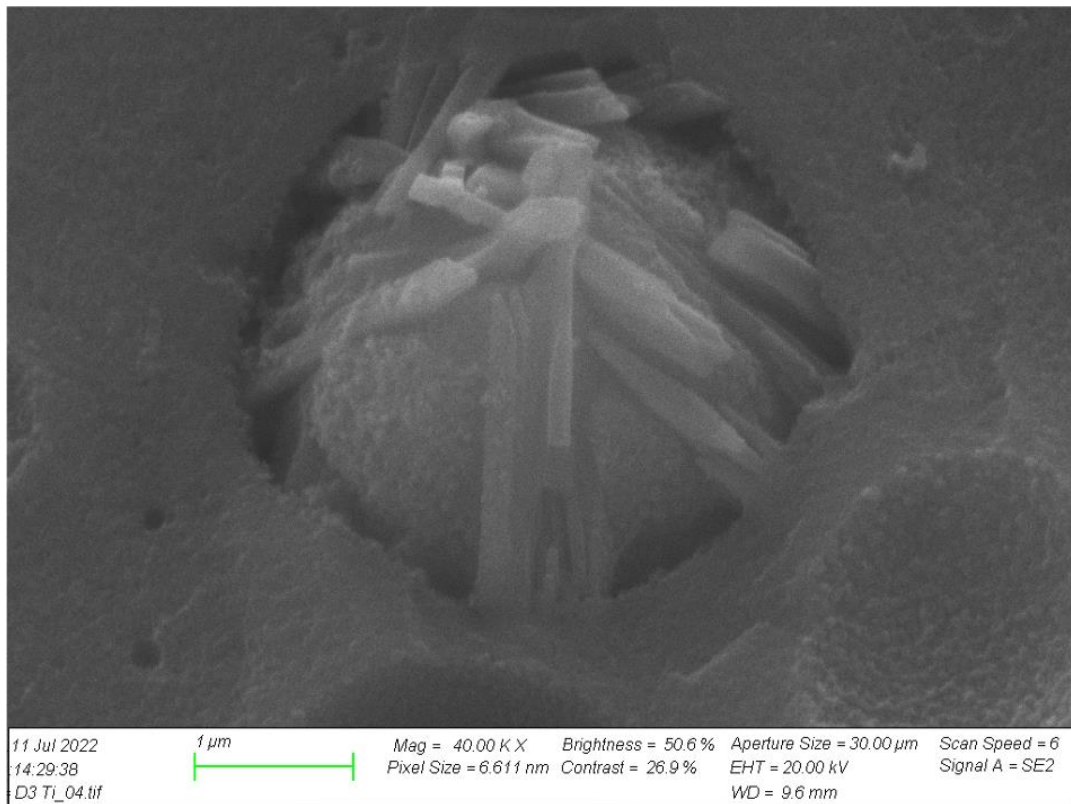


Figure 5.39 SEM images of (a) Geopolymer Reference; (b) Geopolymer Ref. + 0.4g TiO<sub>2</sub> NPs

To have a clear picture of the crystal needles, the “geopolymer reference + 0.4g TiO<sub>2</sub>” sample was further magnified with 40000 times. As shown in **figure 5.40**, several needles are crystallized around the sphere. Structurally, the formation of crystals around the free unreacted fly ash allows enforcing the structure as well as fills the gaps in the geopolymers.



**Figure 5.40 SEM image of crystalized TiO<sub>2</sub> nanoparticles in geopolymer cement**

To summarize, in terms of pore structures, unreacted fly ash and cracks, both geopolymers (with and without TiO<sub>2</sub>) showed all these at the considered SEM analysis points. However, by visual inspection, one can observe the different structures of the unreacted fly ashes and the formation of crystals in TiO<sub>2</sub> blended geopolymer. The presence of crystals around the unreacted fly ash and in the system in general could be the reason for the higher uniaxial strength development as reported in [section 5.4.1](#). Furthermore, the addition of titanium nanoparticles seemed to improve the reduction in pore structure, which could increase the impermeability of the geopolymer cement.

Moreover, one can also interpret that TiO<sub>2</sub> enhance the gelation in geopolymers as also could be observed in neat G-class cement in the next section. However, the degree of gelation is not a linear function of the TiO<sub>2</sub> concentration. The optimum concentration that provides a higher mechanical strength is determined through experimental works. For instance, for the considered TiO<sub>2</sub> concentrations, the 0.4g was found out to be the optimum. In addition, the size of NPs used in this thesis might be appropriate to use in conjunction with geopolymer cement.

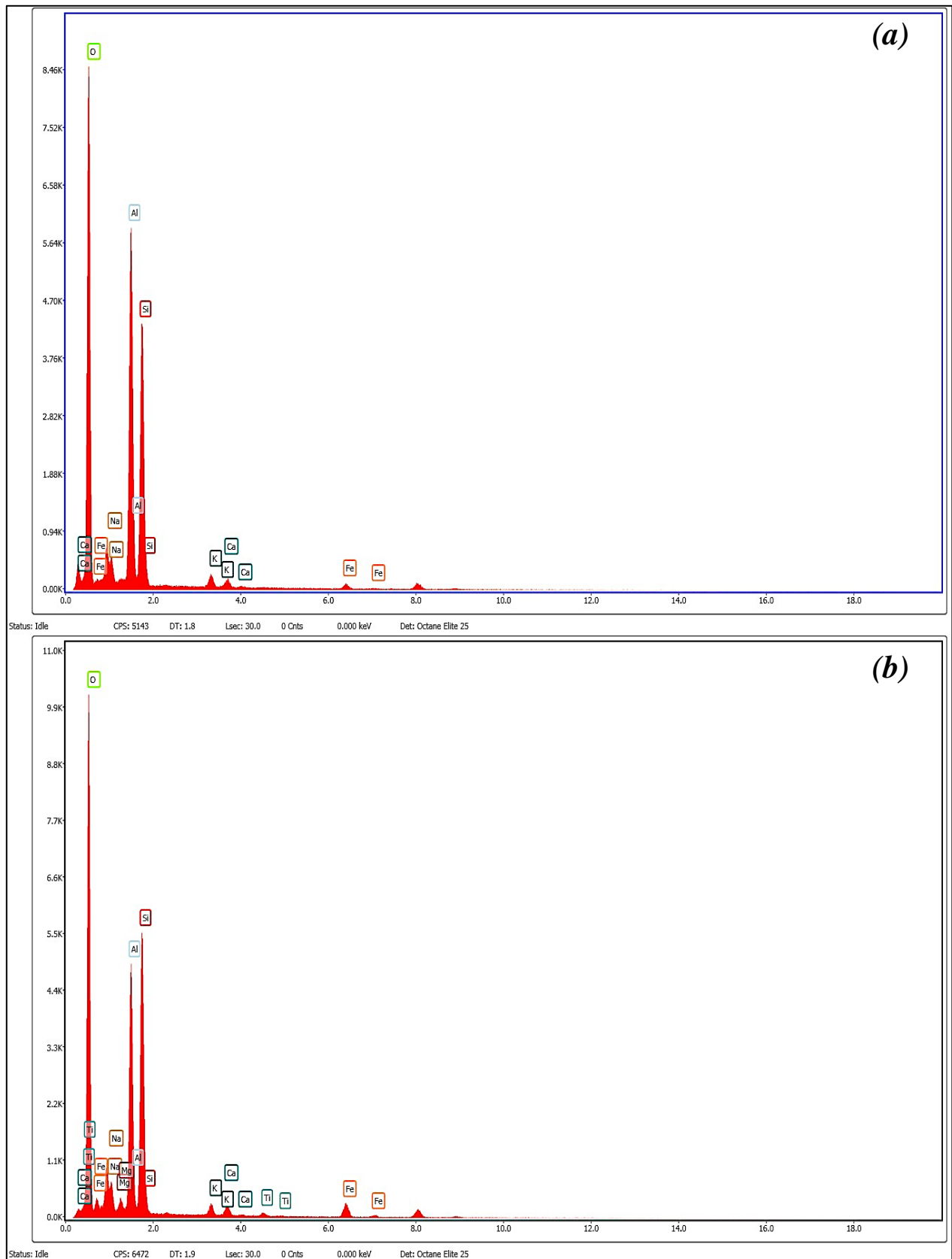
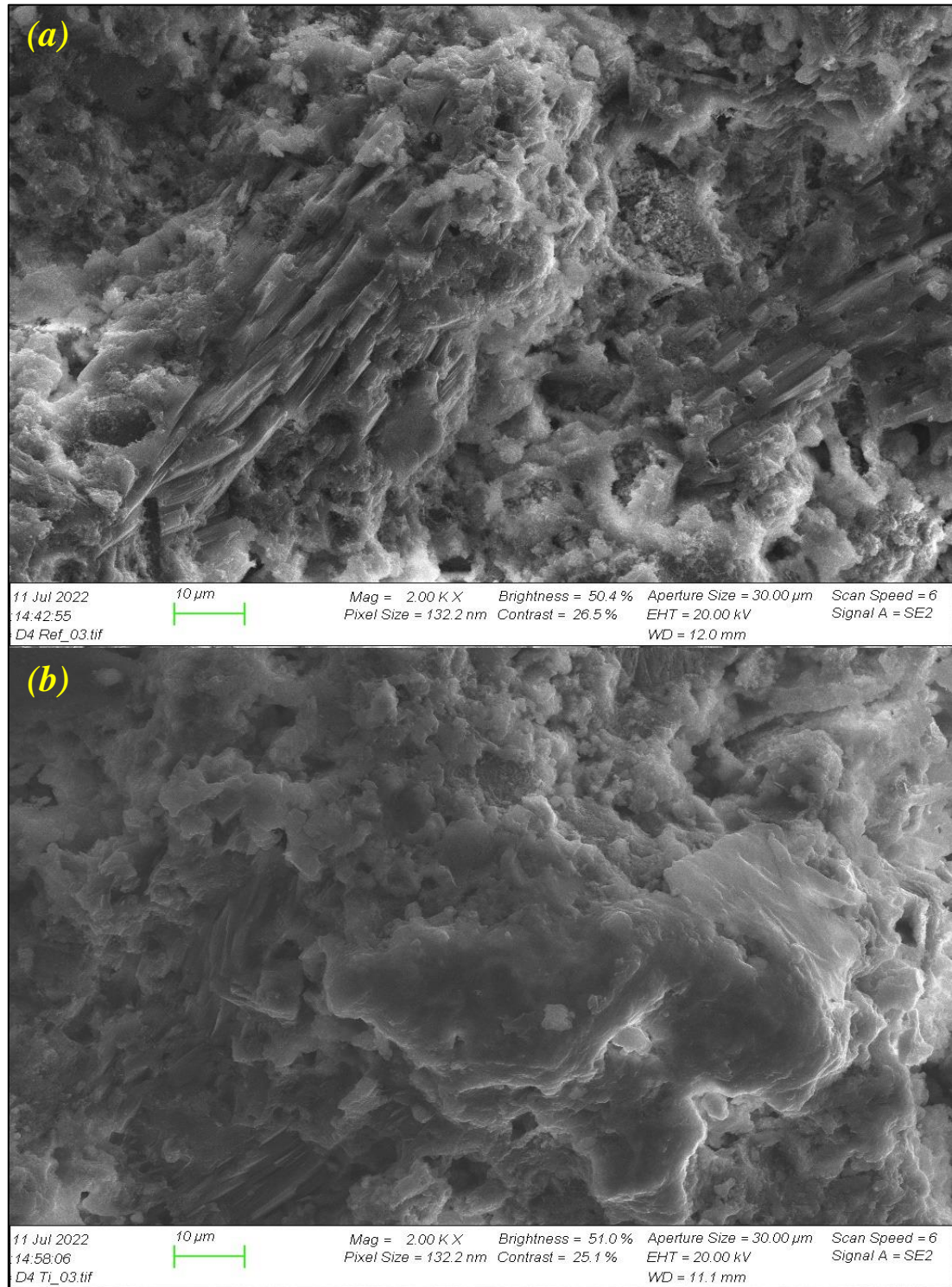


Figure 5.41 EDS results of (a) Geopolymer Reference; (b) Geopolymer Ref. + 0.4g TiO<sub>2</sub> NPs

### 5.8.2 SEM and EDS analyses for TD-4 samples

Samples collected from TD-4 are (a) Reference and (b) Ref. + 0.25g TiO<sub>2</sub> NPs. SEM images taken at the magnification of 2000 times are shown in **figure 5.42**. It should be mentioned that experiments were conducted on OPC with nanoparticles.



**Figure 5.42 SEM images of (a) Reference and (b) Ref. + 0.25g TiO<sub>2</sub> NPs**

As shown in **figure 5.42 (a)**, the reference sample, neat OPC, did not interact very well with the elevated temperature of 80°C, thus showing a very uneven surface, alike dry wax. In other words, the internal structure is not homogeneous. As a result, visibly, neat cement is not showing compact regions with pore spaces.

On the other hand, **figure 5.42 (b)** displays a very compact surface on the sample containing titanium NPs. It exhibits gelled structures, where the microstructures are looked to be fused together compactly. One can decide that under elevated temperatures, nano-Ti performs well in bonding strongly with OPC to reduce pore spaces to improve strength and impermeability. In [section 5.5.1](#), it is observed that oven-cured plugs with 0.25g titania still performed better than the respected reference plug. With this fact, one can be led to believe that internal structure after 28 days at 80°C would potentially look alike. Although, the 0.25g dosage was not the best performing addition in 28 days batch, this could be logical to assume that the best performing sample, which is 0.45g TiO<sub>2</sub>, would have relatively the same topography and bonding features.

In the following **figure 5.43**, the EDS results for localized points on the aforementioned samples will be displayed. The presence of titanium in the nano-added samples supports the strength improvement discussed in [section 5.5.1](#) and the apparent compact internal structure. The low peak is congruent with the relatively low dosage of nano-Ti in **figure 5.43 (b)**.

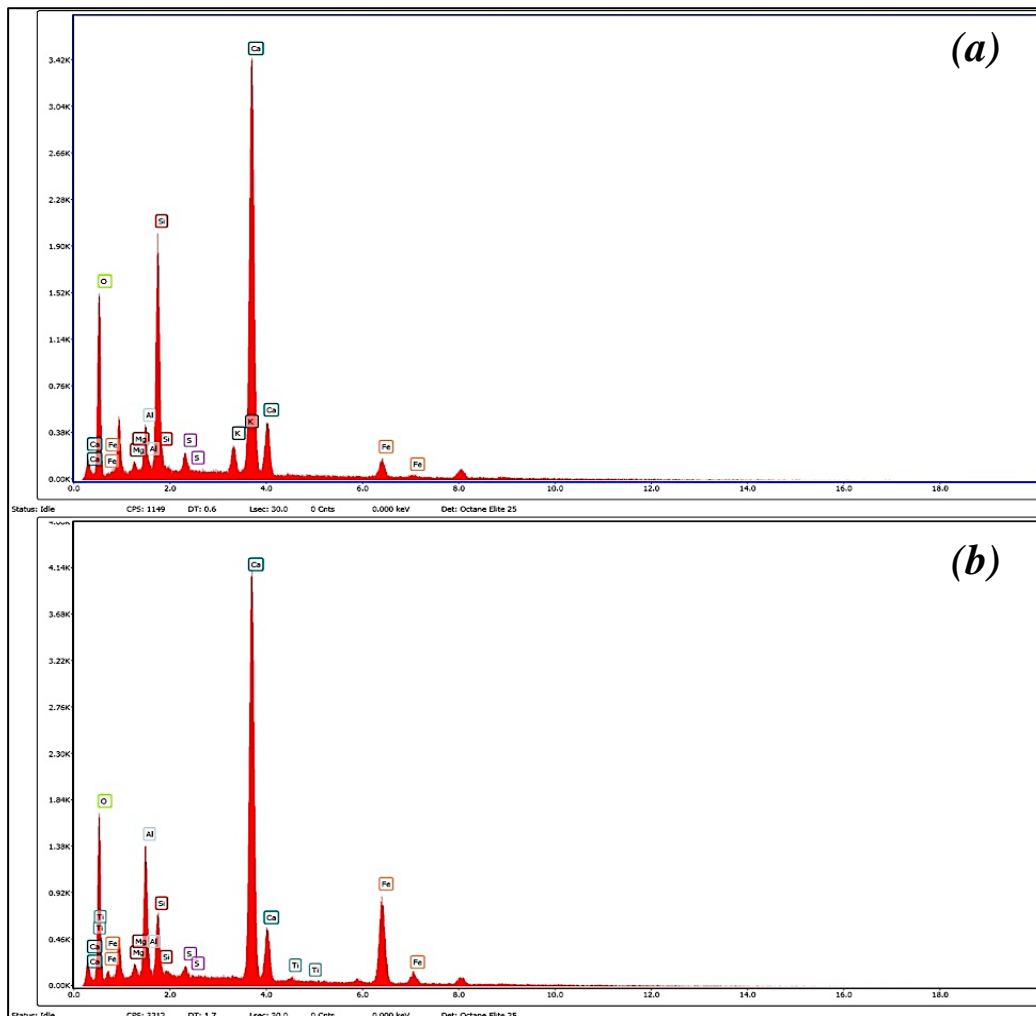


**Figure 5.43 EDS results of (a) Reference and (b) Ref. + 0.25g TiO<sub>2</sub> NPs**



In order to have even closer inspection of the internal structure, an SEM image of the nano-added sample was taken at 6000 times magnification. The glued together structure of the sample is shown in *figure 5.44*.

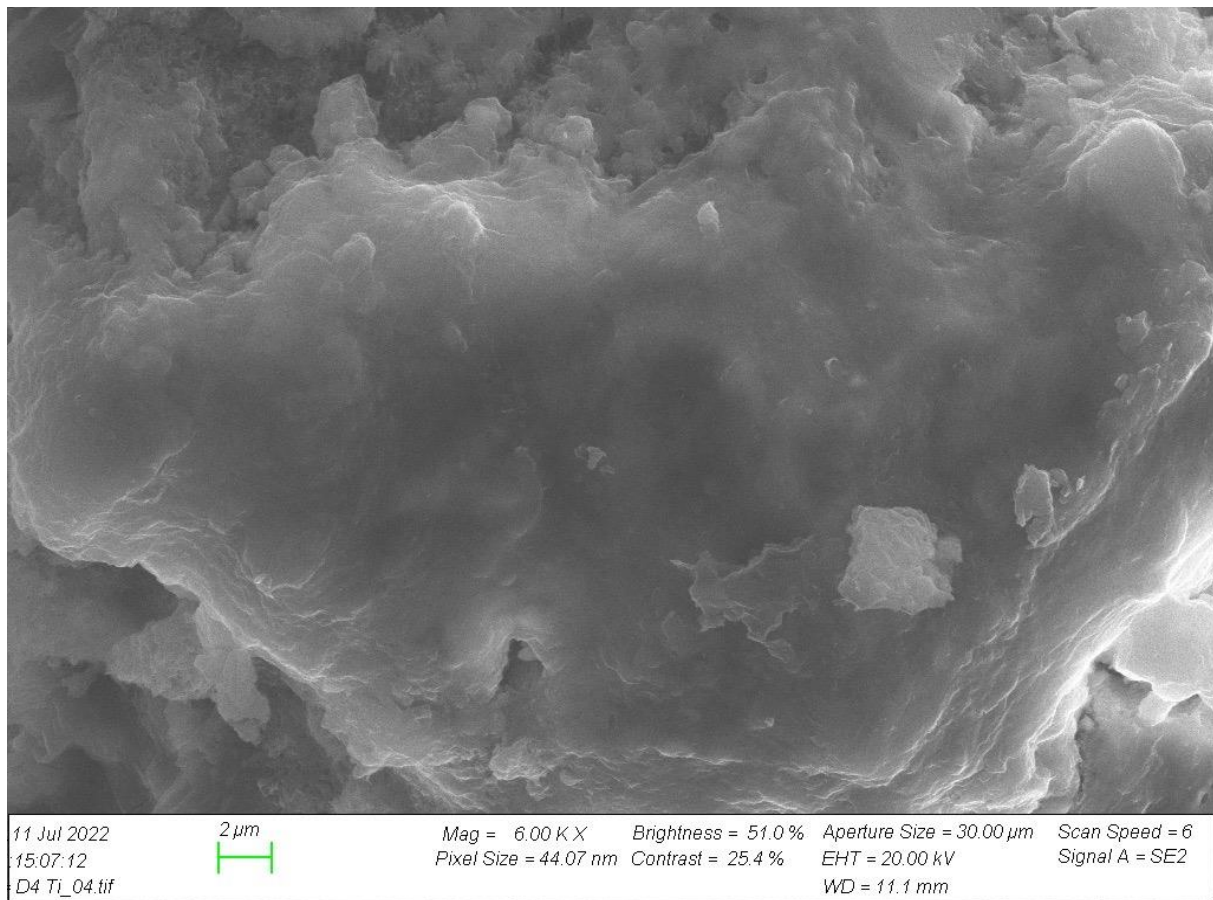


*Figure 5.44 TiO<sub>2</sub> NPs fused OPC sample*

In summary, we can attest that the SEM analysis results indicated that the selected TiO<sub>2</sub> concentration enhanced gel structure in the cement, hence it increased the cement bonding. As a result, the improved internal structure could be the reason for the higher mechanical strength of the nano-reinforced sample. Opposite can be said for the neat OPC sample, as it did not show a highly coherent internal structure.

One can also deduce that the improved internal structure allows to enhance the petrophysical properties such that decrease porosity and permeability as well. These might also be helped in achieving due to NPs size, which could also reduce water absorption and possible shrinkage of OPC improving well integrity.

## **5.9 Uncertainties and challenges**

In the following, we are going to elucidate on some of the potential uncertainties and challenges faced during the experimental phase, which have influenced the test results significantly.

- **Laboratory apparatus:** Various petroleum companies and research organizations supported most of the literature sources utilized in this thesis with substantial financial means. Being a student with no such economic resources, we had to rely on improvisations and over-used equipment, i.e., customized hand-operated shop press to conduct destructive tests instead of an automated compression test apparatus. Due to the hydraulic press being operated manually, sometimes it posed challenges in maintaining constant loading on cement samples.
- **Malfunctioning apparatus:** The hydraulic press used in thesis was fitted with a deformation sensor to measure deformations. There have been quite a few incidences, where it did not record data correctly. This issue proved to be quite challenging as we had to be extra careful when experiments were carried out. It is possible that due to being heavily-used regularly led to this uncertainty.
- **Materials' age:** Another uncertainty that we faced during that might potentially have impacted the test results are how old a certain material was and how long their potential exposure to surrounding was. For example, the cement used in thesis did not have a manufacturing date mentioned, although it was confirmed to be the right kind.
- **Cement slurry synthesis:** All slurries were made using the same techniques and blended by hand with laboratory spoons. Unfortunately, it was noticed while mixing the ingredients that the slurries include air bubbles, which might influence the compressive strength of the hardened plugs. The slurry was repeatedly tapped lightly onto a level surface when pouring the cement to avoid multiple phases in the plugs. It is questionable whether all air bubbles were eliminated by tapping or if it helped to make more homogenous mediums. In addition, it is unknown if the cement powder was entirely dissolved while mixing. There may have been tiny cement lumps in a few samples.
- **Dispersion of nanoparticles and fibers:** Usually in the literature, NPs and fibers are dispersed with ultrasonic dispersion methods to distribute these materials. However, nanoparticles and fibers were dispersed by stirring with hands as evenly as possible. It is debatable, whether these elements are distributed evenly in the cement slurries.
- **Testing preparation for cured plugs:** After the curing periods, cement plugs were polished with sandpaper for various tests. The polishing was done with hands and flatness was checked with a spirit level to avoid point-loading while UCS test. Although, it has been done with great care and focus, there are always some uncertainties about how well they polished. It would certainly increase the possibility of having frequent flat surfaces, if a mechanical device were to be used. Additionally, while taking the plugs out of the plastic moulds, they would stick to inside of the moulds and extra force was applied to get them out, which could initiate some post-curing defects on the surface of the plugs.

- **Repetitions of experiments:** To acquire the most precise findings possible, it is necessary to conduct tests numerous times to assure consistency. Due to time and materials restrictions, two plugs per additive dose were developed. This was done to utilize the mean of the two plugs as the final result. More samples should have been collected to guarantee the most accurate findings. In addition, sensor malfunctioning or human mistakes in measuring deformations caused some findings to be recorded as a single value rather than the average of two. Although this was uncommon, one should endeavour to generate further examples if time and finances permit.
- **Human fallibilities:** Human beings carried out all the experimental and testing activities. As regrettable as it may seem, all of us are susceptible to making mistakes, thus, there is always the risk that human errors might impact the studies. Namely in TD-2, detailed load and deformation data had not been able to be recorded for two of the samples due to a momentary lapse in focus.

## 6 Empirical UCS Modelling

In this chapter, a new model will be developed and tested for UCS estimation. This model will bear a resemblance to Horsrud's (2001) model [121], which was introduced in [section 4.2.1](#). As mentioned before, this model was developed from shale (sedimentary rocks) and this is why the model may not be fully compatible with cementitious materials. Therefore, the model will be examined against actual measured UCS and the newly developed model as well. Nerhus's (2020) [78] and Titlestad's (2021) [79] empirical UCS models will also be studied here.

### 6.1 Development of a new model

To estimate UCS without conducting destructive tests, a new model has been developed utilizing the data acquired in the experimental phases of this thesis. This model was developed from the compressional wave velocities calculated from the ultrasonic measurements of the cement plugs to estimate UCS, which is comparable to Horsrud's model. The detailed discussion on ultrasonic measurements were completed in [section 4.1.2.3](#). The newly designed model is shown in [figure 6.1](#) with the datapoints used in the development of the model.

$$UCS = 5.4857 \cdot v_p^{1.2239} \quad [Equation 6.1]$$

The model can be described fairly convincingly with power law function as seen in [figure 6.1](#), where the coefficient of determination ( $R^2$  value) is 0.9114, which means the data correspond to the regression model very well.

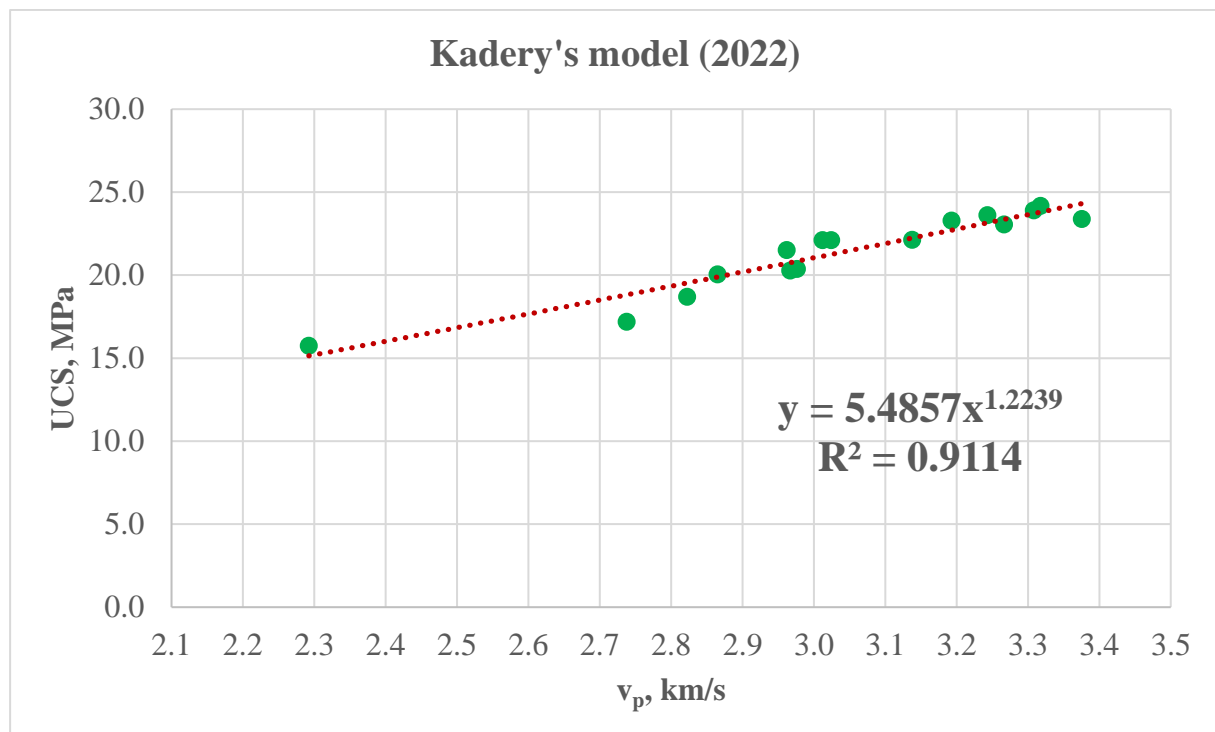


Figure 6.1 Newly developed UCS–v<sub>p</sub> model

## 6.2 Testing of the new model

Testing is an important part of developing a model. It can tell us how it compares with existing models and also with direct experimental data. To test the model from *equation 6.1*, Nerhus's (2020) [78] and Titlestad's (2021) [79] experimental data and their models [section 4.2] will be used, along with Horsrud's (2001) model [121] and unused data in modelling from this thesis. This is to see not only how the models fair against one another, but also to see how the actual UCS experimental data match the three respective models.

### ➤ Model testing with Kadery's (2022) measured dataset

In *figure 6.3*, first testing batch is shown, four models' estimations are displayed against Kadery's (2022) actual UCS data. Model developed in this thesis captures the experimental data better than rest of the models. In this batch, Horsrud's model [121] always underestimated the actual UCS, however by small margins. In contrast, Titlestad [79] and Nerhus [78] reported that when testing their respective models, Horsrud's model [121] overestimated the actual UCS by large margins in both cases. On the other hand, in most cases Titlestad's and Nerhus's underestimated the measured UCS by rather large margins.

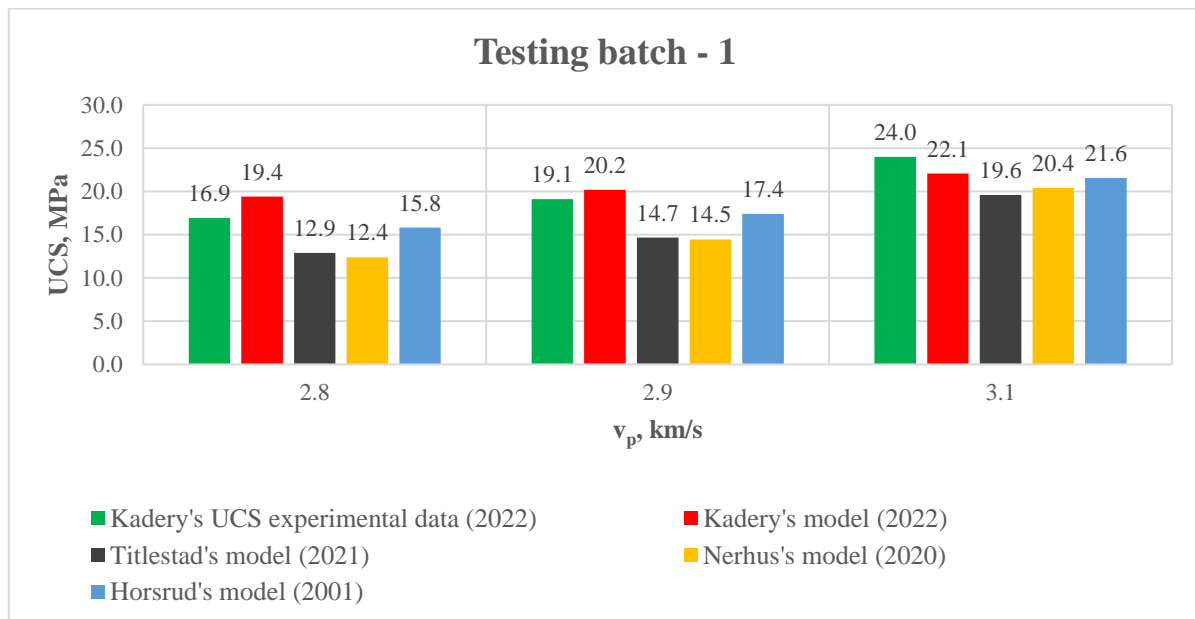


*Figure 6.2 Kadery's UCS experimental data (2022) vs models' estimations*

### ➤ Model testing with Titlestad's (2021) measured dataset

Second testing batch, *figure 6.3*, presents Titlestad's (2021) experimental UCS data with all the models. As expected, Titlestad's own model performed very well in comparison to the actual UCS data. Seemingly, Kadery's model (2022) performed well enough to estimate the actual UCS to acceptable range. Noticeably, Nerhus's model and Horsrud's model [121] overestimated UCS in all of the cases. Titlestad (2021) reported the same types of occurrences for Horsrud's model in his report, albeit in higher amount [79].

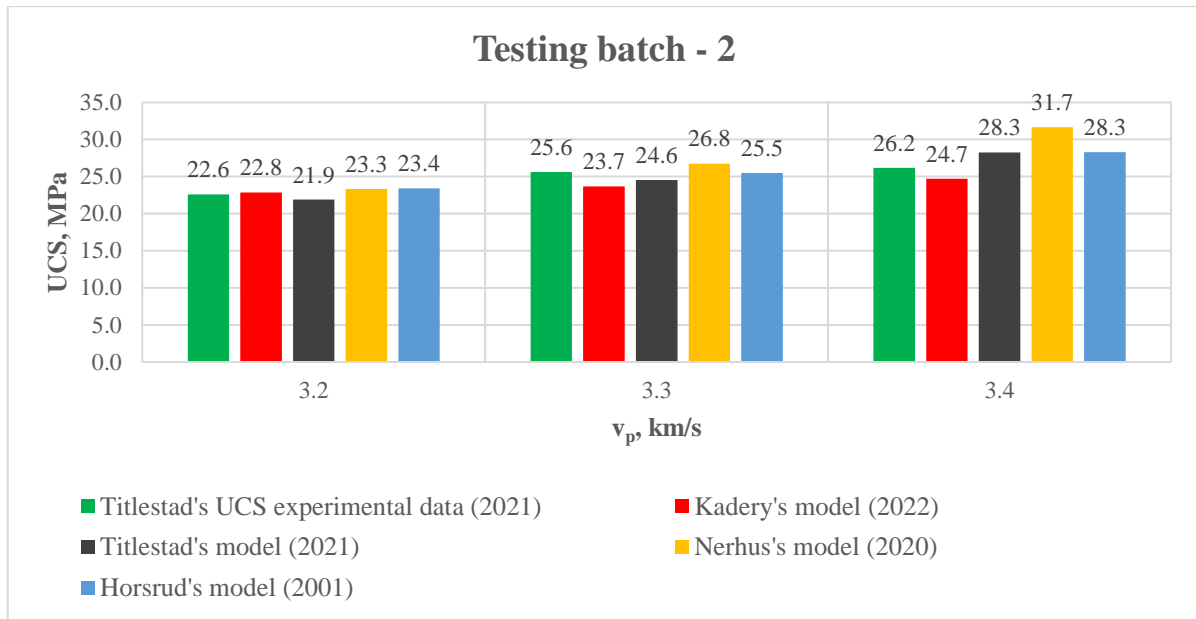


Figure 6.3 Titlestad’s UCS experimental data (2021) vs models’ estimations

➤ Model testing with Nerhus’s (2020) measured dataset

When testing Kadery’s model (2022) with Nerhus’s (2020) UCS experimental data, **figure 6.4**, it is observed that the new model performed reasonably accurately in estimating the actual UCS data, along with Nerhus’s own model, which is expected. It is also apparent that Titlestad’s [79] and Horsrus’s model [121] have also estimated the UCS comparatively well. Although, it was reported by Nerhus, that Horsrud’s model overestimated the UCS by large margins, which can be described as contradictory to what was found in **figure 6.4** [78].

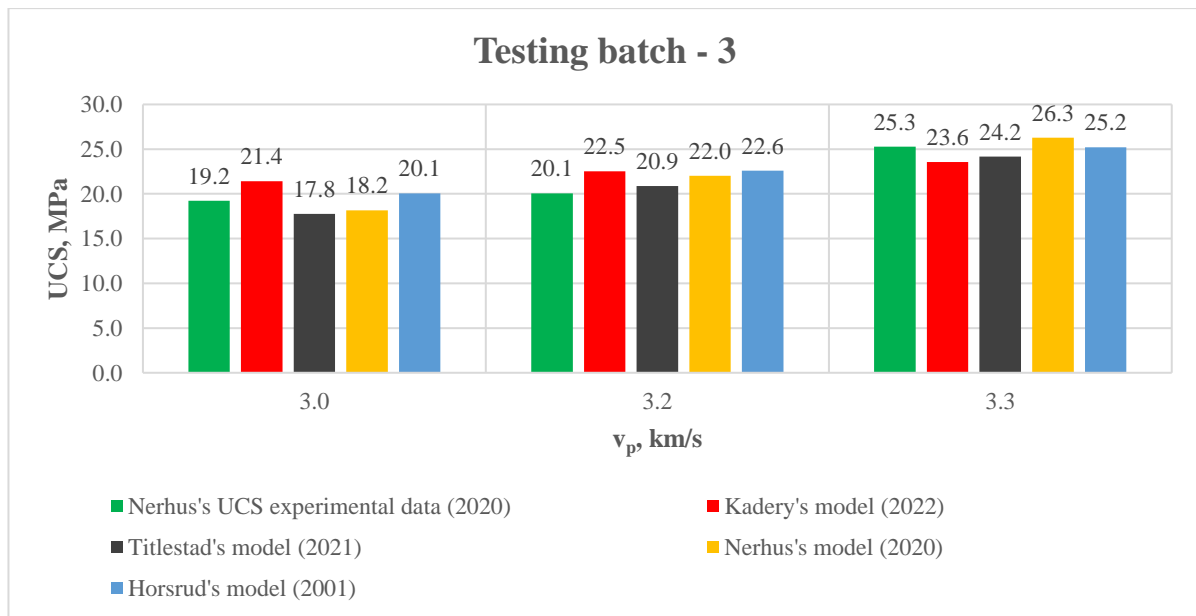


Figure 6.4 Nerhus’s UCS experimental data (2020) vs models’ estimations

The summary from the above discussion is that the model developed in this thesis is more reliable and fitting than Horsrud's model [121] when performing modelling of UCS data from cementitious materials. It is noteworthy that the three models developed from cement samples have a trend of estimating the UCS to the actual UCS value more closely in the majority of the cases. Finally, from all the testing batches above, we can see that the newly developed model had better estimations of the UCS, even when tested with three different sets of experimental UCS data, making it a reliable model for future comparisons.

## 7 Summary and Conclusions

Five experimental test designs were created to study the impact of Al<sub>2</sub>O<sub>3</sub> and TiO<sub>2</sub> nanoparticles on cementitious and non-cementitious material in room temperature of 20°C and at 80°C in an oven. This chapter will summarize the experimental results based on the results obtained from the UCS tests of the samples from every test design and their subsequent test batches. Precisely, the compressive strength developments will be reflected comprehensively with their respective percentile changes in the *table 7.1*, where positive values will indicate strength enhancement and negative values denote strength reduction compared to reference. The reason for selecting the UCS metrics as the markers of efficiency of the cement samples is because the UCS results are more reliable being the direct output of destructive tests.

**Table 7.1 Summary of the experimental results based on UCS developments**

TDs	TBs	Additives			Curing age	Room temperature, 20°C				Oven temperature, 80°C			
						Best dosage of additives, g	Neat Reference UCS, MPa	Best Additives-modified Reference UCS, MPa	Percentile changes against Reference, %	Best dosage of additives, g	Neat Reference UCS, MPa	Best Additives-modified Reference UCS, MPa	Percentile changes against Reference, %
TD-1	TB-1	Al <sub>2</sub> O <sub>3</sub>			3 days	1.4g Al <sub>2</sub> O <sub>3</sub>	18.7	18.0	-3.7	1.6g Al <sub>2</sub> O <sub>3</sub>	20.6	22.0	7.1
	TB-2				7 days	1.6g Al <sub>2</sub> O <sub>3</sub>	29.4	22.1	-24.7	1.6g Al <sub>2</sub> O <sub>3</sub>	22.8	21.8	-4.6
	TB-3				28 days	1.2g Al <sub>2</sub> O <sub>3</sub>	13.9	27.8	100.1	1.2g Al <sub>2</sub> O <sub>3</sub>	20.1	25.0	24.8
TD-2	TB-4	Al <sub>2</sub> O <sub>3</sub> + FA	FA	3 days	1.4g Al <sub>2</sub> O <sub>3</sub> + 1g FA	19.3	20.4	5.8	3g FA	18.7	22.5	20.7	
	TB-5			7 days	3g FA	23.9	24.9	4.1	2g FA	18.0	25.8	43.3	
	TB-6			28 days	1.4g Al <sub>2</sub> O <sub>3</sub> + 2g FA	26.3	32.5	23.6	1g FA	28.9	26.1	-9.7	
TD-3*	TB-7*	TiO <sub>2</sub>			10 days	0.4g TiO <sub>2</sub>	22.6	32.0	41.8	n/a			
TD-4	TB-8	TiO <sub>2</sub>			3 days	0.45g TiO <sub>2</sub>	16.2	16.8	3.4	0.25g TiO <sub>2</sub>	19.1	22.7	18.7
	TB-9				7 days	0.15g TiO <sub>2</sub>	17.6	26.4	49.9	0.25g TiO <sub>2</sub>	25.0	28.4	13.3
	TB-10				28 days	0.15g TiO <sub>2</sub>	21.5	25.6	19.2	0.45g TiO <sub>2</sub>	19.8	28.2	42.1
TD-5	TB-11	TiO <sub>2</sub>	TiO <sub>2</sub> + CF	TiO <sub>2</sub> + WF	3 days	0.45g TiO <sub>2</sub> + 0.3g WF	16.3	19.2	17.8	0.45g TiO <sub>2</sub> + 0.1g CF	18.5	23.3	26.3
	TB-12				7 days	0.45g TiO <sub>2</sub> + 0.3g CF	25.3	27.6	9.1	0.45g TiO <sub>2</sub> + 0.3g CF	27.0	29.6	9.4
	TB-13				28 days	0.45g TiO <sub>2</sub> + 0.3g CF	25.9	31.9	23.2	0.45g TiO <sub>2</sub> + 0.3g CF	21.8	30.8	41.7

**NB.** TD-3\* — It has the same 8 plugs from the room temperature.



Since the completion of experimental works and the subsequent analyses of the experimental data, several observations and interpretations have been made concerning the performances of the samples. These accumulated observations will be outlined according to the characterization methods discussed in [chapter 4](#) and the test designs, where these methods were used in the following with some of their potential utilizations in the industries.

➤ **Test design 1 (Impact of Al<sub>2</sub>O<sub>3</sub> nanoparticles on OPC)**

- It has been observed that relatively lower concentration of 1.2g nano-Al performed gradually better in significantly increasing the UCS of 0.44 WCR OPC in both room temperature and at 80°C than the higher concentrations after 28 days, as shown in [section 5.2.1](#). Thus, showing that it could be used in cementing of both top and bottom sections of a wellbore. As the UCS is the direct results of destructive tests, it can be accepted the most reliable data among other obtained results.
- The E-moduli [[section 5.2.2](#)] and the resilience [[section 5.2.3](#)] did not show clear trends most of the time due to various uncertainties. The E-moduli and reliance of the plugs with 1.2g nano-Al had improved frequently after 28 days in both curing environments indicating stiff, strong and highly resilient samples in practice. Some analyses were incomplete because of data being absent from aforementioned reasons.
- The M-moduli data of the samples modified with nano-Al followed the UCS trends typically, as they are functions of compressive wave velocity. Albeit, few anomalies exist due to plugs' microstructural and surface irregularities, namely 1.2g aluminium modified OPC plug after 28 days at 80°C diverted from the UCS trend, as depicted in [section 5.2.4](#).
- In terms of rheological properties influenced by aluminium NPs, it was observed that 1.2g nano-Al had decreased shear stress of nano-modified OPC slurry with increasing shear rate, however the difference had been very small [[section 5.7.1](#)]. Additionally, it decreased viscosity of the OPC slurry compared to reference OPC making it a pumpable cement slurry increasing its workability for numerous applications, such as, narrow annuli cementing.

➤ **Test design 2 (Impact of Al<sub>2</sub>O<sub>3</sub> nanoparticles and fly ash on OPC)**

- From the UCS results obtained after samples were cured in room temperature for 3, 7 and 28 days, one can come to the possible conclusions that addition of FA with nano-Al of 1.4g could be used in the top sections of a wellbore or in construction activities, where these additions do face high temperature. Because, only FA solitary blend at 80°C had increased OPC's early strength of 3 and 7 days, but failed to do so after 28 days [[section 5.3.1](#)]. Hence, it is evident that high temperature poses a challenge to nano-Al when mixed with FA and OPC, however, it could be claimed that solitary FA might improve concrete strength if cured at elevated temperature for a short period.
- Samples' data analyses of E-modulus and resilience show no clear progression in accordance with UCS results as shown respectively in [section 5.3.2](#) and [section 5.3.3](#). However, it is apparent that the samples internal properties like E-moduli and resilience fared much better in room temperature than their counterparts in 80°C. The best performing samples in 20°C had positive development in these properties compared to oven-cured plugs, as mentioned in [table 7.1](#). It affirms the previously made remarks.

- P-wave moduli for the both curing environments partially follow the UCS trend. The temperature effects are very obvious from the 28 days results of both curing environments [[section 5.3.4](#)]. Most possibly due to being dried of humidity, oven-cured samples had complete positive results than that of room-cured plugs.
- No additives modified-OPC slurry was tested for rheological properties' development, because there were no additives of any dosage that showed an improvement in UCS over their neat references after 28 days of being cured in oven at 80°C. It is considered to be the more realistic downhole surroundings.

➤ **Test design 3 (Impact of TiO<sub>2</sub> nanoparticles on geopolymers cement)**

- The optimum concentration found to have increased the geopolymer cement strength was 0.4g nano-Ti. UCS had been increased by 41.8%. It was also observed that UCS development had a clear trend showing 0.4g TiO<sub>2</sub> to be the best dosage, where highest dosage of 0.5g nano-Ti had reduced UCS significantly [[section 5.4.1](#)]. Since geopolymer samples had been cured mainly in room temperature, it is unclear how they will perform under constant elevated temperatures. It can branch out for a future work the temperature effect on FA based geopolymer cement.
- In [section 5.4.2](#), the stiffness (E-moduli) of the geopolymer plugs had seen enormous reduction, which can be explained due to being more porous medium in nature than OPC plugs. Although, the resilience in [section 5.4.3](#) had been increased in unison with UCS by 48.2%, denoting the samples with higher capacity for deflecting loads before being crushed.
- M-moduli of the samples shown in [section 5.4.4](#) had conveyed the only positive results for plug with 0.4g TiO<sub>2</sub>. This also goes to show that 0.4g might be the optimal dosage for geopolymer with this LSR of 0.54.
- The 0.4g dosage did not perform very well in rheological testing. It made the base slurry so viscous that no practical information could be achieved. Therefore, further analyses were not done [[section 5.7.2](#)].
- SEM analyses were carried out for the 0.4g TiO<sub>2</sub> plug and the base. Although, these analyses sometimes do not represent the whole sample as they are done for few local points in the sample, still they can give us useful indications about the rest of the plug. From the SEM images, it could be seen a lot of unreacted FA that did not possibly contribute to strength build-up. Micro cracks were also noted in the sample. Rather importantly, nano-Ti had been seemed to be forming crystal around these unreacted FA, as well as filling the pore spaces [[section 5.8.1](#)]. These activities could spell out a possible decrease in porosity and permeability. It can be alluded that if the dispersion was made as homogeneous as possible, the potential better gel structure made by nano-Ti could increase UCS even more.

➤ **Test design 4 (Impact of TiO<sub>2</sub> nanoparticles on OPC)**

- The UCS build-up for OPC modified samples showed that 0.15g (19.2% increase) and 0.45g nano-Ti are the best concentrations for improving OPC's mechanical strength in low and high temperature respectively after an extended period of curing. It should be noted that 0.35g NPs addition generally did not have positive effects in either of the curing of the curing system [[section 5.5.1](#)]. From *table 7.1* one can easily see the possible applications of 0.15g nano-Ti in wellbore cementing of various top sections casings and the opposite goes for 0.45g nano-Ti, as it could increase the cement strength around production casings and liner.

- The E-moduli [[section 5.5.2](#)] and resilience [[section 5.5.3](#)] of the samples modified with titanium nanoparticles did not present clear trends. Although, most dosages with best UCS results shown in *table 7.1* had positive developments in both of these properties.
- The P-wave moduli [[section 5.5.4](#)] of the test design were not found to have maintained parallel drifts with that of the UCS. To put it context, among six best dosages with UCS shown in *table 7.1*, only three followed the trend strength build-up trends. One possible way to justify these inconsistencies is that the plugs are not homogeneous inside, because of which sonic propagation is often unpredictable.
- The addition of 0.45g nano-Ti in OPC slurry had decreased shear stress and viscosity, however increased yield strength as compared to neat OPC slurry. It signifies that more pump pressure might be needed to start pumping the slurry but being a low viscosity slurry would help with its pumpability [[section 5.7.3](#)].
- SEM images were taken to analyse the microstructure of the cement matrix. Due to the unavailability of 0.45g nano-Ti plug during the time of the sample collection, we had to pick 0.25g nano-Ti plug with still better UCS than reference from the oven temperature. It was observed that the NPs were very compactly fused together with OPC elements in the matrix. The created gelled structure could lead one to believe that nano-Ti bonds well with OPC under elevated temperature. In comparison, the neat OPC sample was found to have a very scrambled surface, in other words the medium was not very homogenous [[section 5.8.2](#)].

➤ **Test design 5 (Impact of TiO<sub>2</sub> nanoparticles, CF and WF on OPC)**

- NPs and CF reinforced OPC plugs were found to be predominantly better performing than WF and NPs induced cement samples in the UCS developments of this test design. Particularly, OPC plugs modified with 0.45g nano-Ti and 0.3g CF showed the most noteworthy improvements in both curing environments [[section 5.6.1](#)]. The ability to withstand different temperature effects could render this dosage to be quite versatile in terms of applying them in complete cementing of wellbores and also in construction industry.
- The stiffness [[section 5.6.2](#)] and capacity for energy absorption [[section 5.6.3](#)] for the TD-5 samples had no concrete trends to be deciphered. These contradictions in data could be the results of incorrect data recording by the deformation sensor. It was observed that the often plugs with best UCS strengths in respective batches would have inconsistent E-moduli and resilience data, in terms of the UCS oscillations of the samples.
- The samples with the best UCS, as shown in *table 7.1*, generally had shown higher M-moduli compared to the respective reference. It is to say that most M-moduli data had followed parallelly with UCS, with a few exceptions resulting from internal anomalies [[section 5.6.4](#)].
- The rheological study performed on OPC slurry modified with 0.45g nano-Ti and 0.3g CF could be employed for hole cleaning and cutting transport, as shear stress and viscosity had been increased by the additions in comparison with the neat reference. However, the increase in viscosity and decrease in yield stress might reduce the pumpability of the slurry. For a particular well operation, the WCR could be manipulated to satisfy the corroborating slurry requirements for that operation [[section 5.7.3](#)].

➤ **Empirical UCS model**

- An empirical UCS model was developed to estimate UCS from the compressional wave velocity ( $v_p$ ) without conducting the destructive tests. To clarify, the coefficient of determination ( $R^2$  value) was found to be 0.9114, which attests to the efficacy of the newly developed model. Furthermore, while testing the model with three different previously developed empirical models, it had captured very fittingly the UCS trends. To conclude, with further improvements, this model could prove to be a very competent technique to determine strength of cement plugs without permanently crushing the plugs [[chapter 6](#)].

It is noteworthy to mention that the obtained results are only valid for the cement slurry compositions and their curing process and environments, including with their measurement methods considered in this thesis. Manipulating these parameters could reflect different outcomes than what is presented here. In addition, these investigations were carried out to provide answers to the research questions cited in [section 1.3](#).

## 8 Future Work Recommendations

From the experiences gathered during the course of this thesis, various ideas for future experimental activities were brought about that could potentially enhance the cement's mechanical, rheological and petrophysical properties and enhance the quality of data as well. Some of these opinions are recommended to carry out during future experiments.

- **Broader quantities of cement samples:** During the experimental activities, the cement samples' current size presented several obstacles. Owing to the fact of constricted time and materials, only two plugs were created per concentrations of additives. Because the specimens' quantities are relatively small, they are significantly impacted by even the slightest defects and therefore are more susceptible to uncertainty. It is possible that increasing the quantities of the cement samples will make the measurements more consistent while also simplifying many other parts of the experiment. In addition, this should result in reduced variance in the data, which will make the destructive test results even more accurate by mitigating the unpredictability created from small numbers of samples.
- **SEM and EDS analyses:** Only for two samples with additives and their references were studied by SEM and EDS analyses to characterize the internal structure of the plugs, however initially both analyses were planned for all the best performing additions from all of the test designs. Unfortunately, the plan did not come to fruition due to shortage of time and miscalculations in sample collections. This is why it is highly recommended to carry out extensive SEM imaging and element analysis to study pore spaces, microcracks, amalgamation of the additives with both cementitious and non-cementitious materials.
- **Brazilian tensile strength testing:** The results of an inquiry into the effects that the additives being evaluated might have on tensile strength could give pertinent information. Because cement in a wellbore environment is subjected to forces coming from all directions, it is crucial to investigate this aspect of the material.
- **Leakage and shrinkage testing:** It is required by NORSOK D-010 for the cementitious materials to be impermeable and non-shrinking in the long run. Studies on how nanoparticles, carbon fiber, glass fibers etc. can reduce these phenomena could harvest valuable data regarding these additives' sustainability.
- **UCS prediction using Kadery's model (2022):** As developed in [chapter 6](#), it would be fascinating and extremely advantageous to improve this model to the point, where destructive UCS testing of cement specimens becomes unnecessary, saving the industry a lot in time and resources.
- **Chemical resistance study:** Cement faces a lot of corrosive chemicals and gases in downhole environments. Although, it had not been in the scope of this thesis, undoubtedly, it will be beneficial to study if and how nanoparticles could increase the chemical resistance to preserve the cement integrity and in turn, well integrity.

## References

- [1] *Well integrity in drilling and well operations*, NORSOK Standard D-010, Rev. 4, Standards Norway, Lysaker, Norway, 2013.
- [2] E. B. Nelson and D. Guillot, Eds. *Well Cementing*, 2nd ed. Sugar Land, Texas, USA: Schlumberger, 2006. [Online]. Available: <https://www.slb.com/resource-library/book/well-cementing>
- [3] B. Vignes and B. S. Aadnøy, “Well-Integrity Issues Offshore Norway,” presented at the IADC/SPE Drilling Conference, Orlando, Florida, USA, Mar. 2008, Paper SPE-112535-MS, doi: 10.2118/112535-MS. [Online]. Available: <https://onepetro.org/SPEDC/proceedings/08DC/All-08DC/SPE-112535-MS/143821> [Accessed: Aug. 07, 2022]
- [4] B. S. Aadnøy, *Modern Well Design*, 2nd ed. Leiden, The Netherlands; Boca Raton [Fla.]: CRC Press/Balkema, 2011.
- [5] T. J. Considine, R. W. Watson, N. B. Considine, and J. P. Martin, “Environmental regulation and compliance of Marcellus Shale gas drilling,” *Environmental Geosciences*, vol. 20, no. 1, pp. 1–16, Mar. 2013, doi: 10.1306/eg.09131212006. [Online]. Available: <https://pubs.geoscienceworld.org/eg/article-standard/20/1/1/138134/Environmental-regulation-and-compliance-of> [Accessed: Aug. 07, 2022]
- [6] A. Wigston, J. Williams, L. Davies, and D. Ryan, “Technology Roadmap to Improve Wellbore Integrity: Summary Report,” Natural Resources Canada, Canada, Technical Report Cat. No. M134-59/2019E-PDF, Apr. 2019. [Online]. Available: <http://rgdoi.net/10.13140/RG.2.2.36212.30081> [Accessed: Aug. 07, 2022]
- [7] *Well integrity — Part 2: Well integrity for the operational phase*, ISO/TS 16530-2:2013(E), ISO, Switzerland, 2013.
- [8] SPE International. “Cementing operations.” PetroWiki. [Online]. Available: [https://petrowiki.spe.org/Cementing\\_operations](https://petrowiki.spe.org/Cementing_operations) [Accessed: Aug. 07, 2022]
- [9] M. Khalifeh and A. Saasen, *Introduction to Permanent Plug and Abandonment of Wells*, 1st ed., vol. 12. Cham: Springer Nature Switzerland AG, 2020. [Online]. Available: <https://doi.org/10.1007/978-3-030-39970-2> [Accessed: Aug. 05, 2022]
- [10] M. Recasens, S. Garcia, E. Mackay, J. Delgado, and M. M. Maroto-Valer, “Experimental Study of Wellbore Integrity for CO<sub>2</sub> Geological Storage,” *Energy Procedia*, vol. 114, pp. 5249–5255, Jul. 2017, doi: 10.1016/j.egypro.2017.03.1681. [Online]. Available: <https://linkinghub.elsevier.com/retrieve/pii/S1876610217318829> [Accessed: Aug. 07, 2022]
- [11] SPE International. “Surface casing vent flow (SCVF).” PetroWiki. [Online]. Available: [https://petrowiki.spe.org/Surface\\_casing\\_vent\\_flow\\_\(SCVF\)](https://petrowiki.spe.org/Surface_casing_vent_flow_(SCVF)) [Accessed: Aug. 07, 2022]
- [12] T. L. Watson and S. Bachu, “Evaluation of the Potential for Gas and CO<sub>2</sub> Leakage Along Wellbores,” *SPE Drilling & Completion*, vol. 24, no. 01, pp. 115–126, Mar. 2009, Paper SPE-106817-PA, doi: 10.2118/106817-PA. [Online]. Available: <https://onepetro.org/DC/article/24/01/115/191763/Evaluation-of-the-Potential-for-Gas-and-CO2> [Accessed: Aug. 07, 2022]

- [13] R. J. Davies *et al.*, “Oil and gas wells and their integrity: Implications for shale and unconventional resource exploitation,” *Marine and Petroleum Geology*, vol. 56, pp. 239–254, Sep. 2014, doi: 10.1016/j.marpetgeo.2014.03.001. [Online]. Available: <https://linkinghub.elsevier.com/retrieve/pii/S0264817214000609> [Accessed: Aug. 08, 2022]
- [14] “Sustained Casing Pressure.” Drilling Industry Glossary. [Online]. Available: <https://www.pvisoftware.com/drilling-glossary/sustained-casing-pressure.html> [Accessed: Aug. 08, 2022]
- [15] “Statistical Review of World Energy,” BP p.l.c., Energy economics, 71st edition, 2022. [Online]. Available: <https://www.bp.com/en/global/corporate/energy-economics/statistical-review-of-world-energy.html> [Accessed: Aug. 08, 2022]
- [16] Schlumberger. “Blaine fineness.” Energy Glossary. [Online]. Available: [https://glossary.slb.com/en/Terms/b/blaine\\_fineness.aspx](https://glossary.slb.com/en/Terms/b/blaine_fineness.aspx) [Accessed: Aug. 08, 2022]
- [17] G. Liu, Ed. *Applied Well Cementing Engineering*. Cambridge, MA, USA: Gulf Professional Publishing, 2021. [Online]. Available: <https://doi.org/10.1016/C2019-0-03030-0> [Accessed: Aug. 05, 2022]
- [18] P. K. Mehta, “Natural pozzolans: Supplementary cementing materials in concrete,” *CANMET Special Publication*, vol. 86, pp. 1–33, 1987.
- [19] R. Snellings, G. Mertens, and J. Elsen, “Supplementary Cementitious Materials,” *Reviews in Mineralogy and Geochemistry*, vol. 74, no. 1, pp. 211–278, Jan. 2012, doi: 10.2138/rmg.2012.74.6. [Online]. Available: <https://pubs.geoscienceworld.org/rimg/article/74/1/211-278/140929> [Accessed: Aug. 08, 2022]
- [20] M. Amran, S. Debbarma, and T. Ozbakkaloglu, “Fly ash-based eco-friendly geopolymer concrete: A critical review of the long-term durability properties,” *Construction and Building Materials*, vol. 270, p. 121857, Feb. 2021, doi: 10.1016/j.conbuildmat.2020.121857. [Online]. Available: <https://linkinghub.elsevier.com/retrieve/pii/S0950061820338617> [Accessed: Aug. 08, 2022]
- [21] R. M. Andrew, “Global CO<sub>2</sub> emissions from cement production,” *Earth System Science Data*, vol. 10, pp. 195–217, Jan. 2018, doi: 10.5194/essd-10-195-2018. [Online]. Available: <https://essd.copernicus.org/articles/10/195/2018/> [Accessed: Aug. 08, 2022]
- [22] J. Davidovits, “Geopolymer Cement: a review,” *Geopolymer Science and Technics*, Technical Paper nr. 21, Geopolymer Institute Library, Saint-Quentin, France, Jan. 2013. [Online]. Available: <https://www.geopolymer.org/library/technical-papers/21-geopolymer-cement-review-2013/>
- [23] T. J. Van Dam, “TechBrief: Geopolymer Concrete,” U.S. Federal Highway Administration, Research Publication Number: FHWA-HIF-10-014, Mar. 2010. [Online]. Available: [https://www.fhwa.dot.gov/pavement/pub\\_details.cfm?id=665](https://www.fhwa.dot.gov/pavement/pub_details.cfm?id=665) [Accessed: Aug. 08, 2022]

- [24] S. Adjei, S. Elkatatny, W. N. Aggrey, and Y. Abdelraouf, “Geopolymer as the future oil-well cement: A review,” *Journal of Petroleum Science and Engineering*, vol. 208, Part B, p. 109485, Jan. 2022, doi: 10.1016/j.petrol.2021.109485. [Online]. Available: <https://linkinghub.elsevier.com/retrieve/pii/S092041052101127X> [Accessed: Aug. 08, 2022]
- [25] R. R. Suppiah, S. H. A. Rahman, S. Irawan, and N. Shafiq, “Development of New Formulation of Geopolymer Cement for Oil Well Cementing,” presented at the International Petroleum Technology Conference, Bangkok, Thailand, Nov. 2016, Paper IPTC-18757-MS, doi: 10.2523/IPTC-18757-MS. [Online]. Available: <https://onepetro.org/IPTCONF/proceedings/16IPTC/3-16IPTC/Bangkok,%20Thailand/153951> [Accessed: Aug. 08, 2022]
- [26] R. R. Suppiah, S. H. A. Rahman, N. Shafiq, and S. Irawan, “Uniaxial compressive strength of geopolymer cement for oil well cement,” *Journal of Petroleum Exploration and Production Technology*, vol. 10, no. 1, pp. 67–70, Jan. 2020, doi: 10.1007/s13202-019-0704-z. [Online]. Available: <https://link.springer.com/10.1007/s13202-019-0704-z> [Accessed: Aug. 08, 2022]
- [27] S. Salehi, C. P. Ezeakacha, and M. J. Khattak, “Geopolymer Cements: How Can You Plug and Abandon a Well with New Class of Cheap Efficient Sealing Materials,” presented at the SPE Oklahoma City Oil and Gas Symposium, Oklahoma City, Oklahoma, USA, Mar. 2017, Paper SPE-185106-MS. [Online]. Available: <https://doi.org/10.2118/185106-MS> [Accessed: Aug. 08, 2022]
- [28] M. Criado, A. Palomo, A. Fernández-Jiménez, and P. F. G. Banfill, “Alkali activated fly ash: effect of admixtures on paste rheology,” *Rheologica Acta*, vol. 48, no. 4, pp. 447–455, May 2009, doi: 10.1007/s00397-008-0345-5. [Online]. Available: <http://link.springer.com/10.1007/s00397-008-0345-5> [Accessed: Aug. 08, 2022]
- [29] R. K. Chouhan, M. Mudgal, A. Bisarya, and A. K. Srivastava, “Rice-husk-based superplasticizer to increase performance of fly ash geopolymer concrete,” *Emerging Materials Research*, vol. 7, no. 3, pp. 169–177, Sep. 2018, doi: 10.1680/jemmr.18.00035. [Online]. Available: <https://www.icevirtuallibrary.com/doi/10.1680/jemmr.18.00035> [Accessed: Aug. 08, 2022]
- [30] A. Chaudhary, V. Gupta, S. Teotia, S. Nimanpure, and D. K. Rajak, “Electromagnetic Shielding Capabilities of Metal Matrix Composites,” in *Encyclopedia of Materials: Composites*, vol. 1, 3 vols, D. Brabazon, Ed., Amsterdam: Elsevier, 2021, pp. 428–441. [Online]. Available: <https://doi.org/10.1016/B978-0-12-803581-8.11828-4> [Accessed: Aug. 08, 2022]
- [31] “Carbon fibers.” Wikipedia. [Online]. Available: [https://en.wikipedia.org/wiki/Carbon\\_fibers](https://en.wikipedia.org/wiki/Carbon_fibers) [Accessed: Aug. 08, 2022]
- [32] C. Wang, K.-Z. Li, H.-J. Li, G.-S. Jiao, J. Lu, and D.-S. Hou, “Effect of carbon fiber dispersion on the mechanical properties of carbon fiber-reinforced cement-based composites,” *Materials Science and Engineering: A*, vol. 487, no. 1–2, pp. 52–57, Jul. 2008, doi: 10.1016/j.msea.2007.09.073. [Online]. Available: <https://linkinghub.elsevier.com/retrieve/pii/S0921509307016978> [Accessed: Aug. 08, 2022]



- [33] Y. Yu, J. Fu, C. Zhang, F. Qi, M. Li, and J. Yang, “Mechanical Properties and Enhancement Mechanism of Oil-Well Cement Stone Reinforced with Carbon Fiber Surfaces Treated by Concentrated Nitric Acid and Sodium Hypochlorite,” *International Journal of Polymer Science*, vol. 2020, 10 pages, Nov. 2020, Art. ID 8214549, doi: 10.1155/2020/8214549. [Online]. Available: <https://www.hindawi.com/journals/ijps/2020/8214549/> [Accessed: Aug. 08, 2022]
- [34] J. J. Martín-Del-Río *et al.*, “Comparing Mechanical Behavior of API H-Class Cement Reinforced with Carbon, Mineral or Polypropylene Fiber Additions,” *Arabian Journal for Science and Engineering*, vol. 44, no. 6, pp. 6119–6125, Jun. 2019, doi: 10.1007/s13369-018-3671-7. [Online]. Available: <http://link.springer.com/10.1007/s13369-018-3671-7> [Accessed: Aug. 08, 2022]
- [35] “Glass fiber.” Wikipedia. [Online]. Available: [https://en.wikipedia.org/wiki/Glass\\_fiber](https://en.wikipedia.org/wiki/Glass_fiber) [Accessed: Aug. 08, 2022]
- [36] T. Sathishkumar, S. Satheeshkumar, and J. Naveen, “Glass fiber-reinforced polymer composites – a review,” *Journal of Reinforced Plastics and Composites*, vol. 33, no. 13, pp. 1258–1275, Jul. 2014, doi: 10.1177/0731684414530790. [Online]. Available: <http://journals.sagepub.com/doi/10.1177/0731684414530790> [Accessed: Aug. 08, 2022]
- [37] M. B. Volf, *Technical approach to glass*. Amsterdam ; New York: Elsevier, 1990.
- [38] V. B. Gupta and V. K. Kothari, Eds. *Manufactured Fibre Technology*, 1st ed. Dordrecht: Springer Netherlands, 1997. [Online]. Available: <https://doi.org/10.1007/978-94-011-5854-1> [Accessed: Aug. 09, 2022]
- [39] “Properties, Manufacturing and Application of Fiberglass.” Textile Blog, Aug. 19, 2021. [Online]. Available: <https://www.textileblog.com/fiberglass-properties-manufacturing/> [Accessed: Aug. 09, 2022]
- [40] J. W. S. Hearle, Ed. *High-performance fibres*. Cambridge, England: Woodhead Publishing, 2001.
- [41] A. H. Assi, F. H. M. Almahdawi, and Q. A. Khalti, “The Influence of Glass Fiber and Milled Glass Fiber on the Performance of Iraqi Oil Well Cement,” *Journal of Petroleum Research and Studies*, vol. 11, no. 2, pp. 30–48, Jun. 2021. [Online]. Available: <https://doi.org/10.52716/jprs.v11i2.496> [Accessed: Aug. 09, 2022]
- [42] L. F. Lalinde, A. Mellado, M. V. Borrachero, J. Monzó, and J. Payá, “Durability of Glass Fiber Reinforced Cement (GRC) Containing a High Proportion of Pozzolans,” *Applied Sciences*, vol. 12, no. 7, p. 3696, Apr. 2022, doi: 10.3390/app12073696. [Online]. Available: <https://www.mdpi.com/2076-3417/12/7/3696> [Accessed: Aug. 09, 2022]
- [43] K. E. Drexler, *Nanosystems: molecular machinery, manufacturing, and computation*. New York: Wiley, 1992.
- [44] K. E. Drexler, *Engines of Creation: The Coming Era of Nanotechnology*, 6th ed. [print]. New York: Doubleday, 1990.

- [45] “Nanotechnology.” Wikipedia. [Online]. Available: <https://en.wikipedia.org/wiki/Nanotechnology> [Accessed: Aug. 09, 2022]
- [46] “What Is Nanotechnology? | National Nanotechnology Initiative.” [Online]. Available: <https://www.nano.gov/nanotech-101/what/definition> [Accessed: Aug. 09, 2022]
- [47] S. Panneerselvam and S. Choi, “Nanoinformatics: Emerging Databases and Available Tools,” *International Journal of Molecular Sciences*, vol. 15, no. 5, pp. 7158–7182, Apr. 2014, doi: 10.3390/ijms15057158. [Online]. Available: <http://www.mdpi.com/1422-0067/15/5/7158> [Accessed: Aug. 09, 2022]
- [48] F. Allhoff, P. Lin, and D. Moore, *What Is Nanotechnology And Why Does It Matter?: From Science To Ethics*. Chichester, UK ; Malden, MA: Wiley- Blackwell, 2010.
- [49] “Different types of nanomaterials.” Anton Paar Wiki. [Online]. Available: <https://wiki.anton-paar.com/no-en/different-types-of-nanomaterials/> [Accessed: Aug. 09, 2022]
- [50] *Nanotechnologies - Vocabulary - Part 2: Nano-objects*, ISO/TS 80004-2:2015(E), ISO, Switzerland, 2015.
- [51] M. Vert *et al.*, “Terminology for biorelated polymers and applications (IUPAC Recommendations 2012),” *Pure and Applied Chemistry*, vol. 84, no. 2, pp. 377–410, Jan. 2012, doi: 10.1351/PAC-REC-10-12-04. [Online]. Available: <https://www.degruyter.com/document/doi/10.1351/PAC-REC-10-12-04/html> [Accessed: Aug. 09, 2022]
- [52] “Nanoparticle.” Wikipedia. [Online]. Available: <https://en.wikipedia.org/wiki/Nanoparticle> [Accessed: Aug. 09, 2022]
- [53] “Characterization of nanoparticles.” Wikipedia. [Online]. Available: [https://en.wikipedia.org/wiki/Characterization\\_of\\_nanoparticles](https://en.wikipedia.org/wiki/Characterization_of_nanoparticles) [Accessed: Aug. 09, 2022]
- [54] “Nanoparticle synthesis.” Nature. [Online]. Available: <https://www.nature.com/subjects/nanoparticle-synthesis> [Accessed: Aug. 09, 2022]
- [55] “Nanoparticle Synthesis.” Nanoscience Instruments. [Online]. Available: <https://www.nanoscience.com/techniques/nanoparticle-synthesis/> [Accessed: Aug. 09, 2022]
- [56] J. Turkevich, P. C. Stevenson, and J. Hillier, “A study of the nucleation and growth processes in the synthesis of colloidal gold,” *Discussions of the Faraday Society*, vol. 11, pp. 55–75, May 1951. [Online]. Available: <https://doi.org/10.1039/DF9511100055> [Accessed: Aug. 09, 2022]
- [57] M. Huston, M. DeBella, M. DiBella, and A. Gupta, “Green Synthesis of Nanomaterials,” *Nanomaterials*, vol. 11, no. 8, p. 2130, Aug. 2021, doi: 10.3390/nano11082130. [Online]. Available: <https://www.mdpi.com/2079-4991/11/8/2130> [Accessed: Aug. 09, 2022]
- [58] SPE International. “Applications of nanotechnology.” PetroWiki. [Online]. Available: [https://petrowiki.spe.org/Applications\\_of\\_nanotechnology](https://petrowiki.spe.org/Applications_of_nanotechnology) [Accessed: Aug. 09, 2022]

- [59] T. A. Saleh, Ed. *Nanotechnology in Oil and Gas Industries: Principles and Applications*, 1st ed. Cham, Switzerland: Springer International Publishing, 2018. [Online]. Available: <https://doi.org/10.1007/978-3-319-60630-9> [Accessed: Aug. 09, 2022]
- [60] M. T. Alsaba, M. F. Al Dushaishi, and A. K. Abbas, “A comprehensive review of nanoparticles applications in the oil and gas industry,” *Journal of Petroleum Exploration and Production Technology*, vol. 10, no. 4, pp. 1389–1399, Apr. 2020, doi: 10.1007/s13202-019-00825-z. [Online]. Available: <https://link.springer.com/10.1007/s13202-019-00825-z> [Accessed: Aug. 09, 2022]
- [61] A. S. Hogeweg, R. E. Hincapie, H. Foedisch, and L. Ganzer, “Evaluation of Aluminium Oxide and Titanium Dioxide Nanoparticles for EOR Applications,” presented at the SPE Europec featured at 80th EAGE Conference and Exhibition, Copenhagen, Denmark, Jun. 2018, Paper SPE-190872-MS, doi: 10.2118/190872-MS. [Online]. Available: <https://doi.org/10.2118/190872-MS> [Accessed: Aug. 09, 2022]
- [62] Y. Ding, S. Zheng, X. Meng, and D. Yang, “Low Salinity Hot Water Injection with Addition of Nanoparticles for Enhancing Heavy Oil Recovery under Reservoir Conditions,” presented at the SPE Western Regional Meeting, Garden Grove, California, USA, Apr. 2018, Paper SPE-190132-MS, doi: 10.2118/190132-MS. [Online]. Available: <https://doi.org/10.2118/190132-MS> [Accessed: Aug. 10, 2022]
- [63] O. Mahmoud, H. A. Nasr-El-Din, Z. Vryzas, and V. C. Kelessidis, “Effect of Ferric Oxide Nanoparticles on the Properties of Filter Cake Formed by Calcium Bentonite-Based Drilling Muds,” *SPE Drilling & Completion*, vol. 33, no. 04, pp. 363–376, Dec. 2018, Paper SPE-184572-PA, doi: 10.2118/184572-PA. [Online]. Available: <https://onepetro.org/DC/article/33/04/363/207522/Effect-of-Ferric-Oxide-Nanoparticles-on-the> [Accessed: Aug. 10, 2022]
- [64] M. A. Alvi, M. Belayneh, A. Saasen, and B. S. Aadnøy, “The Effect of Micro-Sized Boron Nitride BN and Iron Trioxide Fe<sub>2</sub>O<sub>3</sub> Nanoparticles on the Properties of Laboratory Bentonite Drilling Fluid,” presented at the SPE Norway One Day Seminar, Bergen, Norway, Apr. 2018, Paper SPE-191307-MS doi: 10.2118/191307-MS. [Online]. Available: <https://doi.org/10.2118/191307-MS> [Accessed: Aug. 10, 2022]
- [65] M. T. Alsaba, A. Al Fadhli, A. Marafi, A. Hussain, F. Bander, and M. F. Al Dushaishi, “Application of Nanoparticles in Improving Rheological Properties of Water Based Drilling Fluids,” presented at the SPE Kingdom of Saudi Arabia Annual Technical Symposium and Exhibition, Dammam, Saudi Arabia, Apr. 2018, Paper SPE-192239-MS, doi: 10.2118/192239-MS. [Online]. Available: <https://doi.org/10.2118/192239-MS> [Accessed: Aug. 10, 2022]
- [66] M. R. Gurluk, H. A. Nasr-El-Din, and J. B. Crews, “Enhancing the Performance of Viscoelastic Surfactant Fluids Using Nanoparticles,” presented at the EAGE Annual Conference & Exhibition incorporating SPE Europec, London, UK, Jun. 2013, Paper SPE-164900-MS, doi: 10.2118/164900-MS. [Online]. Available: <https://doi.org/10.2118/164900-MS> [Accessed: Aug. 10, 2022]
- [67] R. Singh, S. Tong, K. Panthi, and K. Mohanty, “Nanoparticle-Encapsulated Acids for Stimulation of Calcite-Rich Shales,” presented at the SPE/AAPG/SEG Unconventional Resources Technology Conference, Houston, Texas, USA, Jul. 2018, Paper URTEC-2897114-MS, doi: 10.15530/urtec-2018-2897114. [Online]. Available: <https://onepetro.org/URTECONF/proceedings-abstract/18URTC/2-18URTC/D023S029R002/157436> [Accessed: Aug. 10, 2022]

- [68] M. F. Fakoya and S. N. Shah, "Effect of Silica Nanoparticles on the Rheological Properties and Filtration Performance of Surfactant-Based and Polymeric Fracturing Fluids and Their Blends," *SPE Drilling & Completion*, vol. 33, no. 02, pp. 100–114, Jun. 2018, Paper SPE-163921-PA, doi: 10.2118/163921-PA. [Online]. Available: <https://doi.org/10.2118/163921-PA> [Accessed: Aug. 10, 2022]
- [69] H. C. Lau, M. Yu, and Q. P. Nguyen, "Nanotechnology for oilfield applications: Challenges and impact," *Journal of Petroleum Science and Engineering*, vol. 157, pp. 1160–1169, Aug. 2017, doi: 10.1016/j.petrol.2017.07.062. [Online]. Available: <https://linkinghub.elsevier.com/retrieve/pii/S0920410516304016> [Accessed: Aug. 10, 2022]
- [70] C. Vipulanandan, A. Mohammed, and A. S. Ganpatye, "Smart Cement Performance Enhancement with Nano Al<sub>2</sub>O<sub>3</sub> for Real Time Monitoring Applications Using Vipulanandan Models," presented at the Offshore Technology Conference, Houston, Texas, USA, Apr. 2018, Paper OTC-28880-MS, doi: 10.4043/28880-MS. [Online]. Available: <https://onepetro.org/OTCONF/proceedings-abstract/18OTC/4-18OTC/D041S056R007/179164> [Accessed: Aug. 10, 2022]
- [71] M. Alkhamis and A. Imqam, "New Cement Formulations Utilizing Graphene Nano Platelets to Improve Cement Properties and Long-Term Reliability in Oil Wells," presented at the SPE Kingdom of Saudi Arabia Annual Technical Symposium and Exhibition, Dammam, Saudi Arabia, Apr. 2018, Paper SPE-192342-MS, doi: 10.2118/192342-MS. [Online]. Available: <http://www.onepetro.org/doi/10.2118/192342-MS> [Accessed: Aug. 10, 2022]
- [72] P. E. Mabeyo and J. Gu, "Coupled effects of hydrophilic nano silica oxide and anatase nano titanium oxide on strengths of oilwell cement," *Tanzania Journal of Science*, vol. 47, no. 2, pp. 568–582, May 2021, doi: 10.4314/tjs.v47i2.13. [Online]. Available: <https://www.ajol.info/index.php/tjs/article/view/207038> [Accessed: Aug. 10, 2022]
- [73] M. T. Baig, M. K. Rahman, and A. Al-Majed, "Application of Nanotechnology in Oil Well Cementing," presented at the SPE Kuwait Oil & Gas Show and Conference, Kuwait City, Kuwait, Oct. 2017, Paper SPE-187543-MS, doi: 10.2118/187543-MS. [Online]. Available: <https://onepetro.org/SPEKOGS/proceedings-abstract/17KOGS/3-17KOGS/D031S011R001/194891> [Accessed: Aug. 10, 2022]
- [74] C. Huh, H. Daigle, V. Prigiobbe, and M. Prodanović, *Practical Nanotechnology for Petroleum Engineers*, 1st ed. Boca Raton: CRC Press, Taylor and Francis Group, 2019. [Online]. Available: <https://doi.org/10.1201/9781351210362> [Accessed: Aug. 10, 2022]
- [75] A. Nazari and S. Riahi, "Improvement compressive strength of concrete in different curing media by Al<sub>2</sub>O<sub>3</sub> nanoparticles," *Materials Science and Engineering: A*, vol. 528, no. 3, pp. 1183–1191, Jan. 2011, doi: 10.1016/j.msea.2010.09.098. [Online]. Available: <https://linkinghub.elsevier.com/retrieve/pii/S0921509310011445> [Accessed: Aug. 10, 2022]
- [76] A. Santra, P. J. Boul, and X. Pang, "Influence of Nanomaterials in Oilwell Cement Hydration and Mechanical Properties," presented at the SPE International Oilfield Nanotechnology Conference and Exhibition, Noordwijk, The Netherlands, Jun. 2012, Paper SPE-156937-MS, doi: 10.2118/156937-MS. [Online]. Available: <https://onepetro.org/speionc/proceedings-abstract/12IONC/All-12IONC/SPE-156937-MS/158482> [Accessed: Aug. 10, 2022]

- [77] C. A. Franco, C. A. Franco, R. D. Zabala, Í. Bahamón, Á. Forero, and F. B. Cortés, “Field Applications of Nanotechnology in the Oil and Gas Industry: Recent Advances and Perspectives,” *Energy & Fuels*, vol. 35, no. 23, pp. 19266–19287, Dec. 2021, doi: 10.1021/acs.energyfuels.1c02614. [Online]. Available: <https://pubs.acs.org/doi/10.1021/acs.energyfuels.1c02614> [Accessed: Aug. 10, 2022]
- [78] H. Nerhus, “Effect of nanoparticles and elastomers on the mechanical and elastic properties of G-class Portland cement: Experimental and Modelling studies.” M.S. thesis, Department of Energy and Petroleum Engineering (IEP), University of Stavanger, Stavanger, Norway, 2020. [Online]. Available: <https://uis.brage.unit.no/uis-xmlui/handle/11250/2685503> [Accessed: Jul. 12, 2022]
- [79] H. Titlestad, “Effect of nano-SiO<sub>2</sub>, nano-Al<sub>2</sub>O<sub>3</sub>, MWCNT and FA on properties of Portland G-class cement,” M.S. thesis, Department of Energy and Petroleum Engineering (IEP), University of Stavanger, Stavanger, Norway, 2021. [Online]. Available: <https://uis.brage.unit.no/uis-xmlui/handle/11250/2788247> [Accessed: Jul. 12, 2022]
- [80] N. Farzadnia, A. A. Abang Ali, and R. Demirboga, “Characterization of high strength mortars with nano alumina at elevated temperatures,” *Cement and Concrete Research*, vol. 54, pp. 43–54, Dec. 2013, doi: 10.1016/j.cemconres.2013.08.003. [Online]. Available: <https://linkinghub.elsevier.com/retrieve/pii/S0008884613001750> [Accessed: Aug. 10, 2022]
- [81] M. Genedy, U. F. Kandil, E. N. Matteo, J. Stormont, and M. M. Reda Taha, “A new polymer nanocomposite repair material for restoring wellbore seal integrity,” *International Journal of Greenhouse Gas Control*, vol. 58, pp. 290–298, Mar. 2017, doi: 10.1016/j.ijggc.2016.10.006. [Online]. Available: <https://linkinghub.elsevier.com/retrieve/pii/S1750583616306843> [Accessed: Aug. 10, 2022]
- [82] M. T. Maagi, S. D. Lupyana, and J. Gu, “Effect of Nano-SiO<sub>2</sub>, Nano-TiO<sub>2</sub> and Nano-Al<sub>2</sub>O<sub>3</sub> Addition on Fluid Loss in Oil-Well Cement Slurry,” *International Journal of Concrete Structures and Materials*, vol. 13, no. 62, Dec. 2019, doi: 10.1186/s40069-019-0371-y. [Online]. Available: <http://link.springer.com/10.1186/s40069-019-0371-y> [Accessed: Aug. 10, 2022]
- [83] F. Khan, H. Kesarwani, G. Kataria, G. Mittal, and S. Sharma, “Application of titanium dioxide nanoparticles for the design of oil well cement slurry – a study based on compressive strength, setting time and rheology,” *Journal of Adhesion Science and Technology*, to be published, Jun. 2022, doi: 10.1080/01694243.2022.2087963. [Online]. Available: <https://www.tandfonline.com/doi/full/10.1080/01694243.2022.2087963> [Accessed: Aug. 10, 2022]
- [84] M. S. Döndüren and M. G. Al-Hagri, “A review of the effect and optimization of use of nano-TiO<sub>2</sub> in cementitious composites,” *Research on Engineering Structures and Materials*, vol. 8, no. 2, pp. 283–305, Jan. 2022, doi: 10.17515/resm2022.348st1005. [Online]. Available: <http://www.jresm.org/archive/resm2022.348st1005.html> [Accessed: Aug. 10, 2022]
- [85] M. Khalifeh, S. Salehi, A. Jamrozik, R. Kimanzi, and S. Abdollahpour, “Nano-Modified Rock-Based Geopolymers as Supplement to Portland Cement for Oil Well Cementing,” presented at the ASME 2019 38th International Conference on Ocean, Offshore and Arctic Engineering, Glasgow, Scotland, UK, Jun. 2019, Paper OMAE2019-95380, doi: 10.1115/OMAEE2019-95380. [Online]. Available: <https://doi.org/10.1115/OMAEE2019-95380> [Accessed: Aug. 10, 2022]

- [86] N. H. Jumaa, I. M. Ali, M. S. Nasr, and M. W. Falah, “Strength and microstructural properties of binary and ternary blends in fly ash-based geopolymer concrete,” *Case Studies in Construction Materials*, to be published, vol. 17, no. e01317, Dec. 2022, doi: 10.1016/j.cscm.2022.e01317. [Online]. Available: <https://linkinghub.elsevier.com/retrieve/pii/S2214509522004491> [Accessed: Aug. 10, 2022]
- [87] Z. Xu *et al.*, “Research progress on key problems of nanomaterials-modified geopolymer concrete,” *Nanotechnology Reviews*, vol. 10, no. 1, pp. 779–792, Aug. 2021, doi: 10.1515/ntrev-2021-0056. [Online]. Available: <https://www.degruyter.com/document/doi/10.1515/ntrev-2021-0056/html> [Accessed: Aug. 10, 2022]
- [88] A. M. Hunashyal, J. M. Suman, N. R. Banapurmath, S. S. Quadri, and A. S. Shettar, “Experimental Investigation on the Effect of Titanium dioxide and Carbon fibers on the Mechanical and Microstructural Properties of Cement Beams,” *SOP Transactions on Nanotechnology*, vol. 2, no. 1, Feb. 2015, doi: 10.15764/NANO.2015.01001. [Online]. Available: <https://www.semanticscholar.org/paper/Experimental-Investigation-on-the-Effect-of-dioxide-Hunashyal-Suman/72c506d48a12214e3af66e895f1a4075fd6fd1ec> [Accessed: Aug. 10, 2022]
- [89] A. Joshaghani, “Evaluating the effects of titanium dioxide (TiO<sub>2</sub>) and carbon-nanofibers (CNF) as cement partial replacement on concrete properties,” *MedCrave Online Journal of Civil Engineering*, vol. 4, no. 1, pp. 29–38, Jan. 2018, doi: 10.15406/mojce.2018.04.00094. [Online]. Available: <https://medcraveonline.com/MOJCE/evaluating-the-effects-of-titanium-dioxide-tio2-and-carbon-nanofibers-cnf-as-cement-partial-replacement-on-concrete-properties.html> [Accessed: Aug. 10, 2022]
- [90] J.-J. Park, S. Kim, W. Shin, H.-J. Choi, G.-J. Park, and D.-Y. Yoo, “High-Performance Photocatalytic Cementitious Materials Containing Synthetic Fibers and Shrinkage-Reducing Admixture,” *Materials*, vol. 13, no. 8, p. 1828, Apr. 2020, doi: 10.3390/ma13081828. [Online]. Available: <https://www.mdpi.com/1996-1944/13/8/1828> [Accessed: Aug. 10, 2022]
- [91] “Norwell.” [Online]. Available: <https://www.norcem.no/en/norwell> [Accessed: Aug. 04, 2022]
- [92] “Aluminum Oxide Al<sub>2</sub>O<sub>3</sub> Nanopowder / Nanoparticles Water Dispersion (Alpha, 20 wt%, 30 nm).” [Online]. Available: <https://www.us-nano.com/inc/sdetail/623> [Accessed: Aug. 03, 2022]
- [93] “Titanium Oxide (TiO<sub>2</sub>) Nanopowder / Nanoparticles Dispersion (TiO<sub>2</sub> Nanoparticles Aqueous Dispersion, Anatase, 15 wt%, 5-15 nm).” [Online]. Available: <https://www.us-nano.com/inc/sdetail/630> [Accessed: Aug. 03, 2022]
- [94] A. Bahadori, Ed. *Essentials of coating, painting, and lining for the oil, gas and petrochemical industries*, 1st ed. Amsterdam: Gulf Professional Publishing, an imprint of Elsevier, 2015 [Online]. Available: <https://doi.org/10.1016/C2013-0-19127-1>
- [95] The American Concrete Institute. “Silica Fume Topic.” [Online]. Available: <https://www.concrete.org/topicsinconcrete/topicdetail/Silica%20Fume?search=Silica%20Fume> [Accessed: Aug. 04, 2022]

- [96] VWR International. “Sodium hydroxide 98.5-100.5%, pellets, AnalaR NORMAPUR® Reag. Ph. Eur. analytical reagent.” [Online]. Available: <https://cz.vwr.com/store/product/en/781220/sodium-hydroxide-98-5-100-5-pellets-analar-normapur-reag-ph-eur-analytical-reagent> [Accessed: Aug. 04, 2022]
- [97] PQ Corporation. “Sodium Silicate Liquids.” [Online]. Available: <https://www.pqcorp.com/products/sodium-silicate-liquids> [Accessed: Aug. 04, 2022]
- [98] ZOLTEK. “What is Carbon Fiber?” [Online]. Available: <https://zoltek.com/carbon-fiber/what-is-carbon-fiber/> [Accessed: Aug. 04, 2022]
- [99] R. Worst. “17 Types of Fiberglass & Their Various Properties & Applications.” Worst Room. [Online]. Available: <https://worstroom.com/types-of-fiberglass/> [Accessed: Aug. 05, 2022]
- [100] P. A. Bjørkum and P. H. Nadeau, “Temperature Controlled Porosity/Permeability Reduction, Fluid Migration, and Petroleum Exploration in Sedimentary Basins,” *The APPEA Journal*, vol. 38, no. 1, pp. 453–464, Mar. 1998, doi: 10.1071/AJ97022. [Online]. Available: [https://www.researchgate.net/publication/285729785\\_Temperature\\_controlled\\_porositypermeability\\_reduction\\_fluid\\_migration\\_and\\_petrolium\\_exploration\\_in\\_sedimentary\\_basins](https://www.researchgate.net/publication/285729785_Temperature_controlled_porositypermeability_reduction_fluid_migration_and_petrolium_exploration_in_sedimentary_basins) [Accessed: Aug. 10, 2022]
- [101] A. Palomo, M. W. Grutzeck, and M. T. Blanco, “Alkali-activated fly ashes: A cement for the future,” *Cement and Concrete Research*, vol. 29, no. 8, pp. 1323–1329, Aug. 1999, doi: 10.1016/S0008-8846(98)00243-9. [Online]. Available: <https://linkinghub.elsevier.com/retrieve/pii/S0008884698002439> [Accessed: Aug. 04, 2022]
- [102] “Geopolymer cement.” Wikipedia. [Online]. Available: [https://en.wikipedia.org/wiki/Geopolymer\\_cement](https://en.wikipedia.org/wiki/Geopolymer_cement) [Accessed: Aug. 04, 2022]
- [103] Schlumberger. “Uniaxial Compressive Strength.” Energy Glossary. [Online]. Available: [https://glossary.slb.com/en/Terms/u/uniaxial\\_compressive\\_strength.aspx](https://glossary.slb.com/en/Terms/u/uniaxial_compressive_strength.aspx) [Accessed: Aug. 04, 2022]
- [104] E. Fjær, R. M. Holt, P. Horsrud, A. M. Raaen, and R. Risnes, Eds. *Petroleum related rock mechanics*, 2nd ed., vol. 53. Amsterdam ; Boston: Elsevier, 2008.
- [105] B. S. Aadnøy and R. Looyeh, *Petroleum rock mechanics: Drilling Operations and Well Design*, 2nd ed. Cambridge, MA: Gulf Professional Publishing, 2019. [Online]. Available: <https://doi.org/10.1016/C2017-0-03371-2>
- [106] D. R. Askeland and W. J. Wright, *The Science and Engineering of Materials*, 7th ed. Boston, MA: Cengage Learning, 2016.
- [107] W. D. Callister and D. G. Rethwisch, *Materials Science and Engineering: An Introduction*, 10th ed. Hoboken, NJ, USA: Wiley, 2018.
- [108] T. Editors of Encyclopaedia Britannica, Eds. “Young’s modulus.” Encyclopaedia Britannica. [Online]. Available: <https://www.britannica.com/science/Youngs-modulus> [Accessed: Aug. 05, 2022]

- [109] “Young’s modulus.” Wikipedia. [Online]. Available: [https://en.wikipedia.org/wiki/Young%27s\\_modulus](https://en.wikipedia.org/wiki/Young%27s_modulus) [Accessed: Aug. 05, 2022]
- [110] University of Washington. “Young’s Modulus.” [Online]. Available: [https://depts.washington.edu/matseed/mse\\_resources/Webpage/Biomaterials/young%27s\\_modulus.htm](https://depts.washington.edu/matseed/mse_resources/Webpage/Biomaterials/young%27s_modulus.htm) [Accessed: Aug. 05, 2022]
- [111] R. C. Hibbeler, *Mechanics of Materials*, 8th ed. Boston: Prentice Hall, 2011.
- [112] “Scanning electron microscope.” Wikipedia. [Online]. Available: [https://en.wikipedia.org/wiki/Scanning\\_electron\\_microscope](https://en.wikipedia.org/wiki/Scanning_electron_microscope) [Accessed: Aug. 05, 2022]
- [113] Purdue University. “Scanning Electron Microscope.” Radiological and Environmental Management. [Online]. Available: <https://www.purdue.edu/ehps/rem/laboratory/equipment%20safety/Research%20Equipment/sem.html> [Accessed: Aug. 05, 2022]
- [114] G. Mavko, T. Mukerji, and J. Dvorkin, *The Rock Physics Handbook: Tools for Seismic Analysis of Porous Media*, 2nd ed. Cambridge, UK; New York, USA: Cambridge University Press, 2009.
- [115] G. Mavko, T. Mukerji, and J. Dvorkin, *The Rock Physics Handbook*, 3rd ed. United Kingdom: Cambridge University Press, 2020. [Online]. Available: <https://doi.org/10.1017/9781108333016> [Accessed: Aug. 05, 2022]
- [116] Schlumberger. “Viscosity.” Energy Glossary. [Online]. Available: <https://glossary.slb.com/en/terms/v/viscosity> [Accessed: Aug. 05, 2022]
- [117] Schlumberger. “Plastic Viscosity.” Energy Glossary. [Online]. Available: [https://glossary.slb.com/en/terms/p/plastic\\_viscosity](https://glossary.slb.com/en/terms/p/plastic_viscosity) [Accessed: Aug. 05, 2022]
- [118] Schlumberger. “Shear Stress.” Energy Glossary. [Online]. Available: [https://glossary.slb.com/en/terms/s/shear\\_stress](https://glossary.slb.com/en/terms/s/shear_stress) [Accessed: Aug. 05, 2022]
- [119] Schlumberger. “Yield Stress.” Energy Glossary. [Online]. Available: [https://glossary.slb.com/en/terms/y/yield\\_stress](https://glossary.slb.com/en/terms/y/yield_stress) [Accessed: Aug. 05, 2022]
- [120] Schlumberger. “Shear Rate.” Energy Glossary. [Online]. Available: [https://glossary.slb.com/en/terms/s/shear\\_rate](https://glossary.slb.com/en/terms/s/shear_rate) [Accessed: Aug. 05, 2022]
- [121] P. Horsrud, “Estimating Mechanical Properties of Shale from Empirical Correlations,” *SPE Drilling & Completion*, vol. 16, no. 02, pp. 68–73, Jun. 2001, Paper SPE-56017-PA, doi: 10.2118/56017-PA. [Online]. Available: <https://onepetro.org/DC/article/16/02/68/75206/Estimating-Mechanical-Properties-of-Shale-From> [Accessed: Jul. 12, 2022]
- [122] G. Mishra. “Why Do We Test Concrete Compressive Strength After 28 Days?” *The Constructor*. [Online]. Available: <https://theconstructor.org/concrete/why-we-test-concrete-strength-after-28-days/6060/> [Accessed: Aug. 11, 2022]



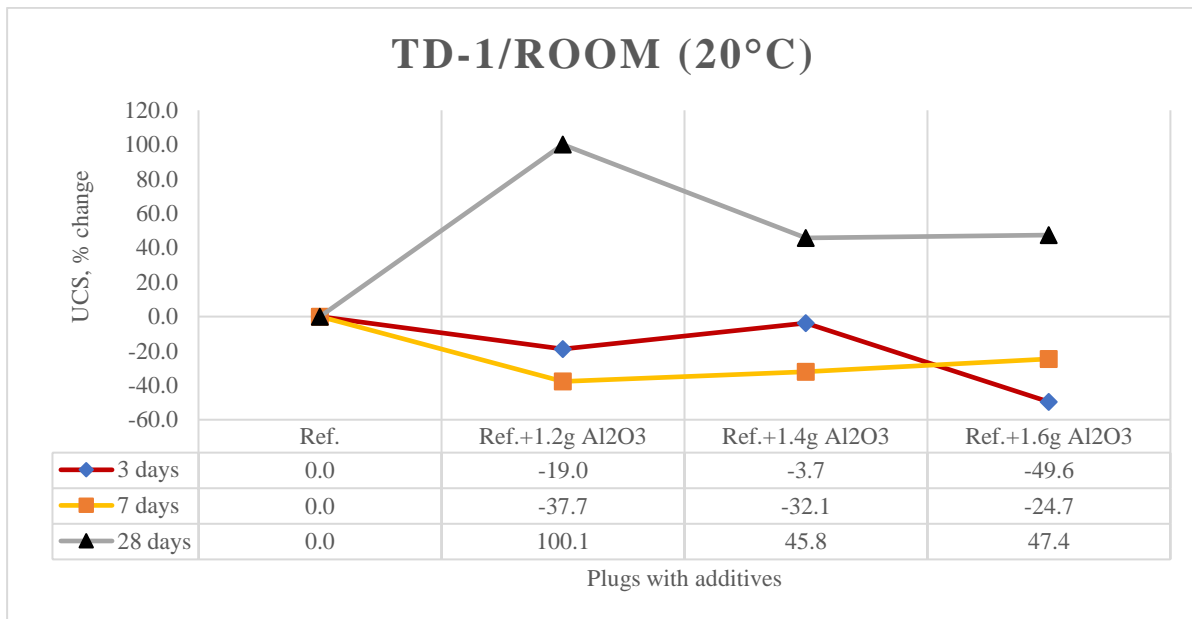
[123] R. Campbell and S. Lauper, “Low Viscosity Cement Slurry for Improved Placement in Narrow Annuli,” presented at the SPE Western Regional Meeting, Anchorage, Alaska, USA, May 2016, Paper SPE-180427-MS, doi: 10.2118/180427-MS. [Online]. Available: <https://onepetro.org/SPEWRM/proceedings-abstract/16WRM/All-16WRM/SPE-180427-MS/188175> [Accessed: Aug. 11, 2022]

[124] S. Aarnes, “A comprehensive experimental investigation of MWCNTs in oil-well cementing and the development of a new empirical model for UCS estimation,” M.S. thesis, Department of Energy and Petroleum Engineering (IEP), University of Stavanger, Stavanger, Norway, 2018. [Online]. Available: <https://uis.brage.unit.no/uis-xmlui/handle/11250/2568579> [Accessed: Jul. 12, 2022]

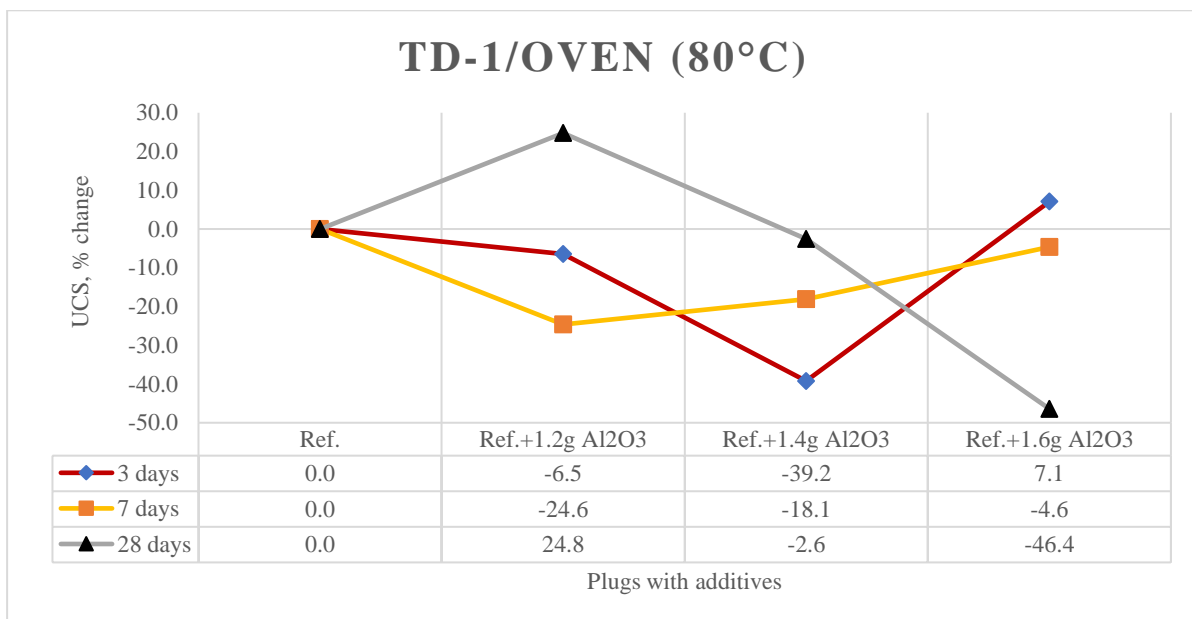
## Appendix A – Percentile changes in the results

In the following, changes in the parameter will be shown in percentile. It is arranged by designs, curing environments and various characterization parameters. It can be observed that some data are absent here just as they were absent in [section 5](#) due to the same reason of deformation sensor not performing correctly.

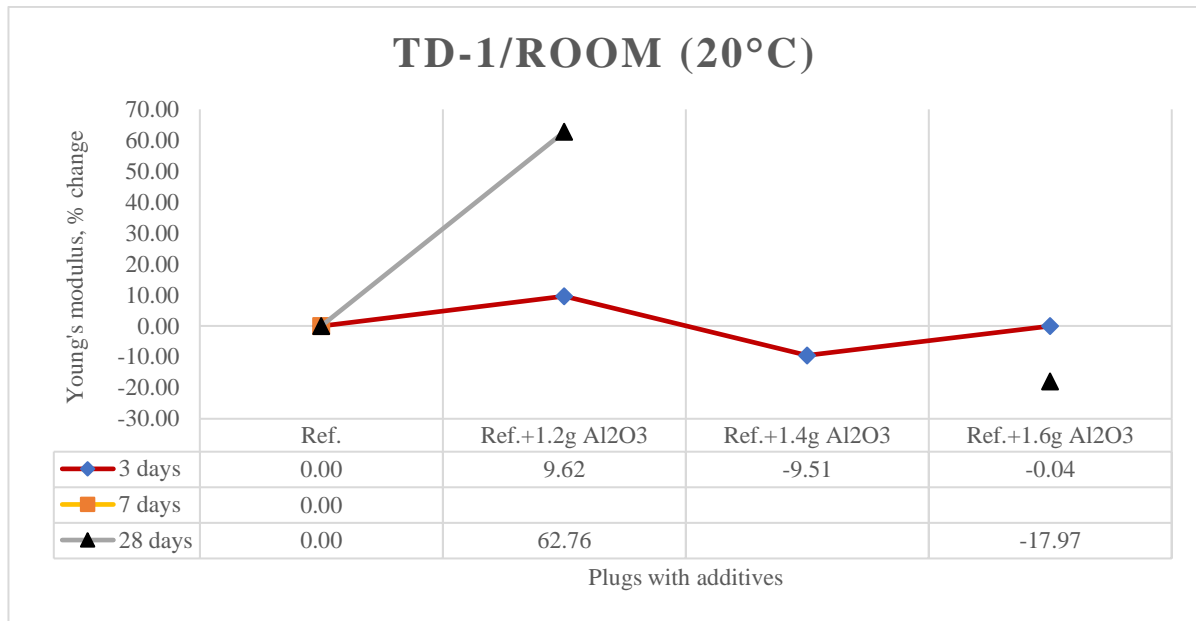
### ➤ TD-1 – Room – UCS



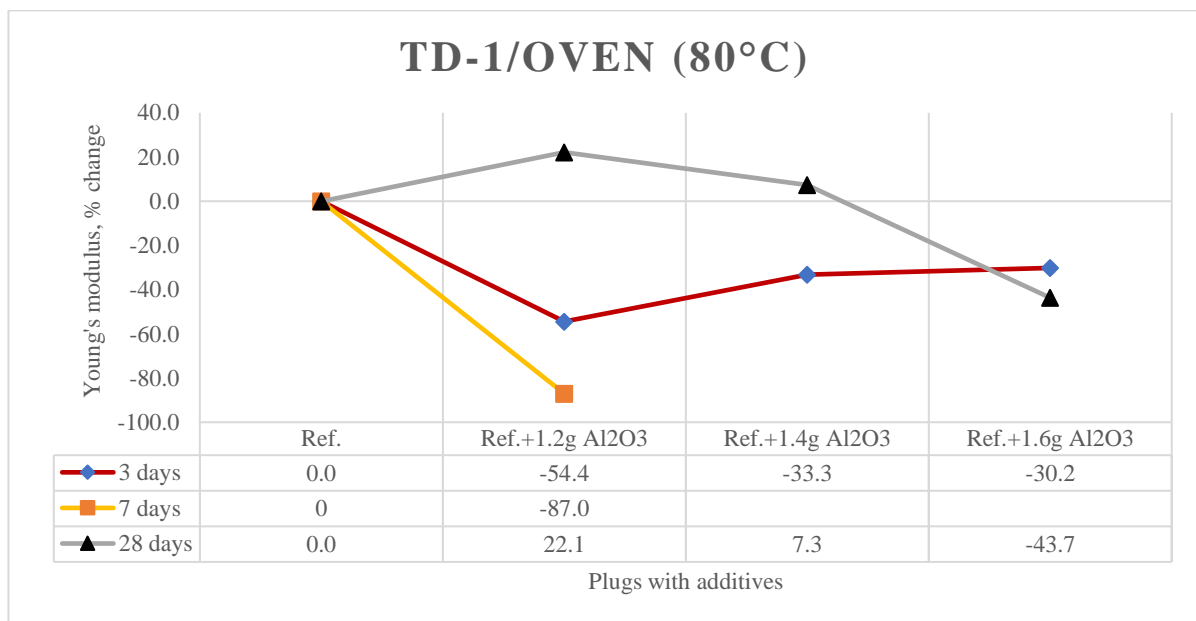
### ➤ TD-1 – Oven – UCS



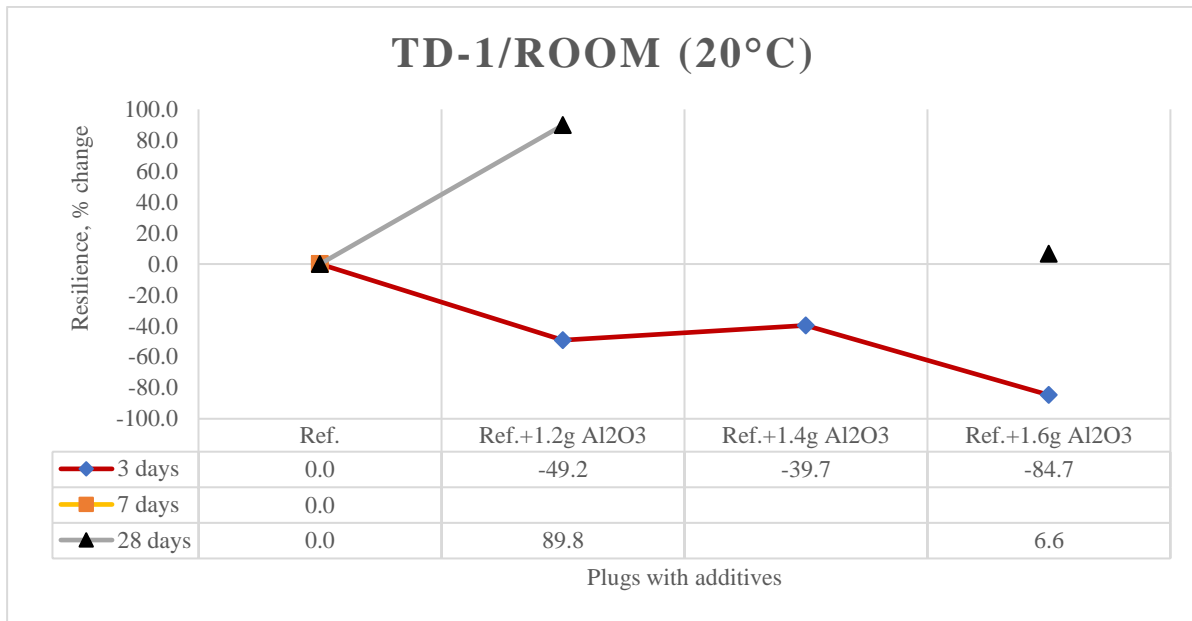
➤ **TD-1 – Room – Young’s modulus**



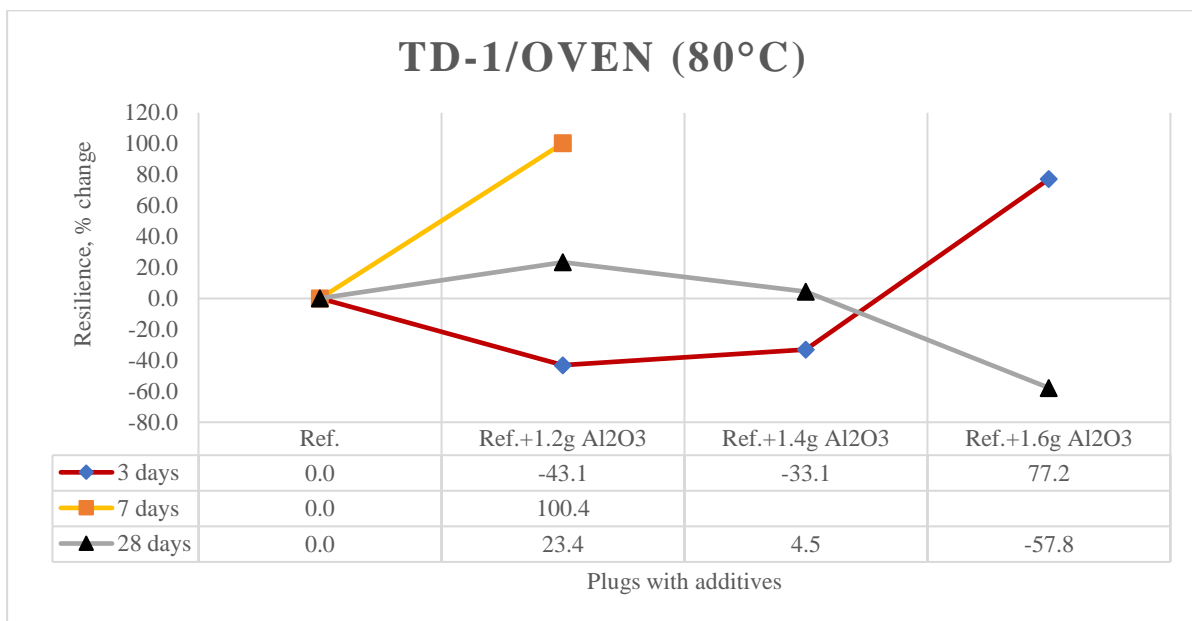
➤ **TD-1 – Oven – Young’s modulus**



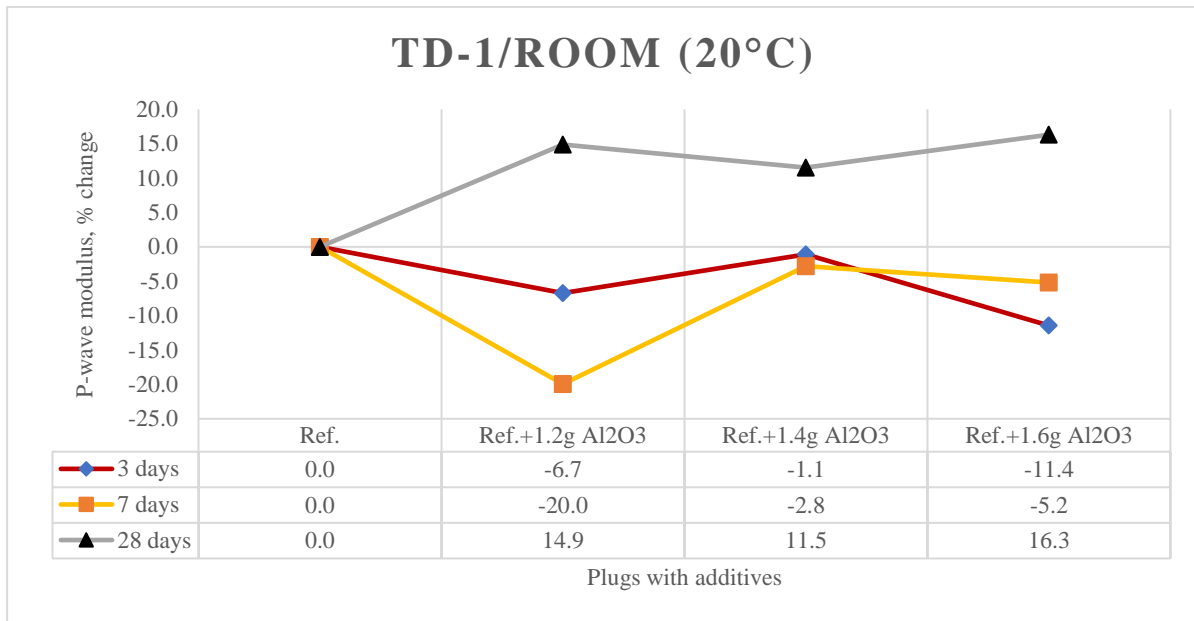
➤ **TD-1 – Room – Resilience**



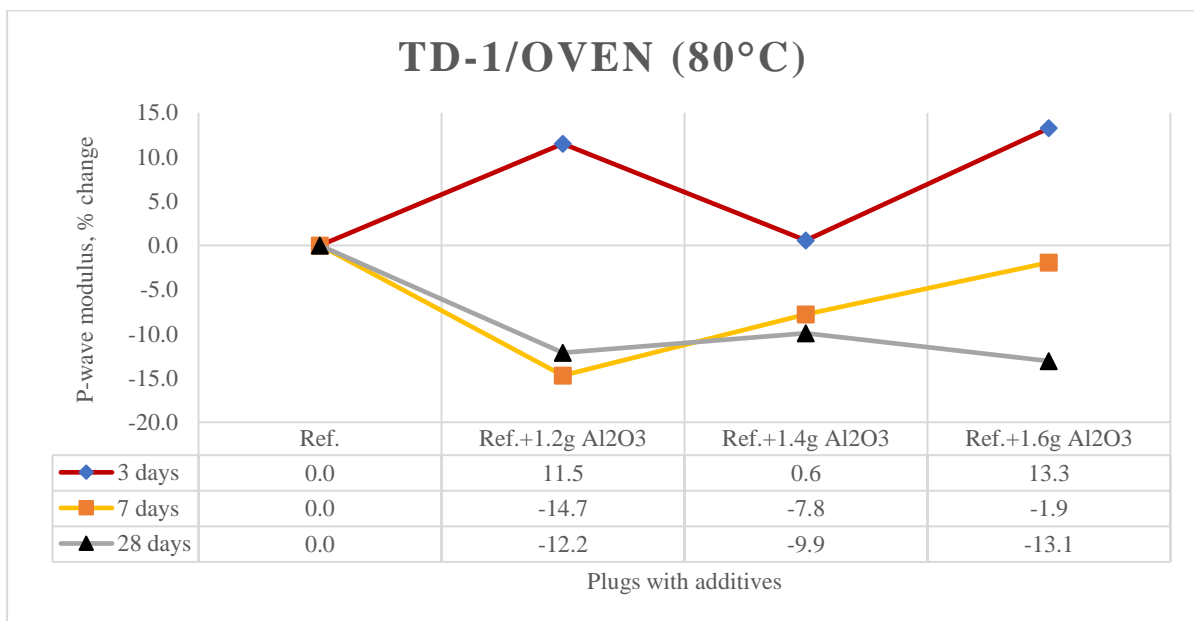
➤ **TD-1 – Oven – Resilience**



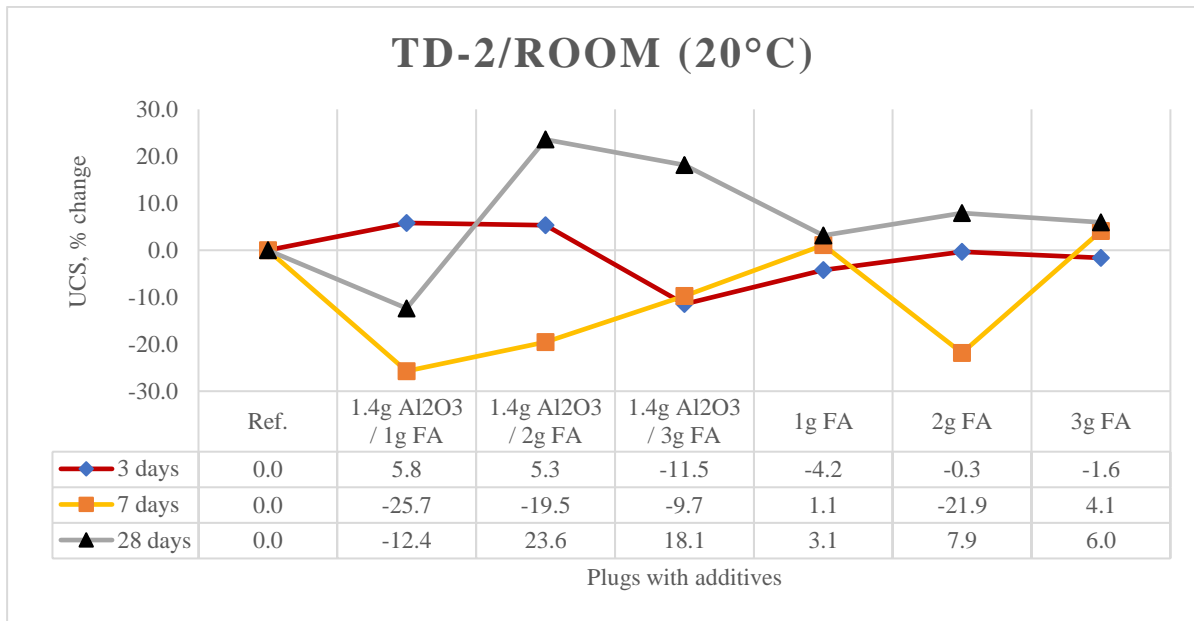
➤ **TD-1 – Room – P-wave modulus**



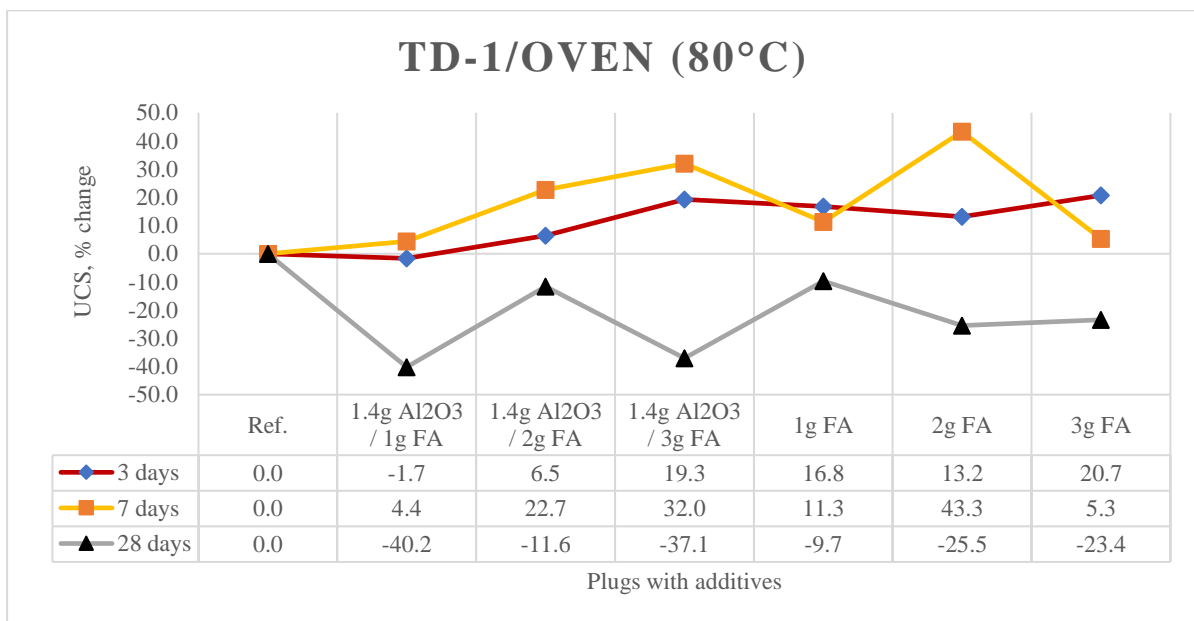
➤ **TD-1 – Oven – P-wave modulus**



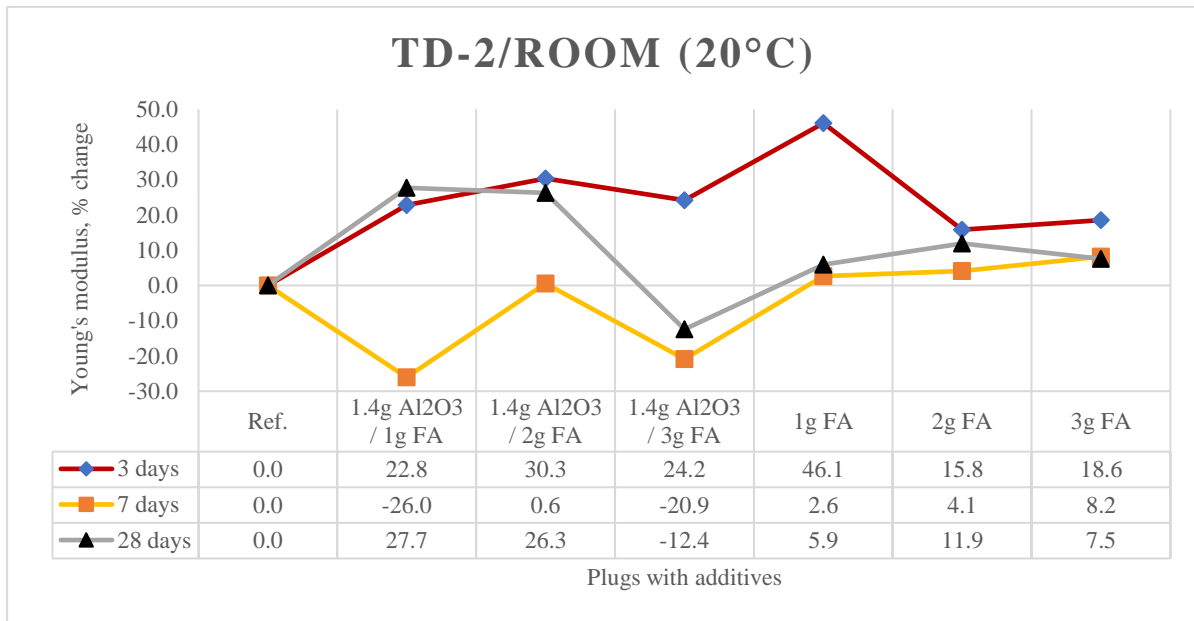
➤ TD-2 – Room – UCS



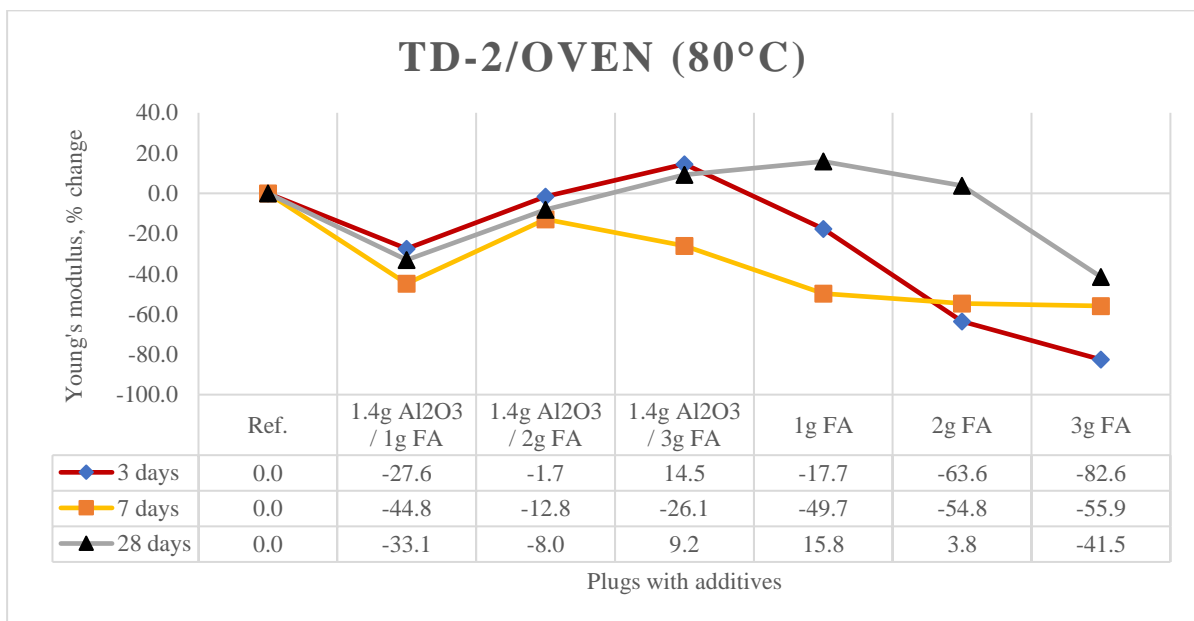
➤ TD-2 – Oven – UCS



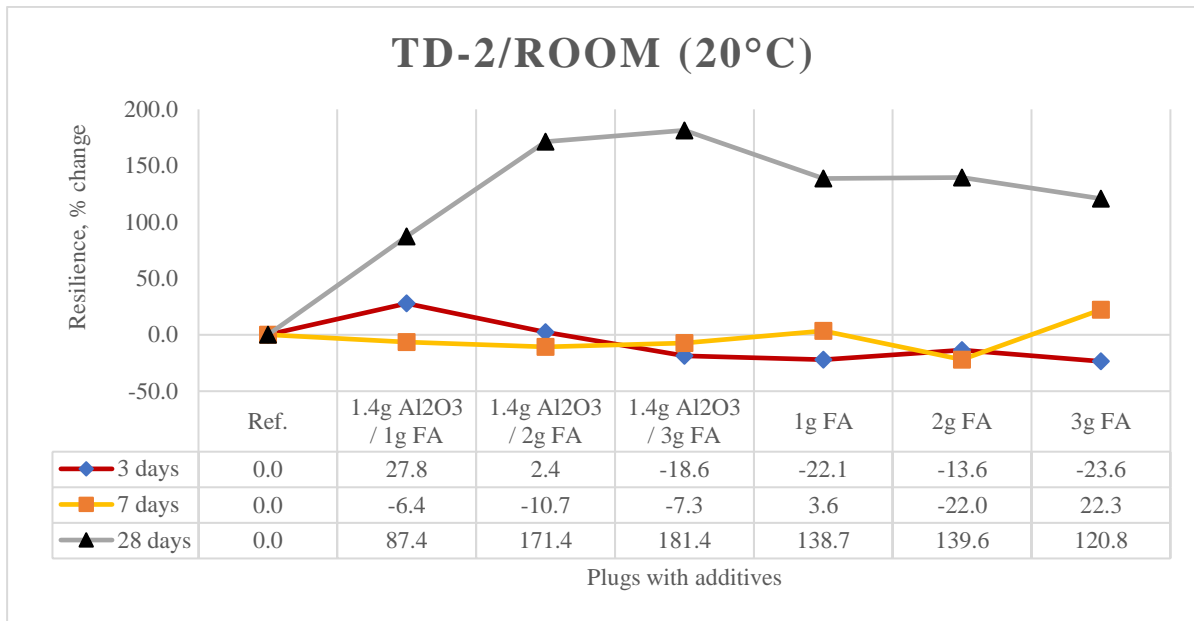
➤ **TD-2 – Room – Young’s modulus**



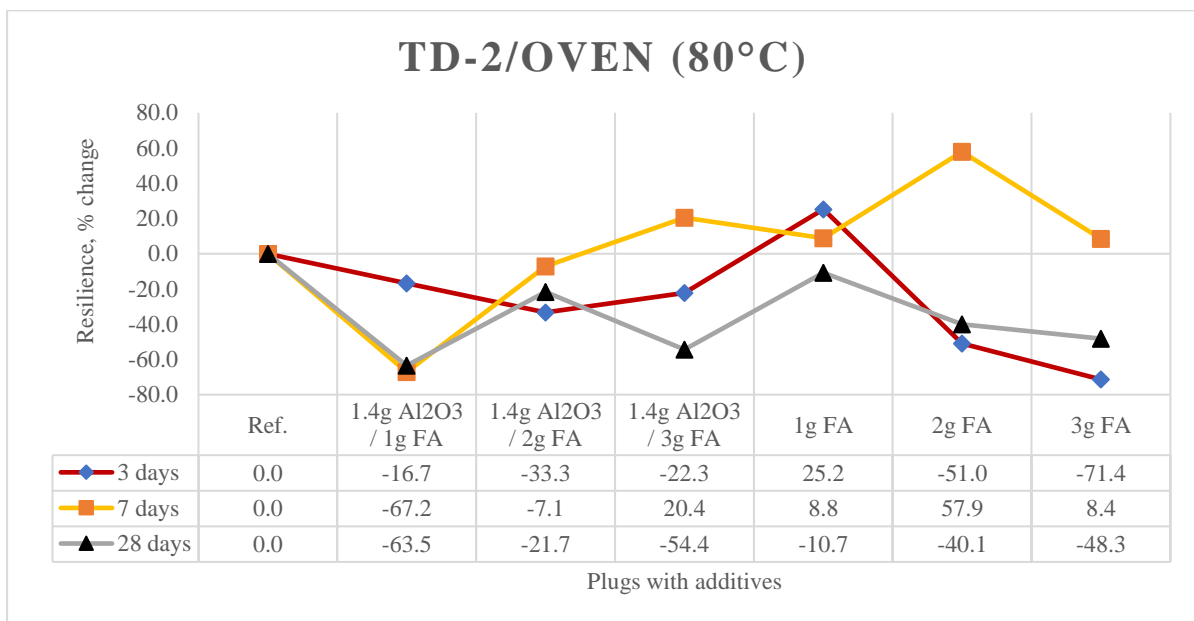
➤ **TD-2 – Oven – Young’s modulus**



➤ TD-2 – Room – Resilience

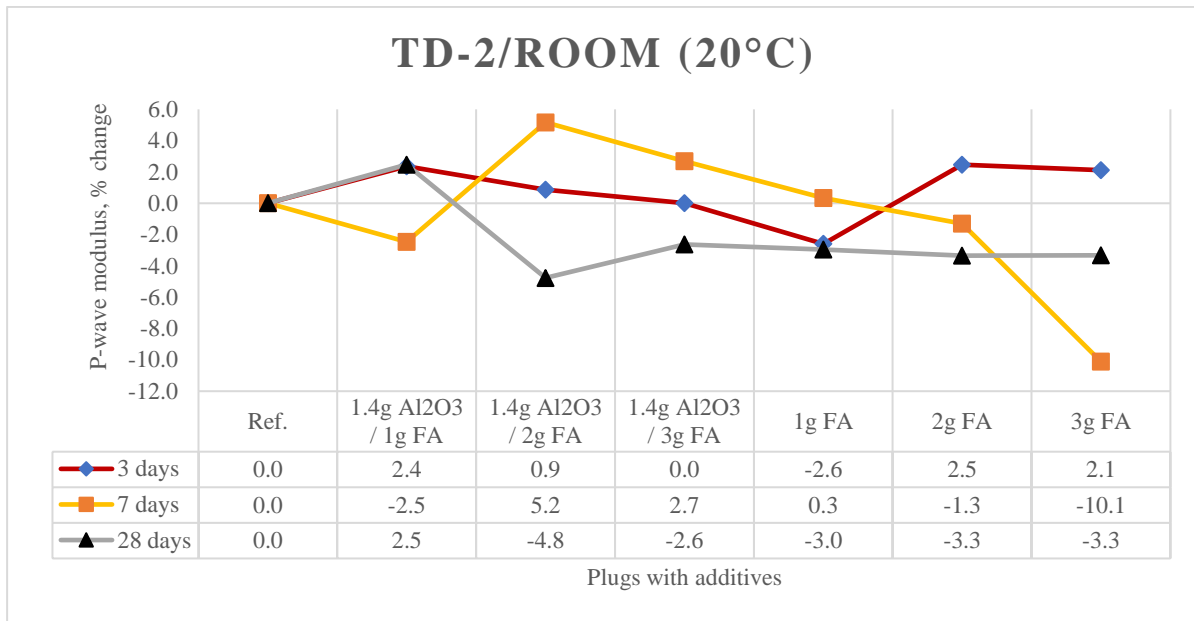


➤ TD-2 – Oven – Resilience

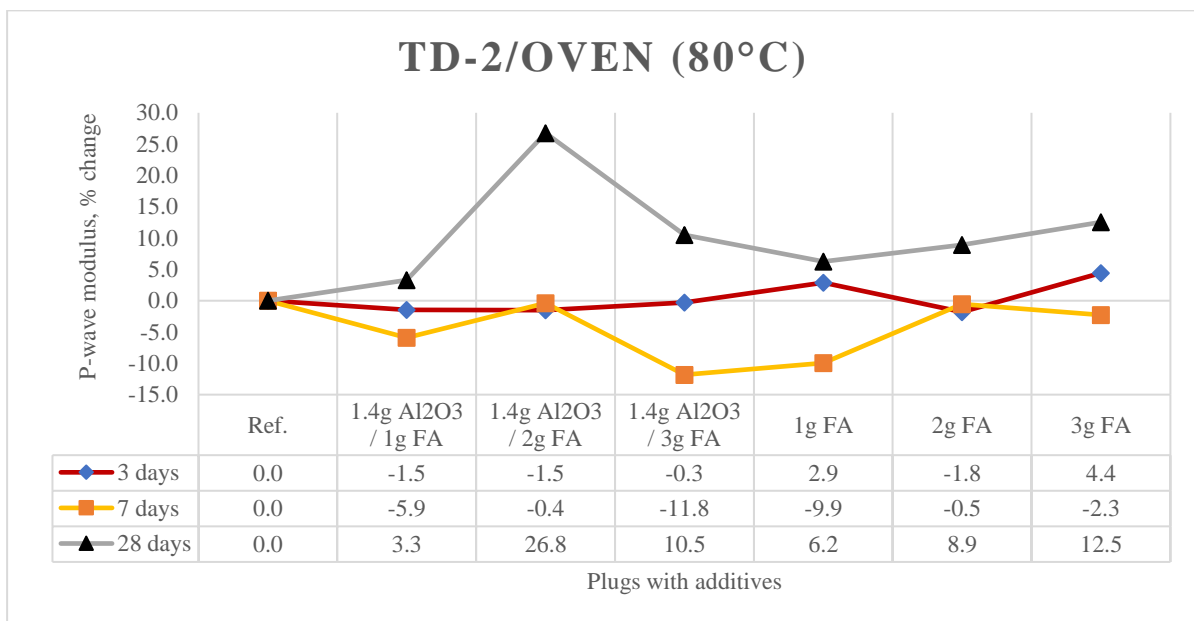




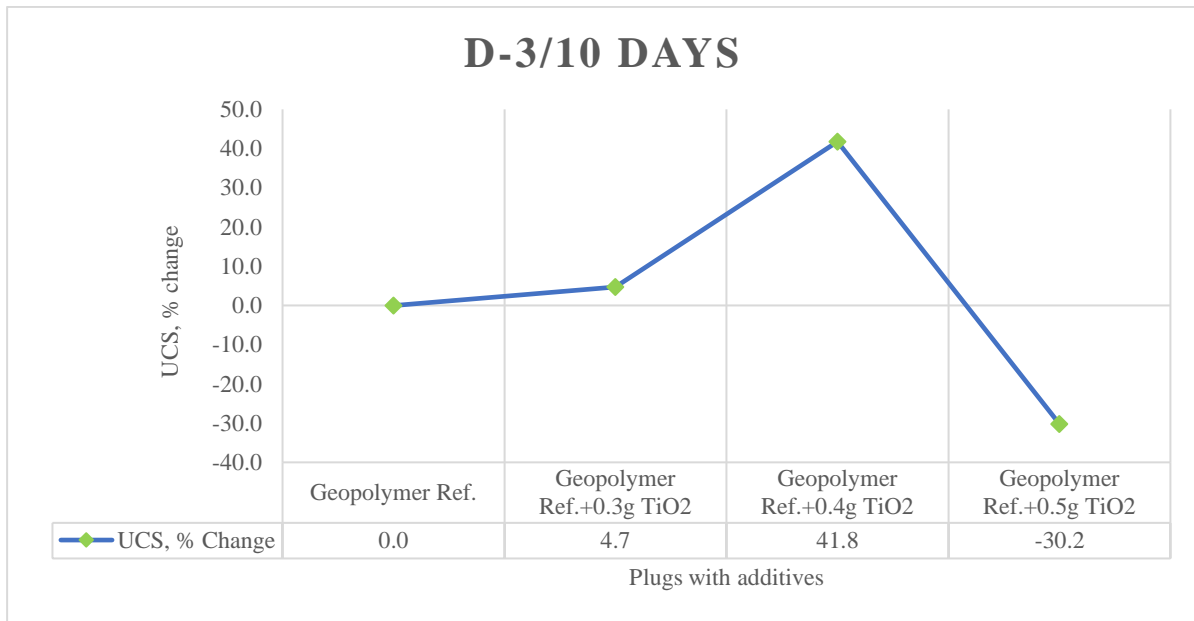
➤ **TD-2 – Room – P-wave modulus**



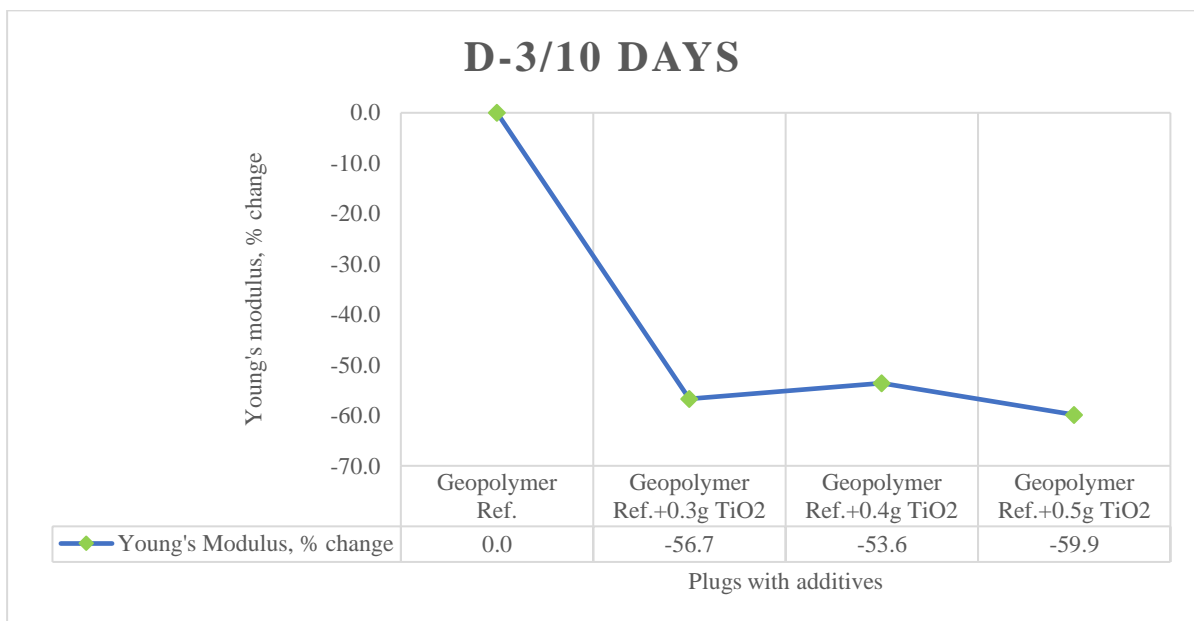
➤ **TD-2 – Oven – P-wave modulus**



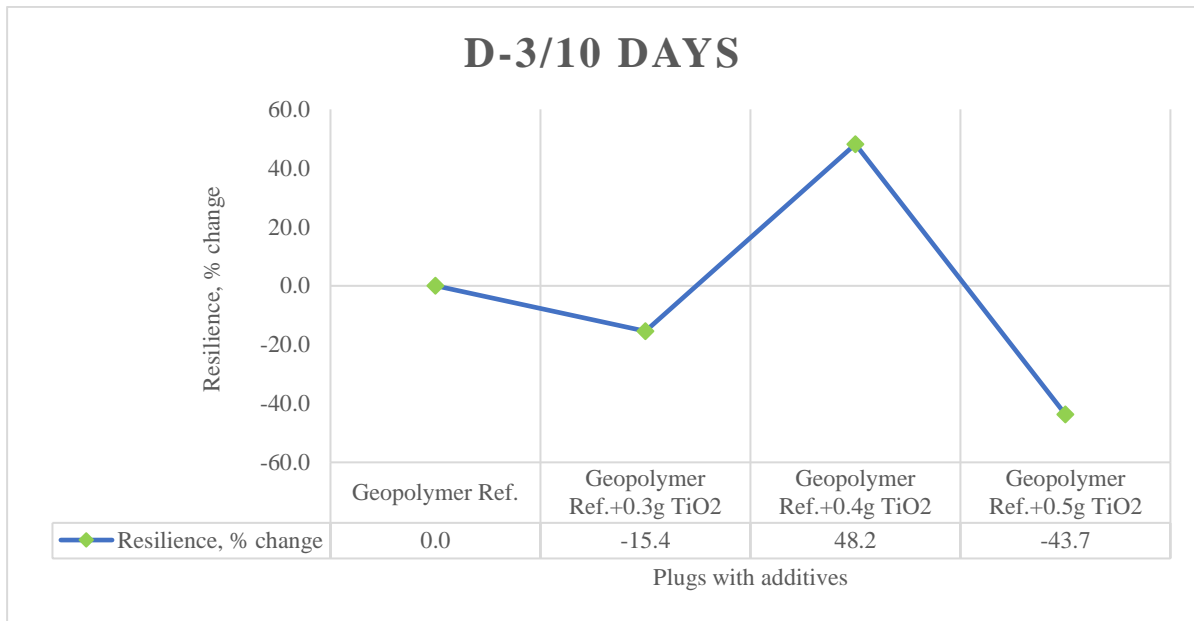
➤ **TD-3 – UCS**



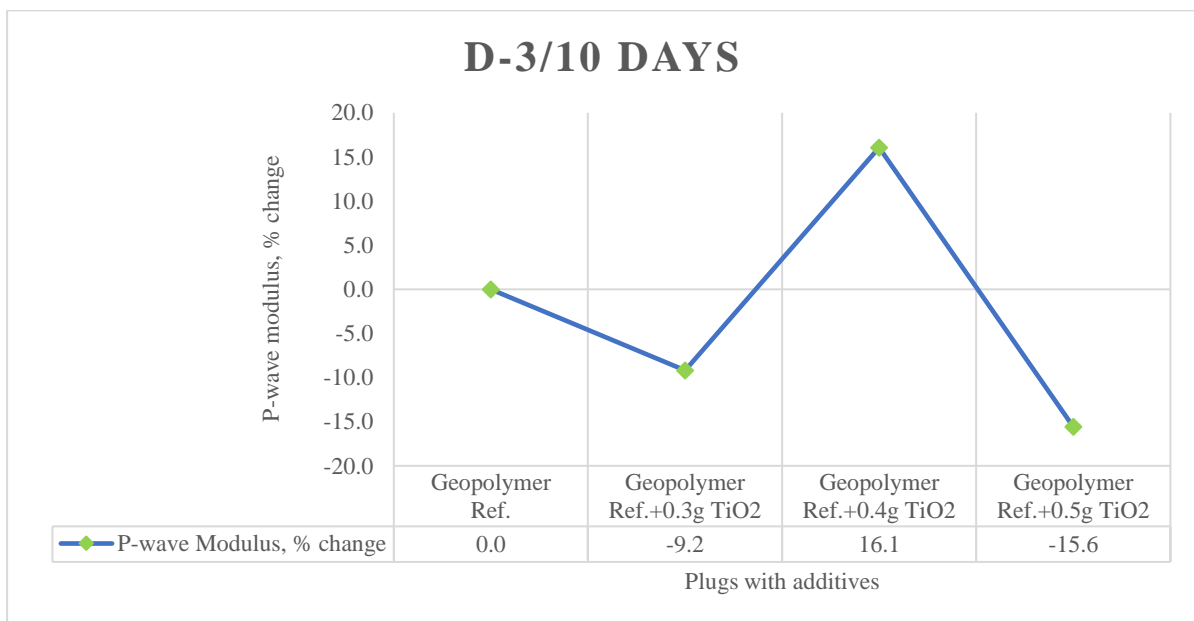
➤ **TD-3 – Young's modulus**



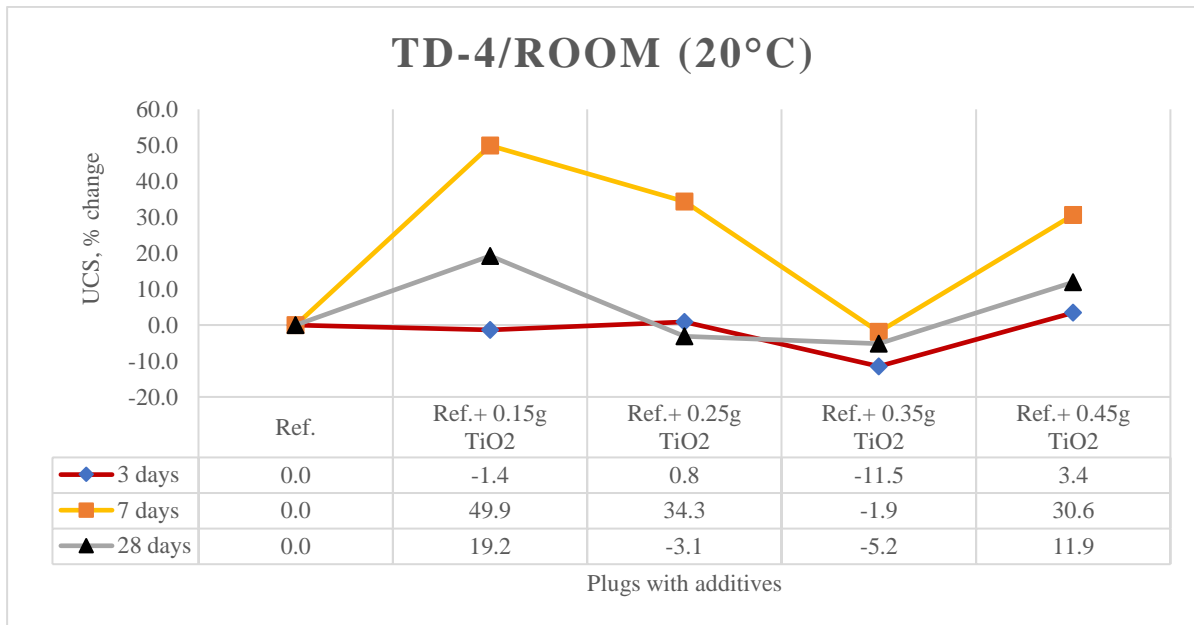
➤ **TD-3 – Resilience**



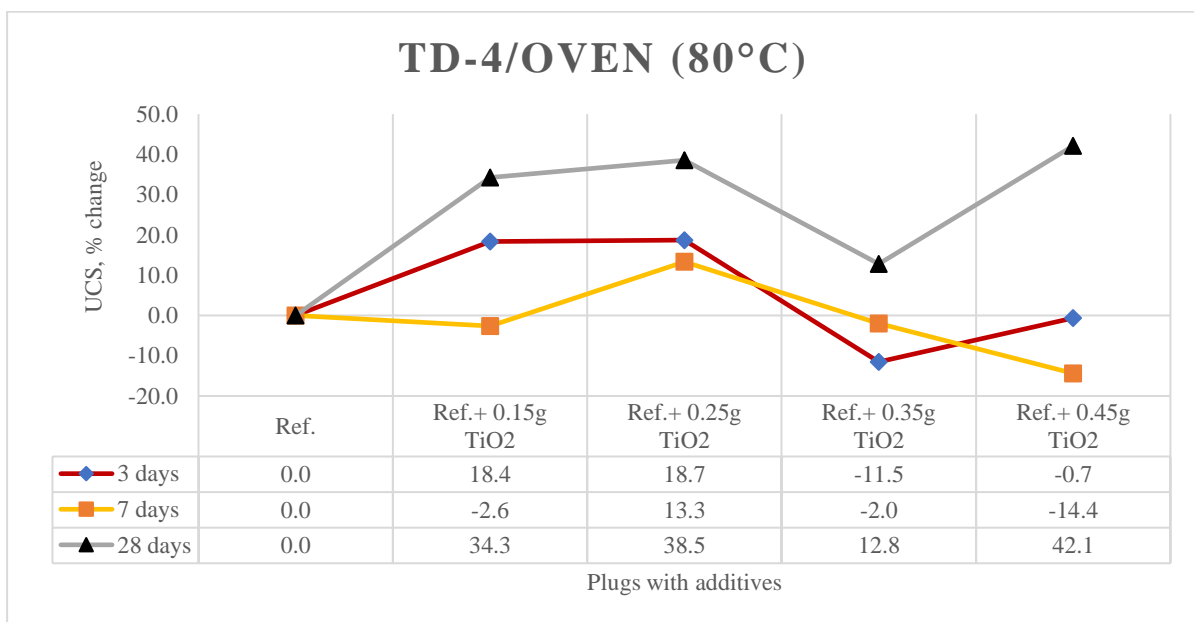
➤ **TD-3 – P-wave modulus**



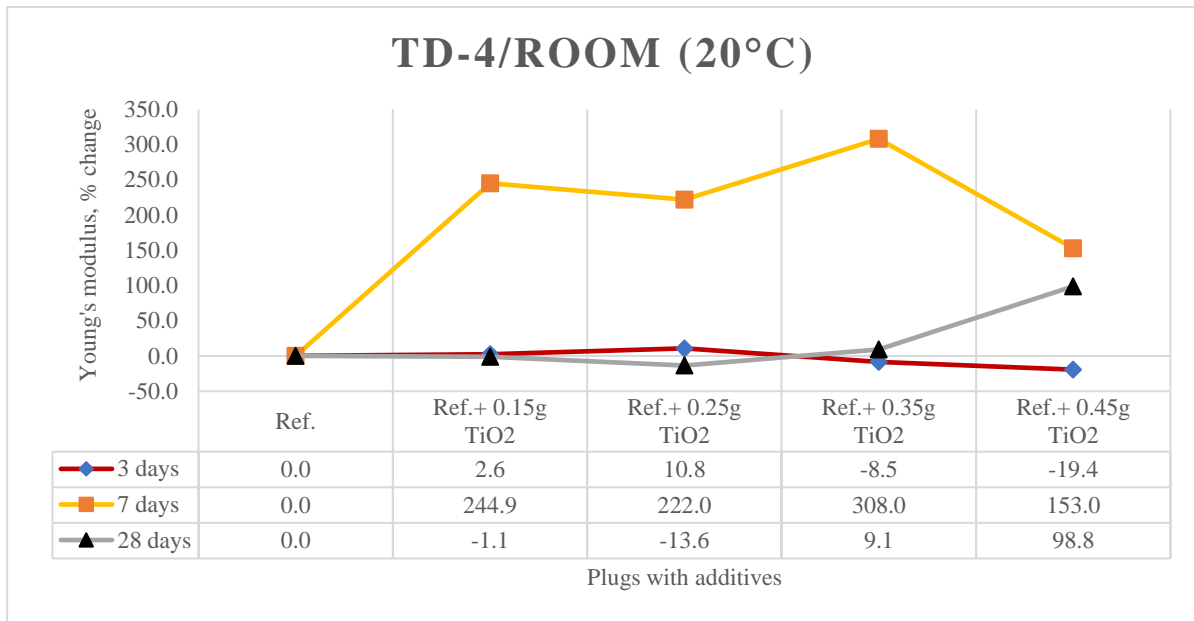
➤ TD-4 – Room – UCS



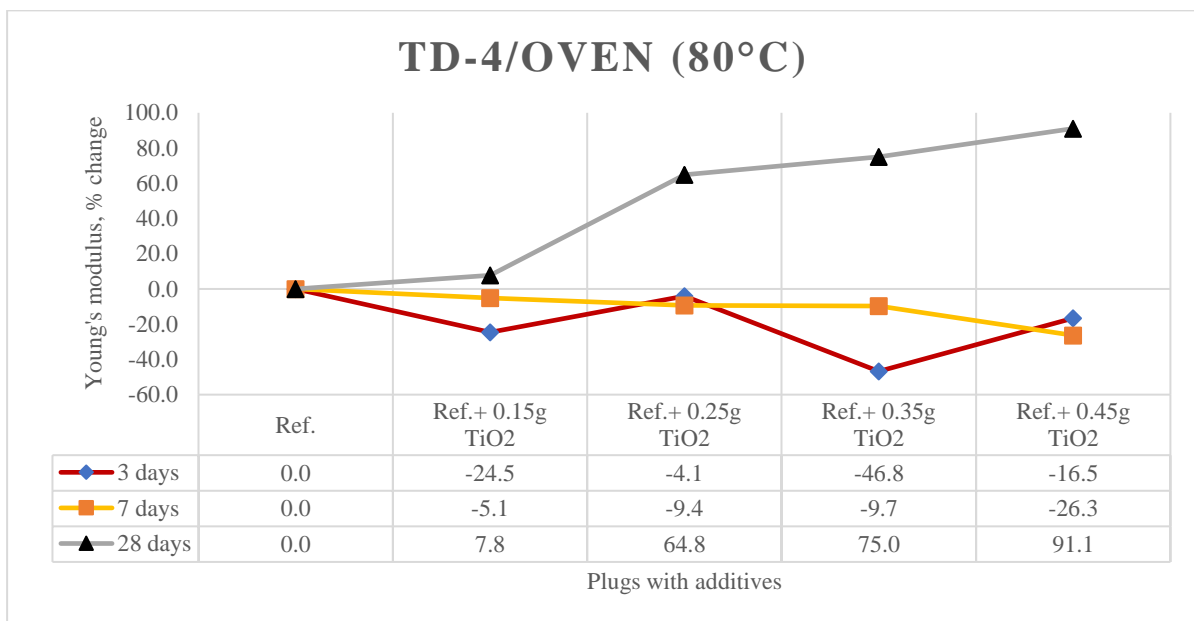
➤ TD-4 – Oven – UCS



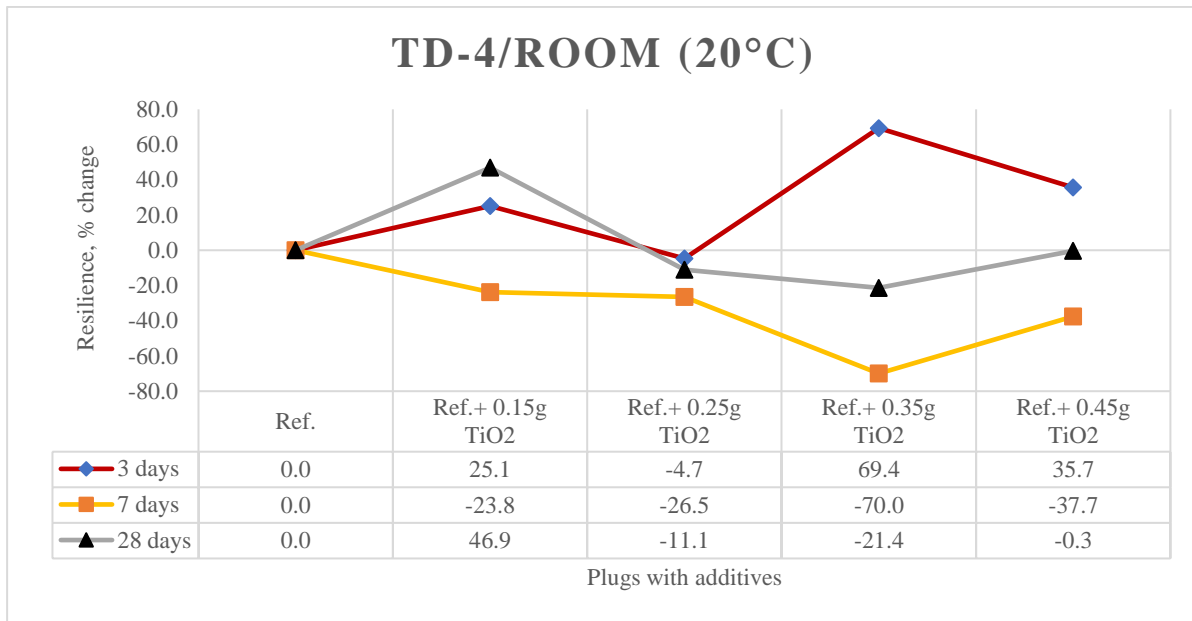
➤ **TD-4 – Room – Young’s modulus**



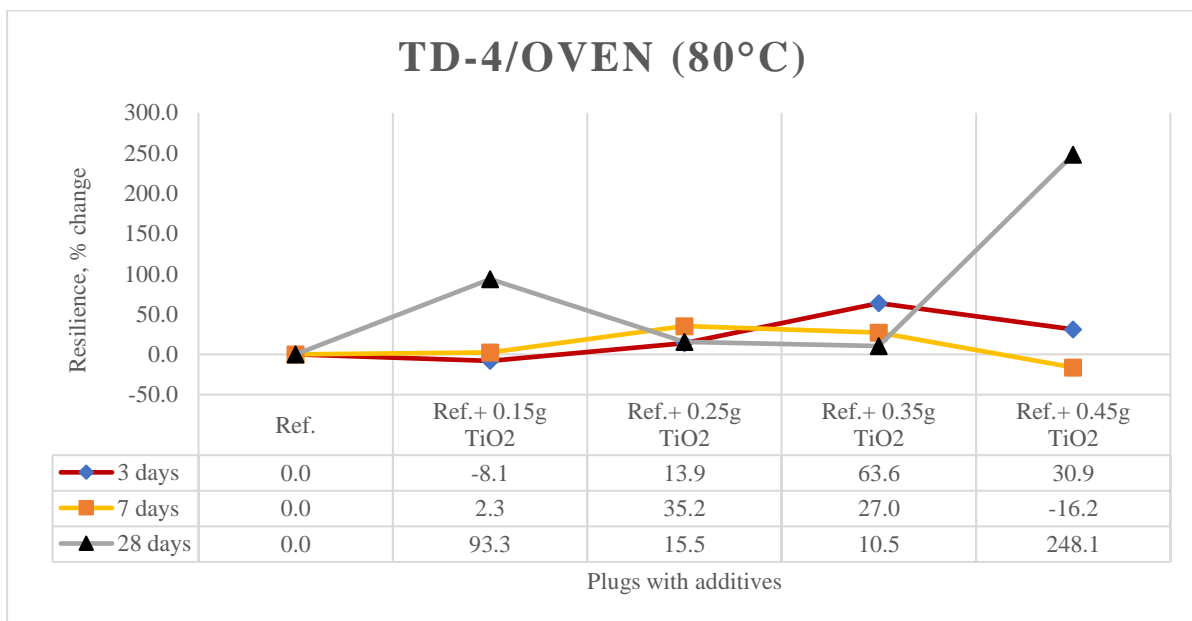
➤ **TD-4 – Oven – Young’s modulus**



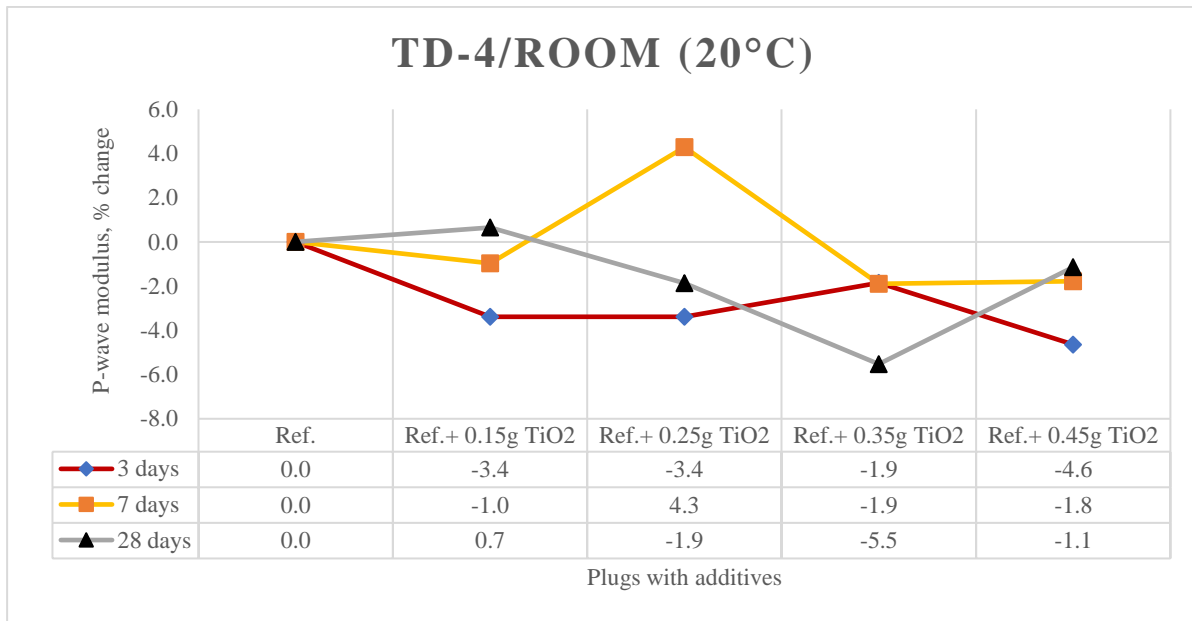
➤ **TD-4 – Room – Resilience**



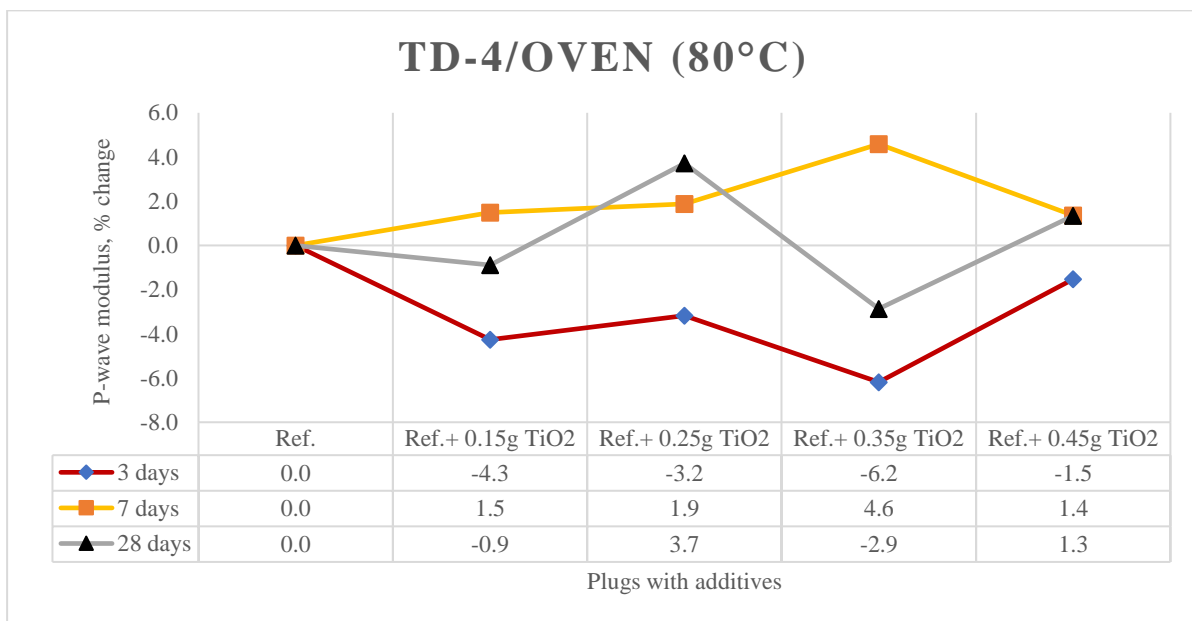
➤ **TD-4 – Oven – Resilience**



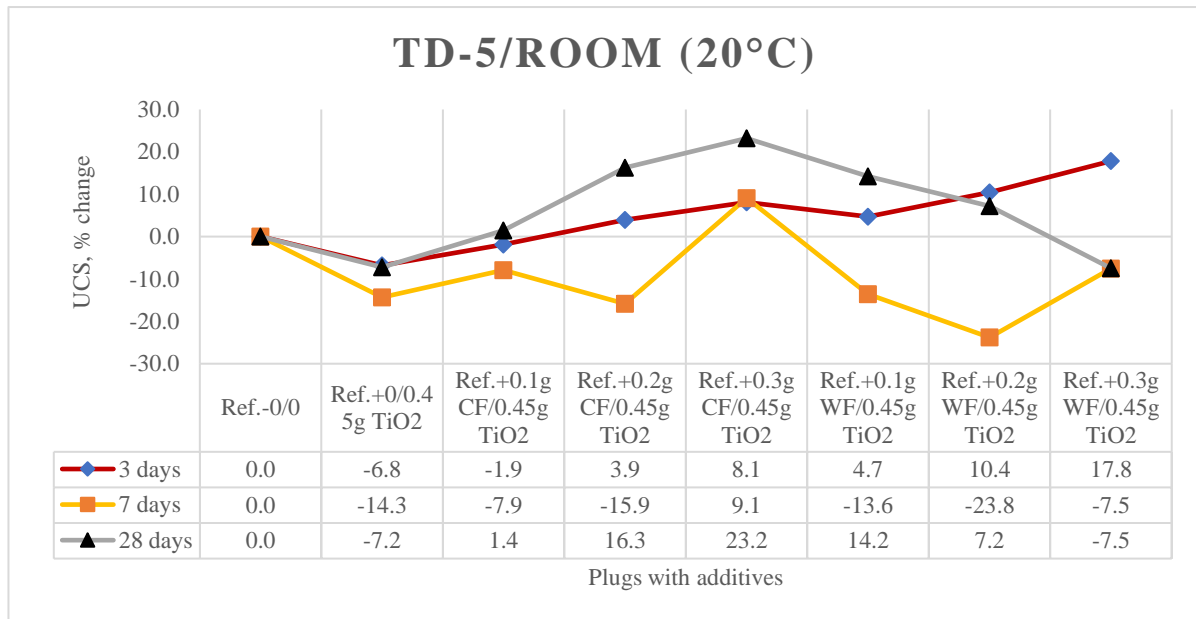
➤ **TD-4 – Room – P-wave modulus**



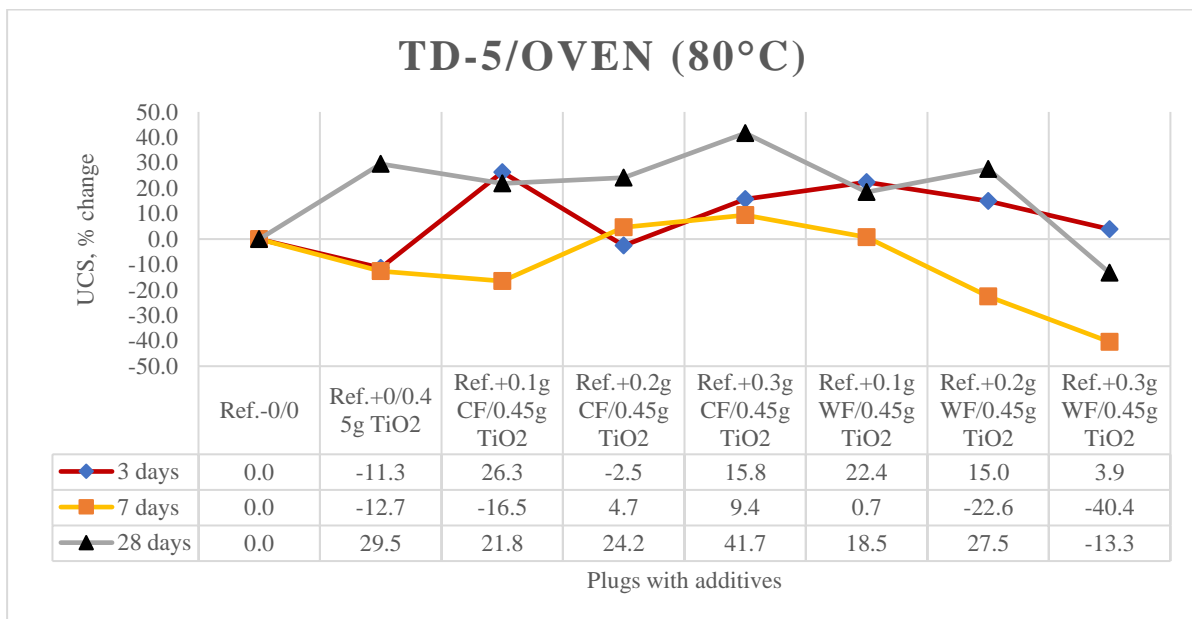
➤ **TD-4 – Oven – P-wave modulus**



➤ TD-5 – Room – UCS

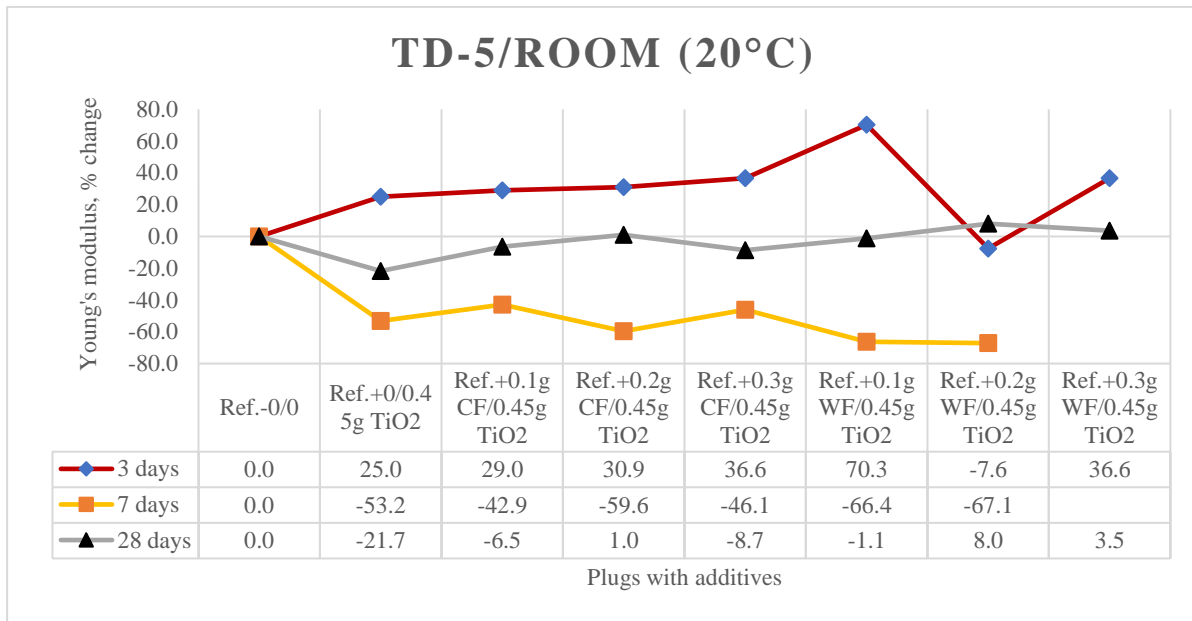


➤ TD-5 – Oven – UCS

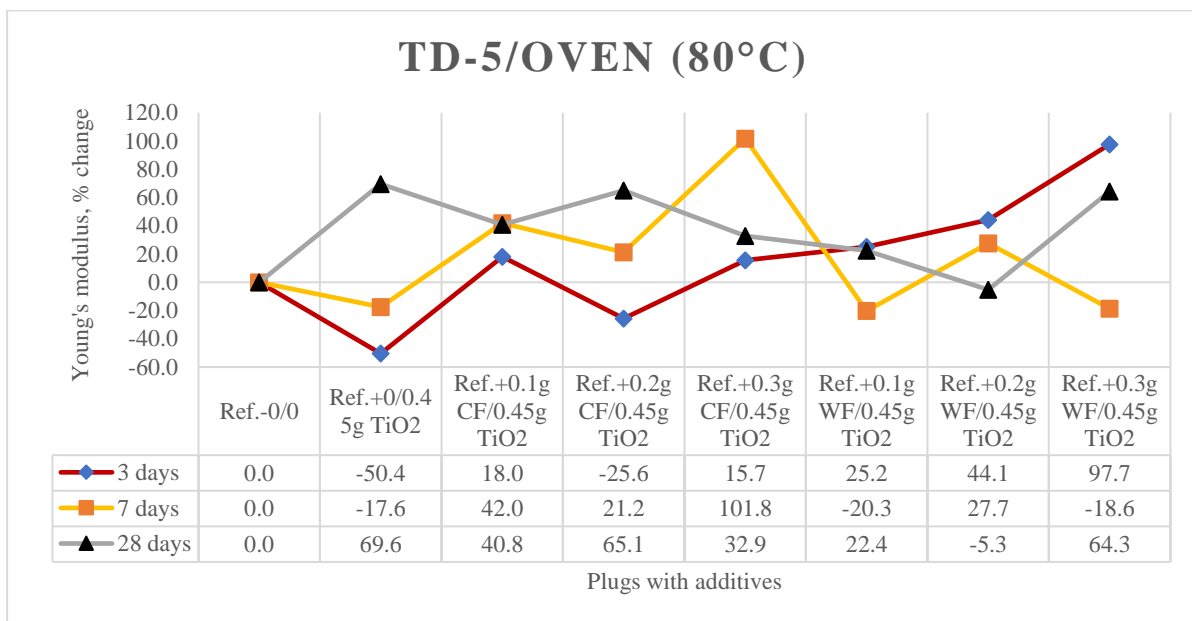




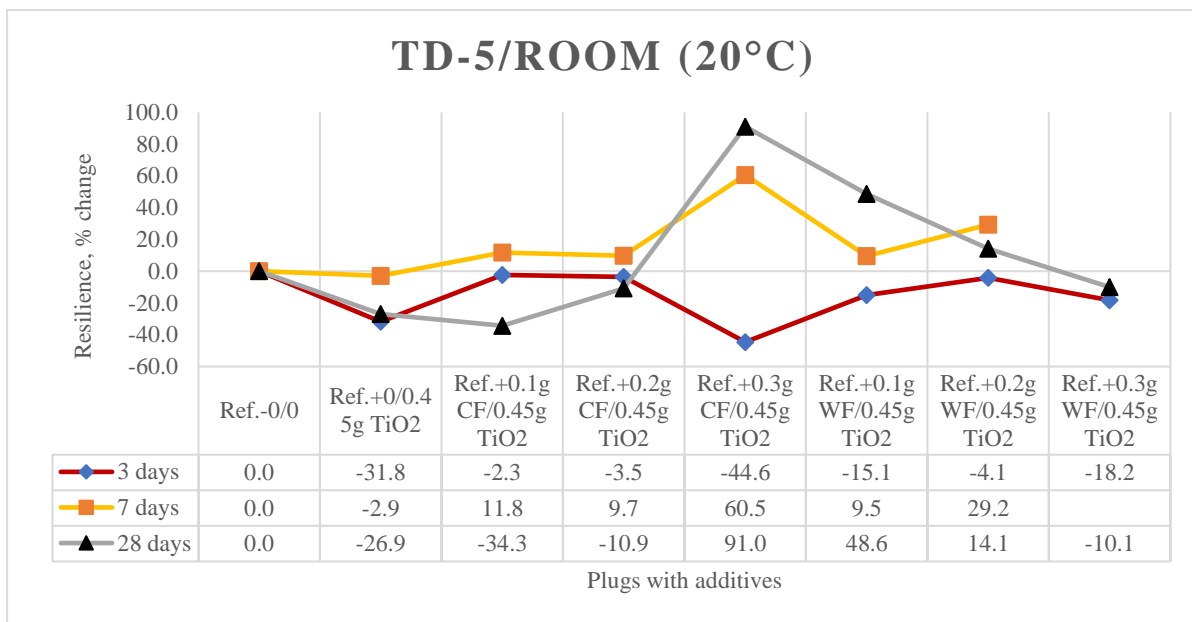
➤ TD-5 – Room – Young’s modulus



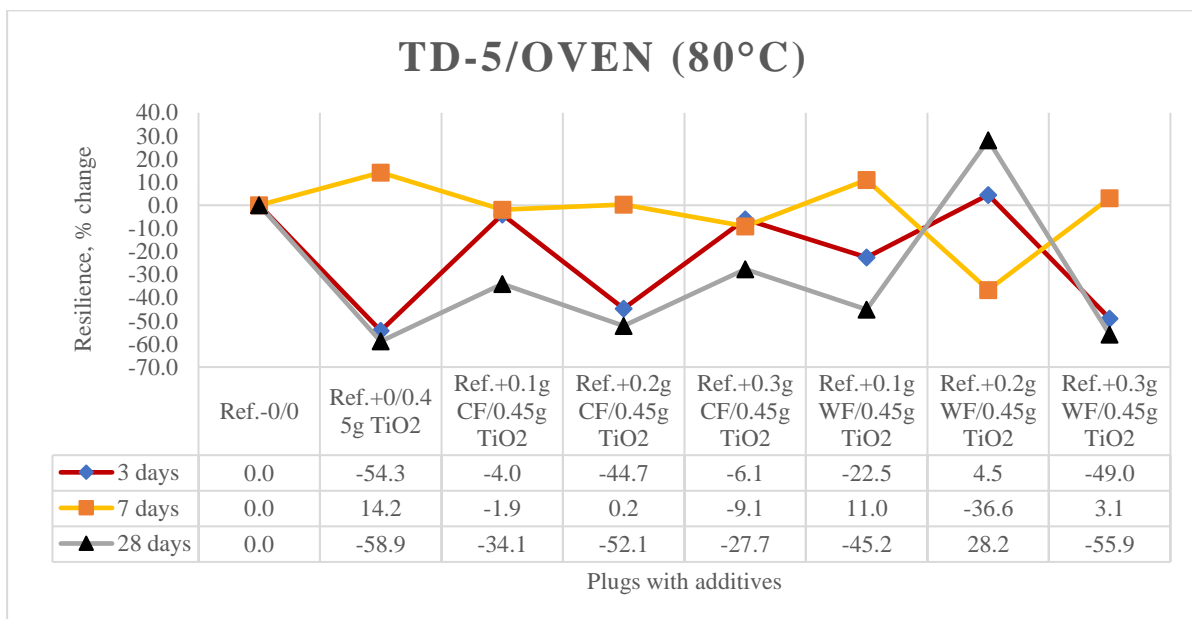
➤ TD-5 – Oven – Young’s modulus



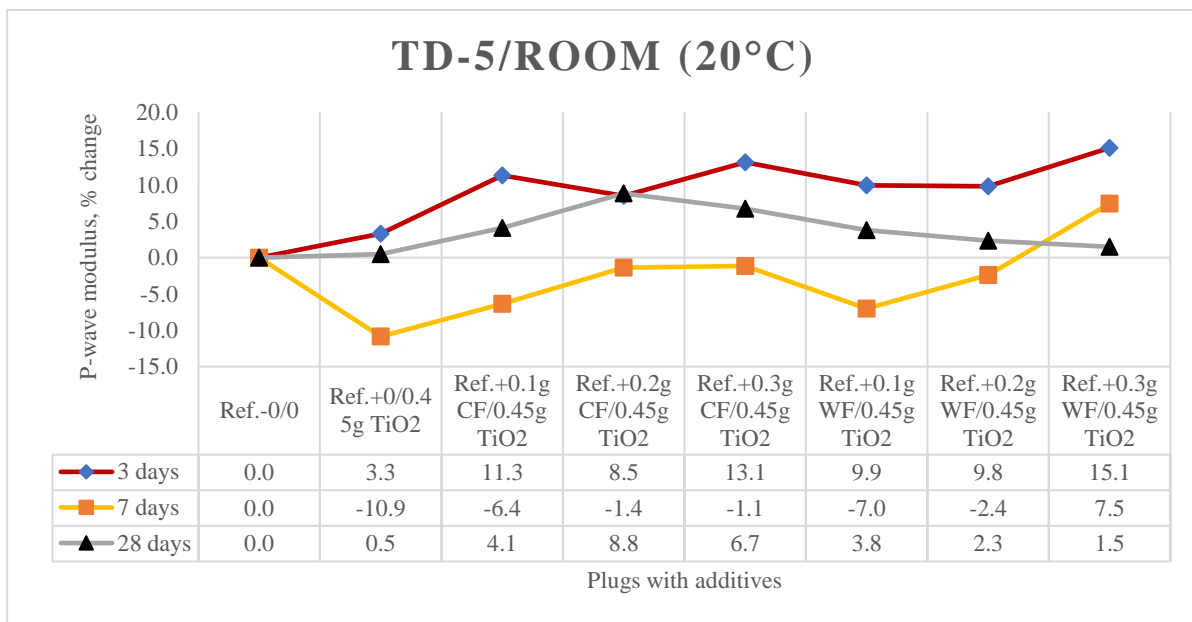
➤ TD-5 – Room – Resilience



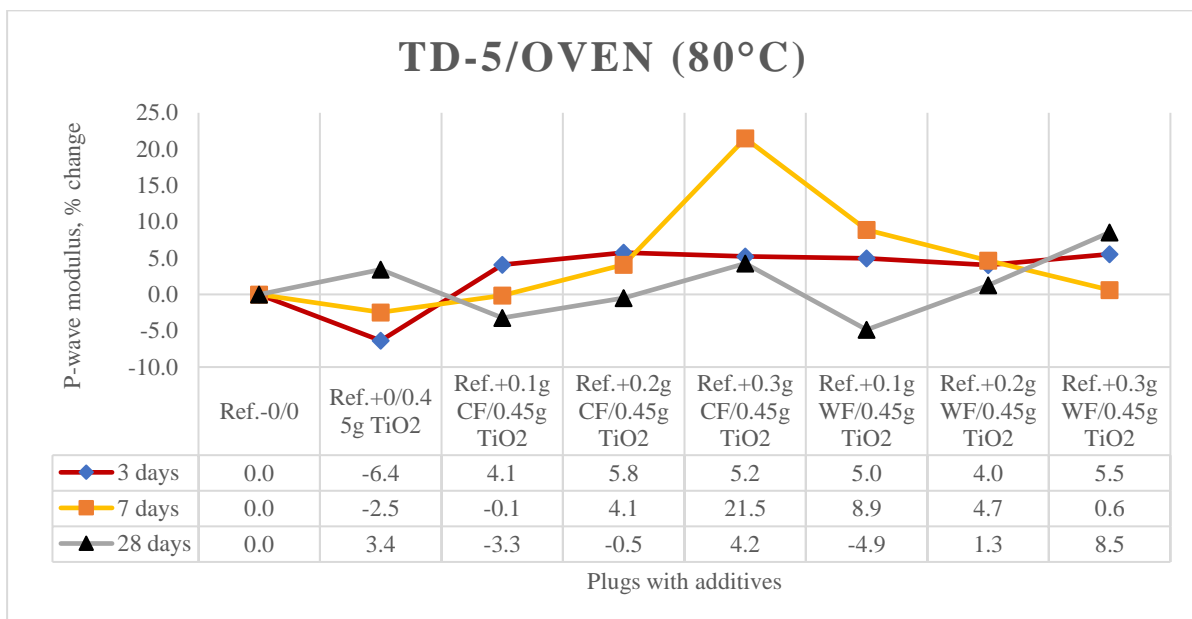
➤ TD-5 – Oven – Resilience



➤ **TD-5 – Room – P-wave modulus**



➤ **TD-5 – Oven – P-wave modulus**



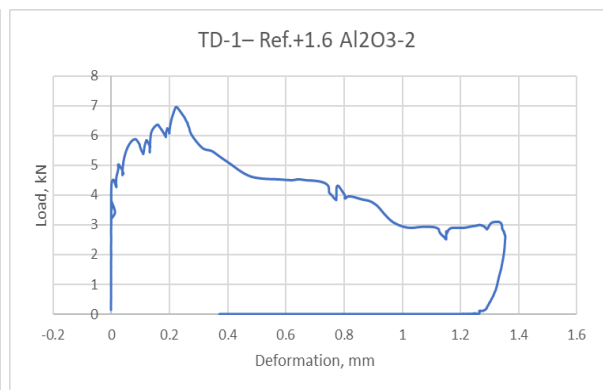
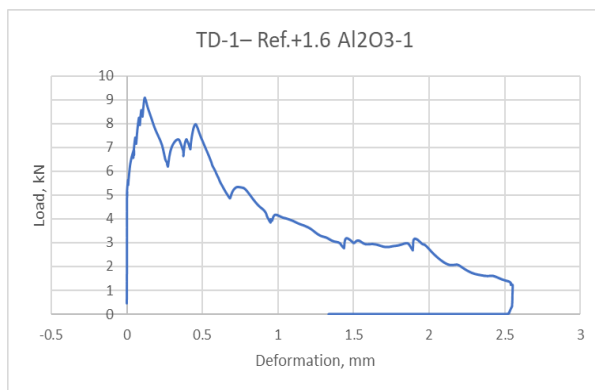
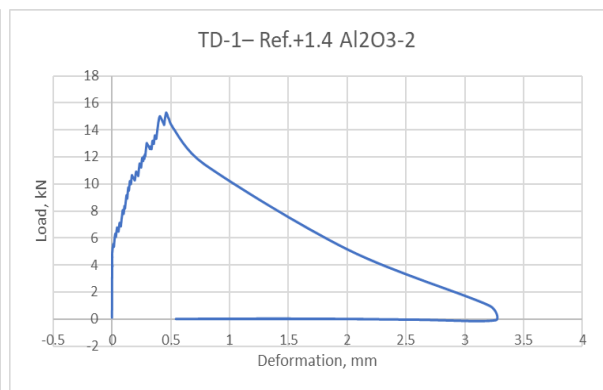
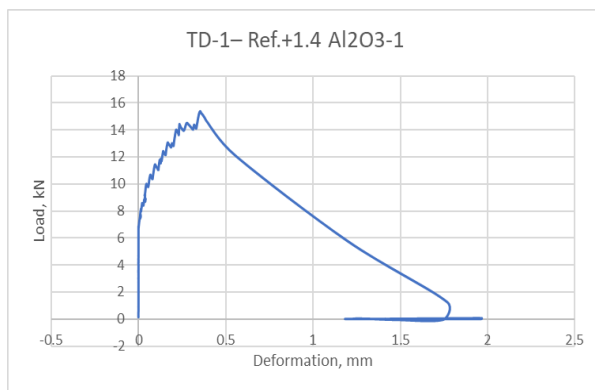
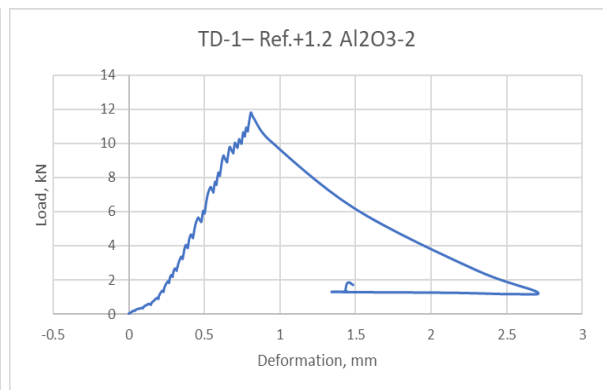
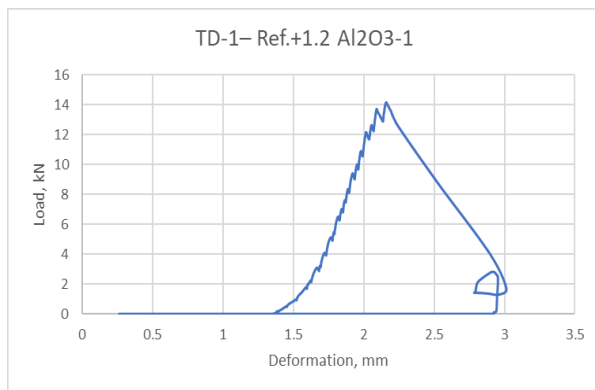
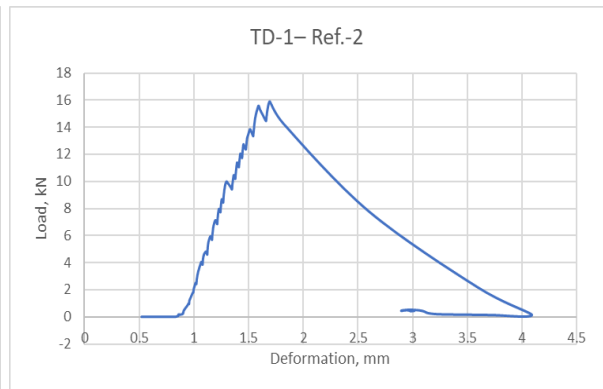
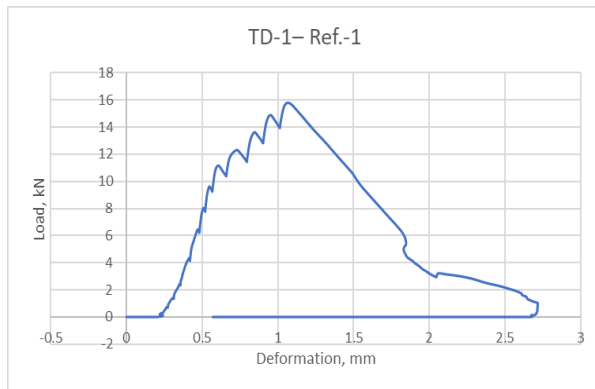
## **Appendix B – Load vs deformation diagrams**

In this appendix, load vs deformation curves will be shown. Load (kN) will be on x-axis and deformation (mm) on y-axis.

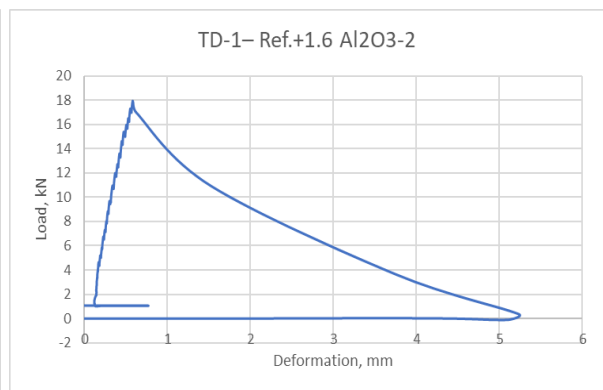
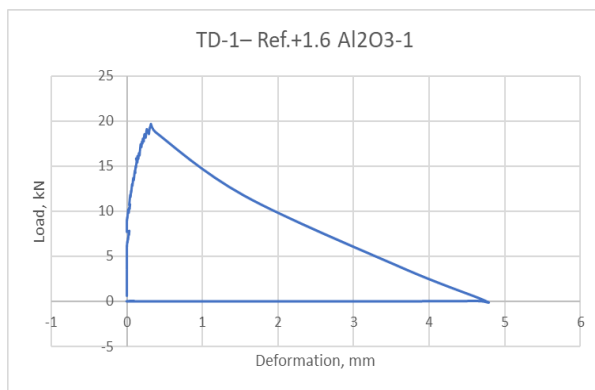
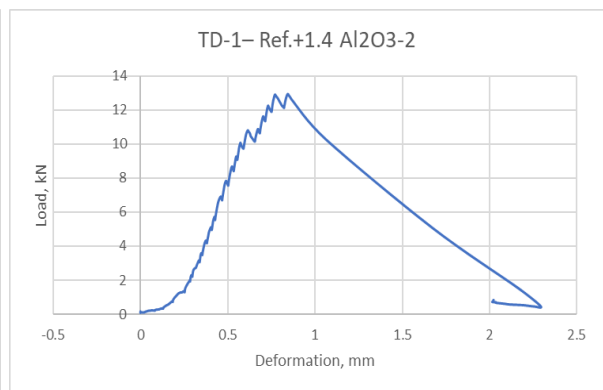
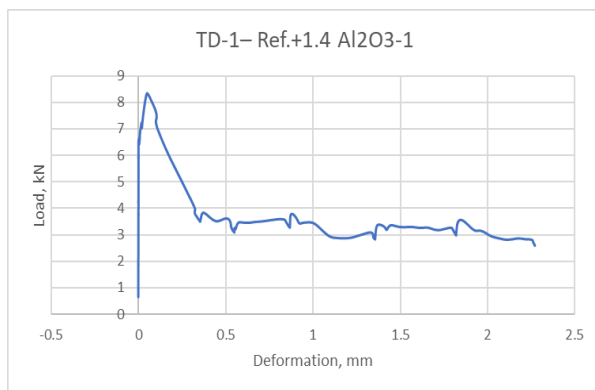
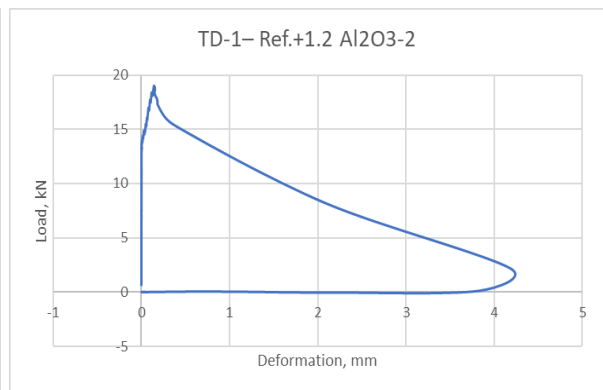
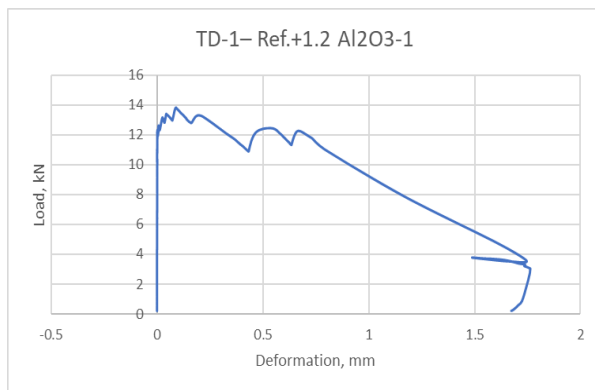
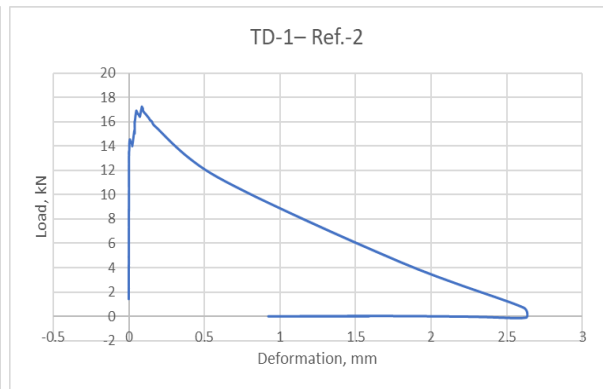
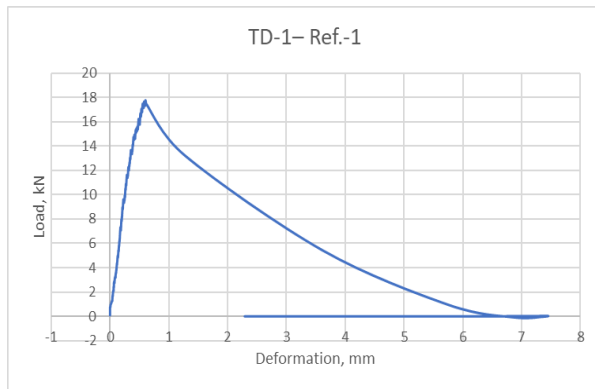
It is to be noted that some samples might be missing because of them being defective, since this happened occasionally but rarely. A few unfortunate human mistakes in measuring deformation may account for their absence. There will be diagrams of such samples as well, where only load was properly measured but deformation was not due to malfunction in the deformation sensor.

The diagrams are arranged by their test designs, test batches with their curing environments and curing ages as described in [section 3.2.1](#).

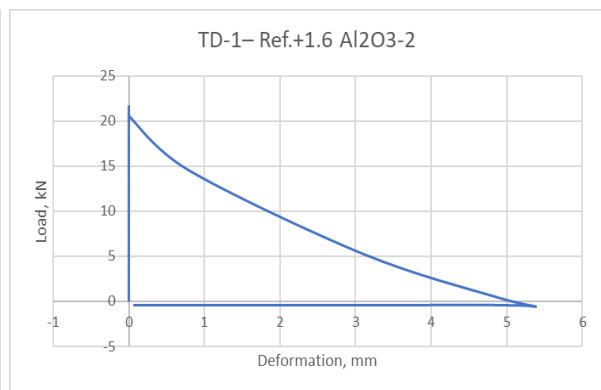
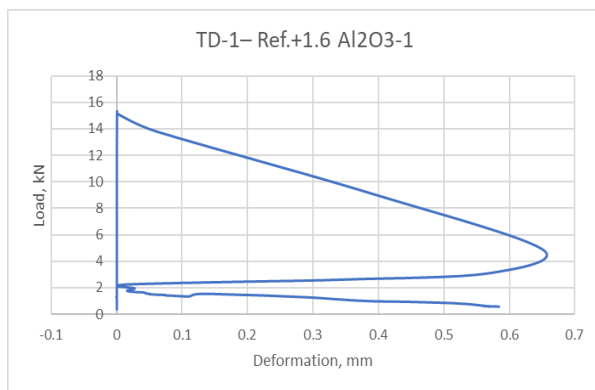
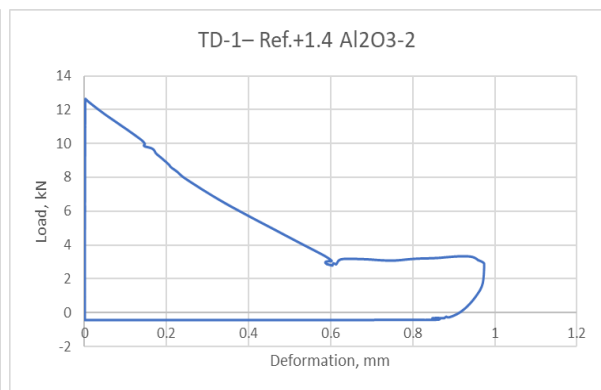
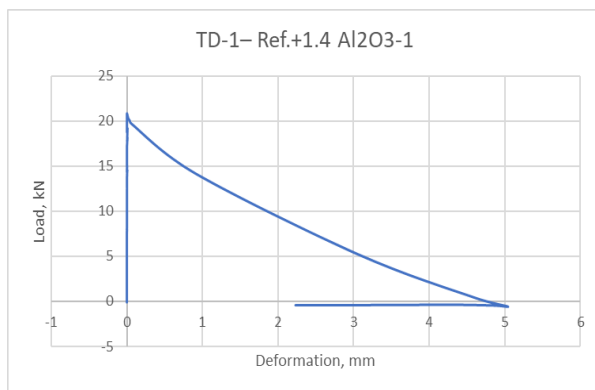
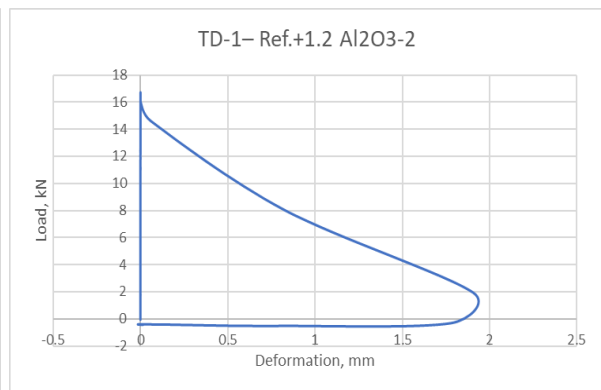
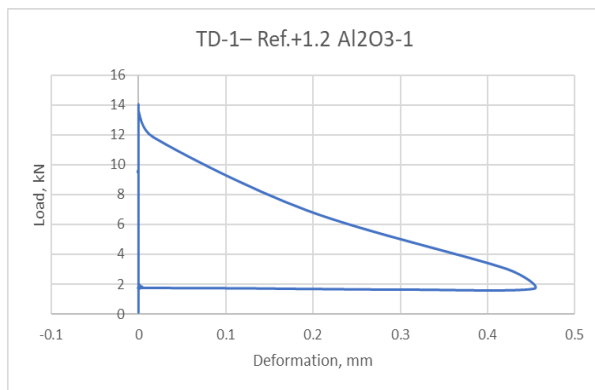
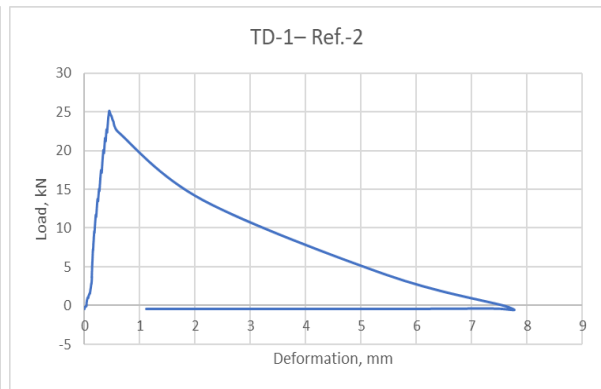
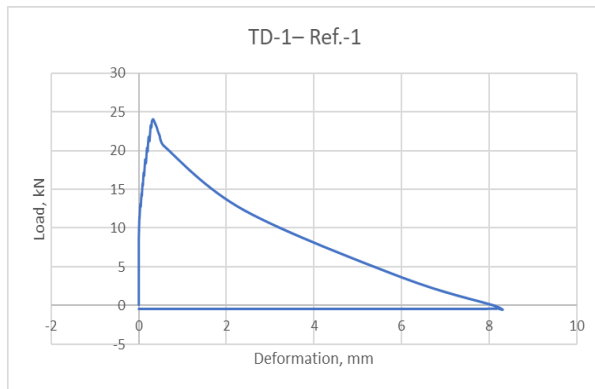
➤ **TD-1 – TB-1-R – 3 days**



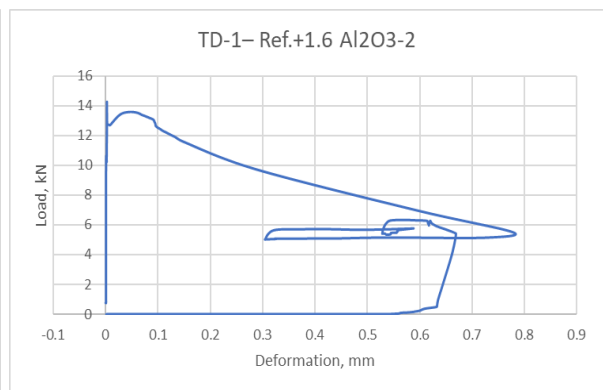
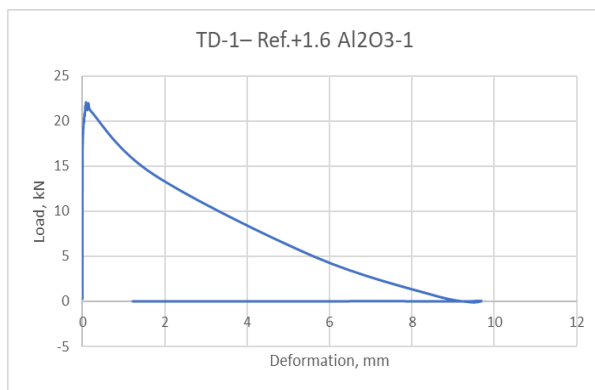
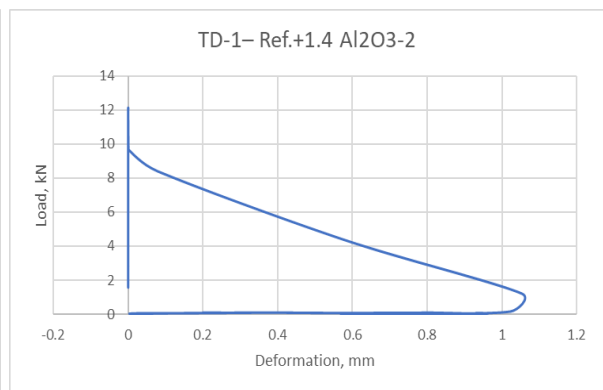
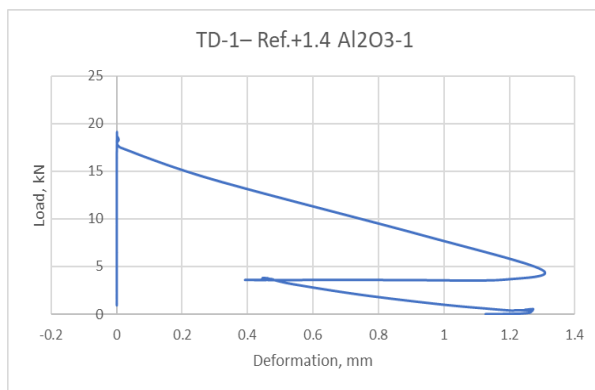
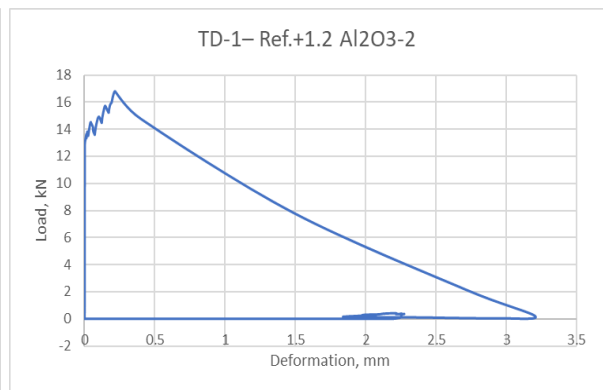
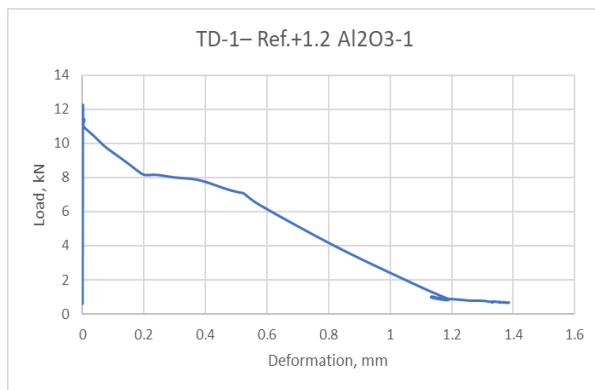
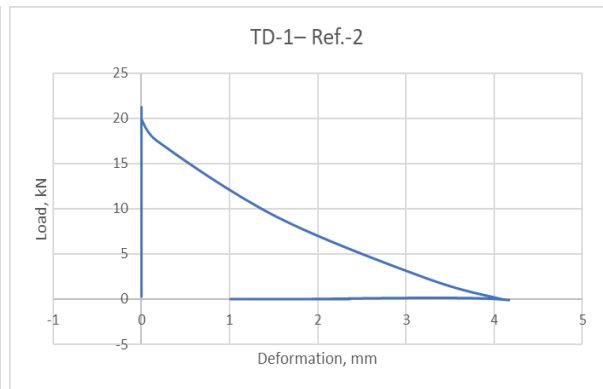
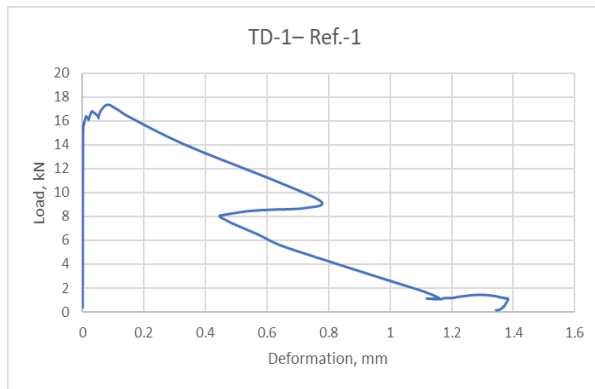
➤ **TD-1 – TB-1-O – 3 days**



➤ TD-1 – TB-2-R – 7 days

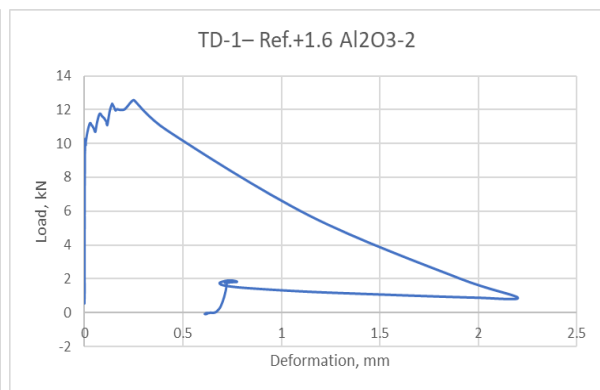
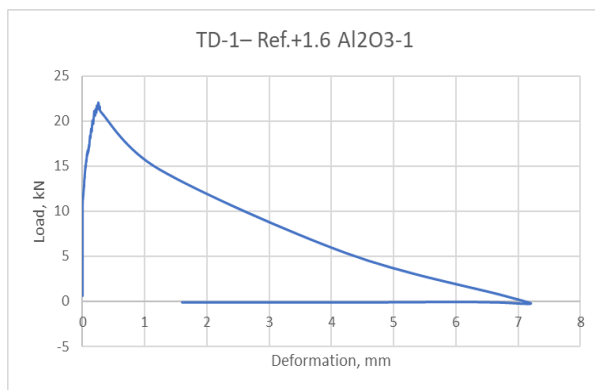
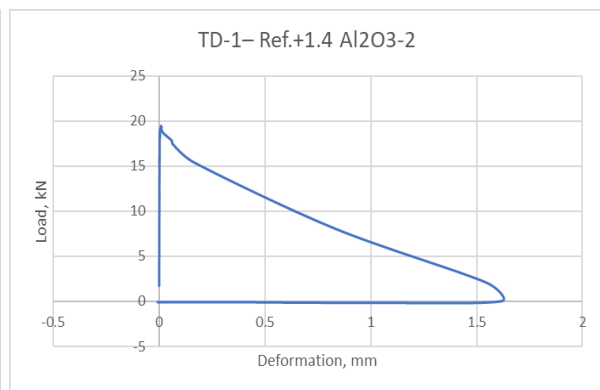
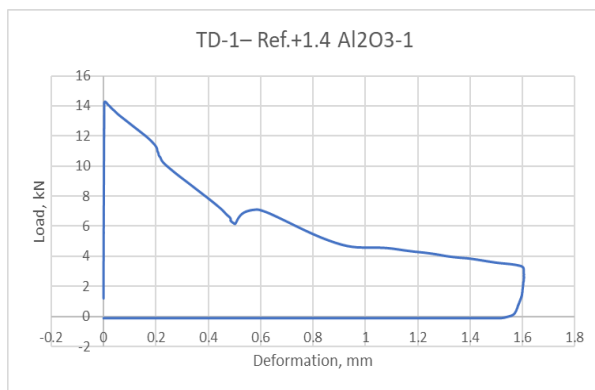
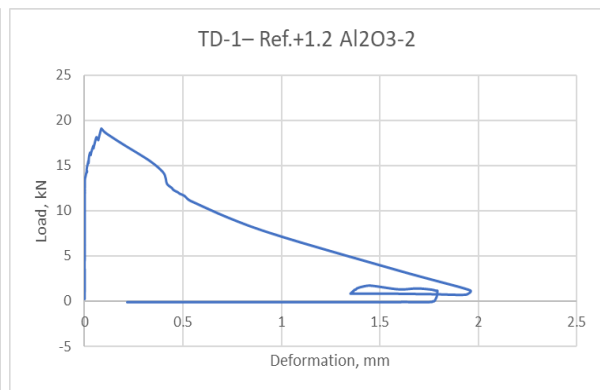
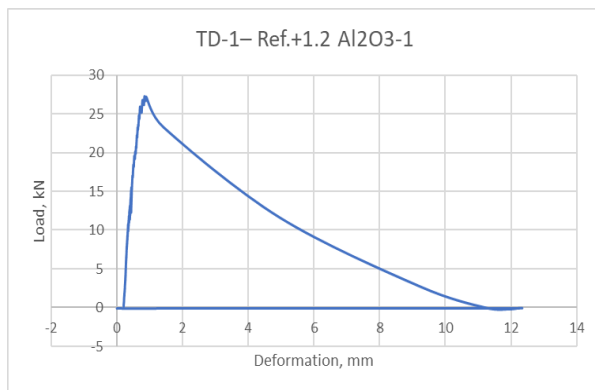
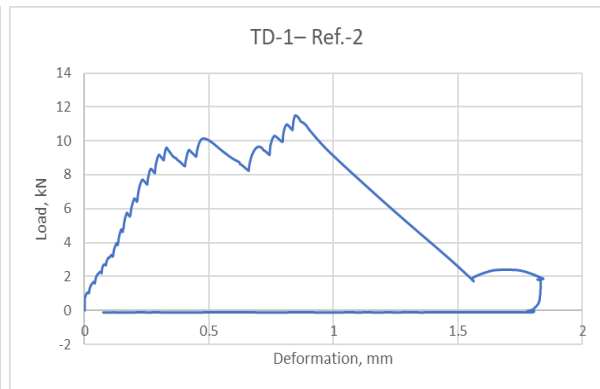
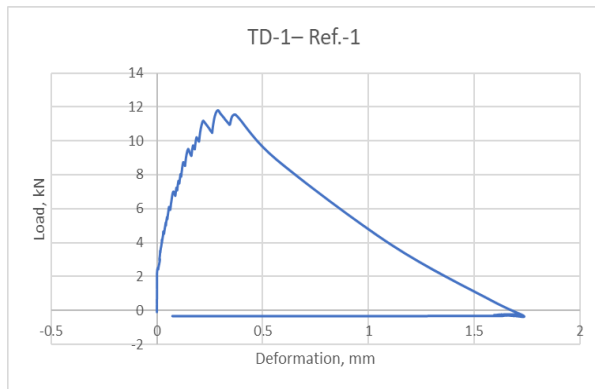


➤ **TD-1 – TB-2-O – 7 days**

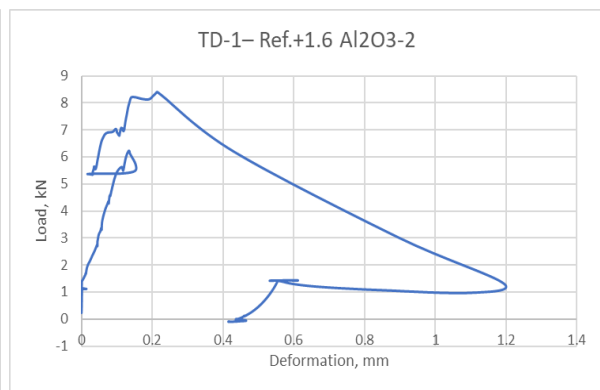
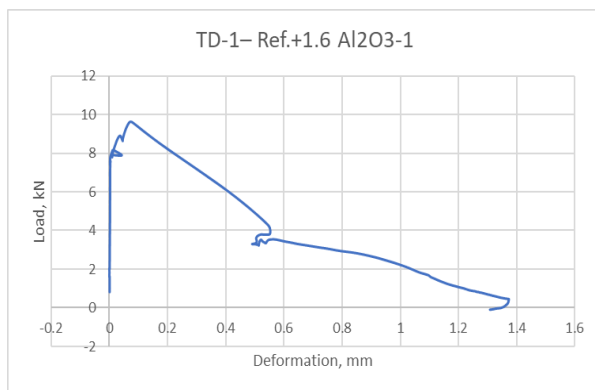
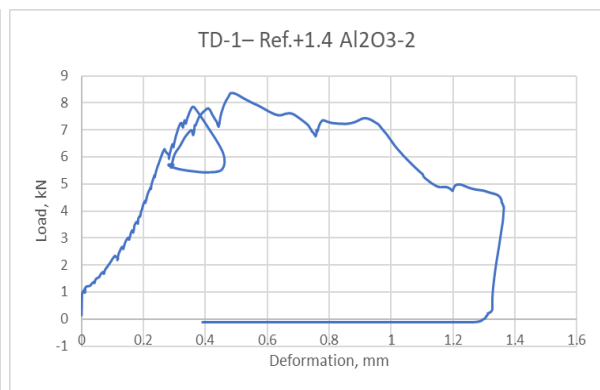
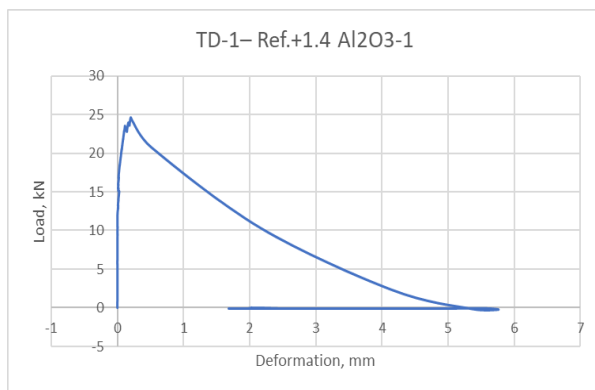
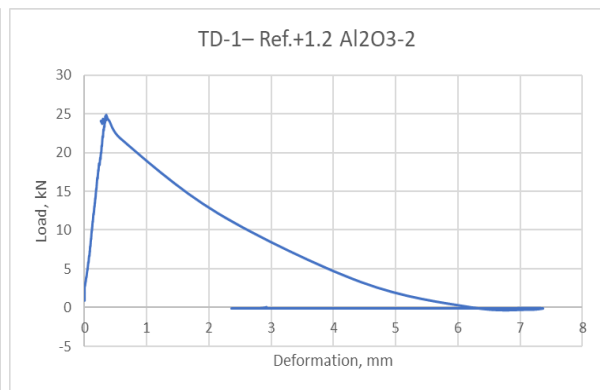
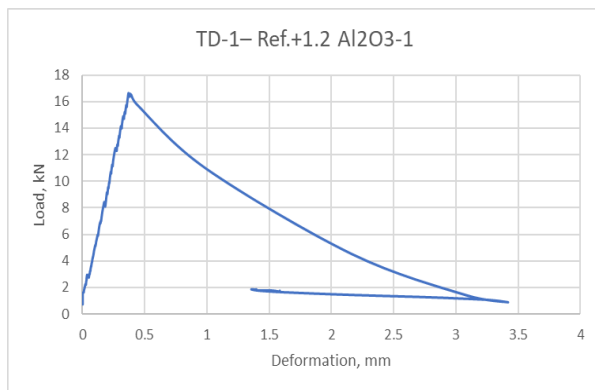
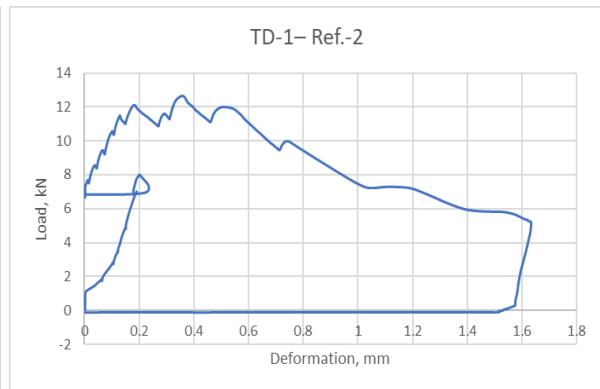
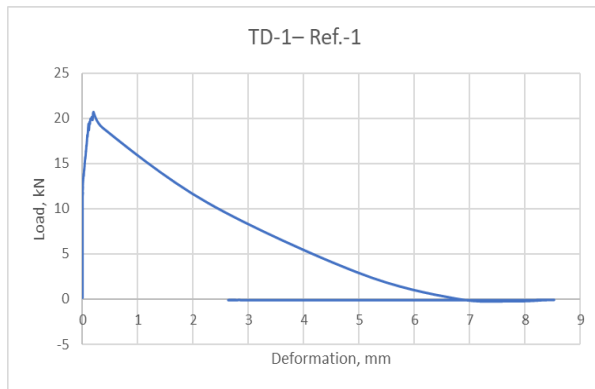




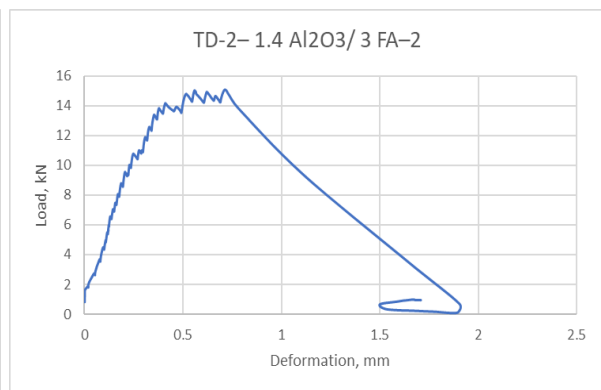
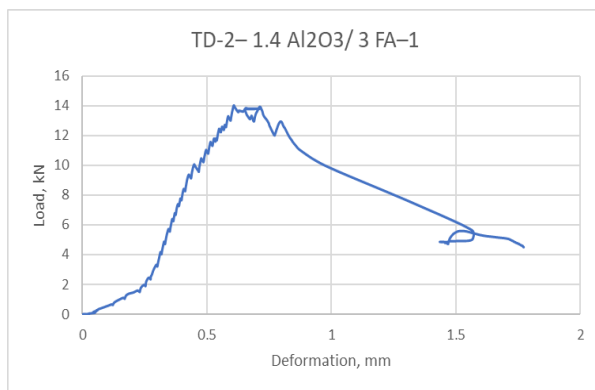
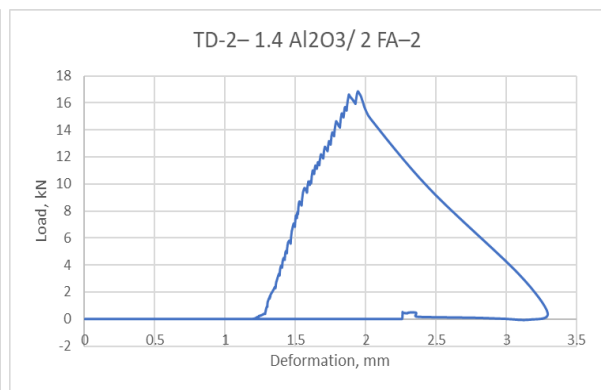
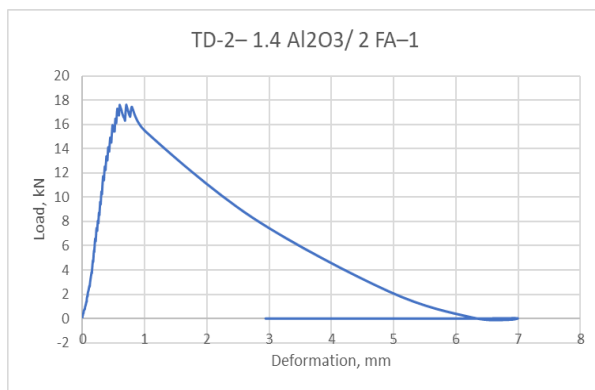
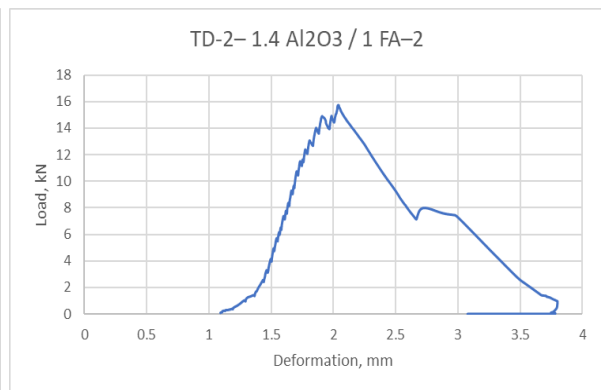
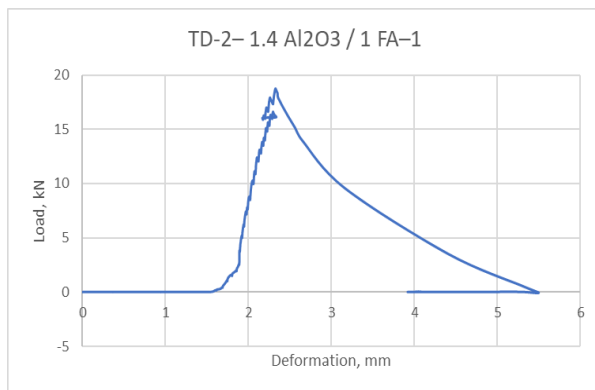
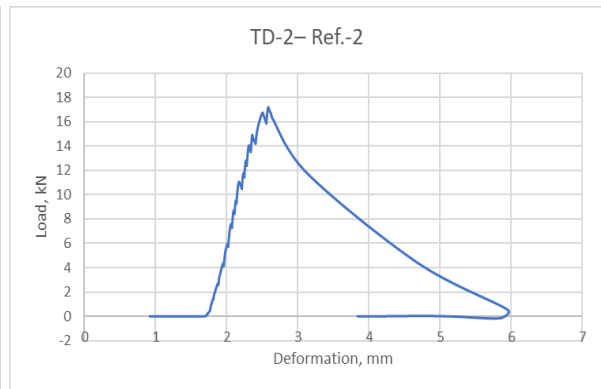
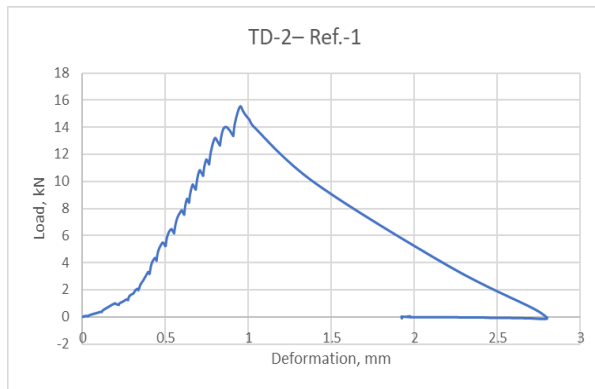
➤ **TD-1 – TB-3-R – 28 days**



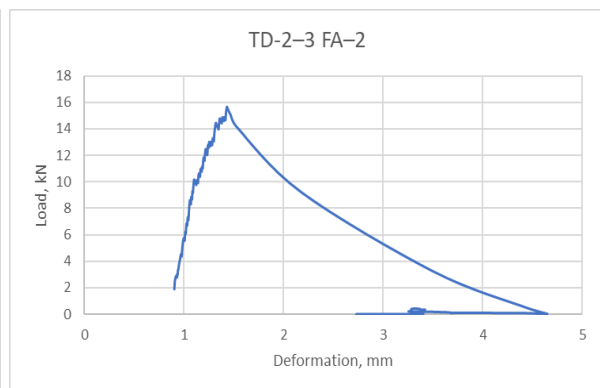
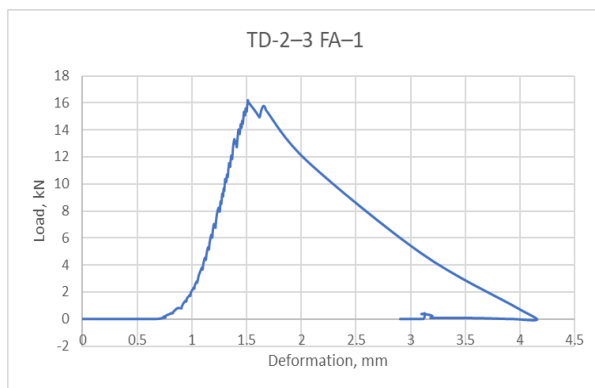
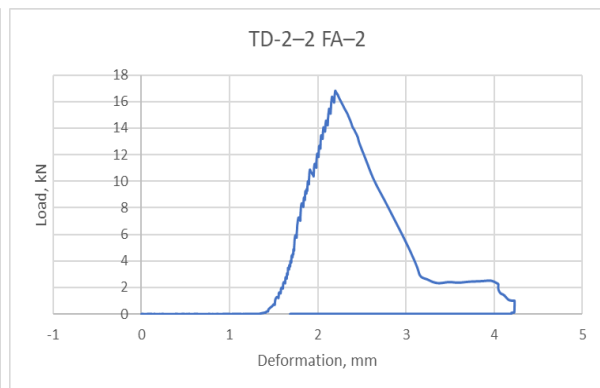
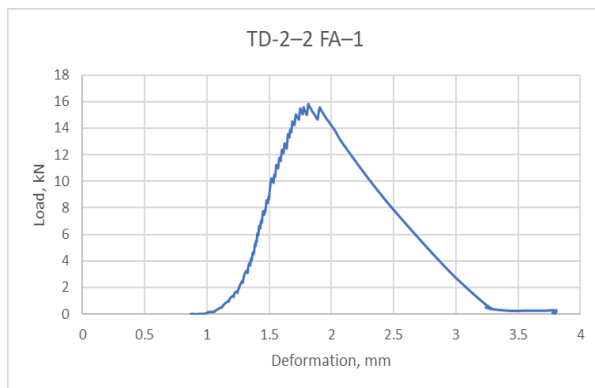
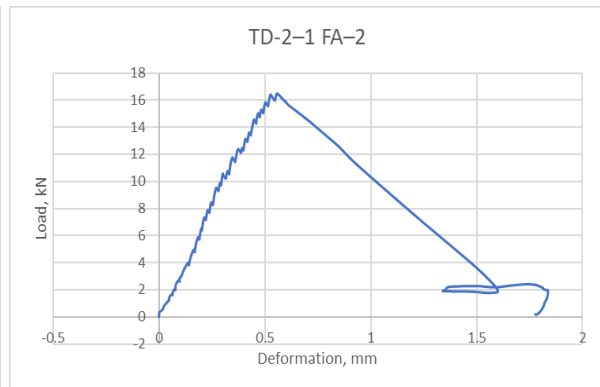
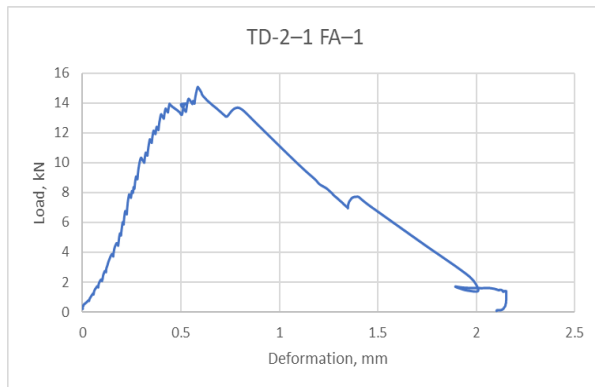
➤ TD-1 – TB-3-O – 28 days



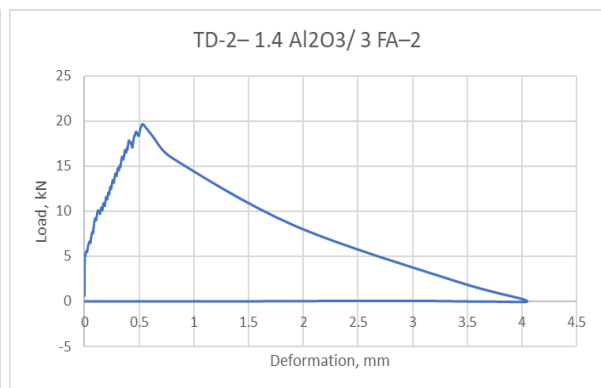
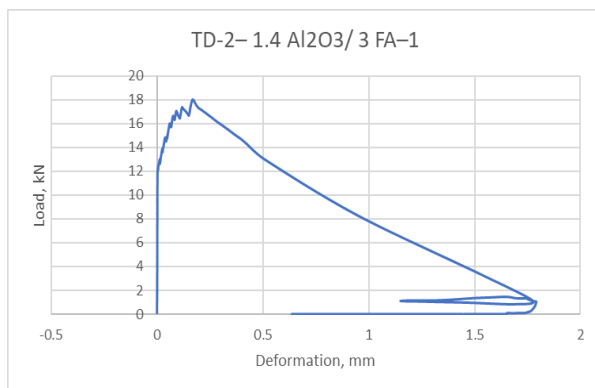
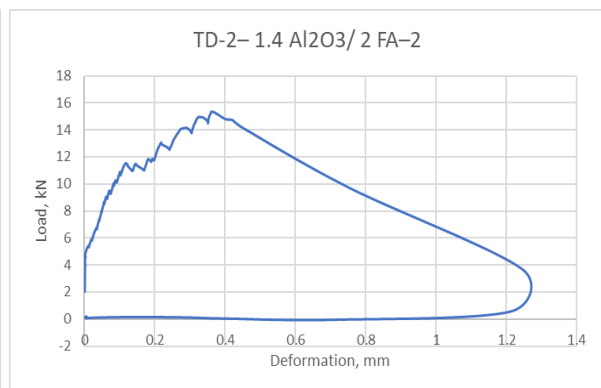
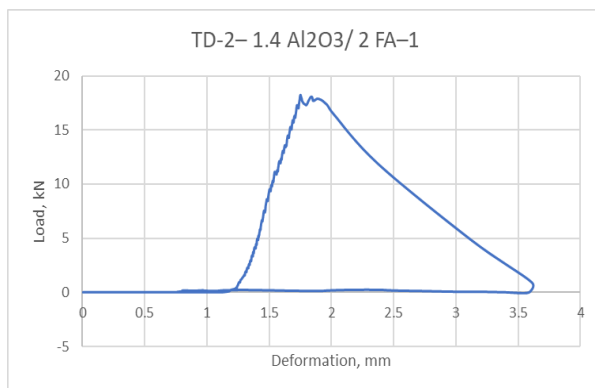
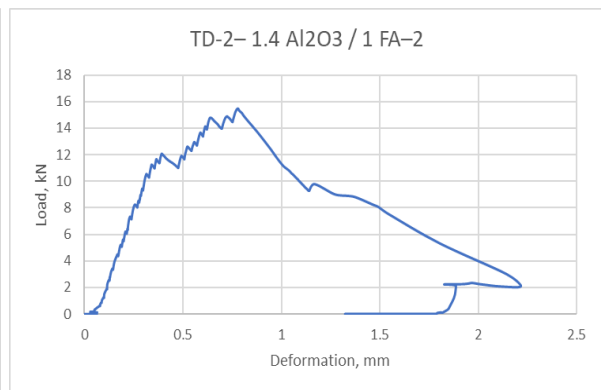
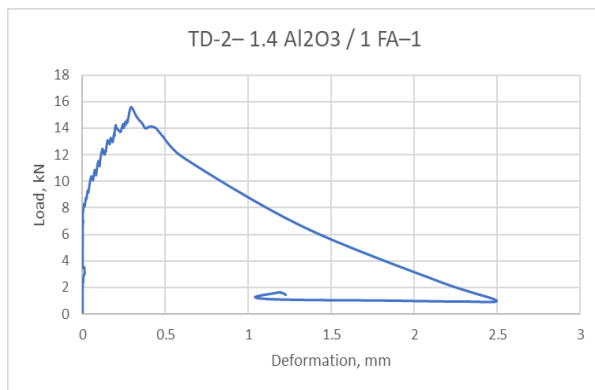
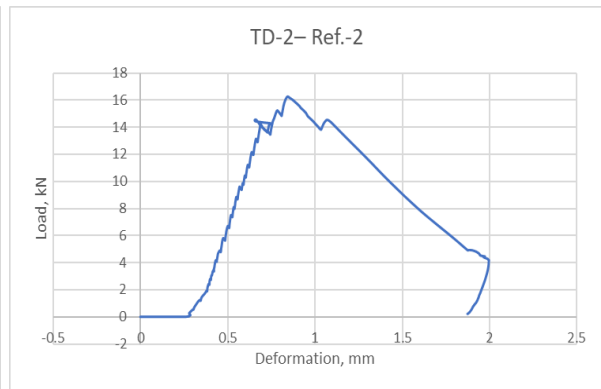
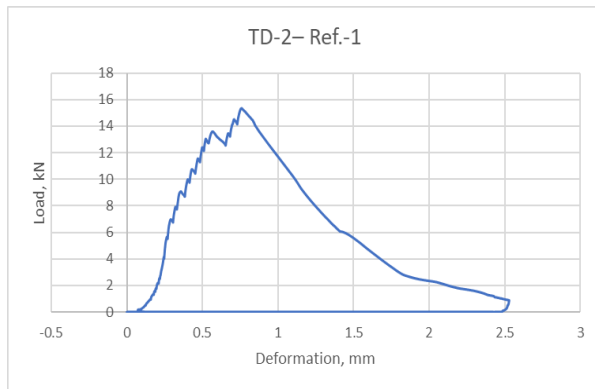
➤ TD-2 - TB-4-R – 3 days



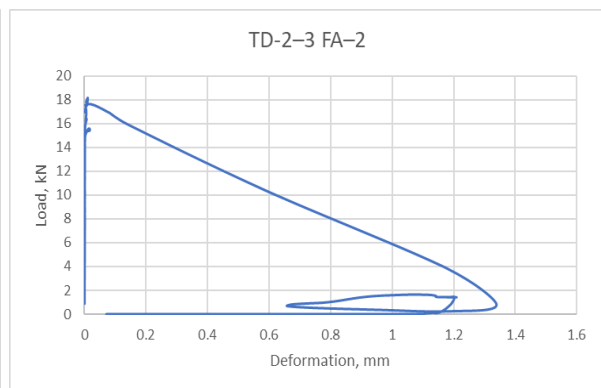
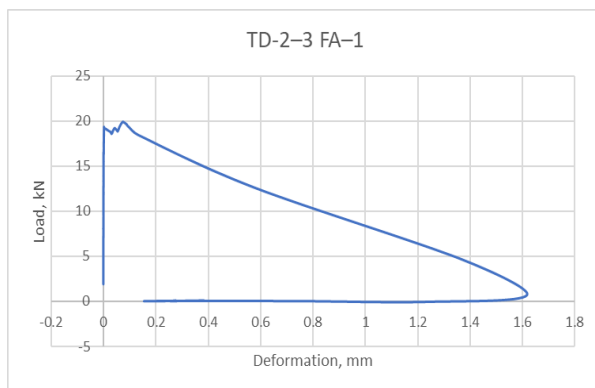
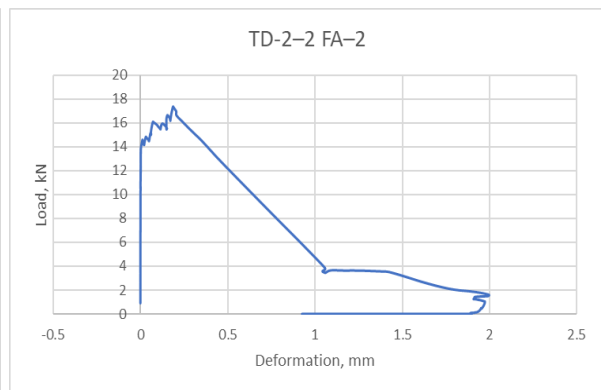
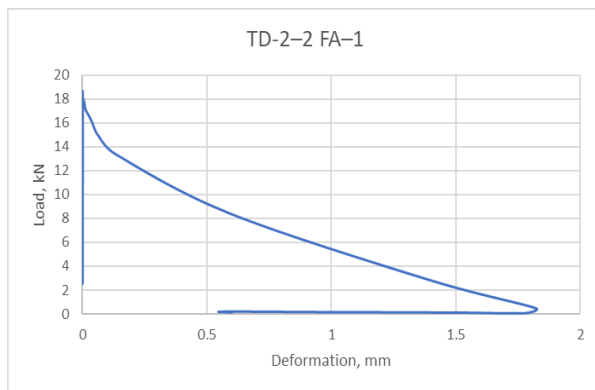
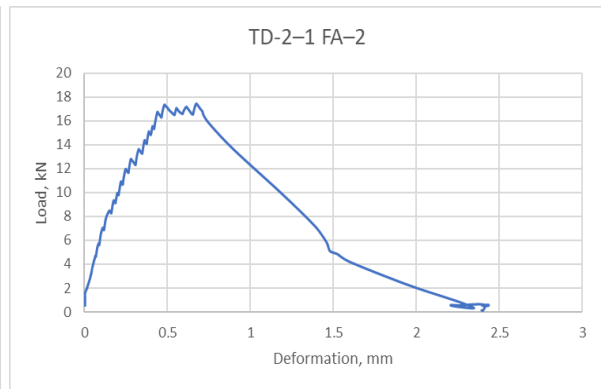
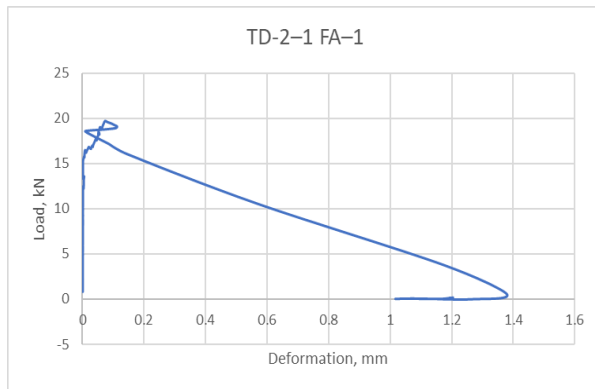
➤ **TD-2 - TB-4-R – 3 days: Continuation**



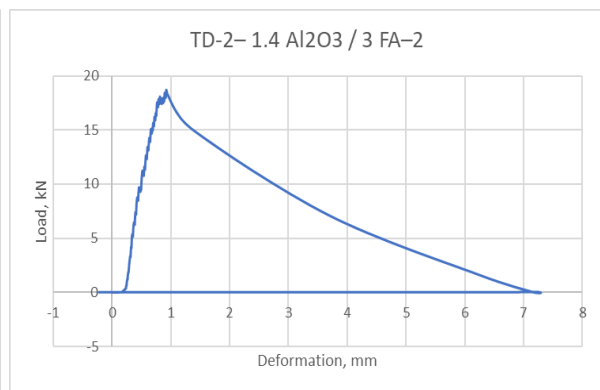
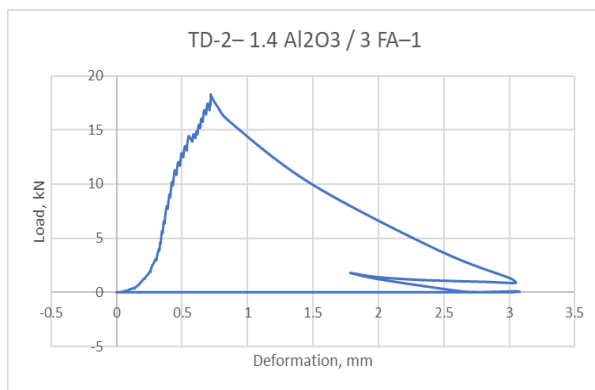
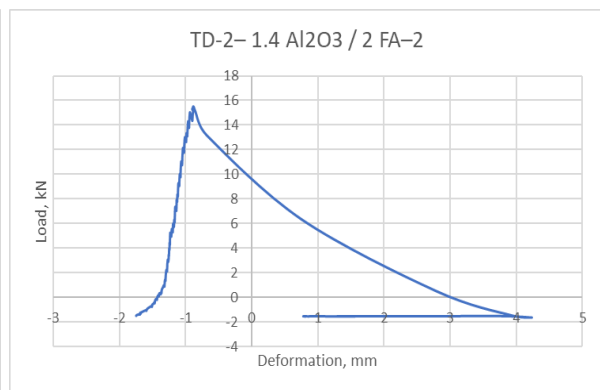
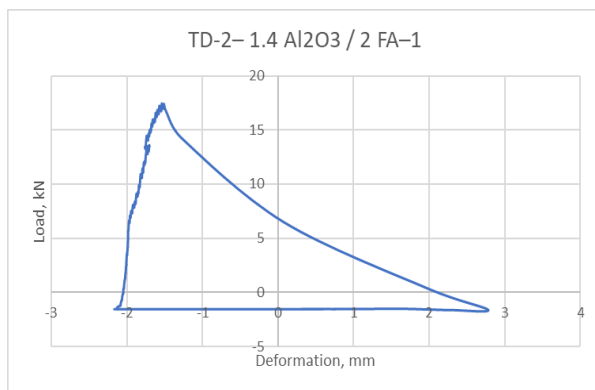
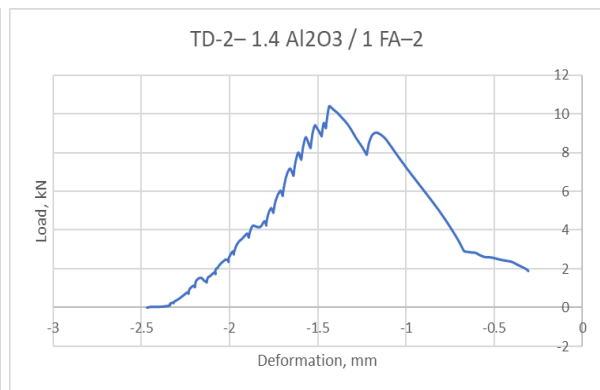
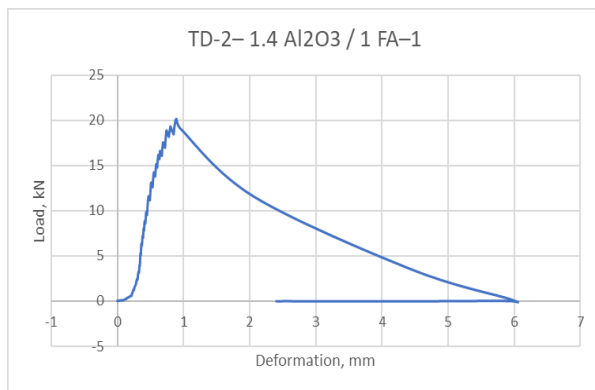
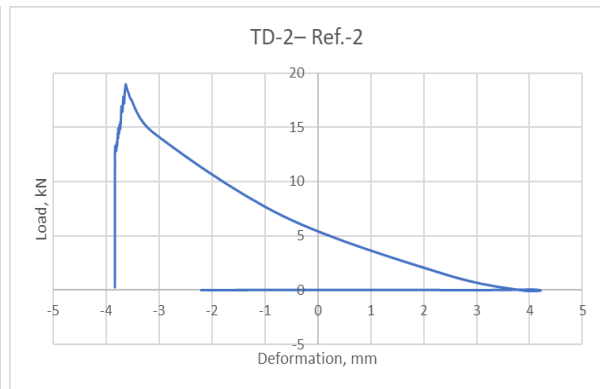
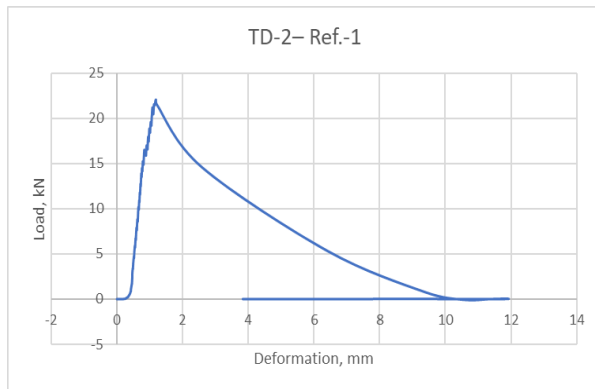
➤ TD-2 – TB-4-O – 3 days



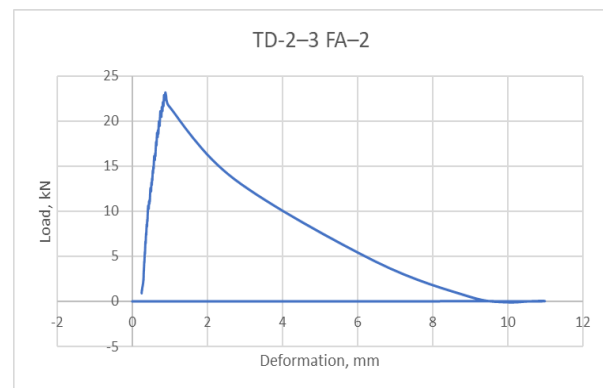
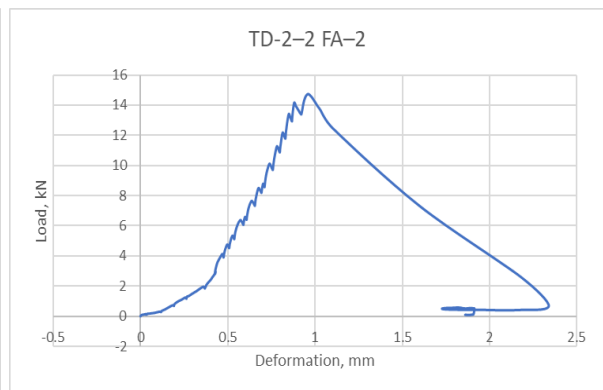
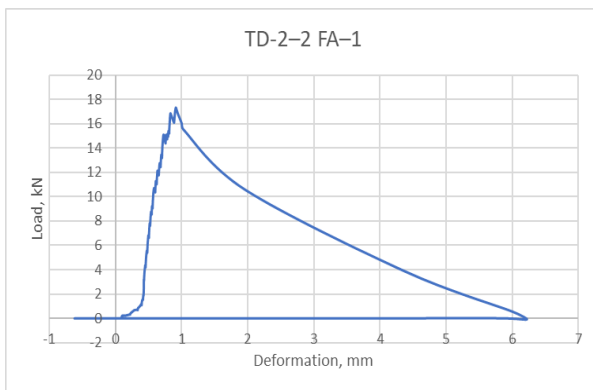
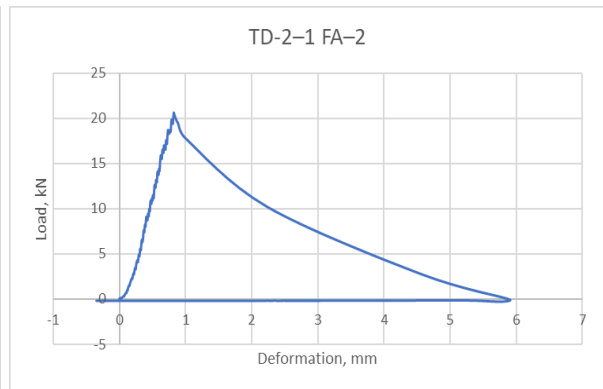
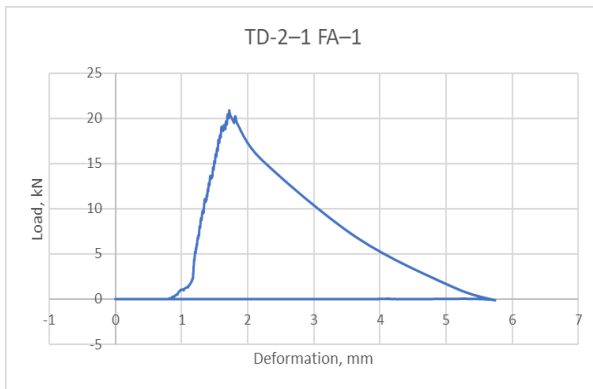
➤ TD-2 – TB-4-O – 3 days: Continuation



➤ **TD-2 – TB-5-R – 7 days**

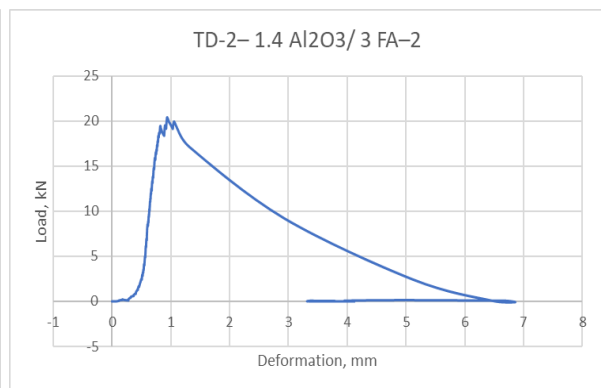
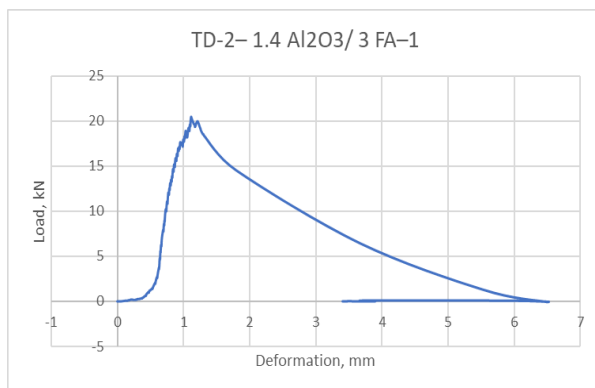
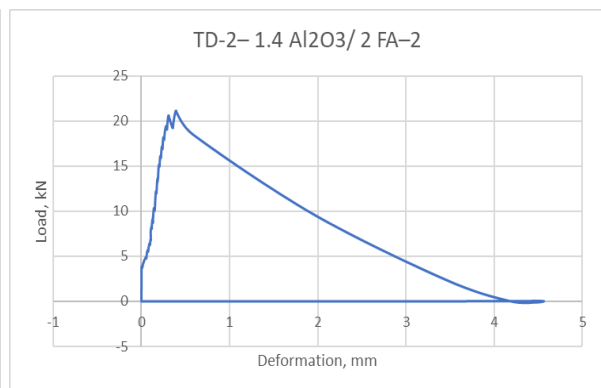
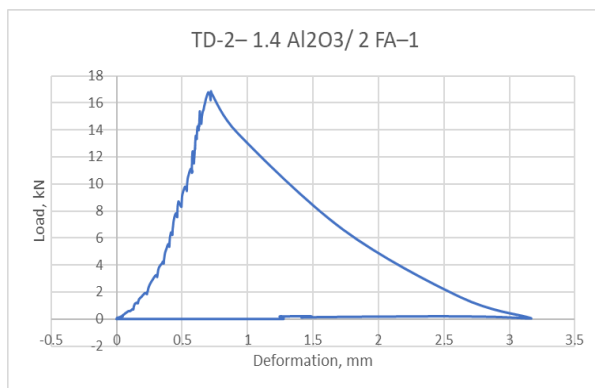
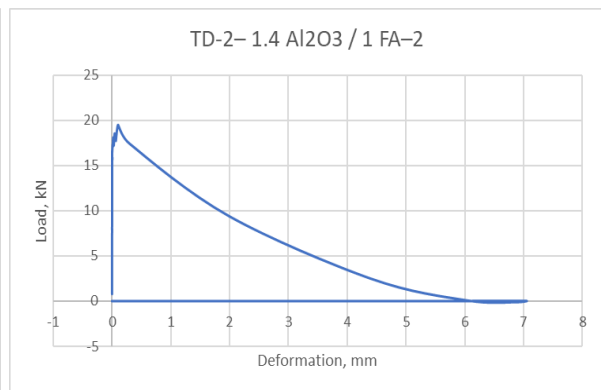
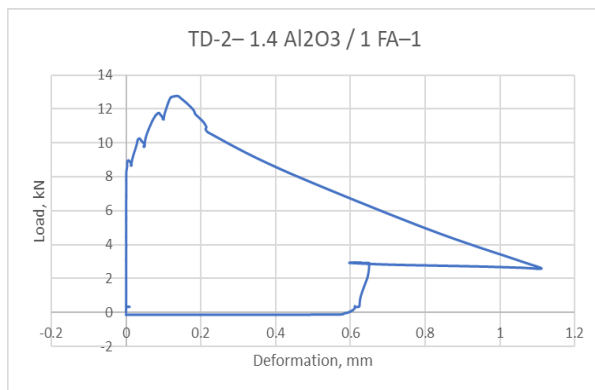
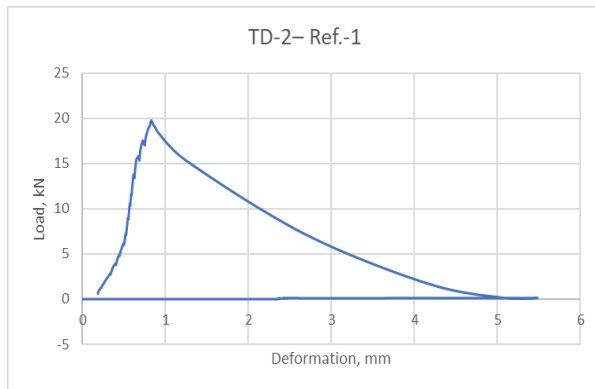


➤ **TD-2 – TB-5-R – 7 days: Continuation**

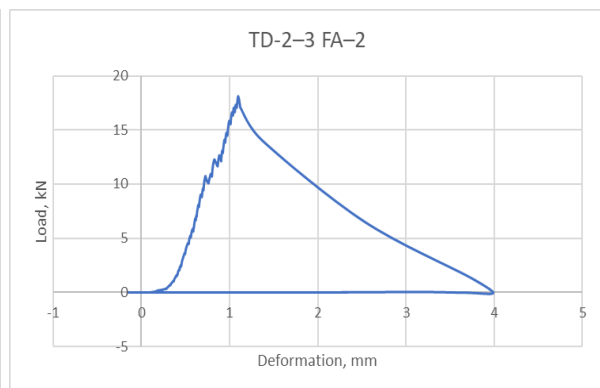
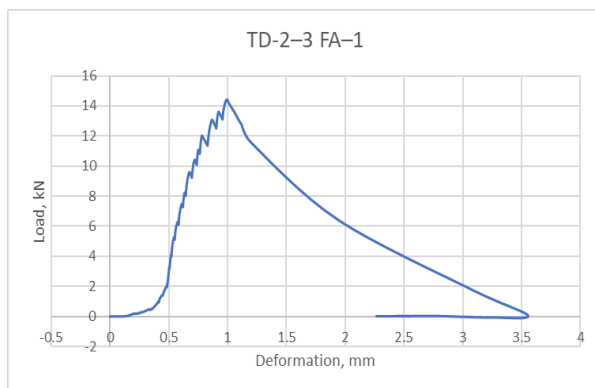
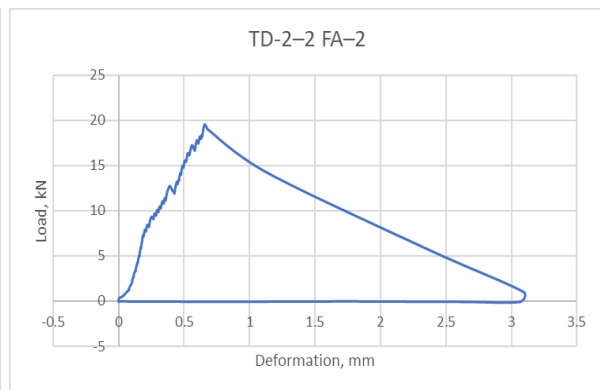
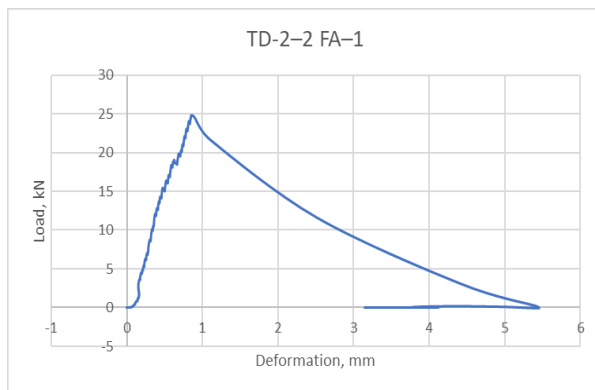
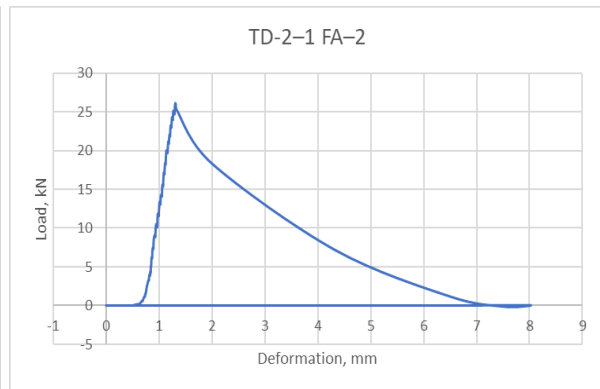
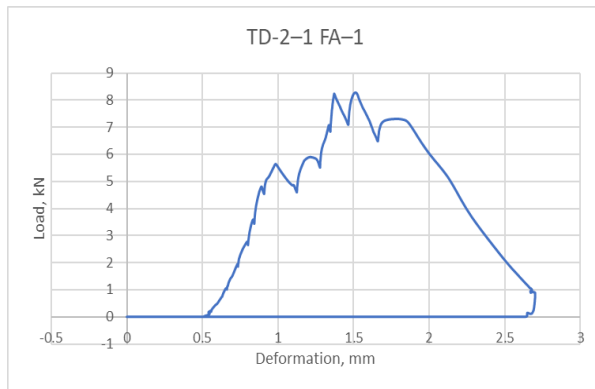




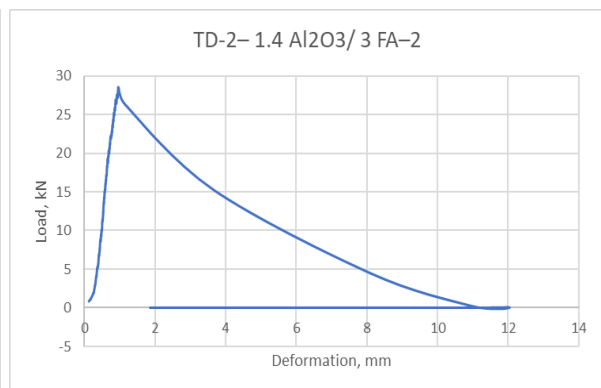
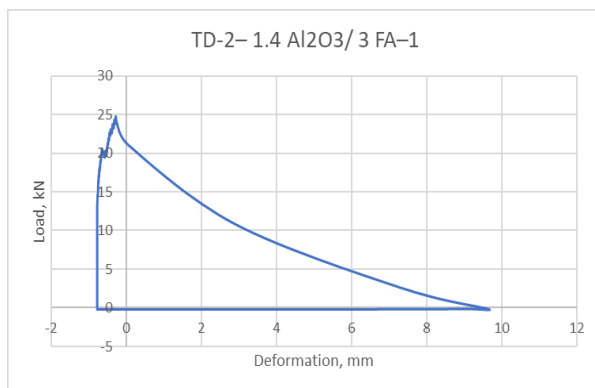
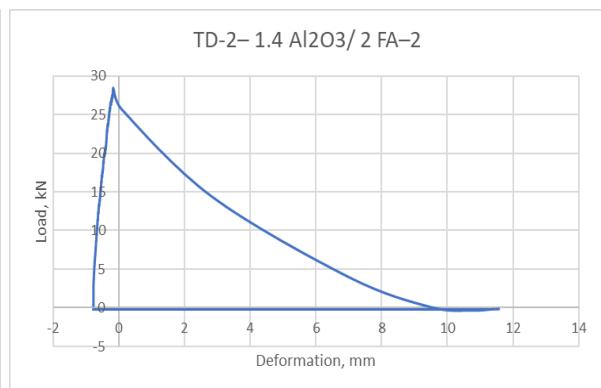
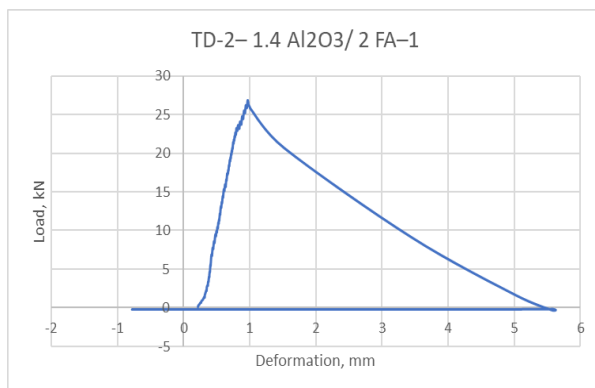
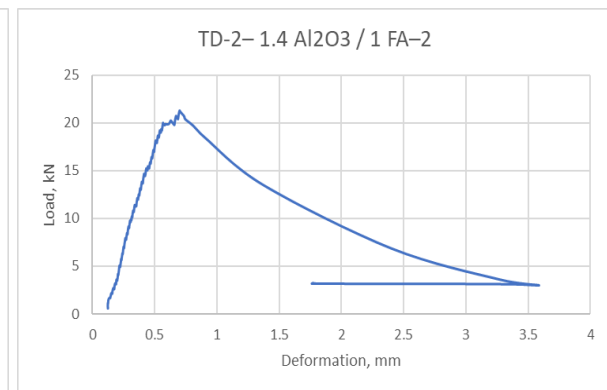
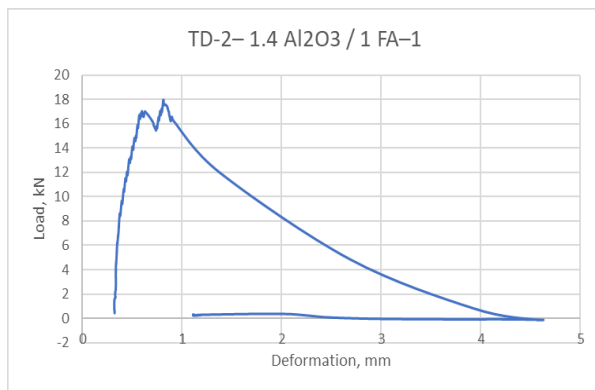
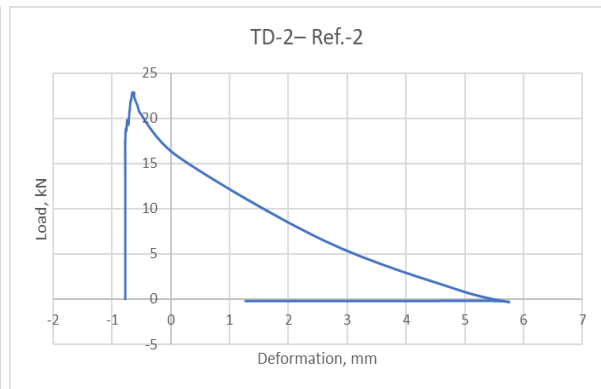
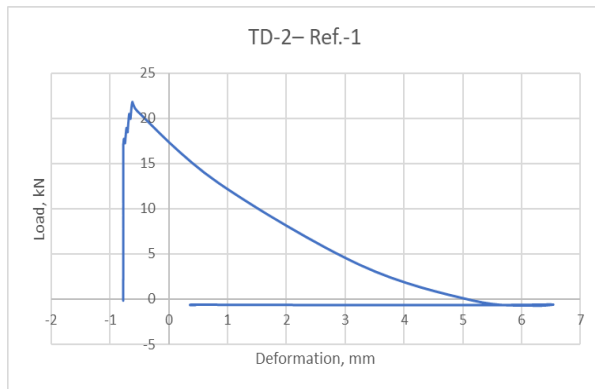
➤ TD-2 – TB-5-O – 7 days



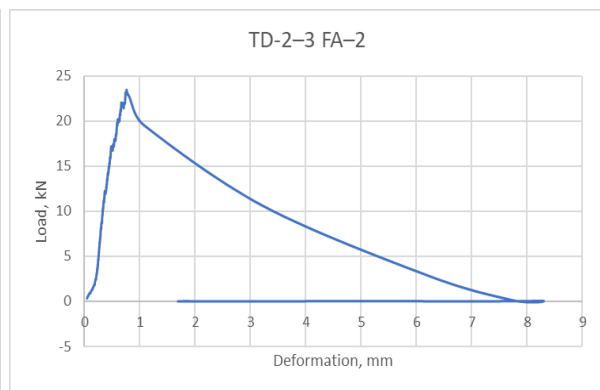
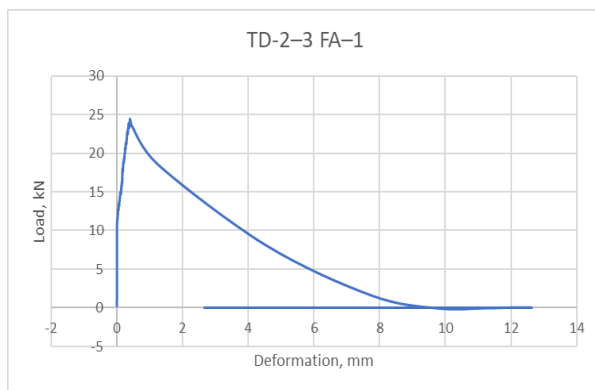
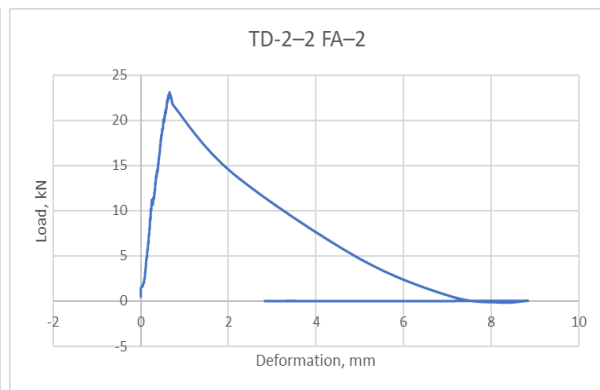
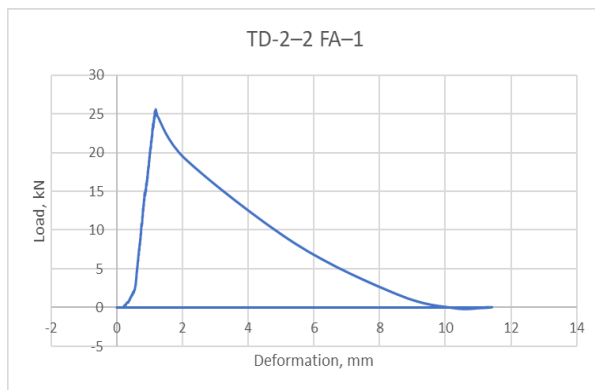
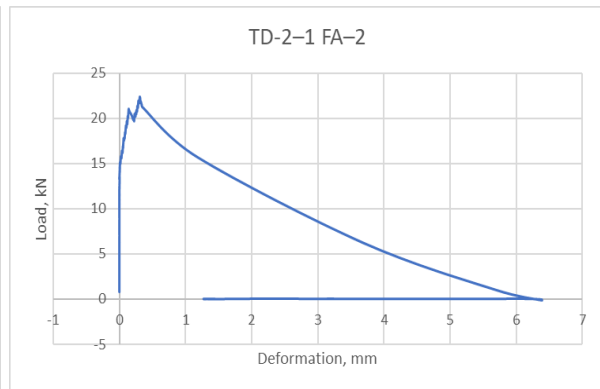
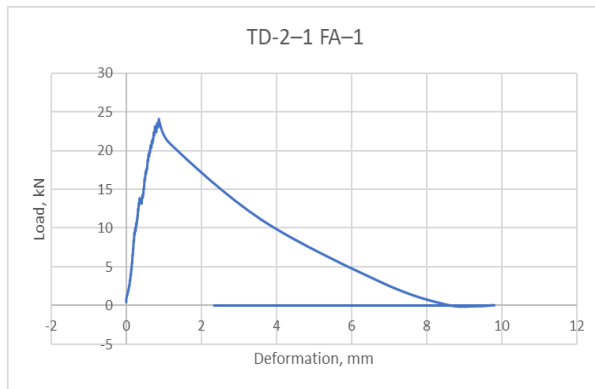
➤ TD-2 – TB-5-O – 7 days: Continuation



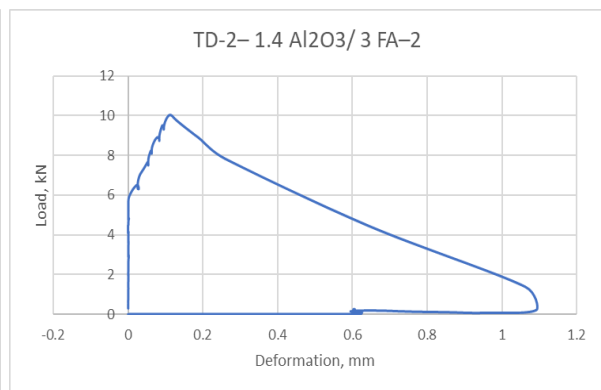
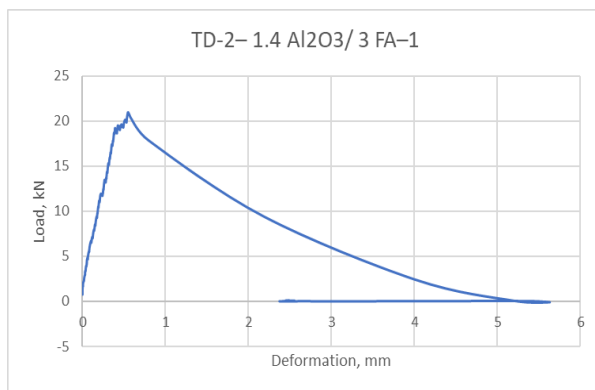
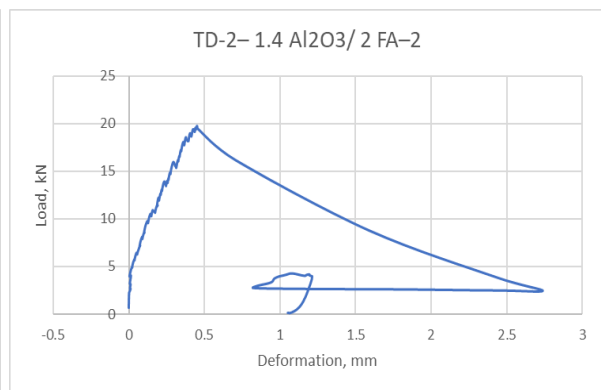
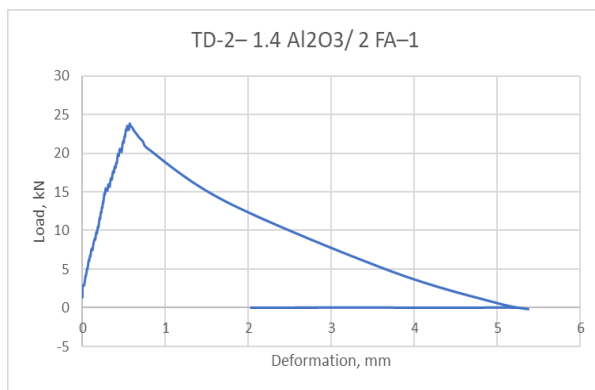
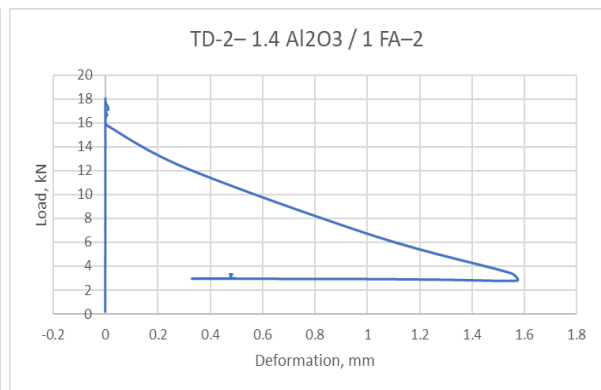
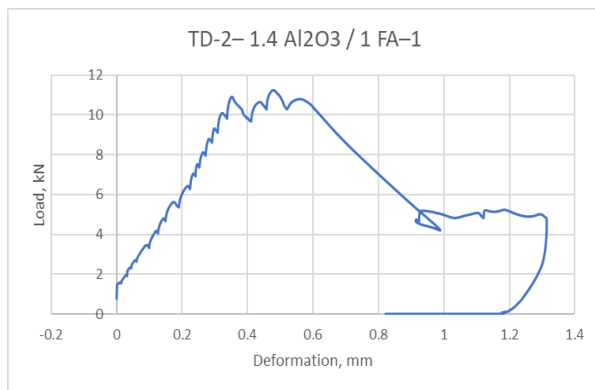
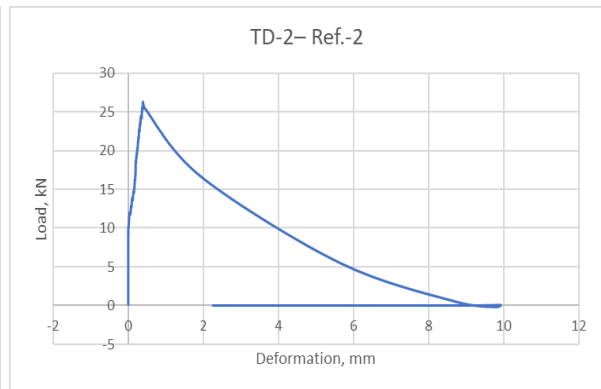
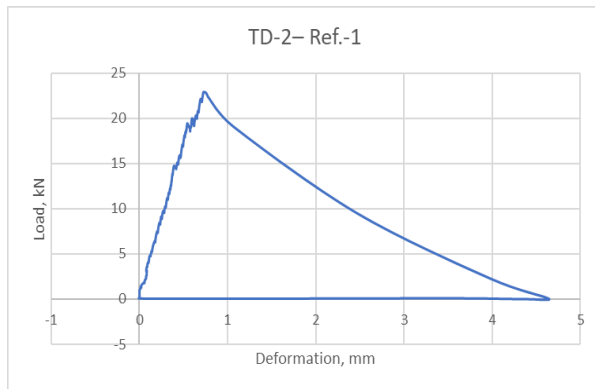
➤ TD-2 – TB-6-R – 28 days



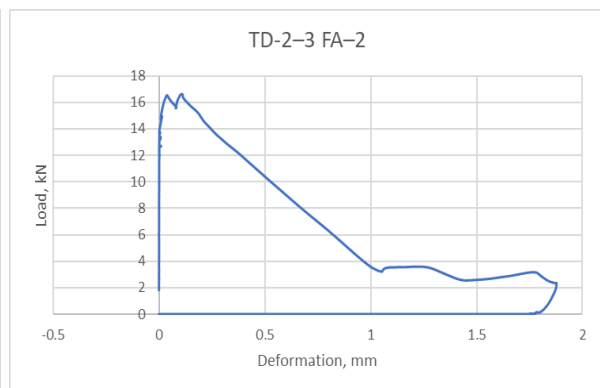
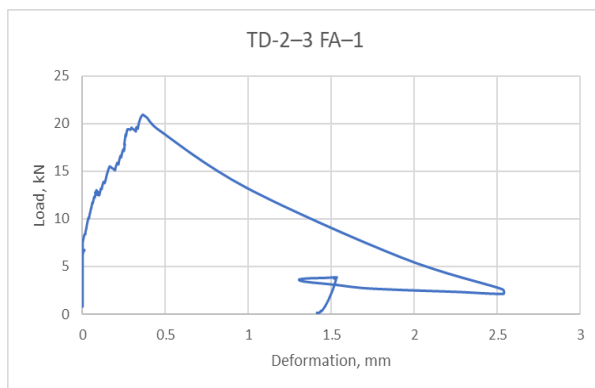
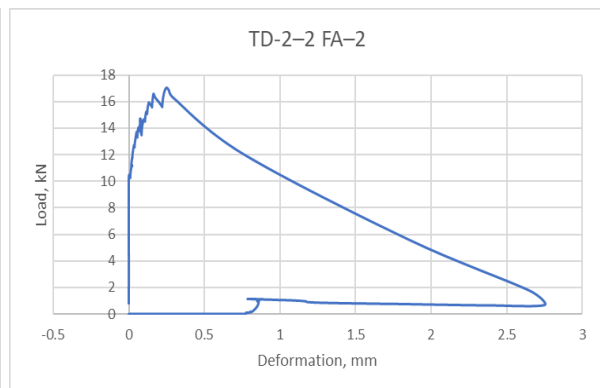
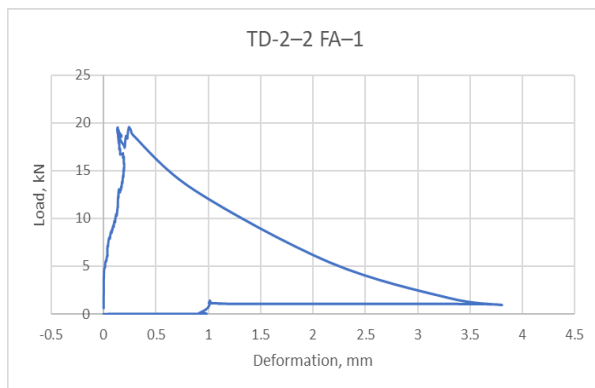
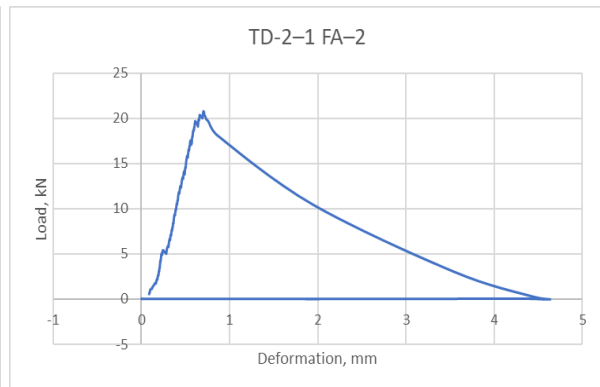
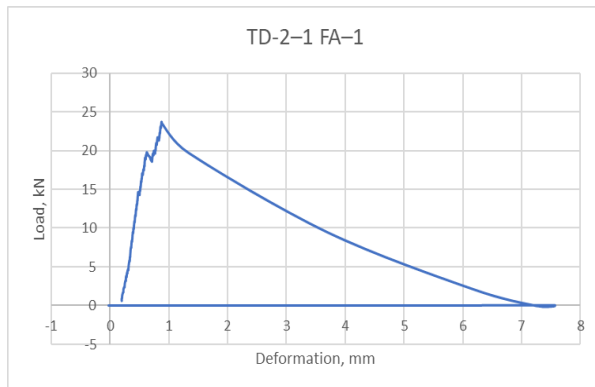
➤ TD-2 – TB-6-R – 28 days: Continuation



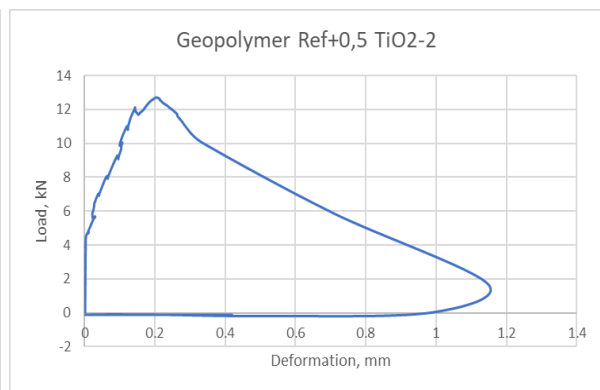
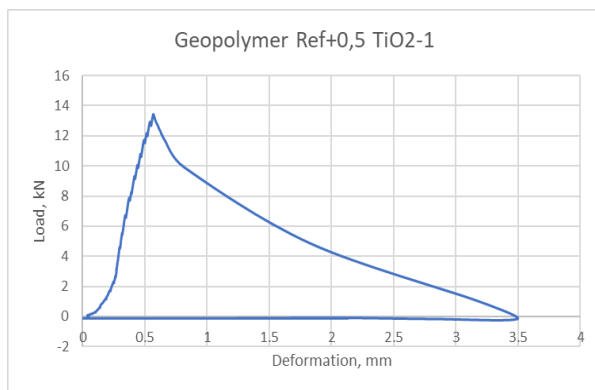
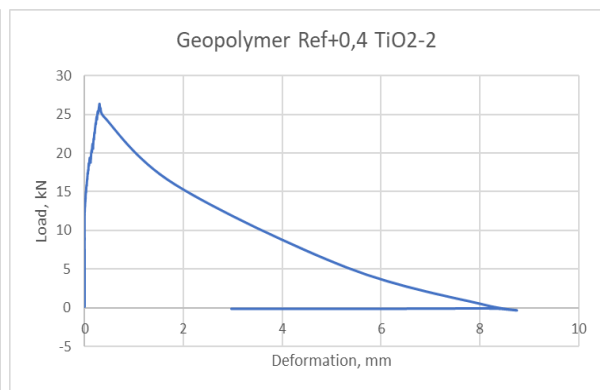
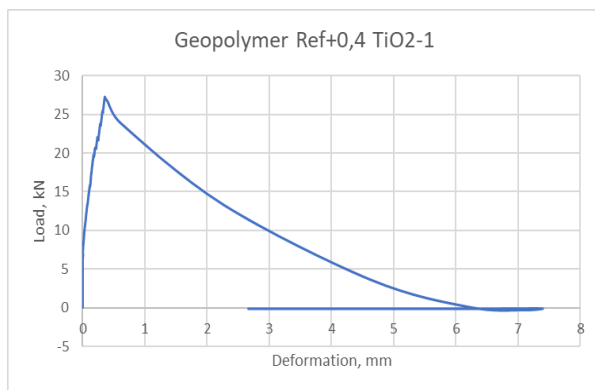
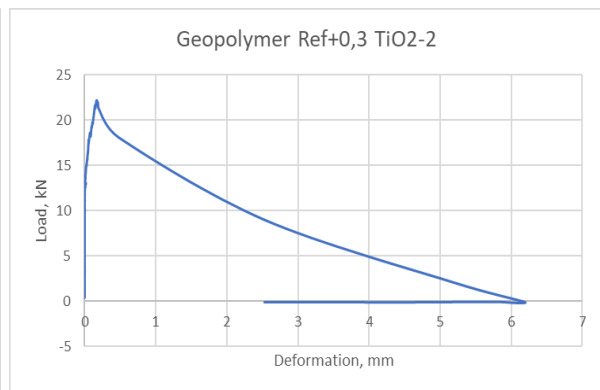
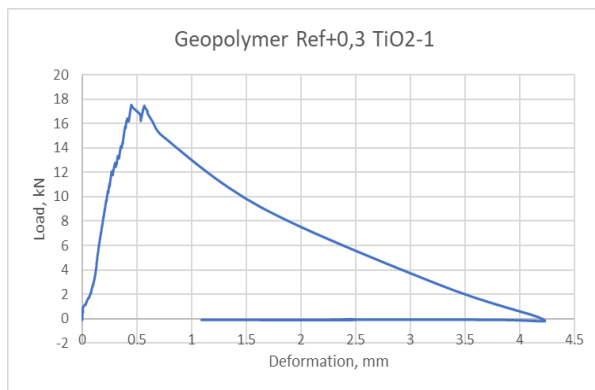
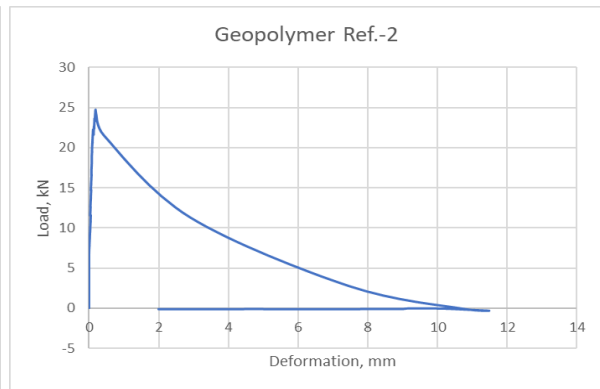
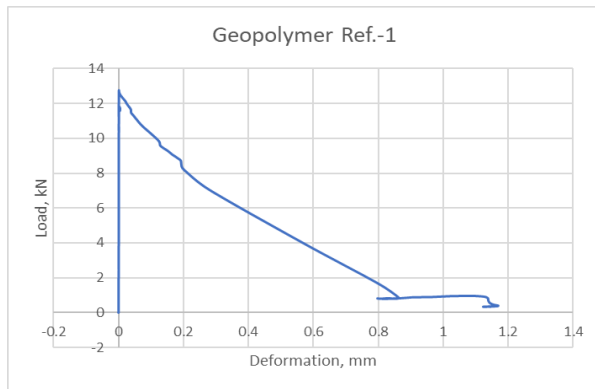
➤ TD-2 – TB-6-O – 28 days



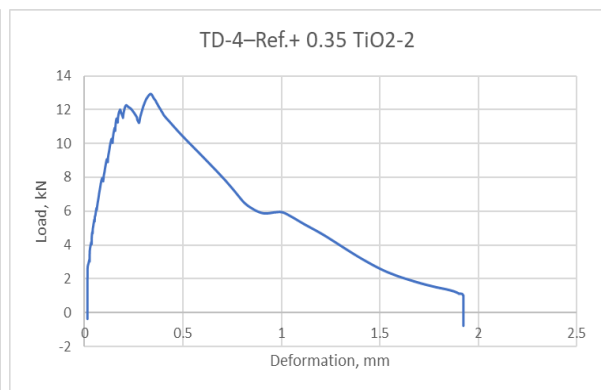
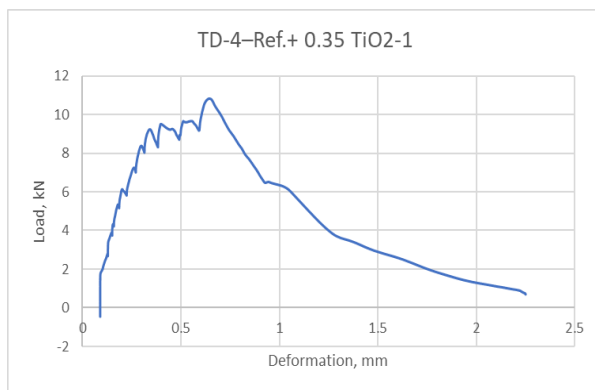
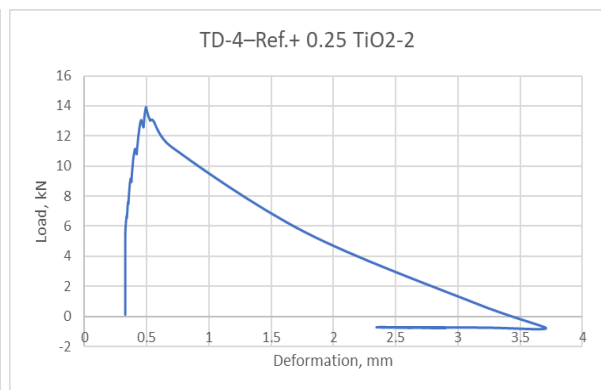
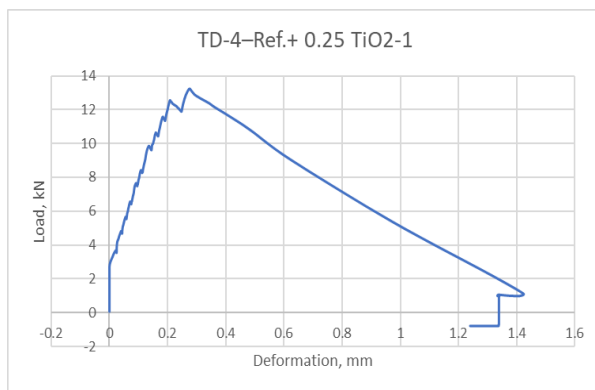
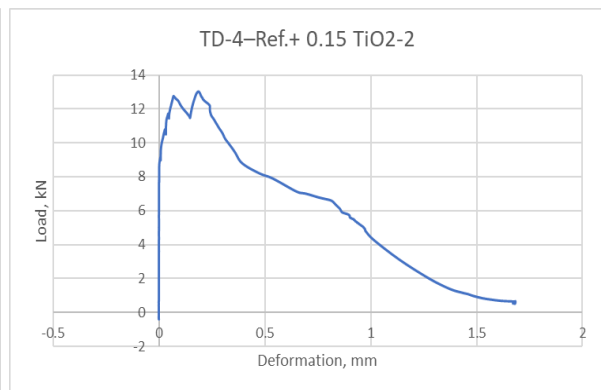
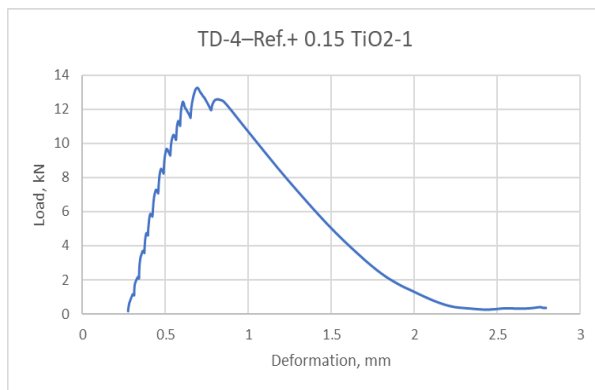
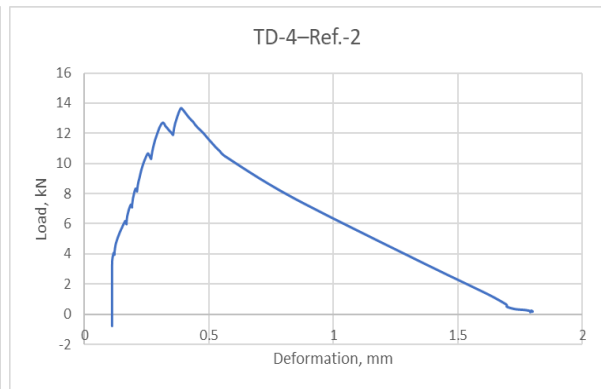
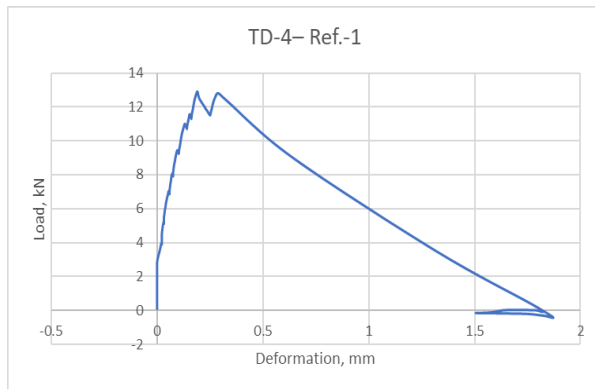
➤ **TD-2 – TB-6-O – 28 days: Continuation**



➤ TD-3\* – TB-7-R\* – 10 days

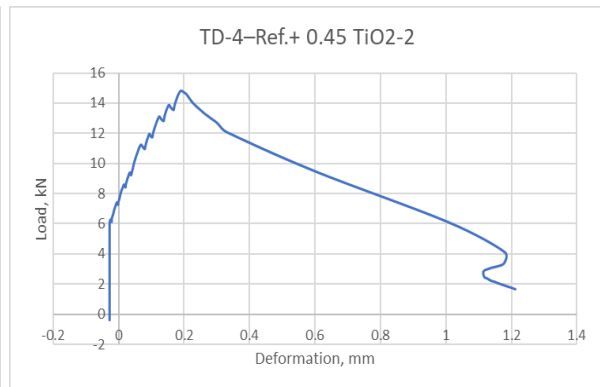
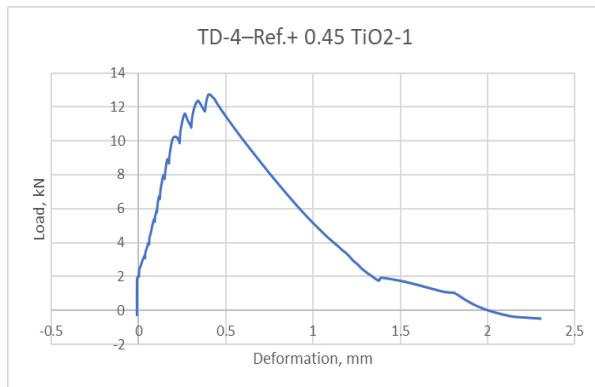


➤ TD-4 – TB-8-R – 3 days

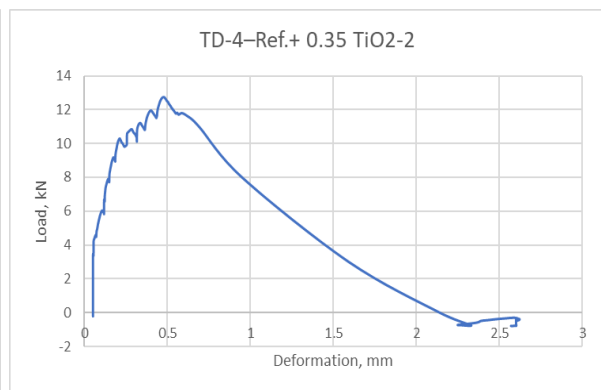
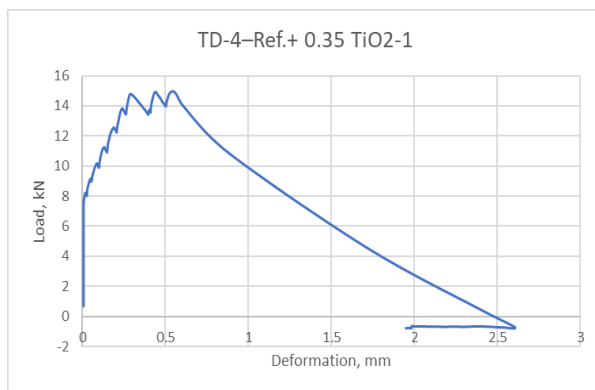
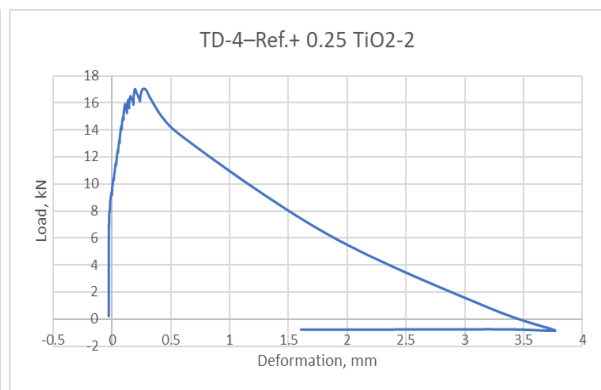
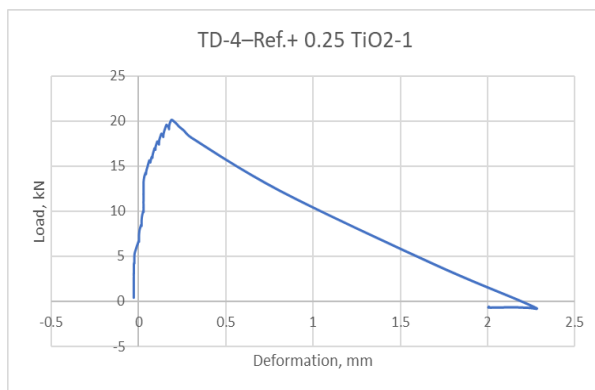
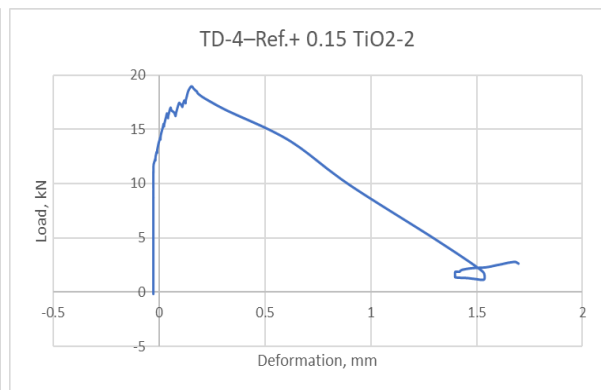
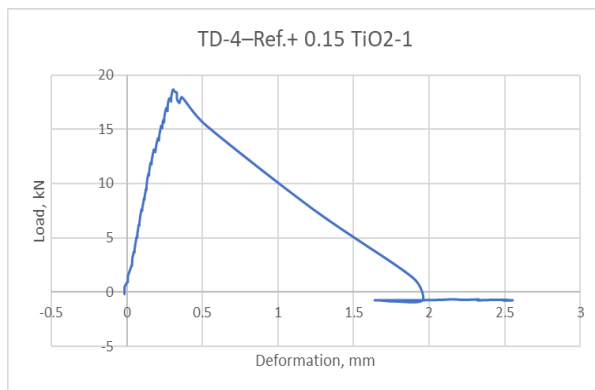
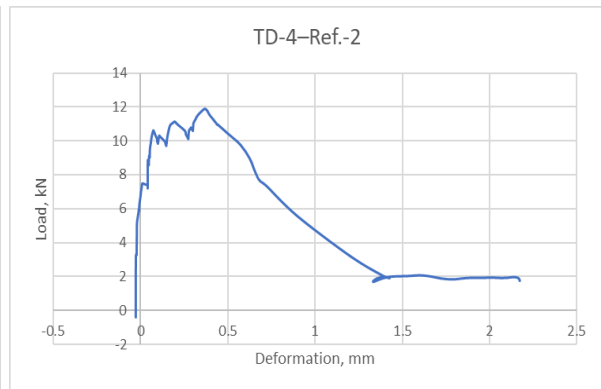
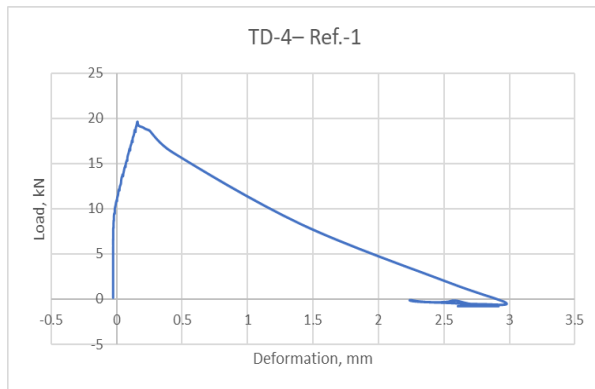




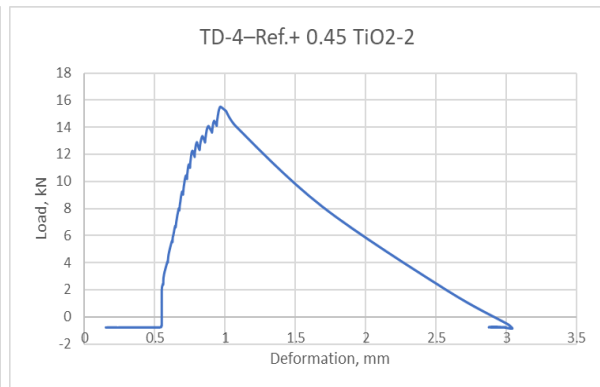
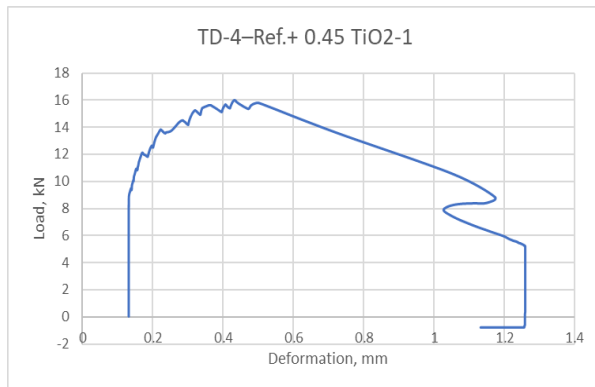
➤ **TD-4 – TB-8-R – 3 days: Continuation**



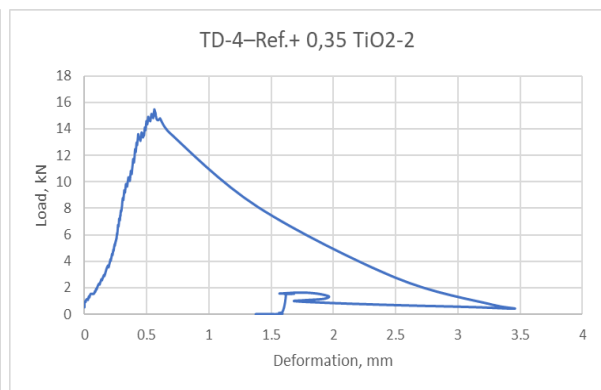
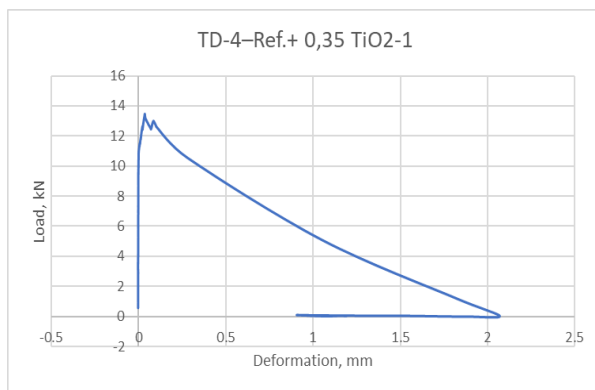
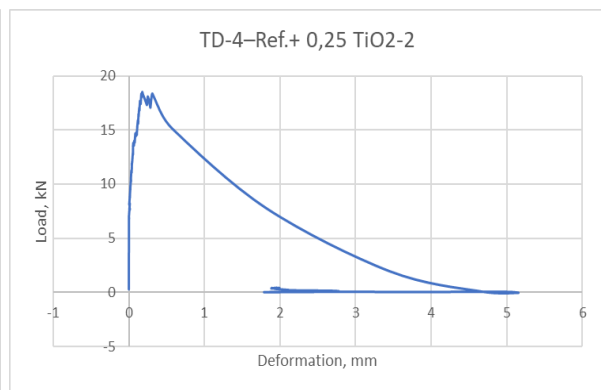
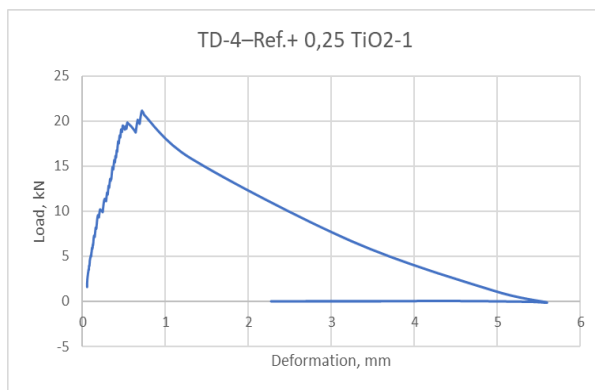
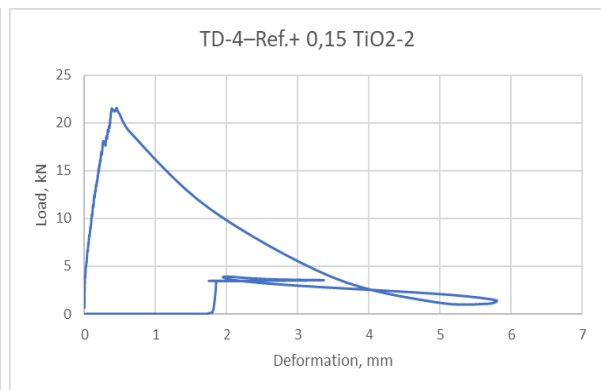
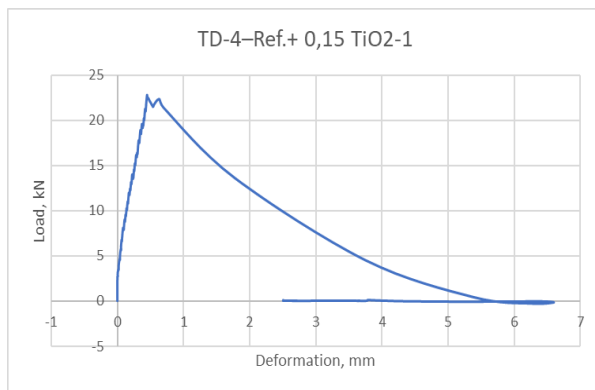
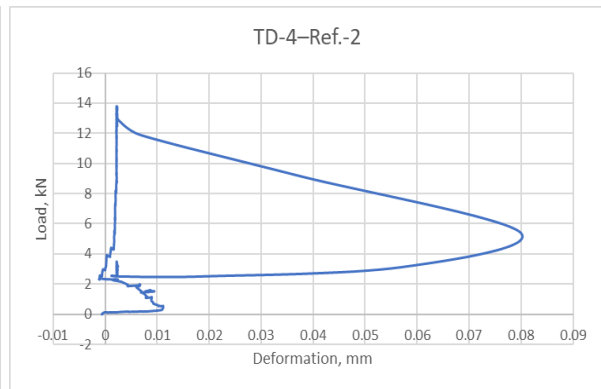
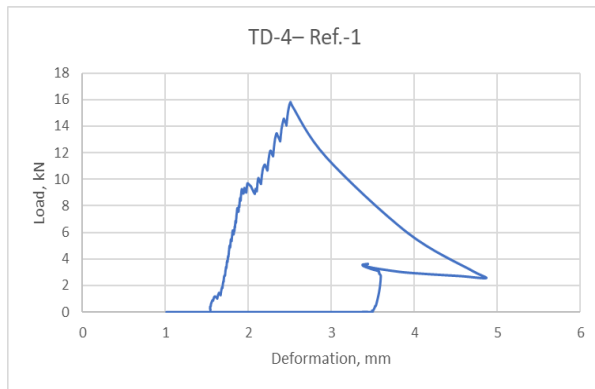
➤ TD-4 – TB-8-O – 3 days



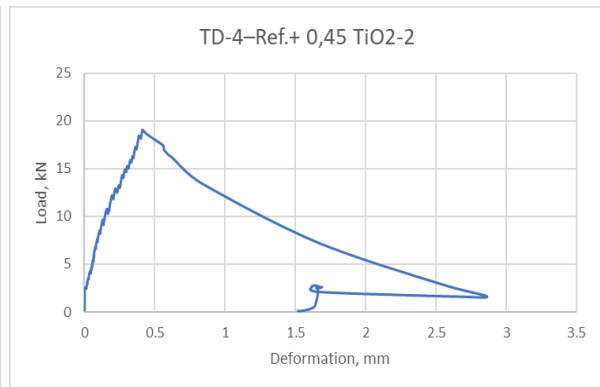
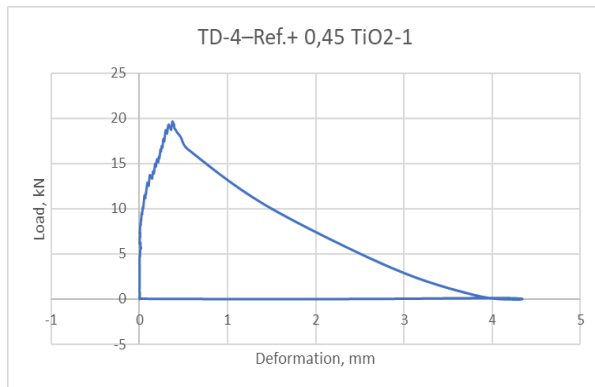
➤ **TD-4 – TB-8-O – 3 days: Continuation**



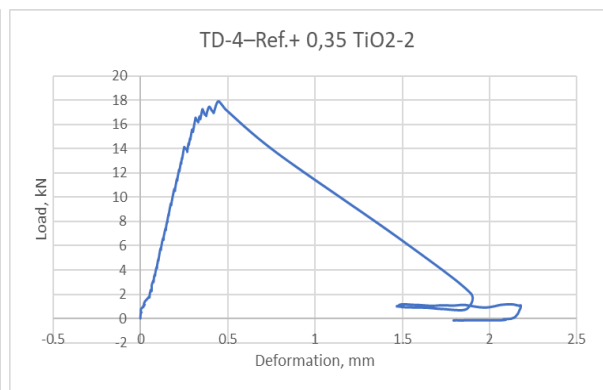
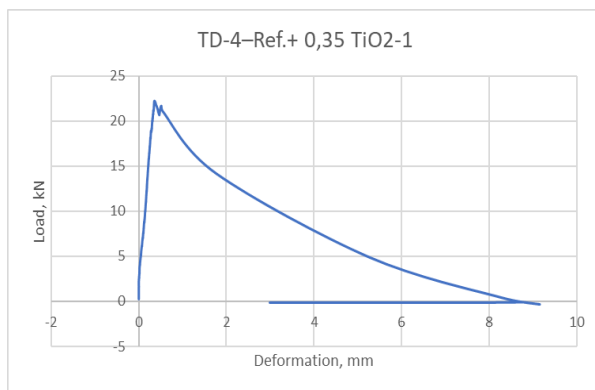
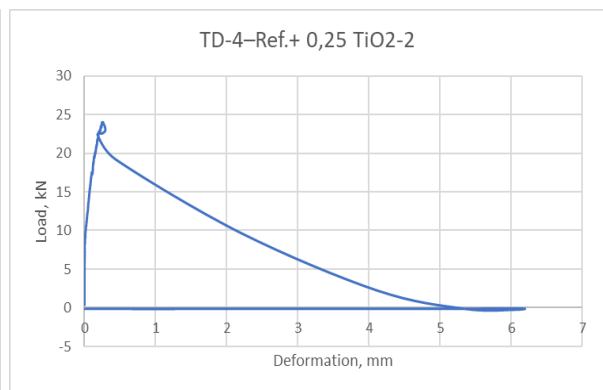
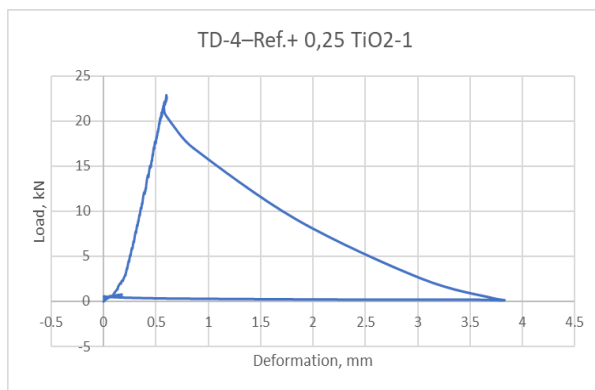
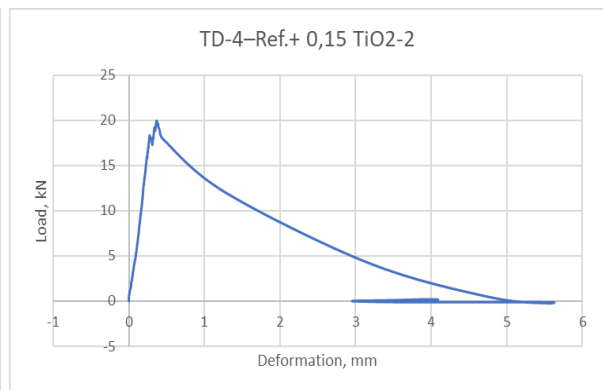
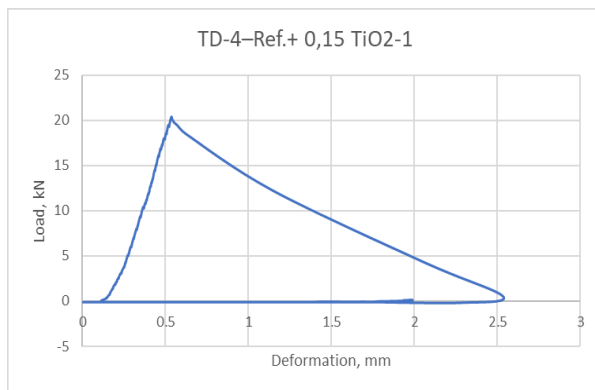
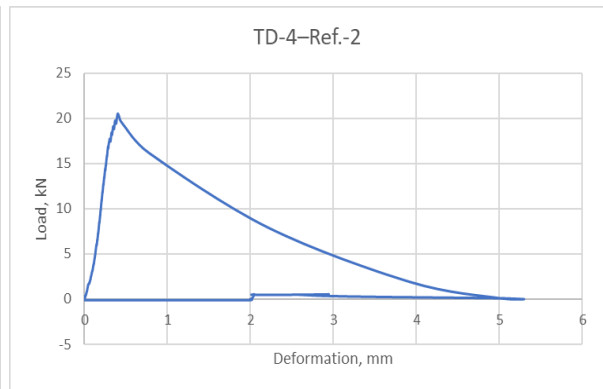
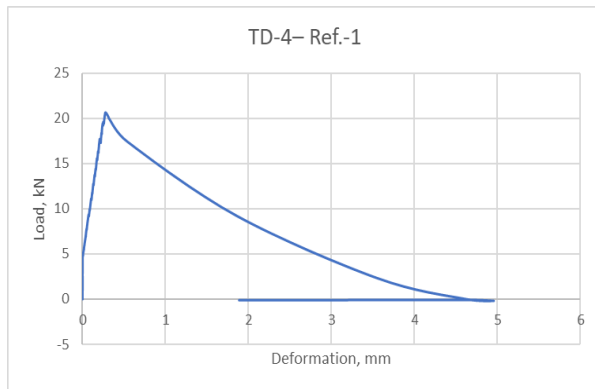
➤ **TD-4 – TB-9-R – 7 days**



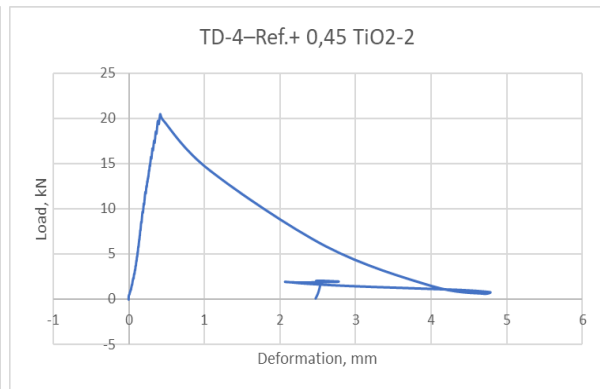
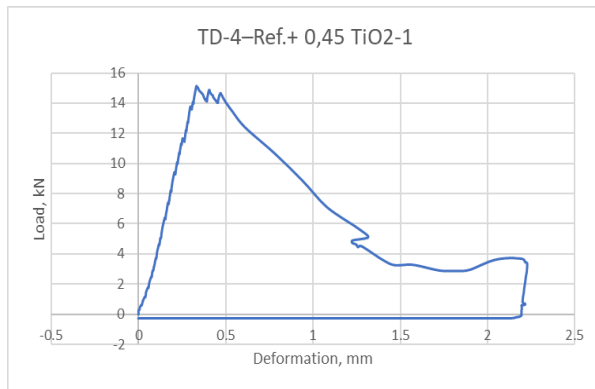
➤ **TD-4 – TB-9-R – 7 days: Continuation**



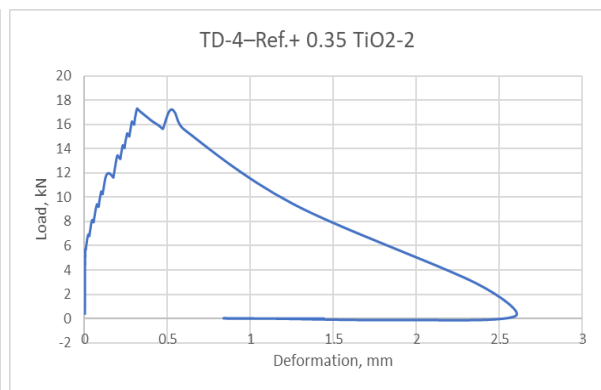
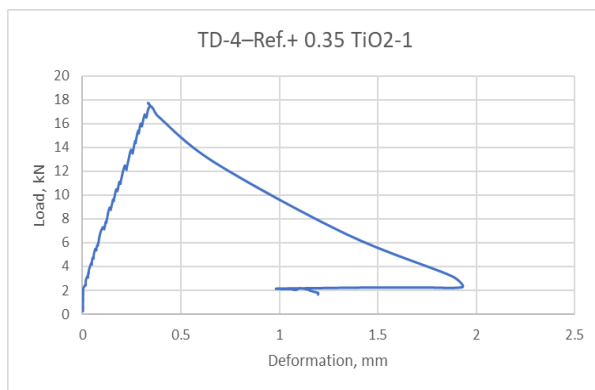
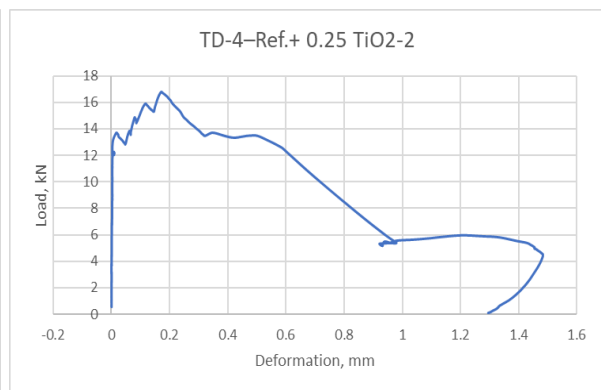
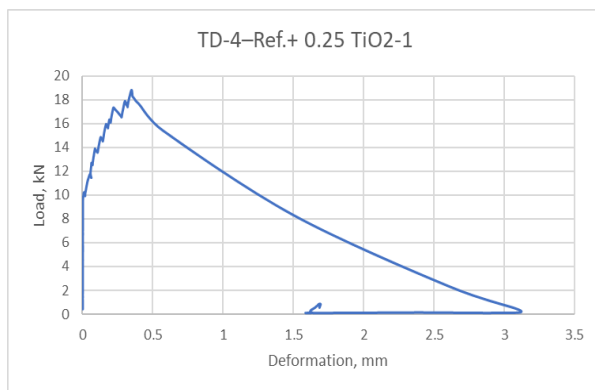
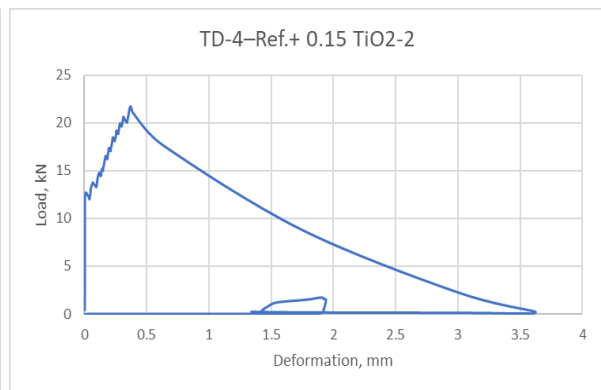
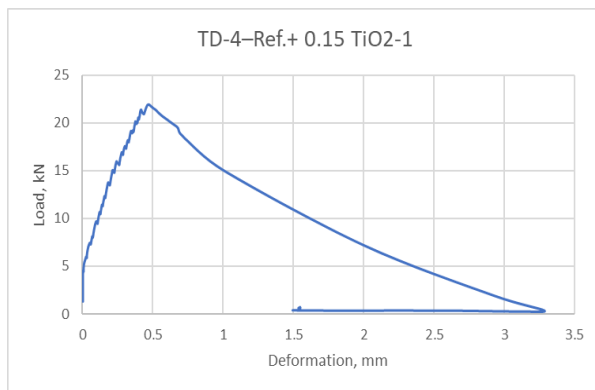
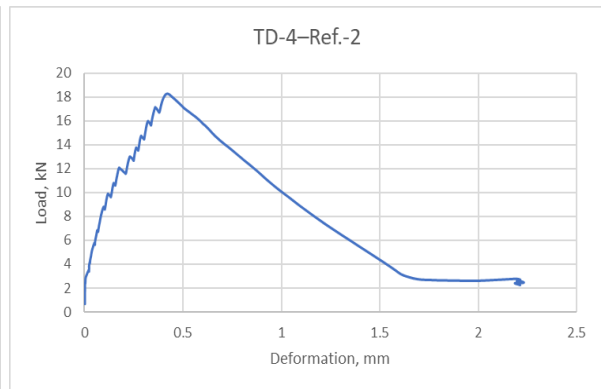
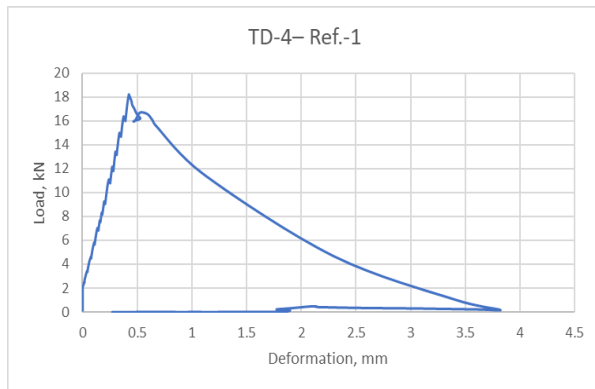
➤ **TD-4 – TB-9-O – 7 days**



➤ **TD-4 – TB-9-O – 7 days: Continuation**

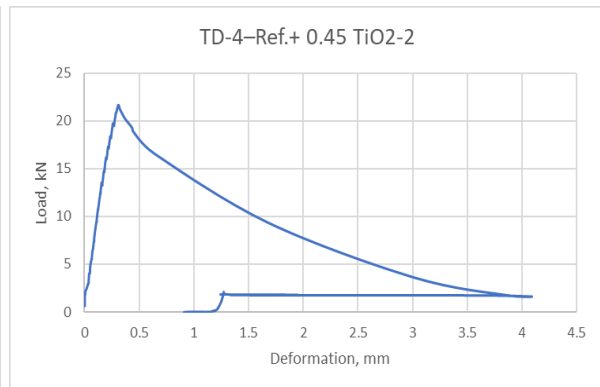
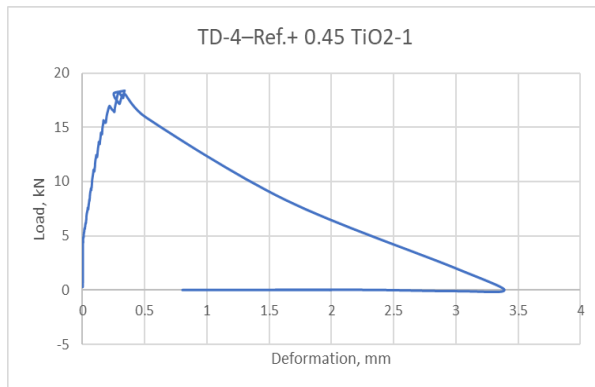


➤ TD-4 – TB-10-R – 28 days

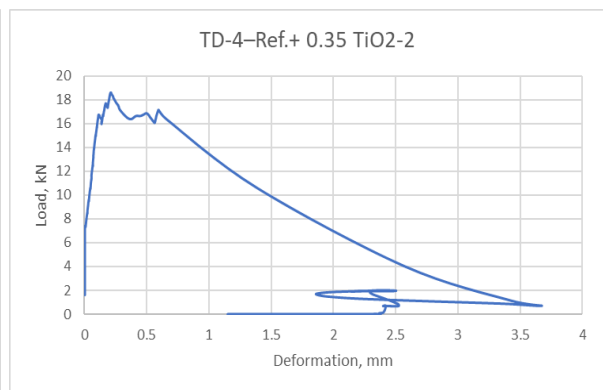
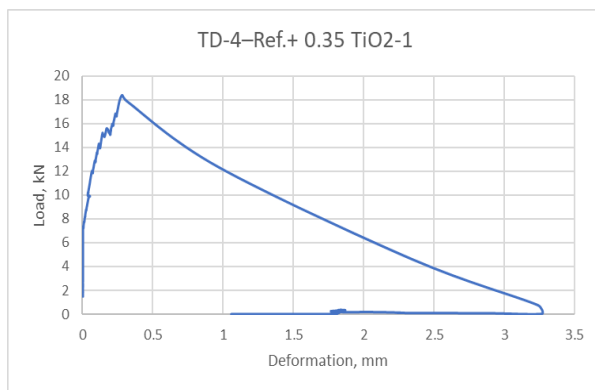
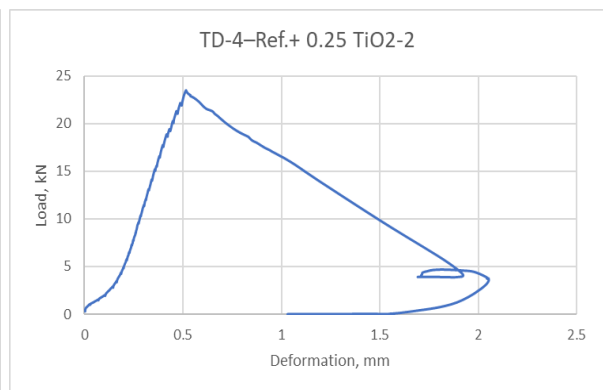
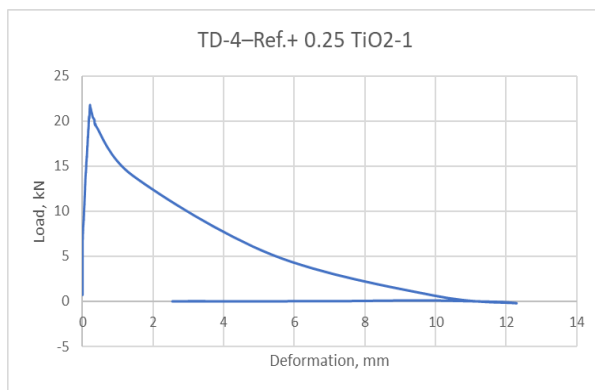
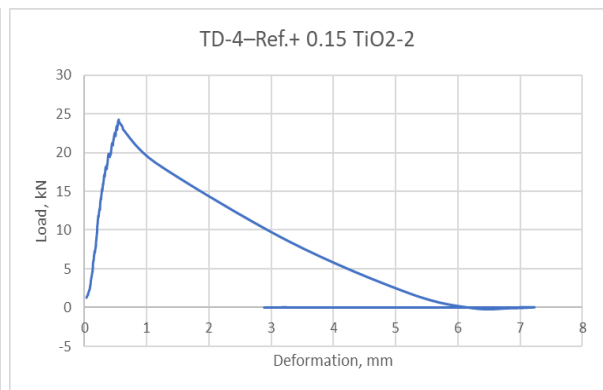
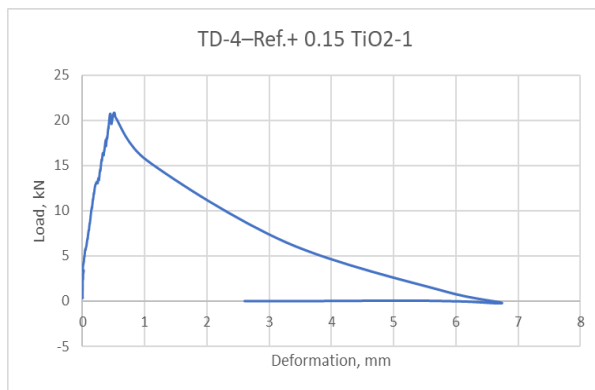
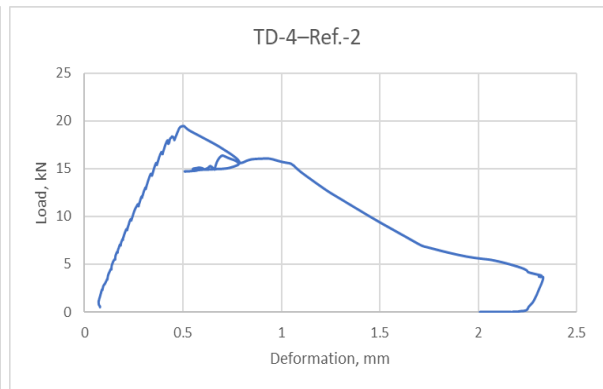
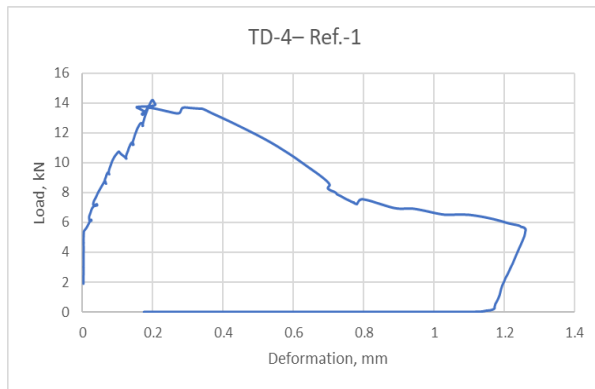




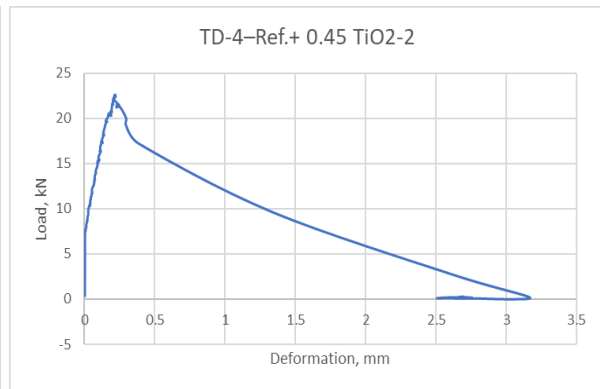
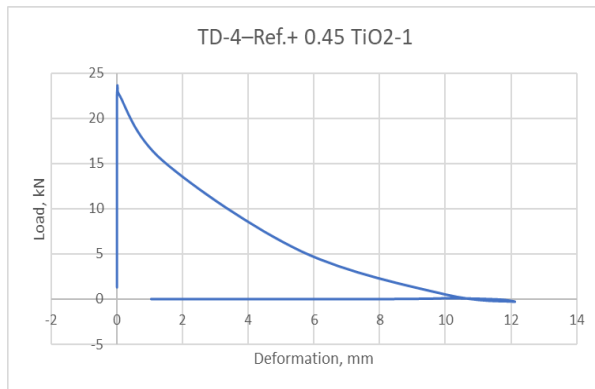
➤ **TD-4 – TB-10-R – 28 days: Continuation**



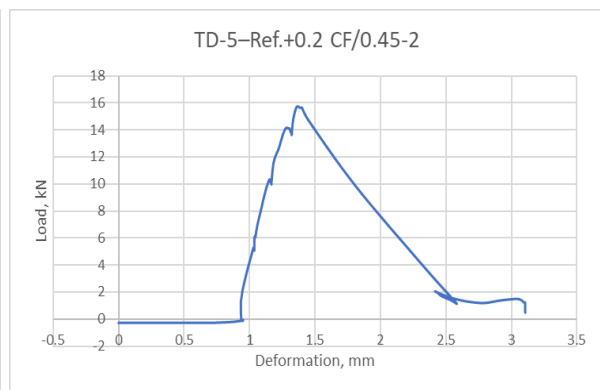
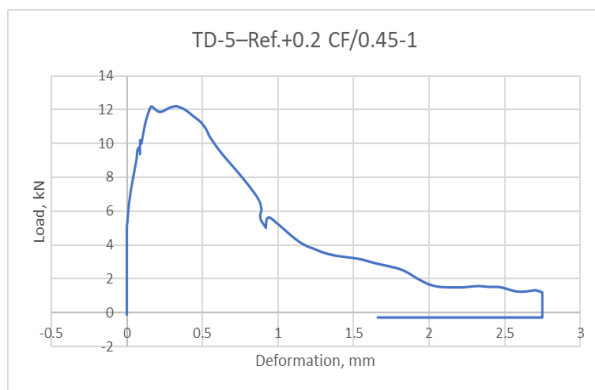
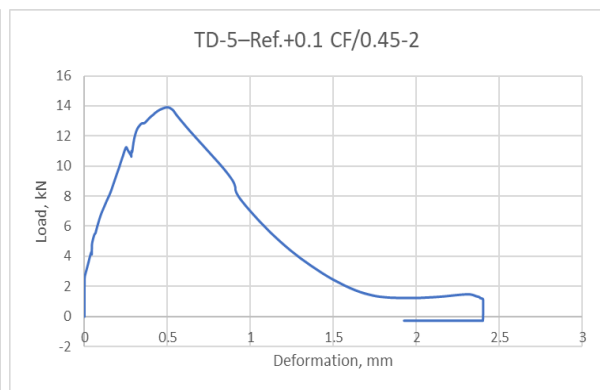
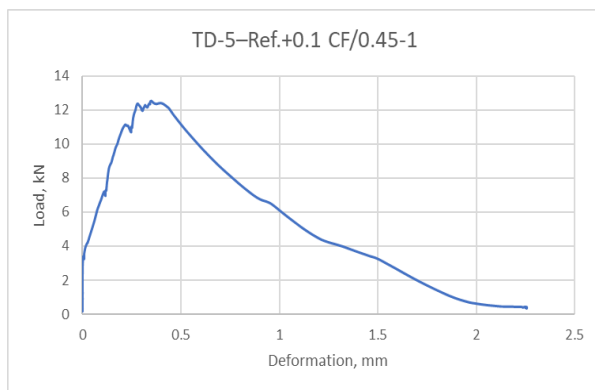
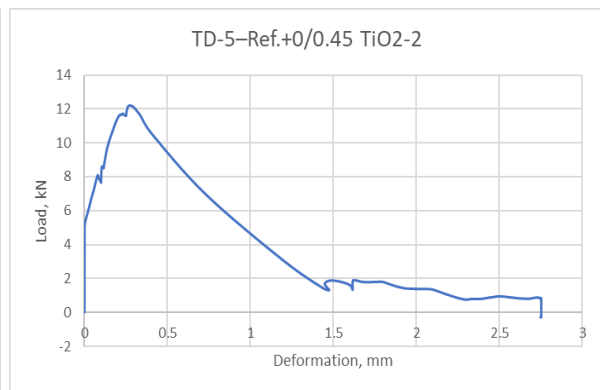
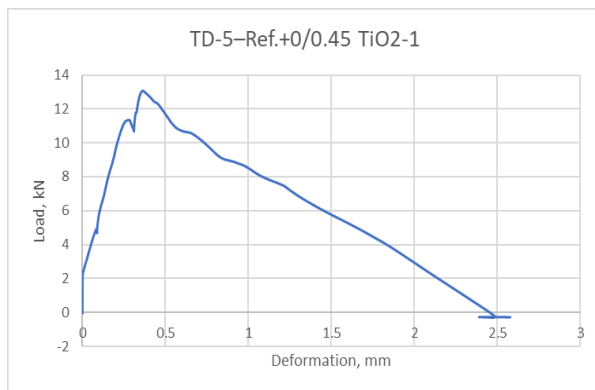
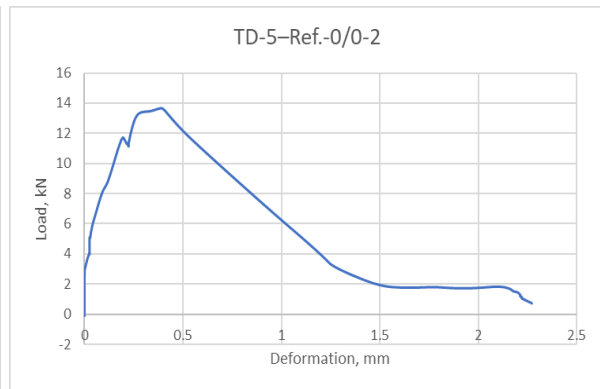
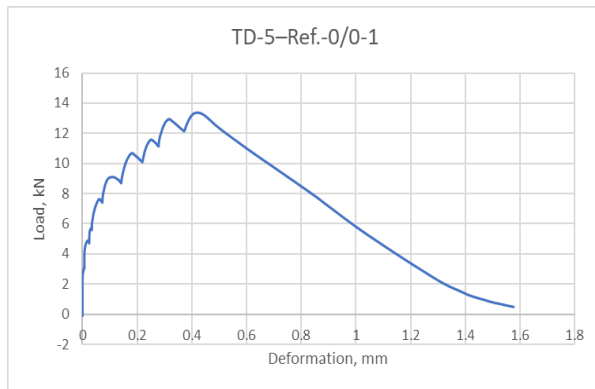
➤ **TD-4 – TB-10-O – 28 days**



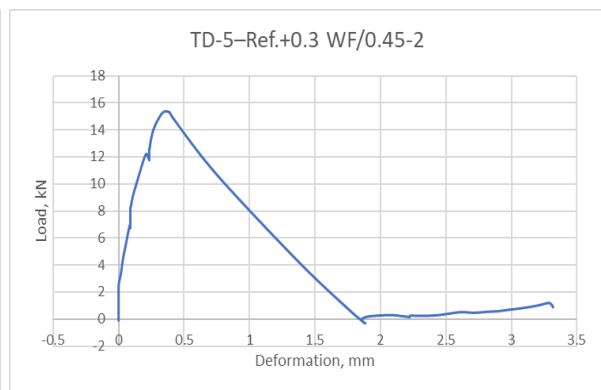
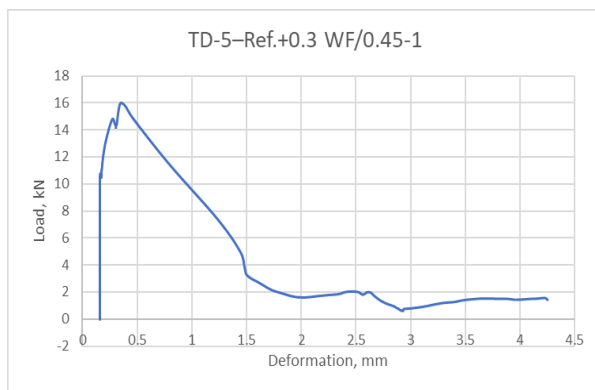
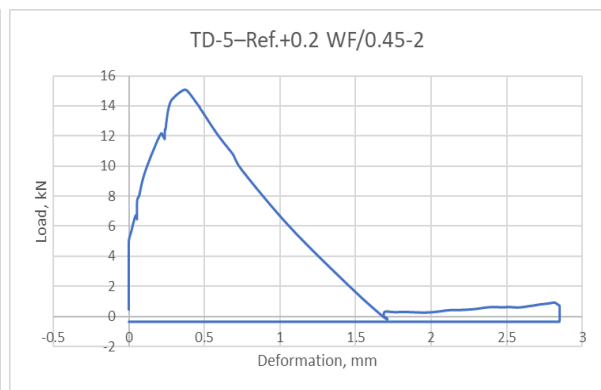
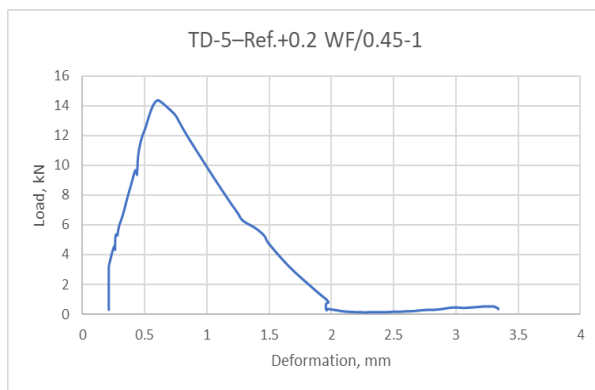
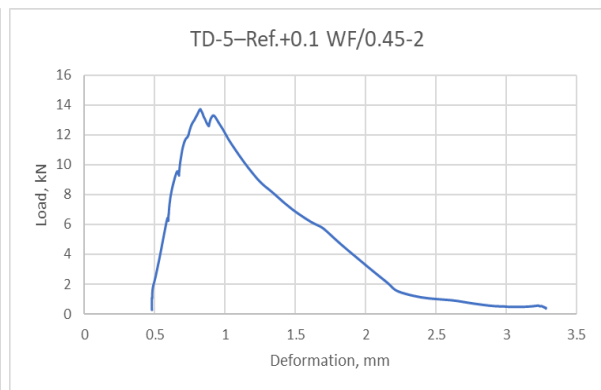
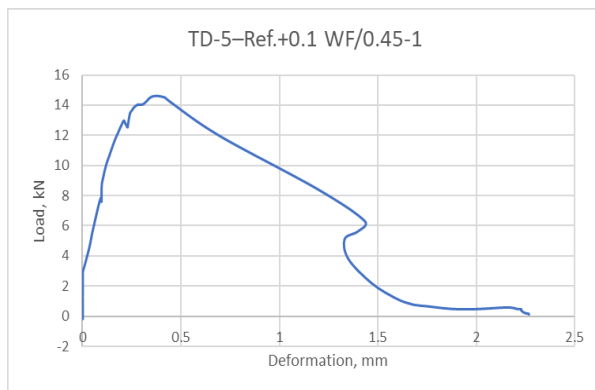
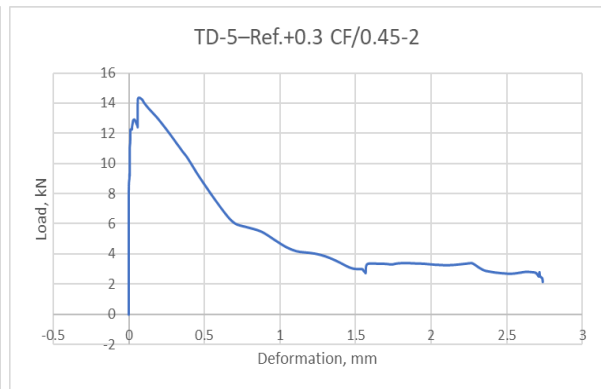
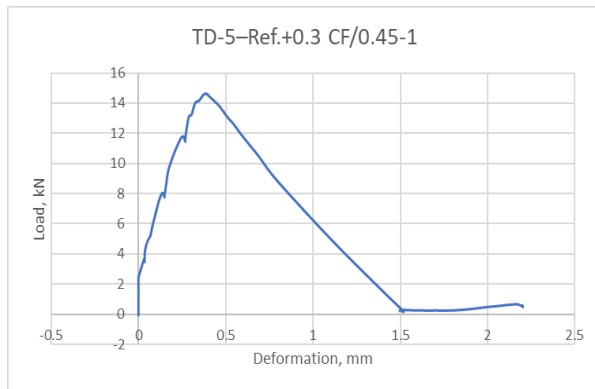
➤ **TD-4 – TB-10-O – 28 days: Continuation**



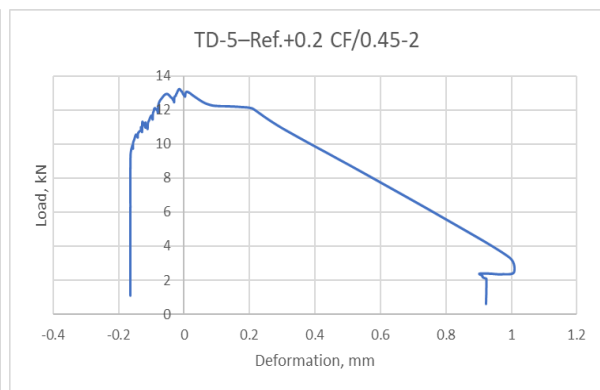
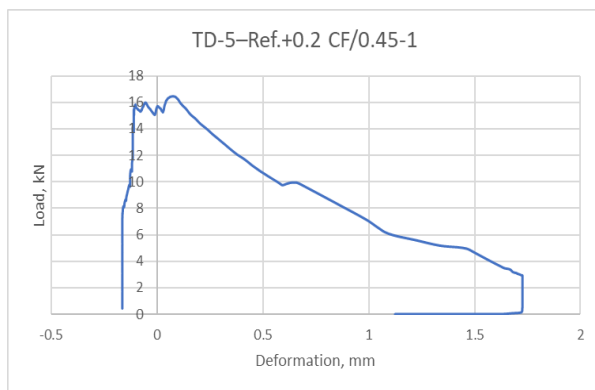
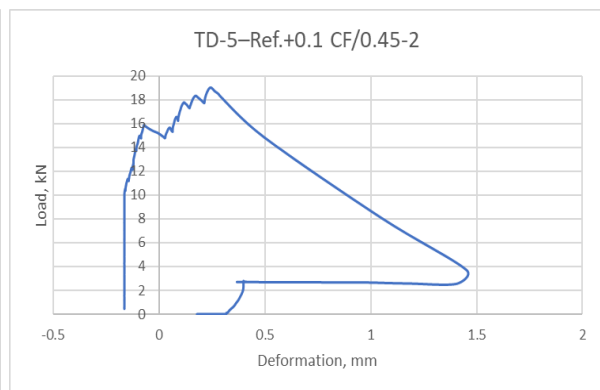
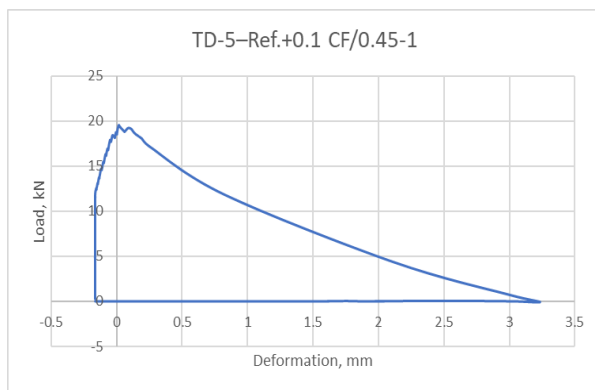
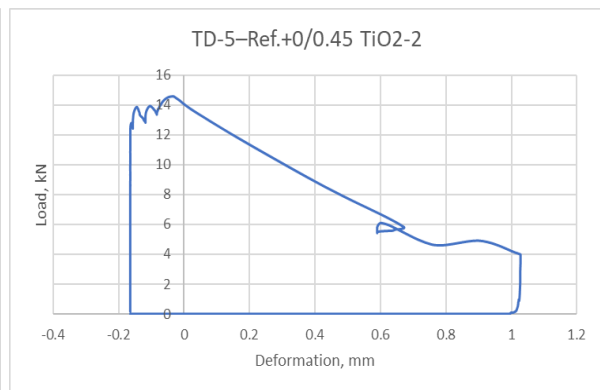
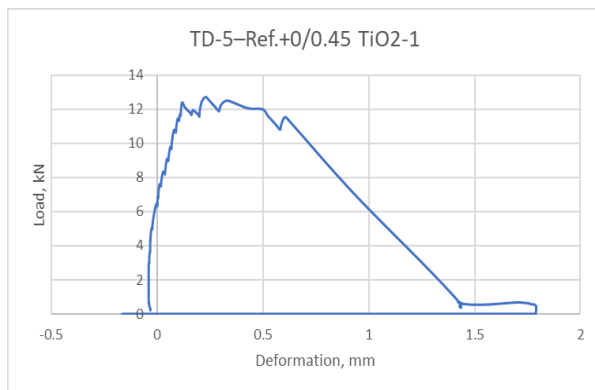
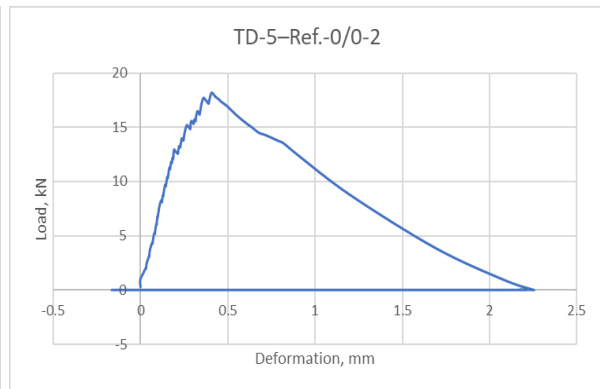
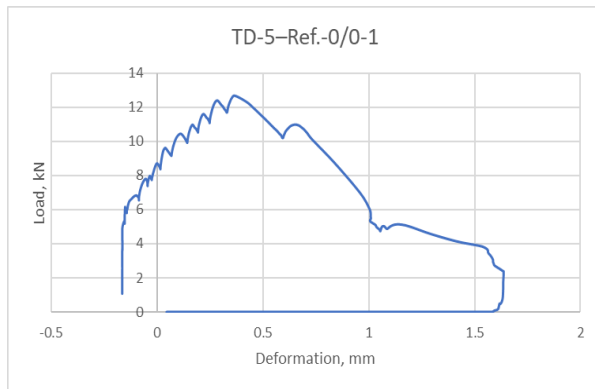
➤ TD-5 – TB-11-R – 3 days



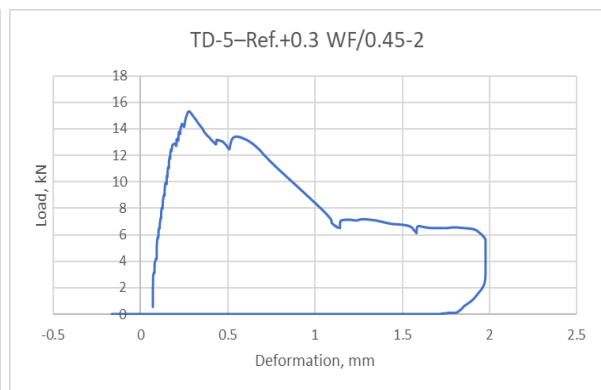
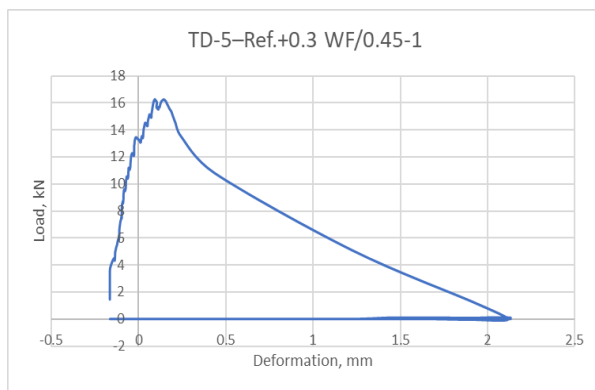
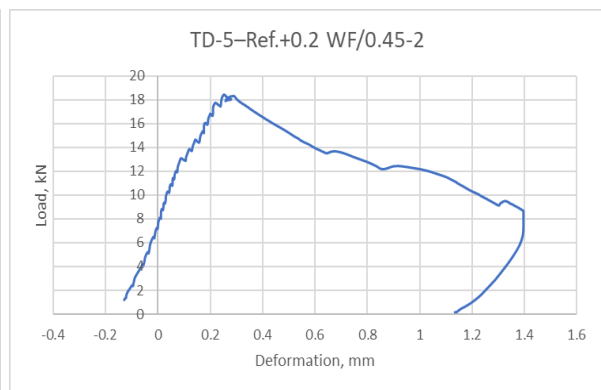
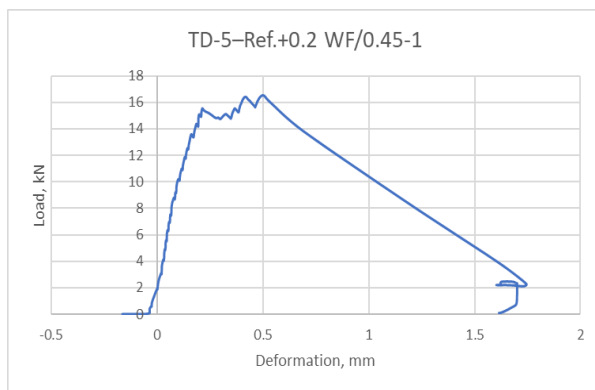
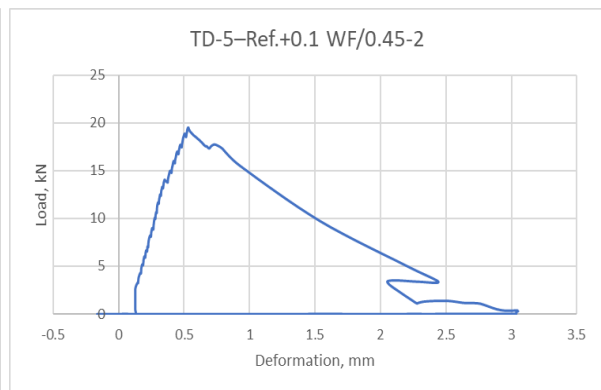
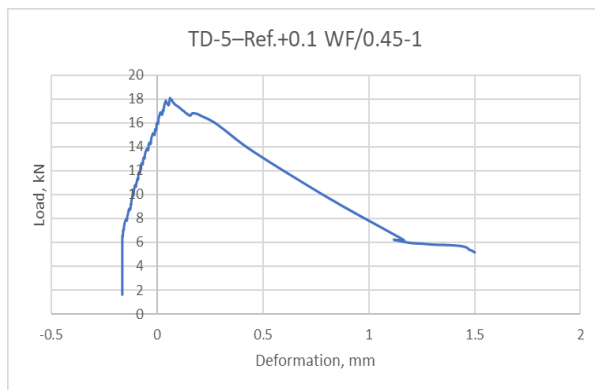
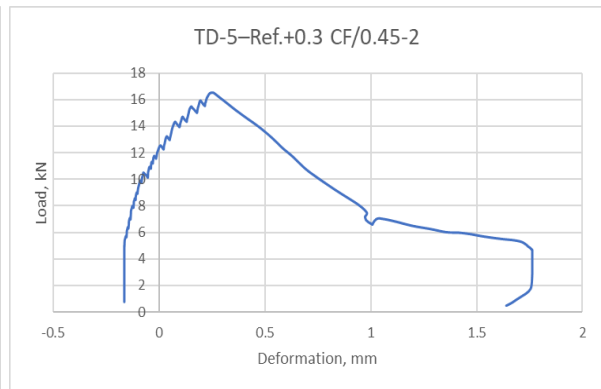
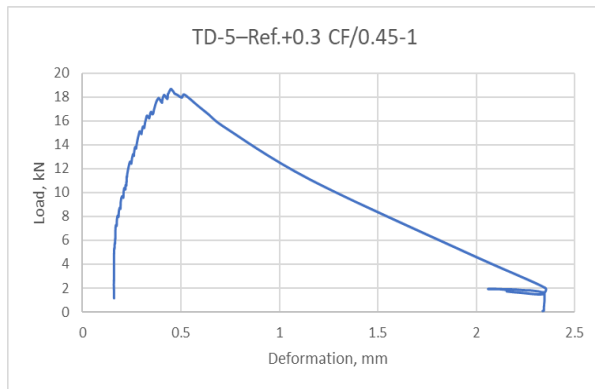
➤ **TD-5 – TB-11-R – 3 days: Continuation**



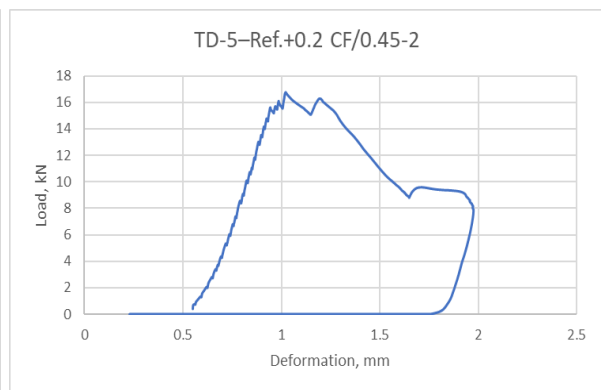
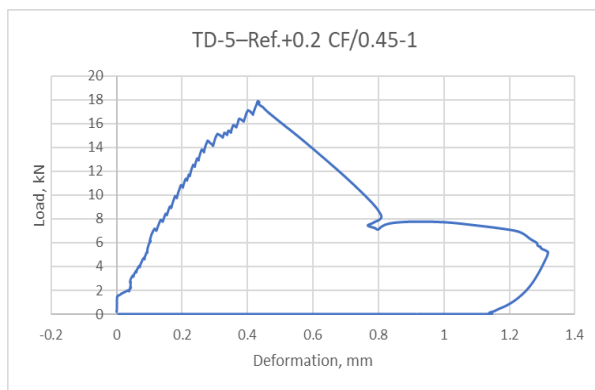
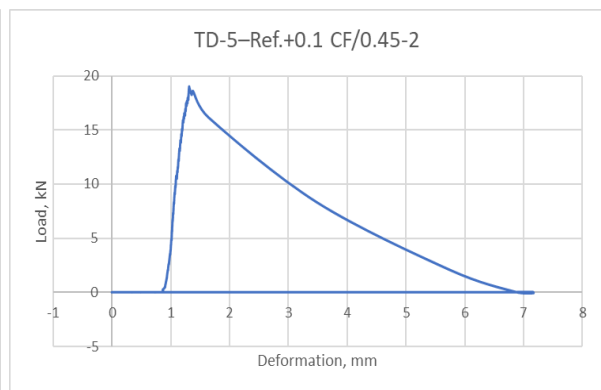
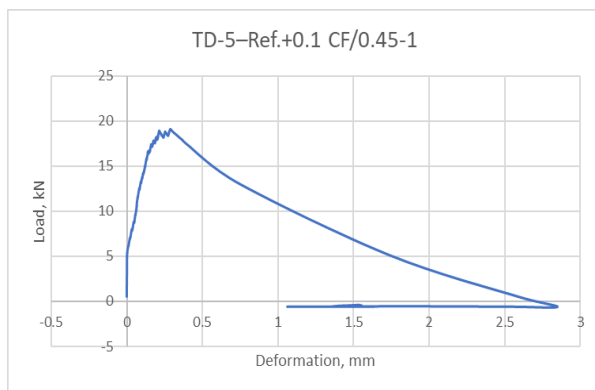
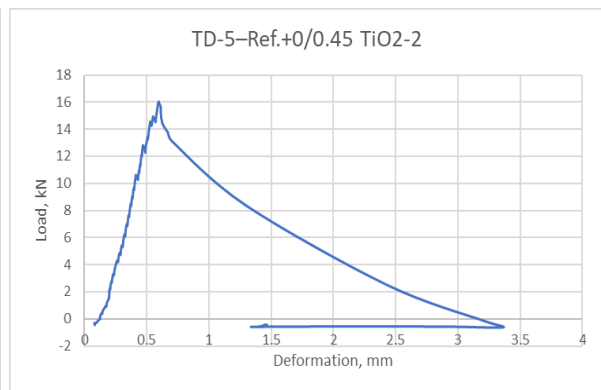
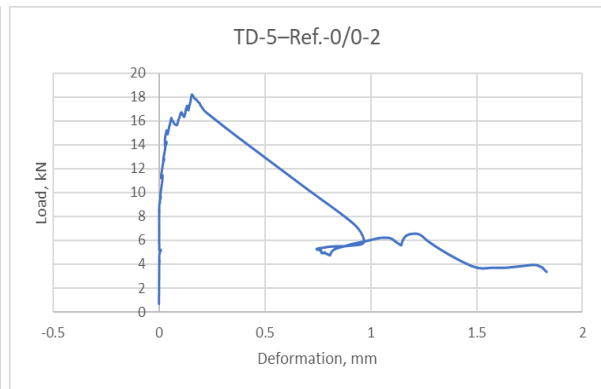
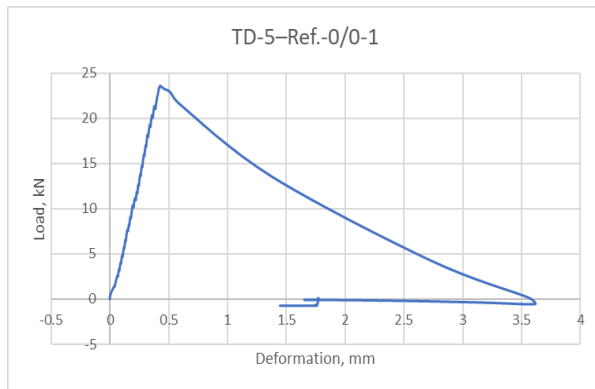
➤ TD-5 – TB-11-O – 3 days



➤ **TD-5 – TB-11-O – 3 days: Continuation**

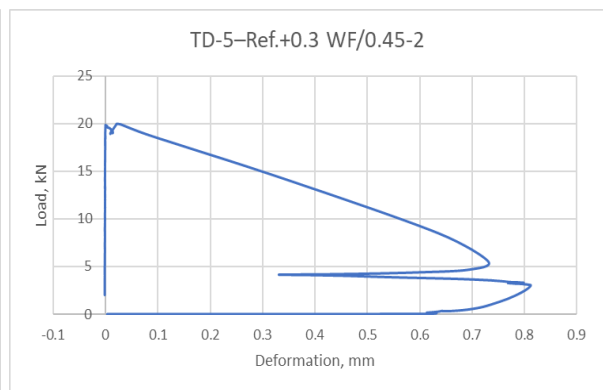
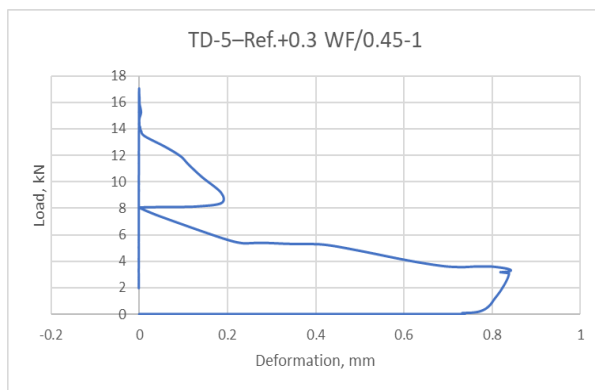
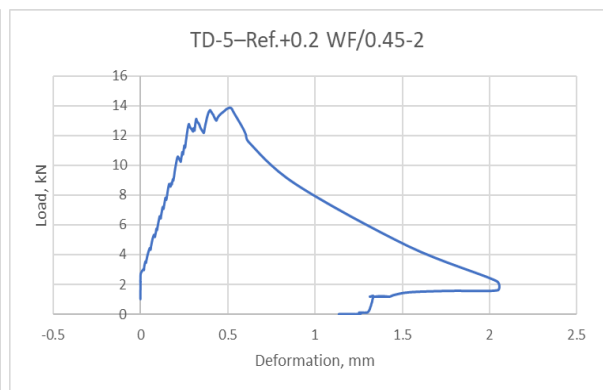
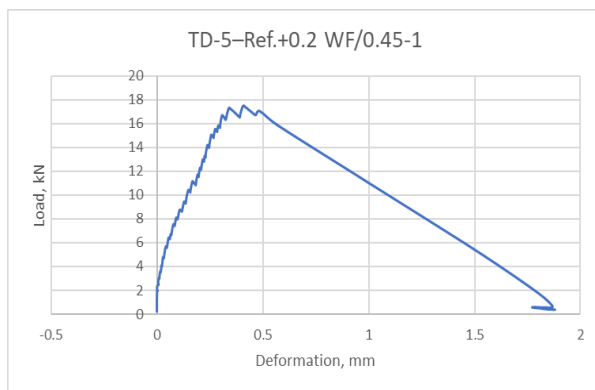
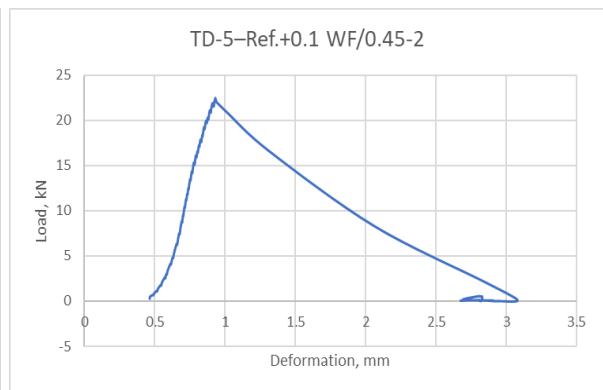
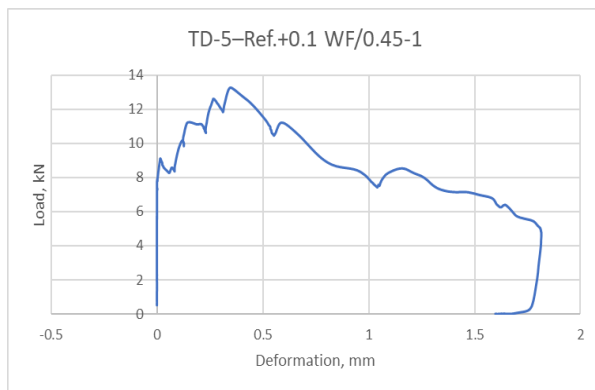
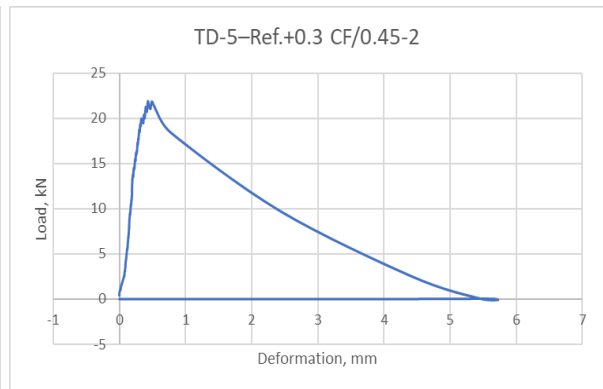
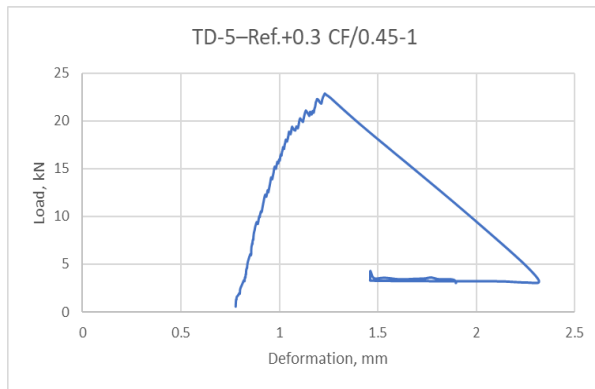


➤ **TD-5 – TB-12-R – 7 days**

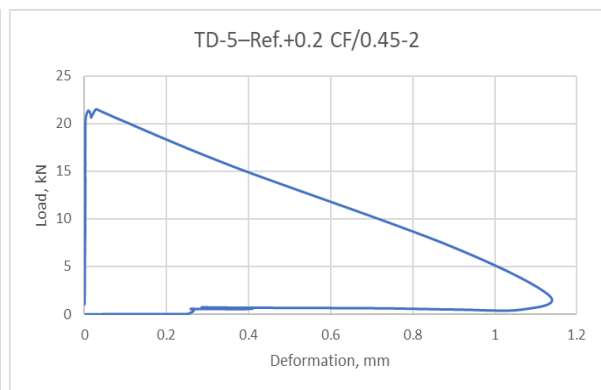
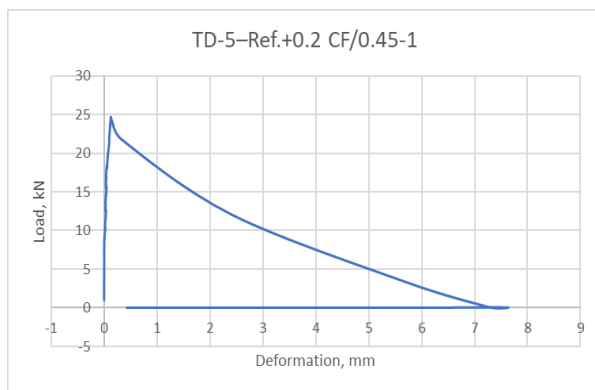
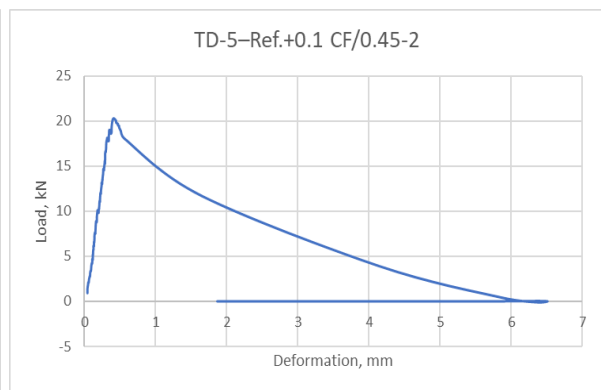
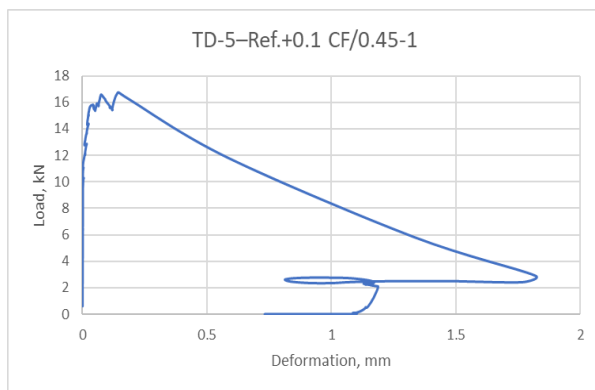
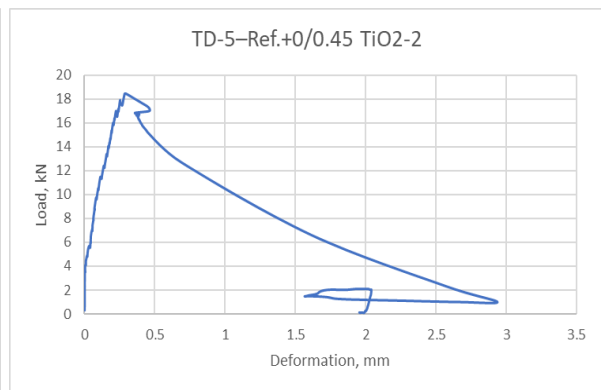
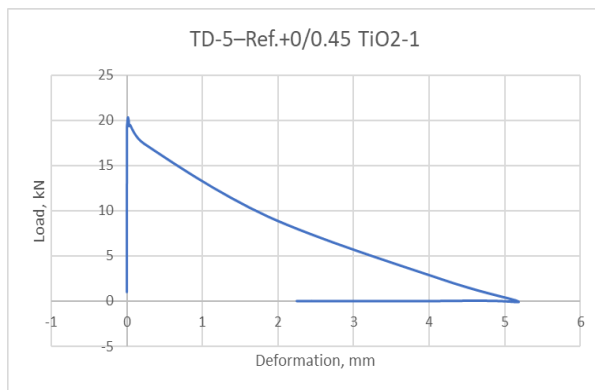
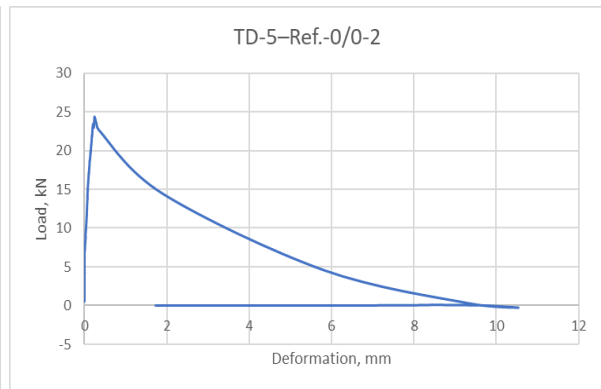
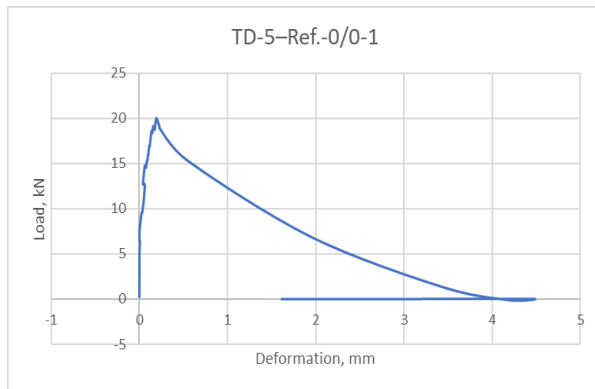




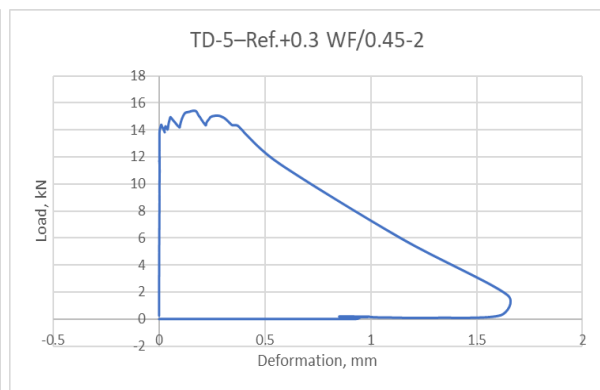
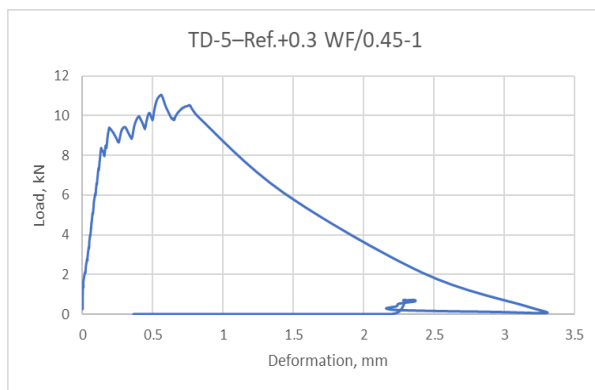
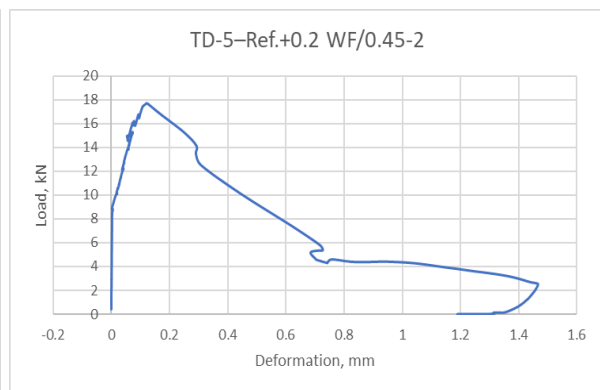
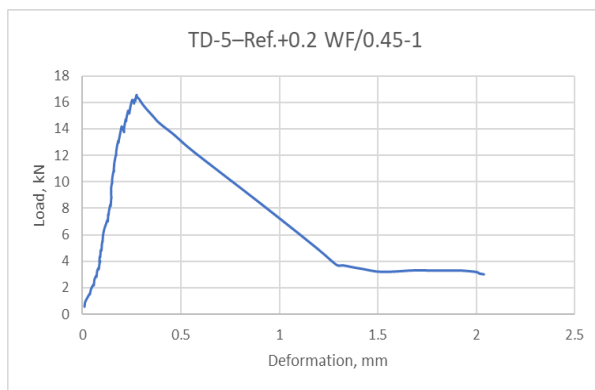
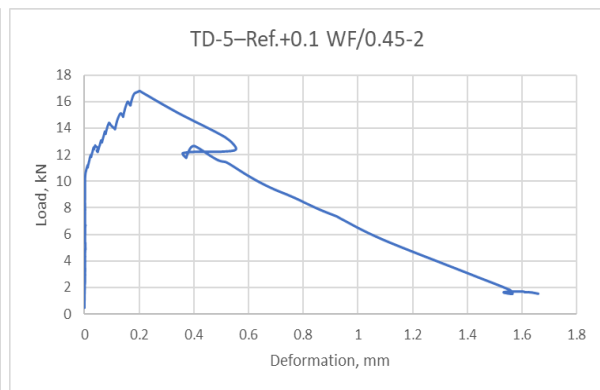
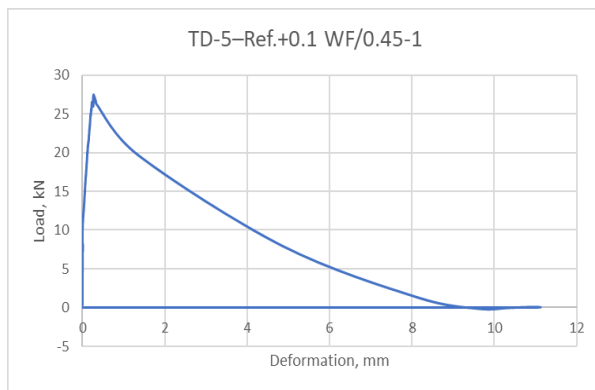
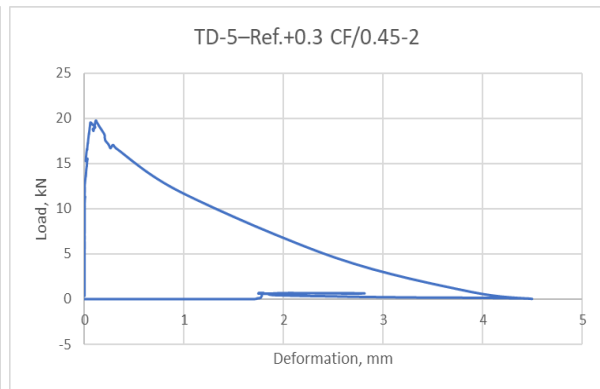
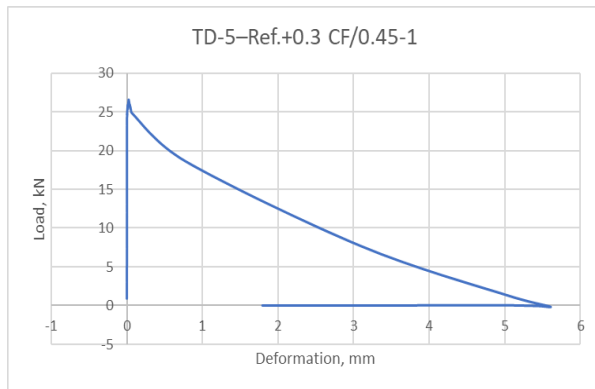
➤ **TD-5 – TB-12-R – 7 days: Continuation**



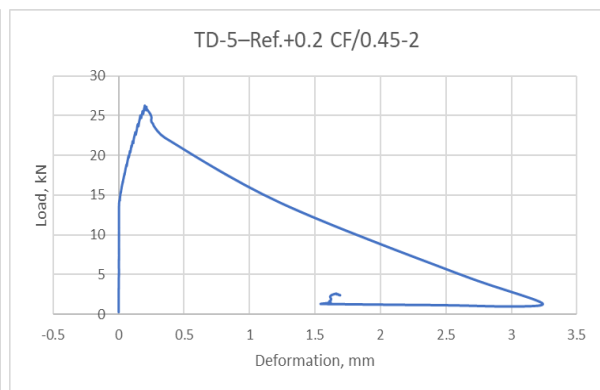
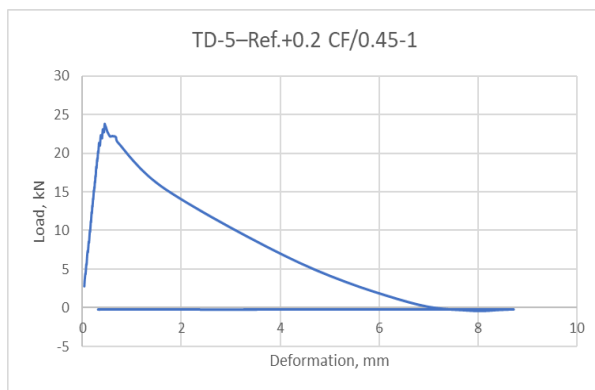
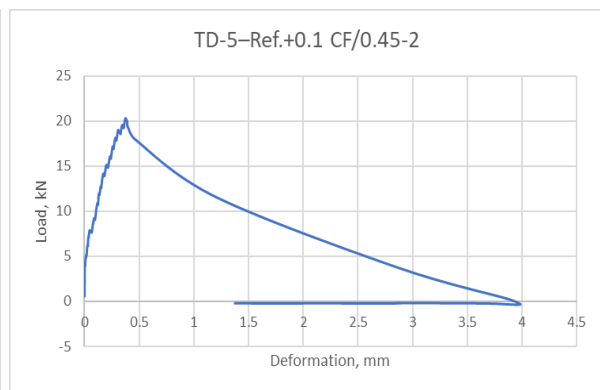
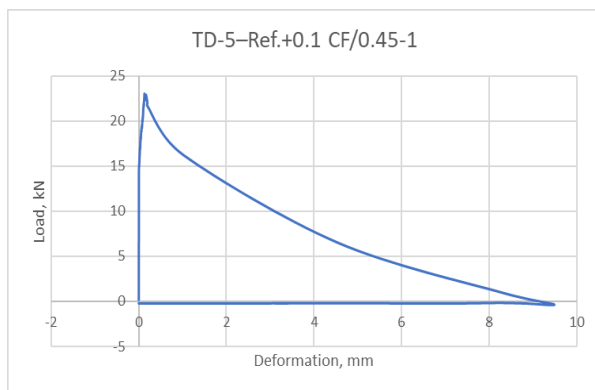
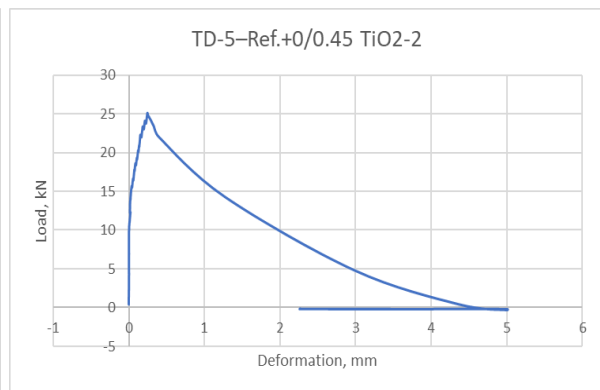
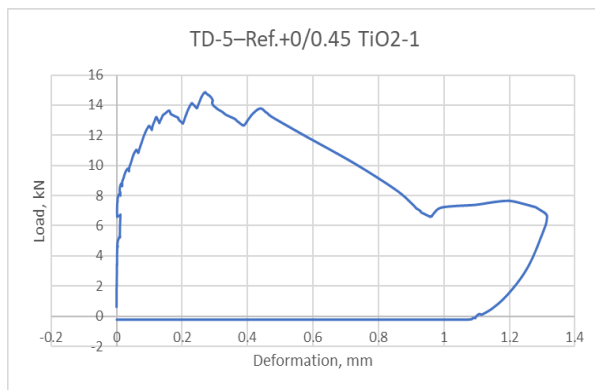
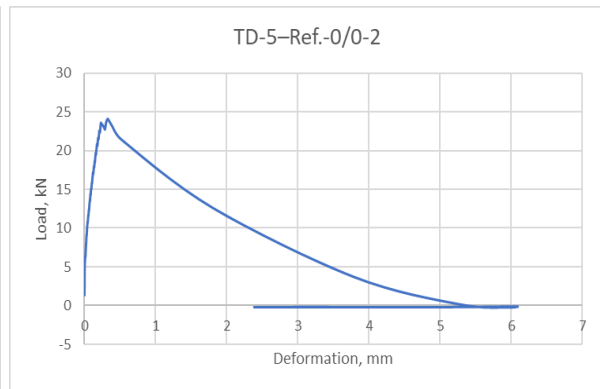
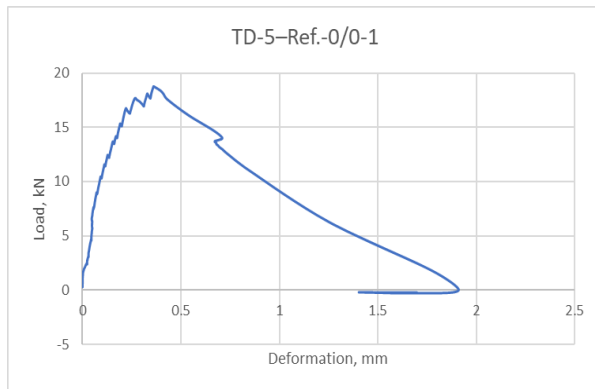
➤ TD-5 – TB-12-O – 7 days



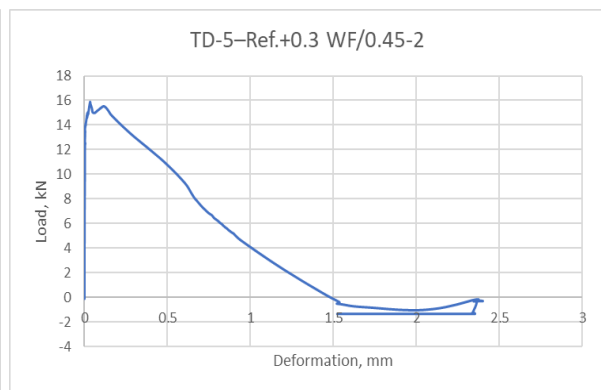
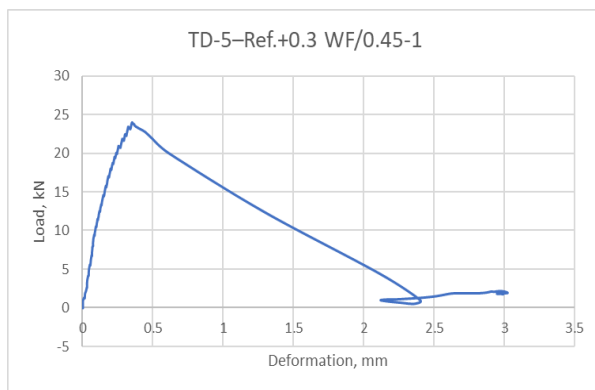
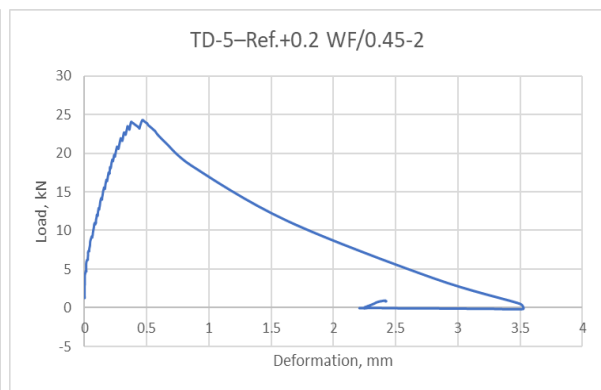
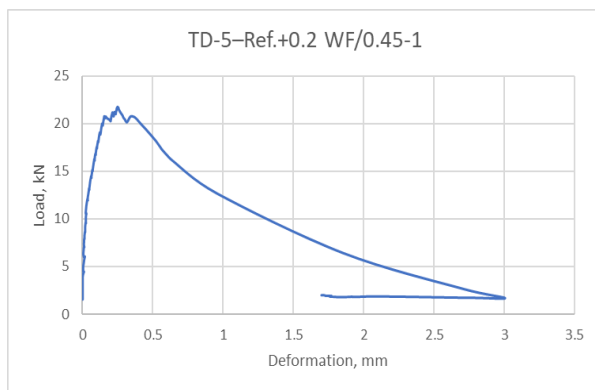
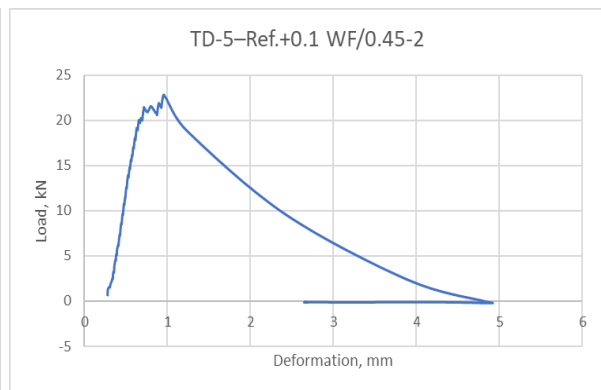
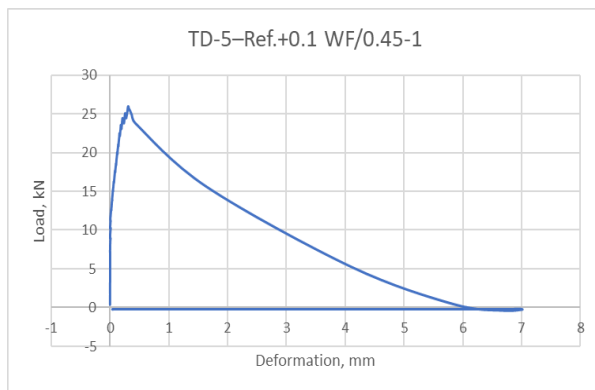
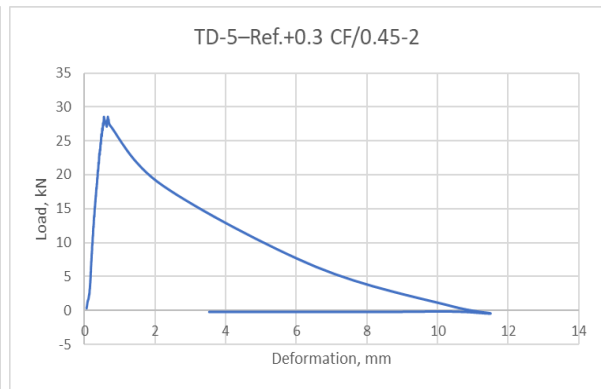
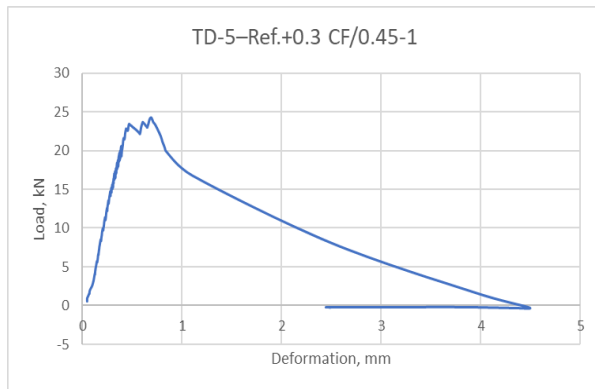
➤ **TD-5 – TB-12-O – 7 days: Continuation**



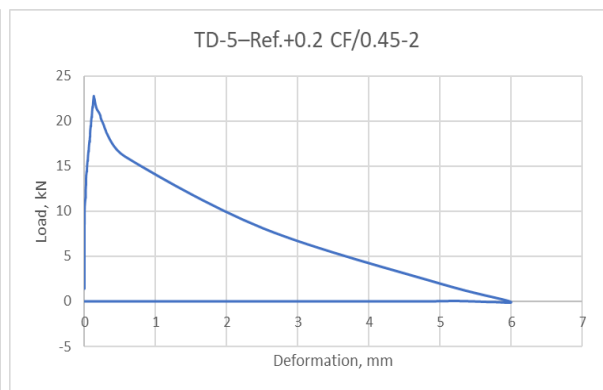
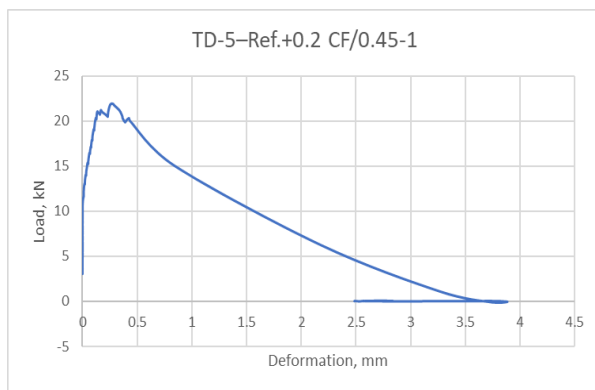
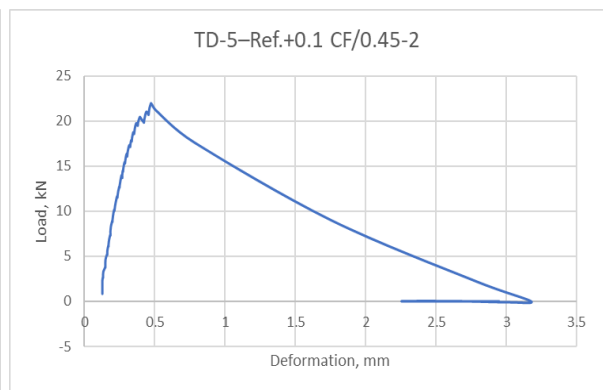
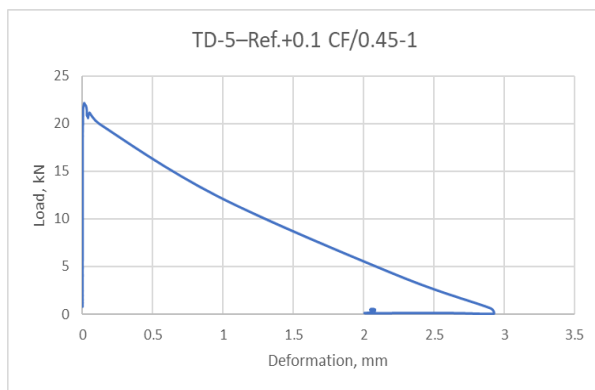
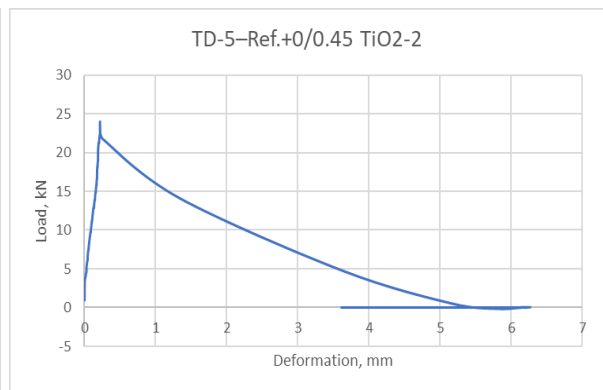
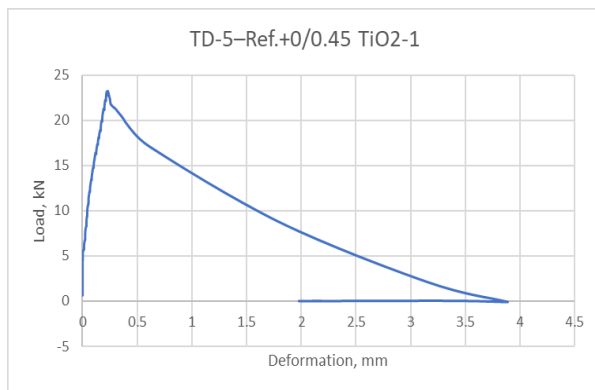
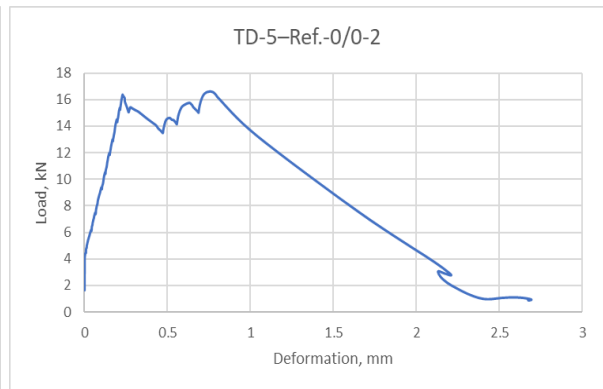
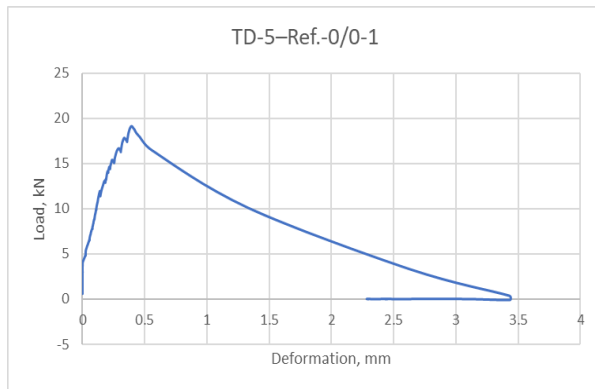
➤ **TD-5 – TB-13-R – 28 days**



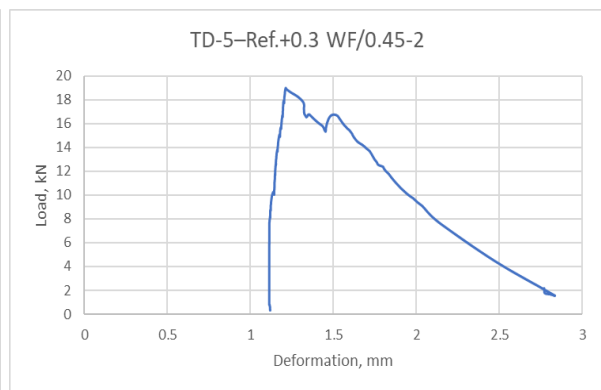
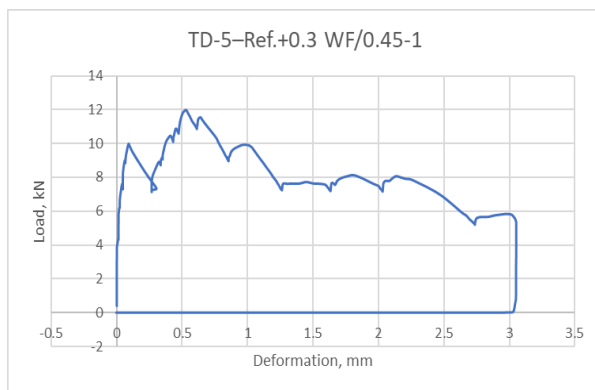
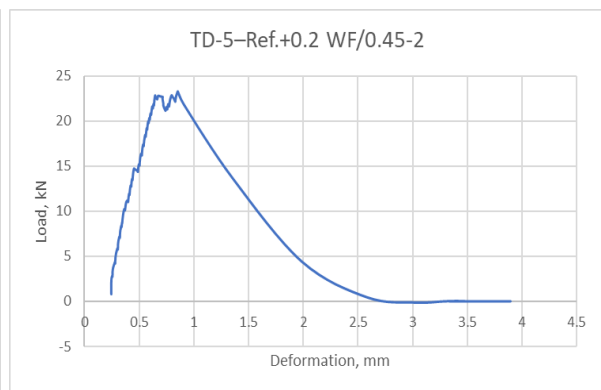
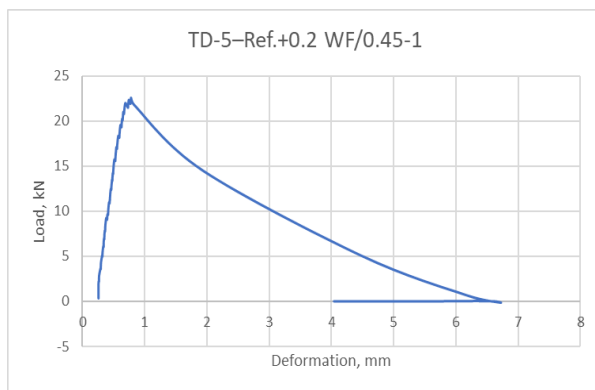
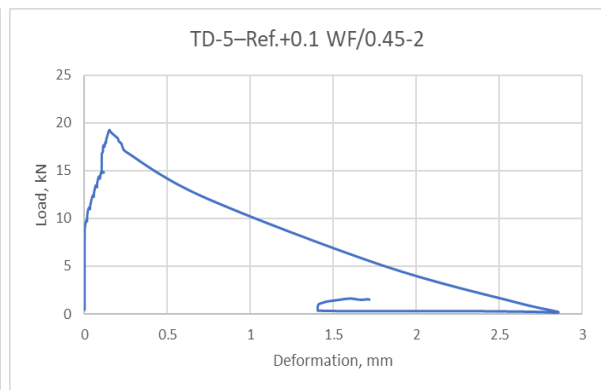
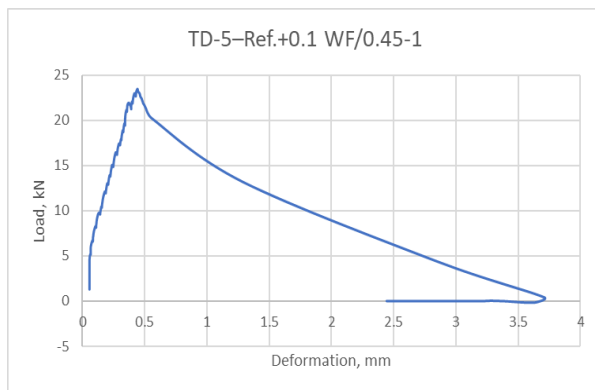
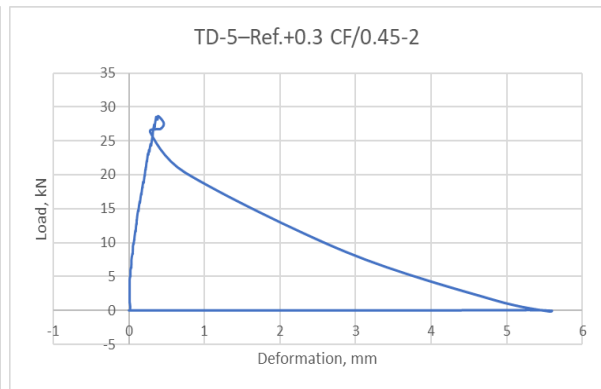
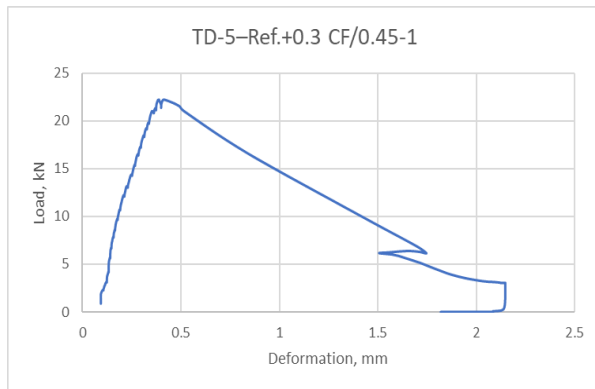
➤ **TD-5 – TB-13-R – 28 days: Continuation**



➤ **TD-5 – TB-13-O – 28 days**



➤ TD-5 – TB-13-O – 28 days: Continuation



## Appendix C – Measured non-destructive test results

Appendix C contains raw data like outer diameter, length, mass, sonic transit time that were obtained before destructive testing of the specimens. These values are used to calculate volume, density, compressional wave velocity and M-modulus.

The diagrams are arranged by their test designs, test batches with their curing environments and curing ages as described in [section 3.2.1](#).

### ➤ TD-1 – TB-1-R – 3 days

Plugs	OD, mm	Length, mm	Mass, g	Sonic, $\mu$ s	Area, m <sup>2</sup>	Volume, m <sup>3</sup>	Density, kg/m <sup>3</sup>	v <sub>p</sub> , m/s	M-modulus, GPa
TD-1– Ref.-1	32.73	67.2	107.04	21.9	0.000841	5.65E-05	1893.19	3068.49	17.83
TD-1– Ref.-2	32.98	67.35	106.23	22.2	0.000854	5.75E-05	1846.37	3033.78	16.99
TD-1– Ref.+1.2g Al <sub>2</sub> O <sub>3</sub> -1	33.1	67.13	106.82	22.2	0.000860	5.78E-05	1849.23	3023.87	16.91
TD-1– Ref.+1.2g Al <sub>2</sub> O <sub>3</sub> -2	32.94	67.42	106.81	23.3	0.000852	5.75E-05	1859.03	2893.56	15.57
TD-1– Ref.+1.4g Al <sub>2</sub> O <sub>3</sub> -1	32.91	67.11	106.79	22.2	0.000851	5.71E-05	1870.67	3022.97	17.09
TD-1– Ref.+1.4g Al <sub>2</sub> O <sub>3</sub> -2	32.95	67.3	107.38	22.1	0.000853	5.74E-05	1871.15	3045.25	17.35
TD-1– Ref.+1.6g Al <sub>2</sub> O <sub>3</sub> -1	32.89	67.72	107.32	24.3	0.000850	5.75E-05	1865.29	2786.83	14.49
TD-1– Ref.+1.6g Al <sub>2</sub> O <sub>3</sub> -2	32.96	67.28	106.83	22.7	0.000853	5.74E-05	1860.99	2963.88	16.35

### ➤ TD-1 – TB-1-O – 3 days

Plugs	OD, mm	Length, mm	Mass, g	Sonic, $\mu$ s	Area, m <sup>2</sup>	Volume, m <sup>3</sup>	Density, kg/m <sup>3</sup>	v <sub>p</sub> , m/s	M-modulus, GPa
TD-1– Ref.-1	32.85	66.71	99.38	23.8	0.000848	5.65E-05	1757.71	2802.94	13.81
TD-1– Ref.-2	32.95	67.2	100.12	24.9	0.000853	5.73E-05	1747.23	2698.80	12.73
TD-1– Ref.+1.2g Al <sub>2</sub> O <sub>3</sub> -1	33.09	67.31	100.88	23.2	0.000860	5.79E-05	1742.78	2901.29	14.67
TD-1– Ref.+1.2g Al <sub>2</sub> O <sub>3</sub> -2	32.85	67.59	100.7	23.2	0.000848	5.73E-05	1757.87	2913.36	14.92
TD-1– Ref.+1.4g Al <sub>2</sub> O <sub>3</sub> -1	32.98	67.53	101.42	24	0.000854	5.77E-05	1758.07	2813.75	13.92
TD-1– Ref.+1.4g Al <sub>2</sub> O <sub>3</sub> -2	32.85	66.71	99.75	24.8	0.000848	5.65E-05	1764.25	2689.92	12.77
TD-1– Ref.+1.6g Al <sub>2</sub> O <sub>3</sub> -1	32.97	67.68	101.26	23.1	0.000854	5.78E-05	1752.47	2929.87	15.04
TD-1– Ref.+1.6g Al <sub>2</sub> O <sub>3</sub> -2	32.95	67.15	100.85	23	0.000853	5.73E-05	1761.28	2919.57	15.01



➤ **TD-1 – TB-2-R – 7 days**

Plugs	OD, mm	Length, mm	Mass, g	Sonic, $\mu$ s	Area, m <sup>2</sup>	Volume, m <sup>3</sup>	Density, kg/m <sup>3</sup>	v <sub>p</sub> , m/s	M-modulus, GPa
TD-1– Ref.-1	32.62	66.64	103.58	20.6	0.000836	5.57E-05	1.86E+03	3.23E+03	1.95E+01
TD-1– Ref.-2	32.65	66.59	103.05	20.8	0.000837	5.58E-05	1.85E+03	3.20E+03	1.89E+01
TD-1– Ref.+1.2g Al <sub>2</sub> O <sub>3</sub> -1	32.73	66.78	102.91	23.1	0.000841	5.62E-05	1.83E+03	2.89E+03	1.53E+01
TD-1– Ref.+1.2g Al <sub>2</sub> O <sub>3</sub> -2	32.71	66.38	102.48	22.9	0.000840	5.58E-05	1.84E+03	2.90E+03	1.54E+01
TD-1– Ref.+1.4g Al <sub>2</sub> O <sub>3</sub> -1	32.77	65.26	100.42	20.6	0.000843	5.50E-05	1.82E+03	3.17E+03	1.83E+01
TD-1– Ref.+1.4g Al <sub>2</sub> O <sub>3</sub> -2	32.56	66.26	101.37	20.6	0.000833	5.52E-05	1.84E+03	3.22E+03	1.90E+01
TD-1– Ref.+1.6g Al <sub>2</sub> O <sub>3</sub> -1	32.51	66.2	102.33	20.8	0.000830	5.50E-05	1.86E+03	3.18E+03	1.89E+01
TD-1– Ref.+1.6g Al <sub>2</sub> O <sub>3</sub> -2	32.67	66.18	101.82	21.4	0.000838	5.55E-05	1.84E+03	3.09E+03	1.76E+01

➤ **TD-1 – TB-2-O – 7 days**

Plugs	OD, mm	Length, mm	Mass, g	Sonic, $\mu$ s	Area, m <sup>2</sup>	Volume, m <sup>3</sup>	Density, kg/m <sup>3</sup>	v <sub>p</sub> , m/s	M-modulus, GPa
TD-1– Ref.-1	32.5	66.05	91.89	22.1	0.000830	5.48E-05	1.68E+03	2.99E+03	1.50E+01
TD-1– Ref.-2	33.08	66.66	95.37	22.7	0.000859	5.73E-05	1.66E+03	2.94E+03	1.44E+01
TD-1– Ref.+1.2g Al <sub>2</sub> O <sub>3</sub> -1	32.88	66.15	94.3	23.6	0.000849	5.62E-05	1.68E+03	2.80E+03	1.32E+01
TD-1– Ref.+1.2g Al <sub>2</sub> O <sub>3</sub> -2	32.75	66	92.1	24.7	0.000842	5.56E-05	1.66E+03	2.67E+03	1.18E+01
TD-1– Ref.+1.4g Al <sub>2</sub> O <sub>3</sub> -1	32.6	66.1	93.82	22.3	0.000835	5.52E-05	1.70E+03	2.96E+03	1.49E+01
TD-1– Ref.+1.4g Al <sub>2</sub> O <sub>3</sub> -2	32.65	66.48	93.8	24.8	0.000837	5.57E-05	1.69E+03	2.68E+03	1.21E+01
TD-1– Ref.+1.6g Al <sub>2</sub> O <sub>3</sub> -1	32.56	66	94.82	22.3	0.000833	5.50E-05	1.73E+03	2.96E+03	1.51E+01
TD-1– Ref.+1.6g Al <sub>2</sub> O <sub>3</sub> -2	32.69	66.01	92.61	23.1	0.000839	5.54E-05	1.67E+03	2.86E+03	1.36E+01

➤ **TD-1 – TB-3-R – 28 days**

Plugs	OD, mm	Length, mm	Mass, g	Sonic, $\mu$ s	Area, m <sup>2</sup>	Volume, m <sup>3</sup>	Density, kg/m <sup>3</sup>	v <sub>p</sub> , m/s	M-modulus, GPa
TD-1– Ref.-1	32.64	66.29	101.143	21.7	0.000837	5.55E-05	1.82E+03	3.05E+03	1.70E+01
TD-1– Ref.-2	32.66	66.16	100.682	22.9	0.000838	5.54E-05	1.82E+03	2.89E+03	1.52E+01
TD-1– Ref.+1.2g Al <sub>2</sub> O <sub>3</sub> -1	32.46	64.07	98.497	19.3	0.000828	5.30E-05	1.86E+03	3.32E+03	2.05E+01
TD-1– Ref.+1.2g Al <sub>2</sub> O <sub>3</sub> -2	32.69	66.08	100.465	21.9	0.000839	5.55E-05	1.81E+03	3.02E+03	1.65E+01
TD-1– Ref.+1.4g Al <sub>2</sub> O <sub>3</sub> -1	32.68	66.41	100.412	22.9	0.000839	5.57E-05	1.80E+03	2.90E+03	1.52E+01
TD-1– Ref.+1.4g Al <sub>2</sub> O <sub>3</sub> -2	32.43	66.02	100.648	19.7	0.000826	5.45E-05	1.85E+03	3.35E+03	2.07E+01
TD-1– Ref.+1.6g Al <sub>2</sub> O <sub>3</sub> -1	32.7	65.89	101.269	20	0.000840	5.53E-05	1.83E+03	3.29E+03	1.99E+01
TD-1– Ref.+1.6g Al <sub>2</sub> O <sub>3</sub> -2	32.89	65.98	100.687	21.1	0.000850	5.61E-05	1.80E+03	3.13E+03	1.76E+01

➤ **TD-1 – TB-3-O – 28 days**

Plugs	OD, mm	Length, mm	Mass, g	Sonic, $\mu$ s	Area, m <sup>2</sup>	Volume, m <sup>3</sup>	Density, kg/m <sup>3</sup>	v <sub>p</sub> , m/s	M-modulus, GPa
TD-1– Ref.-1	32.27	66.33	86.619	21.2	0.000818	5.42E-05	1.60E+03	3.13E+03	1.56E+01
TD-1– Ref.-2	32.94	65.62	86.426	20.4	0.000852	5.59E-05	1.55E+03	3.22E+03	1.60E+01
TD-1– Ref.+1.2g Al <sub>2</sub> O <sub>3</sub> -1	32.43	65.62	86.021	22.9	0.000826	5.42E-05	1.59E+03	2.87E+03	1.30E+01
TD-1– Ref.+1.2g Al <sub>2</sub> O <sub>3</sub> -2	32.51	65.76	86.842	21.6	0.000830	5.46E-05	1.59E+03	3.04E+03	1.47E+01
TD-1– Ref.+1.4g Al <sub>2</sub> O <sub>3</sub> -1	32.73	66.01	86.899	21.2	0.000841	5.55E-05	1.56E+03	3.11E+03	1.52E+01
TD-1– Ref.+1.4g Al <sub>2</sub> O <sub>3</sub> -2	32.9	65.19	86.333	22.3	0.000850	5.54E-05	1.56E+03	2.92E+03	1.33E+01
TD-1– Ref.+1.6g Al <sub>2</sub> O <sub>3</sub> -1	32.75	65.78	86.235	21.2	0.000842	5.54E-05	1.56E+03	3.10E+03	1.50E+01
TD-1– Ref.+1.6g Al <sub>2</sub> O <sub>3</sub> -2	32.55	64.35	85.536	23	0.000832	5.35E-05	1.60E+03	2.80E+03	1.25E+01

➤ **TD-2 – TB-4-R – 3 days**

Plugs	OD, mm	Length, mm	Mass, g	Sonic, $\mu$ s	Area, m <sup>2</sup>	Volume, m <sup>3</sup>	Density, kg/m <sup>3</sup>	$v_p$ , m/s	M-modulus, GPa
TD-2– Ref.-1	32.92	67.38	106.406	23.2	0.000851	5.74E-05	1.86E+03	2.90E+03	1.56E+01
TD-2– Ref.-2	32.88	67.78	106.027	22.7	0.000849	5.76E-05	1.84E+03	2.99E+03	1.64E+01
TD-2– 1.4g Al <sub>2</sub> O <sub>3</sub> /1g FA-1	32.9	67.25	105.264	23	0.000850	5.72E-05	1.84E+03	2.92E+03	1.57E+01
TD-2– 1.4g Al <sub>2</sub> O <sub>3</sub> /1g FA-2	32.75	67.55	105.994	22.3	0.000842	5.69E-05	1.86E+03	3.03E+03	1.71E+01
TD-2– 1.4g Al <sub>2</sub> O <sub>3</sub> /2g FA-1	32.86	67.5	104.909	22.7	0.000848	5.72E-05	1.83E+03	2.97E+03	1.62E+01
TD-2– 1.4g Al <sub>2</sub> O <sub>3</sub> /2g FA-2	32.92	66.31	104.026	22.4	0.000851	5.64E-05	1.84E+03	2.96E+03	1.62E+01
TD-2– 1.4g Al <sub>2</sub> O <sub>3</sub> /3g FA-1	32.89	67.03	104.446	22.5	0.000850	5.69E-05	1.83E+03	2.98E+03	1.63E+01
TD-2– 1.4g Al <sub>2</sub> O <sub>3</sub> /3g FA-2	33.02	67.16	104.741	22.8	0.000856	5.75E-05	1.82E+03	2.95E+03	1.58E+01
TD-2–1g FA-1	33	67.2	104.52	22.7	0.000855	5.75E-05	1.82E+03	2.96E+03	1.59E+01
TD-2–1g FA-2	33.01	67.14	104.11	23.1	0.000856	5.75E-05	1.81E+03	2.91E+03	1.53E+01
TD-2–2g FA-1	32.98	65.32	101.98	21.5	0.000854	5.58E-05	1.83E+03	3.04E+03	1.69E+01
TD-2–2g FA-2	32.82	66.18	103.52	22.5	0.000846	5.60E-05	1.85E+03	2.94E+03	1.60E+01
TD-2–3g FA-1	32.69	66.29	103.46	22.6	0.000839	5.56E-05	1.86E+03	2.93E+03	1.60E+01
TD-2–3g FA-2	32.76	66.24	103.18	22	0.000843	5.58E-05	1.85E+03	3.01E+03	1.68E+01

➤ **TD-2 – TB-4-O – 3 days**

Plugs	OD, mm	Length, mm	Mass, g	Sonic, $\mu$ s	Area, m <sup>2</sup>	Volume, m <sup>3</sup>	Density, kg/m <sup>3</sup>	$v_p$ , m/s	M-modulus, GPa
TD-2– Ref.-1	32.86	67.25	99.34	23.7	0.000848	5.70E-05	1.74E+03	2.84E+03	1.40E+01
TD-2– Ref.-2	32.82	66.98	91.5	22.2	0.000846	5.67E-05	1.61E+03	3.02E+03	1.47E+01
TD-2– 1.4g Al <sub>2</sub> O <sub>3</sub> /1g FA-1	32.81	66.99	100.32	23.1	0.000845	5.66E-05	1.77E+03	2.90E+03	1.49E+01
TD-2– 1.4g Al <sub>2</sub> O <sub>3</sub> /1g FA-2	32.85	67.03	98.46	24.1	0.000848	5.68E-05	1.73E+03	2.78E+03	1.34E+01
TD-2– 1.4g Al <sub>2</sub> O <sub>3</sub> /2g FA-1	32.89	66.77	97.46	23.9	0.000850	5.67E-05	1.72E+03	2.79E+03	1.34E+01
TD-2– 1.4g Al <sub>2</sub> O <sub>3</sub> /2g FA-2	32.72	66.94	97.16	22.8	0.000841	5.63E-05	1.73E+03	2.94E+03	1.49E+01
TD-2– 1.4g Al <sub>2</sub> O <sub>3</sub> /3g FA-1	32.88	67.12	98.79	23.3	0.000849	5.70E-05	1.73E+03	2.88E+03	1.44E+01
TD-2– 1.4g Al <sub>2</sub> O <sub>3</sub> /3g FA-2	32.78	67.3	98.75	23.5	0.000844	5.68E-05	1.74E+03	2.86E+03	1.43E+01
TD-2–1g FA-1	32.91	66.84	97.81	23.1	0.000851	5.69E-05	1.72E+03	2.89E+03	1.44E+01
TD-2–1g FA-2	32.98	66.62	100.05	22.7	0.000854	5.69E-05	1.76E+03	2.93E+03	1.51E+01
TD-2–2g FA-1	32.96	66.8	97.74	23.3	0.000853	5.70E-05	1.71E+03	2.87E+03	1.41E+01
TD-2–2g FA-2	32.96	66.72	97.96	23.3	0.000853	5.69E-05	1.72E+03	2.86E+03	1.41E+01
TD-2–3g FA-1	32.9	67.04	99.27	23.1	0.000850	5.70E-05	1.74E+03	2.90E+03	1.47E+01
TD-2–3g FA-2	32.71	66.37	98.23	22.5	0.000840	5.58E-05	1.76E+03	2.95E+03	1.53E+01

➤ **TD-2 – TB-5-R – 7 days**

Plugs	OD, mm	Length, mm	Mass, g	Sonic, $\mu$ s	Area, m <sup>2</sup>	Volume, m <sup>3</sup>	Density, kg/m <sup>3</sup>	$v_p$ , m/s	M-modulus, GPa
TD-2– Ref.-1	33.05	66.95	105.508	19.8	0.000858	5.74E-05	1.84E+03	3.38E+03	2.10E+01
TD-2– Ref.-2	33.06	67.29	105.707	20.8	0.000858	5.78E-05	1.83E+03	3.24E+03	1.92E+01
TD-2– 1.4g Al <sub>2</sub> O <sub>3</sub> / 1g FA-1	33.1	67.19	105.411	20.5	0.000860	5.78E-05	1.82E+03	3.28E+03	1.96E+01
TD-2– 1.4g Al <sub>2</sub> O <sub>3</sub> / 1g FA-2	33.07	66.54	104.144	20.3	0.000859	5.72E-05	1.82E+03	3.28E+03	1.96E+01
TD-2– 1.4g Al <sub>2</sub> O <sub>3</sub> / 2g FA-1	33.03	66.9	105.785	19.5	0.000857	5.73E-05	1.85E+03	3.43E+03	2.17E+01
TD-2– 1.4g Al <sub>2</sub> O <sub>3</sub> / 2g FA-2	33.03	66.74	105.331	20	0.000857	5.72E-05	1.84E+03	3.34E+03	2.05E+01
TD-2– 1.4g Al <sub>2</sub> O <sub>3</sub> / 3g FA-1	33.03	66.63	104.944	20	0.000857	5.71E-05	1.84E+03	3.33E+03	2.04E+01
TD-2– 1.4g Al <sub>2</sub> O <sub>3</sub> / 3g FA-2	33.05	67.44	105.997	20	0.000858	5.79E-05	1.83E+03	3.37E+03	2.08E+01
TD-2–1g FA-1	33.08	67.36	105.742	20.3	0.000859	5.79E-05	1.83E+03	3.32E+03	2.01E+01
TD-2–1g FA-2	33.04	67	105.359	20.2	0.000857	5.74E-05	1.83E+03	3.32E+03	2.02E+01
TD-2–2g FA-1	33.06	67.35	105.04	20.2	0.000858	5.78E-05	1.82E+03	3.33E+03	2.02E+01
TD-2–2g FA-2	33.05	67.25	105.229	20.6	0.000858	5.77E-05	1.82E+03	3.26E+03	1.94E+01
TD-2–3g FA-1	33.06	67.21	105.789	21.2	0.000858	5.77E-05	1.83E+03	3.17E+03	1.84E+01
TD-2–3g FA-2	33.05	67.54	105.667	21.7	0.000858	5.79E-05	1.82E+03	3.11E+03	1.77E+01

➤ **TD-2 – TB-5-O – 7 days**

Plugs	OD, mm	Length, mm	Mass, g	Sonic, $\mu$ s	Area, m <sup>2</sup>	Volume, m <sup>3</sup>	Density, kg/m <sup>3</sup>	$v_p$ , m/s	M-modulus, GPa
TD-2– Ref.-1	33.1	67.39	95.784	22.7	0.000860	5.80E-05	1.65E+03	2.97E+03	1.46E+01
TD-2– Ref.-2	33.05	64.62	94.659	21.3	0.000858	5.54E-05	1.71E+03	3.03E+03	1.57E+01
TD-2– 1.4g Al <sub>2</sub> O <sub>3</sub> / 1g FA-1	33.03	66.67	96.896	24.2	0.000857	5.71E-05	1.70E+03	2.75E+03	1.29E+01
TD-2– 1.4g Al <sub>2</sub> O <sub>3</sub> / 1g FA-2	33.04	66.89	95.985	21.9	0.000857	5.73E-05	1.67E+03	3.05E+03	1.56E+01
TD-2– 1.4g Al <sub>2</sub> O <sub>3</sub> / 2g FA-1	33.06	66.9	95.693	22.2	0.000858	5.74E-05	1.67E+03	3.01E+03	1.51E+01
TD-2– 1.4g Al <sub>2</sub> O <sub>3</sub> / 2g FA-2	33.08	67.37	94.42	22.2	0.000859	5.79E-05	1.63E+03	3.03E+03	1.50E+01
TD-2– 1.4g Al <sub>2</sub> O <sub>3</sub> / 3g FA-1	33.06	66.84	94.814	24.1	0.000858	5.74E-05	1.65E+03	2.77E+03	1.27E+01
TD-2– 1.4g Al <sub>2</sub> O <sub>3</sub> / 3g FA-2	33.08	67.15	95.493	23.1	0.000859	5.77E-05	1.65E+03	2.91E+03	1.40E+01
TD-2–1g FA-1	33.07	67.01	96.249	23.6	0.000859	5.76E-05	1.67E+03	2.84E+03	1.35E+01
TD-2–1g FA-2	33.04	67.06	94.831	23.2	0.000857	5.75E-05	1.65E+03	2.89E+03	1.38E+01
TD-2–2g FA-1	33.07	66.86	95.828	21.7	0.000859	5.74E-05	1.67E+03	3.08E+03	1.58E+01
TD-2–2g FA-2	33.08	66.19	94.642	22.6	0.000859	5.69E-05	1.66E+03	2.93E+03	1.43E+01
TD-2–3g FA-1	33.04	67.16	94.876	22.5	0.000857	5.76E-05	1.65E+03	2.98E+03	1.47E+01
TD-2–3g FA-2	33.05	67.55	94.127	22.3	0.000858	5.80E-05	1.62E+03	3.03E+03	1.49E+01

➤ **TD-2 – TB-6-R – 28 days**

Plugs	OD, mm	Length, mm	Mass, g	Sonic, $\mu$ s	Area, m <sup>2</sup>	Volume, m <sup>3</sup>	Density, kg/m <sup>3</sup>	$v_p$ , m/s	M-modulus, GPa
TD-2– Ref.-1	32.88	67.31	104.319	21	0.000849	5.72E-05	1.83E+03	3.21E+03	1.88E+01
TD-2– Ref.-2	32.87	67.32	104.155	20.7	0.000849	5.71E-05	1.82E+03	3.25E+03	1.93E+01
TD-2– 1.4g Al <sub>2</sub> O <sub>3</sub> / 1g FA-1	32.95	67.42	104.219	20.8	0.000853	5.75E-05	1.81E+03	3.24E+03	1.90E+01
TD-2– 1.4g Al <sub>2</sub> O <sub>3</sub> / 1g FA-2	32.9	67.47	105.53	20.5	0.000850	5.74E-05	1.84E+03	3.29E+03	1.99E+01
TD-2– 1.4g Al <sub>2</sub> O <sub>3</sub> / 2g FA-1	32.96	67.38	104.583	21.5	0.000853	5.75E-05	1.82E+03	3.13E+03	1.79E+01
TD-2– 1.4g Al <sub>2</sub> O <sub>3</sub> / 2g FA-2	32.86	67.37	104.835	21.3	0.000848	5.71E-05	1.83E+03	3.16E+03	1.84E+01
TD-2– 1.4g Al <sub>2</sub> O <sub>3</sub> / 3g FA-1	33.09	67.22	104.79	21.5	0.000860	5.78E-05	1.81E+03	3.13E+03	1.77E+01
TD-2– 1.4g Al <sub>2</sub> O <sub>3</sub> / 3g FA-2	33.01	66.57	103.358	20.4	0.000856	5.70E-05	1.81E+03	3.26E+03	1.93E+01
TD-2–1g FA-1	33	67.09	103.249	21.2	0.000855	5.74E-05	1.80E+03	3.16E+03	1.80E+01
TD-2–1g FA-2	33.03	66.88	103.712	20.7	0.000857	5.73E-05	1.81E+03	3.23E+03	1.89E+01
TD-2–2g FA-1	33.01	67.11	103.921	20.7	0.000856	5.74E-05	1.81E+03	3.24E+03	1.90E+01
TD-2–2g FA-2	33.06	67.05	104.033	21.4	0.000858	5.76E-05	1.81E+03	3.13E+03	1.77E+01
TD-2–3g FA-1	33.04	67.13	103.773	21.5	0.000857	5.76E-05	1.80E+03	3.12E+03	1.76E+01
TD-2–3g FA-2	33.1	67.34	104.087	20.6	0.000860	5.79E-05	1.80E+03	3.27E+03	1.92E+01

➤ **TD-2 – TB-6-O – 28 days**

Plugs	OD, mm	Length, mm	Mass, g	Sonic, $\mu$ s	Area, m <sup>2</sup>	Volume, m <sup>3</sup>	Density, kg/m <sup>3</sup>	$v_p$ , m/s	M-modulus, GPa
TD-2– Ref.-1	32.96	67.15	89.679	23.7	0.000853	5.73E-05	1.57E+03	2.83E+03	1.26E+01
TD-2– Ref.-2	32.91	66.99	90.179	23.7	0.000851	5.70E-05	1.58E+03	2.83E+03	1.26E+01
TD-2– 1.4g Al <sub>2</sub> O <sub>3</sub> / 1g FA-1	32.84	66.88	89.854	24.2	0.000847	5.66E-05	1.59E+03	2.76E+03	1.21E+01
TD-2– 1.4g Al <sub>2</sub> O <sub>3</sub> / 1g FA-2	32.88	67.62	90.06	22.7	0.000849	5.74E-05	1.57E+03	2.98E+03	1.39E+01
TD-2– 1.4g Al <sub>2</sub> O <sub>3</sub> / 2g FA-1	32.97	67.04	89.558	21.1	0.000854	5.72E-05	1.56E+03	3.18E+03	1.58E+01
TD-2– 1.4g Al <sub>2</sub> O <sub>3</sub> / 2g FA-2	32.96	67.1	90.63	21	0.000853	5.73E-05	1.58E+03	3.20E+03	1.62E+01
TD-2– 1.4g Al <sub>2</sub> O <sub>3</sub> / 3g FA-1	32.95	66.99	89.001	22.2	0.000853	5.71E-05	1.56E+03	3.02E+03	1.42E+01
TD-2– 1.4g Al <sub>2</sub> O <sub>3</sub> / 3g FA-2	32.99	66.95	89.114	22.6	0.000855	5.72E-05	1.56E+03	2.96E+03	1.37E+01
TD-2–1g FA-1	32.94	66.57	88.47	22.6	0.000852	5.67E-05	1.56E+03	2.95E+03	1.35E+01
TD-2–1g FA-2	32.97	65.72	87.16	22.5	0.000854	5.61E-05	1.55E+03	2.92E+03	1.33E+01
TD-2–2g FA-1	32.84	67.07	89.109	22.3	0.000847	5.68E-05	1.57E+03	3.01E+03	1.42E+01
TD-2–2g FA-2	32.97	67.07	89.326	23	0.000854	5.73E-05	1.56E+03	2.92E+03	1.33E+01
TD-2–3g FA-1	32.91	66.64	88.567	23	0.000851	5.67E-05	1.56E+03	2.90E+03	1.31E+01
TD-2–3g FA-2	32.86	66.91	88.523	21.4	0.000848	5.67E-05	1.56E+03	3.13E+03	1.53E+01

➤ **TD-3 – TB-7-R – 10 days**

Plugs	OD, mm	Length, mm	Mass, g	Sonic, $\mu$ s	Area, m <sup>2</sup>	Volume, m <sup>3</sup>	Density, kg/m <sup>3</sup>	v <sub>p</sub> , m/s	M-modulus, GPa
<b>Geopolymer Ref.-1</b>	32.55	67.01	97.021	26.5	0.000832	5.58E-05	1.74E+03	2.53E+03	1.11E+01
<b>Geopolymer Ref.-2</b>	32.52	66.01	94.789	26.7	0.000831	5.48E-05	1.73E+03	2.47E+03	1.06E+01
<b>Geopolymer Ref.+0.3g TiO<sub>2</sub>-1</b>	32.8	65.6	96.26	27.2	0.000845	5.54E-05	1.74E+03	2.41E+03	1.01E+01
<b>Geopolymer Ref.+0.3g TiO<sub>2</sub>-2</b>	32.65	65.4	94.95	27.8	0.000837	5.48E-05	1.73E+03	2.35E+03	9.60E+00
<b>Geopolymer Ref.+0.4g TiO<sub>2</sub>-1</b>	32.61	66.17	99.272	25	0.000835	5.53E-05	1.80E+03	2.65E+03	1.26E+01
<b>Geopolymer Ref.+0.4g TiO<sub>2</sub>-2</b>	32.74	66.53	99.6	25	0.000842	5.60E-05	1.78E+03	2.66E+03	1.26E+01
<b>Geopolymer Ref.+0.5g TiO<sub>2</sub>-1</b>	32.64	65.33	94.784	29.1	0.000837	5.47E-05	1.73E+03	2.25E+03	8.74E+00
<b>Geopolymer Ref.+0.5g TiO<sub>2</sub>-2</b>	32.38	65.05	93.656	27.8	0.000823	5.36E-05	1.75E+03	2.34E+03	9.57E+00

➤ **TD-4 – TB-8-R – 3 days**

Plugs	OD, mm	Length, mm	Mass, g	Sonic, $\mu$ s	Area, m <sup>2</sup>	Volume, m <sup>3</sup>	Density, kg/m <sup>3</sup>	v <sub>p</sub> , m/s	M-modulus, GPa
TD-4- Ref.-1	32.26	66.22	100.731	21.5	0.000817	5.41E-05	1.86E+03	3.08E+03	1.77E+01
TD-4-Ref.-2	32.38	66.43	101.018	22.8	0.000823	5.47E-05	1.85E+03	2.91E+03	1.57E+01
TD-4-Ref.+ 0.15g TiO <sub>2</sub> -1	32.34	66	100.482	22.4	0.000821	5.42E-05	1.85E+03	2.95E+03	1.61E+01
TD-4-Ref.+ 0.15g TiO <sub>2</sub> -2	32.39	66.09	100.803	22.4	0.000824	5.45E-05	1.85E+03	2.95E+03	1.61E+01
TD-4-Ref.+ 0.25g TiO <sub>2</sub> -1	32.74	66.21	100.837	22.7	0.000842	5.57E-05	1.81E+03	2.92E+03	1.54E+01
TD-4-Ref.+ 0.25g TiO <sub>2</sub> -2	32.35	66.57	101.399	22.1	0.000822	5.47E-05	1.85E+03	3.01E+03	1.68E+01
TD-4-Ref.+ 0.35g TiO <sub>2</sub> -1	32.46	66.33	101.263	22.3	0.000828	5.49E-05	1.84E+03	2.97E+03	1.63E+01
TD-4-Ref.+ 0.35g TiO <sub>2</sub> -2	32.49	66.55	100.639	22.2	0.000829	5.52E-05	1.82E+03	3.00E+03	1.64E+01
TD-4-Ref.+ 0.45g TiO <sub>2</sub> -1	32.45	66.42	100.625	23.4	0.000827	5.49E-05	1.83E+03	2.84E+03	1.48E+01
TD-4-Ref.+ 0.45g TiO <sub>2</sub> -2	32.29	66.36	100.768	21.9	0.000819	5.43E-05	1.85E+03	3.03E+03	1.70E+01

➤ **TD-4 – TB-8-O – 3 days**

Plugs	OD, mm	Length, mm	Mass, g	Sonic, $\mu$ s	Area, m <sup>2</sup>	Volume, m <sup>3</sup>	Density, kg/m <sup>3</sup>	v <sub>p</sub> , m/s	M-modulus, GPa
TD-4- Ref.-1	32.41	65.76	92.781	22.6	0.000825	5.43E-05	1.71E+03	2.91E+03	1.45E+01
TD-4-Ref.-2	32.39	65.81	91.215	22.8	0.000824	5.42E-05	1.68E+03	2.89E+03	1.40E+01
TD-4-Ref.+ 0.15g TiO <sub>2</sub> -1	32.49	65.97	91.7	23.2	0.000829	5.47E-05	1.68E+03	2.84E+03	1.36E+01
TD-4-Ref.+ 0.15g TiO <sub>2</sub> -2	32.59	65.99	92.57	23.1	0.000834	5.50E-05	1.68E+03	2.86E+03	1.37E+01
TD-4-Ref.+ 0.25g TiO <sub>2</sub> -1	32.34	66.07	92.966	23.5	0.000821	5.43E-05	1.71E+03	2.81E+03	1.35E+01
TD-4-Ref.+ 0.25g TiO <sub>2</sub> -2	32.25	66.09	92.665	23.1	0.000817	5.40E-05	1.72E+03	2.86E+03	1.41E+01
TD-4-Ref.+ 0.35g TiO <sub>2</sub> -1	32.26	66.04	91.991	23.3	0.000817	5.40E-05	1.70E+03	2.83E+03	1.37E+01
TD-4-Ref.+ 0.35g TiO <sub>2</sub> -2	32.36	66.32	92.378	23.9	0.000822	5.45E-05	1.69E+03	2.77E+03	1.30E+01
TD-4-Ref.+ 0.45g TiO <sub>2</sub> -1	32.7	66.07	94.02	22.7	0.000840	5.55E-05	1.69E+03	2.91E+03	1.44E+01
TD-4-Ref.+ 0.45g TiO <sub>2</sub> -2	32.32	66.3	92.082	23.3	0.000820	5.44E-05	1.69E+03	2.85E+03	1.37E+01

➤ **TD-4 – TB-9-R – 7 days**

Plugs	OD, mm	Length, mm	Mass, g	Sonic, $\mu$ s	Area, m <sup>2</sup>	Volume, m <sup>3</sup>	Density, kg/m <sup>3</sup>	$v_p$ , m/s	M-modulus, GPa
TD-4- Ref.-1	32.75	63.97	98.851	20.1	0.000842	5.39E-05	1.83E+03	3.18E+03	1.86E+01
TD-4-Ref.-2	32.75	65.83	100.81	20.3	0.000842	5.55E-05	1.82E+03	3.24E+03	1.91E+01
TD-4-Ref.+ 0.15g TiO <sub>2</sub> -1	32.77	66.32	102.949	21.1	0.000843	5.59E-05	1.84E+03	3.14E+03	1.82E+01
TD-4-Ref.+ 0.15g TiO <sub>2</sub> -2	32.69	64.56	101.573	20.2	0.000839	5.42E-05	1.87E+03	3.20E+03	1.91E+01
TD-4-Ref.+ 0.25g TiO <sub>2</sub> -1	32.6	65.52	102.893	20	0.000835	5.47E-05	1.88E+03	3.28E+03	2.02E+01
TD-4-Ref.+ 0.25g TiO <sub>2</sub> -2	32.81	66.14	103.726	20.6	0.000845	5.59E-05	1.85E+03	3.21E+03	1.91E+01
TD-4-Ref.+ 0.35g TiO <sub>2</sub> -1	32.81	66.24	101.21	21.9	0.000845	5.60E-05	1.81E+03	3.02E+03	1.65E+01
TD-4-Ref.+ 0.35g TiO <sub>2</sub> -2	32.58	65.53	100.972	19.7	0.000834	5.46E-05	1.85E+03	3.33E+03	2.05E+01
TD-4-Ref.+ 0.45g TiO <sub>2</sub> -1	32.83	65.72	103.08	20.5	0.000847	5.56E-05	1.85E+03	3.21E+03	1.90E+01
TD-4-Ref.+ 0.45g TiO <sub>2</sub> -2	32.7	65.8	103.158	21.2	0.000840	5.53E-05	1.87E+03	3.10E+03	1.80E+01

➤ **TD-4 – TB-9-O – 7 days**

Plugs	OD, mm	Length, mm	Mass, g	Sonic, $\mu$ s	Area, m <sup>2</sup>	Volume, m <sup>3</sup>	Density, kg/m <sup>3</sup>	$v_p$ , m/s	M-modulus, GPa
TD-4- Ref.-1	32.31	66.4	86.937	23.2	0.000820	5.44E-05	1.60E+03	2.86E+03	1.31E+01
TD-4-Ref.-2	32.41	64.44	87.335	22.6	0.000825	5.32E-05	1.64E+03	2.85E+03	1.34E+01
TD-4-Ref.+ 0.15g TiO <sub>2</sub> -1	32.62	64.69	88.64	22.7	0.000836	5.41E-05	1.64E+03	2.85E+03	1.33E+01
TD-4-Ref.+ 0.15g TiO <sub>2</sub> -2	32.3	64.79	87.311	22.6	0.000819	5.31E-05	1.64E+03	2.87E+03	1.35E+01
TD-4-Ref.+ 0.25g TiO <sub>2</sub> -1	32.54	65.23	87.818	23.2	0.000832	5.42E-05	1.62E+03	2.81E+03	1.28E+01
TD-4-Ref.+ 0.25g TiO <sub>2</sub> -2	32.35	64.53	87.147	22	0.000822	5.30E-05	1.64E+03	2.93E+03	1.41E+01
TD-4-Ref.+ 0.35g TiO <sub>2</sub> -1	32.31	64.74	87.571	22.8	0.000820	5.31E-05	1.65E+03	2.84E+03	1.33E+01
TD-4-Ref.+ 0.35g TiO <sub>2</sub> -2	32.24	64.75	86.756	21.9	0.000816	5.29E-05	1.64E+03	2.96E+03	1.43E+01
TD-4-Ref.+ 0.45g TiO <sub>2</sub> -1	32.58	65.15	87.844	22.2	0.000834	5.43E-05	1.62E+03	2.93E+03	1.39E+01
TD-4-Ref.+ 0.45g TiO <sub>2</sub> -2	32.49	64.88	86.98	23	0.000829	5.38E-05	1.62E+03	2.82E+03	1.29E+01



➤ **TD-4 – TB-10-R – 28 days**

Plugs	OD, mm	Length, mm	Mass, g	Sonic, $\mu$ s	Area, m <sup>2</sup>	Volume, m <sup>3</sup>	Density, kg/m <sup>3</sup>	$v_p$ , m/s	M-modulus, GPa
TD-4- Ref.-1	32.78	66.23	100.89	21.3	0.000844	5.59E-05	1.81E+03	3.11E+03	1.75E+01
TD-4-Ref.-2	32.94	65.98	100.546	21.3	0.000852	5.62E-05	1.79E+03	3.10E+03	1.72E+01
TD-4-Ref.+ 0.15g TiO <sub>2</sub> -1	32.91	67.07	102.215	21.9	0.000851	5.71E-05	1.79E+03	3.06E+03	1.68E+01
TD-4-Ref.+ 0.15g TiO <sub>2</sub> -2	32.92	65.2	99.896	20.6	0.000851	5.55E-05	1.80E+03	3.17E+03	1.80E+01
TD-4-Ref.+ 0.25g TiO <sub>2</sub> -1	33.07	66.07	100.793	21.8	0.000859	5.67E-05	1.78E+03	3.03E+03	1.63E+01
TD-4-Ref.+ 0.25g TiO <sub>2</sub> -2	32.89	67.05	102.439	21.4	0.000850	5.70E-05	1.80E+03	3.13E+03	1.77E+01
TD-4-Ref.+ 0.35g TiO <sub>2</sub> -1	33.11	66.96	102.003	22.1	0.000861	5.77E-05	1.77E+03	3.03E+03	1.62E+01
TD-4-Ref.+ 0.35g TiO <sub>2</sub> -2	33.04	66.73	101.405	21.9	0.000857	5.72E-05	1.77E+03	3.05E+03	1.65E+01
TD-4-Ref.+ 0.45g TiO <sub>2</sub> -1	32.63	65.45	98.672	21.8	0.000836	5.47E-05	1.80E+03	3.00E+03	1.63E+01
TD-4-Ref.+ 0.45g TiO <sub>2</sub> -2	32.48	65.89	99.611	21	0.000829	5.46E-05	1.82E+03	3.14E+03	1.80E+01

➤ **TD-4 – TB-10-O – 28 days**

Plugs	OD, mm	Length, mm	Mass, g	Sonic, $\mu$ s	Area, m <sup>2</sup>	Volume, m <sup>3</sup>	Density, kg/m <sup>3</sup>	$v_p$ , m/s	M-modulus, GPa
TD-4- Ref.-1	33.06	66.14	86.517	23.5	0.000858	5.68E-05	1.52E+03	2.81E+03	1.21E+01
TD-4-Ref.-2	32.71	67.19	88.797	23.2	0.000840	5.65E-05	1.57E+03	2.90E+03	1.32E+01
TD-4-Ref.+ 0.15g TiO <sub>2</sub> -1	32.87	67	87.877	23.5	0.000849	5.69E-05	1.55E+03	2.85E+03	1.26E+01
TD-4-Ref.+ 0.15g TiO <sub>2</sub> -2	32.78	66.98	88.27	23.7	0.000844	5.65E-05	1.56E+03	2.83E+03	1.25E+01
TD-4-Ref.+ 0.25g TiO <sub>2</sub> -1	32.43	66.07	85.244	23.2	0.000826	5.46E-05	1.56E+03	2.85E+03	1.27E+01
TD-4-Ref.+ 0.25g TiO <sub>2</sub> -2	32.32	65.61	85.659	22.5	0.000820	5.38E-05	1.59E+03	2.92E+03	1.35E+01
TD-4-Ref.+ 0.35g TiO <sub>2</sub> -1	32.37	66.19	84.599	22.8	0.000823	5.45E-05	1.55E+03	2.90E+03	1.31E+01
TD-4-Ref.+ 0.35g TiO <sub>2</sub> -2	32.49	66.11	84.775	24.3	0.000829	5.48E-05	1.55E+03	2.72E+03	1.14E+01
TD-4-Ref.+ 0.45g TiO <sub>2</sub> -1	32.33	66.31	84.79	23.5	0.000821	5.44E-05	1.56E+03	2.82E+03	1.24E+01
TD-4-Ref.+ 0.45g TiO <sub>2</sub> -2	32.27	65.01	84.812	22.6	0.000818	5.32E-05	1.60E+03	2.88E+03	1.32E+01

➤ **TD-5 – TB-11-R – 3 days**

Plugs	OD, mm	Length, mm	Mass, g	Sonic, $\mu$ s	Area, m <sup>2</sup>	Volume, m <sup>3</sup>	Density, kg/m <sup>3</sup>	$v_p$ , m/s	M-modulus, GPa
TD-5-Ref.-0/0-1	32.51	66.5	99.823	24.4	0.000830	5.52E-05	1.81E+03	2.73E+03	1.34E+01
TD-5-Ref.-0/0-2	32.48	66.47	99.934	25.2	0.000829	5.51E-05	1.81E+03	2.64E+03	1.26E+01
TD-5-Ref.+0/0.45g TiO <sub>2</sub> -1	32.6	66.36	100.228	24.3	0.000835	5.54E-05	1.81E+03	2.73E+03	1.35E+01
TD-5-Ref.+0/0.45g TiO <sub>2</sub> -2	32.49	66.4	99.783	24.4	0.000829	5.51E-05	1.81E+03	2.72E+03	1.34E+01
TD-5-Ref.+0.1g CF/0.45g TiO <sub>2</sub> -1	32.45	66.17	99.677	23.6	0.000827	5.47E-05	1.82E+03	2.80E+03	1.43E+01
TD-5-Ref.+0.1g CF/0.45g TiO <sub>2</sub> -2	32.44	66.26	100.31	23.4	0.000827	5.48E-05	1.83E+03	2.83E+03	1.47E+01
TD-5-Ref.+0.2g CF/0.45g TiO <sub>2</sub> -1	32.37	65.88	99.164	24.1	0.000823	5.42E-05	1.83E+03	2.73E+03	1.37E+01
TD-5-Ref.+0.2g CF/0.45g TiO <sub>2</sub> -2	32.42	66	100.041	23.4	0.000825	5.45E-05	1.84E+03	2.82E+03	1.46E+01
TD-5-Ref.+0.3g CF/0.45g TiO <sub>2</sub> -1	32.39	65.95	99.759	23.2	0.000824	5.43E-05	1.84E+03	2.84E+03	1.48E+01
TD-5-Ref.+0.3g CF/0.45g TiO <sub>2</sub> -2	32.36	66.15	99.709	23.4	0.000822	5.44E-05	1.83E+03	2.83E+03	1.46E+01
TD-5-Ref.+0.1g WF/0.45g TiO <sub>2</sub> -1	32.61	66.49	100.317	23.7	0.000835	5.55E-05	1.81E+03	2.81E+03	1.42E+01
TD-5-Ref.+0.1g WF/0.45g TiO <sub>2</sub> -2	32.4	66.55	99.552	23.6	0.000824	5.49E-05	1.81E+03	2.82E+03	1.44E+01
TD-5-Ref.+0.2g WF/0.45g TiO <sub>2</sub> -1	32.28	66.77	99.577	24.1	0.000818	5.46E-05	1.82E+03	2.77E+03	1.40E+01
TD-5-Ref.+0.2g WF/0.45g TiO <sub>2</sub> -2	32.26	66.32	99.597	23.5	0.000817	5.42E-05	1.84E+03	2.82E+03	1.46E+01
TD-5-Ref.+0.3g WF/0.45g TiO <sub>2</sub> -1	32.26	66.5	100.031	23.1	0.000817	5.44E-05	1.84E+03	2.88E+03	1.53E+01
TD-5-Ref.+0.3g WF/0.45g TiO <sub>2</sub> -2	32.25	66.11	99.737	23.4	0.000817	5.40E-05	1.85E+03	2.83E+03	1.47E+01

➤ **TD-5 – TB-11-O – 3 days**

Plugs	OD, mm	Length, mm	Mass, g	Sonic, $\mu$ s	Area, m <sup>2</sup>	Volume, m <sup>3</sup>	Density, kg/m <sup>3</sup>	$v_p$ , m/s	M-modulus, GPa
TD-5-Ref.-0/0-1	32.69	63.57	88.296	22.6	0.000839	5.34E-05	1.65E+03	2.81E+03	1.31E+01
TD-5-Ref.-0/0-2	32.56	64.68	89.665	22.9	0.000833	5.39E-05	1.66E+03	2.82E+03	1.33E+01
TD-5-Ref.+0/0.45g TiO <sub>2</sub> -1	32.56	65.98	90.5	24.1	0.000833	5.49E-05	1.65E+03	2.74E+03	1.23E+01
TD-5-Ref.+0/0.45g TiO <sub>2</sub> -2	32.56	65.94	91.326	24.2	0.000833	5.49E-05	1.66E+03	2.72E+03	1.23E+01
TD-5-Ref.+0.1g CF/0.45g TiO <sub>2</sub> -1	32.49	65.7	90.315	22.9	0.000829	5.45E-05	1.66E+03	2.87E+03	1.36E+01
TD-5-Ref.+0.1g CF/0.45g TiO <sub>2</sub> -2	32.36	65.86	90.381	22.9	0.000822	5.42E-05	1.67E+03	2.88E+03	1.38E+01
TD-5-Ref.+0.2g CF/0.45g TiO <sub>2</sub> -1	32.56	66	91.352	22.9	0.000833	5.50E-05	1.66E+03	2.88E+03	1.38E+01
TD-5-Ref.+0.2g CF/0.45g TiO <sub>2</sub> -2	32.19	65.97	91.115	22.9	0.000814	5.37E-05	1.70E+03	2.88E+03	1.41E+01
TD-5-Ref.+0.3g CF/0.45g TiO <sub>2</sub> -1	32.36	66.65	91.079	23.1	0.000822	5.48E-05	1.66E+03	2.89E+03	1.38E+01
TD-5-Ref.+0.3g CF/0.45g TiO <sub>2</sub> -2	32.38	65.79	91.411	22.9	0.000823	5.42E-05	1.69E+03	2.87E+03	1.39E+01
TD-5-Ref.+0.1g WF/0.45g TiO <sub>2</sub> -1	32.5	65.96	91.407	23.1	0.000830	5.47E-05	1.67E+03	2.86E+03	1.36E+01
TD-5-Ref.+0.1g WF/0.45g TiO <sub>2</sub> -2	32.56	66.46	92.434	22.9	0.000833	5.53E-05	1.67E+03	2.90E+03	1.41E+01
TD-5-Ref.+0.2g WF/0.45g TiO <sub>2</sub> -1	32.53	66.11	92.23	23.3	0.000831	5.49E-05	1.68E+03	2.84E+03	1.35E+01
TD-5-Ref.+0.2g WF/0.45g TiO <sub>2</sub> -2	32.22	66.24	92.262	23.2	0.000815	5.40E-05	1.71E+03	2.86E+03	1.39E+01
TD-5-Ref.+0.3g WF/0.45g TiO <sub>2</sub> -1	32.23	65.74	91.568	22.9	0.000816	5.36E-05	1.71E+03	2.87E+03	1.41E+01
TD-5-Ref.+0.3g WF/0.45g TiO <sub>2</sub> -2	32.51	66.18	92.111	23.1	0.000830	5.49E-05	1.68E+03	2.86E+03	1.38E+01

➤ **TD-5 – TB-12-R – 7 days**

Plugs	OD, mm	Length, mm	Mass, g	Sonic, $\mu$ s	Area, m <sup>2</sup>	Volume, m <sup>3</sup>	Density, kg/m <sup>3</sup>	$v_p$ , m/s	M-modulus, GPa
TD-5-Ref.-0/0-1	32.5	63.68	98.499	19.4	0.000830	5.28E-05	1.86E+03	3.28E+03	2.01E+01
TD-5-Ref.-0/0-2	32.35	66.43	101.407	20.2	0.000822	5.46E-05	1.86E+03	3.29E+03	2.01E+01
TD-5-Ref.+0/0.45g TiO <sub>2</sub> -1	32.33	66.29	99.559	21.4	0.000821	5.44E-05	1.83E+03	3.10E+03	1.76E+01
TD-5-Ref.+0/0.45g TiO <sub>2</sub> -2	32.55	65.64	100.119	20.8	0.000832	5.46E-05	1.83E+03	3.16E+03	1.83E+01
TD-5-Ref.+0.1g CF/0.45g TiO <sub>2</sub> -1	32.35	65.71	99.305	20.5	0.000822	5.40E-05	1.84E+03	3.21E+03	1.89E+01
TD-5-Ref.+0.1g CF/0.45g TiO <sub>2</sub> -2	32.21	64.88	97.905	20.4	0.000815	5.29E-05	1.85E+03	3.18E+03	1.87E+01
TD-5-Ref.+0.2g CF/0.45g TiO <sub>2</sub> -1	32.33	65.47	98.575	20.4	0.000821	5.37E-05	1.83E+03	3.21E+03	1.89E+01
TD-5-Ref.+0.2g CF/0.45g TiO <sub>2</sub> -2	32.04	64.48	96.547	19.3	0.000806	5.20E-05	1.86E+03	3.34E+03	2.07E+01
TD-5-Ref.+0.3g CF/0.45g TiO <sub>2</sub> -1	32	64.34	96.084	19.3	0.000804	5.17E-05	1.86E+03	3.33E+03	2.06E+01
TD-5-Ref.+0.3g CF/0.45g TiO <sub>2</sub> -2	32.26	64.96	97.958	20.2	0.000817	5.31E-05	1.84E+03	3.22E+03	1.91E+01
TD-5-Ref.+0.1g WF/0.45g TiO <sub>2</sub> -1	32.19	66.31	100.154	20.7	0.000814	5.40E-05	1.86E+03	3.20E+03	1.90E+01
TD-5-Ref.+0.1g WF/0.45g TiO <sub>2</sub> -2	32.29	64.8	98.167	20.6	0.000819	5.31E-05	1.85E+03	3.15E+03	1.83E+01
TD-5-Ref.+0.2g WF/0.45g TiO <sub>2</sub> -1	32.03	65.48	99.346	20.2	0.000806	5.28E-05	1.88E+03	3.24E+03	1.98E+01
TD-5-Ref.+0.2g WF/0.45g TiO <sub>2</sub> -2	32.38	64.75	98.835	20	0.000823	5.33E-05	1.85E+03	3.24E+03	1.94E+01
TD-5-Ref.+0.3g WF/0.45g TiO <sub>2</sub> -1	31.87	65.12	97.303	19.6	0.000798	5.19E-05	1.87E+03	3.32E+03	2.07E+01
TD-5-Ref.+0.3g WF/0.45g TiO <sub>2</sub> -2	31.64	64.79	97.507	18.9	0.000786	5.09E-05	1.91E+03	3.43E+03	2.25E+01

➤ **TD-5 – TB-12-O – 7 days**

Plugs	OD, mm	Length, mm	Mass, g	Sonic, $\mu$ s	Area, m <sup>2</sup>	Volume, m <sup>3</sup>	Density, kg/m <sup>3</sup>	$v_p$ , m/s	M-modulus, GPa
TD-5-Ref.-0/0-1	32.28	65.75	86.334	22.8	0.000818	5.38E-05	1.60E+03	2.88E+03	1.33E+01
TD-5-Ref.-0/0-2	32.37	65.24	87.005	23.5	0.000823	5.37E-05	1.62E+03	2.78E+03	1.25E+01
TD-5-Ref.+0/0.45g TiO <sub>2</sub> -1	32.32	65.7	86.505	23.6	0.000820	5.39E-05	1.60E+03	2.78E+03	1.24E+01
TD-5-Ref.+0/0.45g TiO <sub>2</sub> -2	32.35	64.51	85.245	22.9	0.000822	5.30E-05	1.61E+03	2.82E+03	1.28E+01
TD-5-Ref.+0.1g CF/0.45g TiO <sub>2</sub> -1	32.3	65.18	85.997	23	0.000819	5.34E-05	1.61E+03	2.83E+03	1.29E+01
TD-5-Ref.+0.1g CF/0.45g TiO <sub>2</sub> -2	32.35	64.61	85.063	22.8	0.000822	5.31E-05	1.60E+03	2.83E+03	1.29E+01
TD-5-Ref.+0.2g CF/0.45g TiO <sub>2</sub> -1	32.54	64.78	85.505	23.1	0.000832	5.39E-05	1.59E+03	2.80E+03	1.25E+01
TD-5-Ref.+0.2g CF/0.45g TiO <sub>2</sub> -2	31.89	63.85	84.883	21.7	0.000799	5.10E-05	1.66E+03	2.94E+03	1.44E+01
TD-5-Ref.+0.3g CF/0.45g TiO <sub>2</sub> -1	31.37	63.7	84.19	20.3	0.000773	4.92E-05	1.71E+03	3.14E+03	1.68E+01
TD-5-Ref.+0.3g CF/0.45g TiO <sub>2</sub> -2	31.84	64.61	85.17	21.8	0.000796	5.14E-05	1.66E+03	2.96E+03	1.45E+01
TD-5-Ref.+0.1g WF/0.45g TiO <sub>2</sub> -1	32.18	65.43	86.592	21.7	0.000813	5.32E-05	1.63E+03	3.02E+03	1.48E+01
TD-5-Ref.+0.1g WF/0.45g TiO <sub>2</sub> -2	32.18	65.46	86.858	22.9	0.000813	5.32E-05	1.63E+03	2.86E+03	1.33E+01
TD-5-Ref.+0.2g WF/0.45g TiO <sub>2</sub> -1	32.28	64.15	85.133	21.5	0.000818	5.25E-05	1.62E+03	2.98E+03	1.44E+01
TD-5-Ref.+0.2g WF/0.45g TiO <sub>2</sub> -2	32.27	65.39	86.295	23.4	0.000818	5.35E-05	1.61E+03	2.79E+03	1.26E+01
TD-5-Ref.+0.3g WF/0.45g TiO <sub>2</sub> -1	32.44	63.97	84.634	22.4	0.000827	5.29E-05	1.60E+03	2.86E+03	1.31E+01
TD-5-Ref.+0.3g WF/0.45g TiO <sub>2</sub> -2	32.28	63.6	84.232	22.5	0.000818	5.20E-05	1.62E+03	2.83E+03	1.29E+01

➤ **TD-5 – TB-13-R – 28 days**

Plugs	OD, mm	Length, mm	Mass, g	Sonic, $\mu$ s	Area, m <sup>2</sup>	Volume, m <sup>3</sup>	Density, kg/m <sup>3</sup>	$v_p$ , m/s	M-modulus, GPa
TD-5-Ref.-0/0-1	32.48	65.95	97.943	21.5	0.000829	5.46E-05	1.79E+03	3.07E+03	1.69E+01
TD-5-Ref.-0/0-2	32.47	64.55	96.66	20.5	0.000828	5.35E-05	1.81E+03	3.15E+03	1.79E+01
TD-5-Ref.+0/0.45g TiO <sub>2</sub> -1	32.63	66.25	99.263	21.3	0.000836	5.54E-05	1.79E+03	3.11E+03	1.73E+01
TD-5-Ref.+0/0.45g TiO <sub>2</sub> -2	32.52	66.26	99.315	21.2	0.000831	5.50E-05	1.80E+03	3.13E+03	1.76E+01
TD-5-Ref.+0.1g CF/0.45g TiO <sub>2</sub> -1	32.45	65.98	99.513	20.8	0.000827	5.46E-05	1.82E+03	3.17E+03	1.84E+01
TD-5-Ref.+0.1g CF/0.45g TiO <sub>2</sub> -2	32.4	66.51	99.513	21.2	0.000824	5.48E-05	1.81E+03	3.14E+03	1.79E+01
TD-5-Ref.+0.2g CF/0.45g TiO <sub>2</sub> -1	32.59	66.38	100.576	20.5	0.000834	5.54E-05	1.82E+03	3.24E+03	1.90E+01
TD-5-Ref.+0.2g CF/0.45g TiO <sub>2</sub> -2	32.51	66.25	99.133	20.5	0.000830	5.50E-05	1.80E+03	3.23E+03	1.88E+01
TD-5-Ref.+0.3g CF/0.45g TiO <sub>2</sub> -1	32.58	65.45	98.674	20.4	0.000834	5.46E-05	1.81E+03	3.21E+03	1.86E+01
TD-5-Ref.+0.3g CF/0.45g TiO <sub>2</sub> -2	32.39	63.94	96.41	20.1	0.000824	5.27E-05	1.83E+03	3.18E+03	1.85E+01
TD-5-Ref.+0.1g WF/0.45g TiO <sub>2</sub> -1	32.49	66.02	98.306	20.8	0.000829	5.47E-05	1.80E+03	3.17E+03	1.81E+01
TD-5-Ref.+0.1g WF/0.45g TiO <sub>2</sub> -2	32.35	65.62	97.624	20.8	0.000822	5.39E-05	1.81E+03	3.15E+03	1.80E+01
TD-5-Ref.+0.2g WF/0.45g TiO <sub>2</sub> -1	32.54	65.98	99.527	20.8	0.000832	5.49E-05	1.81E+03	3.17E+03	1.83E+01
TD-5-Ref.+0.2g WF/0.45g TiO <sub>2</sub> -2	32.48	65.73	99.22	21.3	0.000829	5.45E-05	1.82E+03	3.09E+03	1.73E+01
TD-5-Ref.+0.3g WF/0.45g TiO <sub>2</sub> -1	32.46	65.8	98.702	20.8	0.000828	5.45E-05	1.81E+03	3.16E+03	1.81E+01
TD-5-Ref.+0.3g WF/0.45g TiO <sub>2</sub> -2	32.73	66.27	98.952	21.3	0.000841	5.58E-05	1.77E+03	3.11E+03	1.72E+01

➤ **TD-5 – TB-13-O – 28 days**

Plugs	OD, mm	Length, mm	Mass, g	Sonic, $\mu$ s	Area, m <sup>2</sup>	Volume, m <sup>3</sup>	Density, kg/m <sup>3</sup>	$v_p$ , m/s	M-modulus, GPa
TD-5-Ref.-0/0-1	32.38	65.66	84.176	22.9	0.000823	5.41E-05	1.56E+03	2.87E+03	1.28E+01
TD-5-Ref.-0/0-2	32.27	66.28	85.376	22.4	0.000818	5.42E-05	1.57E+03	2.96E+03	1.38E+01
TD-5-Ref.+0/0.45g TiO <sub>2</sub> -1	32.7	66.21	84.838	22.1	0.000840	5.56E-05	1.53E+03	3.00E+03	1.37E+01
TD-5-Ref.+0/0.45g TiO <sub>2</sub> -2	32.6	64.86	83.625	21.7	0.000835	5.41E-05	1.54E+03	2.99E+03	1.38E+01
TD-5-Ref.+0.1g CF/0.45g TiO <sub>2</sub> -1	32.66	65.8	84.07	22.9	0.000838	5.51E-05	1.53E+03	2.87E+03	1.26E+01
TD-5-Ref.+0.1g CF/0.45g TiO <sub>2</sub> -2	32.42	66.03	84.6	22.7	0.000825	5.45E-05	1.55E+03	2.91E+03	1.31E+01
TD-5-Ref.+0.2g CF/0.45g TiO <sub>2</sub> -1	32.46	66.09	85.516	22.7	0.000828	5.47E-05	1.56E+03	2.91E+03	1.33E+01
TD-5-Ref.+0.2g CF/0.45g TiO <sub>2</sub> -2	32.42	66.24	85.54	22.8	0.000825	5.47E-05	1.56E+03	2.91E+03	1.32E+01
TD-5-Ref.+0.3g CF/0.45g TiO <sub>2</sub> -1	32.37	66.02	86.55	22.5	0.000823	5.43E-05	1.59E+03	2.93E+03	1.37E+01
TD-5-Ref.+0.3g CF/0.45g TiO <sub>2</sub> -2	32.44	66.39	86.682	22.3	0.000827	5.49E-05	1.58E+03	2.98E+03	1.40E+01
TD-5-Ref.+0.1g WF/0.45g TiO <sub>2</sub> -1	32.42	66.07	84.627	23.2	0.000825	5.45E-05	1.55E+03	2.85E+03	1.26E+01
TD-5-Ref.+0.1g WF/0.45g TiO <sub>2</sub> -2	32.54	65.97	84.761	23	0.000832	5.49E-05	1.54E+03	2.87E+03	1.27E+01
TD-5-Ref.+0.2g WF/0.45g TiO <sub>2</sub> -1	32.47	66.08	85.388	22.6	0.000828	5.47E-05	1.56E+03	2.92E+03	1.33E+01
TD-5-Ref.+0.2g WF/0.45g TiO <sub>2</sub> -2	32.38	65.85	85.993	22.5	0.000823	5.42E-05	1.59E+03	2.93E+03	1.36E+01
TD-5-Ref.+0.3g WF/0.45g TiO <sub>2</sub> -1	32.44	66.06	85.545	21.8	0.000827	5.46E-05	1.57E+03	3.03E+03	1.44E+01
TD-5-Ref.+0.3g WF/0.45g TiO <sub>2</sub> -2	32.25	64.78	84.36	21.5	0.000817	5.29E-05	1.59E+03	3.01E+03	1.45E+01

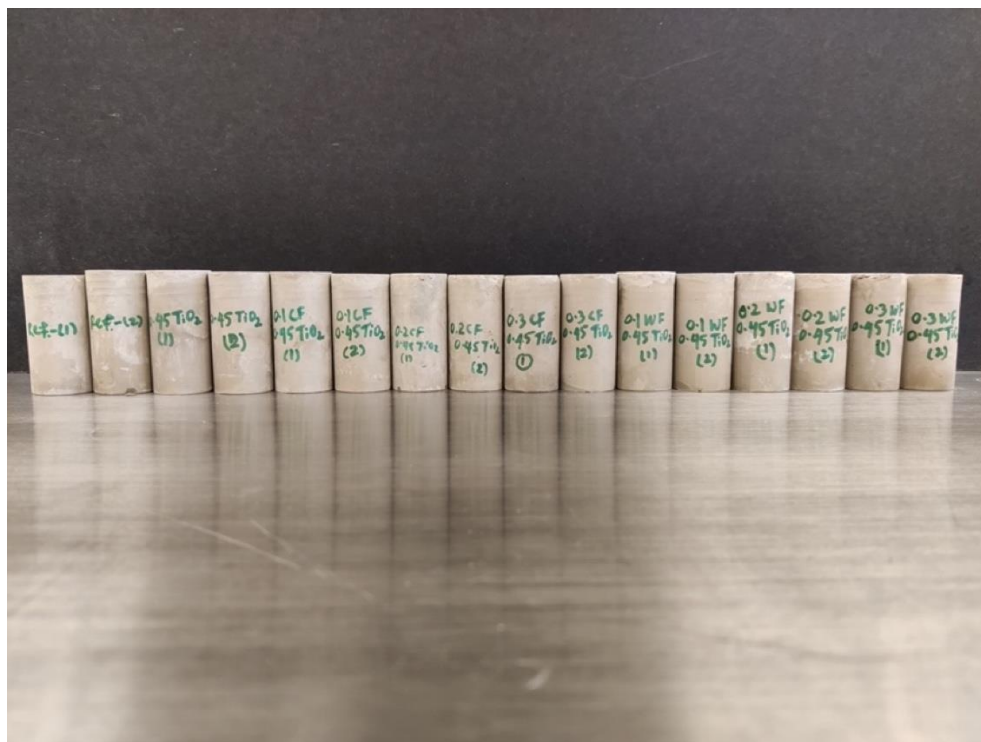
## Appendix D – Supplementary pictures of cement plugs and equipment from the experiments

This section includes various auxiliary photographs taken over the course of this thesis. The following pictures are going to demonstrate the cement samples in various conditions.

- *Geopolymer plugs retrieved from the moulds, labelled and ready for testing*

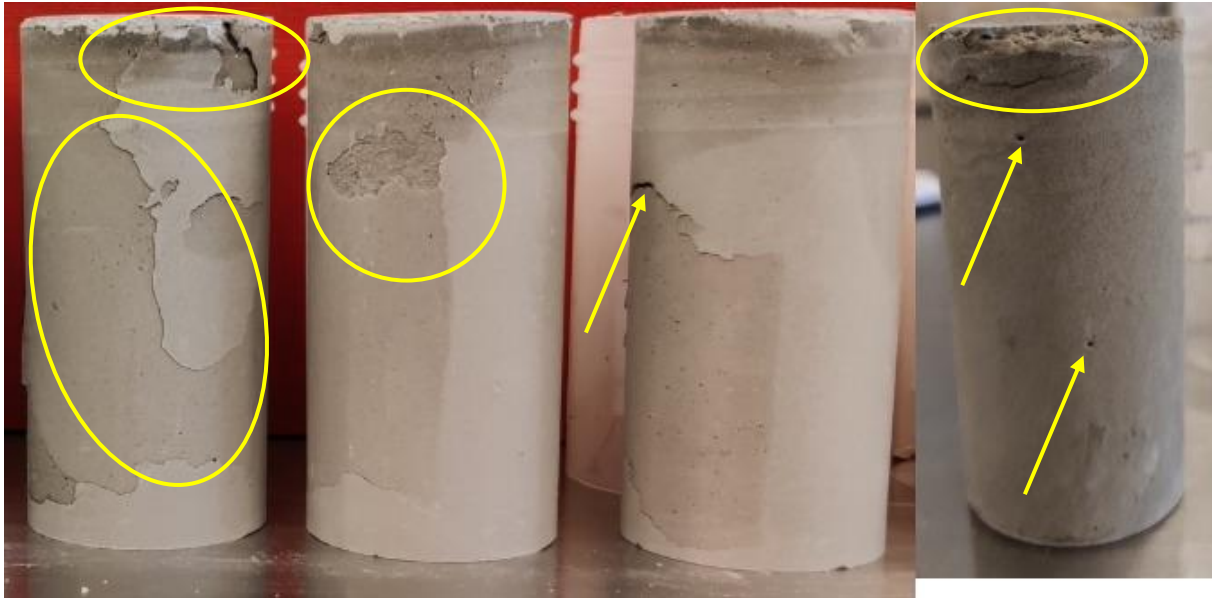


- *OPC plugs reinforced with TiO<sub>2</sub> NPs, carbon fibers and white glass fibers labelled, polished and prepared to be tested*





- *Samples with various defects visible on the surface, as such incidences occasionally ensued*



- *Visible differences: Left– Room-cured plug; Right– Oven-cured plug*



- *Samples inside an oven being cured at 80°C*



- *Example of a good sample*



- *Additives are properly measured and ready to be mixed with OPC– This is how additives were prepared every time before slurry synthesis*

